

Ajith Abraham · Sergey Kovalev
Valery Tarassov · Vaclav Snasel
Margreta Vasileva · Andrey Sukhanov *Editors*

Proceedings of the Second International Scientific Conference “Intelligent Information Technologies for Industry” (IITI’17)

Volume 2

Advances in Intelligent Systems and Computing

Volume 680

Series editor

Janusz Kacprzyk, Polish Academy of Sciences, Warsaw, Poland
e-mail: kacprzyk@ibspan.waw.pl

About this Series

The series “Advances in Intelligent Systems and Computing” contains publications on theory, applications, and design methods of Intelligent Systems and Intelligent Computing. Virtually all disciplines such as engineering, natural sciences, computer and information science, ICT, economics, business, e-commerce, environment, healthcare, life science are covered. The list of topics spans all the areas of modern intelligent systems and computing.

The publications within “Advances in Intelligent Systems and Computing” are primarily textbooks and proceedings of important conferences, symposia and congresses. They cover significant recent developments in the field, both of a foundational and applicable character. An important characteristic feature of the series is the short publication time and world-wide distribution. This permits a rapid and broad dissemination of research results.

Advisory Board

Chairman

Nikhil R. Pal, Indian Statistical Institute, Kolkata, India

e-mail: nikhil@isical.ac.in

Members

Rafael Bello Perez, Universidad Central “Marta Abreu” de Las Villas, Santa Clara, Cuba

e-mail: rbellop@uclv.edu.cu

Emilio S. Corchado, University of Salamanca, Salamanca, Spain

e-mail: escorchado@usal.es

Hani Hagrass, University of Essex, Colchester, UK

e-mail: hani@essex.ac.uk

László T. Kóczy, Széchenyi István University, Győr, Hungary

e-mail: koczy@sze.hu

Vladik Kreinovich, University of Texas at El Paso, El Paso, USA

e-mail: vladik@utep.edu

Chin-Teng Lin, National Chiao Tung University, Hsinchu, Taiwan

e-mail: ctlin@mail.nctu.edu.tw

Jie Lu, University of Technology, Sydney, Australia

e-mail: Jie.Lu@uts.edu.au

Patricia Melin, Tijuana Institute of Technology, Tijuana, Mexico

e-mail: epmelin@hafsamx.org

Nadia Nedjah, State University of Rio de Janeiro, Rio de Janeiro, Brazil

e-mail: nadia@eng.uerj.br

Ngoc Thanh Nguyen, Wroclaw University of Technology, Wroclaw, Poland

e-mail: Ngoc-Thanh.Nguyen@pwr.edu.pl

Jun Wang, The Chinese University of Hong Kong, Shatin, Hong Kong

e-mail: jwang@mae.cuhk.edu.hk

More information about this series at <http://www.springer.com/series/11156>

Ajith Abraham · Sergey Kovalev
Valery Tarassov · Vaclav Snasel
Margreta Vasileva · Andrey Sukhanov
Editors

Proceedings of the Second International Scientific Conference “Intelligent Information Technologies for Industry” (IITI’17)

Volume 2

 Springer

Editors

Ajith Abraham
Scientific Network for Innovation
and Research Excellence
Machine Intelligence Research Labs
(MIR labs)
Auburn, WA
USA

Sergey Kovalev
Rostov State Transport University
Rostov-on-Don
Russia

Valery Tarassov
Bauman Moscow State Technical University
Moscow
Russia

Vaclav Snašel
VSB-Technical University of Ostrava
Ostrava
Czech Republic

Margreta Vasileva
Department Electrical Power Engineering
Technical University of Varna
Varna
Bulgaria

Andrey Sukhanov
Rostov State Transport University
Rostov-on-Don
Russia

ISSN 2194-5357

ISSN 2194-5365 (electronic)

Advances in Intelligent Systems and Computing

ISBN 978-3-319-68323-2

ISBN 978-3-319-68324-9 (eBook)

DOI 10.1007/978-3-319-68324-9

Library of Congress Control Number: 2017953420

© Springer International Publishing AG 2018

This work is subject to copyright. All rights are reserved by the Publisher, whether the whole or part of the material is concerned, specifically the rights of translation, reprinting, reuse of illustrations, recitation, broadcasting, reproduction on microfilms or in any other physical way, and transmission or information storage and retrieval, electronic adaptation, computer software, or by similar or dissimilar methodology now known or hereafter developed.

The use of general descriptive names, registered names, trademarks, service marks, etc. in this publication does not imply, even in the absence of a specific statement, that such names are exempt from the relevant protective laws and regulations and therefore free for general use.

The publisher, the authors and the editors are safe to assume that the advice and information in this book are believed to be true and accurate at the date of publication. Neither the publisher nor the authors or the editors give a warranty, express or implied, with respect to the material contained herein or for any errors or omissions that may have been made. The publisher remains neutral with regard to jurisdictional claims in published maps and institutional affiliations.

Printed on acid-free paper

This Springer imprint is published by Springer Nature

The registered company is Springer International Publishing AG

The registered company address is: Gewerbestrasse 11, 6330 Cham, Switzerland

Preface

This volume of *Advances in Intelligent Systems and Computing* contains papers presented at IITI 2017, the Second International Conference on Intelligent Information Technologies for Industry, which will be held on September 14–16 in Varna, Bulgaria. The conference was jointly co-organized by Technical University of Varna (Bulgaria), Technical University of Sofia (Bulgaria), VŠB Technical University of Ostrava (Czech Republic), and Rostov State Transport University (Russia).

The purpose of IITI 2017 was to bring together international researchers and industrial practitioners interested in the development and implementation of modern technologies for automation, informatization, computer science, artificial intelligence, transport, and power electrical engineering. The conference aimed at advancing both fundamental research and innovative applications, and sought to establish a new dissemination platform and an international network of researchers in these fields. Innovative information technologies were of particular interest to the conference. There were 235 paper submissions from 13 countries. Each submission was reviewed by at least three Chairs or PC members. The conference was selective and accepted 106 regular papers (45%) for presentation. Unfortunately, due to limitations of conference topics and edited volumes, the Program Committee was forced to reject some interesting papers which did not satisfy these topics or publisher requirements. We would like to thank all authors and reviewers for their work and valuable contributions. The friendly and welcoming attitude of conference supporters and contributors made this event a success!

July 2017

Ajith Abraham
Sergey Kovalev
Valery Tarassov
Václav Snášel
Margreta Vasileva
Andrey Sukhanov

Organization

Conference Chairs

Rosen Vasilev	Technical University of Varna, Bulgaria
Václav Snášel	VŠB-TU Ostrava, Czech Republic
Sergey M. Kovalev	Rostov State Transport University, Russia
Alexander N. Guda	Rostov State Transport University, Russia

Conference Vice-chairs

Margreta Vasileva	Technical University of Varna, Bulgaria
Lačezar Ličev	VŠB-TU Ostrava, Czech Republic

International Program Committee

Aboul Ella Hassanien	Cairo University, Egypt
Aleksandr Nazarchev	PEIPK, Russia
Alexander I. Dolgiy	JSC “NIIAS”, Rostov branch, Russia
Alexander L. Tulupyev	St. Petersburg Institute for Informatics and Automation of the Russian Academy of Sciences, Russia
Alexander N. Shabelnikov	JSC NIIAS, Russia
Alexander P. Ereemeev	Moscow Power Engineering Institute, Russia
Alexander V. Smirnov	St. Petersburg Institute for Informatics and Automation of the Russian Academy of Sciences, Russia
Alexey B. Petrovsky	Institute for Systems Analysis of Russian Academy of Sciences, Russia

Alexey N. Averkin	Dorodnitsyn Computing Centre of Russian Academy of Sciences, Russia
Alla V. Zaboлева-Zotova	Volgograd State Technical University, Russia
Anton Beláň	Slovak University of Technology in Bratislava, Slovakia
Angel Colov	Technical University of Sofia, Bulgaria
Bakytzhan Kuanyshhev	Kazakh Academy of Transport and Communications named after M. Tynyshpayev, Kazakhstan
Bronislav Firago	Belarusian National Technical University, Belarus
Dilyana Gospodinova	Technical University of Sofia, Bulgaria
Dimitar Bogdanov	Technical University of Sofia, Bulgaria
Dimo Stoilov	Technical University of Sofia, Bulgaria
Dusan Husek	Institute of Computer Science, Academy of Sciences of the Czech Republic
Eid Emary	Cairo University, Egypt
Eliska Ochodkova	VŠB-TU Ostrava, Czech Republic, Czech Republic
Emil Panov	Technical University of Varna, Bulgaria
František Janíček	Slovak University of Technology in Bratislava, Slovakia
Gennady S. Osipov	Institute for Systems Analysis of Russian Academy of Sciences, Russia
Habib M. Kammoun	University of Sfax, Tunisia
Igor B. Fominykh	Moscow Power Engineering Institute, Russia
Igor D. Dolgiy	Rostov State Transport University, Russia
Igor Kurytnik	University of Bielsko-Biała, Poland
Ildar Batyrshin	National Polytechnic Institute, Mexico
Ivan Angelov	Technical University of Sofia, Bulgaria
Ivan Zelinka	VŠB-TU Ostrava, Czech Republic, Czech Republic
Ján Vittek	University of Žilina, Slovakia
Jana Nowakova	VŠB-TU Ostrava, Czech Republic, Czech Republic
Jaroslav Kultán	University of Economics in Bratislava, Slovakia
Jiří Bouchala	VŠB-TU Ostrava, Czech Republic, Czech Republic
Jiří Hammerbauer	University of West Bohemia, Czech Republic
Josef Paleček	VŠB-TU Ostrava, Czech Republic, Czech Republic
Juan Velasquez	University of Chile, Chile
Konrad Jackowski	Wrocław University of Technology, Poland
Krum Gerasimov	Technical University of Varna, Bulgaria
Leszek Pawlaczek	Wrocław University of Technology, Poland

Marcin Paprzycki	IBS PAN and WSM, Poland
Marinela Yordanova	Technical University of Varna, Bulgaria
Michał Wozniak	Wrocław University of Technology, Poland
Mikołaj Bartłomiejczyk	Gdansk University of Technology, Poland
Milan Dado	University of Žilina, Slovakia
Mohamed Mostafa	Arab Academy for Science, Technology, and Maritime Transport, Egypt
Nadezhda G. Yarushkina	Ulyanovsk State Technical University, Russia
Nashwa El-Bendary	SRGE (Scientific Research Group in Egypt), Egypt
Nedyalko Nikolov	Technical University of Varna, Bulgaria
Nikolay Matanov	Technical University of Sofia, Bulgaria
Oleg P. Kuznetsov	Institute of Control Sciences of Russian Academy of Sciences
Pavol Špánik	University of Žilina, Slovakia
Petar Nakov	Technical University of Sofia, Bulgaria
Petr Saloun	VŠB-TU Ostrava, Czech Republic, Czech Republic
Rad Stanev	Technical University of Sofia, Bulgaria
Santosh Nanda	Eastern Academy of Science and Technology, Bhubaneswar, Odisha, India
Stanislav Kocman	VŠB-TU Ostrava, Czech Republic, Czech Republic
Stanislav Rusek	VŠB-TU Ostrava, Czech Republic, Czech Republic
Svatopluk Stofa	VŠB-TU Ostrava, Czech Republic, Czech Republic
Svetlana Cvetkova	Technical University of Sofia, Bulgaria
Teresa Orłowska-Kowalska	Wrocław University of Technology, Poland
Todor Ganchev	Technical University of Varna, Bulgaria
Vadim L. Stefanuk	Institute for Information Transmission Problems, Russia
Vadim N. Vagin	Moscow Power Engineering Institute, Russia
Valentin Kolev	Technical University of Sofia, Bulgaria
Valery B. Tarassov	Bauman Moscow State Technical University, Russia
Viktor M. Kureychik	Southern Federal University, Russia
Vladimir V. Golenkov	Belarus State University of Informatics and Radioelectronics, Belarus
Vladimír Vašínek	VŠB-TU Ostrava, Czech Republic, Czech Republic
Vladmir V. Kureychik	Southern Federal University, Russia

Yerzhan Syrgaliyev	Almaty University of Power Engineering & Telecommunication, Kazakhstan
Yuri I. Rogozov	Southern Federal University, Russia
Zdeněk Peroutka	University of West Bohemia, Czech Republic

Organizing Committee Chair

Mediha Mehmed-Hamza	Technical University of Varna, Bulgaria
---------------------	---

Conference Organizers

Andrey Sukhanov	Rostov State Transport University, Russia
Andrey V. Chernov	Rostov State Transport University, Russia
Aleksandr Nazarchev	PEIPK, Russia
Elena Racheva	Technical University of Varna, Bulgaria
Hristo Valchanov	Technical University of Varna, Bulgaria
Jan Platoš	VŠB-TU Ostrava, Czech Republic, Czech Republic
Joncho Kamenov	Technical University of Varna, Bulgaria
Maria Butakova	Rostov State Transport University, Russia
Mariana Todorova	Technical University of Varna, Bulgaria
Milena Ivanova	Technical University of Varna, Bulgaria
Pavel Krömer	VŠB-TU Ostrava, Czech Republic, Czech Republic
Todorka Georgieva	Technical University of Varna, Bulgaria
Valentin Gurov	Technical University of Varna, Bulgaria
Violeta Bojikova	Technical University of Varna, Bulgaria
Vitezslav Styskala	VŠB-TU Ostrava, Czech Republic, Czech Republic
Vladislav Kovalev	JSC NIAS
Zdravko Ivanov	Technical University of Varna, Bulgaria

Contents

Hybrid Expert Systems and Intelligent Decision Support Systems in Design and Engineering	
Approach to the Search for Similar Software Projects Based on the UML Ontology	3
Gleb Guskov, Alexey Namestnikov, and Nadezda Yarushkina	
Intelligent Support of Educational Process Basing on Ontological Approach with Use of Tutoring Integrated Expert Systems	11
Galina V. Rybina, Victor M. Rybin, Yury M. Blokhin, and Elena S. Sergienko	
Expert System with Extended Knowledge Acquisition Module for Decision Making Support	21
Alexander Tselykh, Larisa Tselykh, Vladislav Vasilev, and Simon Barkovskii	
Trajectory-Tracking Control of Mobile Robot via Feedback Linearization	32
Aleksey A. Kabanov, Svilen Stoyanov, and Ekaterina N. Kabanova	
Optimization of Design Opportunities and Transfer of Information Between Data 3D Graphics Program Blender and Solidworks CAD System for Use in Dental Industry	42
Rosen Vasilev, Hristo Skulev, and Tihomir Dovramadjiev	
Method for Conceptual Presentation of Subject Tasks in Knowledge Engineering for Computer-Aided Design Systems	50
Anatoly Korobeynikov, Michael Fedosovsky, Igor Zharinov, Vladimir Polyakov, Anatoly Shukalov, Andrey Gurjanov, and Sergey Arustamov	
Energy Meter for Smart Home Purposes	57
Zdenek Slanina and Tomas Docekal	

Decision Models for Volume Plans in Mechanical Engineering 67
Georgy Burdo

Algorithm for Building Recommendations for Intelligent Systems 76
S.B. Kartiev and V.M. Kureychick

**Reconfigurable Distributed Information and Control System
Multiagent Management Approach** 84
E. Melnik, A. Klimenko, and V. Korobkin

**Intelligent System for Technological Adjustment of the Harvesting
Machines Parameters** 96
Lyudmila Borisova, Valery Dimitrov, and Inna Nurutdinova

**Multi-Criteria Decision Making Using AHP to Select the Best
CAD Software** 106
Omar Bataineh, Dina Abu Hjeelah, and Sereen Arabiat

Intelligent and Fuzzy Railway Systems

**Dynamic Programming for Automatic Positioning of Wheel
Chocks on Marshalling Yards** 119
Sergey M. Kovalev, Alexander N. Shabelnikov, and Andrey V. Sukhanov

**Mobile Smart Objects for Incidents Analysis in Railway
Intelligent Control System** 128
Andrey V. Chernov, Maria A. Butakova, Vladimir D. Vereskun,
and Oleg O. Kartashov

**Intellectualization of Sorting Processes Control on the Basis
of Instrumental Determination of Analogies** 138
A.N. Shabelnikov and N.N. Lyabakh

Evaluation of the Intelligence Degree of Systems 146
M.V. Kolesnikov and Ya. M. Gibner

**Transport Systems Intellectualization Based on Analytical Control
Synthesis of Angular Velocities for the Axisymmetric Spacecraft** 154
Vladimir Taran and Vladimir Trofimenko

**Executable Logic Prototypes of Systems Engineering Complexes
and Processes on Railway Transport** 161
Alexander N. Guda, Vera V. Ilicheva, and Oleg N. Chislov

**Intellectualization of Monitoring Vibroacoustic Characteristics
of the Permanent Way and Passing Rolling Stock** 171
O.A. Belyak, A.E. Larin, and T.V. Suvorova

Intelligent Security Analysis of Railway Transport Infrastructure Components on the Base of Analytical Modeling 178
 Igor Kottenko, Andrey Chechulin, and Mikhail Bulgakov

Applied Systems

Sensing Thermal Processes with Piezoelectric Film Elements 191
 Iliya Hadzhidimov and Emil Rosenov

Reliability Estimation of Electricity Distribution Substation Surge Protection System Composed by Surge Arresters with Different Operational Parameters 201
 Nikolay Nikolov, Neli Dimitrova, Anton Georgiev, and Margreta Vasileva

Approximate Solutions of Timoshenko’s Differential Equation for the Free Transverse Vibration of Stubby Beams 210
 Victor A. Chirikov

A Computing Approach to Risk Assessment Related to Electromagnetic Field Exposure from Overhead Power Lines 220
 Marinela Yordanova and Mediha Mehmed-Hamza

Modified Scheduler for Traffic Prioritization in LTE Networks 228
 Veneta Aleksieva and Aydan Haka

Multithreaded Hybrid Library 239
 Hristo Valchanov and Simeon Andreev

Opportunities for Application of TCSC in Low Voltage Power Supply Systems as Technical Solution for Improving of Power Quality 247
 Valentin Gyurov and Yuliyana Yordanov

Simulation Modeling of Stormwater Sewage Discharge and Dispersion in the Bulgarian Black Sea Coastal Waters 254
 Tatyana Zhekova, Anna Simeonova, and Nikolay Nikov

A Computing Approach for Determination of the Magnetic Flux Density Under Transmission Power Lines 264
 Emil Panov, Mediha Mehmed-Hamza, and Marinela Yordanova

An Approach for Monitoring Transport and Delivery Chain of Liquid Fuels in Bulgaria 271
 Todorka Georgieva, Siyka Demirova, and Penka Zlateva

On the Electrodynamics of Moving Bodies According to the Rotary Theory 280
 Emil Panov

On the Electromagnetic Radiation from a Short Electric Dipole According to the Rotary Theory	290
Emil Panov	
Verification of SVD Based Algorithm for Voltage Stability Assessment Against Other Methods	301
Nikolay Nikolaev	
Application of Principal Component Analysis for Fault Detection of DC Motor Parameters	312
Nasko Atanasov, Zhivko Zhekov, Ivan Grigorov, and Mariela Alexandrova	
Automated Stress Level Monitoring in Mobile Setup	323
Valentina Markova, Kalin Kalinkov, Petar Stanev, and Todor Ganchev	
Evaluation of Sandstone Internal Structure with Application of Micro-CT and FOTOM System	332
Lačezar Ličev, Jakub Hendrych, Radim Kunčický, Kateřina Kovářová, and Ivana Kumpová	
Operational Reliability Assessment of Systems Containing Electronic Elements	340
Julia Garipova, Anton Georgiev, Toncho Papanchev, Nikolay Nikolov, and Dimitar Zlatev	
Sensorless Control of the High-Speed Switched-Reluctance Generator for the Steam Turbine	349
Pavel G. Kolpakhchyan, Alexey R. Shaikhiev, and Alexander E. Kochin	
Design and Implementation of High Speed AES on a RISC Microcontroller	359
Plamen Stoianov	
An Algorithm for Generating Optimal Toolpaths for CNC Based Ball-Burnishing Process of Planar Surfaces	365
Stoyan Slavov	
Improvement Aspects in Teaching Analog Electronics	376
Ekaterina Dimitrova, Dimitar Kovachev, and Vencislav Valchev	
Increasing the Education Quality by Means of Computer-Aided Visualization of the Processes in Electric Power Systems	386
Mediha Mehmed-Hamza, Margreta Vasileva, and Plamen Stanchev	
Project of Experimental Complex for Power System Stability Studies . . .	396
Yulian Rangelov, Nikolay Nikolaev, Yoncho Kamenov, and Krum Gerasimov	

Determination of the Temperature of Cathode Unit of Indirect Plasma Burner Through a Computer Simulation Model 403
 Krastin Yordanov, Tatyana Mechkarova, Aneliya Stoyanova, and Penka Zlateva

Modeling, Measurement and Management of Business Processes in Organization 410
 Krasimira Dimitrova

Application of Recursive Methods for Parameter Estimation in Adaptive Control of DC Motor 420
 Ivan V. Grigorov, Nasko R. Atanasov, Zhivko Zhekov, and Mariela Alexandrova

Electronic Differentials with Active Torque Distribution for IWD Vehicles 428
 Petr Simonik, Tomas Mrovec, and Samuel Przewczek

EMG as Objective Method for Revealed Mistakes in Sport Shooting 439
 Lucie Svecova, David Vala, and Zdenek Slanina

Compensation of Nonlinear Distortions in Telecommunication Systems with the Use of Functional Series of Volterra 449
 N.D. Pirogova and I.O. Neches

Improving the Reliability of Busbar Protection System with IEC 61850 GOOSE Based Communication 459
 Dimitar Bogdanov, Georgi Dimitrov, and Francisco Gonzalez-Longatt

Author Index 469

**Hybrid Expert Systems and Intelligent
Decision Support Systems in Design
and Engineering**

Approach to the Search for Similar Software Projects Based on the UML Ontology

Gleb Guskov^(✉), Alexey Namestnikov, and Nadezda Yarushkina

Ulyanovsk State Technical University, Ulyanovsk, Russia
guskovgleb@gmail.com, am.namestnikov@gmail.com, jng@ulstu.com

Abstract. In this paper proposes an approach to the search for program solutions for software project or module. The initial data for the search are the class diagram of the developing project and the names of the public libraries structural elements. Search can be carried out among projects from public repositories and organizations internal repositories. The paper contains the structure of the ontology of the UML language and several design patterns presented in the ontology. The rules, nuances and examples of transferring an architectural solution to ontology are given. An example of proposed approach applying to the problem of searching architectural solutions for integration with the social network API is considered. The paper comprises an analysis of the results, conclusions and directions for further research.

Keywords: Ontology · Software design · UML class diagram · Design patterns

1 Introduction

In software development, it is important to use the time of developers optimally, because it is a key resource. Temporary development costs can very often be reduced by reusing the code. But finding an appropriate architectural solution is not always easy. The necessary solution can be kept in project implemented a long time ago or it can be implemented by another developer.

Search by keywords does not always give an acceptable result. For example, on request “social network name + api”, a result was obtained containing 900 projects. Searching for a solution manually in this case is a fairly nontrivial and time-consuming task. Based on the results of our previous research [1], we can conclude that the developers adhere to completely different development styles and use different sets of structural elements. The selection of projects based on their architectural solutions is a promising approach. To implement a filtering by projects based on their architecture, it is needed to be able to analyze it.

In other words, it is necessary to determine the elements on which the analysis will be built. Minimal structural elements of object-oriented programming, such as classes, interfaces, objects, etc. are not the best way for this task. The combination of such elements is much better describes the architecture, semantics and designation of the project. Sustainable combination of structural elements, known as design

patterns. The design patterns have appeared relatively long time ago at information technology and are still relevant. The design patterns are actively used by the community of developers, thereby representing a reliable reference point in the analysis of the project.

There are many works devoted to the integration of software development with ontologies [2, 3]. There is a whole approach to information system development – ontology-based software engineering [4]. There are approaches to the analysis of artifacts obtained during the creation of information systems [5–7]. Attempts to integrate ontologies into software development were undertaken at different levels: technical documents [8–10], source code maintenance and testing [11, 12], UML diagrams [13, 14]. Recently, the tendency of ontologies fuzzification is very popular [15, 16], since it's necessary to deal with vague information.

2 Description of UML Based Ontology

As a structure for storing design patterns was chosen an OWL ontology, because this format is the most modern and expressive for representation of knowledge from complex subject areas. The structure of the ontology used is based on the UML meta-scheme and presented at Fig. 1. Such a structure is convenient, because any of the design patterns are typically described as a small structural diagram.

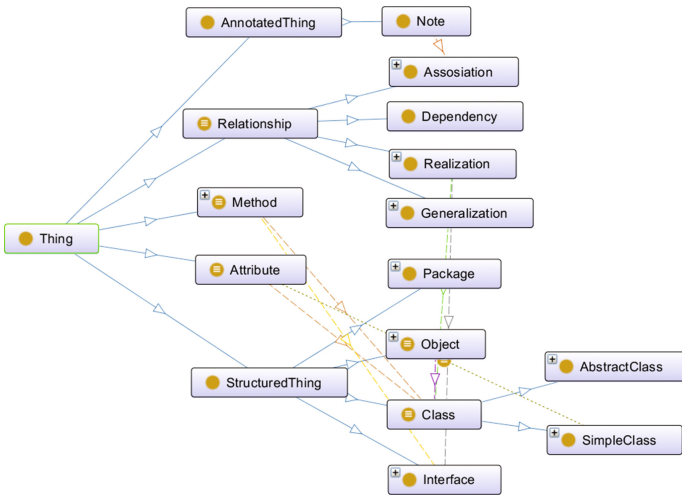


Fig. 1. UML based ontology graph from protégé.

2.1 Rules for the Conversion of Class Diagram Elements to the Ontology

The class diagram elements should be translated into ontology as concepts with considering to their semantics. Semantics of the whole diagram is being formed from the semantics of diagram elements and the semantics of their interaction. Ontology contains

concepts that describe the most basic elements of the class diagram, but it can be expanded if necessary.

Elements and Relationship

The element is root concepts in UML and all UML-diagrams consist from elements. At current stage ontology contains next elements: class, abstract class, interface, object, package, method and attribute. Such set of attributes is sufficient to represent most design patterns.

In UML meta-model the relationship is an element that specifies some kind of relation between other elements. Relationships: generalization, association, realization and dependency were selected and transferred to ontology, as the most common.

Type and Datatype

To determine the elements such as a class with its attributes and methods, it is necessary to correlate the data types of UML and OWL. Basic types of OWL and UML based on XSD it means that types can be transformed directly without additional transformation.

Unique data types in OWL and UML was obtained by using constraints on the basic types that means such types are also compatible.

2.2 Example of Adding an Adapter Design Pattern to an Ontology

Design patterns are insert into ontology as a set of individuals based only on the ontology classes described above. Semantic constraints and properties of design patterns are specified with by the object properties and datatype properties of ontology. Since many design patterns are stored in the ontology at the same time, it is necessary to enter naming rules for their elements to avoid duplicate names. The name of the design pattern element begins with the design pattern name, and then if the element is the class, its name is

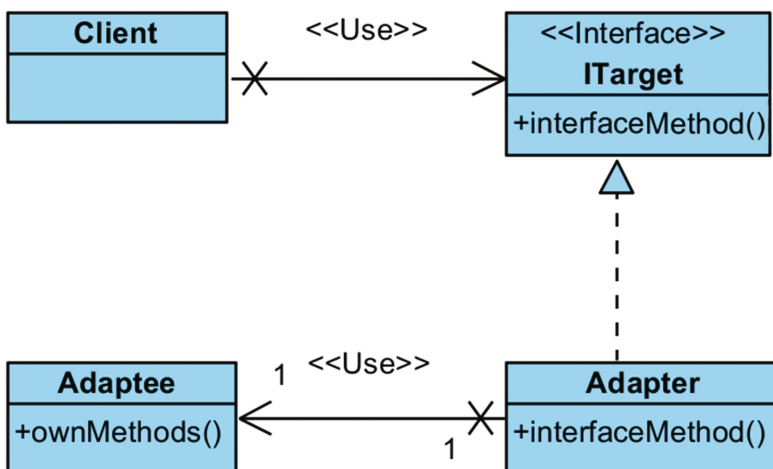


Fig. 2. Design pattern adapter UML-diagram.

written. If the element is a relationship, then the names of the elements that it connects are written through the underscore.

One of the most commonly used design patterns is the adapter [17] whose UML diagram is shown in Fig. 2. The adapter allows change the interface of interaction with Adaptee class to more convenient for Client class, without making any changes Adaptee class behavior.

Examples of naming the elements of design pattern Adapter are shown in Fig. 3.

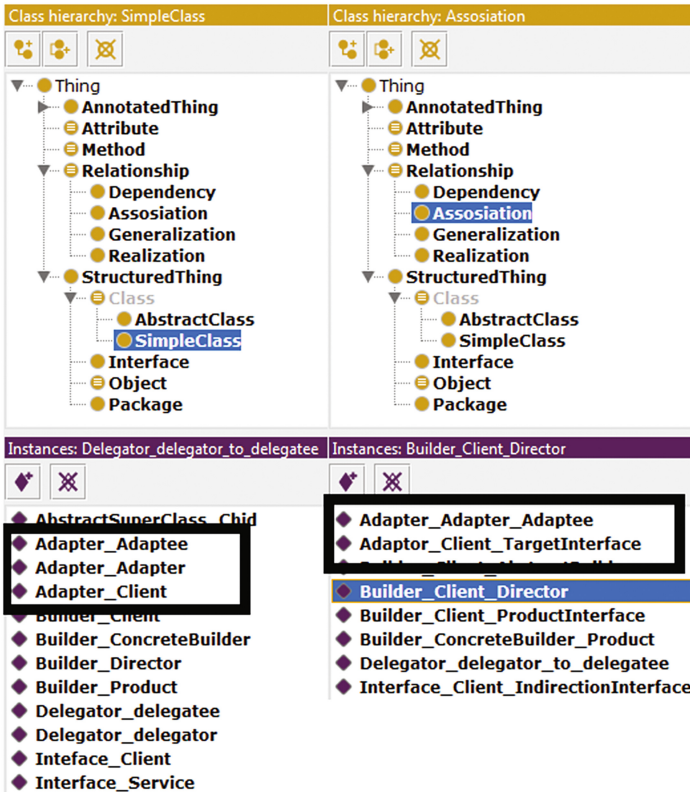


Fig. 3. Elements of design patterns translated into ontology.

3 An Example Applying Approach to Open Source Repository GitHub

3.1 Initial Data and Experimental Limitations

To evaluate the proposed approach, an experiment was conducted. Experiment target was searching design patterns in the open source repository GitHub. For searching, the following 10 design patterns were added to the ontology:

- Delegation
- Interface
- Abstract superclass
- Builder
- Adaptor
- Singleton
- Bridge
- Façade
- Decorator
- Observer

Selected design patterns are different by complexity. They consist of a set element from 3 to 20 and differ in its internal connections.

For the search, only projects in the Java programming language will be used, since the used design patterns were considered in this language. Ideally, the design pattern should be completely independent of the programming language, at least if language is an object-oriented language. But in practice, the implementations of object-oriented programming in different languages still have differences.

3.2 The Results of Applying the Approach When Searching for Design Patterns

Since the number of projects in the Java language in GitHub is extremely large, it is necessary to limit the initial projects for the search. In order to limit the entire set of projects, we use the text inquiries “vk api” and “design patterns”. As a result of the “vk api” request was obtained 108 projects related to this social network were received. And as a result of the

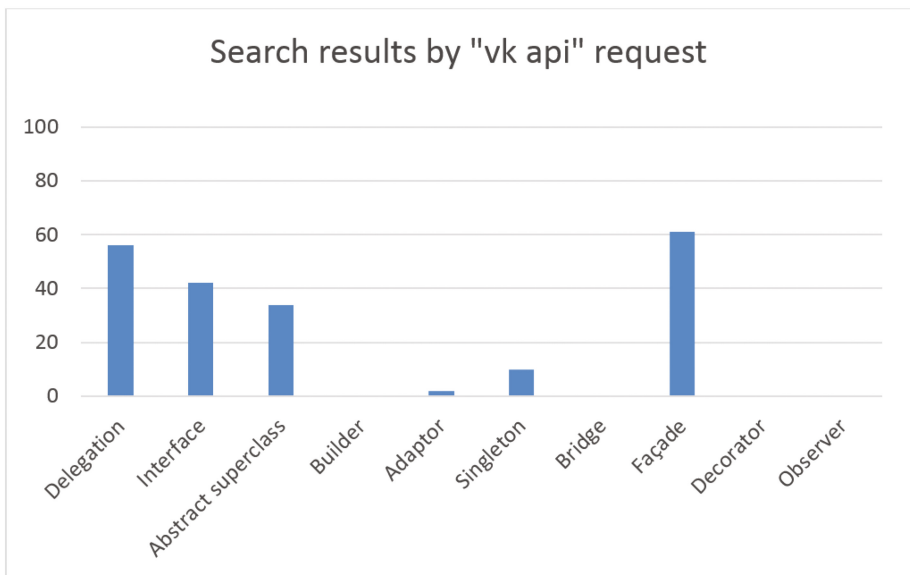


Fig. 4. The results of the search for design patterns in the projects on request “vk api”.

query “design patterns”, we received 6516 projects, for test the results was limited by 100 projects. These projects are likely to contain a large number of templates.

The search for design patterns was carried out by the coincidence of the structure, without taking into account the names of the elements and elements relationship outside the structure (Figs. 4 and 5).

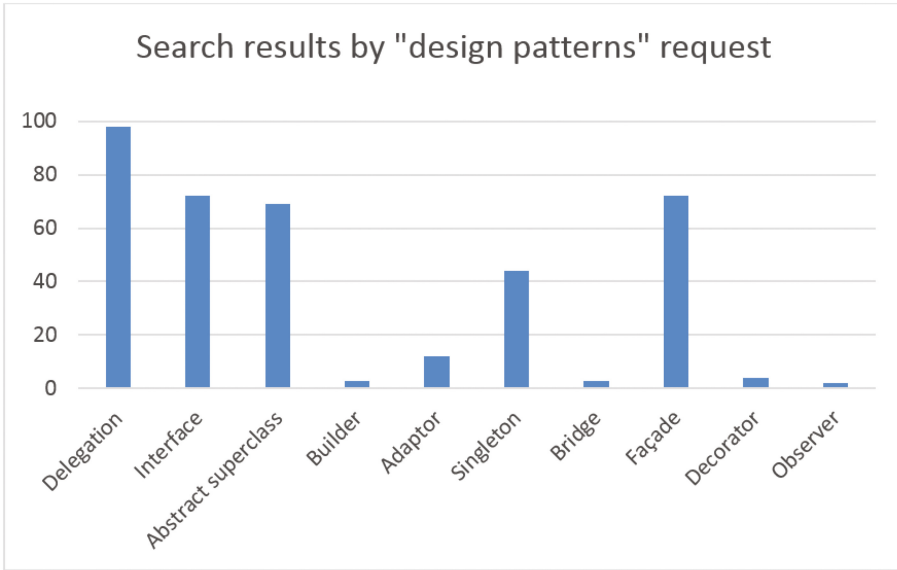


Fig. 5. The results of the search for design patterns in the projects on request “design patterns”

4 Conclusion

The results of the experiments performed are quite realistic in the current state of implementation of the approach. High results of the Delegation, Interface, Abstract superclass and Facade design patterns can be explained by their relatively simple structure. Developers could use them unconsciously, or these design patterns can be part of a more complex structure.

Builder, Adapter, Bridge, Decorator and Observer templates are much less common due to the large number of internal elements. The rarity of detecting a complex design patterns is also explained by the fact that a large count of elements must coincide at once. Since at the current realization the search was carried out by complete coincidence.

Further ways of development of the approach are follows:

- fuzzy assessment of compliance with the design pattern,
- adding strictly fixed by name elements to design pattern,
- adding new design patterns,
- adding new restrictions for design patterns,
- more detailed set of ontology axioms.

Acknowledgements. The authors acknowledge that this paper was supported by the project no. 16-47-730742 and 16-47-732033 of the Russian Foundation for Basic Research and project no. 2.1182.2017 of the Ministry of Education and Science of the Russian Federation.

References

1. Guskov, G., Namestnikov, A.: Ontological mapping for conceptual models of software system. In: Proceedings of Seventh Conference on OSTIS 2017, Minsk, Belarus, 18–20 February 2017, pp. 111–117 (2017)
2. Wongthongtham, P., Pakdeetrakulwong, U., Marzooq, S.: Ontology annotation for software engineering project management in multisite distributed software development environments. In: Mahmood, Z. (ed.) Software Project Management for Distributed Computing, pp. 315–343. Springer, Cham (2017)
3. Emdad, A.: Use of ontologies in software engineering. In: Al-Mubaid, H., Zalila-Wenkstern, R. (eds.) SEDE, pp. 145–150. ISCA (2008)
4. Dillon, T., Chang, E., Wongthongtham, P.: Ontology-based software engineering - software engineering 2.0. In: Australian Software Engineering Conference, pp. 13–23. IEEE Computer Society (2008)
5. Novák, V., Perfilieva, I., Jarushkina, N.: A general methodology for managerial decision making using intelligent techniques. In: Recent Advances in Decision Making. Series Studies in Computational Intelligence, vol. 222, pp. 103–120 (2009)
6. Hossein, S., Sartipi, K.: Dynamic analysis of software systems using execution pattern mining. In: ICPC, pp. 84–88. IEEE Computer Society (2006)
7. Marcus, A., Rajlich, V., Buchta, J., Petrenko, M., Sergejev, M.: Static techniques for concept location in object-oriented code. In: Proceedings of 13th International Workshop on Program Comprehension, pp. 33–42. IEEE, May 2005
8. Namestnikov, A., Filippov, A., Avvakumova, V.: An ontology based model of technical documentation fuzzy structuring. In: SCAKD 2016, Russian Federation, Moscow, vol. 1687, pp. 63–74. CEUR Workshop Proceedings (2016)
9. Goy, A., Magro, D.: Towards an ontology-based software documentation management - a case study. In: Liu, K., Filipe, J. (eds.) KMIS, pp. 125–131. SciTePress (2012)
10. Koukias, A., Nadoveza, D., Kiritsis, D.: An ontology-based approach for modelling technical documentation towards ensuring asset optimization. *Int. J. Prod. Lifecycle Manag.* **8**(1), 24–45 (2015)
11. Carvalho, N.R., Almeida, J.J., Henriques, P.R., Pereira, M.J.V.: Conclave: ontology-driven measurement of semantic relatedness between source code elements and problem domain concepts. In: Murgante, B., et al. (eds.) ICCSA 2014, pp. 116–131. Springer, Cham (2014)
12. Happel, H., Seedorf, S.: Applications of ontologies in software engineering. In: Proceedings of International Workshop on Semantic Web Enabled Software Engineering (SWESE 2006), Athens, USA (2006)
13. Ma, Z., Zhang, F., Yan, L., Cheng, J.: Representing and reasoning on fuzzy UML models: a description logic approach. *Expert Syst. Appl.* **38**(3), 2536–2549 (2011)
14. Zedlitz, J., Jorke, J., Luttenberger, N.: From UML to OWL 2. In: Proceedings of Knowledge Technology Week 2011. Springer (2012)
15. Almeida Ferreira, D., Silva, A.: UML to OWL mapping overview an analysis of the translation process and supporting tools. In: 7th Conference of Portuguese Association of Information Systems (2013)

16. Bobillo, F., Straccia, U.: Representing fuzzy ontologies in OWL 2. In: WCCI IEEE World Congress on Computational Intelligence, Barcelona, Spain, pp. 2696–2700, 18–23 July 2009
17. Grand, M.: Java Enterprise Design Patterns: Patterns in Java (Patterns in Java). Wiley, London (2002)

Intelligent Support of Educational Process Basing on Ontological Approach with Use of Tutoring Integrated Expert Systems

Galina V. Rybina^(✉), Victor M. Rybin, Yury M. Blokhin,
and Elena S. Sergienko

National Research Nuclear University MEPHI (Moscow Engineering Physics Institute), Kashiskoe sh. 31, Moscow 115409, Russian Federation
galina@ailab.mephi.ru

Abstract. Experience of development and usage in education process in NRNU MEPhI of tutoring integrated expert systems is analyzed. These systems are developed basing on problem-oriented methodology and AT-TECHNOLOGY workbench. This work is focused on value, role and peculiarities of ontologies integration with other components of tutoring integrated expert systems.

Keywords: Problem-oriented methodology · Tutoring integrated expert systems · Standard design procedures · Reusable components · Student model · Tutoring model · Ontology model · Basic intelligent tutoring problems · AT-TECHNOLOGY workbench

1 Introduction

Interest in intelligent tutoring systems (ITS) arose at the turn of the XX and XXI centuries, and now they occupy a significant place in a wide scope of intelligent systems issues. Educational sphere is a good “ground” for the application of artificial intelligence methods and tools, giving rise to a considerable number of approaches and system architectural solutions for intellectualization, individualization and web orientation of learning and training processes. Now, there is an “information explosion” of publications both in Russia and abroad on the subject of ITS. Without claiming to be exhaustive in our review of works in the field of ITS, we will mention only a few papers [2, 7–9, 13], reflecting the results of researches that were conducted in NRNU MEPhI and other universities. The laboratory “Intelligent Systems and Technologies” department of Cybernetics at NRNU MEPhI has accumulated a lot of experience in the development and use of tutoring integrated expert systems (IES) based on problem-oriented methodology [10, 15] and powerful modern tools such as AT-TECHNOLOGY workbench [10, 12, 15].

This work was supported by the MEPhI Academic Excellence Project (agreement with the Ministry of Education and Science of the Russian Federation of August 27, 2013, project no. 02.a03.21.0005).

Tutoring IES and web-based IES (web-IES) are fully functional ITS of the new generation, ensuring the implementation of all the basic models of the ITS (student model, tutoring model, model of the problem domain, ontologies of several types, etc.), as well as the solution of the complex basic intelligent tutoring problems, containing [13, 15]: individual planning of course/discipline study; intelligent analysis of tutoring tasks solutions; intelligent decision support.

Therefore, to support the construction of tutoring IES on the basis of problem-oriented methodology (AT-TECHNOLOGY workbench) was created and tested in practice in the educational process of NRNU MEPhI and other universities special funds that implement “manual” methods of solution of various non-formalised problems, in particular, is presented in [4]. As shown in [13, 15], ontologies and ontological engineering become particularly relevant in the integrated intelligent systems, in particular in the IES, intelligent decision support system (IDSS) and ITS. In then architectures both components as a simple expert systems (ES), intended for solving non-formalised problems and any other components and software implementing solving formalized problems are used together. Here, the main role of an ontology is to create a common basis for the explicit description of the semantics of knowledge and data, which essentially simplifies the integration processes in such systems as the ITS or IES.

By now, there have already been gained considerable experience related to the development and the use of ontologies of different types (top-level ontologies, domain ontologies, representation ontologies, application ontologies etc.), created a number of ways, scripts and methodologies for the appliance of ontologies, developed many languages, tools and platforms for designing intelligent systems based on ontologies. The most detailed and systematic analysis of the models, methods, tools and examples of implementation of the ontological approach is given in [4], as well as these issues are dedicated to [3, 15, 20–22], and others.

The primary focus of this work are questions of modeling of educational activities, in particular the educational process in higher educational institutions, with ontological approach. It is largely attributed to the current stage of the evolution methods of intelligent tutoring and the creation of new ITS architectures based on the ideas of tutoring IES [10, 11, 15, 18], when development of which is based on the problem-oriented methodology and supporting it AT-TECHNOLOGY workbench [10, 12, 15].

Today tutoring IES and web-IES, operate on the basis of generalized ontology [15] “Intelligent Systems and Technologies” and a set of ontologies for specific courses/disciplines. They were created with help of special tools of AT-TECHNOLOGY workbench and basic educational materials provided by the FSES (Federal State Educational Standards).

In general, long-term experience in the development and application in the educational process of NRNU MEPhI of tutoring IES and web-IES is described in detail in monographs [10, 15] and other works, for example, [11, 13, 18], and others. This paper is focused on the methods of integration of ontologies of particular courses/disciplines with other components of the architecture of the tutoring IES, like an individual network student model and adaptive tutoring

model. Their construction is carried out in the context of the requirements of a heuristic model of the solution of the typical education problem, as well as the methods of its implementation by AT-TECHNOLOGY workbench [10, 15].

Another important aspect of research and development in the field of ITS is connected with development of tools and technologies for automated support of ITS development. Currently there is no big diversity and innovation of tools and researchers are focused the focus is on reengineering and development of the existing tools. It should be noted that currently there is no standard technology of ITS development, so workbench of general purpose is often used for ITS, for example, [5, 6, 20] The focus of this work is the further development of methods and tools for automated construction of tutoring IES with use of intelligent software environment components.

2 General Characteristics of the Components of an Intelligent Software Environment of the AT-TECHNOLOGY Workbench

The AT-TECHNOLOGY workbench is a modern tool that supports intelligent software technology for automated construction of IES of different types and levels of difficulty. The conceptual base for the integration of methods of knowledge engineering, ontological engineering, intelligent planning and traditional programming is the concept of “intelligent environments” first introduced in [10] and studied experimentally in the process of developing a number of applied IES, including tutoring IES [10–12, 15, 17, 19]. The basic role in the intellectual software environment belongs to the intelligent planner, which manages IES and web-IES development projects. Different versions of the scheduler are described in detail in [10, 15–17] and other works.

Therefore, this work is focused on questions related to the methods of implementation of the above-mentioned tasks of intelligent training with the help of other, equally important components of an intelligent software environment of the AT-TECHNOLOGY workbench. As shown in [10], the main components of an intelligent software environment used for construction and execution of plans for the development of prototypes of applied IES include standard design procedures (SDP) and reusable components (RUC). In accordance with [10], SDP model for tutoring IES is represented as

$$SDP_T = \langle C_T, L_T, T_T \rangle \quad (1)$$

where C_T is a set of conditions, which ensure SDP invocation; L_T - an execution scenario described with internal SDP actions description language; T_T - a set of parameters initialized by the intelligent planner when SDP is included into an IES prototype development plan. Every RUC, involved in IES prototype development is defined as

$$RUC = \langle N, Arg, F, PINT, FN \rangle \quad (2)$$

N in this model is the name of the component, by which it is registered in the workbench. $Arg = \{Arg_i\}, i = 1...l$ - set of arguments containing current project database subtree serving as input parameters for the functions from the set. $F = \{F_i\}, i = 1...s$ - a variety of methods (RUC interfaces) for this component at the implementation level. $PINT$ - a set of other kinds of RUC interfaces, used by the methods of the RUC. $FN = \{FN_i\}, i = 1...v$ - set of functions names performed by this RUC. The main algorithm element used during development plan generation process of the IES prototype is SDP. By SDP we mean a set of elementary instructions (steps) which are traditionally executed by a knowledge engineer at every development lifecycle stage. The intelligent planner of the AT-TECHNOLOGY workbench has knowledge about all available SDPs, and based on this knowledge it forms a set of tasks for any IES prototype development (accordingly to a current lifecycle stage). Then, basing on special requirements specified at the system requirements analysis stage, the planner decomposes the plan into smaller tasks (subtasks).

All the workbench SDPs are classified in the following manner: problem independent SDPs (for example, “knowledge acquisition from database”), problem dependent SDPs (for example forming tutoring IES components), SDPs related with RUC, i.e. procedures, that contain knowledge about RUC lifecycle from its configuring up to including it into the IES prototype model. Latter SDPs also contain knowledge about problems solved with this RUC and its necessary configurations. The general architecture of the AT-TECHNOLOGY workbench is built in such manner, that all functionality is distributed between the components registered in the workbench and acting under intelligent development environment. In other words, these components are reusable components of the workbench, and they are developed in accordance with some workbench rules [10].

There are SDPs related to distributed knowledge acquisition from different knowledge sources, dynamic IES development SDP and the most complicated SDP for tutoring IES construction [10] in the experimental stage. The difficulties of the tutoring IES development technology are caused by supporting two different work modes - DesignTime, oriented to work with teachers (course/discipline ontology creating processes, different typed training impacts creating, etc.) and Runtime, for working with students (current student model construction processes, including psychological model, etc.).

In the RunTime mode the following AT-TECHNOLOGY workbench instruments are used: training impact construction tools (hypertext textbook, educational-training tasks), basic core workbench tools for IES prototype construction, student psychological model construction tool, tools for course/discipline ontology construction, individual tutoring strategy former, tutoring strategy realization component, different skills level elicitation components, component for mapping a current student model to course/discipline ontology.

The student model construction (student model current knowledge, student model current skills, psychological model components) is directly connected to the tools for construction and realization of the tutoring model, as well as to

the component for mapping a current student model to course/discipline ontology. The mapping component is also connected to the individual tutoring strategy forming component. The peculiarity of a tutoring web-IES developed with AT-TECHNOLOGY workbench is a presence of some components of skill level detection and of the component for construction a student's psychological model (as an aggregate of personal characteristics which are collected as a results of psychological testing).

The most difficult and complicated stage is the construction of the "Training with IES" training impact, which includes a comprehensive problem of the applied IES development for a certain problem. This IES is developed using AT-TECHNOLOGY workbench core. For example, almost all the courses of the "Intelligent systems and technologies" specialization require some knowledge of engineering methods. These methods are presented as non-formalized tasks and non-formalized methods such as "System analysis of the problem domain about applicability of the ES technology", "Choosing knowledge representation formalism", "Choosing development tools" and other tasks requiring expert knowledge [10]. The aggregate of the listed non-formalized tasks and their logical relations are the base for the problem domain construction. The model of problem domain is constructed with the knowledge representation language used in the AT-TECHNOLOGY workbench.

3 Features of Realization of Some Intelligent Training Tasks Based on the Use of Operational and Informational RUC

In accordance with problem-oriented methodology for constructing IES [10], one of the important components of a generalized model of a typical tutoring problem is the network student model, the construction and renovation of which is carried out dynamically by implementing control measures, provided by the curriculum of each course/discipline. For these purposes, as a part of the subsystem of construction of tutoring IES/web-IES, which works in both (basic and web version) of AT-TECHNOLOGY workbench, there are special tools for construction student model.

As described above, the set of SDP and RUC are components of intellectual technological knowledge base [10, 15] providing the intellectualization of the creation and operation of a wide class of ITS, including tutoring IES. Detailed description of the intelligent software environment model and the means of its implementation are given in [10, 15–17, 19]. Specifications of operational and informational RUC's that copes with major issues of intellectual tutoring are presented in this work. Brief description of these RUC's is given below.

Since the models and methods for constructing of training IES and web-IES on the basis of the problem-oriented methodology and the AT-TECHNOLOGY workbench that supports this methodology are described in detail in two monographs [10, 15], we will focus on the analysis of the experience of developing and using training IES in the educational process and creating a single ontological

space in the context of solving basic intelligent tutoring problems. The unifying basis for the basic intelligent tutoring problems [15] is the use of IES of different architectural typology (tutoring IES, ITS on the basis of intellectual agents, etc.) are processes of elicitation knowledge (declarative knowledge of a specific course/discipline) and skills (procedural knowledge that allows to demonstrate how the declarative knowledge of the trainees is used in practice). When these processes are implemented in the tutoring IES (in the RunTime mode), the current competence-oriented student model [10] is dynamically formed, which is based on the analysis of answers to questions from special web tests. Generating of test case variants is performed before the beginning of web testing by applying the genetic algorithm to the specific ontology of the course/discipline or to its fragment [15] in accordance with the curriculum for carrying out control activities.

In the current version of the tools for generating test case variants, the following requirements are supported: the generated question test should cover the specified fragment of the ontology of the course/discipline; in each of the options there should not be the same questions; the number of questions in each option should be the same; the aggregate level of complexity of each option should be approximately equal; So-called “cluster issues” should not be in one version. As for the methodology for evaluating knowledge, it is based on the calculation of the resulting estimate for the complete test (described in detail in [10,15]). Then the current student model is compared with the ontology of the course/discipline, as a result of which so-called “problem zones” are elicitation in the students’ knowledge of the individual sections and topics of the course/discipline and the corresponding current competence. Thus, ontologies of courses/disciplines be key in revealing the level of knowledge of students and construction competence-oriented students models.

Now consider the place and role of ontologies in the processes of computer-based elicitation of students abilities to solve tutoring problems. As it was shown in [10,18], today in the higher educational process two groups of courses/disciplines are distinguished: strongly and medium-formalized (mathematics, physics, theoretical mechanics, etc.) and poorly formalized (non-formalized) humanitarian, engineering and special courses/disciplines. For the first of them, questions of the creation of computer tools reflecting the teaching methodology, the specifics of the requirements for tutoring tasks, methods of evaluation, etc., are well developed and rely on ready-made solutions and standards.

Concerning the second group of courses/disciplines, the situation is much more complicated, since for such unofficial courses/disciplines, the process of elicitation skills to solve tutoring problems is related to modeling the reasoning of the person (student), and other approaches are already required related, in particular, to the methods and means of traditional ES and IES. For example, the tutoring of special courses/disciplines in the areas of training “Applied Mathematics and Informatics” and “Software Engineering” (“Introduction to Intellectual Systems”, “Expert Systems”, “Intelligent Information Systems”, “Intel-

ligent Dialogue Systems”, etc.) is impossible today without elicitation the skills and abilities of students to solve following problems [11, 13–15, 18]: the ability to construct on the basis of the “self-expert” models of the simplest situations of the problem domain based on frames and semantic networks, simulate strategies of direct/reverse reasoning in the ES, construction the components of the linguistic model of business prose sublanguage, and others. The training tasks listed above are based on non-formalized expert methods, the experience of which has been accumulated in the technologies of traditional ES and IES, in particular, in knowledge engineering [4, 14].

As shown in [11, 14, 15, 18], in order to determine the skills/abilities of students to solve the training non-formalized from the six courses/disciplines presented in the generalized ontology “Intellectual Systems and Technologies”, it is used the simulation of the reasoning process of students solving four types of the following training tasks: simulate strategies of direct/reverse reasoning; simulation of the simplest situations of the problem domain with the use of frames and semantic networks; construction components of the linguistic model of business prose sublanguage.

For several years of experimental software research on several generations of students and continuous improvement of the methodical, algorithmic and software of all the above RUC, it was possible to create quite unique methods and software to elicitation and evaluate the skills of students to solve informal practical problems within the ontology of a specific subject area. Since all RUCs were developed and operated autonomously without connection with the corresponding ontology of courses/disciplines, special algorithms and tools were developed to integrate the ontology elements of courses/disciplines with a variety of RUCs to identify the student’s ability to solve tutoring tasks.

Typically, in the context of the ontological approach, a conceptually close problem arose in the construction of an adaptive tutoring model that, in accordance with [10, 15], contains knowledge of the planning and organization of the tutoring process, depending on the individual tutoring models. An important feature is that each strategy (plan) of education consists of a certain sequence of learning impacts of different types, the application of which is completely determined by the state of the current student model (in particular, by “problem zones” and other parameters). At the present time, it were developed, decorated as a RUC and have undergone experimental testing such classes of teaching influences such [10, 15] as the solution of educational-training tasks (ETT) [1] of several types, reading sections of the hypertext textbook (HT-textbook) and “training with ES/IES”.

The greatest expansion of applied ontologies of courses/disciplines was associated with the implementation of the integration of ontology elements of courses/disciplines with a set of the following ETTs, designed as operational RUCs [15]: “Arrangement of correspondences between blocks”, “Filling in blanks in the text”, “Marking or correction of the text”, “Choosing answer options”, “Arranging graphic images”.

3.1 Individual Planning of Course/Discipline Study

Main operational RUCs for this task are the means of construction the ontology of a course/discipline [15]. Also it uses about ten informational RUC's, associated with fragments of HT-textbooks for specific courses/disciplines, and several informational RUC's for construction a generalized ontology "Intelligent systems and technologies".

Each tutoring strategy includes a specific sequence of training impacts such as: reading of a hypertext book; solution of several types of ETT ("Construction relationships between elements of the graphical representation", "Organizing graphics", "Enter a numeric value for the interval", "graphic analysis", "The mapping and sequencing of the blocks", "Formation of the answer by selecting its components from the proposed list", "Marking the correction of the text", "Filling the gaps in the text", "Setting correspondences between blocks", "Enter the answer to the open question"); implementation of training impact "Training with IES"; explanation of the obtained results; tips; localization of errors made; control of the correct solutions, etc. Any tutoring strategy is characterized by a specific set of procedures and application of training impacts, the content of which is determined by the degree of destabilization of the problem, depending on the level of knowledge and skills of a student and his or her psychological portrait. The process of formation and implementation of all relevant tutoring impacts is supported by special operational and informational RUC's.

3.2 Intelligent Analysis of Tutoring Tasks Solutions

To elicitation the skills and abilities of students to solve tutoring non-formalized problems from six courses/disciplines represented in a generalized ontology "Intelligent Systems and Technologies" [14,15] a simulation of student's reasoning for solving four types of learning tasks was used: simulate strategies of direct/reverse reasoning, simulation of simplest situations of problem domain with frames and semantic networks, construction the components of a linguistic model of business prose sublanguage.

3.3 Intelligent Decision Support

It is important to note that in the development of tutoring impacts such as "Training with IES" for different formalized courses/disciplines the most important task is construction of problem domain models (including those based on knowledge, containing certain types of NEG-factors [10]). Another important task is implementation of "consultation with IES" mode, in which there are scenarios of dialogues with the student. In this dialogues a considerable attention is given to explanations, tips and/or verification of the next stage of solving the problem, etc. Here we could apply multiple operational RUC's from the basic AT-TECHNOLOGY workbench (communication subsystem, universal AT-SOLVER, an explanation subsystem, etc.), as the development of training

impact is a task of creating a complete IES. Informational RUC's are also used (knowledge based fragments from previously created teaching operations "Training with IES", fragments of user dialogue scenarios in "Consultation with IES" mode, etc.) and operational RUC "Explanation component" provides assistance at every stage of the solution of educational problems particularly, gives hints of the next stage, gives explanations like "how" and "why" as well as makes at visualization of inference.

4 Conclusion

Educational process automation basing on intelligent software environment of AT-TECHNOLOGY workbench was discussed. Basic components of technological knowledge base of AT-TECHNOLOGY workbench were described including reusable components and standard design procedures. Standard design procedure for tutoring integrated expert systems construction was briefly described in context of onthological approach. Basic intelligent tutoring problems and their implementation were analysed. For all three basic intelligent tutoring problems the software components developed for its support are briefly described.

References

1. Bashmakov, A.I., Bashmakov, I.A.: The Development of Computer Textbooks and Training Systems. Informational-Publishing House 'Filin', Moscow (2003)
2. Bonner, D., Walton, J., Dorneich, M.C., Gilbert, S.B., Winer, E., Sottolare, R.A.: The development of a testbed to assess an intelligent tutoring system for teams. In: Workshops at the 17th International Conference on Artificial Intelligence in Education, AIED-WS 2015. CEUR Workshop Proceedings (2015)
3. De Moor, A., De Leenheer, P., Meersman, R.: DOGMA-MESS: a meaning evolution support system for inter organizational ontology engineering. In: 14th International Conference on Conceptual Structures, ICCS. Lecture Notes in Computer Science (2006)
4. Gavrilova, T.A., Kudryavtsev, D.V., Muromtsev, D.I.: Knowledge Engineering. Models and Methods: A Textbook. Lan, Saint Petersburg (2016)
5. Gribova, V.V., Kleshev, A.S., Krylov, D.A., Moscalenko, F.M.: The basic technology development of intelligent services on cloud platform IACPAAS. Part 1. The development of a knowledge base and a solver of problems. *Softw. Eng.* **12**, 3–11 (2015)
6. Gribova, V.V., Ostrovskiy, G.E.: Intelligent learning environment for the diagnosis of acute and chronic diseases. In: Proceedings of the XV National Conference on Artificial Intelligence with International Participation KII 2016 (2016)
7. Grivokostopoulou, F., Perikos, I., Hatzilygeroudis, I.: An educational system for learning search algorithms and automatically assessing student performance. *Int. J. Artif. Intell. Educ.* **27**(1), 207–240 (2017)
8. Nye, B.D.: Intelligent tutoring systems by and for the developing world: a review of trends and approaches for educational technology in a global context. *Int. J. Artif. Intell. Educ.* **25**, 177–203 (2015)

9. Rahman, A.A., Abdullah, M., Alias, S.H.: The architecture of agent-based intelligent tutoring system for the learning of software engineering function point metrics. In: 2nd International Symposium on Agent, Multi-Agent Systems and Robotics, ISAMSR 2016, pp. 139–144 (2016)
10. Rybina, G.V.: Theory and Technology of Construction of Integrated Expert Systems. Monography. Nauchtehlitizdat, Moscow (2008)
11. Rybina, G.V.: Tutoring integrated expert systems: some results and prospects. *Artif. Intell. Decis. Making* **1**, 22–46 (2008)
12. Rybina, G.V.: AT-TECHNOLOGY workbench to support building integrated expert systems: general characteristics and development prospects. *Instr. Syst. Monit. Control Diagn.* **11**, 17–40 (2011)
13. Rybina, G.V.: Intelligent tutoring systems based on integrated expert systems: the experience of the development and use. *Inf. Measuring Control Syst.* **10**, 4–16 (2011)
14. Rybina, G.V.: Fundamentals of building intelligent systems. Tutorial Finance and Statistics, Moscow (2014)
15. Rybina, G.V.: Intelligent Systems: From A to Z. Monography series in 3 books, vol. 1. Knowledge-Based Systems. Integrated Expert Systems. Nauchtehlitizdat, Moscow (2014)
16. Rybina, G.V., Blokhin, Y.M.: Modern automated planning methods and tools and their use for control of process of integrated expert systems construction. *Artif. Intell. Decis. Making* **1**, 75–93 (2015)
17. Rybina, G.V., Blokhin, Y.M.: Use of intelligent planning for integrated expert systems development. In: 8th IEEE International Conference on Intelligent Systems, IS 2016, Sofia, Bulgaria, 4–6 September 2016, pp. 295–300 (2016)
18. Rybina, G.V., Rybin, V.M., Sergienko, E.S., Sorokin, I.A.: Some aspects of intelligent tutoring through the use of tutoring integrated expert systems. *Inf. Measuring Control Syst.* **8**, 3–8 (2016)
19. Rybina, G., Rybin, V., Blohin, Y., Sergienko, E.: Intelligent technology for integrated expert systems construction. In: *Advances in Intelligent Systems and Computing*, vol. 451, pp. 187–197. Springer, Cham (2016)
20. Sosnovsky, S., Mitrovic, A., Lee, D., Brusilovsky, P., Yudelson, M.: Ontology-based integration of adaptive educational systems. In: 16th International Conference on Computers in Education (ICCE 2008) (2008)
21. Surez-Figueroa, M.C., Gmez-Prez, A., Motta, E., Gangemi, A.: *Ontology Engineering in a Networked World*. Springer Science & Business Media, Heidelberg (2012)
22. Telnov, Y.F., Kazakov, V.A.: Ontology modeling network interactions organizations in informatively-educational space. In: *Proceedings of the XV National Conference on Artificial Intelligence with International Participation KII-2016* (2016)

Expert System with Extended Knowledge Acquisition Module for Decision Making Support

Alexander Tselykh¹, Larisa Tselykh^{2(✉)}, Vladislav Vasilev¹,
and Simon Barkovskii¹

¹ SFEDU, Taganrog, Russia

{ant,vsvasilev}@sfedu.ru, kharitonov.simon@yandex.ru

² RSUE, Taganrog, Russia

l.tselykh58@gmail.com

Abstract. This study is an attempt to develop an expert system containing an advanced knowledge acquisition module to support decision-making in socio-economic systems. In this article, we demonstrate the operation of the effective controls algorithm for generating the attributes of expert systems. The selection of factors for the creation of production rules is automated and is based on the discovery of knowledge from fuzzy cognitive map, which is a system representation of the problem being solved, using numerical methods of linear algebra. The synergy of three tools - fuzzy cognitive maps, numerical methods and fuzzy inference - is realized in the architecture of the expert system.

Keywords: Expert system · Effective controls · Knowledge acquisition · Knowledge discovery

1 Introduction

The most successful implementation of artificial intelligence have been in expert systems (ES), which first appeared in the 70 s of the last century. During the entire period of their development, there have been periods of intense interest in them as well as some cooling. The latter is primarily due to the internal problems of expert systems themselves. The main difficulties encountered in the design and promotion of ES show three aspects: the domain area, the structure of the ES and the process of developing an ES. As William P. Wagner noted in his study [1], expert systems are best developed in those functional areas where the problems being addressed can be presented in a well-structured form. Such areas include diagnostics (medicine, technology), planning and settlement operations (accounting, finance), monitoring, including the use of sensor data. Many problem areas remain not covered by ES applications. Broad prospects for the development of ES are decision support systems. Of these, the most neglected with respect to software applications are the areas of management in socio-economic systems.

In the structure of ES, the most problematic and most complex element is the knowledge base. The quality of the knowledge base must satisfy certain requirements

specified in the work of Adelman [2] in 1989. The classical type of the expert system underwent certain changes connected with the use of several sources of knowledge used to form the knowledge base. To date, two types of knowledge sources have been identified: the knowledge of the human expert, and data sets, including those obtained from the Internet. Methods that draw on the deep knowledge that human experts possess have not so far received proper development in expert systems applications. Two of the five determinants of the quality of the knowledge base specified in [2] remain largely relevant today. These are methods of knowledge acquisition (KA) and problem domains. It can be said that the development of ES is currently restrained mainly by the level of development of methods for extracting deep and implicit knowledge and transforming it into a knowledge base.

In their study, Leu G. and Abbass H. [3] stated that the degree of human participation in the process of knowledge acquisition varied over time from complete and exclusive to partial, and up to the complete replacement of the human expert with unstructured artifact data. However, as noted by the researchers in [3], in the process of extracting, knowledge is modified in human perception, which entails a change not only in the ontological construction of knowledge, but also a change in one's own level of knowledge. This property implies the development of a new group of methods that would take into account such a change in the cognition of the entity.

Our research focuses on the development of an ES for poorly formalized area under a high degree of uncertainty – decision-making support for management in socio-economic systems. The high degree of complexity and variability of the object and the subjects of such an ES requires the development of new approaches and methods. We propose a new approach for the development of the knowledge base of the production expert system on the basis of the properties of cause-effect relations between the attributes of inference. Fuzzy cognitive maps, representing fuzzy directed signed weighted graphs with feedback cycles, will form the basis for generating a set of antecedents and consequents to be used in the fuzzy rule based ES. Two new aspects were taken into account in the design of the ES: (1) the modification of the ES structure with an expanded knowledge acquisition module based on knowledge discovery methods; (2) the ability of ES to process knowledge induction.

2 Related Work

The selection of works in this article was made from the point of view of the development of the ES structure and its knowledge acquisition module. The main range of issues that determined the search for related research:

- approaches to the selection of variable attributes for the inference engine;
- formation of the structure of the ES knowledge acquisition module;
- experience of applying FCM to ES.

The central problem to be resolved in the study [4] is to minimize the interference of knowledge engineers (KE) into the process of knowledge acquisition from domain experts (DE). The ES proposed in [4] provides the domain expert with the tools using problem solving methods to obtain “knowledge of the processes” as a knowledge type.

It should be noted that knowledge of the process is characteristic of the areas that provide the opportunity for structuring and knowledge of exact (or at least possible) sequence of actions. The examples given in the article are mainly suitable for chemistry, physics, biology, and engineering. For business, this approach seems acceptable at the production level, when the decision has already been made and is being implemented. Until the decision is made, the use of this approach is not possible in a complex unstructured environment with multiple variables, feedbacks and changing external and internal conditions.

In [5], a specialized ES (NFES, NFPEM) is presented for estimating and predicting the expected efficiency of the Distributed Software System Architecture at the level of planning its architecture. The basis for this estimate is the neuro-fuzzy hybrid model integrated into the Inference Engine. The article notes that with the number of attributes greater than 150 the system becomes unfriendly to the user. The preliminary selection of variables included a questionnaire and exploratory factor analysis using maximum likelihood extraction method. Summarizing the structure of this ES, it can be noted that the knowledge acquisition module has a two-stage structure: a questionnaire and factor analysis based on the factor model on the data. The requirements to data significantly limits the scope of application of this ES.

Studies [5, 6] state the problem of the “oversized rule base” due to the large number of attributes, which confirms the need to allocate a small number of basic components for ES and to model the cause-effect relationships between them. The proposed prototype - a belief rule based expert system uses method of artificial intelligence of the same name (the belief rule based (BRB) system). This method requires the data of the observed parameters for the extraction of the factor. For control tasks in the socio-economic system, firstly, qualitative variables are characteristic, and secondly, there is a large lag of the system response. The absence of observable variables is a critical obstacle to the application of the system proposed in [6].

In [7], a CAKES-ISTS expert system that uses a simple type of cognitive model is presented. Obtaining a model of this kind requires preliminary processing, extraction of attributes and relationships between them.

In the original development [8], an ES is proposed based on deductive resolution of ambiguity in the meaning of a word when translated with the data-mining module. From the point of view of the ES structure, this proposal adds new elements to the classical ES. The knowledge acquisition unit is supplemented by a data mining module, and the knowledge base by a module of association rules. However, it should be noted that this system has the same limitation as [5] – the necessity of data availability.

In [9], a broad overview of the application of FCM in expert systems in medical diagnostics, treatment planning, etc., based on FCM’s unique ability to model complex systems is given. Despite the presence of 12 kinds of FCM, practically in all the applications given in [9], FCM is applied in its classical form, that is, with a pre-known typing of concepts (factor, selector, output). With all the variety of methods developed for algorithmic processing of FCM, their scope of application is limited to learning of the weighted matrix.

In view of the foregoing, the task of improving the quality of the knowledge base based on the methods of acquisition deep and implicit knowledge remains relevant today. Our study shows a new approach to the formation of the knowledge acquisition

module based on system representation of a complex domain system, allowing to identify implicit knowledge and transform it into a knowledge base. Mathematical support tools are presented below.

3 The Structure of the Proposed EC Knowledge Acquisition Module

3.1 ES Architecture with the FCM Discovery Module

Proceeding from the arguments the previous sections, the design of the ES must have three important characteristics: system approach, mathematical support, and automation. As stated in [2], the quality of the knowledge base depends on five quality determinants. In the proposed ES, each of them received certain development.

Our approach is implemented through FCM discovery module, which includes a FCM engine, Math engine, FCM learning engine, FCM redesigning engine, and Equivalent graph engine. In the “FCM engine”, the system representation of the domain is formed in the form of a fuzzy cognitive model in two variants: either through loading the finished matrix representation of the model or through the introduction of data for the formation of the matrix representation using FCM Editor. The entered data is converted by the FCM converter into the form required for algorithmic processing. The formation of the cognitive model is not the subject of our research, so the deployment of its development block is not included in our ES. The Math engine block includes three components that provide mathematical support for processing the cognitive model of the system under consideration: cluster analysis, influence analysis, and equivalent graph modeling.

The creation of the cognitive model has two stages of its learning: verification and validation. The scheme for implementing the described approach to the development of ES attributes is shown in Fig. 1. The proposed ES is based on the use of FCM (initial knowledge), as a mental representation of the work of the system as a whole, and on the discovery of new knowledge in it, which is further considered as attributes of production rules. The framework of the ES is shown in Fig. 2. The working components of the ES include seven modules that solve the main functional tasks and have an internal structure. The expert system is located on the remote server [Backend], the database and the knowledge base are on the data server [Data server]. The user accesses the server of the expert system via the browser and logs in. Next, the user will be able to create a project and upload original data to the server. Figure 3 shows a sequence diagram that displays the life cycle of objects on a time axis. The objects displayed in the diagram are: the Domain expert, FCM engine, Math engine, Equivalent graph engine, Knowledge acquisition module.

The diagram includes the learning process of the FCM model [FCM learning] in which the user enters the original data and gets a list of concepts (graph vertices) from the Math engine arranged in descending order.

The equivalent graph represents the system as a whole at the level of the value of its potential (set by the expert or the user). The equivalent graph data represents the required attributes (consequents, antecedents) for production rules of inference. Then

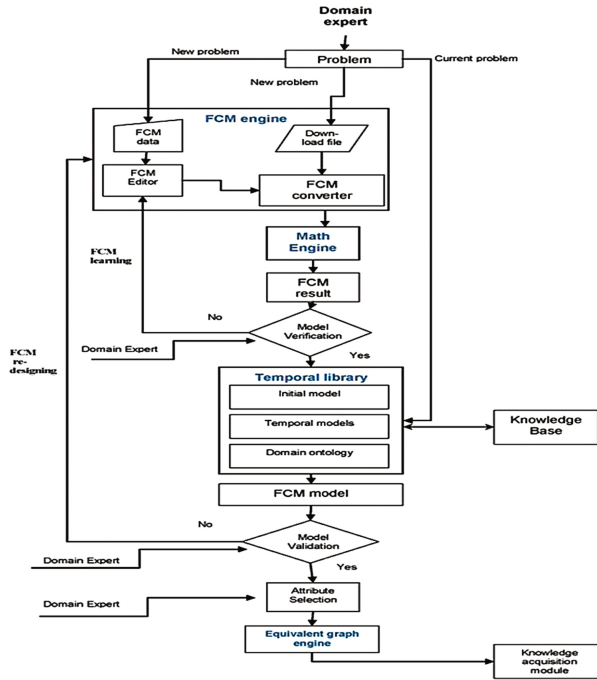


Fig. 1. The scheme of ES attribute generation in the FCM discovery module.

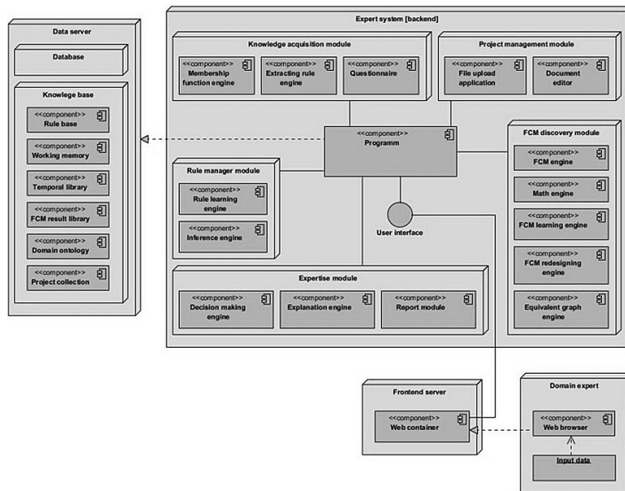


Fig. 2. System deployment diagram

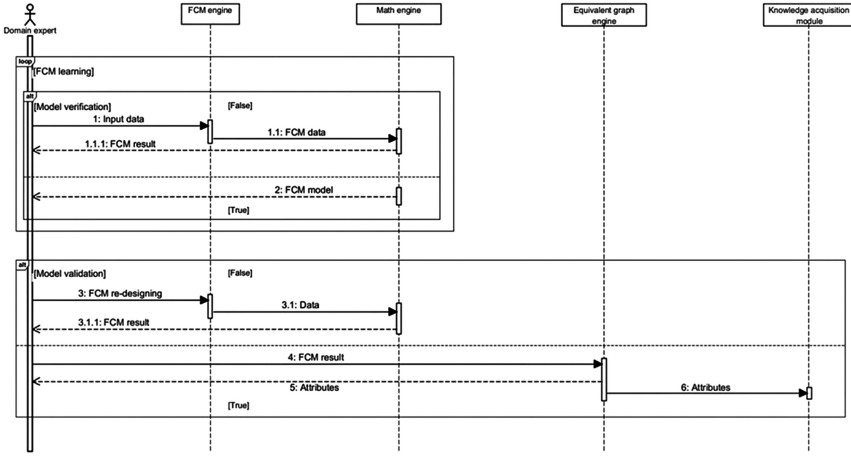


Fig. 3. Sequence diagram

the data is transferred into the Knowledge acquisition module. At all stages, the engineer receives information about the operation of all the engines of the system.

3.2 Algorithmic Support

Consider a finite graph $G = \langle V, E \rangle$, where $V = \{v_1, v_2, \dots, v_n\}$ – is a finite set of vertices, n – the number of vertices, $E = \{ \langle v_i, v_j \rangle | v_i \in V, v_j \in V \}$ – a finite set of arcs. The graph G is set by the adjacency matrix $\mathbf{A} = \|a_{ij}\|_{n \times n}$, where the weight a_{ij} of the arc $\langle v_i, v_j \rangle$ can express the presence of an arc (Boolean value), arc multiplicity, arc weight, fuzzy measure of the contiguity of the vertices v_i and v_j etc.

The method is based on the following model of the control system [10]:

$$x_j = \sum_{i=1}^n a_{ij} \left(u_i + \delta \sum_{k=1}^m a_{ki} x_k \right) \quad (1)$$

where x_j is the relative increment of the vertex v_j ; a_{ij} is the weight of the arc directed from vertex v_i to vertex v_j , $-1 \leq a_{ij} \leq 1$; n is the number of vertices in the graph; u_i is the component of the control vector for the vertex exponent v_i ; δ is the damping factor, $0 \leq \delta \leq 1$; a_{ki} is the weight of the arc directed from vertex v_k to vertex v_i , $-1 \leq a_{ki} \leq 1$; x_k is the value of the relative energy increment of the vertices not directly related to the vertex v_j ; or in matrix form:

$$\mathbf{x} = \mathbf{A}^T (\mathbf{u} + \delta \mathbf{A}^T \mathbf{x}) \quad \text{or} \quad (\mathbf{E} - \delta \mathbf{A}^T \mathbf{A}^T) \mathbf{x} = \mathbf{A}^T \mathbf{u} \quad (2)$$

In the control system model above, the delay effect is realized, which is expressed in the acceptance of only all preceding effects on the vertices of the graph. The following explains Eq. (1). From the expression of model (1) it follows that the relative energy increment x_j of vertex v_j equals to the adjusted for the weight of arc a_{ij} sum of

the relative increments under the corresponding controls from: (1) direct impacts u_i on the connected vertices (the first summand), and (2) impacts $(\delta \sum_{k=1}^n a_{ki}x_k)$, transferred from the remaining vertices (the second summand). Control impact u_i is transferred through arcs a_{ij} and changes the parameter of vertex x_j . In this case, the change in the value x_j of vertex v_j is taken into account in calculating the relative energy increment of the subsequent vertex.

The action of the model can be demonstrated by a simple example. Let the graph be represented by four vertices and three arcs (Fig. 4).

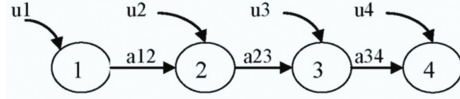


Fig. 4. Demonstration model of influence transmission: $\{1, 2, 3, 4\}$ is a set of vertices, a_{12}, a_{23}, a_{34} are weights of the arcs, u_1, u_2, u_3, u_4 are control impacts on the vertices.

Then, according to (1), the value of the relative energy increment of the vertex will be as follows: $x_2 = a_{12} \cdot u_1$; $x_3 = a_{23} \cdot (u_2 + a_{12} \cdot x_1)$; $x_4 = a_{34} \cdot (u_3 + a_{23} \cdot x_2)$, which corresponds to our explanation above.

For model (1), the task is to find the vector(s) of external impacts that maximizes the accumulated growth of the vertex indices. The proposed approach is that the vector of control impacts is determined from the solution of the optimization problem of maximization R , where R is the ratio of the squares of the norms of responses (controls) $\|\mathbf{x}\|^2$ and impacts $\|\mathbf{u}\|^2$, and the problem takes the form:

$$R = \frac{\|\mathbf{x}\|^2}{\|\mathbf{u}\|^2} = \frac{\left((\mathbf{E} - \delta \mathbf{A}^T \mathbf{A}^T)^{-1} \mathbf{A}^T \mathbf{u}, (\mathbf{E} - \delta \mathbf{A}^T \mathbf{A}^T)^{-1} \mathbf{A}^T \mathbf{u} \right)}{(\mathbf{u}, \mathbf{u})} = \frac{(\mathbf{B}\mathbf{u}, \mathbf{u})}{(\mathbf{u}, \mathbf{u})} \rightarrow \rightarrow \max, \tag{3}$$

where $\mathbf{B} = \mathbf{A}(\mathbf{E} - \delta \mathbf{A}\mathbf{A})^{-1}(\mathbf{E} - \delta \mathbf{A}^T \mathbf{A}^T)^{-1} \mathbf{A}^T = \mathbf{A}(\mathbf{Z}^T \mathbf{Z})^{-1} \mathbf{A}^T$ is a symmetric positive definite (semidefinite) matrix. Matrix \mathbf{B} is defined as the product $\mathbf{B} = \mathbf{A}\mathbf{F}$, and $\mathbf{F} = (\mathbf{Z}^T \mathbf{Z})^{-1} \mathbf{A}^T$ is found from SLE solutions with a unified matrix $(\mathbf{Z}^T \mathbf{Z})$, but with different right parts: the j -th column of matrix \mathbf{F} is the SLE solution with the right part – the j -th line of the adjacency matrix \mathbf{A} . Such a scalar formulation leads to symmetrization of the matrix of the fundamental quadratic form of the problem. The symmetry of the matrix will ensure that its eigenvalues and the components of its eigenvectors are real. Moreover, the eigenvectors corresponding to different eigenvalues are orthogonal. To find \mathbf{u}_i from the SLE (2) solution, we find \mathbf{x}_i .

In this formulation, the task is related to the task of determining the resonance properties of a system described by the adjacency matrix of a directed signed graph, namely, finding the eigenvalues and eigenvectors of the adjacency matrix. Separation of successively calculated eigenvectors is performed using the Gram-Schmidt orthogonalization process [11]. Of practical interest are not all, but only a few

directions, corresponding to several first eigenvalues with the largest values. The substantiation of the selection of control and impact components is achieved by determining the accumulated shares $r_{i,j}^2$ and $v_{i,j}^2$ (the performance index and the controllability index, respectively) of the overall system control, which are defined as follows:

$$v_{i,j}^2 = \frac{u_{i,j}^2}{u_{i,1}^2 + u_{i,2}^2 + \dots + u_{i,n}^2} \quad \text{and} \quad r_{i,j}^2 = \frac{x_{i,j}^2}{x_{i,1}^2 + x_{i,2}^2 + \dots + x_{i,n}^2} \quad (4)$$

Algorithm for finding relevant components of effective controls:

- (1) Entering matrix \mathbf{A} and damping factor δ .
- (2) Computation of matrix: $\mathbf{Z} = \mathbf{E} - \delta\mathbf{A}$.
- (3) Computation: $\mathbf{F} = (\mathbf{Z}^T\mathbf{Z})^{-1}\mathbf{A}^T$.
- (4) Computation of the quadratic matrix: $\mathbf{B} = \mathbf{A}\mathbf{F}$.
- (5) Computation of (several first) eigenvalues and the corresponding eigenvectors of matrix \mathbf{B} , $\mathbf{u}_1, \mathbf{u}_2, \dots, \mathbf{u}_n, R_1, R_2, \dots, R_n$.
- (6) Selection of relevant controls $\mathbf{u}_1, \mathbf{u}_2, \dots, \mathbf{u}_l$.
- (7) Computation of vectors of growth of indicators of vertices $\mathbf{x}_1, \mathbf{x}_2, \dots, \mathbf{x}_l$, (SLE (2)).
- (8) For each relevant control \mathbf{u}_i and vector \mathbf{x}_j :
 - (a) calculation of $v_{i,j}^2$ and $r_{i,j}^2$ and their components (4);
 - (b) sorting in descending order of $v_{i,j}^2$ and $r_{i,j}^2$ and their components;
 - (c) selection of relevant components \mathbf{u}_i and \mathbf{x}_j .

Presentation of results $u_{i,j}, x_{i,q}, 1 \leq i \leq l, 1 \leq j \leq k_u(i), 1 \leq q \leq k_x(i)$.

4 Experiment

A numerical experiment of finding the relevant components of effective controls is shown for six cognitive models, which are directed signed weighted graphs with cause-effect relations having cycles. In the Math engine, the ordered absolute values of the components of the impact and control are formed, shown in Fig. 5a. The results of processing showed that the functioning of the system is determined by several leading factors, which strongly prevail over the others. For more effective control, it is possible to select those factors that are in a noticeable separation from the others and provide a significant part of the maximum growth.

Figure 5b shows the accumulation of shares and effectiveness indices $r_{i,j}^2$, and controllability indices $v_{i,j}^2$ for a reasoned selection of components of control and impact. Thus, for models 1, 2, 5, and 6, the growth of indices will immediately identify several (1–3) most significant components of control, which encompass a significant potential of the system (more than 40%). In other models, the number of such control components increases to factors of 4–10. In all the cases, the selection is carried out by setting the level of system control potential, which is sufficient for the decision-maker.

The results show the hidden knowledge extracted from the fuzzy cognitive model of the domain. The selected data then is transferred to the Knowledge acquisition module for the development of production rules.

Thus, it has been shown that there is a reasonable possibility of selecting ES attributes based on mechanisms of detecting hidden knowledge in fuzzy cognitive models.

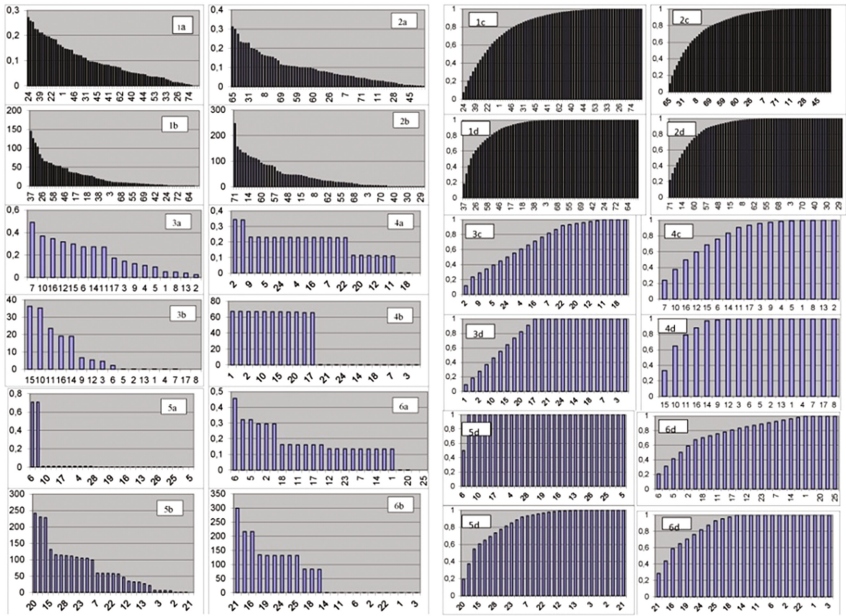


Fig. 5. Ordered components of impact vectors (a), control vectors (b), ensuring controllability indices (c) and effectiveness indices (d) for the six examples.

5 Discussion of the Results

The results are considered with respect to two groups of tools used in the knowledge discovery process: (1) the use of FCM as the basis for selecting attributes, and (2) the quality of the resultant work of the Math engine and the Equivalent graph engine. The use of FCM is justified by several considerations:

- the work of the system can be presented as a whole (taking into account all possible factors) at the mental level;
- construction of fuzzy cognitive model of the system does not require special (mathematical) knowledge;
- the process of construction is easy to carry out;
- no strict hierarchy of model construction is required.

The problem with using the FCM is how to estimate the validity and correctness of the constructed model at the current time and after the expiration of the relevant period. The solution to this issue is proposed to be carried out in two stages using the Math engine toolkit, the FCM learning engine, and the FCM redesigning engine. Based on the results of the solution, the expert (user) can estimate the correspondence of the received model to his or her mental representations. The FCM is widely used to represent knowledge and inference, but, as pointed out in [12], the theory of fuzzy cognitive maps itself needs improvement. From this point of view, an effective control algorithm was developed, presented in the Math engine, which is a new example of changing the usual mathematical processing of cognitive maps.

The next question to be discussed and assessed is how to select the most significant concepts. This issue is solved in the Equivalent graph engine, in which the conditionally equivalent graph is formed by the solution of the conditional optimization problem. In our case, this task is extracting the target set of nodes in such a way that it gives the largest expected coverage of the system's performance. The presentation of this algorithm is the goal of our future work.

The reliability and quality of the resulting solution is ensured by solving the mathematical problem excluding intuitive and empirical considerations.

6 Conclusion

The purpose of our research was to make significant changes to the process of generating the attributes of product rules for ES based on the expansion of the knowledge acquisition module. The task of designing a special knowledge discovery tool lay in the field of solving control tasks in socio-economic systems. The expansion of the knowledge acquisition module is implemented by adding a knowledge discovery module from FCM, which is a system representation of the task being solved.

The employed mathematical tools reduce the subjectivity of the domain expert by revealing tacit knowledge, and at the same time, it combines the system representation with the specific properties of the domain. In the ES, we presented a method of maximizing the spread of influence in models of socio-economic systems. The application of this method provides an opportunity to define the main concepts of the system that provide its main potential, and the possibility to select the object of the control action with a system response forecast. The resulting objects are induced by hidden knowledge extracted from the FCM. They can be used as attributes to develop production rules for inference, or for independent use in the decision-making process. Thus, the application of the approach combining the acquisition and discovery of knowledge increases the quality of the Knowledge base and allows to make well-grounded managerial decisions.

Acknowledgements. This work was supported by the Russian Foundation for Basic Research [grant number № 17-01-00076].

References

1. Wagner, W.P.: Trends in expert system development: a longitudinal content analysis of over thirty years of expert system case studies. *Expert Syst. Appl.* **76**, 85–96 (2017). doi:[10.1016/j.eswa.2017.01.028](https://doi.org/10.1016/j.eswa.2017.01.028)
2. Adelman, L.: Measurement issues in knowledge engineering. *IEEE Trans. Syst. Man Cybern.* **19**, 483–488 (1989)
3. Leu, G., Abbass, H.: A multi-disciplinary review of knowledge acquisition methods: from human to autonomous eliciting agents. *Knowl. Based Syst.* **105**, 1–22 (2016). doi:[10.1016/j.knosys.2016.02.012](https://doi.org/10.1016/j.knosys.2016.02.012)
4. Gomez-Perez, J.M., Erdmann, M., Greaves, M., Corcho, O., Benjamins, R.: A framework and computer system for knowledge-level acquisition, representation, and reasoning with process knowledge. *Int. J. Hum Comput Stud.* **68**, 641–668 (2010). doi:[10.1016/j.ijhcs.2010.05.004](https://doi.org/10.1016/j.ijhcs.2010.05.004)
5. Akinuwesi, B., Uzoka, F.-M., Osamiluyi, A.: Neuro-fuzzy expert system for evaluating the performance of distributed software system architecture. *Expert Syst. Appl.* **40**, 3313–3327 (2013). doi:[10.1016/j.eswa.2012.12.039](https://doi.org/10.1016/j.eswa.2012.12.039)
6. Yang, Y., Fu, C., Chen, Y.-W., Xu, D.-L., Yang, S.-L.: A belief rule based expert system for predicting consumer preference in new product development. *Knowl. Based Syst.* **94**, 105–113 (2016). doi:[10.1016/j.knosys.2015.11.012](https://doi.org/10.1016/j.knosys.2015.11.012)
7. Lee, K.C., Lee, S.: A causal knowledge-based expert system for planning an Internet-based stock trading system. *Expert Syst. Appl.* **39**, 8526–8635 (2012). doi:[10.1016/j.eswa.2012.01.191](https://doi.org/10.1016/j.eswa.2012.01.191)
8. Fakhrahmad, S., Sadreddini, M., Jahrom, M.Z.: A proposed expert system for word sense disambiguation: deductive ambiguity resolution based on data mining and forward chaining. *Expert Syst.* **32**, 178–191 (2015). doi:[10.1111/exsy.12075](https://doi.org/10.1111/exsy.12075)
9. Amirkhani, A., Papageorgiou, E.I., Mohseni, A., Mosavi, M.: A review of fuzzy cognitive maps in medicine: taxonomy, methods, and applications. *Comput. Meth. Prog. Biomed.* **142**, 129–145 (2017). doi:[10.1016/j.cmpb.2017.02.021](https://doi.org/10.1016/j.cmpb.2017.02.021)
10. Tselykh, A., Vasilev, V., Tselykh, L., Barkovskii, S.: Method maximizing the spread of influence in directed signed weighted graphs. *Adv. Electric. Electron. Eng.* **15**, 203–214 (2017)
11. Horn, R., Johnson, C.: *Matrix Analysis*, 2nd edn. Cambridge University Press, New York (2013). ISBN-13: 978-0521548236
12. Gomez, A., Morenoa, A., Parosa, J., Sierra-Alonso, A.: Knowledge maps: an essential technique for conceptualization. *Data Knowl. Eng.* **33**, 169–190 (2000). doi:[10.1016/S0169-023X\(99\)00050-6](https://doi.org/10.1016/S0169-023X(99)00050-6)

Trajectory-Tracking Control of Mobile Robot via Feedback Linearization

Aleksey A. Kabanov^{1,2(✉)}, Svilen Stoyanov³,
and Ekaterina N. Kabanova⁴

¹ FRC CSC RAS, Moscow, Russian Federation
kabanovaleksey@gmail.com

² Sevastopol State University, Sevastopol, Russian Federation

³ Technical University of Varna, Varna, Bulgaria
svilen.stoyanov@tu-varna.bg

⁴ Nakhimov Black Sea Higher Naval School, Sevastopol, Russian Federation

Abstract. This paper is devoted to the designing of a trajectory-tracking control system for a unicycle-type mobile robot. Synthesis of the trajectory control law is based on the feedback linearization method and a canonical similarity transformation of nonlinear affine system in state-dependent coefficient form. Proposed system has two control loops: trajectory control loop and velocity control loop. Based on this, the structure of the control system consists of two modules: the reference and the executive. The result of experimental test of the trajectory control system for mobile robot Rover5 is presented.

Keywords: Mobile robot · Trajectory-tracking · Feedback linearization · MIMO system · Similarity transformation

1 Introduction

The problem of mobile robot (MR) control is relevant over the years because of the wide range of theoretical problems and practical applications associated with it. There is a great number of works in the field of motion control of MR that are published in recent decades. Their reviews can be founded in [1–4].

Trajectory-tracking control problem is a typical control problem for MR. It is mainly concerned with the design of control laws that force a MR to reach and follow a time parameterized reference trajectory [5]. Thus, as a rule, simple nonlinear models are operated, which characterize only the kinematic relationship between the MR's motion parameters and parameters that are predetermined by a reference trajectory.

At this point it is possible to mark out two basic approaches to design the trajectory-tracking system. The first approach is based on linear control design methods and tangent linearization of system model about the reference trajectory. At that, a pole placement method or linear optimal control method are usually used to adjust controller parameters [6–8]. Another approaches is based on nonlinear control design methods, such as feedback linearization (FL), Lyapunov techniques [9–11].

A lot of publications are devoted to the trajectory-tracking control problem for MR with nonholonomic constraints by means of FL (static and dynamic). In [9]

applicability of static FL for setpoint regulation problems and for trajectory-tracking problems is considered. In [11] the trajectory-tracking control problem based on dynamic FL is considered. It is shown that dynamic FL is an efficient design tool leading to a solution simultaneously valid for both trajectory tracking and setpoint regulation problems. The main drawback of such solution is aligned with the raise of the system order and the order of the dynamic feedback.

In this paper, we propose another approach for static FL control design for trajectory-tracking, based on representing the original nonlinear system into a state-dependent coefficient (SDC) form and applying the canonical similarity transformation, that allow getting the system to canonical form. This similarity transformation allow accomplishing linearization of a system without determining of a virtual system output.

The remaining sections of the paper proceed as follows: Sect. 2 describes the trajectory-tracking control problem statement; Sect. 3 is devoted to the problem of designing of trajectory control system for MR based on FL method; Sect. 4 describes the structure of the trajectory control system, results of experimental tests for MR Rover5; some conclusions are shown in Sect. 5.

2 Formulation of a Trajectory-Tracking Control Problem for MR

The simplest model of a nonholonomic MR is the unicycle. Let us consider the kinematic model of a unicycle-type MR motion in a horizontal plane (Fig. 1a) [1–4]:

$$\begin{aligned} \dot{X} &= V \cos \varphi = 0,5 \cdot \cos \varphi (V_1 + V_2), & \dot{Y} &= V \sin \varphi = 0,5 \cdot \sin \varphi (V_1 + V_2), \\ \dot{\varphi} &= \omega = 0,5 \cdot d^{-1} \cdot (V_2 - V_1), \end{aligned} \quad (1)$$

where X , Y are coordinates of MR posture in the earth coordinate system; V_1 , V_2 , V are linear velocities of left and right wheels and velocity of MR; ω is a MR angular velocity; φ is an angle between the vector V and the axis OX .

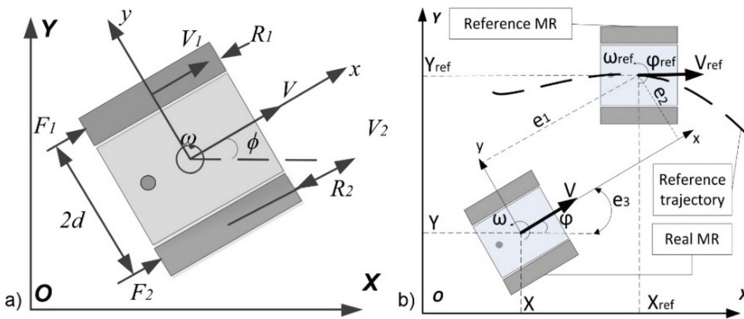


Fig. 1. a) The MR on a plane. b) Statement of the trajectory-tracking control problem for MR

We suppose that there is a given trajectory $p_{ref}(t) = (X_{ref}(t), Y_{ref}(t), \varphi_{ref}(t))$. MR trajectory-tracking errors (Fig. 1b) is defined as [1–4]

$$\begin{aligned} e_x &= X_{ref} - X, \quad e_y = Y_{ref} - Y, \quad e_\varphi = \varphi_{ref} - \varphi, \\ e_1 &= e_x \cos \varphi + e_y \sin \varphi, \quad e_2 = e_y \cos \varphi - e_x \sin \varphi, \quad e_3 = e_\varphi. \end{aligned} \quad (2)$$

Differentiating (2), we obtain the dynamic model of MR trajectory following errors:

$$\begin{aligned} \dot{e}_1 &= \omega_{ref} \cdot e_2 + u_1, \quad \dot{e}_2 = -\omega_{ref} \cdot e_1 + V_{ref} \cdot \sin e_3, \\ \dot{e}_3 &= u_2, \quad u_1 = V_{ref} \cdot \cos e_3 - V, \quad u_2 = \omega_{ref} - \omega. \end{aligned} \quad (3)$$

The problem is to find control inputs u_1 and u_2 , such that system (3) be an asymptotically stable, i.e. $e_i \rightarrow 0, i = 1, 2, 3$ for $t \rightarrow \infty$.

3 Control Law Design

3.1 Feedback Linearization of MIMO Nonlinear System

Nonlinear MIMO system in state-dependent coefficient form is considered:

$$\dot{x}(t) = A(x)x + B(x)u, \quad (4)$$

where $x \in R^n$ is a state vector; $u \in R^r$ is a control vector; matrix $A(x) - (n \times n)$ and $B(x) - (n \times r)$ are continuous differentiable matrices and have bounded derivatives. Let us suppose that the system (4) is controllable.

The feedback linearization problem of the system (4) consists in searching a nonsingular similarity transformation $z = T(x)x$ and a control input $u = u_{FL}$ by means of which the system (4) can be transformed into a linear canonical form.

The procedure of constructing the similarity transformation is given in detail in [12]. Here is an example of the system conversion for the case $u \in R^2$.

Applying the similarity transformation $z = T(x)x$ to the system (4) we get

$$\dot{z} = A_C(z)z + B_C(z)u, \quad A_C = TAT^{-1} + \dot{T}T^{-1}, \quad B_C = TB, \quad (5)$$

$$\begin{aligned} A_C &= \left(\begin{array}{c|c} J_{r_0} & E_{r_0 r_1} \\ \hline E_{r_1 r_0} & J_{r_1} \end{array} \right), \quad B_C = \left(\begin{array}{c|c} e_{p_1 p_1} & B_{12} \\ \hline 0 & e_{p_2 p_2} \end{array} \right), \quad J_k = \left(\begin{array}{c|c} 0 & I \\ \hline a_{k1} & a_{k2} \dots a_{kk} \end{array} \right), \quad E_{kl} = \left(\begin{array}{c} 0 \\ \hline a_{k1} \dots a_{kl} \end{array} \right), \\ B_{12} &= \left(\begin{array}{c} 0 \\ \hline b_{12} \end{array} \right), \quad I = \text{diag}(1, \dots, 1); J_k - (k \times k), \quad E_{kl} - (k \times l), \quad B_{12} - (r_0 \times 1), \\ &I - (k-1, k-1), \quad k = r_0, r_1; \quad l = r_0, r_1; \quad m = 2. \end{aligned}$$

Matrix B_C can be presented in terms of

$$B_C = \bar{B}C, \quad C - (2 \times 2), \quad \bar{B} = \begin{pmatrix} e_{p_1} & 0 \\ 0 & e_{p_2} \end{pmatrix}, \quad C = \begin{pmatrix} 1 & b_{12} \\ 0 & 1 \end{pmatrix}.$$

Since C is nonsingular, there is a new equivalent input $\bar{u} = Cu$. Feedback linearizing control for system (4) can be defined in the next form

$$u = u_{FL} + v = C^{-1}(K_{FL}z + v), \quad K_{FL} = -\begin{pmatrix} k_{11} & k_{12} & \dots & k_{1n} \\ k_{21} & k_{22} & \dots & k_{2n} \end{pmatrix}.$$

Instead of elements k_{ij} , it is necessary to take corresponding elements of J_k , E_{kl} .

3.2 Design of Trajectory-Tracking Control Law

Trajectory-tracking control loop is designed on the basis of FL method (4) and (5) for tracking error dynamic system (3), which can be written in a state-dependent coefficient form:

$$\dot{e} = A(e)e + Bu, \quad e = (e_1 \ e_2 \ e_3)^T, \quad u_K = (u_1 \ u_2)^T, \quad (6)$$

$$A(e) = \begin{pmatrix} 0 & \omega_{ref} & 0 \\ -\omega_{ref} & 0 & V_{ref}e_3^{-1} \sin e_3 \\ 0 & 0 & 0 \end{pmatrix}, \quad B = \begin{pmatrix} 1 & 0 \\ 0 & 0 \\ 0 & 1 \end{pmatrix}.$$

The similarity transformation for system (6) under condition of controllability of pair of matrices $(A(e), B)$ (holds for all V_{ref} , ω_{ref} , except $V_{ref} = 0$, $\omega_{ref} = 0$) is

$$\tilde{e} = T(e)e, \quad T(e) = \begin{pmatrix} 0 & -\omega_{ref}^{-1} & 0 \\ 1 & \dot{\omega}_{ref}\omega_{ref}^{-2} & a_{23}\omega_{ref}^{-1} \\ 0 & 0 & 1 \end{pmatrix}, \quad a_{23} = \frac{V_{ref} \sin(e_3)}{e_3}. \quad (7)$$

Under transformation (7), the system (6) takes the form

$$\dot{\tilde{e}} = \tilde{A}(e)\tilde{e} + \tilde{B}\bar{u}, \quad u = C^{-1}\bar{u},$$

$$\tilde{A}(e) = \begin{pmatrix} 0 & 1 & 0 \\ \tilde{a}_{21} & \tilde{a}_{22} & \tilde{a}_{23} \\ 0 & 0 & 0 \end{pmatrix}, \quad \tilde{B} = \begin{pmatrix} 0 & 0 \\ 1 & 0 \\ 0 & 1 \end{pmatrix}, \quad C = \begin{pmatrix} 1 & \tilde{b}_{22} \\ 0 & 1 \end{pmatrix},$$

$$\tilde{a}_{21} = -\frac{\omega_{ref}\dot{\omega}_{ref} - \dot{\omega}_{ref}^2 + \omega_{ref}^4}{\omega_{ref}^2}, \quad \tilde{a}_{22} = -\frac{\dot{\omega}_{ref}}{\omega_{ref}},$$

$$\tilde{a}_{23} = \frac{\sin(e_3)(\dot{\omega}_{ref}V_{ref} - \tilde{V}_{ref}\dot{\omega}_{ref})}{e_3\omega_{ref}^2}, \quad \tilde{b}_{22} = \frac{V_{ref} \sin e_3}{\omega_{ref}e_3}.$$

The resulting control law is

$$u = C^{-1}(K_{FL} + G_{ST})T(e)e,$$

$$K_{FL} = -\begin{pmatrix} \tilde{a}_{21} & \tilde{a}_{22} & \tilde{a}_{23} \\ 0 & 0 & 0 \end{pmatrix}, \quad G_{ST} = -\begin{pmatrix} g_{11} & g_{12} & 0 \\ 0 & 0 & g_{23} \end{pmatrix}, \quad g_{11}, g_{12}, g_{23} > 0. \quad (8)$$

Numerical values of g_{11} , g_{12} , g_{23} may be calculated by a pole placement method. When $V_{ref} = const$, $\omega_{ref} = const \neq 0$ we have a special case:

$$T(e) = \begin{pmatrix} 0 & -\omega_{ref}^{-1} & 0 \\ 1 & 0 & a_{23}\omega_{ref}^{-1} \\ 0 & 0 & 1 \end{pmatrix}, \quad (9)$$

$$u_1 = \omega_{ref}e_2 - g_{12}e_1 + \frac{g_{11}e_2 + g_{12}V_{ref}\sin(e_3) - g_{23}V_{ref}\sin(e_3)}{\omega_{ref}}, \quad u_2 = -g_{23}e_3.$$

The control law (9) is not applicable when $\omega_{ref} = 0$. So on the basis of this law it is impossible to realize a tracking along a straightforward trajectory. To overcome this disadvantage, it is possible to change the similarity transformation:

$$\tilde{e} = T(e)e, \quad T(e) = \begin{pmatrix} 0 & -1 & 0 \\ \omega_{ref} & 0 & a_{23} \\ 0 & 0 & 1 \end{pmatrix},$$

which leads to transformed system

$$\dot{\tilde{e}} = \tilde{A}(e)\tilde{e} + \tilde{B}C^{-1}\tilde{u}, \quad \tilde{a}_{21} = -\omega_{ref}^2, \quad \tilde{b}_{22} = -a_{23},$$

$$\tilde{A}(e) = \begin{pmatrix} 0 & 1 & 0 \\ \tilde{a}_{21} & 0 & 0 \\ 0 & 0 & 0 \end{pmatrix}, \quad \tilde{B} = \begin{pmatrix} 0 & 0 \\ \omega_{ref} & \tilde{b}_{22} \\ 0 & 1 \end{pmatrix}, \quad C^{-1} = \begin{pmatrix} \omega_{ref} & -\tilde{b}_{22} \\ 0 & 1 \end{pmatrix}.$$

In this case, the resulting control law has the form (8) where $\tilde{a}_{22} = \tilde{a}_{23} = 0$. It can be written in a scalar form

$$u_1 = \omega_{ref}(e_2 + g_{11}e_2 + g_{12}V_{ref}\sin(e_3)) - g_{12}e_1\omega_{ref}^2 - g_{23}V_{ref}\sin(e_3), \quad (10)$$

$$u_2 = -g_{23}e_3.$$

Finally, for the required values of MR linear and angular velocities, we have:

$$V_{req} = V_{ref}\cos(e_3) - u_1, \quad \omega_{req} = \omega_{ref} - u_2.$$

4 Experimental Test

4.1 Description of the Experimental MR

Object of the study is a MR Rover5 by DAGU (Fig. 2a) [8]. Power section of robot includes two electric drives based on the DC Motors. As a control unit Arduino UNO controller is used. To control the motors Rover5 Explorer PCB board is used. It is equipped with two FET H-bridges rated at 4A. Wireless communication interface is implemented through the usb-programmable wireless module Wixel.

Some parameters of the Rover5: track length $l = 0,245$, m; driving wheel's radius $r_w = 0,03$, m; robot's mass $m = 0,83$, kg; distance between tracks $d = 0,19$, m. Motor parameters: rated voltage: $U_{\mathcal{H}} = 7,2$, V; armature resistance $R_m = 100$, Ohm; armature inductance $L = 0,00123$, H; gear ratio $n_g = 86,8$. For measuring the motor's

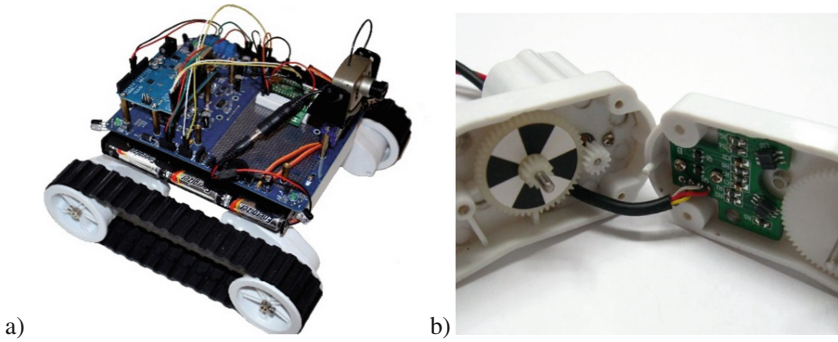


Fig. 2. a MR Rover5. b MR Rover5 quadrature encoder.

speed MR Rover5 is equipped with two quadrature encoders (Fig. 2b). Encoder's resolution is 1000 pulses for 3 turns of the driving wheel.

4.2 Structure of the Trajectory-Tracking Control System

Trajectory-tracking control system for Rover5 has a two-level architecture (Fig. 3).

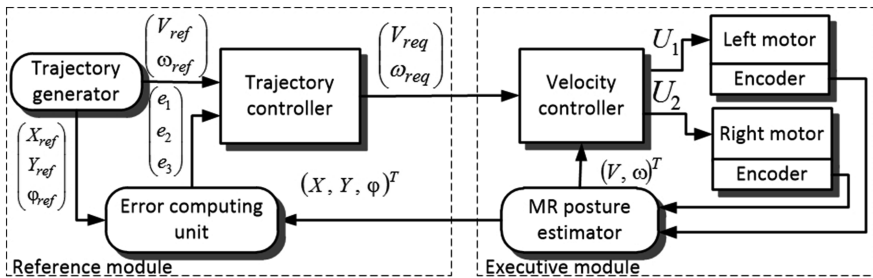


Fig. 3. Structural diagram of the MR control system.

Proposed two-level structure of the control system consists of two modules: a reference module and an executive module. The reference module is installed on a personal computer. It contains a trajectory generator, a trajectory control loop and an errors computing unit. The executive module includes a velocity control loop and an estimator of the robot posture. It is installed on the MR board.

4.3 Rover5 Dynamic Model and Velocity Control Loop

The dynamic model of the MR motion in the horizontal plane including the robot motors dynamic (it is assumed that both motors are identical) is [8]:

$$\frac{dx}{dt} = Ax + Bu, \quad x(0) = x_0, \quad y = Cx,$$

where is denoted

$$x = \begin{pmatrix} V \\ \omega \\ I_1 \\ I_2 \end{pmatrix}, \quad u = \begin{pmatrix} U_1 \\ U_2 \end{pmatrix}, \quad B = \begin{pmatrix} 0 & 0 \\ 0 & 0 \\ b_1 & 0 \\ 0 & b_1 \end{pmatrix}, \quad A = \begin{pmatrix} 0 & 0 & a_1 & a_1 \\ 0 & 0 & -a_2 & a_2 \\ -a_3 & -a_4 & -a_5 & 0 \\ -a_3 & a_4 & 0 & -a_5 \end{pmatrix}, \quad (11)$$

$$a_1 = \frac{c_m n_g}{r_w m}, \quad a_2 = a_1 \cdot \frac{d \cdot m}{J}, \quad a_3 = \frac{c_e n_g}{r_w L}, \quad a_4 = a_3 \cdot d, \quad a_5 = \frac{R_m}{L}, \quad b_1 = \frac{1}{L},$$

$$y = \begin{pmatrix} \omega_{r1} \\ \omega_{r2} \end{pmatrix}, \quad C = \frac{n_g}{r_w} \begin{pmatrix} 1 & d & 0 & 0 \\ 1 & -d & 0 & 0 \end{pmatrix}.$$

where J is a moment of inertia of the robot; c_m is a motor torque constant; I_i , $i = 1, 2$ is a current in the armature winding of the motor; U_i is a voltage in the motor armature; c_e is a motor e.m.f. constant; other variables are defined earlier.

The velocity control loop we develop using suboptimal control techniques [13]:

$$\begin{aligned} u &= -R^{-1} B_s^T P_s C_1^{-1} y, \\ 0 &= -A_s^T P_s - P_s A_s + P_s B_s^T R^{-1} B_s P_s - Q_s, \\ R &= \text{diag}(r_{U1}, r_{U2}) > 0, \quad Q_s = \text{diag}(q_1, q_2) \geq 0, \\ A_s &= -A_{12} A_{22}^{-1} A_{21}, \quad B_s = -A_{12} A_{22}^{-1} B_2, \\ A_{12} &= \begin{pmatrix} a_1 & a_1 \\ -a_2 & a_2 \end{pmatrix}, \quad A_{21} = \begin{pmatrix} -\bar{a}_3 & -\bar{a}_4 \\ -\bar{a}_3 & \bar{a}_4 \end{pmatrix}, \quad A_{22} = \begin{pmatrix} -\bar{a}_5 & 0 \\ 0 & -\bar{a}_5 \end{pmatrix}, \\ B_2 &= \begin{pmatrix} 1 & 0 \\ 0 & 1 \end{pmatrix}, \quad C_1 = \frac{n_g}{r_w} \begin{pmatrix} 1 & d \\ 1 & -d \end{pmatrix}, \quad \bar{a}_3 = \frac{c_e n_g}{r_w}, \quad \bar{a}_4 = \bar{a}_3 \cdot d, \quad \bar{a}_5 = R_m. \end{aligned} \quad (12)$$

The formula (12) is the mathematical basis for the synthesis of the sub-optimal velocity control loop for MR Rover5.

4.4 Trajectory Generator for MR

The reference trajectory is defined by the coordinates X_{ref} , Y_{ref} of an arbitrary reference robot's point M. Projections of the point's M velocity on the fixed axes are continuous functions of time:

$$V_{Xref} = \dot{X}_{ref}, \quad V_{Yref} = \dot{Y}_{ref}.$$

The considered MR is a nonholonomic system. So, there is a nonholonomic constraint: $-V_X \sin \varphi + V_Y \cos \varphi = 0$. This constraint does not allow setting arbitrarily the angular coordinate φ of robot, which in such a situation must be a solution of the differential equation [8]

$$\dot{\varphi}_{ref} = \frac{-V_{Xref} \sin \varphi + V_{Yref} \cos \varphi}{b_M \cos \gamma}, \quad \varphi_{ref}(0) = \varphi_0, \quad (13)$$

where $b_M \cos \gamma$ and $b_M \sin \gamma$ are constant coordinates of a point M in the coordinate system associated with the robot. Integrating (13), we find the law for φ_{ref} changes.

4.5 The Estimator of MR's Posture

The estimation of a MR posture is calculated according to the measurements of MR motors angular velocities ω_{r1} and ω_{r2} . Further, from (11) linear and angular velocities are calculated:

$$V = \frac{r}{2 \cdot n} (\omega_{r1} + \omega_{r2}), \quad \omega = \frac{r}{2 \cdot d \cdot n} (\omega_{r1} - \omega_{r2}).$$

The current position of the robot is determined from (1), by using the Euler approximation:

$$X = X_p + V \cdot \cos \varphi_p \cdot T_s, \quad Y = Y_p + V \cdot \sin \varphi_p \cdot T_s, \quad \varphi = \varphi_p + \omega \cdot T_s,$$

where T_s is a sample period, index «p» matches a value corresponding to the last sampling point.

4.6 The Experimental Results

An eight-shaped reference trajectory was taken as a test trajectory. At the initial time the robot is at the point with coordinates (0,25; -0,25), the trajectory starts to move from the point (0, 0).

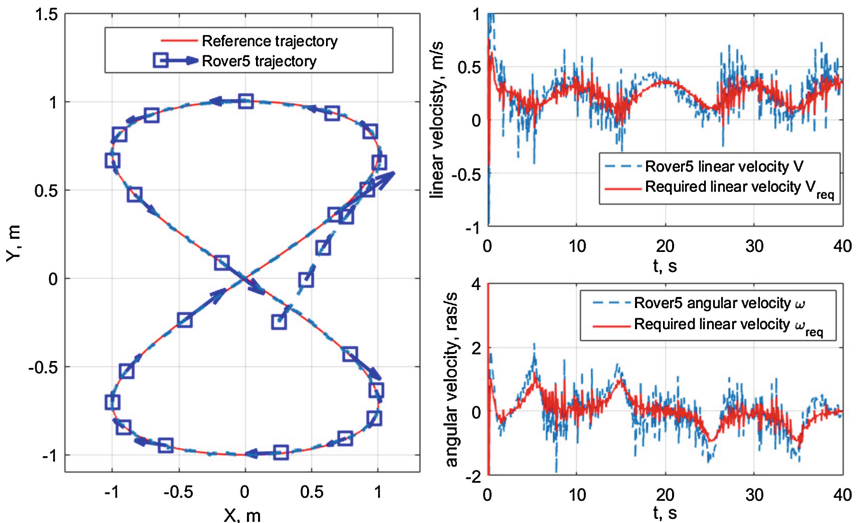


Fig. 4. The experimental results: reference and real trajectory of MR Rover5.

The frequency of harmonic signals $X_{ref}(t)$ and $Y_{ref}(t)$ is set so that the trajectory $p_{ref}(t)$ forms an “eight” for 40 s.

The experimental results on a real Rover5 robot are shown in Fig. 4, where are shown reference and real Rover5’s trajectories, required V_{req} and real V linear velocities, required ω_{req} and real ω robot’s angular velocities.

The results show us that the system has an acceptable quality. Robot enters the reference trajectory for 5 s, then deviations are $|e_x| \leq 0.015$, m, $|e_y| \leq 0.01$, m, $|e_\varphi| \leq 0.05$, rad, the relative tracking error doesn’t exceed 2% after the robot reached reference trajectory.

5 Conclusions

The problem of MR trajectory-tracking control was considered. The proposed system consists of two modules (reference and executive) and has, accordingly, two control loops: the first – trajectory control loop, the second – velocity control loop.

The design of trajectory control loop is based on FL problem for tracking error dynamic. In general case, the control law is a tracking error feedback with time-varying coefficients. Non-stationary nature of the problem is determined by the time-varying values of reference linear and angular velocities of the robot. In such a case when these velocities are constant, the problem becomes stationary and the feedback’s coefficients also become time-invariant.

Experimental verification of developed trajectory-tracking control system was performed on mobile robot Rover5. The results of experiment confirm the acceptable quality of designed control system.

The disadvantage of the proposed method is that it is not applicable if $V_{ref} = 0$, $\omega_{ref} = 0$ (“zero velocity” problem), i.e. this approach in this form is not applicable to the posture stabilization problem. Future research will be focused on developing the FL approach to MR control problem. In particular, the designing of a static FL for a kinematic model (1) for solving the problem of posture stabilization and point-to-point moving of MR.

Acknowledgments. This work was supported by the Russian Science Foundation (Project No.17-11-01220).

References

1. Siciliano, B., Khatib, O.: Springer Handbook of Robotics. Springer, Heidelberg (2016)
2. Siciliano, B., Sciavicco, L., Villani, L., Oriolo, G.: Robotics: Modelling, Planning and Control. Springer, London (2009)
3. Kozłowski, K.: Robot Motion and Control: Recent Developments. Springer, London (2006)
4. Cook, G.: Mobile Robots: Navigation, Control and Remote Sensing, Wiley-IEEE Press, Hoboken (2011)

5. Aguiar, A.P., Hespanha, J.P.: Trajectory-tracking and path-following of underactuated autonomous vehicles with parametric modeling uncertainty. *IEEE Trans. Autom. Contr.* **52**(8), 1362–1379 (2007). doi:[10.1109/TAC.2007.902731](https://doi.org/10.1109/TAC.2007.902731)
6. Klančar, G., Matko D., Blazič, S.: Mobile robot control on a reference path. In: Proceedings of the 13th Mediterranean Conference on Control and Automation, Limassol, Cyprus, 27–29 June, pp. 1343–1348 (2005). doi:[10.1109/2005.1467211](https://doi.org/10.1109/2005.1467211)
7. Charalambous, C.D., Lambis, A., Li, X.: Optimal control of a two-wheeled mobile robot via finite capacity communication channel. In: Proceedings of 16th Mediterranean Conference on Control and Automation, Ajaccio, France, pp. 946–951 (2008). doi:[10.1109/MED.2008.4602187](https://doi.org/10.1109/MED.2008.4602187)
8. Kabanov, A.A.: Optimal control of mobile robot's trajectory movement. *WSEAS Trans. Syst. Contr.* **9**, 408–414 (2014)
9. D'Andréa-Novel, B., Campion, G., Bastin, G.: Control of nonholonomic wheeled mobile robots by state feedback linearization. *Int. J. Rob. Res.* **14**(6), 543–559 (1995). doi:[10.1177/027836499501400602](https://doi.org/10.1177/027836499501400602)
10. Dixon, W.E., Dawson, D.M., Zergeroglu, E.: *Nonlinear Control of Wheeled Mobile Robots*. Springer, London (2001)
11. Oriolo, G., Luca, A.D., Vendittelli, M.: WMR control via dynamic feedback linearization: design, implementation and experimental validation. *IEEE Trans. Contr. Syst. Technol.* **10**(6), 835–852 (2002). doi:[10.1109/TCST.2002.804116](https://doi.org/10.1109/TCST.2002.804116)
12. Kabanov, A.A.: Full-state linearization of systems via feedback using similarity transformation. In: International Siberian Conference on Control and Communications (SIBCON). Proceedings of National Research University Higher School of Economics, Russia, Moscow, 12–14 May 2016. doi:[10.1109/SIBCON.2016.7491724](https://doi.org/10.1109/SIBCON.2016.7491724)
13. Kabanov, A.A.: Suboptimal robust system for mobile robot motion control. *Mekhatronika, Avtomatizatsiya, Upravlenie* **4**, 14–19 (2013)

Optimization of Design Opportunities and Transfer of Information Between Data 3D Graphics Program Blender and Solidworks CAD System for Use in Dental Industry

Rosen Vasilev, Hristo Skulev, and Tihomir Dovramadjiev^(✉)

Technical University of Varna, Varna, Bulgaria
{rosen.vasilev,hristo.skulev}@tu-varna.bg,
dr.tihomir.dovramadjiev@gmail.com

Abstract. Dental industry is making great progress recent years. Increasing opportunities and best applied practices to a large extent is due to the improvement in the technology toolbox. At the design stage there are various technological tools that possess one or another positive quality and are in progressive competition. Using the resources of specialized 3D graphics application Blender, for producing dental biological and implant elements and components is a very good opportunity in terms of designing complex 3D geometric models. Modifying the developed polygonal models into ones with solid bodies is successfully implemented in an environment of SolidWorks, a leader in the field of CAD systems. By using appropriate methodology the information data of 3D models is transferred between systems and is optimized in an appropriate form.

Keywords: Dental · 3D · CAD

1 Introduction

Despite the availability of specialized software packages with dental focus, they are more or less limited in their informational, structural, parametrical and other options covering a particular segment or group of activities [1]. Sometimes providing this type of software systems requires the availability of financial security. This is a feature that must be provided by companies that develop professional activity in the dental industry. In recent years, with the improvement of the technology hardware base, the progress of “open source” programs in design significantly improved [2]. This opens a new opportunity for further or fully covering activities at the stage of computer design of the developed 3D virtual dental models. This is the stage of construction, which is of great importance in future development of the actual manipulation, prosthetics and other activities set for implementation. The concept of modeling 3D dental models is determined based on the specific requirements, factors and capabilities. Good basis for establishing the virtual dental models can be merging the resources of “open software” as Blender [3] and the programming language Python [4] combined with specialized CAD system SolidWorks [5], which significantly improve the modeling process. This article

aims to systematize the methodology which synchronizes the transfer of information data by bringing together various technology software into unified system that greatly enhance the development of dental models for the needs of the dental industry.

Often the production of dental models is preceded by simulation processes, analyzing the strength of virtual samples. This is possible in the CAE environment [6], wherein the patterns are examined by the finite element method [7]. To make this possible it is necessary virtual models to have solid bodies [8]. This in turn poses a number of questions arising during the construction of 3D models. The quality of design of the developed templates depends on precise work of geometry and compliance with the structural features. From a design standpoint it is known that solid and mesh modeling have their big advantages or disadvantages depending on the further use of the developed 3D models. The modeling of solid forms provides an opportunity to direct study of the quality and strength of the developed models but has its limitations in the design process where the design of certain specific geometric elements is problematic. This can be solved if we use the resources of 3D graphics programs working with polygonal meshes and curves [9]. A good opportunity is the Blender software, which besides its free license, provides a good environment for the development of 3D geometric models by meshes using curves, parametrically through specialized applications and also by applying the programming language Python.

For the purposes of this study there will be a systematic methodology developed that includes milestones transfer information data for the needs of the dental industry (Fig. 1).

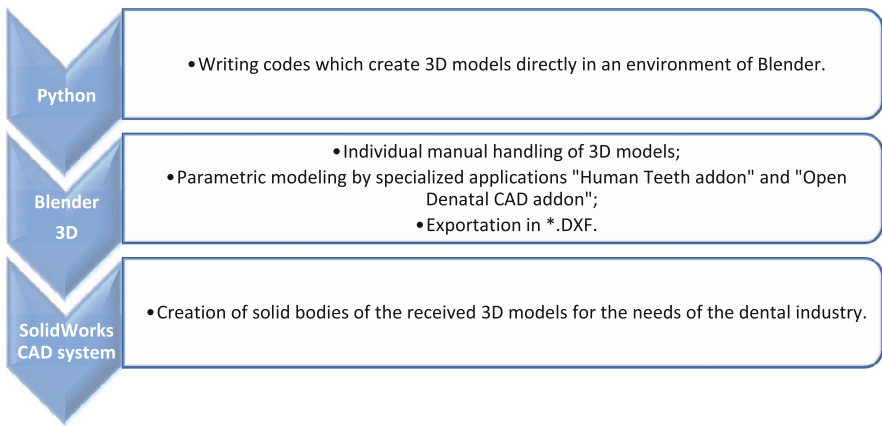


Fig. 1. Methodology for transfer of information data for the needs of the dental industry, containing creation of 3D geometry of dental models, data transfer and the creation of solid bodies in a CAD environment

The methodology includes:

- Creating 3D geometric objects in the environment of Blender, using the programming language Python and writing codes;

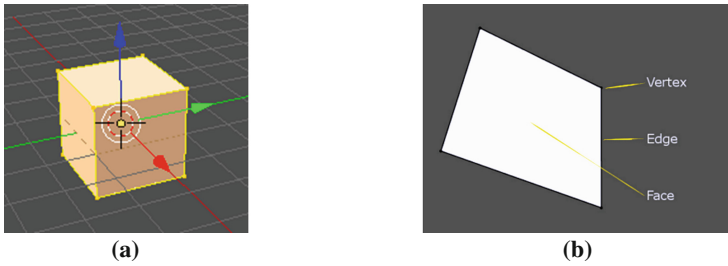


Fig. 3. Model of 3D primitive cube (a) Edit Mode; (b) The three bases forming the mesh in Blender: vertex, edges и faces

```
bpy.ops.object.mode_set(mode='EDIT')
bpy.ops.mesh.subdivide()
bpy.ops.mesh.subdivide()
bpy.ops.mesh.subdivide()
bpy.ops.object.mode_set(mode='OBJECT')
```

1.2 Modeling and Parametric Design Capabilities with Additional Applications Addons

Depending on the task what the 3D model should be, it can be in a different geometric shape. It is considered that 3D primitive cube has such a base geometry that through processing it can acquire a desired final model as tooth, crown, implant component, etc. Getting the final dental model of primitive cubic subject results of successive steps combining different modeling techniques such as working with the mesh and/or specific capability for 3D sculpts in Blender with “Sculpt Mode” [11]. Using the appropriate tools sculpts (Fig. 4(a)) a model of a dental crown or a tooth was constructed (Fig. 4(b)) [12].

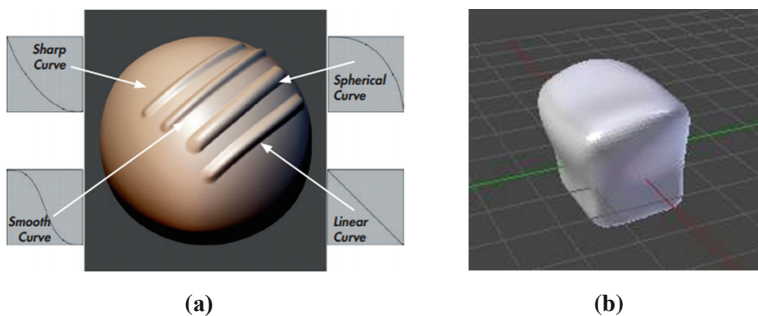


Fig. 4. The process of creating a 3D model of a crown (a) modeling capabilities of Sculpt Mode; (b) a process of construction of a dental crown or tooth

To achieve quality results it is desirable to apply combined techniques including working with mesh, modifiers, sculpting as well as specialized tools and modular

applications containing ready-developed dental samples. Fully available with a free license are “Human Teeth addon” [13] and “Open Dental CAD addon” [14]. These are applications that are specifically designed for the needs of 3D modeling of tooth, jaws, tissue and dental implants, abutments and crowns, and compatible with the latest version of Blender 2.78c.

1.3 Creating Solid Models

Polygonal meshes and curves make it possible to construct three-dimensional models with complex geometry. This is a good opportunity to supplement the design possibilities in the CAD system, where the development of dental components containing many crooked shapes, curves and surfaces is difficult. This is due to the solid body of the models that are used for research and production purposes and needs. Referring to modern dental implantology, the need to optimize the design possibilities for the development of implant components designed for three-dimensional printing is of good importance, where the presence of anatomical data is necessary. Figure 5 shows the implant models: standard - screw developed by the Straumann Company [15] and produced by 3D printing [16].



Fig. 5. Implant models (a) standard - screw; (b) relative to the shape of the root

From the photographs of the samples shown in Fig. 5 it is apparent that the implant of Fig. 5(a) has a straight shape, while that of Fig. 5(b) has a curved shape. This is a feature which is successfully implemented in environment of Blender using methodological guidelines described in Sects. 1.1 and 1.2. When work on the construction of 3D models is done, the finished geometry is transformed into solid body in an environment of SolidWorks. This is done by transferring the data in a file format *.DXF and subsequent processing in the CAD system, following the methodological requirements for working with curves, surfaces, scaling and creating solid bodies. For research purposes and objectives there are material samples set (physical materials), respectively of titanium (Ti), zirconium (Zr), etc. The process for transferring geometry data from Blender in the CAD system SolidWorks is shown in Fig. 6.



Fig. 6. The process of transfer of geometric data from Blender into the CAD system SolidWorks

2 Solid Models and Mesh Visualization

Modern dental industry covers various activities and applications. One of them is the development of dental crowns for teeth and implant structures. Unlike the implant

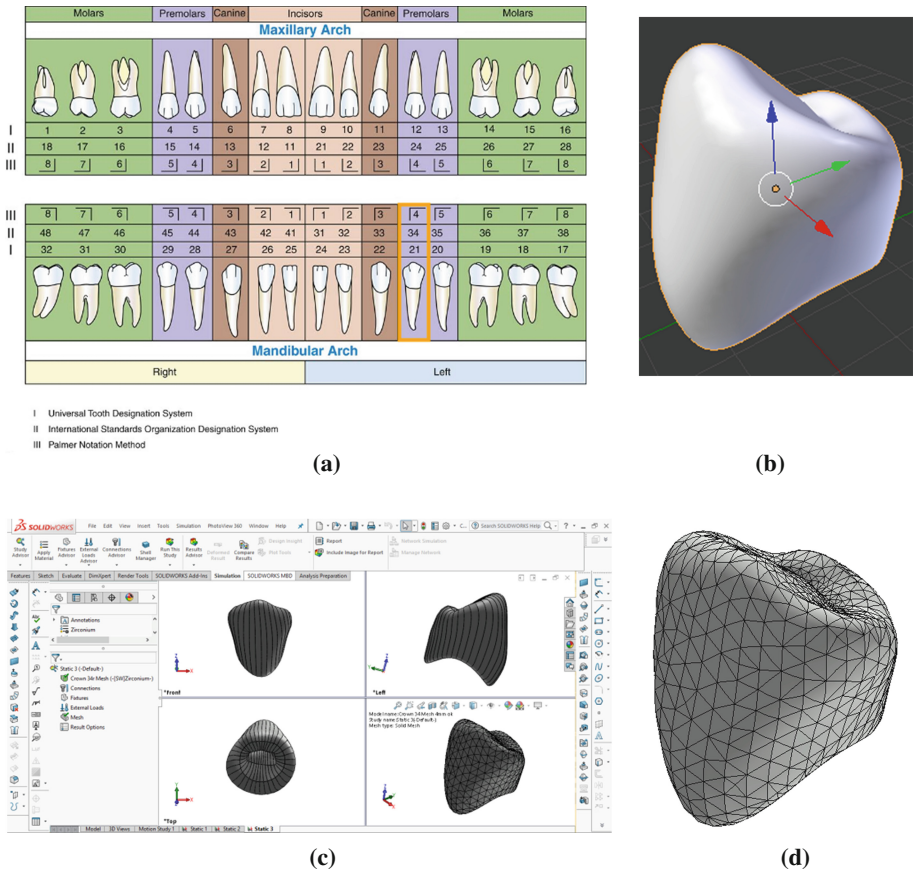


Fig. 7. Receiving solid model and mesh visualization (a) a complete set of human teeth, numbered in the international standards [17]; ISO 3950 [18]: I. Universal Tooth Designation System; II. International Standards Organization Designation System; III. Palmer Notation Method; (b) 3D.blend model of dental crown (N21 – I, N34 – II, N4 – III); (c) 3D solid model of dental zirconium crown created in the CAD system Solid Works; (d) detailed visualization of the resulting solid mesh (curvature-based mesh)

structures, three-dimensional geometry of the drill bit must have similar anatomical geometry of the tooth shape. It contains a complex combination of geometric forms. Respecting the procedure of Sect. 1 in sequence a 3D model of the dental crown is constructed (Fig. 7).

The resulting solid model in SolidWorks allows due to its discretion to investigate static, fatigue, non-linear loads and others. The results of the studies will be with good accuracy, based on the precisely crafted geometry model. The creation of this and other dental components with the developed methodology will significantly facilitate and improve the dental industry.

3 Conclusion

The actual production of dental components includes different technologies depending on the specific tasks and activities. The availability of regular geometric data for 3D dental models has big importance for the quality of real-manufactured components and the process of study the design strength in CAE systems. Given the complex solid modeling in CAD systems due to the specifics of the three dimensional shape of the models, it is a good opportunity to use the resources of 3D graphics programs, where the modeling of specific geometric elements is facilitated by using polygonal meshes and curves. This helps to build accurate 3D geometry of dental components which through the use of specific modeling techniques are converted into solid models that can be applicable to the dental industry. The optimization of this process can be improved by pre-building database of 3D models of dental components by writing programming codes. In a similar way applications addons can be created, by means of which parametrically to design three-dimensional dental components.

In the present article a fully operational methodology in structured stages is developed. Through it the projection opportunities and transfer data at 3D dental components are optimized for the needs of the dental industry. The stages of the construction of a specific three-dimensional geometry and the associative interaction program resources, leading to the improvement of research and production results are explained in details.

References

1. Rjakhovsky, A.: Use of computer 3D-technologies on the stage of planning and realization of dental implantation. In: CRID, Stomatologija (Mosk), Moscow, vol. 2, pp. 85–88 (2011)
2. Amrollahi, A., Khansari, M., Manian, A.: How open source software succeeds? A review of research on success of open source software. *IJICTR* **6**(2), 67–77 (2014). ISSN 2223-4985. (Spring)
3. Chronister, J.: Blender Basics 2.6, 4th edn., p. 178. Cdschools eBook Online (2011)
4. Prohorenok, N., Dronov, V.: Python 3. Samoe neobhodimoe, p. 482. BVH-Petersburg, Saint Petersburg (2014). ISBN: 978-5-97060-315-4
5. Tickoo, S.: SOLIDWORKS 2016 for Designers, 14th edn, p. 1715. CAD/CIM Technologies, Schererville (2016). ISBN 978-1-942689-18-8
6. Aliamovski, A.: SolidWorks Simulation. Kak reshat prakticheskie zadachi. – SPb, p. 448. BVH-Petersburg, Saint Petersburg (2012). ISBN 978-5-9775-0763-9

7. Hutton, D.: Fundamentals of Finite Element Analysis, 1st edn., p. 494. The McGraw-Hill Companies, New York (2004). ISBN-10: 0072395362
8. Gavrilov, V.: Teoreticheskie osnovi geometricheskogo modelirovaniya. Trehmerno modelirovanie (uch. Pos.). Izd-vo Samar gos. aerocosm. un-ta, Chap. 2, p. 80, Samar. ISBN 978-5-7883-0639-1
9. Botsch, M., Pauly, M., Kobbelt, L., Alliez, P., Lévy, B., Bischoff, S., Rössl, C.: Geometric modeling based on polygonal meshes. In: Eurographics, p. 180. ETH Zurich (2008)
10. Christen, M.: 3D Computer Graphics with Python, p. 58. Institut Vermessung und Geoinformation, Switzerland (2016)
11. Simonds, B.: Blender Master Class, p. 267. William Pollock, Baltimore (2013). ISBN-10: 1-59327-477-7
12. Dovramadjiev, T.: Advanced creating of 3D dental models in Blender software. In: MTM (s. 2016), pp. 32–33. STUME, Bulgaria (2016). ISSN 1310-3946
13. Human teeth addon. <http://byaapplication3d.blogspot.bg/p/ents-3d.html>
14. Open Dental CAD. <https://sites.google.com/site/blenderdental/home>
15. Straumann Produktkatalog (2017). <http://www.straumann.de>
16. Natural Dental Implants AG. 3D Printed REPLICATE™ Tooth. Germany (2017). <http://www.prnewswire.com/news-releases/natural-dental-implants-ag-announces-3d-printed-replicate-tooth-at-the-international-dental-show-in-cologne-300426972.html>
17. Pocket Dentistry. Overview of the Dentitions. <http://pocketdentistry.com/15-overview-of-the-dentitions/>
18. ISO 3950. Dentistry – Designation system for teeth and areas of the oral cavity. <https://www.iso.org/standard/68292.html>

Method for Conceptual Presentation of Subject Tasks in Knowledge Engineering for Computer-Aided Design Systems

Anatoly Korobeynikov^{1,2(✉)}, Michael Fedosovsky¹, Igor Zharinov^{1,3},
Vladimir Polyakov¹, Anatoly Shukalov¹, Andrey Gurjanov³,
and Sergey Arustamov¹

¹ ITMO University, 49, Kronverksky Pr., 197101 St. Petersburg, Russia
v_i_polyakov@mail.ru, sergey.arustamov@gmail.com

² SPBF IZMIRAN, University Emb., Building 5, letter B,
199034 St. Petersburg, Russia
office@izmiran.spb.ru

³ JSC Elektroavtomatika Design Bureau n.a. P.A. Efimov,
40, Marshala Govorova Street, 198095 St. Petersburg, Russia

Abstract. Currently, the basic paradigm of intelligent technology is a knowledge processing approach. A knowledge database that constitutes a core of intelligent systems must meet certain requirements such as availability, flexibility, consistency, and the others. These requirements can be satisfied with the aid of Knowledge Engineering. Due to the fact that the automation of the design process of complex technical systems is considered as one of the main approached increasing the efficiency of designer's activity simultaneously improving the quality and reliability of the projects, the development of knowledge representation techniques in knowledge engineering appears to be a topical task.

The paper deals with the method of conceptual presentation of application tasks for knowledge presentation in a consistency with the development of complex engineering systems supported by the category theory apparatus. Such presentation can be used to integrate and coordinate the common knowledge within the computer-aided design cycle. We adduce here the results of universal theoretical categorical semantic mathematical models of this representation.

Keywords: Knowledge engineering · Information technologies · Computer-aided design · Mathematical model · Conceptual modeling · Category theory

1 Introduction

Currently, all countries that are technologically advanced in the field of knowledge engineering are intensively conducting research in the development and implementation of new information technology (IT) processes in computer-aided design (CAD) [1]. This trend is giving rise to more rigid requirements to operation of modern complex technical systems (CTS) and, therefore, put up fundamentally new tasks that

require their solutions in the process of implementation CAD for CTS. It should be noted that existence of more rigid requirements quite often requires the denial of classic CTS design principles formulated half a century ago. That is why we are facing the task of creating the modern CTS design technologies, through which we can meet all the requirements specified. These technologies are based on the idea to form initially quite a large set of mathematical models (MM) with the obligatory presence of the toolkit performing various step by step transformations of the MM [2–4]. These technologies are presented in domain engineering, distributed computing, model-driven engineering (MDE), aspect-oriented software development (AOSD) [5–8].

To deploy the technologies listed above to operate of a large variety of flexible heterogeneous and complex MM for CAD CTS we have to carry out a specific scaling procedure [9]. The possibility is guaranteed when strait-through automation is taken place. Therefore, in the process of development of a modern CAD CTS technology we are facing a problem of elaboration of unified theoretical framework, based on which we permit to register scaling mechanisms, formulate and prove the basic properties, without going into details of the structure of specific MM.

Usage of these general-purpose technologies gives way to generate standard solutions, that typically appear as an ad hoc solutions [10, 11]. Consequently, the task of designing and developing a theoretical framework for CAD STK technology, that would have no above mentioned drawbacks, is a topical scientific problem. In other words, it can be stated the following way: the task of creation of a single universal formalism to describe a variety of technologies, suitable for CAD for complex heterogeneous systems and their integration and coordination is really urgent.

It is clear that a solution to this problem depends on the mathematical tools used for the simulation and analysis of the above technologies. Differential equations or minimizing composing functions, used for solutions, for example, to physical problems, is of no sense for the simulation of the required technology due to the lack of suitable analogues of conservation laws, statistical laws, variation based principles [12]. Therefore, an alternative approach can be used assuming the following principle: “for the most systems the history of assembly for some of their primary components either available or easily recoverable” [13].

If we know the MM of components and process steps required in the development of the system, the designer can calculate the integral characteristics of the designed system using the formal analogy of assembly drawings or “megamodels”, that can be formally described by means of directed graphs (diagrams). With this description, nodes will correspond to the components, and edges to technological operations. It is obvious that in case of CAD CTS generation and processing of large graphs would be required.

Therefore, we may face situations when there is no way to represent these graphs in details. In this case, structural limitations could be introduced. Currently, for the synthesis and analysis of graphs based on category theory a powerful mathematical tool, a division of a higher algebra, has been developed [13]. At same time a modern universal algebra, according to the formal provisions is a part of the theory of heterogeneous (or polybasic-sorted) algebraic systems with arbitrary signature and forming a family of suitable mathematical categories. Sticking to this standpoint we can assume there is a way to combine the theory of abstract data types with the AP theory.

In this case the algebraic systems provide a sufficiently large set of MM and methods of their design [13]. Meanwhile, a mathematical logic would provide an apparatus for constructing a theory of MM. Thus, using the theory of the categories, we can explore the family of sorted algebraic systems as not a random collection of MM but as a new and reasonably organized algebraic system.

Thus, following the above, we can use the apparatus of the theory of categories for clear and compact formalization of a problem for CAD CTS [14].

This article deals with a method for operating the models at the stage of conceptual representation of the subject task (CRST), defining the construction of a knowledge system for a specific subject task (ST).

2 Development of a Method of Conceptual Modeling for a Subject Tasks

Initial conceptual look at a subject task solves the problem of determining the basis to interpret the data used in the process of computer-aided solutions. In addition, the problem of semantic integrity for any formal linguistic representations of the task is being solved.

At CRST stage we will work with component-wise related conceptual models of the object and the specific levels of abstraction. Consequently, CRST for the n -th problem can be represented as follows:

$$CRST(n) = (CRST_1(n), \{CRST_2(n)\}),$$

where $CRST_1(n)$ - a conceptual model of n -th substantive task at the object level of abstraction;

$\{CRST_{2k}\} = (CRST_{21}, CRST_{21}, \dots, CRST_{2k})$ - conceptual models at specific level for the k -th implementation of the n -th subject task;

$$CRST_1(n) = Ob_CRST_1(n) \cup Mor_CRST_1(n),$$

where $Ob_CRST_1(n)$ - subject objects (SO);

$$Mor_CRST_1(n) = S_CRST_1(n) \cup D_CRST_1(n);$$

$S_CRST_1(n) = (B_CRST_1(n), P_CRST_1(n), BP_CRST_1(n))$ - a set of static relations on objects;

$B_CRST_1(n) \subset Ob_CRST_1(n) \times Ob_CRST_1(n)$ - a set of binary relations on $Ob_CRST_1(n)$;

$P_CRST_1(n)$ - a set of schemas on $Ob_CRST_1(n)$;

$BP_CRST_1(n) \subset P_CRST_1(n) \times P_CRST_1(n)$ - a set of binary relations on $P_CRST_1(n)$;

$D_CRST_1(n) = (V_CRST_1(n) \cup, BV_CRST_1(n))$ - a set of dynamic relations on objects;

$V_CRST_1(n)$ - a set of constraints on the object level of abstraction

$BV_CRST_1(n) \subset V_CRST_1(n) \times V_CRST_1(n)$ – a set of binary relations on $V_CRST_1(n)$;

$$CRST_{2i}(n) = Ob_CRST_{2i}(n) \cup Mor_CRST_{i1}(n),$$

where $Ob_CRST_{2i}(n)$ – representatives of subject objects (RSO);

$$Mor_CRST_{2i}(n) = S_CRST_{2i}(n) \cup D_CRST_{2i}(n);$$

$S_CRST_{2i}(n) = (B_CRST_{2i}(n), P_CRST_{2i}(n), BP_CRST_{2i}(n))$ – a set of static relations on objects;

$B_CRST_{2i}(n) \subset Ob_CRST_{2i}(n) \times Ob_CRST_{2i}(n)$ – a set of binary relations on $Ob_CRST_{2i}(n)$;

$P_CRST_{2i}(n)$ – a set of schemas on $Ob_CRST_{2i}(n)$;

$BP_CRST_{2i}(n) \subset P_CRST_{2i}(n) \times P_CRST_{2i}(n)$ – a set of binary relations on $P_CRST_{2i}(n)$;

$D_CRST_{2i}(n) = (V_CRST_{2i}(n) \cup, BV_CRST_{2i}(n))$ – a set of dynamic relations on objects;

$V_CRST_{2i}(n)$ – a set of object level constraints on abstraction that are representatives of subject dependencies (RSD);

$BV_CRST_{2i}(n) \subset V_CRST_{2i}(n) \times V_CRST_{2i}(n)$ – binary relations on $V_CRST_{2i}(n)$.

Schematically $CRST_1(n)$ for the n-th task looks as presented on Fig. 1.

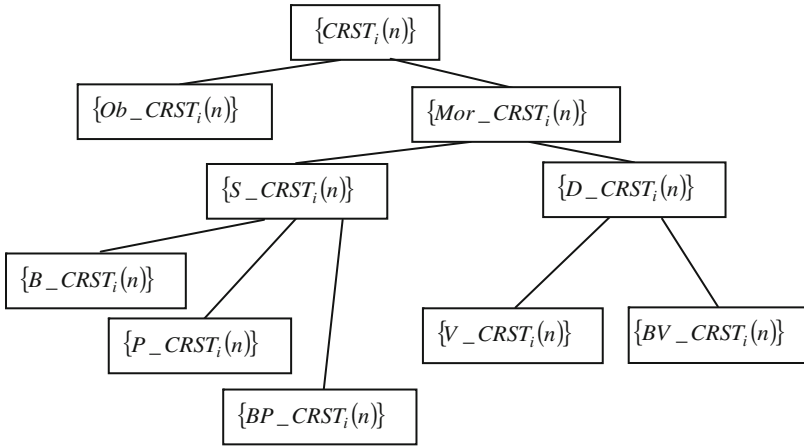


Fig. 1. Conceptual representation of a subject task $CRST_1(n)$ for the n-th task

Figure brackets note there may be either one conceptual model of the n-th object tasks or a set of conceptual models of specific level for the k-th implementation of the n-th task

$$\{CRST_{2k}\} = (CRST_{21}, CRST_{21}, \dots, CRST_{2k}).$$

We specify dependencies between sets of objects and constraints as follows:

$V_CRST_1(n) = (m_{1,1}, m_{1,2}, \dots, m_{1,k}) \& W(n)$ – a set of relations between SO and representation of the task (RT) at the object level,

$$\text{where } m_{1,i} \in Ob_CRST_1(n), i = 1, \dots, k; k = |Ob_CRST_1(n)|,$$

$W(n)$ – conditions defining the links in SO,

$$W(n) = \left\{ \left(\left\{ m_{1,i}^{(j)} \right\} \in Ob_CRST_1(n) \right), \left(\left\{ m_{1,i}^{(j)}, m_{1,i}^{(r)} \right\} \in B_CRST_1(n) \right), \right. \\ \left. \left(\left\{ p_{1,i}^{(j)} \right\} \in P_CRST_1(n) \right), \left(\left\{ p_{1,i}^{(j)}, p_{1,i}^{(r)} \right\} \in BP_CRST_1(n) \right) \right\}.$$

$V_CRST_2(n) = \left\{ v_{2,i}^{(j,r)}(n) \right\} = \left\{ m_{2,1}^{(j,l)}, m_{2,2}^{(j,l)}, \dots, m_{2,r}^{(j,l)} \right\} \& Q(n)$ – a set of relations between RSD and representatives of representations of a task at specific level,

where $\left\{ m_{2,i}^{(j,l)} \right\} \in Ob_CRST_2(n), i = 1, \dots, k; k = |Ob_CRST_2(n)|,$

$$Q(n) = \left\{ \left(\left\{ m_{2,i}^{(j,l)} \right\} \in \{Ob_CRST_2(n)\} \right), \left(\left\{ m_{2,i}^{(j,l)}, m_{2,u}^{(s,r)} \right\} \in \{B_CRST_2(n)\} \right), \right. \\ \left. \left(\left\{ p_{2,i}^{(j,l)} \right\} \in P_CRST_2(n) \right), \left(\left\{ p_{2,i}^{(j,l)}, p_{2,u}^{(s,r)} \right\} \in \{BP_CRST_2(n)\} \right) \right\}.$$

In this case the dependence may be presented as follows:

$$CRST_1(n) \rightarrow \{CRST_2(n)\},$$

i.e. $Ob_CRST_1(n) \rightarrow \{Ob_CRST_2(n)\}, P_CRST_1(n) \rightarrow \{P_CRST_2(n)\},$

$BP_CRST_1(n) \rightarrow \{BP_CRST_2(n)\}, V_CRST_1(n) \rightarrow \{V_CRST_2(n)\},$

$BV_CRST_1(n) \rightarrow \{BV_CRST_2(n)\}.$

With the use of apparatus of relational algebra we can formally justify the interlinks between the models at different levels:

$$B_CRST_{2,j}(n) = Ob_CRST_1(n) \bullet Ob_CRST_{2,j}(n) \bullet B_CRST_1(n),$$

$S_CRST_{2,j}(n) = S_CRST_1(n) \bullet B_CRST_1(n) \bullet B_CRST_{2,j}(n)$ – static relations,

$BV_CRST_{2,j}(n) = V_CRST_1(n) \bullet V_CRST_{2,j}(n) \bullet BV_CRST_1(n)$ – dynamic relations.

We can define formal rules for transition from object level to specific one for $CRST$ based on a formal approach defined above.

In a formal way the integration at the object level may be presented as follows:

$$\begin{aligned} Ob_CRST_1^0 &= \bigcup_n Ob_CRST_1(n), B_CRST_1^0 = \bigcup_n B_CRST_1(n), \\ P_CRST_1^0 &= \bigcup_n P_CRST_1(n), BP_CRST_1^0 = \bigcup_n BP_CRST_1(n), \\ V_CRST_1^0 &= \bigcup_n V_CRST_1(n), BV_CRST_1^0 = \bigcup_n BV_CRST_1(n). \end{aligned}$$

In a formal way the integration at the specific level may be presented as follows:

$$\begin{aligned} Ob_CRST_2^0 &= \bigcup_{n,m} Ob_CRST_{2,m}(n), B_CRST_2^0 = \bigcup_{n,m} B_CRST_{2,m}(n), \\ P_CRST_2^0 &= \bigcup_{n,m} P_CRST_{2,m}(n), BP_CRST_2^0 = \bigcup_{n,m} BP_CRST_{2,m}(n), \\ V_CRST_2^0 &= \bigcup_{n,m} V_CRST_{2,m}(n), BV_CRST_2^0 = \bigcup_{n,m} BV_CRST_{2,m}(n). \end{aligned}$$

3 Conclusion

The solution of the problem of uniform presentation of sets heterogeneous models reflecting different level of generalization or abstraction for application tasks gave way to formulate general definition of models disclosing their structure.

The research conducted aimed to implement developed method CRST for various CAD tasks is based on the modern information technologies that made possible to reveal uniform semantic foundation in a form of categories and assess the level of their formalization.

In the course of further research in the area of knowledge engineering we expect a development of CAD methods that presumes generation of mathematical categories (models) for a stage of so called infological simulation. The main target of such simulation is a creation of most natural and convenient methods for a designer and presentation of information required for knowledge databases are being developed.

References

1. Korobeynikov, A.G., Fedosovsky, M.E., Maltseva, N.K., Baranova, O.V., Zharinov, I.O., Gurjanov, A.V., Zharinov, O.O.: Use of information technologies in design and production activities of instrument making plants. *Indian J. Sci. Technol.* **9**(44), 1–8 (2016). <http://www.indjst.org/index.php/indjst/article/view/104708/75206>
2. Morin, B., Barais, O., Nain, G., Jézéquel, J.-M.: Taming dynamically adaptive systems using models and aspects. In: *Proceedings of 31st International Conference on Software Engineering, ICSE 2009, Vancouver*, pp. 122–132 (2009)
3. Korobeynikov, A.G.: *Design and research of mathematical models in the environments MATLAB and MAPLE*, 160 p. ITMO University, St. Petersburg, Russia (2012)
4. Korobeynikov, A.G., Grishentsev, A.Y.: *Development and a research of multivariate mathematical models with use of systems of computer algebra*, 100 p. ITMO University, St. Petersburg, Russia (2013)

5. Kiczales, G., Lamping, J., Mendhekar, A., Maeda, C., Lopes, C.V., Loingtier, J.-M., Irwin, J.: Aspect-oriented programming. In: Proceedings of 11th European Conference on Object-Oriented Programming, ECOOP 1997, Jyväskylä, Finland, 9–13 June 1997. Lecture Notes in Computer Science, vol. 1241, pp. 220–242. Springer, Heidelberg (1997)
6. Gatchin, Y.A., Zharinov, I.O., Korobeynikov, A.G., Zharinov, O.O.: Theoretical estimation of Grassmann's transformation resolution in avionics color coding systems. *Mod. Appl. Sci.* **9**(5), 197–210 (2015). ISSN 1913-1844
7. Korobeynikov, A.G., Aleksanin, S.A., Perezyabov, O.A.: Automated image processing using magnetic defectoscopy. *ARPN J. Eng. Appl. Sci.* **10**(17), 7488–7493 (2015). ISSN 1819-6608
8. Aleksanin, S.A., Zharinov, I.O., Korobeynikov, A.G., Perezyabov, O.A., Zharinov, O.O.: Evaluation of chromaticity coordinate shifts for visually perceived image in terms of exposure to external illuminance. *ARPN J. Eng. Appl. Sci.* **10**(17), 7494–7501 (2015). ISSN 1819-6608
9. Kolovos, D.S., Paige, R.F., Polack, F.A.C.: The grand challenge of scalability for model driven engineering. *Lecture Notes in Computer Science*, vol. 5421, pp. 48–53 (2009)
10. Diskin, Z., Maibaum, T.S.E.: Category theory and model-driven engineering: from formal semantics to design patterns and beyond. In: Proceedings of 7th Workshop ACCAT 2012, Electronic Proceedings in Theoretical Computer Science, vol. 93, pp. 1–21 (2012)
11. Korobeynikov, A.G., Grishentsev, A.Y., Velichko, E.N., Korikov, C.C., Aleksanin, S.A., Fedosovskii, M.E., Bondarenko, I.B.: Calculation of regularization parameter in the problem of blur removal in digital image. *Opt. Memory Neural Netw. (Information Optics)* **25**(3), 184–191 (2016)
12. Sommerville, I.: *Software Engineering*, 9th edn., 790 pp. Pearson Education, Inc., Publishing as Addison-Wesley, Boston (2011)
13. https://www.homeworkmarket.com/sites/default/files/q5/19/07/cis_421_sommerville_9e_ch1-3.pdf
14. Cohn, P.: *Universal Algebra*, p. 412. Springer, Heidelberg (2012)
15. Mac Lane, S.: *Categories for the Working Mathematician*, 2nd edn., p. 314. Springer, New York (1998)

Energy Meter for Smart Home Purposes

Zdenek Slanina^(✉) and Tomas Docekal

Department of Cybernetics and Biomedical Engineering, VSB - Technical University
of Ostrava, 17. listopadu 15, 70833 Ostrava, Czech Republic
zdenek.slanina@vsb.cz

Abstract. This paper describes smart energy meter electronics design and implementation with later realization with real time operating system FreeRTOS. The main areas to use this energy meter are charging stations (stands) for electric vehicle (follows as EV) charging support and possible embedding into current smart building technology. In described module there was required measurement of voltage, electric current and frequency of power network. After integration into smart buildings (home automation, parking houses) there are pros and cons of such solution mentioned.

1 Introduction

Nowadays there are still primarily internal combustion engine used in passenger transport vehicles. Especially in big cities this is the main problem of heavy traffic due over limit level of toxic exhaust fumes. A good alternative is the offer of alternative technologies as the electric or hydrogen powered vehicles [9–12].

This article is mainly oriented to electric vehicles application for change of this bad situation. The truth is that it brings many problems associated with the wrong idea of their use, their manufacturing and maintenance and especially development of the infrastructure for their use which lags behind the mainstream for decades. Leaving aside the possibility of replacing the batteries pack when they are depleted the only way to recharge energy is using electricity at home or public grid.

The second option means the need to measure the amount of electric energy in case of commercial use and also the need to regulate the charging current to prevent overloading of electric network.

At the Department of Cybernetics and Biomedical Engineering there were developed several charging stations for testing and commercial purposes. Current version allows charging from an electric network 400 VAC which does not meet the requirements in the preceding paragraph on possibility of energy regulation used for charging due to lack of communication interface.

Based on past experience and current demands for enhanced solution there was developed energy measuring module which can be integrated into existing technology of charging stand and which can expand the possibilities of communication ([3–5, 13]) towards the electric car and energy infrastructure of smart building [1, 2, 6–8].

2 Energy Meter Design

The whole device was divided into several sections, which provide comprehensive functions and could work independently. With this solution, there can be minimum of compromises when selecting the components. There is no need to find one universal part for doing all tasks, but specialized parts with better performances and features can be chosen. The division is shown in the block diagram on Fig. 1. The main idea is to separate digital part, which is intended for controlling, and analog part, which is designed for measuring.

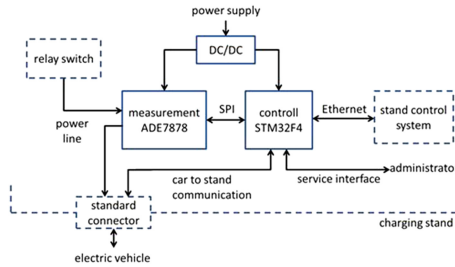


Fig. 1. Block design

The specialized circuit ADE7878 was selected for purposes of measurement. This chip is made by company Analog Devices. It is prepared for measuring in three phase electricity network, which can be realized by three or four wires. The voltage and the current are measured in each phase and also the current in the neutral conductor. The circuit includes seven independent analog to digital convertors for this purpose. Each of these convertors is high accuracy sigma-delta type with 24 bit resolution and 1.024 MHz sampling rate. The measuring circuit does not require many external components, there have to be only several blocking capacitors and accurate crystal clock with frequency 16.384 MHz.

The other values are calculated from measured currents and voltages. Firstly, the RMS values for measured signals are calculated, and then the active, reactive and apparent powers and energies for each phase. It is also possible to measure the frequency of electricity network and to compute the phase shift between current and voltage in single phase or for example between voltages from different phases.

The external circuit between current sensors and the ADE7878 circuit is necessary, because this circuit is able to measure voltage signals only. The structure of this circuit depends on type of the current sensor. The variant for the current transformer is shown on the Fig. 2. The transfer from current (on transformer's output) to voltage is ensured by the resistors R_1 and R_2 . There are two low pass filters in each way – positive and negative, but for current transformers only one is used in each way. They are anti-aliasing filters for attenuating high

frequencies of the signals before their sampling. The cut off frequency of these filters is following:

$$f_c = \frac{1}{2\pi R_5 C_3} = \frac{1}{2\pi \cdot 1 \cdot 10^3 \cdot 22 \cdot 10^{-3}} = 7234.316 \text{ Hz}$$

As it was mentioned above, measuring circuit sample the signals with frequency 1.024 MHz, so this anti-aliasing filter is sufficient. There is the digital filter with cut off frequency 256 kHz inside the circuit and also additional low pass filter, which limits the frequency range of signals to the interval 40 Hz–2 kHz.

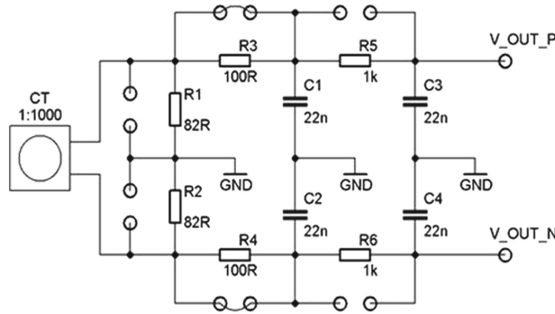


Fig. 2. The circuit for the current sensor

The part for measuring the phase voltage uses the series connection of the resistors as the voltage divider. It decreases the value of the voltage to the interval $\pm 0.5 \text{ V}$, which is allowed on the input of the analog to digital converter. This circuit is shown on Fig. 3. As you can see, there is the anti-aliasing filter too. Its cut off frequency is the same as in the case of current sensing.

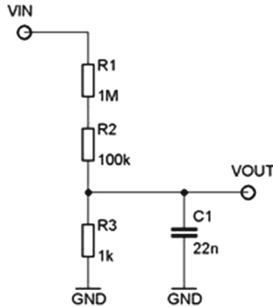


Fig. 3. The circuit for the voltage measurement

The 32 bit microcontroller (MCU) with ARM core was chosen as the main control element, MCU STM32F407 from STMicroelectronics. There are several reasons for this choice. The first and very important is presence of periphery for the communication via Ethernet network. It is required to add external chip for realization of physical layer only. The connection between MCU and this external chip may use the MII (Media Independent Interface) or RMII (Reduced Media Independent Interface) interface. The second reason is presence of the many sources, which can be used for the implementation of the special and complicated functions. These sources include for example large RAM and flash memory or digital signal processor (DSP). In the same way as the measuring circuit, the MCU require some blocking capacitors and accurate crystal. The frequency of the crystal can be various, there is not only one correct value, because of internal PLL. The physical layer is realized by the integrated circuit LAN8720.

The final firmware, which is implemented in the control MCU, is based on real time operating system FreeRTOS. It allows separation of different task into integrated and enclosed parts. The interactions between these tasks are realized as the communication, which uses the parts of FreeRTOS for inter process communication (IPC).

The independent module was designed for realization of communication with the electric vehicle. The advantage is that this module has not to be the part of the whole energy meter in each applications and it may be removed. The simplified schematic is shown on Fig. 4. The PWM (Pulse Width Modulation) with range $\pm 12V$ is used for the communication with the vehicle. The duty of the signal corresponds to the maximal current, which can be used for charging by the electric vehicle. According to the state of charging process, there can be also 12 VDC signal.

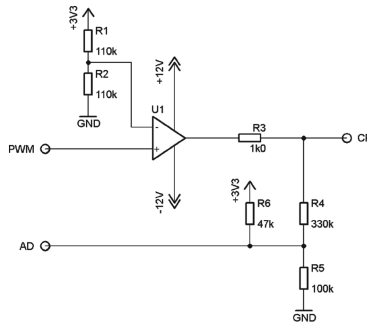


Fig. 4. The circuit for the current sensor

The MCU operates with 3V3 logic levels, so it was necessary to ensure the conversion of generated PWM signal to the required level. This is done by the operating amplifier, which is used as the comparator. Its output is connected with specific connector by 1 k Ω resistor according to the documentation.

The voltage value of this output is measured by the control MCU, because the vehicle is able to connect the additional resistors to this communication line according to the state of the charging. Due to this action the +12 V level is decreased. This value provides for MCU the information about the connection of electric vehicle, if it is ready for charging, if the charging is completed or if there are some errors. The transfer to the range 0–3.3 V is ensured by three resistors according to the Fig. 4.

During the design of whole device, the attention was aimed on the safety, because one of the parts of the energy meter is in contact with the line voltage. This was the reason for galvanic isolation of all parts, as can be seen on Fig. 5. The digital control part is isolated from measuring parts with use of digital isolators ADMU1401 from Analog Devices. It is possible to transfer high frequency digital signals through these isolators. They are based on the transformer principles. Similar circuit is used to isolate connection with module for Mennekes communication and to service interface too. The connection to Ethernet network is using connector, which includes transformers and which isolated the energy meter from other parts of network.

The energy meter is powered from 12 V source. The required voltage levels for powering each part are obtained from galvanically isolated DC/DC converters. It is evidential from the Fig. 5 that the control part is isolated from all other parts as well as the measuring part, except the power lines, which are measured. The device is safety internally, that means problems from one part should not damage another parts, and also externally for another connected devices.

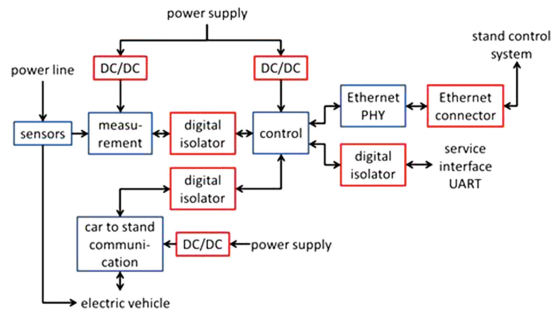


Fig. 5. The galvanic isolation of the energy meter parts

3 Experiment with Boiling Water

This early experiment deals with the water heating. This activity is related to the energy transfer from some heating source to the heating medium. The intention is to use the electric kettle to boil one litre of the water and measure the energy consumption over time.

In terms of physics, we are speaking about heating the substance in a liquid state from one temperature (indoor temperature) to the second (the boiling point). The electric kettle will stop automatically after reaching the boiling point, but temperature of the water may not be the same in the entire volume and some amount can change the physical state. So the premise is that the measured amount of consumed energy has to be in the range between calculated energy needed for heat the water and this energy plus the energy necessary for change the physical state of small amount of the original water quantity. It is also appropriate to consider the efficiency of the electric kettle, which is approximately 90%.

On the start of the experiment the initial values of variables were measured, the temperature of water before heating t_1 and the weight of the volume of water m_1 . The temperature of the boiling point t_2 was calculated based on the measured atmospheric pressure p_1 . This temperature is relative, because the real temperature of water will vary in volume.

$$\begin{aligned}t_1 &= 20.6^\circ\text{C} \\p_1 &= 98.994\text{ kPa} \\t_2 &= 71.6 + \frac{7}{25}p_1 = 99.32^\circ\text{C} \\m_1 &= 1.002\text{ kg} \\c &= 4180\text{ Jkg}^{-1}\text{ K}^{-1} \\l &= 2260 \cdot 10^3\text{ Jkg}^{-1}\end{aligned}$$

The amount of energy for water heating is calculated from following equation.

$$\begin{aligned}Q &= m_1c\Delta t = m_1c(t_2 - t_1) \\Q &= 1.002 \cdot 4180 \cdot (99.32 - 20.6) = 329708\text{ J} \\Q &= 91.586\text{ Wh}\end{aligned}$$

The second amount of energy (for change the physical state) can be calculated based on the weight of water in the electric kettle m_2 measured after the experiment.

$$\begin{aligned}m_2 &= 0.994\text{ kg} \\L &= (1.002 - 0.992) \cdot 2260 \cdot 10^3 = 18080\text{ J} = 5.022\text{ Wh}\end{aligned}$$

The final value of energy E_1 was read out of the energy meter at the end of experiment. The chart of energy consumptions change during time is on Fig. 6. The values were read out each two seconds.

$$E_1 = 101.365\text{ Wh}$$

If we calculate the estimated kettle efficiency, we obtain the measured energy E_2 transferred to the water without losses.

$$E_2 = E_1 \cdot \eta = 101.365 \cdot 0.9 = 91.229 \text{ Wh}$$

As you can see, the difference between the measured and calculated energy is approximately 4.7 Wh excluding the kettle efficiency or 5.4 Wh including it. This can be caused by different efficiency, inaccurately determined final temperature (we do not know how exactly the kettle estimate the end of heating) or by another influences.

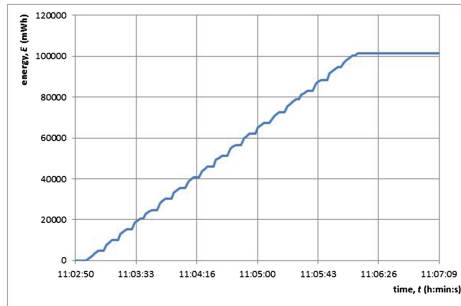


Fig. 6. Measured energy in time for boiling water experiment

4 Real Measurement with Electric Car

Another experiment was to measure the charge of a real electric car. For this measurement, an electric stand was used to charge the electric vehicles, which was developed at the same department. This is a version that allows only AC charging, either single-phase or three-phase. The energy consumed can then be compared with an industrial electricity meter installed in the stand. Several cars were used for the measurements, in this particular case, the Peugeot 106, which was reconstructed for electric drive. From Fig. 7, the maximum possible accumulated energy of the car is visible, which is currently at the lower limit of installed batteries in mass-produced wagons. Original batteries capacity was about 10 kWh, graphs show about 6 kWh because a part of batteries is depleted. On this graph we can see time (11:35) where balancing unit begins to work and input power is decreasing too.

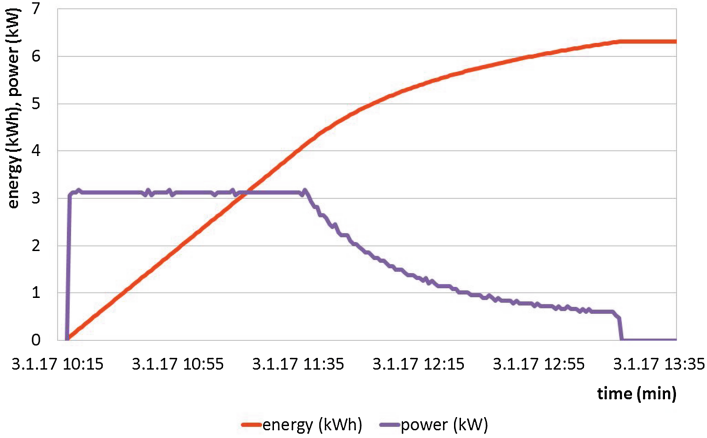


Fig. 7. Real experiment with electric Peugeot car prototype

5 Conclusion

Introduced solution of energy measurement for smart home purposes was described. This meter (Fig. 9) makes easy to connect electric car to your home network and, in conjunction with the switching elements, allows to control the charging or discharging process of an electric car mentioned in the references in the first chapters in this article. The next step is to integrate communication elements that can match the charging process with own car control system or car charger needs. There is already a broad horizon for expanding the smart energy meter with other features to address the charge rate depending on the needs of the power network from the macro point of view or inside the off grid network.

The information about charging was read by computer connected to Ethernet. The control application provided the information about electric energy according to the sequential diagram on Fig. 8.

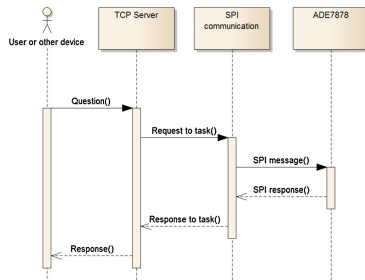


Fig. 8. Sequence diagram of communication

Based on message from client, the TCP Server inserts requests into the queue. Then the SPI communication task starts, sends the request to measuring circuit and after that provides the response from ADE7878 to TCP Server, which transform this data into the message for client.

Key benefits were mentioned in the text above. Among them there is the communication with superior system based on Ethernet. It is also possible to connect proposed solution with smart buildings technology and to control energy according to the electric network state.

The last benefit is that it should be used for possibility of bidirectional flows of electric energy between the electric vehicle and energy networks which is nowadays much welcome feature of charging stands and electric vehicles combination. Respectively it is possible to use electric vehicles as an energy container in grid-off technologies (Fig. 9).

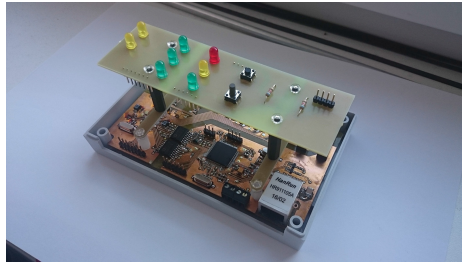


Fig. 9. Open energy meter box

Acknowledgement. This work was supported by the project SP2017/158, “Development of algorithms and systems for control, measurement and safety applications III” of Student Grant System, VSB-TU Ostrava.

References

1. Misak, S., Prokop, L.: Off-grid power systems. In: 9th Conference on Environment and Electrical Engineering, EEEIC 2010, pp. 14–17 (2010)
2. Prokop, L., Misak, S.: Off-grid energy concept of family house. In: Proceedings of the 13th International Scientific Conference Electric Power Engineering, EPE 2012, pp. 753–758 (2012)
3. Ozana, S., Pies, M., Hajovsky, R., Koziorek, J., Horacek, O.: Application of PIL approach for automated transportation center. Lecture Notes in Computer Science, vol. 8838, pp. 501–513 (2014)
4. Bradac, Z., Kaczmarczyk, V., Fiedler, P.: Optimal scheduling of domestic appliances via MILP. *Energies* **8**(1), 217–232 (2015)
5. Leseck, F., Stastny, L., Bradac, Z.: Modelling transmission lines for the purpose of data transmission over power lines. *Procedia Eng.* **100**(January), 1381–1388 (2015)
6. Kaczmarczyk, V., Fiedler, P., Stohl, R., Bradac, Z.: Electric vehicles charger as a part of home area network. *IFAC Proc. Vol. (IFAC-PapersOnline)* **11**(PART 1), 180–185 (2012)

7. Zezulka, F., Sajdl, O., Bradac, Z., Sembera, J.: Experimental smart grid. IFAC Proc. Vol. (IFAC-PapersOnline) **4**(PART 1), 416–419 (2012)
8. Friedrischkova, K., Vala, D.: Energy-independent concept of a house using an electric vehicle traction. IFAC-PapersOnLine **49**(25), 535–540 (2016)
9. Friedrischkova, K., Vala, D., Horak, B.: Accumulation system of electric vehicle and its secondary exploitation. In: IYCE 2015 - Proceedings: 2015 5th International Youth Conference on Energy (2015)
10. Friedrischkova, K., Vala, D., Horak, B.: Testing of the traction batteries in electric vehicles and their further use. IFAC-PapersOnLine **28**(4), 272–277 (2015)
11. Friedrischkova, K., Vala, D., Horak, B.: The use an Electric vehicle as a power source. In: ICINCO 2015-12th International Conference on Informatics in Control, Automation and Robotics Proceedings, pp. 164–170 (2015)
12. Horak, B., Minarik, D., Friedrischkova, K., Vala, D., Kazarik, J.: The development of drive units for electric cars Kaipan voltage. In: 14th International Scientific Conference on Electric Power Engineering 2013, pp. 753–758 (2013)
13. Franek, L., Stastny, L., Bradac, Z.: Power line communication parameters of multi conductor power line. IFAC-PapersOnLine **49**(25), 212–217 (2016)

Decision Models for Volume Plans in Mechanical Engineering

Georgy Burdo^(✉)

Tver State Technical University, A. Nikitin Emb., 22, Tver, Russia
gbtms@yandex.ru

Abstract. Multiproduct mechanical engineering, where, as a rule, first samples of high-tech and science intensive products are produced, is characterized by a great number of orders having to be done simultaneously and to be renewed continually as well as by simplified process-layout preparation (predetermining the approximation of standard time for production steps). Therefore, manufacturing systems work under uncertainty when their current state cannot be identified and which leads to some difficulties in determining the way of corrective control action. One of the critical stages in determining manufacturing system capacity is volume planning which, consequently, influences the whole system of division plans. The uncertainty in decision-making can be decreased with “advice” automated systems when Control Subjects are making agreed decisions. The research describes the problem of making agreed decisions for volume manufacturing plans. An automated technological process control system generates options of control actions, with experts analyzing and assessing them, then choosing the most feasible one with fuzzy sets. The method developed was piloted at the base plant.

Keywords: Automated technological process control system · Manufacturing process · Artificial intelligence · Mechanical engineering · Expert judgments · Decision-making · Fuzzy sets

1 Introduction

Multiproduct mechanical engineering, where, as a rule, first samples of high-tech and science intensive products are produced, is characterized by a great number of orders having to be done simultaneously and to be renewed continually as well as by simplified process-layout preparation (predetermining the approximation of standard time for production steps). Therefore, manufacturing systems work under uncertainty when their current state cannot be identified and which leads to some difficulties in determining the way of corrective control action. One of the critical stages in determining manufacturing system capacity is volume planning which, consequently, influences the whole system of division plans [1, 2]. The uncertainty in decision-making can be decreased with “advice” automated systems when Control Subjects are making agreed

The work is done with funding from RFBR, project 17-01-00566.

decisions [3]. It should be noted that the task of volume plans for production divisions is, in many respects, a low-formalized multichoice one, therefore, according to the authors, the integration of different level staff managers' natural intelligence with an automated technological process control system having the elements of artificial intelligence helps overcome the difficulties outlined above. Therefore, the aim of the study was to develop a decision-making procedures for production planning targeted at the plan quality improvement by means of the system users' knowledge.

2 Decision-Making in Automated Technological Process Control System

2.1 General Structure and Functions of Automated Technological Process Control System

General functions of automated technological process control system in multiproduct mechanical engineering are the following: (1) volume (annual, quarterly, and monthly) production planning; (2) planned scheduling (quarterly, monthly) with production being based on the time; (3) operation scheduling (decade, as a rule) of piece making and dispatching production control (technological process regulation) following the actual timing of the schedule. The source data for the automated technological process control system are based on an organizations' tactical production and sales plans made under contractual liabilities and CAM data on labor and tool intensity by equipment types and groups [4–6]. Volume planning is the highest level of an organization's tactical plans, with its proper elaboration, in many respects, determining positive technical and economic indices of the company. It should be noted that the proposed hierarchy of planning procedures in the automated technological process control system fully defines an organization's adopted plan structures. It should be emphasized that the algorithms of the automated technological process control systems must agree with "just in time" ideology [7, 8].

2.2 Procedures of Volume Planning

The prerequisite for the effective control of manufacturing systems is the apportionment (due to the available facility and time) of the whole volume of work planned for a sufficiently large period (a year, a quarter, etc.), or period parts relevant to the planned time intervals (a quarter, a month) established in the organization. The work allocation between the technological divisions (TD), or spatial distribution, and by time, or time distribution, is achieved in line with the period of contract execution. The procedures discussed below are actively controlled by the staff making an agreed decision (as a rule, they are Deputy Director for Production (Subject 1), Head of the Production System Department (Subject 2) and Head of the Dispatch Service (Subject 3).

The plan establishment level is determined through meeting contractual obligations [3] with the definite coefficient of facilities and area utilization (K_{zq} and K_{zs}). Initially, the coefficient is recommended to range from 0.85 to 0.9 at the stage of volume planning (VP) and to take into account some uncertainty of technological production

cycles (determined at the stage of scheduling) and the necessity to have capacity reserves for rush orders. The choice of K_{zq} and K_{zs} less than 0.8 will result in guaranteed execution of plan targets but may cause the underutilization of facilities and areas and will lead to unreasonable outsourcing.

The authors recommend an iteration algorithm of volume planning. It can provide gradual detailed elaboration and “fine” tuning for the available production capacities (facilities and areas) calculated by the formulas:

$$P_{qj} = C_j \times F_{rj}; \quad P_s = V_a \times F_a \tag{1}$$

where C_j is the number of facility units of the j -th type; F_{rj} is a real annual period of equipment duty, hour; V_a is a manufacturing area of assembly divisions, m^2 ; F_a is a real annual period of assemblers’ work, hour.

Step 1. Based on the contracts effective during a year the iteration synthesizes an annual volume plan (OP_g) at the plant in general. The function of working out an original $OP_g \{OP_{gm}, OP_{ga}\}$:

$$F : K\{C, N\} \times \{T_{mN}\} \rightarrow OP_{gm}; K\{C, N\} \times \{T_{aN}\} \rightarrow OP_{ga} \tag{2}$$

where $K\{C, N\}$ are the contracts specified with terms (C) and listed products (N); $\{T_{mN}, T_{aN}\}$ are the data on a set of machine-tool and labour intensities of piece machining and assembly; OP_{gm}, OP_{ga} are annual volume data on machining and assembly. The essence of procedure at Step 1 is to compare the total labour intensity of machining (Q_m) and tool capacity (P_g); available (Q_s) and required (P_s) areas. If the Subjects made an agreed decision about contract corrections (ΔK) or the number of machine-tools (ΔC), the actions connected with the precise definition of the number of contracts, the recalculation of equipment capacities are performed.

Step 2. OP_{gm} is distributed among major technological processes, if there are any. The distribution is made due to the specialization on products and (or) types of work. With the specialization on types of work (blanking, machining, welding, etc.) the transfer function is of the form:

$$\varphi_1 : OP_{gm} \times \{\{B_{ij}\}\} \times \{C_i\} \rightarrow \{OP_{gmj}\} \tag{3}$$

where $\{\{B_{ij}\}\}$ is a set of types of work performed by the j -th TD; $\{OP_{gmj}\}$ are annual volume machining plans of the j -th TD; $\{C_i\}$ is the timing of the i -th types of work. With the specialization on products (types of pieces) the function is of the form:

$$\varphi_2 : OP_{gm} \times \{\{BP_m\}_k\} \times \{C_m\} \rightarrow \{OP_{gmk}\} \tag{4}$$

where $\{\{BP_m\}_k\}$ is a set of types of pieces manufactured by the k -th TD; OP_{gmk} are annual volume machining plans of the k -th TD on the m -th pieces; $\{C_m\}$ is the delivery date of the m -th pieces. If there is only one division, it complies with OP_{gm} . In formulas

(3) and (4) a set of parameters $\{C_i\}$ and $\{C_m\}$ is introduced in order to uniformly provide TD with work during a calendar year. Further, speaking about OP_{gmi} of the i -th TD, we will denote it as OP_{gti} without distinguishing how it is obtained. When a set $\{OP_{gti}\}$ is formed, the conditions determining the avoidance of distribution duplication must be provided. Then the plans are analyzed for each TD, the type of available metal cutting equipment being considered:

$$OP_{gt} \times \{T_i\} \rightarrow \{OP_{gti}\}, \quad (6)$$

where $\{T_j\}$ is a set of metal cutting equipment types (turning, milling, drilling, etc.); OP_{gti} is a TD annual plan by the j -th type of equipment (kind of machining works). The capacities of the j -th type of work are determined with an above mentioned formula, the quantitative equipment composition is determined according to the planned population of workers and standards of equipment service. Further, the equipment loading is determined for the organization in general, each TD, and a type of machine tools:

$$K_{zmi} = OP_{gm}/P_g; \{K_{zmi}\} = \{OP_{gti} / \sum (M_i \times F_{ri}); \{K_{zaj}\} = \{OP_{gti}/P_{gi}\},$$

where M_i is a number of piece of equipment by the i -th technological process.

At this step the senior management of organization may provide the information on changing the list of contracts being executed. Such correction is introduced in order to have the opportunity of changing the list of valid contracts after the initial distribution of volume of work among TD. In this case the procedure is carried out by formulas being similar to the ones mentioned above. The actions are aimed at achieving a balance in volume of work across the whole organization. At the second step the procedures can be repeated by the subjects of decision-making. The following steps are done when there is no possibility to achieve an agreed decision at this step.

Step 3. The type of work or (and) the type of products (workpieces) are tried to be changed (with the possibility to transfer them from one TD to another). The type of work covers types of machining operations for manufacturing specific pieces and their assemblies. The work schedule is specified by TD and then by types of machining operations. Several cycles can be executed at the third step. The main task is to provide the uniform equipment utilization within a specific TD.

Step 4. Parts of the work (as labor intensities) ΔOP_{gt} are transferred from one (the p -th TD) to the other (the q -th TD) covering the manufacturing of workpiece assemblies. Part of the work covers the types of machine-tool operations for the production of workpiece assemblies. The fourth step is useful if the discreteness of the plan change at step 3 does not lead to the desired results.

Step 5. The amount $\{\Delta OP_{gtj}\}$ of the machine work of j -type (for specific assemblies or (and) individual pieces) are transferred from one TD (p) to the other (q). Step 5 can cover several cycles with the consequent diminishing amount of the transferred work. The same can be referred to the previous 3 and 4 steps where the sets of

redistributed groups and types of machining operations can be gradually reduced to the machining of one assembly or a set of pieces, while the assembly operations – to the assembly of one workpiece. At the end of the five-step iteration the spatial structure of the volume plan for each TD will be formed.

2.3 Development Models of Control Actions

At the plan development stage, the significance of probable control actions comes down to the plan formation in accordance with capabilities of the enterprise and on the basis of analysis K_{zm} as well as the load factor of assembly areas K_{za} .

To set up a system one has to determine the allowed intervals Δ_{zi} and Δ_{za} of load deviations from the planned values K_{zm}^p and K_{za}^p . It is advisable to take them at the level of 0.8, with Δ_{zm} and Δ_{za} being equal to 0.1 (± 0.05).

Probable control actions are synthesized by using production models.

1. IF (K_{zm} differs from K_{zm}^p by more than Δ_{zm}) AND (contracts cannot be changed), THEN (it is necessary to correct the employee population ΔP) OR (to replace the equipment ΔM).
2. IF (K_{zm} differs from K_{zm}^p by more than Δ_{zm}) AND (contracts can be changed), THEN (it is necessary to change the list of contracts ΔK).
3. IF (K_{zm} differs from K_{zm}^p by more than Δ_{zm}) AND (it is impossible to change contracts in the required volumes), THEN (it is necessary to change the list of contracts ΔK) AND (to change the employee population ΔP or to replace the equipment ΔM).
4. IF (K_{zm} differs from K_{zm}^p by no more than Δ_{zm}), THEN (it is necessary to pass on to Step 2 of Stage 1, to the volume planning). The actions are identical at the 2nd–5th steps. At these steps the equipment loading is analyzed for every TD (K_{zmt}) and grouped by types ($K_{z oj}$). The allowed intervals for planned loadings are set for a technological division as a whole; the same is true of each type of machines.
5. IF (for the i -st/ i -th TD, K_{zmt} differs from K_{zmt}^p by no more than Δ_{zmt}), THEN (it is necessary to analyze the equipment loading for each type of machines inside the specific TD, see Rules 7 and 8).
6. IF (for the i -st/ i -th TD, K_{zmt} differs from K_{zmt}^p by more than Δ_{zmt}), THEN (it is necessary to reallocate the types of work ΔV OR workpieces ΔI between the TDs). The information is transferred to Step 3; the work is reallocated on the basis of value K_{zmt} .
7. IF (for the i -st/ i -th TD, K_{zmt} differs from K_{zmt}^p by no more than Δ_{zmt} , AND for all the j -th equipment groups $K_{z oj}$ differs from $K_{z oj}^p$ by no more than Δ_{zmt}) THEN (it is necessary to proceed to the scheduling stage).
8. IF (for some j -th equipment groups, $K_{z oj}$ differs from $K_{z oj}^p$ by more than $\Delta_{z mj}$), THEN (it is necessary to proceed to Step 5, that is, to reallocate the j -th machine work between the i -th TDs).

9. IF (after iterations L at Steps 1–3, the difference between actual and planned equipment load factors does not decrease by more than 10%), THEN (it is necessary to change the method of reallocation).

This means moving to the next step.

2.4 Decision-Making in Volume Planning

Probable control actions are estimated by a team of experts, i.e. representatives of an organization according to the following procedure.

It is necessary:

1. To assign weight to every expert, with weight assignment sum being 1, in view of a. the expert degree of responsibility for decision-making; b. the expert qualification in the solution domain.
2. To determine a lower tolerance limit of the expert confidence in the effectiveness of the control action (recommended experience-based value ≥ 0.7).
3. To determine the periodicity of adjustments (as soon as the recommendations are given by the automated technological process control system).
4. To discuss and assess the control action option (confidence in achieving the result by implementing a control action) numerically (from 0 to 1) by each expert.
5. To get a weighted estimate of the experts' general confidence in achieving the result by implementing a control action.
6. The person responsible for decision-making should take it (to translate a decision into practice or not).
7. Go to the next estimation point.

Special attention should be paid to the method of determining the weighted confidence of all experts. For this purpose, an intelligent database built on fuzzy sets was developed following on from the expert estimates [11]. It looks like this:

IF (confidence of expert 1 with weight P_1 is equal to A_1) AND IF (confidence of expert 2 with weight P_2 is equal to A_2), AND IF (confidence of expert n with weight P_n is equal to A_n), THEN (the weighted confidence of all experts results in A_i).

The linguistic variable A_i has 3 terms: insufficient, mean, sufficient [12] as it is shown in Fig. 1.

The linguistic variable B_i has 5 terms: quite unreliable, unreliable, doubtful, reliable, most reliable (see Fig. 2). The following fuzzy production rules determining the value of the linguistic variable B_i (experts' weighted confidence) are formed with the help of experts' estimates. Preliminarily, subconditions containing opposite values of linguistic variable A_i (sufficient \Leftrightarrow insufficient) are eliminated from the production rule. So, as a result there appear the production rules with adjacent values of linguistic variable A_i .

1. IF (all subconditions contain the *sufficient* value of linguistic variable A_i), THEN (the value of the linguistic variable B_i is *most reliable*).
2. IF (all subconditions contain the *insufficient* value of the linguistic variable B_i), THEN (the value of the linguistic variable B_i is *quite unreliable*).

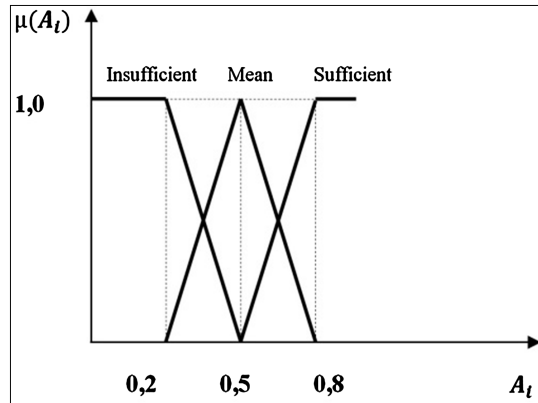


Fig. 1. The function of membership to linguistic variable A_i

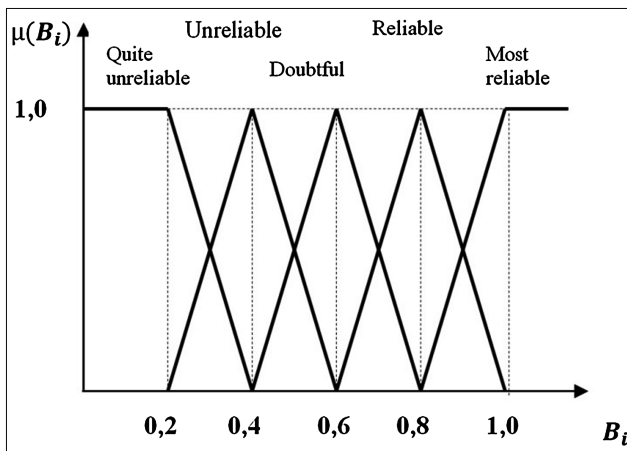


Fig. 2. The function of membership to linguistic variable B_i

3. IF (the number of subconditions with the *mean* value of the linguistic variable A_i exceeds the number of subconditions with the *sufficient or insufficient* value of the linguistic variable A_i) OR (the number of subconditions is by no more than one fewer the number of subconditions with the *sufficient or insufficient* value of the linguistic variable A_i), THEN (the linguistic variable B_i is *doubtful*).
4. IF (the number of subconditions with the *sufficient or insufficient* value of the linguistic variable A_i is by more than one higher the number of subconditions with the *mean* value of the linguistic variable A_i), THEN (the linguistic variable B_i is *reliable or unreliable*, respectively).

For example: IF (the confidence of expert 1 is *sufficient* AND the confidence of the expert 3 is *sufficient*, AND the confidence of expert 3 is *sufficient*, AND the confidence of expert 4 is *mean*), THEN (the value of the linguistic variable B_i is *reliable*).

The fuzzy-logic conjunction of subconditions is carried out according to the minimum rule. The function of joint membership is carried out according to the Mamdani fuzzy implication rule. Defuzzification of the weighted estimates of experts' confidence (the result) is carried out according to the centroid method.

3 Conclusions

The proposed method of synthesizing the volume plans of technological divisions provides the quite complete realization of their production capacities due to a multi-step iteration algorithm with a gradually decreasing step. The hybrid way of building the automated technological process control system, where probable control actions are generated by the automated system itself and their estimates and decision-making are carried out under the active participation of experts, has a number of advantages. The use of this method leads to realization of Ackoff participatory principle [13] in creating the automated technological process control system. Even more, it takes into account the experience of specialists and the production system subsets the connection of which with the controlling actions is largely difficult to formalize. The test approval of system models was a success at some machine-building enterprises of the Tver Region.

References

1. Burdo, G.B., Isayev, A.A.: Modeli tselevoy funktsii pri podgotovke mnogonomenklaturnogo proizvodstva. B: Trudy kongressa po intellektual'nym sistemam i iskusstvennomu intellektu, IS&IT 2014, pp. 345–351. Fizmatlit, Tom 1. Moskva (2014)
2. Burdo, G.B., Isayev, A.A.: Opredeleniye tselevoy funktsii pri tekhnologicheskoy podgotovke na osnove analiza situatsii v firme. B: Trudy 6-oi Vserossiyskoy nauchno-prakticheskoy konferentsii po nechetkim sistemam i myagkim vychisleni-yam (NSMV-2014), pp. 80–89. Politekhnik- servis, Tom 2. SPb (2014)
3. Burdo, G.B., Vinogradov, G.P., Isayev, A.A.: Soglasovannoye prinyatiye reshe-niy v proizvodstvennykh sistemakh izgotovleniya naukoymkikh izdeliy. B: Pro-grammnyye produkty i sistemy 2(110), 75–82 (2015)
4. Allan, J.J., et al.: A Survey of Commercial Turnkey CAD/CAM Systems, 2nd edn. Productivity International Inc., Dallas (1990)
5. Groover, M.P.: Automation, Production Systems and Computer-Aided Manufacturing. Co Prentice-Hall Inc., Englewood Cliffs (1985). Chap. 10
6. Amirouche, M.L.: Computer-Aided Design and Manufacturing. Co Prentice-Hall, Englewood Cliffs (1993)
7. Womack, J.P., Jones, D.T.: Lean Thinking, 2nd edn. Free Press, New York (2003)
8. Shingo, S.: Kaizen and the Art of Creative Thinking. Enna Product Corporation and PCS Inc., Bellingham (2007)
9. O'Leary, D.L.: Enterprise Resource Planning Systems. Cambridge University Press, New York (2000). 232 p.
10. Leon, A.: Enterprise Resource Planning, 2nd edn. McGraw-Hill, New Dehli (2008). 500 p.
11. Zadeh, L.: Fuzzy Sets. Inf. Control 8, 338–353 (1965)

12. Burdo, G.B., Palyukh, B.V., Semenov, N.A.: Podderzhka prinyatiya resheniy pri dispetchirovaniy tekhnologicheskikh protsessov v mashinostroyenii. B: Trudy pyatnadsatoy natsional'noy konferentsii po iskusstvennomu intellektu s mezh-dunarodnym uchastiyem. Rossiyskaya assotsiatsiya iskusstvennogo intellekta. Tom 1, pp. 231–238 (2016)
13. Ackoff, R.: Ackoff's Best: His Classic Writings on Management. Wiley, New York (2003). 356 p.

Algorithm for Building Recommendations for Intelligent Systems

S.B. Kartiev and V.M. Kureychick^(✉)

Institute of Computer Technologies and Information Security, Southern Federal
University, via Chekhova Street 2, 34722 Taganrog, Russia
mlarningsystems@gmail.com, kur@srfedu.ru

Abstract. At present, when developing intellectual systems, one of the most important questions is the construction of a formal description of the data domain. This allows to improve the quality of development. The ontological models are currently used for these purposes. The paper describes the development of a model of the recommendation system based on the ontological approach. When developing recommendatory systems, the usual methods of describing objects are applied, which leads to the impossibility of configuring the system being developed. The purpose of this study was to develop an ontological model for configurable recommender systems. An introduction is given to the topic of ontological modeling, sufficient for understanding the main material of the article. The formal ontology model is presented, the main ontology classes, ontology levels, ontology usage objectives are described. The main principle of modeling the domain object-oriented design is described. Next, the application of ontologies in the recommendation system is described. It describes the conceptual model of the system with UML. A model of the ontology of the data domain description for the development of the recommendatory system was developed. The principal difference of this model from existing models is its customization on the data domain. Using the developed model, it is possible to develop configurable advisory systems. A recommendatory system has been developed using the Python programming language to solve the problem of making recommendations using the developed ontological model of the domain model presentation. Studies were conducted on the effectiveness of modeling the subject area with regard to the compilation of requirements for the recommendation system.

Keywords: Recommended system · Ontological modeling · Semantic web

1 Introduction

In this paper, we propose a model for designing an recommender system (RS) based on ontologies. The main objective of determining the design of the RS models is a unification of basic objects and relations between them in the form of a graph RDF (Resource Description Framework), whose purpose is the formal description of the semantic web resources. The ontological approach itself allows us to describe the conceptual model in the form of a series of specifications based on the data domain of the system being developed. It also allows to determine the basic concepts of the

system, regardless of the current configuration. Ontologies are used to describe the data domain in the third-generation recommendation systems.

Recommendation systems are representatives of the class of decision-making systems that use knowledge about the interests and preferences of a person to assess and predict his response to recommendations. The human response is evaluated by the system using a certain metric, which is usually measured in the ordinal scale [1].

Recommendation systems are designed to predict the interests of users based on their preferences, which can be extracted from their history of interaction with the system. There are two main templates for building first-recommendation systems: collaborative filtering, content filtering.

- Collaborative filtration uses the information about Procedure the user had in the past.
- By content filtering is performed on the basis of the Mechanism of creation of users “profiles” that may be formed by means of answers in questionnaires or based on geographical regulations [2].

Recommendations can be divided into 3 levels of personalization

- Not personalized recommendations.
- Partially-personalized.
- Fully personalized.

The second generation was represented by RS, based on machine learning methods and taking into account the context. At the moment, 2-generation recommendatory systems are practically being implemented, but for researchers the problem of creation of the 3-generation recommendation systems is great interest now. These systems will have to take into account the context, including ontologies, including the semantic aspects of interest models and the construction of a user profile. Let us consider the basic methods of making recommendations.

2 The Main Algorithms for Developing Recommendations

Collaborative filtering is the main method of making recommendations. Its generalized operation algorithm is represented in the following form [3];

- View large groups of sampling units
- Finding or creating a group, corresponding to the interests
- Combining of preferences
- Creation of a ranked list of preferences

The models for implementing collaborative filtering are divided into groups:

- Filtering by the principle of the nearest neighbors.
- Filtering based on models.

The second method of making recommendations is the recommendation algorithm based on the data.

The third method is the algorithm for developing recommendations, based on the knowledge developed by the intellectual system.

Algorithms for machine learning are often used to implement the mechanism of recommendations. The main task of machine learning is the process of issuing a forecast or solution based on the training sample, mainly by maximizing the mathematical goal of how the algorithm should behave. There are different types of learning tasks - classification, regression analysis, clustering. Classification is a task whose purpose is to determine the belonging of an element to a particular category on the basis of marked copies of similar elements. Regression is the method of analysis. All algorithms of machine learning require to define a set of characteristic features that will be transmitted to the learning function for each element. Training should be done using a training sample, which contains the rules described by means of ontologies.

3 Ontological Principles of Modeling Systems

The term “ontology” can be interpreted as one of two meanings:

- Ontology is a philosophical discipline that studies the most common x Characteristics of being and entities.
- Ontology is a structure, describing the values of the system elements [4].

In engineering, in the IP construction process, ontology allows the subject domain. We will describe the term ontology (ONT) in the form of a formal model. The ONT model is described as follows:

$$\text{OHT} = \{C, R, T, D, A, F, A_x\}.$$

Where $C = \{C_1, \dots, C_n\}$ - is a finite set of classes that describe the main objects of the domain.

$R = \{R_1, \dots, R_n\}$ - a set of relations defined on classes.

$T = \{T_1, \dots, T_n\}$ - set of fundamental object data types.

D is the set of a subject area domains.

A is a finite set of attributes describing properties of classes C and relations R.

F is the set of constraints on the values of the attributes of classes and relations.

A_x - a set of axioms determining the semantics of relations ont [5].

In the theory of object-oriented design classes are descriptive units for creating objects with standardized behavior [6]. In ontologies, classes are also characterized as concepts. Concepts are the conceptualization of a class, the whole group of a certain entity or phenomenon, where each class describes a group of entities with an individual principle of behavior combined on the basis of the availability of common properties. The designation C is the representation of the complete collection of objects of the data domain (DD), the designation R is the relation, which indicates the existence of a connection between the objects.

The purpose of this article is to develop a model and ONT of the description of the PR for the advisory system. The principal difference of this model from existing models

is its customization on the subject area. This difference implies the configurability of the RC, that allows you to reconfigure RS easily with changing rules and objects.

The use of the ONT model in IS is assumed using three levels of ontology representations.

- Informal level is the level of users representations. On this level of ONT are presented in a form convenient for the user-expert in the subject area of the system being developed.
- Formal level is the level of representations ONT Programmers and level Inter-machine Exchange of ONT.
- Structural level - level representation ONT at view [7].

The goals of using ontologies in the process of designing RS are:

- The common use of the general comprehension of information structure by the data domain experts and programmers.
- The ability to re-use knowledge in a DD.
- Analysis of knowledge and separation of DD knowledge and operational knowledge and operational knowledge which are not displayed on ontological model.

Let us consider the basic ways of describing the domain model on the basis of ontologies.

4 Description of the Data Domain Model Using Ontologies for the Advisory System

Ontological knowledge model allows to describe the whole data domain in their own language (RDF) originally.

The ONT model is used in all limited contexts of the system being developed.

Figure 1 shows the effect of ontologies on a limited context, is objects and their connections are described in the form of ontologies.

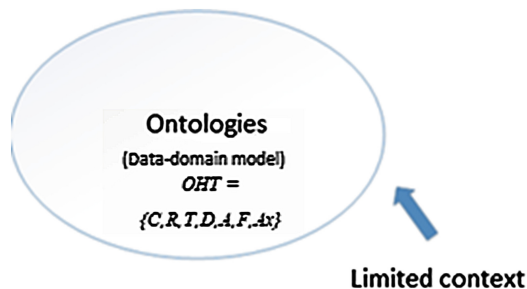


Fig. 1. Conditional description of the data domain model within a limited context

With the use of ONT, there is no need to describe the DD for each limited context. ONT can fully describe the subject domain of IS. This implies storing an ontological model in the core of the system or as a separate module, available to other modules. The domain-driven design (DDD) is used to form such a picture [8]. In the context of DDD, a DD model is formed, in the form of ontologies. In the future, this model can be used in any subsystems of the RS, if it does not have architectural features that interfere with the application of the general model of the domain. By introducing this model into the basis of the RS, it is possible to avoid the complexity of logic with a multitude of rules and conditions that describe the various uses and features of the system's behavior. The given decision provides the creation of a network of the interconnected objects. Each of them is a kind of meaningful entity, which can be both a large object

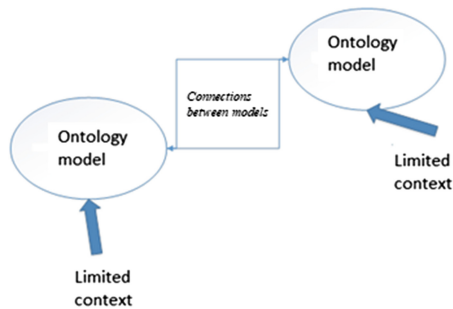


Fig. 2. Application of the ontological model to represent the data domain within two limited contexts

of the description of the data domain, and an entity that describes a single row of the table (Fig. 2).

5 Microservice Architecture and Its Integration with the Data Domain Model Based on Ontologies

The micro-service architecture is a lightweight implementation of service-oriented architecture (SOA). The basic idea of microservices is the partitioning of a system into a number of separate services that communicate with each other using messages [9].

What are the advantages of microservice architecture?

- Decomposition problem is solved: micro service usually contains small number of lines.
- All tasks are distributed: handy distribution of the tasks among services.
- Independence from development tools: for each service you can use the programming language which suits best for effective solution of the task.
- Fail-safety: Micro service usage brings horizontally scalable and fail-safe code.

When designing the RS using microservices the construction controllers and views can be automated with the use of metamodels. The meta-model should contain information about the supported functions and data required to form views. Metadata can determine the functional of the RS in individual subsystems [11].

There are two approaches to the functioning of MS:

- Generation of the IS logic is based on the ONT.
- IP operates on the basis of interpretation of the ONT models of data domain.

The first approach allows to improve the system performance due to the absence of logical output operations during system operation. All logical conclusion is made at the stage of RS assembly. The second approach mean that the system will require more resources by producing a process of logical inference, which can be facilitated using the caching procedure of previous results. In the case of the second approach, the system can dynamically change the data domain model without reassembling the RS [12]. Consider the software implementation of the developed RS.

The data access service of the database allows you to configure the RS using different ontological models to configure the RS for a specific subject area. To implement advisory systems, it is necessary to describe the subject area with sufficient accuracy. To describe the subject area, we will use the authors developed ontological approach to the modeling of the domain (Fig. 3).

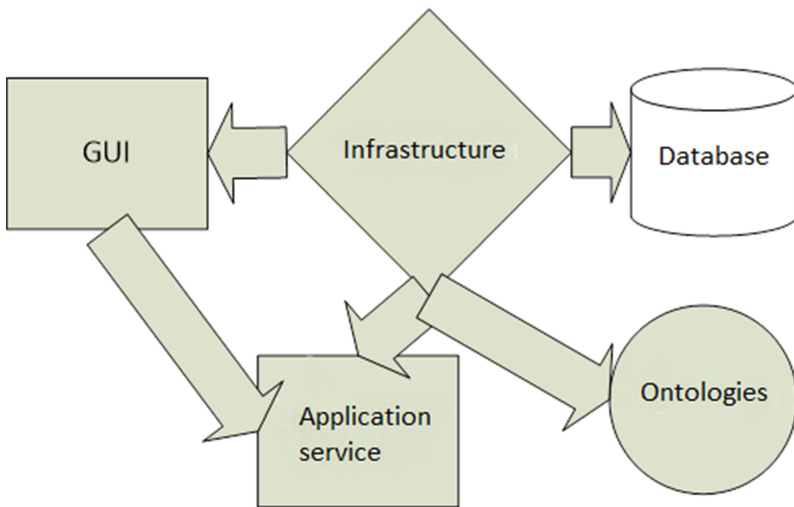


Fig. 3. An example of the architecture of a RS based on ontologies.

6 Program Implementation of the Recommendation System

This RS is developed using the Python programming language and the Django web development technology.

The RS web interface is built on the principles of the request-response. As a document-oriented database MongoDB was selected. The main advantages of this database are to support the transaction, the full-text search using Apache Lucense, completely safe data management and ease of use [13].

For example, we describe the basic model of the main data domain.

```
Public Class Card
{
    Public int CardId {get; set; }
    Public string Name {get; set; }
    Public DateTime DueDate {get; set; }
    Public DateTime CreatedAt {get; set; }
    Public string Description {get; set; }
    Public List CurrentList {get; set; }
    Public List <User> Members {get; set; }
    Public List <string> Comments {get; set; }
```

Where Name is a property describing the name of the card, DueDate is the date of expiry of the card, Description is the description of the map. This model describes the main fields related to the model of the map, which is a task. This model allows the user to manipulate data which will influence model with use of the controller by means of representation. As a target, we will set the problem of forecasting the state of a complex technical system. Solving the problem of making recommendations for decision making will allow us to recognize the state of a complex technical system, relying on the RS and using the ontological model as the basis for knowledge of the system analysis conditions. When solving the task of making recommendations, the subject area affects the decision-making process. For example, the forecasting of technogenic processes [15] requires careful elaboration of the data domain, and the system should be developed with the participation of a working group of experts [16].

7 Conclusion

The research on the ontology application in simulation of data domain for the RS development has been made in this paper. The bases of ontological modeling, connection with the data domain model are described. An example of the construction of the PC architecture using design pattern Model-View-Controller was given. The influence of data domain models on the decision-making process in the context of the forecasting problem is described. The effectiveness of the application of the ontological approach to the modeling of the data domain is shown.

The study was partially carried out at the expense of the RFBR grant (project No. 15-07-05523) at the Southern Federal University) and the Ministry of Education and Science of the Russian Federation “Organization of Scientific Research” code 2.5537. 2017/VU at the Southern Federal University.

References

1. Gorodetsky, O.N.T.: Ontology and personification of the user profile in the recommended third generation systems. *J. Ontol. Des.* **3**, 7–31 (2014)
2. Korolev, D.E., Filippov, M.V.: Analysis of collaborative learning algorithms recommendatory systems. *Eng. J. Sci. Innovation* **6** (2013)
3. Seguran, T.: *Programmable collective mind. M: symbol - Plus* (2008)
4. Regents, A.M.: *Meta-level Informational Ensuring the CAD: From Theory to Practice*, 176 p. Ulstu, Ulyanovsk (2015)
5. Ciorascu, C., Ciorascu, I.: Ontological support for information retrieval systems. In: *Proceedings of 26th Annual International ACM SIGIR Conference, Workshop on Semantic Web, Toronto, Canada* (2003)
6. Lapshin, V.A.: *Ontologies at Computer Systems. Science of World, Moscow* (2010)
7. Butch, G.: *Object-Oriented Analysis and Design from Examples of Applications for C++*, 2nd edn., 560 p. Nevsky Dialect, St. Petersburg (2001). Transl. from Eng. M. - Publisher Bean
8. Esposito, D., Saltarello, A.: *The Microsoft .NET Architecture of Enterprise Applications*, 362 p. (2015). Williams, M.
9. Muromtsev, D.I.: *Ontological Engineering Knowledge at System. SPb SU ITMO, St. Petersburg* (2007)
10. Evans, E.: *Domain-Driven Design (DDD). Structuring of Complex Programs*, 448 p. (2010). Williams, M.
11. Fowler, M., Sadaladzh, G.P.: *NoSQL Distilled*, 192 p. (2012). The ISBN 978-5-8459-1829-1, Williams, M.
12. Meijer, H.J.M.: *The model key to the object of value-mapping the model the data - US patent the App. 12/938.168. The Google Patents* (2010)
13. Fowler, M.: *Patterns of Enterprise Application Architecture (Addison-Wesley Signature Series)*, 544 p. Addison-Wesley, Boston (2003)
14. Fielding, R., Taylor, R.: *Principled design of the modern web architecture. ACM Trans. Inter. Technol.* **2**, 115–150 (2002)
15. Shapkin, P.A.: Using ontologies at development of web - applications, custom on substantive area. *Inf. Technol. Comput. Syst.* **2**(C), 44–50 (2009)
16. DeCandia, G., Hastorun, D., Jampani, M., Kakulapati, G., Lakshman, A., Pilchin, A., Sivasubramanian, S., Vosshall, P., Vogels, W.: *Dynamo is: Amazon's highly available market of value-the key store. In: The ACM Symposium on 21st The Operating Systems' Principles. Stevenson, The WA* (2007)
17. Kartiev, S.B., Kureichik, V.M., Martynov, A.V.: *A parallel algorithm for prediction of short time series. In: Proceedings of the Congress by intelligent systems and Information technology. The IS & of IT 2015. Scientific publication in the 4x volumes, FIZMATLIT the M, pp. 27–47c* (2015)
18. Kartiev, S.B., Kureichik, V.M., Pisarenko, I.: *Prediction of time series for analysis of technological processes. In: Actual Problems Hydrolithosphere, pp. 323–331c* (2015)
19. Kureichik, V.M.: *Information processing based on ontologies. In: Proceedings of the Congress by Intelligent Systems and Information Technology, the IS & of IT 2015. Scientific publication in the 4x volumes, FIZMATLIT the M, pp. 63–75c* (2015)
20. Kartiev, S.B., Kureichik, V.M.: *Classification algorithm, based on the principles of random forests for solving the problem of forecasting. Softw. Prod. Syst.* **2016**(g2), 11–15c (2016)

Reconfigurable Distributed Information and Control System Multiagent Management Approach

E. Melnik¹, A. Klimenko^{2(✉)}, and V. Korobkin³

¹ Southern Scientific Centre of the Russian Academy of Sciences,
Rostov-on-Don, Russia

² SFedU Acad. Kalyaev Scientific Research Institute of Multiprocessor
Computer Systems, Taganrog, Russia
anna_klimenko@mail.ru

³ Scientific-Research Institute of Multiprocessor Computing
and Control Systems, Taganrog, Russia

Abstract. The paper is devoted to the fully distributed reconfigurable information and control system management implemented by multiagent concept. The key issues of ICS management related to the system reliability and fault-tolerance are outlined. The new configuration forming problem is presented, and the new problem-oriented solving approach is given. The reconfigurable distributed information and control system multiagent management approach is a complex one: it is based on robust distributed algorithms and the new approach of the configuration forming. The simulation results are given and discussed briefly.

Keywords: Multiagent system · Information and control system · Reconfigurable industrial control systems · Multicriteria search · Simulated annealing

1 Introduction

Information and control systems (ICSs) are the basis of wide range of mechatronic complexes nowadays. Some of ICSs perform in the lack of time conditions (aircraft, for instance), some of them are the part of autonomous objects, which operates for a long time periods without any maintenance, and, of course, there is a plenty of large and complex objects, which are failure-critical due to the possible casualties and environmental disasters. So, the ICS dependability is the extremely important issue of the contemporary science [1–4].

As it was shown in [5–7], the ICSs with performance redundancy and fully decentralized dispatching, implemented by software agents, might have the acceptable levels of reliability and fault-tolerance. The reconfiguration procedure assumes that in case of computational unit (CU) failure monitoring and control tasks (MCTs) are relocated to the operational CUs, taking into consideration system constraints.

Systems mentioned above are in the scope of the current paper.

In some cases, when, for example, the set of CUs is not large, each state of the system with possible failures can be described by the set of configurations (MCT distribution among the CUs), and the reconfiguration proceeds with the new configuration choice. Sometimes it is impossible to describe all states of the system, so, the new configuration should be formed through the reconfiguration itself in “on-line” mode.

The configuration forming problem is described in details in [7, 8]. It is multicriteria, multiconstraint and, in the reason of resource allocation problem as a component, has too complex solution space to make its analytical research. At the same time, configurations effect onto the system dependability [9], so their qualities must be as good as possible.

Hence, we can outline at least two key issues of the reconfigurable ICS management:

- configurations must be formed as fast as possible and be of acceptable quality;
- the management system of ICS must be implemented on basis of cooperation and coordination principles taking into account the need to use techniques of distributed computing.

Within this paper the new reconfigurable distributed ICS multiagent management approach is presented. The approach is complex, it includes the set of different approaches and algorithms, and is directed to the solution of two issues outlined above.

The main idea is to involve the software agents to the configuration forming through the simplification of the criterion set and cooperative solution search. Sections of this paper contain:

- the new generalized model of configuration forming problem;
- the new approach to improve the configuration quality, we called it the “criterion delegating” approach;
- the generalized algorithms of multiagent management of ICS with fully decentralized dispatching;
- the results of simulation of the “criterion delegating” approach;
- the simulation results of the hybrid search technique;
- the brief discussion of the results and future work.

2 The Model of Configuration Forming Problem

Previous works [7, 8] contain the configuration forming problem in details, but the formal model seems to be a little bit cluttered. So, to make the problem model more clear and comprehensive, the new generalized and simplified formalization of the configuration forming problem was made.

There are N MCTs with computational complexities g_i , M CUs with equal performance m_j , $U = \{u_{ij}\}$ – the percentage of j CU performance allocated for the i MCT, T – planned completion time for the N MCTs, $F = \{f_k\}$, $k \in \{1, \dots, M\}$, – the set of simultaneously failed CUs.

Through the resource allocation every MCT links to the CU, and it can be described by the following tuple:

$a_i = \langle j, u_{ij}, t_i \rangle$, where j – the CU identifier, u_{ij} – the allocated resource ratio, t_i – the time of MCT i start.

So, the set $A = \{a_i\}$ determines the configuration of ICS before failure, the set $A' = \{a'_i\}$ determines the configuration of ICS after the reconfiguration. In fact, A' is the solution of configuration forming problem, and a'_i – the tuples which describe the new MCT assignments.

The objective functions are the following.

Firstly, the number of MCTs relocated from the operational nodes must be minimized. In other words, if there is a solution where the MCT's new assignment propose the relocation of tasks from the operational node, we should choose the solution, where there is no relocation at all. This objective function can be described with the expressions given below.

Let's determine the subtraction operator for sets A and A' so that:

$$a_i - a'_i = \begin{cases} 0, & \text{if } j \text{ is equal to } j'; \\ 1, & \text{otherwise.} \end{cases} \quad (1)$$

Then

$$F_1 = \sum_{i=1}^N (a_i - a'_i) \rightarrow \text{MIN} \quad (2)$$

The optimal location in the search space of this objective function means that only MCTs from the faulted node are launched on other nodes.

The second objective function is the minimization of the eliminated MCTs. On practice some MCTs are critical and must be saved during the reconfiguration, and some MCTs are non-critical. But from the system survivability point of view it is extremely preferable to save as much MCTs as possible. So,

$$F_2 = |A| - |A'| \rightarrow \text{MIN} \quad (3)$$

And, finally, the dispersion of CU loadings must be minimized:

$$F_3 = \sum_{k=1}^K u'_{kj} - \sum_{l=1}^L u'_{lq} \rightarrow \text{MIN}, \quad \forall j, q \quad (4)$$

where K is the number of MCTs assigned to the CU j , L is the number of MCTs assigned to the CU q .

The main constraint is that all MCTs must be accomplished within the planned completion time T :

$$t'_i + \frac{g_i}{u'_{ij} \cdot m_j} \leq T, \forall i, j. \quad (5)$$

Also the failed CUs must be taken into consideration:

$$M' = M - F, \quad (6)$$

where M' , M and F are the sets of CUs.

And, lastly, the bordering conditions are: all variable values are positive, $u_{ij} < 1$, $u'_{ij} < 1$, $\forall i, j$. So, the vector objective function contains objective functions (2–4), with constrains (5, 6).

At the first glance the problem is similar to the k -partition problem, which has a suitable solving method [10], but vector objective function makes the problem np -hard with complex and non-trivial search space. Also it must be mentioned that with the increasing of objective function number the quality of solution degrades, in general.

As the preferable attribute of the system is the load balancing [9], the goal of the configuration forming is to get solutions with as good load balancing as possible. At the same time the other objective functions must be taken into consideration.

Also it must be mentioned that Service Oriented Architecture (SOA) concept is used in contemporary ICSs too. Services can be relocated, hence for the SOA-based ICSs there is no need to keep the MCT relocation criterion, but some preparation of the relocation is needed.

3 Criterion Delegating Approach

There are at least three well-known ways to solve the multicriteria problem.

- To transfer the vector objective function to the scalar form with appropriate weight ratios for each vector component, as it was done in [8];
- To choose one criterion for the solution, while the others become the constraints, as it was done in [5];
- To solve the multicriteria problem through the Pareto front search (or, at least, through the search of single solution which belongs to Pareto front).

The approach of “criterion delegating” is based on two assumptions in the context of ICSs:

1. We can involve the software agents to the MCT context data exchange, storage and delivering to the MCTs which are activated by the reconfiguration;
2. If we “delegate” the semantic of the task relocation, the solutions become better from the load balancing point of view.

Based on assumptions listed above, the configuration forming problem can be solved without the objective function (4).

To approve the practicability of such configuration forming approach some simulations were made. We solved the configuration forming problem in two ways: like a three criteria optimization problem and like a two criteria one. The quality of the results was evaluated from the load-balancing point of view. The optimization problems were solved with the “quenching” technique of simulated annealing [11–13], which allows to solve optimization problems fast enough [11], but gives the local optimums as results. For the simulation a random set of 25 MCTs with computational complexity 10–40 conventional units were generated. MCTs were assigned to the 10 CUs with equal performance. The cases of failures are combinations of one random failure and two random failures simultaneously.

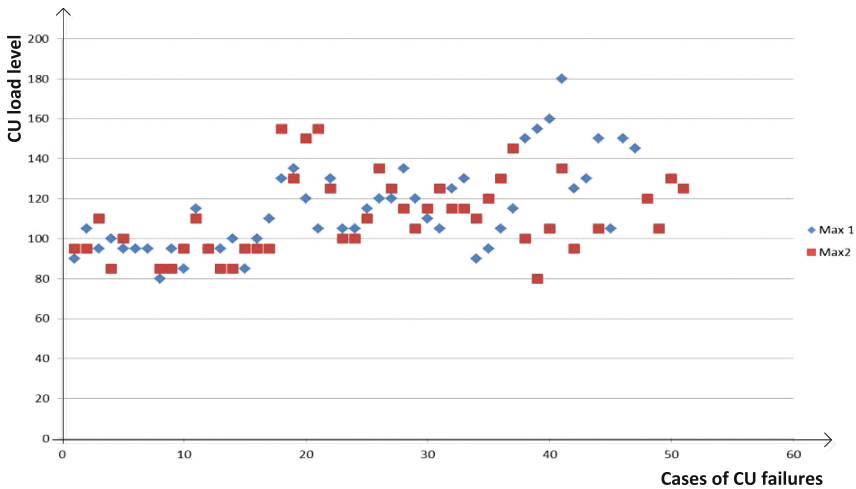


Fig. 1. Maximum CU loadings. The x-axis contains variants of CU failures, y-axis contains the loading values. Max 1 – solutions with objective functions (2, 3, 4). Max 2 – solutions with objective functions (3, 4).

It is seen on Fig. 1 that the elimination of the MCT relocation criterion can produce solutions, which are better then solutions of three-criteria configuration forming problem. Also it is seen that in some cases solutions are rather worth – the consequence of fast SA temperature decreasing and limited iterations number.

So, we can state that it is expediently to eliminate the MCT relocation criterion from the set of objective functions, delegating the operations with the MCT context data to the software agents. As the ICS contains more than one agent, the configuration

forming problem used to solve in cooperative manner [8] with simulated annealing parallelization, and the results were rather prospective.

Considering that criterion delegating approach can improve the results significantly, but, in the reason of stochastic search particularities the result a little bit stochastic too, it is prospective to solve the configuration forming problem in two ways: with MCT relocation criteria and without one. Depending on the particularities of the ICS operational conditions (lack of time, for instance), searches can be made simultaneously or consequently.

4 ICS Multiagent Management Algorithms

When the system with fully-distributed dispatching is implemented as a multiagent system (MAS), each computational node is represented by its own agent, which has a determined functionality including the reconfiguration procedure, regular mode operations and system startup operations.

The main functions of the computational node agent (CNA), taking into account the need to deliver the MCT context data, are:

- to maintain the local CNA knowledge of the system integrity and operability;
- to deliver the periodically data replicas between the agents.
- to implement the reconfiguration procedure and other modes, when it is needed.

The first function – the maintaining of system integrity and operability is achieved by informational messages (IM) exchange between CNAs. The mandatory field of the message data structure is the identifier of CNA, which sends the IM. IMs are sent within chosen time periods, and if one CNA does not receive it, this CNA must initialize the reconfiguration procedure. Taking into account that the dispatching is fully distributed, the reconfiguration procedure must be distributed too.

As we assume that the configuration forming is the online problem, so we don't know where the MCT can be relocated to. This condition has an impressive impact onto the system in general: every CU must keep all MCTs in memory without the resource allocation. Besides this, context data of MCTs will be broadcast to all agents. This is the additional load onto the communication environment, but, if the periods of broadcasting are fixed and not too short, this drawback is neutralized by the dependability and fault-tolerance improvement.

The agent-based reconfiguration includes two major steps:

1. a check of the need of reconfiguration;
2. reconfiguration itself.

The step 1 is needed to check the adequacy of the CNA system local representation to the real system state. For instance, one CNA can loose an IM due to its own fault and initialize a reconfiguration procedure declaring the operable CNA faulted. At the same time other agents handle the IM and suppose that there is no need to reconfigure the system.

The checking of the need of reconfiguration is implemented on the base of polling algorithm [12] with the assumption of the full interconnection between CNAs. The centralized scheme of the polling algorithm is suited for the check because the initiator is the CNA which has not received the IM.

The steps of the generalized algorithm begin at the moment, when the IM from CNA_k has not been received. We assume, that there is a possibility to organize message queues for each computational process which operates as FIFO queue. Also we suppose the local state of the CNA “truthful” if more then $2/3$ of the agents have the same state [12].

1. Begin
2. Int f:=0;
3. If (not_received(CNA_k)) f:= id (CNA_k); *//the message from CNA_k has not been received;*
4. for all neighbours do send f; *//send its number to N-1 neighbours, or 0 if there are no failures;*
5. receive (in_queue); *//check the incoming answers*
6. if number_of_values (f in in_queue) $>2*$ in_queue_size/3 *//if more then 2/3 of CNAs suppose the CNA_k faulted, the reconfiguration is needed*
7. for all neighbours do send reconfig_sign; *//the initialization of reconfiguration*
8. else (stop generate informational messages); *//the agent suppose faulted itself*
9. end.

Described algorithm supposes that in case of normal functioning of the system after the IM the 0-message will be sent. If more than $2/3$ CNAs did not received the message from CNA_k , it means that the CNA is not operable. In this case there are various ways to solve the problem: for example, the agent can begin not to send its own IMs.

The next algorithm describes the distributed reconfiguration procedure.

As the communication network is a clique, the polling algorithm and algorithm based on election problem are usable as a basis too. Moreover, the election problem algorithm is used to choose a leader, which distribute the information between agents, if the configuration forming problem must solved as two- or three-criteria problem.

1. Begin.
2. Leader_id = id; // the agent suppose itself to be the leader
3. For all neighbours do send id;
4. Receive (in_queue); //here all neighbor ids
5. If someone_in_queue>id Leader_id=someone_in_queue;//if the other operational agent has id bigger than current agent
6. If (Leader_id==id)//still leader
7. For all neighbours do {send (random_search_method_choice);} // the leader assign the search method types to the neighbours
8. Own_search_method=random_search_method_choice;//choose its own search method
9. Do get_result = SA_search (own_search_method); //new configuration search according to the method chosen
10. If in_result!=NULL // if someone found the solution earlier and sent its result to the neighbors
11. { Stop_search;
12. Send_neighbours (get_result);
13. If (in_result>get_result) // '>' means 'better'
14. {get_result:=in_result; leader_id:=in_leader_id}} //choose the best solution and the leader
15. If (get_result!=NULL and leader_id==id) do {send_neighbours (result, leader_id);} //stop search when the solution is found and send it to other agents. The agent solved the CSP faster then others.
16. New_config:=get_result;
17. End.

Another way for agents to decide which search method to use is when each agent has a pre-defined search method_id according to its own identificator. This makes the reconfiguration procedure simplified, transferring the algorithm described above to the following:

1. Begin.
2. Leader_id = id; // the agent suppose itself to be the leader
3. Own_search_method=predefined_search_method;//choose its own search method
4. Do get_result = SA_search (own_search_method); //new configuration search according to the method chosen
5. If in_result!=NULL // if someone found the solution earlier and sent its result to the neighbors
6. {
7. Stop_search;
8. Send_neighbours (get_result);
9. If (in_result>get_result) // '>' means 'better'
10. {get_result:=in_result; leader_id:=in_leader_id}} //choose the best solution and the leader
11. If (get_result!=NULL and leader_id==id) do {send_neighbours (result, leader_id);}} //stop search when the solution is found and send it to other agents. The agent solved the CSP faster then others.
12. New_config:=get_result;
13. End.

We assume, that at the beginning of reconfiguration procedure each agent has the following knowledge:

- its own identifier, id;
- a set of operational neighbour's identifiers.

First, if the reconfiguration is initialized, the group of agents must choose the leader, which distribute the method of configuration forming among the neighbours. Here the method of configuration forming can be three- or two-criteria configuration forming problem. After the leader is chosen, and the configuration forming methods are assigned to the other agents, the SA parallel asynchronous search procedure [13–15] is initialized.

If an agent finds the acceptable solution, it broadcasts it, and this means the end of parallel computations. Using the election problem algorithm, we choose the best configuration. It must be mentioned, that with assumption of no initial configurations, the initialization mode of the ICS is equal to reconfiguration procedure.

Through the regular mode the functionality of agents include the IM broadcasting and the context data replicas delivery.

5 Simulation Results

As an experiment, we simulated the configurations with only three-criterion search and with hybrid parallel search strategy. The computations were made for 10 CNAs and fully interconnected communication environment. The configuration qualities are

evaluated from the maximum load spikes point of view: as the spikes are higher the load balancing is worth and visa versa. The computational complexities of the MCTs were the same as in the simulation of Sect. 2.

It is seen on Fig. 2 that a hybrid search allows to get more qualitative solutions of the multicriteria problem from the load balancing point of view in the conditions of

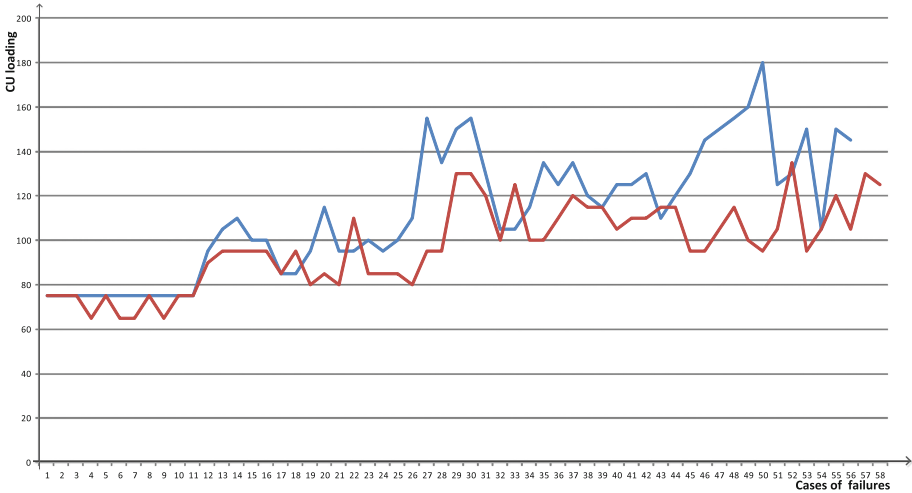


Fig. 2. Maximum loadings of the configurations formed. The first trend shows the results of the parallel SA search with three criteria only. The second trend shows the results of parallel SA search with using “criterion delegating” approach and three criteria objective function in a parallel manner.

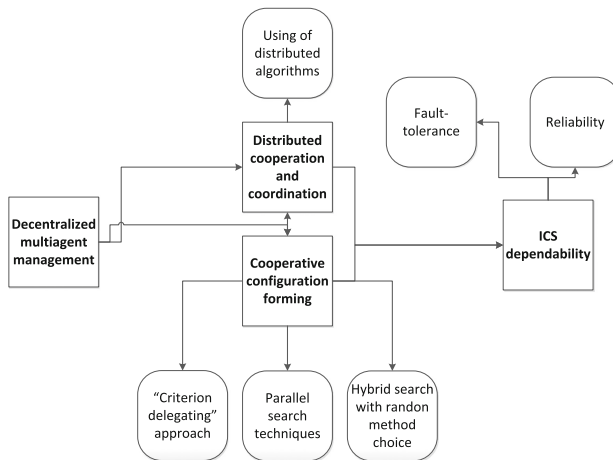


Fig. 3. The schematic representation of the reconfigurable distributed ICS multiagent management approach.

equal iteration number. As the load balancing reduces the failure rate, such approach of multiagent configuration forming is rather prospective.

6 Conclusions and Future Work

Resuming, we suppose that it is rather useful to bring together all proposals, described above, into the schematic representation of reconfigurable distributed ICS multiagent management approach.

As it is shown on the Fig. 3, the management methods have an effect on the ICS dependability issues. At least, they are reliability and fault-tolerance (other dependability attributes and means are out of the scope of this paper). The represented multiagent management approach contains two main blocks: configuration forming block and block of distributed cooperation and coordination based on the reliable and robust distributed algorithms. Blocks of “distributed cooperation and coordination” and “cooperative configuration forming” are connected closely: configuration forming procedures are initialized through the cooperation and coordination of agents, and, at the same time, “criterion delegating” approach using makes the agents responsible for the data replication.

The block “Cooperative configuration forming” includes the set of approaches and techniques, described above. The key idea of “criterion delegating” approach is that we can improve the qualities of configurations assuming that semantic of MCT relocation criterion is delegated to the agents. Simulation results show that the results do become better from the CU loading point of view, but, due to the stochastic nature of SA and limited iteration number it is useful to search in parallel with two different types of complex objective functions and to choose the best solutions. The last proposal is visualized as “Hybrid search with random method choice” block. Simulation results on Fig. 2 show that there is a quality improvement up to 60%. Such results allow us to assume that the complex approach represented is rather prospective.

As to future work directions, first of all it is useful to evaluate and compare the quality of configurations, which are got by approaches of transferring a multiobjective function to the function of one criterion. The second promising direction is to estimate the communicational overheads of the fully online configuration forming and, possibly, evaluate some constraints for hardware and software for fruitful and successful using of “delegating” approach.

Acknowledgement. The reported study was funded by SSC RAS projects 0256-2014-0008, 0256-2015-0082 within the task 007-01114-16 PR and by RFBR project 16-58-00191-Bel-a.

References

1. Laprie, J.C.: Dependable computing and fault tolerance: concepts and terminology. In: Digest of FTCS-15, pp. 2–11, June 1985
2. Laprie, J.C. (ed.): Dependability: Basic Concepts and Terminology. Springer, Heidelberg (1992)

3. Pham, H.: System Software Reliability. Springer Series in Reliability Engineering, p. 440. Springer, London (2006)
4. Zhang, Y., Jiang, J.: Bibliographical review on reconfigurable fault-tolerant control systems. *Annu. Rev. Control* **32**(2), 229–252 (2008)
5. Melnik, E.V., Klimenko, A.B.: Informational and control system configuration generation problem with load-balancing optimization. In: Proceedings of 10th International Conference on Application of Information and Communication Technologies, pp. 492–496 (2016)
6. Melnik, E.V., Klimenko, A.B., Korovin, I.S.: A novel approach to fault tolerant information and control system design. In: Proceedings of 5-th International Conference on Informatics, Electronics and Visualization. University of Dhaka, Dhaka, Bangladesh (2016)
7. Korovin, I., Melnik, E., Klimenko, A.: A recovery method for the robotic decentralized control system with performance redundancy. *Lecture Notes in Computer Science (Including Subseries Lecture Notes in Artificial Intelligence and Lecture Notes in Bioinformatics)*, vol. 9812, pp. 9–17 (2016)
8. Melnik, E., Korobkin, V., Klimenko, A.: System reconfiguration using multiagent cooperative principles. In: Proceedings of the First International Scientific Conference “Intelligent Information Technologies for Industry” (IITI 2016), Series “Advances in Intelligent Systems and Computing”, vol. 451, pp. 385–394 (2016)
9. Melnik, E.V., Gorelova, G.V.: Effect processor computational load balancing devices in highly distributed information management system. *Mechatronics, Automation, Control*, pp. 29–35 (2012)
10. Korf, R.E.: Multi-way number partitioning. In: International Joint Conference on Artificial Intelligence, pp 538–543 (2009)
11. Melnik, E., Klimenko, A., Klimenko, V.: The parallel simulated annealing-based reconfiguration algorithm for the real time distributed control fault-tolerance providing. In: Proceedings of the Application of Information and Communication Technologies, pp. 277–280 (2015)
12. Tel, G.: Introduction to Distributed Algorithms. Cambridge University Press, New York (2000)
13. Ingber, L.: Simulated Annealing: Practice Versus Theory (1993). <http://citeseer.uark.edu/8080/citeseerx/viewdoc/summary?doi=10.1.1.15.1046>
14. Azencott, R. (ed.): Simulated Annealing: Parallelization Techniques, pp. 47–79. Wiley, New York (1992)
15. Crainic, T.G., Toulouse, M.: Parallel Metaheuristics. In: Fleet Management and Logistics, pp. 205–251 (1998)

Intelligent System for Technological Adjustment of the Harvesting Machines Parameters

Lyudmila Borisova^(✉), Valery Dimitrov, and Inna Nurutdinova

Don State Technical University, Rostov-on-Don, Russian Federation
borisovalv09@mail.ru, kaf-qm@donstu.ru, nurut.inna@yandex.ru

Abstract. Some aspects of creating intelligent information system of decision-making support for the problems of technological adjustment of the grain combine harvester tools under field conditions have been considered. The system is intended for retrieving initial values of the harvesting machine adjustable parameters and eliminating troubles with technological process of harvesting, i.e. updating of technological adjustments. The information system architecture includes standard blocks of the expert system and also original subsystems. We present the generalized interrelation diagram of the subsystems: “design”, “setup” and “adjustments updating”. On the basis of linguistic approach a formal-logical scheme of the decision-making process on the account of the analysis of fuzzy expert information has been presented. The algorithm of solving the problem of the harvesting machine preliminary setup has been considered. We suggest the generalized model in the form of composition of fuzzy relations of the considered semantic spaces of environmental factors, adjustable factors and performance indices as a model of knowledge representation of the object domain. Application of the suggested information system makes it possible to reduce information load of an operator and also reduce the time for performing adjustment and, as a consequence, increase the harvesting machine output per shift.

Keywords: Intelligent information system · Grain combine harvester · Technological adjustment · Knowledge representation models · Membership function · Linguistic variable

1 Introduction

When using complex harvesting machinery one of the important problems is technological adjustment of the machine under field conditions. This problem refers to the class of non-formalized problems of decision-making, and its solution is imposed on the operator and depends upon his experience and qualification. The outcome and effectiveness of harvesting directly depend on optimal solution to the problem of technological process control of combine harvesting. Working-out and implementation of new, intellectual-type machines is a prevailing component of the strategy of agricultural engineering development in our country [1]. Grain combine harvester is the main machine used for harvesting many grain crops. In the present paper, we considered the problems of grain combine technological adjustment that doesn't limit the generality of

the suggested approach to the problem of adjustment of any harvesting agricultural machinery.

At present, grain combine harvesters incorporate automation equipment for monitoring and control and they are also integrated into an automated system of “precision agriculture”. Modern combine harvesters (ACROS 530 ... ACROS 595 plus) are equipped with automatic control system. It is permanently modernized, e.g. it uses “Multipurpose terminal module (RSM MTM-02)”. At an undoubted effectiveness of application of automatic systems of control and management in grain combine harvester devices and systems we should notice that the available automatic systems mainly solve the problems of the harvester movement control and doesn't provide the operator with decision support when carrying out technological adjustment of the combine harvester tools. For the purpose of solving the problems of setting up and adjustments updating we have identified the drawbacks of the mentioned automatic system: incomplete description of possible troubles of the technological process; presetting intervals of values change of the adjustable parameters; uncertainty (fuzziness) of initial data; lack of real recommendations on updating etc.

Difficulties of values selection of the harvester adjustable parameters are connected with the ambiguity of information on the external environment factors where a grain combine harvester operate and also with complexity of interrelations among harvesting factors, adjustable parameters and performance indices. Grain losses and rather low output per shift of the combine harvester are often stipulated by wasteful expenditures connected with the necessity of technological adjustment of the harvester tools. It is rather difficult under field conditions to assess certain values of external factors influencing the technological process, and find out their change in due time [2]. It is also complicated to determine point values of the harvester performance indices. And variability of values of the environment factors stipulates expediency of carrying out values updating of the harvester technological parameters under field conditions.

The major part of information, taken into account when making decision on the parameters of technological adjustment, has qualitative or evaluation nature and can be regarded as fuzzy expert information. This stipulates reference to fuzzy simulation, its methodology aims at knowledge fuzziness and also an expert way of providing solution. A promising trend in solving such non-formalized problems of decision-making is the development of intelligent information systems (IIS) of decision support on the basis of fuzzy control [3, 4]. At present, similar systems are used in agricultural industry. They are mainly connected with the analysis of image, weather conditions, processing or sorting agricultural products and also used to determine crop yield, weeds identification, combine harvester positioning in the field, control of its motion etc. [5–12]. We also consider the problems of automatic selection of some parameters of combine harvester operation in terms of performance indices using production rules [13, 14].

2 Problem Solution

2.1 Materials and Method

IIS is necessary for the combine harvester technological adjustment under the conditions of permanently changing external factors. It implements the following functions: description of the grain combine harvester design; preliminary setup of the harvester work tools; technological adjustments updating; explanation of the obtained results; knowledge addition and editing; help to the user while working with IIS.

Figure 1 exemplifies IIS position in the control system of combine harvesting technological process which can be carried out both in automatic mode and can be updated by the operator on the basis of IIS recommendations in accordance with changing environment conditions.

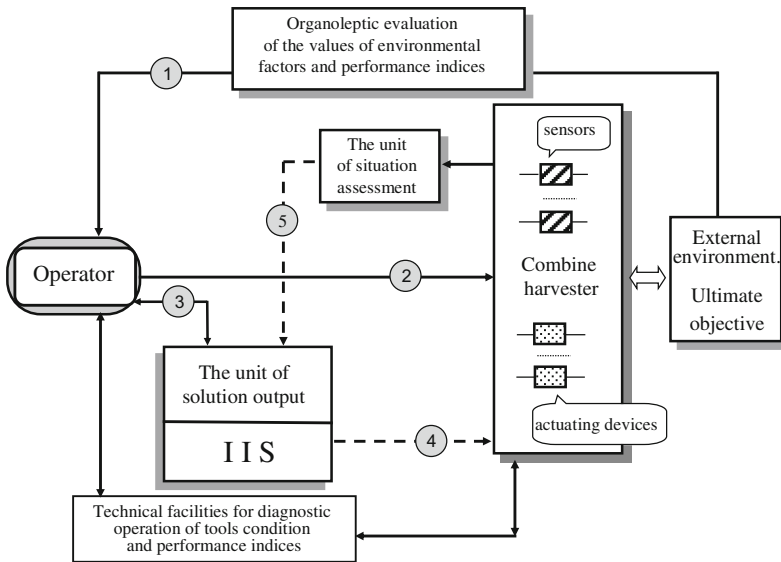


Fig. 1. IIS position in the control system of harvesting technological process. 1 – 2 - conventional relation in the system “man-machine-environment”, 1 – 3 – 2 - advice-giver mode (decision support), 5 – 4 - automatic operation mode.

The structure of the suggested IIS contains both conventional units, being inherent for expert systems, and special ones. Object domain peculiarities and the main requirements for information systems have specified the contents of its components. The IIS under consideration has the following units [15]: the unit of information input; knowledge base; the unit of knowledge acquisition; the output unit; the unit of the decisions interpretation; the unit of resolving contradictions; control unit; the unit of teaching component.

To adapt IIS knowledge base to real conditions, we have provided the possibility of loading into the knowledge system indicated by the expert and also all the standard

functions: knowledge deleting; knowledge editing; knowledge addition; knowledge base reading; knowledge storing.

The most important component of any software product aimed at wide application is user interface. In the IIS under consideration three types of dialogues are used: menu dialogue; question-answer dialogue; dialogue on the basis of screen tips. The script of a dialogue with a user is presented in the form of a tree graph of dialogue procedures where the graph root element is a dialogue initiation point, and terminal elements are output points. The main subsystems relation diagram for the developed IIS: “Design”, “Preliminary setup” and “Technological adjustments updating” is presented in Fig. 2.

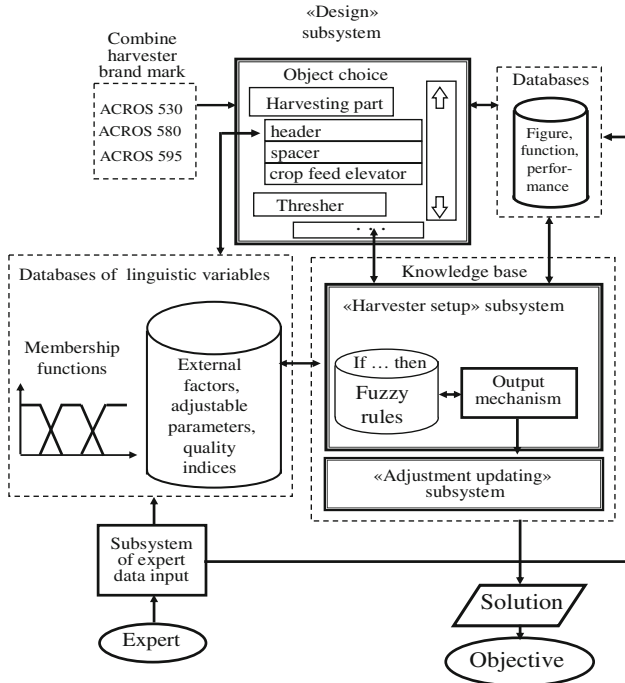


Fig. 2. Relations of IIS subsystems.

While developing the knowledge base the analysis of fulfillment degree of the set of requirements was made. These requirements include feasibility, completeness and consistency.

Software system works in two modes: knowledge acquisition and problem-solving. Herewith, all the stages of linguistic description of input and output attributes and also the analysis of consistency of expert knowledge are carried out [16].

In the mode of knowledge acquisition, the knowledge engineer and the expert form the knowledge base.

In the mode of problem, solving it is the user who interacts with the IIS. Dialogue unit of information input provides natural language interface with the user. Description of technological adjustments of work tools for different conditions of operation is in the

setting-up unit. The unit of the situation analysis contains description of harvesting conditions. The unit of inference mechanisms on the basis of current information, received from the user (or from sensors), rules and general facts about the object domain develops the problem solution. Such explanations to the user as, in which way the solution was obtained, what kind of rules are and why they are used herewith, are incorporated into the unit of decisions interpretation. The unit of the answer synthesis is the final element in IIS functioning. The problem solution can be presented on a display or printed out. The information can be transmitted to the actuating mechanisms in an encoded form.

2.2 Knowledge Formalization

A matter of choice of an adequate formal language is very important, therefore we should point out some advantages of the decision-making process description in a complex multilayer hierarchical system in terms of the theory of fuzzy sets [17]. This approach offers the possibility of representing adequately the essence of the decision making process itself in fuzzy conditions for the multilayer system, work with fuzzy restrictions and objectives and also set them up with the help of linguistic variables. The proposed simulation approach of decision-making processes while carrying out technological adjustment of the combine harvester on the basis of fuzzy models meets the requirements of system analysis – consideration integrity of complex hierarchical system (combine harvester) on the basis of the account of the main elements and processes in the system and relations among them and sufficient degree of simplification during simulation, making it possible to reproduce the real process properly and take into account determining factors in this system.

Description of the harvesting machine design is a connecting link between the subsystems “Preliminary setup” and “Technological adjustments updating.”

A grain combine harvester represents a set K , consisting of finite number of elements. There are different ways of defining sets. Since in our case a set K is finite, then K can be defined by simply enumerating its elements – components (g_i): $K = \{g_1, g_2, \dots, g_i, \dots, g_n\}$. In other words, $K = \{\text{batt, supporting bracket, tooth, finger, } \dots\}$. In addition, the number of elements of the set K is called as its power ($|K|$).

The other way of determining the set K is based on presenting the grain combine harvester as an assemblage of units and systems, for example, header, thresher, chopper etc. In this case, the set K is determined as a union of sets A_i . If A_i is the units the combine harvester consists of, then

$$K = \{A_1, A_2, \dots, A_n\} \text{ or } K = \bigcup_{i=1}^n A_i$$

The set elements reside in some relations among each other or with elements of other sets. So a set of components of the harvesting part, for example, A_i is a subset K , i.e. $A_1 \in K$, or $A_2 \in K$ (where A_2 is a set of elements of an electronic control and management system of the combine harvester work tool parameters). In the same way $A_{11} \in A_1$, i.e. a set of components of a reel (A_{11}) is a subset of the harvesting part (A_1).

When describing a combine harvester design, it is expedient to present information on any object by means of predicates. To describe the content of units and subsystems we used: consist (consists of what); work (how works); function (what function is performed); place (place of location); character (technical data); graphics (graphic display). The given assemblage of expressions represents an object model, presented by a group of predicate formulae. Therefore, information on the design of the object being investigated can be described in an identical form that is very important when formalizing object domain.

Description of the combine harvester operation is presented by a two-place predicate $Q(x, y)$, where Q is predicate to be executed; $x \in K$, and $y \in F$, where F is a multitude of operations performed by different work tools. Predicate Q describes an ordered set, for its assuming we introduce the concept of a tuple (vector). As a matter of fact, predicate Q represents an array of ordered couples: work tool – function, and is named as n -tuple ($n = 2$) or binary tuple. Set C consisting of all n -tuples will be called as the Cartesian product of sets $K \bullet F$.

Expression $\forall x \exists y Q(x, y)$ turns into the statement: any work tool (unit, etc.) fulfils something (true). Herewith an argument x belongs to the described before universe, and $y \in F$. The statement like “header includes reel which provides plants delivery to a cutter bar” in the symbolic language of predicate logics will have the following form: $\exists y$ (includes $(x, y) \wedge$ do (y, z)). Here x is a header; includes (x, y) – header includes y ; do (y, z) – work tool does z ; y is a reel; z is a vocabulary entry with the description of the tool work.

Therefore, the analyzed mathematical apparatus allows us to structure and formalize knowledge of the machine design (concepts and their relations) and present it on the machine-readable storage media in the form of formalisms.

On the basis of the methodology of linguistic approach for investigating complex systems [3, 18] we have developed models of attributes X, Y, V (environment factors, adjusting parameters and the combine harvester performance indices) in the form of semantic spaces and corresponding them membership functions:

$$\begin{aligned} &\{X_i, T(X_i), U, G, M\}, \quad \mu_R(x_1, x_2, \dots, x_n) \in (0, 1), \\ &\{Y_j, T(Y_j), U, G, M\}, \quad \mu_R(y_1, y_2, \dots, y_j) \in (0, 1), \\ &\{V_k, T(V_k), U, G, M\}, \quad \mu_R(v_1, v_2, \dots, v_k) \in (0, 1), \end{aligned}$$

where X, Y, V are names of the linguistic variables, T is a set of its values, or terms, which are the names of the linguistic variables defined over the set U , G is a syntactic procedure describing the process of deriving the new values of linguistic variables from the set T , M is a semantic procedure which makes it possible to map new value generated by procedure G into fuzzy variable, μ is membership functions.

The generalized model of the object domain “technological adjustment” has been adopted in the form of a composition of fuzzy relations of the semantic spaces in question:

$$\begin{aligned} &R_1 \circ R_2 \text{ for } \forall x \in X; \forall y \in Y; \forall v \in V; \\ &\mu_{R_1 \circ R_2}(x, v) \vee (\mu_{R_1}(x, y) \wedge \mu_{R_2}(y, v)) \end{aligned}$$

where R_1 is fuzzy relation “harvesting factors – adjustment parameters,”

$R_1 \{X_i, T(X_i), U, G, M\} \times \{Y_j, T(Y_j), U, G, M\}; \forall(x, y) \in X \times Y; R_2$ is fuzzy relation among adjustment parameters and the combine harvester performance indices,

$R_2 \{Y_j, T(Y_j), U, G, M\} \times \{V_k, T(V_k), U, G, M\}; \forall(y, v) \in Y \times V.$

It is expedient to solve the problems under consideration of preliminary setup and technological adjustments updating in terms of deductive and inductive inference of solutions [18, 19]. Figure 3 presents a general diagram of solutions inference in the problem of combine harvester setup.

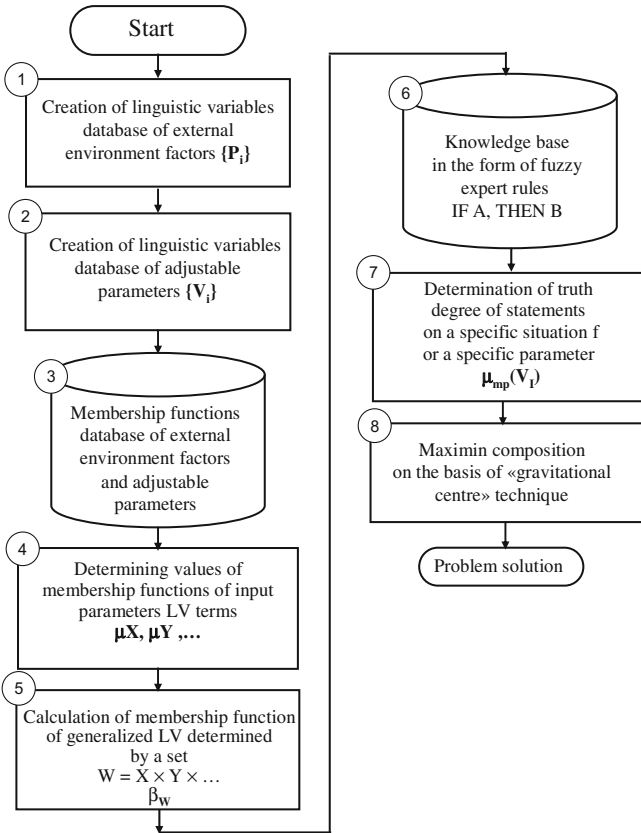


Fig. 3. General diagram of solutions inference in the problem of a combine harvester setup.

The expert system knowledge base presents a set of rules of fuzzy produces with a premise (A) and a consequence (B) [18, 19]:

$$R^{(k)}: A^k \rightarrow B^k, \quad k = 1, \dots, r$$

where r is a number of fuzzy rules; k is a rule number; A^k and B^k are such fuzzy sets that:

$$A^k = A_1^k \times A_2^k \times \dots \times A_n^k, \quad A_i^k \subseteq X_i;$$

$$B^k = B_1^k \times B_2^k \times \dots \times B_m^k, \quad B_j^k \subseteq Y_j,$$

where X_i and Y_j are semantic spaces of input and output attributes, herewith $i = 1, \dots, n$; $j = 1, \dots, m$.

Obtaining a particular solution provides for execution of the determined sequence:

1. Formulation of the generalized linguistic variable on the set of input attributes influencing the value of the output attribute (i.e. aggregation of the left parts of the rules);
2. Computation of membership functions for the generalized linguistic variable;
3. Determination of truth degree of fuzzy rules, in terms of which the selection of the output variable values is performed.

At the heart of the mechanism of IIS solutions inference, there is an object domain model representing a composition of fuzzy relations of semantic spaces of the machine performance indices, environment factors, and the machine adjustable parameters. In general terms, an explicit form of fuzzy logic inference for the system of knowledge of the given kind can be presented in the following way [19]:

$$\mu_{B^k} = \bigvee_{k \in K} (\bigwedge_{j \in J} \mu_{Bkj} y_j) \bigwedge_{i \in I} \mu_{Aki} (x_i')$$

In the final stage of solving the problems with the use of fuzzy logics the determination of exact values of output parameters is produced. One of the most widespread methods applied at the stage of defuzzification is the “gravitational centre” method [4, 20]:

$$y_j' = \left(\int y_j Y_j \mu_{B^k}(y_j) dy_j \right) / \left(\int \mu_{B^k}(y_j Y_j dy_j) \right)$$

A subsystem of obtaining and updating IIS knowledge has been developed for computations automation on estimating compatibility of fuzzy expert information [16]. When introducing new and updating available linguistic variables a computation of additive and multiplicative indices of common compatibility among the models is performed [21].

3 Conclusion

The key advantage of IIS development in terms of logic and linguistic presentation of fuzzy expert knowledge consists in adequate presenting real situations of harvesting machines operation. There is a possibility of accounting qualitative and linguistic attributes of the environment, technical condition parameters, and adjustable parameters of the machine and performance indices on the ground of common formalism.

Application of IIS research prototype under field conditions makes it possible to solve the problem of technological process control when operators have different qualifications. Managerial and engineering assessment of IIS effective application has shown that its usage enables to raise the quality of the adopted decisions; reduce

adjustment time by 1,5 – 4 compared to conventional methods; lessen the spread of values of the time spent depending on the operator working experience and, as a consequence, raise combine harvester output per shift by 8–11%.

For the purpose of implementation of the strategy of producing machines of new generation it is expedient to use IIS for technological adjustment as an element of intelligent system of the combine harvester control.

References

1. Krasnoshchekov, N.V.: Agroinjenernaya strategiya ot mehanizatsii selskogo hozyaistva k ego intellektualizatsii (Agroengineering strategy: from mechanization of agriculture to its intellectualization). *Traktori i selhoz mashini* **8**, 5–7 (2010)
2. Rybalko, A.G.: Osobennosti uborki visokourojainih zernovih kultur (Some features of harvesting high-yield crops). Agropromizdat, Moscow (1988)
3. Averkin, A.N., Batyrshin, I.Z., Blishun, A.F., Silov, V.B., Tarasov, V.B.: Nechetkie mnojestva v modelyah upravleniya i iskusstvennogo intelekta (Fuzzy sets in the models of management and artificial intelligence). Nauka, Moscow (1986)
4. Asai, K., Vatada, D., Sugeno, S.: *Prikladnie nechetkie sistemi (Applied fuzzy systems)*. Mir, Moscow (1993)
5. Omid, M.: Design of an expert system for sorting pistachio nuts through decision tree and fuzzy logic classifier. *Expert Syst. Appl.* **38**, 4339–4347 (2011)
6. Chevalier, R.F., Hoogenboom, G., McClendon, R.W., Paz, J.O.: A web-based fuzzy expert system for frost warnings in horticultural crops. *Environ. Model Softw.* **35**, 84–91 (2012)
7. Sujaritha, M., Annadura, S., Satheeshkuma, J., Sharan, S.K., Mahesh, L.: Weed detecting robot in sugarcane fields using fuzzy real time classifier. *Comput. Electron. Agric.* **134**, 160–171 (2017)
8. Goodridge, W., Bernard, M., Jordan, R., Rampersad, R.: Intelligent diagnosis of diseases in plants using a hybrid multi-criteria decision making technique. *Comput. Electron. Agric.* **133**, 80–87 (2017)
9. Walls III, J.T., Caciagli, P., Tooker, J.F., Russo, J.M., Rajotte, E.G., Rosa, C.: Modeling the decision process for barley yellow dwarf management. *Comput. Electron. Agric.* **127**, 775–786 (2016)
10. Zareiforush, H., Minaei, S., Alizadeh, M.R., Banakar, A., Samani, B.H.: Design, development and performance evaluation of an automatic control system for rice whitening machine based on computer vision and fuzzy logic. *Comput. Electron. Agric.* **124**, 14–22 (2016)
11. Navarro-Hellín, H., Martínez-del-Rincon, J., Domingo-Miguel, R., Soto-Valles, F., Torres-Sánchez, R.: A decision support system for managing irrigation in agriculture. *Comput. Electron. Agric.* **124**, 121–131 (2016)
12. Márquez-Vera, M.A., Ramos-Fernández, J.C., Cerecero-Natale, L.F., Lafont, F., Balmat, J.-F., Esparza-Villanueva, J.I.: Temperature control in a MISO greenhouse by inverting its fuzzy model. *Comput. Electron. Agric.* **124**, 168–174 (2016)
13. Omid, M., Lashgar, M., Mobli, H., Alimardani, R., Mohtasebi, S., Hesamifard, R.: Design of fuzzy logic control system incorporating human expert knowledge for combine harvester. *Expert Syst. Appl.* **37**, 7080–7085 (2010). <http://www.sciencedirect.com/science/article/pii/S0957417410001910>

14. Craessaerts, G., de Baerdemaeker, J., Missotten, B., Saeys, O.: Fuzzy control of the cleaning process on a combine harvester. *Biosyst. Eng.* **106**, 103–111 (2010). <http://www.science-direct.com/science/article/pii/S1537511010000024>
15. Waterman, D.: *Rukovodstvo po ehkspertnym sistemam (Expert systems manual)*. Mir, Moscow (1989)
16. Dimitrov, V.P., Borisova, L.V., Nurutdinova, I.N., Bogatyreva, E.V.: *Programmynaya sistema dlya vvoda ehkspertnih znanii (Software system for inputting expert knowledge)*. *Vestnik DSTU* **11**, 83–90 (2011)
17. Zadeh, L.: Knowledge representation in fuzzy logic. In: Yager, R.R., Zadeh, L.A. (eds.) *An Introduction to Fuzzy Logic Applications in Intelligent Systems*, The Springer International Series in Engineering and Computer Science, vol. 165, pp. 1–27. Springer, New York (1992)
18. Borisov, A.N., Alekseev, A.V., Merkuriev, G.V., et al.: *Obrabotka nechetkoi informacii v sistemah prinyatiya reshenii (Processing of fuzzy data in the systems of decision-making)*. Radio I svyaz, Moscow (1989)
19. Borisova, L.V., Nurutdinova, I.N., Dimitrov, V.P.: Fuzzy logic inference of technological parameters of the combine-harvester. *WSEAS Trans. Syst.* **14**, 278–285 (2015)
20. Makarov, I.M., Lohin, V.M., Man'ko, C.V., Romanov M.P.: *Iskusstvennyj intellekt i intellektual'nye sistemy (Artificial intelligence and intelligent control systems)*. Nauka, Moscow (2006)
21. Borisova, L.V., Nurutdinova, I.N., Dimitrov, V.P.: On creation of expert knowledge base in information systems of decision making support. *Int. J. Fuzzy Syst. Adv. Appl.* **1**, 88–93 (2014)

Multi-Criteria Decision Making Using AHP to Select the Best CAD Software

Omar Bataineh^(✉), Dina Abu Hjeelah, and Sreen Arabiat

Jordan University of Science and Technology, Irbid, Jordan
omarmdb@just.edu.jo

Abstract. One of the important questions that design and manufacturing firms face is which CAD software to use in their product development and realization activities. However, selecting the right CAD software is not a simple task due to the many criteria involved in the selection process such as package cost, ease of use, software popularity, features on offer, and system requirements. What makes it more challenging is the availability of a large number of commercial packages in the market. This constitutes a Multi-Criteria Decision Making (MCDM) problem that is addressed in this study using the Analytic Hierarchy Process (AHP). Because CAD software can be very specialized and vary significantly depending on the area of application, this study is limited to CAD software intended for mechanical design applications. The most popular packages in this regard include CATIA[®], Pro/ENGINEER, SOLIDWORKS, and Inventor[®].

Keywords: Analytic hierarchy process · Multi-Criteria Decision Making · Sensitivity analysis · CAD software

1 Introduction

Making decisions is a practice that is common to everyone and unavoidable in our daily life. Most of these decisions are simple to make and goes without notice. However, certain scenarios occur where decisions involve cases with requirements that are many and conflicting in nature. A special type of these scenarios is when the requirements are qualitative, i.e. not measureable on a numerical scale. This may lead to taking wrong decisions due to subjective judgments that are inconsistent. These types of scenarios, however, can be structured in a way which ensures that judgments are consistent, and improves the chances of taking the right decision. Such structuring can be made according to special techniques such as the AHP, which was first proposed by Saaty [1].

The AHP is very popular method, as evident in the literature through a wide spectrum of decision-making problems and applications. For example, some researchers used AHP to select the best patching material for concrete repair [2], rank airline carriers based on operating costs [3], or select safety devices used in industrial machinery [4]. The use of AHP can be found in decision-making problems related to project management [5, 6], medical and health care [7–10], safety [11, 12] and many other areas. Due

to the importance of the subject, Ho [13] provided a detailed literature review on AHP and its applications.

Not to the surprise, choosing the right software, itself, had its share of interest by researchers. Zaidan et al. [14] integrated between AHP and the Technique for Order of Preference by Similarity to Ideal Solution (TOPSIS) to evaluate and select a suitable open-source EMR software packages. Dorado et al. [15] used AHP to select the best software for engineering education. Eldrandaly [16] tried to find the best Geographic Information System (GIS) software using AHP.

This study is dedicated to aid the decision maker at the generic engineering firm in using the right approach for selecting the best mechanical CAD software to be used in product design and evaluation applications. Once the AHP method is presented, an AHP model of the decision-making problem regarding the selection of the best software is introduced. Then, input of data and implementation of AHP are carried out with the aid of Expert Choice, which is used as the decision-making software. Finally, AHP results and sensitivity analysis are presented.

2 MCDM Methodology Using AHP

The analytic hierarchy process (AHP) is a structured decision making technique for organizing and analyzing complex decisions. AHP works by decomposing a decision problem into a hierarchy of simpler sub-problems, each of which can be analyzed independently. This works by modelling the problem as a hierarchy containing the decision goal, the alternatives for reaching it, and the criteria for evaluating the alternatives [17]. Then, priorities are established among the elements in each level of the hierarchy. This step usually requires data collection by the tasked team through the different sources of information, i.e. through experts and published data. Gathered information are then used to make a series of judgments based on pairwise comparisons of the elements on a 1:9 scale, as summarized in Table 1. Thus, at a given level of the hierarchy, these pairwise comparisons are stored into the matrix

$$A = \begin{bmatrix} a_{11} & a_{12} & \dots & a_{1n} \\ a_{21} & a_{22} & \dots & a_{2n} \\ \vdots & \vdots & & \vdots \\ a_{n1} & a_{n2} & \dots & a_{nn} \end{bmatrix} \quad (1)$$

where

$$a_{ij} = \frac{1}{a_{ji}} \quad (2)$$

Table 1. Relative importance among elements on a 1:9 scale

Intensity of relative importance	Definition	Explanation
1	Equal importance	Two activities contribute equally to objective
3	Moderate importance	Experience and judgment slightly favour one activity over another
5	Strong importance	Experience and judgment strongly favour one activity over another
7	Demonstrated importance	An activity is strongly favoured as can be demonstrated in practice
9	Extreme importance	Evidence favouring the activity is of the highest order of affirmation
2, 4, 6, 8	Intermediate values	When a compromise is needed

Matrix A is then normalized according to

$$a_{ij}^* = \frac{a_{ji}}{\sum_{i=1}^n a_{ji}} \tag{3}$$

for all i and j . Weights w_i resembling priorities of compared elements for the given level of the hierarchy are then calculated as

$$w_i = \frac{\sum_{j=1}^n a_{ij}^*}{n}, \quad i = 1, 2, \dots, n \tag{4}$$

The weights eigenvector w is related to the pairwise comparisons matrix A according to

$$A \cdot w = \lambda_{max} \cdot w \tag{5}$$

where λ_{max} is a scalar used as a reference index that helps indirectly to assess consistency of the judgments. Thus, a consistency index CI is defined as

$$CI = \frac{\lambda_{max} - n}{n - 1} \tag{6}$$

Ultimately, the consistency ratio CR is calculated as

$$CR = \frac{CI}{RI} \tag{7}$$

where RI is the random index, which is a function of the number of compared elements n , as listed in Table 2. The consistency ratio is an important measure of the judgments' consistency. Typically, a CR value of less than 0.1 is reflective of consistent judgments. Higher CR values indicate that inconsistencies exist, which requires looking for sources

of inconsistencies in the judgments and solving the problem before proceeding further with the AHP procedure.

Table 2. List of random inconsistency indices (RI) for n up to 10

n	1	2	3	4	5	6	7	8	9	10
RI	0.00	0.00	0.58	0.90	1.12	1.24	1.32	1.41	1.46	1.49

Once the weights eigenvector w is calculated for each level, judgments are synthesized to yield a set of overall priorities for the hierarchy. This is done by multiplying the elements' weights of the given level by the weight corresponding to the parent element in the upper or main level. Then, desirability of the potential alternatives is established based on the produced weights corresponding to the considered criteria. Finally, a decision is made to achieve the goal set by selecting the alternative that gets the highest weight.

3 Analytic Hierarchy Model

The decision-making problem of selecting the best mechanical CAD software is represented based on the AHP method using a four-level hierarchical model, as shown in Fig. 1. The first level (I) of this model consists of the goal, which is to select the best mechanical CAD software. The second level (II) consists of the main requirements or criteria, which include ease of use, customer satisfaction, cost, system requirements, and features. The third level (III) consists of the sub-criteria. This includes the overall score and popularity for customer satisfaction; initial and license costs for cost; operating system and RAM size for system requirements; and modules and supported languages for features. The fourth level (IV) represents the alternatives, which are CATIA®, Pro/ENGINEER, SOLIDWORKS, and Inventor®. The criteria, sub-criteria, and alternatives were all chosen based on a rigorous study and analysis of the main factors considered when buying a new CAD software, and review of the available software in the market.

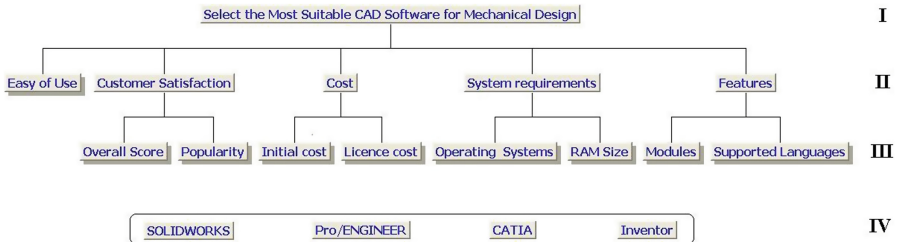


Fig. 1. The analytic hierarchy model for selecting the best mechanical CAD software

3.1 CAD Software Alternatives

CATIA. This software stands for Computer Aided Three-Dimensional Interactive Application. It was developed in 1977 by Avions Marcel Dassault, a French aircraft manufacturer. The software is commonly used by the biggest automotive and airline companies like Toyota, Hyundai, BMW, Ford, Hyundai, Boeing, Airbus. The licensing for CATIA is about \$25,000 per seat, thus it is not usually taught at the college level or used by small businesses. Old versions of CATIA are Unix-based, but new Windows-based versions have become available.

Pro/ENGINEER. It is a parametric feature-based 3D CAD/CAM/CAE modelling software. Its name changed to Creo in late 2010. The software supports Windows operating systems only, and used by many discrete manufacturers for their design and manufacturing applications.

SOLIDWORKS. A Windows-based 3D CAD software that was developed in 1995 by Solid Works Corporation. Then, it was acquired in 1997 by Dassault, which owns CATIA. SOLIDWORKS is currently the most widely used 3D CAD program worldwide. It also features a number of add-on utilities that can be ordered separately from the basic license. SOLIDWORKS is a lot cheaper than the CATIA counterpart.

Inventor. It is a further development to the AutoCAD software created in the early 1980s by Autodesk, which was the most widely used 2D CAD package in the world. This software was first released in 1999 to get a greater share in the 3D modeling market at the time.

3.2 Criteria Pairwise Comparisons

Comparisons were conducted pairwise among the criteria in levels II and sub-criteria in level III. An example of such comparisons is shown in Table 3. This example resembles the pairwise comparisons among the five main criteria of level II in the AHP model. Each entry in the table expresses the relative importance between the corresponding criteria. Thus, “Ease of Use” is 6 times as important to potential customers as “System Requirements”, or “System Requirements” is 1/6 times as important to potential customers as “Ease of Use”. The entries are shown also in Fig. 2, where they are entered

Table 3. Pairwise comparisons among the five main criteria of level II

Criterion	Cost	Customer satisfaction	Ease of use	Features	System requirements
Cost	1	5	3	3	4
Customer satisfaction	1/5	1	8	8	4
Ease of use	1/3	1/8	1	2	6
Features	1/3	1/8	1/2	1	6
System requirement	1/4	1/4	1/6	1/6	1

using Expert Choice to carry out the needed AHP calculations according to Eqs. (1–7). Similar procedure is conducted to compare between the level III sub-criteria specific to a given criterion in level II. This requires four additional pairwise comparison tables.

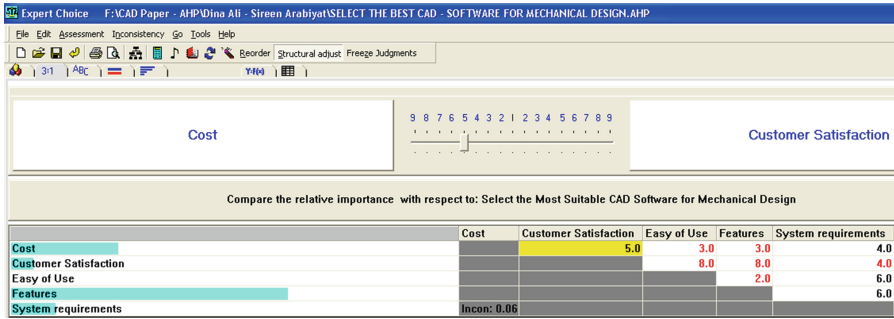


Fig. 2. Using Expert Choice to register entries of the pairwise comparisons among the five main criteria of level II

3.3 Alternatives Evaluation per Each Criteria

An important step of the AHP method is the evaluation of the alternatives with respect to each criteria and sub-criteria listed in the AHP model. This requires collecting data that shows the advantage an alternative may have over another one relative to a specific criteria. For instance, customer reviews of the four mechanical CAD software alternatives are available through several professional online forums. Data available on these forums have been used to assess the software alternatives in terms of the number of users (reflecting popularity of the software) and overall score (reflecting customer satisfaction level). The results are summarized in Table 4. The data related to the overall score in

Table 4. Customer reviews of the four alternative mechanical CAD software

Alternative	Popularity (number of users)	Overall score (out of 10)
SOLIDWORKS	988	8
Pro/ENGINEER	2586	8
CATIA	2097	6
Inventor	1051	8

Table 5. Pairwise comparisons among the software alternatives relative to the overall score

Alternative	SOLDIWORKS	Pro/ENGINEER	CATIA	Inventor
SOLIDWORKS	1	1	4	3
Pro/ENGINEER	1	1	4	3
CATIA	1/4	1/4	1	1/2
Inventor	1/3	1/3	2	1

this table are then used, as shown in Table 5, to generate the pairwise comparisons among the software alternatives in terms of the advantage one possesses over another with respect to the sub-criteria of overall score.

3.4 Ranking of Alternatives and Judgments Consistency

The global importance of each criterion and sub-criterion was calculated based on the procedure outlined in Sect. 2. This was done with the aid of Expert Choice, and the results are summarized in Table 6. It can be seen from Table 6 that features is the most importance criterion with relative importance of $RI = 0.419$, followed by ease of use ($RI = 0.319$). In descending order of importance, cost (initial and licensing), system requirements (operating system and RAM size), and customer satisfaction (popularity and overall score) are much less important. These results are further processed to produce the consistency ratio CR as well as the ranks of the four software alternatives, as shown in Fig. 3. It can be seen from this figure that the consistency ratio is equal to 0.05, which is less than 0.1. This indicates that judgments produced in implementing the AHP method for selecting the best mechanical CAD software were consistent. This improves the credibility of the conclusions to be reached using the AHP method. It can also be seen in Fig. 3 that Pro/ENGINEER gets the highest rank (0.346), followed by Inventor (0.283), SOLIDWORKS (0.275), then CATIA (0.096). This is logical because Pro/

Table 6. Global importance of main criteria in level II as calculated by Expert Choice

Criterion	Global importance
Cost	0.160
Customer satisfaction	0.033
Ease of use	0.319
Features	0.419
System requirements	0.069

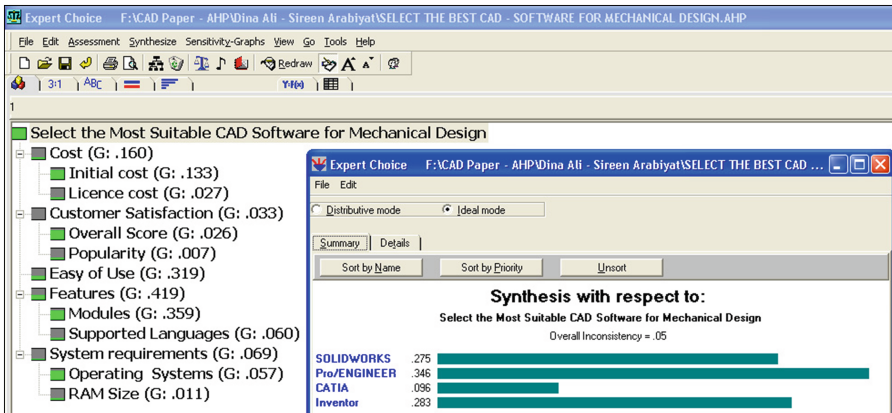


Fig. 3. Criteria’s global importance, consistency ratio, and ranks of the four software alternatives

ENGINEER fared very well in terms of feature and ease of use, which are the most important criteria to customers.

4 Sensitivity Analysis

The previous results were obtained based on fixed input of consistent judgments. Although consistency is an important measure of assuring quality in these judgments, it may still not be enough at all times. One way to give more assurance to the decision maker is by assessing the sensitivity of the outcome to the changes that occur in the relative importance of the various criteria. This was done using Expert Choice, which allows the user to simply dictate the relative importance values for the main criteria. Then, the software displays the ranks of the software alternatives graphically, as shown in Fig. 4. The bar heights in this figure represent the relative importance of the main criteria, and the CAD software with the highest rank is placed on top of the other ones in the right side of the window. By trying to change the relative importance for each criterion by 25%, it was observed that ease of use was the only criterion that could change the outcome of which software will assume the top rank. When the relative importance for the ease of use was increased by 25%, Inventor assumed the top rank instead of Pro/ENGINEER.

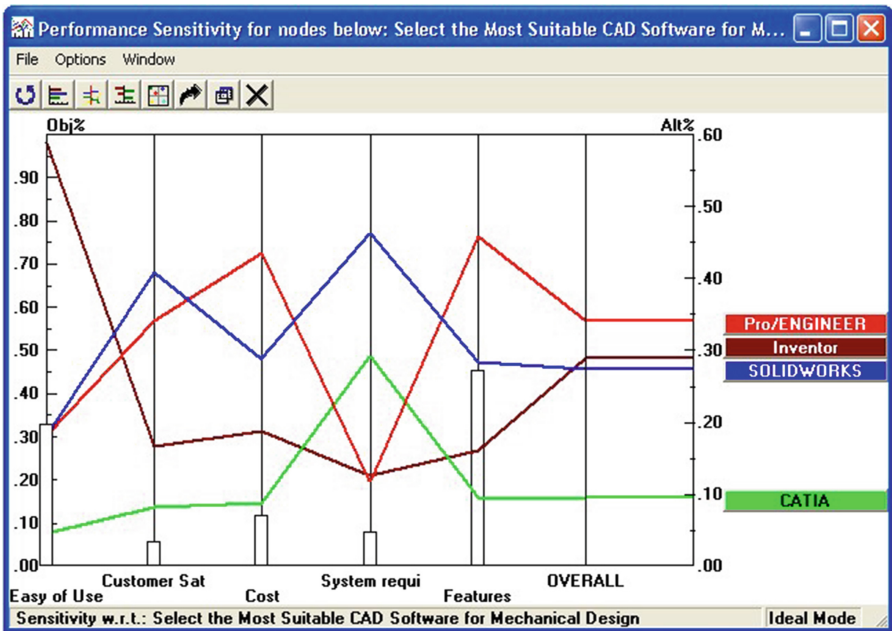


Fig. 4. Sensitivity analysis of the CAD software alternatives using Expert Choice

5 Conclusion

The analytic hierarchy process (AHP) is a structured decision making technique for organizing and analyzing complex decisions. It was used in this study to help provide organizations with the basis for selecting the CAD Software that best fits their needs. AHP works by decomposing a decision problem into a hierarchy of simpler sub-problems, each of which can be analyzed independently. The procedure for applying the AHP can be summarized as follows [T.L. Saaty, *The Analytic Hierarchy Process*].

References

1. Saaty TL. The analytic hierarchy process. *Decis. Anal.* (1980)
2. Do, J.Y., Kim, D.K.: AHP-based evaluation model for optimal selection process of patching materials for concrete repair: focused on quantitative requirements. *Int. J. Concr. Struct. Mater* **6**, 87–100 (2012)
3. Berrittella, M., La Franca, L., Zito, P.: An analytic hierarchy process for ranking operating costs of low cost and full service airlines. *J. Air Transp. Manag.* **15**, 249–255 (2009). Elsevier Ltd.
4. Caputo, A.C., Pelagagge, P.M., Salini, P.: AHP-based methodology for selecting safety devices of industrial machinery. *Saf. Sci.* **53**, 202–218 (2013). Elsevier Ltd.
5. Demirtas, N., Tuzkaya, U.R., Seker, S.: Project management methodology selection using SWOT-fuzzy AHP. *Lect. Notes Eng. Comput. Sci.* p. 1121–1126 (2014)
6. Al, K.M.: Selecting the appropriate project delivery method using AHP. *Int. J. Proj. Manag.* **20**, 464 (2002)
7. Brent, A.C., Rogers, D.E.C., Ramabitsa-Siimane, T.S.M., Rohwer, M.B.: Application of the analytical hierarchy process to establish health care waste management systems that minimise infection risks in developing countries. *Eur. J. Oper. Res.* **181**, 403–424 (2007)
8. Vidal, L.A., Sahin, E., Martelli, N., Berhoune, M., Bonan, B.: Applying AHP to select drugs to be produced by anticipation in a chemotherapy compounding unit. *Expert Syst. Appl.* **37**, 1528–1534 (2010)
9. Danner, M., Hummel, J.M., Volz, F., van Manen, J.G., Wiegard, B., Dintsios, C.-M., et al.: Integrating patients' views into health technology assessment: analytic hierarchy process (AHP) as a method to elicit patient preferences. *Int. J. Technol. Assess. Health Care* **27**, 369–375 (2011)
10. Liberatore, M.J., Nydick, R.L.: The analytic hierarchy process in medical and health care decision making: a literature review. *Eur. J. Oper. Res.* **189**, 194–207 (2008)
11. Gumus, A.T.: Evaluation of hazardous waste transportation firms by using a two step fuzzy-AHP and TOPSIS methodology. *Expert Syst. Appl.* **36**, 4067–4074 (2009)
12. Albert, G., Musicant, O., Oppenheim, I., Lotan, T.: Which smartphone's apps may contribute to road safety? An AHP model to evaluate experts' opinions. *Transp. Policy* **50**, 54–62 (2016). Elsevier
13. Ho, W.: Integrated analytic hierarchy process and its applications - a literature review. *Eur. J. Oper. Res.* **186**, 211–228 (2008)
14. Zaidan, A.A., Zaidan, B.B., Al-Haiqi, A., Kiah, M.L.M., Hussain, M., Abdunabi, M.: Evaluation and selection of open-source EMR software packages based on integrated AHP and TOPSIS. *J. Biomed. Inf.* **53**, 390–404 (2015). Elsevier Inc.
15. Dorado, R., Gómez-Moreno, A., Torres-Jiménez, E., López-Alba, E.: An AHP application to select software for engineering education. *Comput. Appl. Eng. Educ.* **22**, 200–208 (2014)

16. Eldrandaly, K.: GIS software selection: a multi criteria decision making approach. *Appl. GIS* **3**, 1–17 (2007)
17. Saaty, R.W.: The analytic hierarchy process—what it is and how it is used. *Math. Model.* **9**, 161–176 (1987)

Intelligent and Fuzzy Railway Systems

Dynamic Programming for Automatic Positioning of Wheel Chocks on Marshalling Yards

Sergey M. Kovalev¹, Alexander N. Shabelnikov^{1,2},
and Andrey V. Sukhanov^{1,2}(✉)

¹ Rostov State Transport University, Rostov-on-Don, Russia

² JSC “NIIAS” Rostov Branch, Rostov-on-Don, Russia

a.suhanov@rfniias.ru

<http://www.vniias.ru/>

Abstract. Nowadays the problem of automatic control on hump yards is being grown up on railways, because speed of train sorting impacts on efficiency on commodity circulation in country at all. To solve this problem, it is required to have solutions for the local tasks such as automatic uncoupling of cuts on receiving area, automatic hump control with variable speed, automatic chocking of inbound/outbound trains with uncoupled locomotive, etc. This paper presents a decision for automatic chocking of inbound/outbound trains, where automatic positioning of axle chocks is required. The solution is reached utilizing dynamic programming approach for optimal path calculation on weighted directed acyclic graph. The experimental results on a real station are presented.

Keywords: Automation of marshalling yards · Car retarders · Train chocking · Dynamic programming · Directed acyclic graph applications

1 Introduction

Railway traffic is rapidly grown up every year. Nowadays, this growth is defined by various facts, where transport automation plays the key roles, particularly, for marshalling railway stations. This problem is comprehensively revealed in American [1], German [2] and Russian sources [3]. As an example of such railway system, Integrated Automation System for Marshalling Yard Control (IAS MYC) can be presented [4,5]. Unmanned control at marshalling stations is become possible because IAS MYC utilizes modern artificial intelligent technologies and information processing tools.

In spite of progress in IAS MYC development, there are some automation tasks, which are not completely resolved for marshalling yards. This fact does not allow to fully avoid human control under marshalling process. One of such tasks is that handle brake shoes are still used to chock the wheels of train, which is uncoupled from locomotive and should be kept in a position for a while. Train chocking is important action, which helps to avoid unintentional rolling down under gravity force. If unmanned chocking is provided, the referred injuring risks will be excluded. Moreover, it could help to decrease financial and time costs for marshalling process.

2 Problem Statement

2.1 Practical Point of View

Experiments performed by JSC NIIAS (Russia) showed that an optimal solution from physical and economic point of view is piston type retarders (hereafter retarders) installation for chocking (Fig. 1) [6]. The initial purpose of retarders is speed control on hump yards using interaction between the sliding cylinder and the front of car wheel surface.

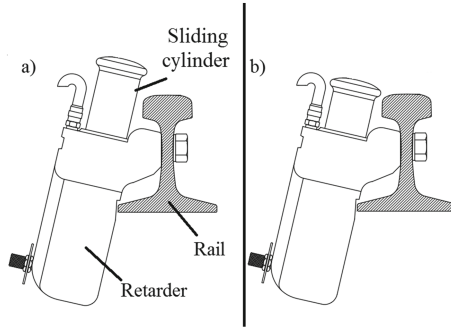


Fig. 1. Piston type retarder (a) Sliding cylinder is pulled, (b) Sliding cylinder is pushed

The main advantage of piston type retarders is that they do not require any additional external power to be applied or released. Retarder chocks a wheel using spring action on sliding cylinder when it is not under the action of external forces. Then, a wheel may be released if enough locomotive power is applied to sufficiently press on retarder.

One retarder can chock a wheel at the rail interval of 70 mm (Here and hereafter all distances are assumed as normalized by 70 mm (Fig. 2)).

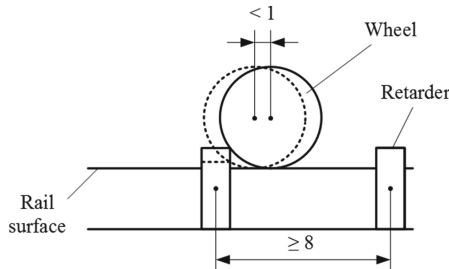


Fig. 2. Schematic illustration of both chocking interval of one retarder and relative disposition of two retarders

As practice shown, it is enough to chock some part $p \in (0, 1)$ of train wheels to avoid its unintentional rolling down under gravity force (the value depends on hump incline).

According to technical documents, chocking is made relatively to first axle of train. It attests to the fact that first axle of train is always chocked at the same point of railway.

There should be noted one natural requirement, according to which retarders should be physically spaced between each other and in relation to sleeper. Neighbour retarders should be spaced by 560 mm (i.e. 70×8 mm) interval at one rail (Fig. 2). Second rail should be provided by the retarders, which are positioned parallel with respect to first ones. Parallel positioning is required to simultaneously chock wheels of one axle.

Therefore, chocking task for inbound/outbound trains is represented as an optimization positioning problem for retarders. To solve this problem, the following natural criteria must be formalized and satisfied:

- (a) The number of possible trains, which are required to chock, is maximal;
- (b) Retarders are physically spaced between each other and relatively to sleeper.

This problem is typical NP complete with exponential complexity, because the brute force algorithm is required to find optimal positions. It means, that the solution is impractical in the initial form.

2.2 Theoretical Point of View

Proposed approach considers weighted directed acyclic graph utilization as the train axle positioning tool, where each train has n cars and each car (which is considered as strictly 4-axle car) is represented by one of m types.

The graph model can be defined as follows [7]:

$$G = \langle X, A, V, C \rangle, \quad (1)$$

where $X = \{x_i \mid i \in [1, 4nm^n]\}$ is the set of graph vertices, where each vertex identifies an axle for certain train (i.e. maps a possible retarder position), $A = \{a_{x,y} \mid x, y \in X\}$ is the set of graph arcs, where each arc represents relative position for axle pair (arc direction is front-to-tail direction of train), $V = \{v_x \mid x \in X\}$ is the set of weights associated with graph vertices ($V : X \rightarrow \mathbb{N}$), $C = \{c_{x,y} \mid x, y \in X\}$ is the set of weights associated with graph arcs ($C : A \rightarrow \mathbb{N}$).

Let the initial arc weight be computed as the physical distance between neighbour vertices (x_i and x_{i+m^n} , subscripts distribution is illustratively shown in Fig. 3):

$$\forall x_i \ i \in [1, (4n-1)m^n] \ j = (i+m^n) : c_{x_i x_j} = dist(i, j), \quad (2)$$

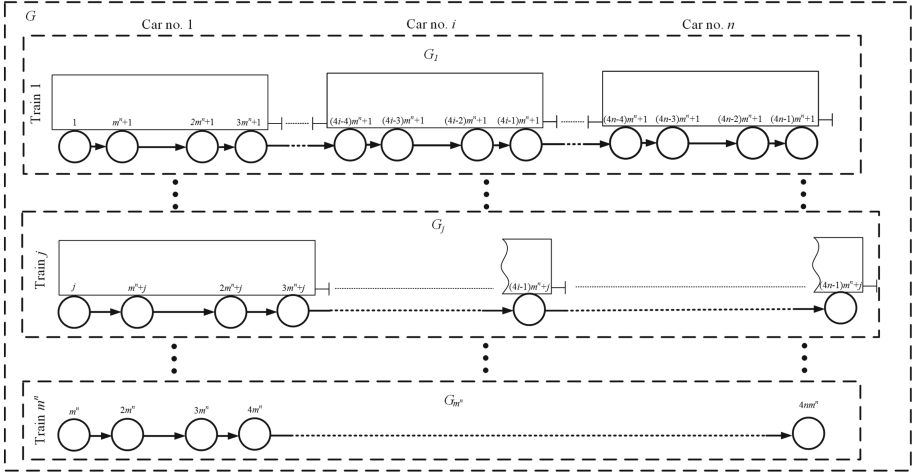


Fig. 3. Graph representation for various axle positions at different trains (here and hereafter only non-zero arcs are traced)

where $dist(i, j)$ is the physical distance (divided by 70 mm) between i th and j th axle of a train.

Let the initial vertex weight be computed as the number of non-zero outgoing arcs of a vertex. According to (2), only one non-zero outgoing arc for all vertices (except sinks) is initialized:

$$\forall x_i \ i \in [1, (4n - 1)m^n] : v_{x_i} = 1. \tag{3}$$

Graph G (Fig. 3) is disconnected, where each connected component $G_j([1, m^n])$ represents j -th variant of train positioning. The task solution based on the presented graph is to find optimal subgraph $G' = \langle X', A', V', C' \rangle$, where every path from source to sink has at least $4pn$ vertices. Here and hereafter path is considered as free from non-zero arcs.

To achieve the solution, the following criterion based on physical spacing of retarders should be satisfied:

$$\forall x \in X' \ \forall y \in X' : (|L_{M(x)} - L_{M(y)}| \geq 8 \vee L_{M(x)} = L_{M(y)}), \tag{4}$$

where $M(x)$ is the path to vertex x from graph source (hereafter path to x), $L_{M(x)}$ is the length of $M(x)$ (physically it is distance between first axle and one mapped to x).

It should be noted that certain vertices included in $M(x)$ from (4) are not specified because physical interpretation for every path to x is the same (in relation to path length).

3 Proposed Approach

In this paper, dynamic programming is proposed to find optimal subgraph as popular tool for similar application [8]. Dynamic programming is a tool for breaking complex NP problem down into polynomial subproblems, where conditions

for i th subproblems are obtained as $(i-1)$ th solution [9]. In present specification, i th task is graph analysis for the train obtained by adding an axle to train under analysis of $(i-1)$ th task.

To avoid exponential complexity, the number of vertices at i th subgraph should be decreased as more as possible. With this purpose, the following assumptions can be made:

1. A vertex is added if and only if it has the path, which contains less than $4pn$ vertices (as $4pn$ vertices are requested to chock a train):

$$\begin{aligned} & \exists M(x) \ ||M(x)| < 4pn \ x \in X' \rightarrow \\ & \rightarrow \left(\forall y = (X \setminus X') \ c_{x,y} \neq 0 : \right. \\ & \left. G' = G' \cup \left\langle y, \{a_{y,x_j} | j \in [1, 4m^n]\}, v_y, \{c_{y,x_j} | j \in [1, 4m^n]\} \right\rangle \right), \end{aligned} \quad (5)$$

where $||M(x)||$ is the number of vertices inside $M(x)$.

2. If pair of vertices has identical path length, then they must be identified (i.e., physically, it means chocking two axles having same position by one retarder):

$$\begin{aligned} & L_{M(x)} = L_{M(y)} \ x \in X' \ y \in X' \rightarrow \\ & \rightarrow \left(\begin{aligned} & v_x = v_x + v_y \wedge \\ & \forall z \in X : (c_{x,z} = c_{y,z}, c_{z,x} = c_{z,y}) \wedge \\ & X' = X' \setminus y \end{aligned} \right), \end{aligned} \quad (6)$$

Obviously, source vertices of all connected components satisfy this assumption (their paths do not contain non-zero arcs) (Fig. 4).

3. The less-weighted vertex from the pair, which does not satisfy condition (4), must be deleted (it cannot be used as retarder position due to physical requirement). To avoid information loss, its edges should be contracted, i.e.

$$\begin{aligned} & (|L_{M(x)} - L_{M(y)}| < 8) \wedge (L_{M(x)} \neq L_{M(y)}) \wedge (v_x > v_y) \ x \in X' \ y \in X' \rightarrow \\ & \rightarrow \left(\begin{aligned} & \forall w \in X' \ \forall z \in X \ c_{w,y} > 0 \ c_{y,z} > 0 : \\ & (c_{w,y} = c_{w,y} + c_{y,z}) \wedge X' = X' \setminus y \end{aligned} \right), \end{aligned} \quad (7)$$

Based on above mentioned, algorithm of dynamical programming for optimal retarder positioning can be presented as Algorithm 1.

4 Experimental Results

As an experimental object, marshalling yard Luzhskaya-Sortirovochnaja is used [10]. This yard is finished for main construction in 2016. It is planned to be one of the most advanced railway hubs not only in Russia, but also in the World. Despite the fact that the yard is enough large railway object, where goods are sorted not only for Russian, but also for Europe companies, which work through Baltic sea using commercial sea port Ust-Luga, it has comparatively small human staff. It is reached by using modern unmanned control tools, which are developed

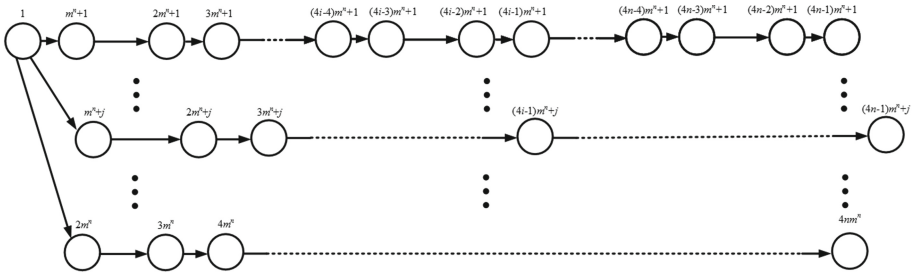


Fig. 4. Source vertices identification

Algorithm 1. Proposed algorithm based on dynamical programming

1: Initialization of graph $G' = \emptyset$ and addition of vertices, which reflect the first axle position ($i = 1$):

$$\begin{aligned} &\forall y \in X c_{y,x \in X} = 0 : \\ &G' = G' \cup \left\langle y, \{a_{y,x_j} | j \in [1, 4m^n]\}, v_y, \{c_{y,x_j} | j \in [1, 4m^n]\} \right\rangle. \end{aligned} \tag{8}$$

- 2: Identification of vertices (Fig. 5) using (6).
- 3: Identification of vertices (Fig. 6) using (7).
- 4: $i = i + 1$, $G_{new} = \emptyset$ (G_{new} is introduced only as the stop criterion).
- 5: Addition of the vertices corresponding i th axle according to (5):

$$\begin{aligned} &\exists M(x) ||M(x)|| < 4pn \ x \in X' \rightarrow \\ &\rightarrow \left(\forall y = (X \setminus X') c_{x,y} \neq 0 : \right. \\ &\left. G_{new} = G_{new} \cup \left\langle y, \{a_{y,x_j} | j \in [1, 4m^n]\}, v_y, \{c_{y,x_j} | j \in [1, 4m^n]\} \right\rangle \right). \end{aligned} \tag{9}$$

6: If $G_{new} = \emptyset$, then algorithm termination. If not, $G' = G' \cup G_{new}$ and go to step 2.

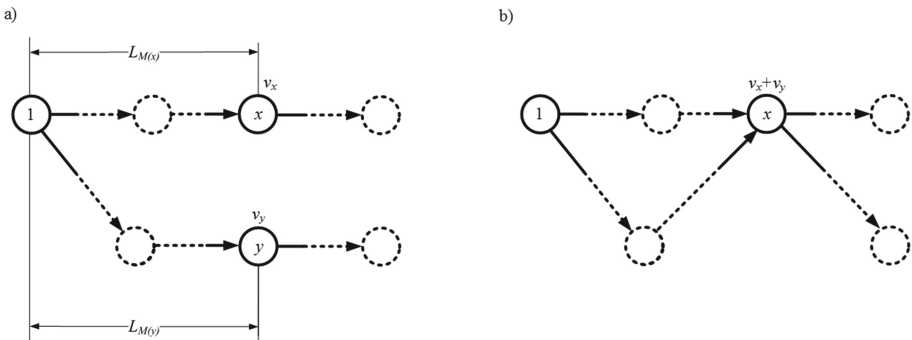


Fig. 5. Vertex identification according (6) (a) vertices before identification, (b) vertices after identification

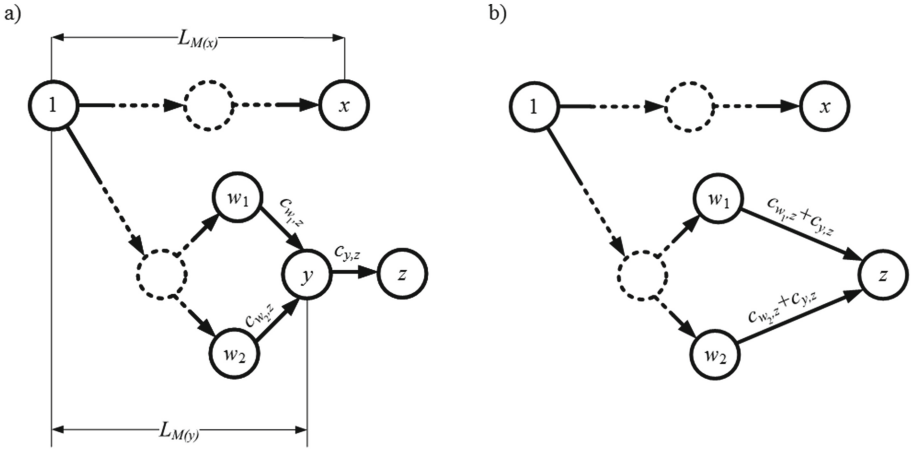


Fig. 6. Edge contraction according (7) (a) vertices before identification, (b) vertices after identification

by Siemens together with JSC “NIIAS”. In these tools, an important role may be played by automatic train chocking system, where proposed approach can be used (Figs. 5 and 6).

According to project documentation of the marshalling yard, average incline is 1%, which referred to (based on empirical calculations) the fact that 20% axles must be chocked to keep a train, i.e. $p = 0.2$.

According to pilot operation programme, the number of all possible car types forming train is 12. The set of car types includes as short cars (wheelbase is from 5950 mm), as long cars (wheelbase is up to 15150 mm). At the same time, to confirm applicability of the proposed technique, it is assumed that trains to be chocked have at least 6 cars. Therefore, $m = 12$, $n = 6$.

To construct graph model, C++ language was used. Time for graph construction was 3 h at processor Intel Core i5-3360M CPU 2.89 GHz. Resulting consisted of 113 vertices.

As the experimental result, it was found that every train, for which $m = 12$ and $n = 6$ with various wheelbases, is impossible to be kept using 20% chocking, because only 84% of various trains get into stopping area. The experiment had been performed for less and less number of car types (each new experiment rejects car with the longest wheelbase for previous one) till 100% result was obtained (Table 1).

Experimental results show that one railway track can be equipped only for trains containing 7 car types with shortest wheelbases. Trains containing the rest part of types can be chocked at the neighbour track, where proposed algorithm is used for positioning.

Table 1. Input data for TD_SAD2 evaluation

Number of car types	Total number of various train formations	Number of retarders for chocking (i.e. vertices of resulted graph)	% of chocked trains (from total number)
12	12 ⁶	113	84
11	11 ⁶	111	88
10	10 ⁶	109	95
9	9 ⁶	109	98
8	8 ⁶	106	99
7	7 ⁶	105	100

5 Conclusions

This paper presents a new approach for automatic chock positioning. Here, retarders are used for unusual purpose, which is to chock inbound/outbound trains with uncoupled locomotive. This is one of key points in the case, when unmanned technology on marshalling yards is required to be provided.

Proposed approach is based on dynamical programming iteration algorithm for optimal subgraph computation at weighted directed acyclic graph, which represents various axle positions. As theoretical and practical analyses showed, dynamical programming allows to present initial NP problem in form of polynomial tasks, where the condition of i th task is obtained as the solution of $(i - 1)$ th one. Polynomiality of subtasks is reached during pairwise identification of vertices when solution of subtask is checked. Presented experimental results illustrate that dynamical programming allows to adequately present the retarders positioning. It is shown that proposed approach helps to make a decision that it is impossible to chock every train, which simultaneously contains long cars as well as short ones. The approach also allows to find an optimal car types set, which forms possible train formations for chocking.

As a future work, algorithm extensions could be specified. From theoretical side, it could be shown more illustratively that NP task is eliminated. From practical side, it could be extended for cases, where number of cars is initially unknown.

Acknowledgement. The work was supported by RFBR (Grants No. 15-07-00112, No. 16-07-00032, No. 17-07-00372, No. 16-07-00086, No. 17-20-02018 and No. 17-20-03063).

References

1. Dick, C.T., Dirnberger, J.R.: Advancing the science of yard design and operations with the CSX hump yard simulation system. In: Proceedings of the 2014 Joint Rail Conference, Colorado Springs, USA (2014)

2. Hansmann, R.S., Zimmermann, U.T.: Optimal sorting of rolling stock at hump yards. In: Mathematics Key Technology for the Future Joint Projects Between Universities and Industry. Springer, Heidelberg (2007)
3. Shabelnikov, A.N.: Integrated automation system for marshalling yard control: problems, functions, main aspects. *Zheleznodorozhny Transp.* **10**, 34–37 (2015). (in Russian)
4. Shabelnikov, A.N.: The intellectual model of control over loose couplings rolling down process based on an indistinct dynamic system. In: Proceedings of IEEE International Conference on Artificial Intelligence Systems, pp. 257–259. IEEE (2002)
5. Shabenikov, A.N., Sukhanov, A.V., Kovalev, S.M.: Intelligent technique for faults prediction on hump yards, *Inenernyj vestnik Dona* 4. <http://ivdon.ru/ru/magazine/archive/n4y2015/3334>. Accessed 11 Nov 2016. (in Russian)
6. Thyssen, C.J.: Shock absorber. Patent US 6,199,671 B1 (2001)
7. Ping, Z.: Handbook of Graph Theory. CRC Press, Florida (2013)
8. Bellman, R.E., Dreyfus, S.E.: Applied Dynamic Programming. Princeton University Press, New Jersey (2015)
9. Dasgupta, S., Papadimitriou, C.H., Vazirani, U.V.: Algorithms. McGraw-Hill Inc., New York (2006)
10. Russia: Marshalling yard Luzhskaya-Sortirovochnaja. <https://www.mobility.siemens.com/mobility/global/SiteCollectionDocuments/en/rail-solutions/rail-automation/references/russia-en.pdf>. Accessed 13 Apr 2017

Mobile Smart Objects for Incidents Analysis in Railway Intelligent Control System

Andrey V. Chernov^(✉), Maria A. Butakova, Vladimir D. Vereskun,
and Oleg O. Kartashov

Rostov State Transport University, Rostov-on-Don, Russia
{avcher,butakova,vvd}@rgups.ru, okrstu@yandex.ru

Abstract. This paper proposes a novel approach to designing an architecture and middleware for a new class of objects, smart mobile objects using in railway intelligent control systems for incident analysis purposes. Architecture, middleware and other related technologies suited for smart objects and current state-of-art in incident analysis and management systems in railway transport are presented. The main existed approaches to smart objects architecture and designing are described. As a possible realization of a new idea, a smart object concept based on reconfigurable hardware is proposed. The paper contains a hardware implementation of a rough-sets based controller for data preprocessing about incidents in the railway infrastructure management system.

Keywords: Incident analysis · Smart objects · Intelligent control system · Railways

1 Introduction

This paper proposes a novel approach to designing an architecture and middleware for a new class of objects, smart mobile objects using in railway intelligent control systems for incident analysis purposes. Architecture, middleware and other related technologies suited for smart objects and current state-of-art in incident analysis and management systems in railway transport are presented. Two main existed approaches to smart objects designing are described. As a possible realization of a new idea, a smart object concept based on reconfigurable hardware is proposed. The paper contains a hardware implementation of a fuzzy-rough controller for data preprocessing about incidents in the railway infrastructure management system.

In recent years we have witnessed a rising interest in smart objects technology. In general case of definition, the “Smart Object” (SO) may refer to rather various objects not strictly technical. However, from the modern point of view,

The work was financially supported by Russian Foundation for Basic Research (projects 15-01-03067-a, 16-01-00597-a, 17-07-00620-a).

we notice that definition of the smart object immediately addresses us to the Internet of Things (IoT) devices, networked or web devices, equipped with sensors and actuators controlled by a microprocessor and with the independent power source. Usually, SOs have small physical size and implement interaction with the physical world through sensors and actuators [1]. Unlike non-smart objects which can also be equipped with sensors and actuators, SOs have some degree of intelligence. This feature allows communication among SOs, perform information handling and decision making at the higher level of intelligence [2]. A lot of SOs in the near future will allow people to interact with their environment, allowing companies to offer “real world” services on request, presenting this “world” in the form of a digital meaning. Nowadays “Machine-to-Machine” (M2M) technology has become is not anything unique. Every day at home, at work or when driving a car many people use smart watches synchronized with smart-phones, locate their way and GPS coordinates synchronized with satellites, operate with network cameras via tablets, etc. The M2M technologies allow to exchange data between objects or to transfer them unilaterally. They automate business processes, improve the efficiency of systems, optimize the interaction between structural elements and, what is of particular importance, make our life more comfortable and safer. It should be noted that now M2M technologies are included in the concept of the IoT, which is gaining popularity all over the world. Let’s briefly introduce the IoT technologies variety underlying SOs.

IoT can conditionally be divided into two categories: the Home-IoT and the Industrial-IoT. Today’s Home-IoT devices are quite familiar most people. They are smartphones, smartwatches, smart-TV sets, smart meteorology stations, systems of smart home automation including ambient light control systems, cooling and conditioning systems, intelligent home security systems, water heating, washing-machine systems and so on. Most of the devices above can be controlled through low range wireless networks, such as Bluetooth, WiFi or RFID and NFC tags. Sometimes these types of networks classify either piconets, in the case of Bluetooth using, or personal area networks (PAN), in the case of providing a low-range WiFi. In the majority of cases, piconets and PANs are temporary networks with master-slave data transmission or temporary access code synchronizing. It should be noted that these network types have a proper autonomy and mobility, but also drawbacks related to low spatial operating range, not so good scalability, vulnerability to computer attacks and in most cases, low data rate performance depending on autonomous power supply. Not so recently we have met the Wireless Body Networks (WBAN) [3], due to the fact the significant advances in miniaturized, lightweight wearable electronics, low power intelligent sensors and specialized systems-on-chips. From the pragmatic point of view, WBANs can find applications in the medical and non-medical area. To improve energy efficiency, extend coverage area and scalability recently Archos announced the PicoWAN technology with Semtech LoRa picocell gateway platform [4] for smart IoT applications. The key to innovation in PicoWAN technology is a unique signal modulation feature and as a consequence, an enhanced wireless transmission protocol implemented in hardware devices, pico-gateways plugged directly into

standard home power supply socket. Pico-gateways are inexpensive, easily being administering, configuring, but covering area guaranteed by devices is comparable with powerful hardware wireless transmitters mounted on the roofs of buildings.

Usually, a characteristic feature of the Home-IoT is the inability of “smart things” to interact with each other without a user actions. Surely, sometimes the interaction among SOs in the Home-IoT can be initiated by programmed events or timers. Other IoT architectures we include into the second IoT category, Industrial-IoT which will be described in the next section.

The rest of the paper is organized as follows. Section 2 focuses on recent advances and works devoted to architecture and middleware of IoT and SOs. Section 3 presents a novel approach to SOs architecture which includes a raw data hardware preprocessor and accelerator, suited for mobile data processing. Section 4 contains new ideas in SOs development based on reconfigurable computing devices, namely Field-Programmable Gate Arrays (FPGA) and focuses on the possible implementation of a hardware accelerator for rough data pre-processing in the railway infrastructure incident management system.

2 Related Work

Due to continuous progress in microelectronics, optoelectronic, wireless and optical data transmission, software and Internet technologies and related improvements, the SOs researching attracts much attention. In recent years the number of research papers significant increase in the number. However, we can distinctly divide them into several groups: the papers concerning general architecture, philosophic, social and other types of the influences SOs to society and environment; SOs communication technologies, that usually includes advances in the wireless data transfer; middlewares for SOs and smart environments and designing various special feature-oriented frameworks for SOs and a group of papers focused on theoretical aspects of SOs functioning, including SOs meta-data modelling, discovery methods and cooperating SOs each other similar to distributed intelligent agents.

The SOs underlying architecture of Industrial-IoT has several alternatives. First alternative states that SOs users interact with “smart things” through local network gateway by the use of OSI (Open Systems Interconnection) protocols stack. In the case of such architecture, nodes can organize broadcast data transmission or be grouped and form communication links in the lack of a gateway. For this purpose, the IEEE 802.15.4 standard is applied widely. The second alternative assumes connecting users to a gateway by the remote proxy server or network also named a cloud. This situation is due to the absence of gateway’s public IP address for security reasons. The user device also has no public IP address necessary for push-messages receiving from “smart thing”. And in the last alternative “smart thing” connected to the Internet directly. This variant requires IP protocol support embedded into the device. Consequently, “thing” may not provide local network access. Obviously, the gateways become a key

component in IoT and solve the main problem of IoT designing related to compatibility among a variety of devices and between a device and corporate network or Internet. The gateway must be not less smart than “smart things” connected and the support of a broad spectrum of wireless and wired protocols is required.

Papers [5, 6] proposes a general architecture of SOs named “Networked Smart objects” which aim to collect data from heterogeneous IoT sources, perform filtering acquired data and then transmitting refined data to middleware for storage and interaction with users through MQTT (Message Queuing Telemetry Transport) protocol. MQTT is designed for low-power embedded devices, so the computational requirements for its implementation are minimal. In addition to the very low system load, the MQTT features high communication efficiency even in networks with low bandwidth. MQTT implements the “Publisher-Subscriber” model, using the minimum number of methods. They serve to indicate the actions to be performed. These activities are reduced to interaction with the broker and to work with topics and messages. Agents connect to the broker, and then either publish topics and messages in them or subscribe to topics and receive messages on these topics published. Having completed the work, the agent disconnects from the broker.

In the white paper [7] one can find the several IoT-focused ITU-T/ISO/IEC standards is being developed refer to Industrial-IoT applications. All standards, namely ISO/IEC 30141 Internet of Things Reference Architecture (IoT RA, working draft) [8], ITU-T Y.2060 [9], and reference architectures, such as the Industrial Internet Consortium Industrial Internet Reference Architecture (IIC IIRA) [10], the Reference Architectural Model Industrie 4.0 (RAMI 4.0) [11], the IoT-A Architectural Reference Model (IoT-A ARM) [12] and the Alliance for Internet of Things Innovation (AIOTI) [13] have at least three-layered structure. The structure contains: device layer with gateway capabilities; network and IoT service support layer; application layer with interfaces which is providing users access to the IoT ecosystem. It is worth to note two extensive surveys [14, 15] devoted to architectural elements, protocols, applications, a vision, and future directions of IoT.

The development of the SOs middleware is attracting much research efforts. SOs middleware in some meaning is based on IoT middleware. The survey in [16] gives us a classification, functional components and IoT middleware comparison. A detailed discussion of the SOs middleware design principles one can find in [17]. One of the main aims of middleware design is organizing so-called Smart Environment (SE) for transparent SOs interaction. Because of heterogeneity of SOs, the middleware should allow abstraction from the concrete sensor, protocol, and platform type. According to [18] there are several abstraction levels SE maintained:

- abstraction over hardware devices with heterogeneous data input and output;
- abstraction over software and hardware interfaces;
- abstraction over data various streams and data types;
- abstraction over physical location and context of individual device.

It is easy to understand that the middleware extends capabilities of hardware and software of SOs and facilitates the use and scalability of SOs ecosystem. The paper [19] make demands to the SOs development which are as following:

- application development must be implemented without reference to specific SOs vendors functions;
- SOs should support augmentation variation;
- management of SOs is required to be performed with environment adaptation feature;
- upgrading and evolution of SOs should be provided in the easy way.

3 A Proposed SOs Architecture

The previous section shows that nowadays there are two main SOs architectures: agent-based SOs architecture [20] and service-oriented SOs architecture [21]. Figure 1 presents a novel SOs architecture which may be characterized as a hybrid architecture. It combines features of approaches above. Architecture has three layers as it was described in the previous section:

1. Physical layer.
2. Smart Object Middleware (Virtualization) layer.
3. Application layer.

Let's describe the feature of proposed architecture in more detail. Agent-based SOs feature with mobile agents can be described in the following way. The mobile SO is a computing module which has the ability to autonomously navigate the network from node to node and perform some calculations required by the user. Before intensive SOs development, a mobile agent has usually represented a software program with some intelligent algorithms implementations. However, now we constitute that mobile agent can be built on highly integrated System-on-Chip. Such ability, surely, increases the area of application of the mobile SOs. Applications from the higher level can inject mobile SO agents into the network, allowing them to navigate the network along a path defined in advance or selected by each agent independently based on the dynamically retrieved information. After completing their mission, mobile SO agents can return to their initial network node to inform the user of the results. Mobile SO agents can autonomously move around the nodes, not maintaining a constant connection with the node that created them. An initial node only creates mobile SO agents and initializes them, and also accepts agents delivering the final result.

The Physical lower layer of proposed SOs architecture performs the data acquire via heterogeneous individual and networked sensors and generate multivariate raw data arrays. The middle layer serves as Smart Object Middleware and performs virtualization functions. Mobile SO consists of sensor provider, sensor manager, and hardware preprocessor and accelerator. The last item will be described in detail in the next section. SO metadata storage is intended to interpret heterogeneous data from lower level onto higher application level in a unified form. The higher Application level is designed to get a unified application program interface to user programs that interacting with mobile SOs.

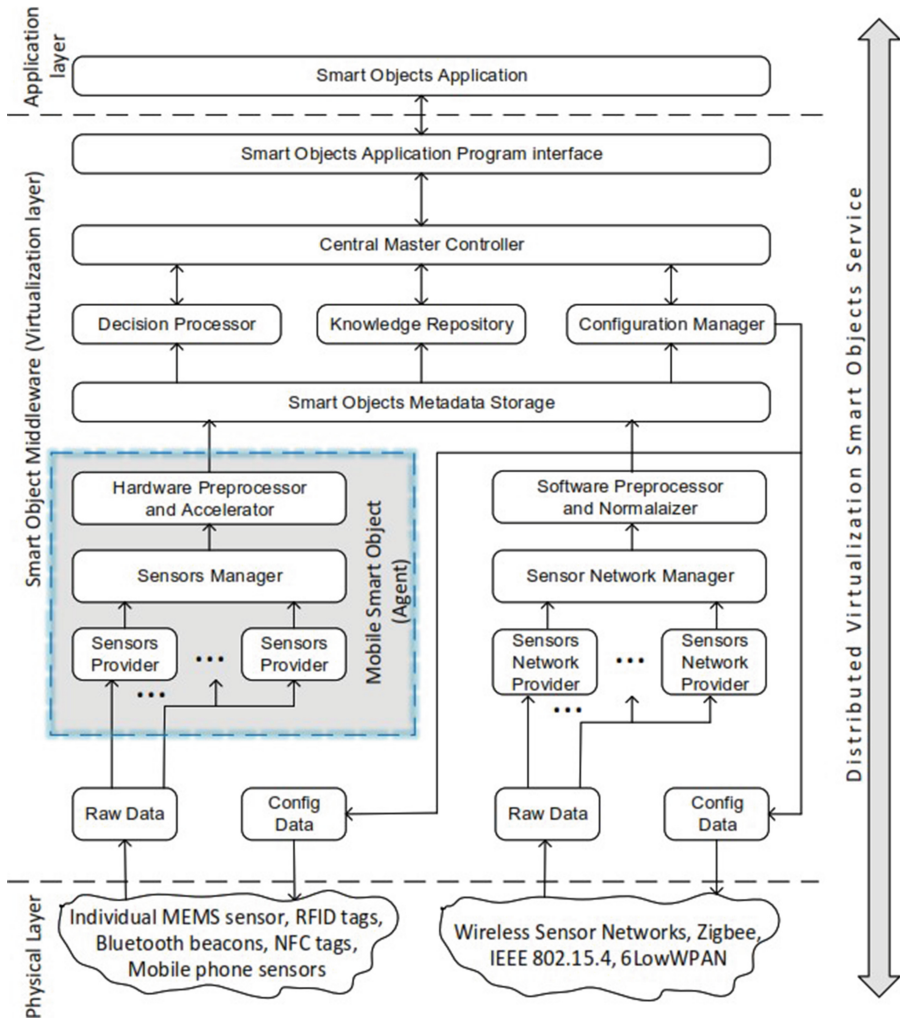


Fig. 1. The proposed SOs hybrid architecture

4 A Hardware Accelerator for Rough Data Preprocessing

The purpose of this section is to present a possible hardware implementation of the acceleration module in mobile SOs architecture (ref. Fig. 1). Hardware acceleration module implementation can be designed in the different ways and purposes related to the SOs applications. In frames of our research, we propose using the mobile SOs in the incident data preprocessing for railway intelligent control systems. In our previous works [22–25], the theoretical basis of security incident identification methods and system structure of railway incident management system was presented.

As the main concept in rough sets theory [26] we consider an information system $S = \langle U, A, V, f \rangle$, where U is a nonempty finite set of objects (universe), $A = C \cup D$ is a finite nonempty set of attributes, C and D are sets conditional and decision attributes respectively, $V = \bigcup_{a \in A} V_a$, V_a is a finite nonempty set of values of some attribute a , $f : U \rightarrow V$ is description function. For each $B \subseteq A$ equivalence relation $R_A(B)$, also called indiscernibility relation is defined as following: $R_A(B) = \{(x, y) \in U^2 \mid \forall a \in B, a(x) = a(y)\}$. If $(x, y) \in R_A(B)$, we conclude that objects x and y are indiscernible relatively to set of attributes B . It should be noted that in the case of changing a set of attributes, for example, increasing their number, objects can become discernible. The notation $[x]_B$ defines an equivalence class of indiscernibility relation $R_A(B)$, and partition $U / R_A(B)$ defines the whole set of equivalence classes $R_A(B)$. For $X \subseteq U$ a set X can be obtained based on information in \underline{B} with B -lower and B -upper approximations, denoted respectively $\underline{B}X$ and $\overline{B}X$, where $\underline{B}X = \{x \mid [x]_B \subseteq X\}$ and $\overline{B}X = \{x \mid [x]_B \cap X \neq \emptyset\}$. Each element of the discernibility $DM(x, y)$ and indiscernibility $IM(x, y)$ matrices $|U| \times |U|$ [27] for given information system S defined as: $DM(x, y) = \{a \in A \mid I_a(x) \neq I_a(y), x, y, \in U\}$, $IM(x, y) = \{a \in A \mid I_a(x) = I_a(y), x, y, \in U\}$, where $I_a(x)$, $I_a(y)$ mean that the x, y have some value of attribute a . Further we define discernibility $f_{dis}(DM)$ and $f_{ind}(IM)$ functions as follows:

$$f_{dis}(DM) = \bigwedge \{\bigvee DM(x, y) \mid x, y \in U, DM(x, y) \neq 0\},$$

$$f_{ind}(IM) = \bigwedge \{\bigvee IM(x, y) \mid x, y \in U, IM(x, y) \neq A\},$$

where \bigwedge and \bigvee a disjunction and a conjunction respectively. Finally, we obtain a reduct, a core set of attributes defined as: $f_{core}(IM, DM) = f_{ind}(IM) \wedge f_{dis}(DM)$.

Several FPGA-based hardware accelerators for rough sets processing are discussed in [28]. Figure 2 presents our proposed hardware implementation based on FPGA. As input values can be used raw data arrays acquired directly from sensor networks or devices.

Due to the fact that the raw data can be continuous, we use the discretization module. Attributes register and its shadow copy serve as a temporary storage of discretized attributes. Attributes register and its shadow copy serve as a temporary storage of discretized attributes. From these registers, data get into two hardware comparator modules for the identifying their equality and inequality each other. Then, for all sets of compared attributes, the OR-operation is executed. The hardware comparator and OR module constitute modules for calculation a discernibility matrix and indiscernibility. The intermediate results of matrices calculations are stored in the parallel registers modules. When we apply AND-operation for all given results we obtain the discernibility and indiscernibility function. After parallel-to-serial transformation through the relevant registers, we can execute resulting AND-operation and provide obtain a resulted irreducible set of attributes, named also reduct or core set of a rough set.

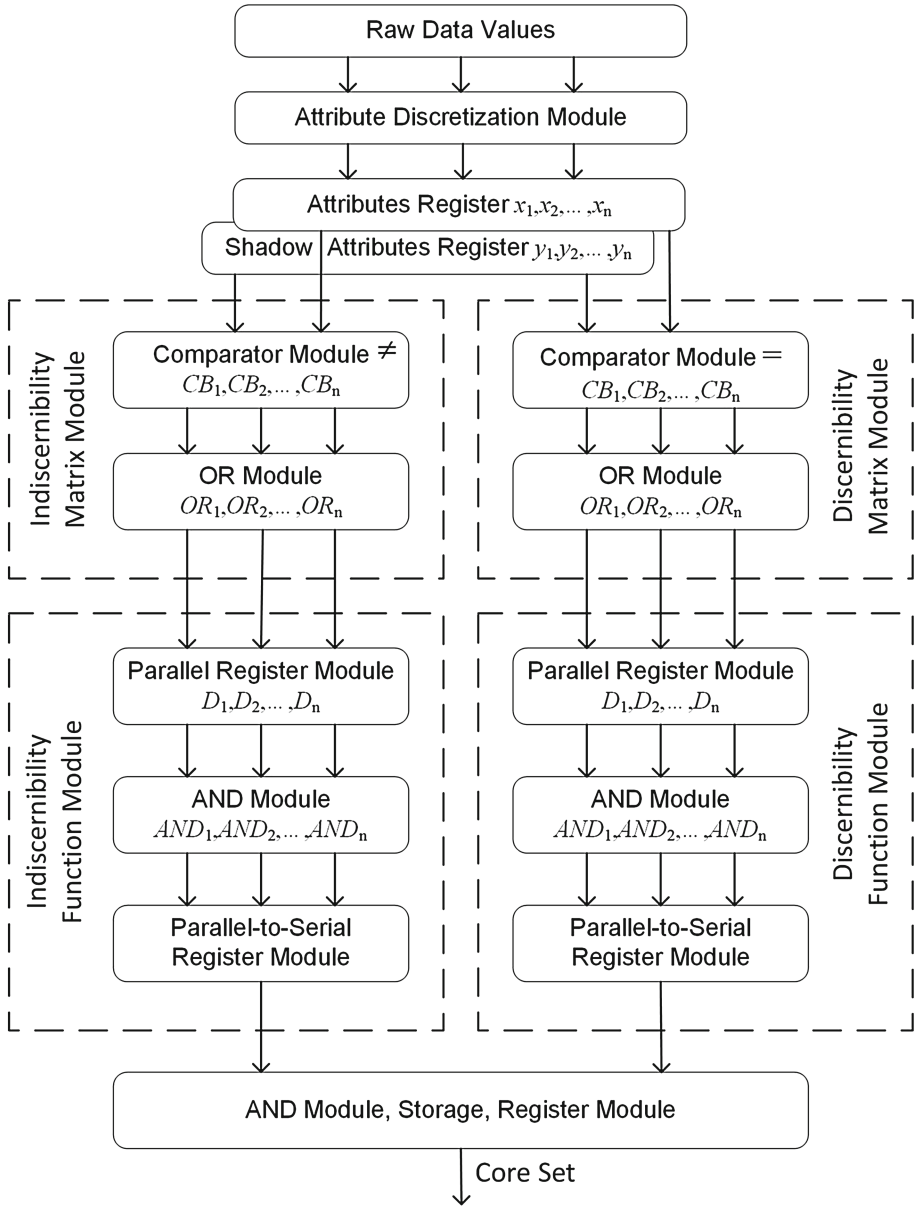


Fig. 2. A hardware implementation of preprocessing accelerator

5 Conclusions

This article has presented a study on various standards focused on SOs underlying architecture including existed middleware. A novel possible hardware


implementation of the FPGA-based acceleration module in mobile SOs architecture has proposed. The essence of the proposed approach is that all the functionality of the application server is divided into independent, loosely-connected, replaceable mobile SOs application services, the communication between which is executes through a special component using messages with predefined protocols. The proposed architecture can also be considered as a specialized information system service for mobile applications.

References

1. Vasseur, J.-P., Dunkels, A.: What are smart objects? In: *Interconnecting Smart Objects with IP. The Next Internet*, pp. 3–20 (2010). doi:[10.1016/B978-0-12-375165-2.00001-6](https://doi.org/10.1016/B978-0-12-375165-2.00001-6)
2. Garcia, C.G., Meana-Llorian, D., G-Bustelo, C.P., Cueva-Lovelle, J.M.: A review about smart objects, sensors, and actuators. *Int. J. Interact. Multimedia Artif. Intell.* **4**(3), 7–10 (2017). doi:[10.9781/ijimai.2017.431](https://doi.org/10.9781/ijimai.2017.431)
3. Ullah, S., Higgins, H., Braem, B., et al.: A comprehensive survey of wireless body area networks. On PHY, MAC, and network layers solutions. *J. Med. Syst.* **36**, 1065–1094 (2012). doi:[10.1007/s10916-010-9571-3](https://doi.org/10.1007/s10916-010-9571-3)
4. Vangelista, L., Zanella, A., Zorzi, M.: Long-range IoT technologies: the dawn of *LoRatm*. In: Atanasovski, V., Leon-Garcia, A. (eds.) *Future Access Enablers for Ubiquitous and Intelligent Infrastructures. LNICS, Social Informatics and Telecommunications Engineering*, vol. 159, pp. 51–58 (2015). doi:[10.1007/978-3-319-27072-2_7](https://doi.org/10.1007/978-3-319-27072-2_7)
5. Sicari, S., Capiello, C., Pellegrini, D., Miorandi, D., Coen-Porisini, A.: A security and quality-aware system architecture for internet of things. *Inf. Syst. Front.* **18**(4), 665–677 (2016). doi:[10.1007/s10796-014-9538-x](https://doi.org/10.1007/s10796-014-9538-x)
6. Rizzardi, A., Miorandi, D., Sicari, S., Capiello, C., Coen-Porisini, A.: Networked smart objects: moving data processing closer to the source. In: Mandler, B., et al. (eds.) *IoT360 2015, Part II. LNICST*, vol. 170, pp. 28–35 (2016). doi:[10.1007/978-3-319-47075-7_4](https://doi.org/10.1007/978-3-319-47075-7_4)
7. IoT 2020: Smart and secure IoT platform. White paper. <http://www.iec.ch/whitepaper/pdf/iecWP-loT2020-LR.pdf>. Accessed 08 Apr 2017
8. ISO/IEC CD 30141: Internet of Things Reference Architecture (IoT RA). <https://www.iso.org/standard/65695.html>. Accessed 08 Apr 2017
9. Y.2060: Overview of the internet of things. <https://www.itu.int/rec/T-REC-Y.2060-201206-I>. Accessed 08 Apr 2017
10. Industrial internet reference architecture V 1.8. <https://www.iiconsortium.org/IIRA.htm>. Accessed 08 Apr 2017
11. Reference Architectural Model Industrie 4.0 (RAMI 4.0). <https://www.plattform-i40.de/I40/Redaktion/EN/Downloads/Publikation/rami40-an-introduction.pdf>. Accessed 08 Apr 2017
12. IoT-A Architectural Reference Model (IoT-A ARM). <http://www.meet-iot.eu/deliverables-IOTA/D1.3.pdf>. Accessed 08 Apr 2017
13. Alliance for Internet of Things Innovation (AIOTI). <https://aioti-space.org/>. Accessed 08 Apr 2017
14. Gubbi, J., Buyya, R., Marusic, S., Palaniswami, M.: Internet of Things (IoT): a vision, architectural elements, and future directions. *Fut. Gen. Comp. Syst.*, **29**(7), 1645–1660 (2013). doi:[10.1016/j.future.2013.01.010](https://doi.org/10.1016/j.future.2013.01.010)

15. Sethi, P., Sarangi, S.R.: Internet of things: architectures, protocols, and applications. *J. Electr. Comp. Eng.* 25 p. (2017). doi:[10.1155/2017/9324035](https://doi.org/10.1155/2017/9324035). Article ID 9324035
16. Roalter L., Kranz M., Mller A.: A middleware for intelligent environments and the internet of things. In: Yu, Z., Liscano, R., Chen, G., Zhang, D., Zhou, X. (eds) *Ubiquitous Intelligence and Computing, UIC 2010*. LNCS, vol. 6406, pp. 267–281 (2010). doi:[10.1007/978-3-642-16355-5_23](https://doi.org/10.1007/978-3-642-16355-5_23)
17. Fortino, G., Guerrieri, A., Russo, W., Savaglio, C.: Middlewares for smart objects and smart environments: overview and comparison. In: *Internet of Things Based on Smart Objects Part of the Series Internet of Things*, pp. 1–27 (2014). doi:[10.1007/978-3-319-00491-4_1](https://doi.org/10.1007/978-3-319-00491-4_1)
18. Roalter, L., Kranz, M., Möller, A.: A middleware for intelligent environments and the internet of things. In: *Proceedings of the 7th International Conference on Ubiquitous Intelligence and Computing, UIC10*, pp. 267–281 (2010). doi:[10.1007/978-3-642-16355-5](https://doi.org/10.1007/978-3-642-16355-5)
19. Kawsar, F., Nakajima, T., Park, J.H., et al.: Design and implementation of a framework for building distributed smart object systems. *J. Supercomput.* **54**(1), 4–28 (2010). doi:[10.1007/s11227-009-0323-4](https://doi.org/10.1007/s11227-009-0323-4)
20. Fortino, G., Guerrieri, A., Russo, W.: Agent-oriented smart objects development. In: *Proceedings of the 2012 IEEE 16th International Conference on Computer Supported Cooperative Work in Design (CSCWD)*, Wuhan, pp. 907–912 (2012). doi:[10.1109/CSCWD.2012.6221929](https://doi.org/10.1109/CSCWD.2012.6221929)
21. Hashimi, S.Y., Steffan, S.J.: Service-oriented architecture. In: *Pro Service-Oriented Smart Clients with .NET 2.0*, pp. 247–268 (2005). doi:[10.1007/978-1-4302-0058-1_9](https://doi.org/10.1007/978-1-4302-0058-1_9)
22. Chernov, A.V., Butakova, M.A., Karpenko, E.V.: Security incident detection technique for multilevel intelligent control systems on railway transport in Russia. In: *2015 23rd Telecommunications Forum Telfor (TELFOR)*, pp. 1–4 (2015). doi:[10.1109/TELFOR.2015.7377381](https://doi.org/10.1109/TELFOR.2015.7377381)
23. Chernov, A.V., Butakova, M.A., Vereskun, V.D., Kartashov, O.O.: Situation awareness service based on mobile platforms for multilevel intelligent control system in railway transport. In: *2016 24th Telecommunications Forum (TELFOR)*, Belgrade, pp. 1–4 (2017). doi:[10.1109/TELFOR.2016.7818714](https://doi.org/10.1109/TELFOR.2016.7818714)
24. Chernov, A.V., Bogachev, V.A., Karpenko, E.V., Butakova, M.A., Davidov, Y.V.: Rough and fuzzy sets approach for incident identification in railway infrastructure management system. In: *2016 XIX IEEE International Conference on Soft Computing and Measurements (SCM)*, St. Petersburg, pp. 228–230 (2016). doi:[10.1109/SCM.2016.7519736](https://doi.org/10.1109/SCM.2016.7519736)
25. Chernov, A.V., Guda, A.N., Kartashov, O.O.: Cloud-assisted middleware for intelligent distributed and mobile objects. In: Abraham, A., Kovalev, S., Tarassov, V., Snel, V. (eds.) *Proceedings of the First International Scientific Conference “Intelligent Information Technologies for Industry” (IITI16)*. AISC, vol. 451, pp. 271–280 (2016). doi:[10.1007/978-3-319-33816-3_27](https://doi.org/10.1007/978-3-319-33816-3_27)
26. Pawlak, Z.: *Rough Sets: Theoretical Aspects of Reasoning About Data*. Kluwer Academic Publishing, Dordrecht (1991). doi:[10.1007/978-94-011-3534-4](https://doi.org/10.1007/978-94-011-3534-4). 231 p
27. Skowron, A., Rauszer, C.: The discernibility matrices and functions in information systems. In: *Intelligent Decision Support. Theory and Decision Library*, vol. 11, pp. 331–362 (1992). doi:[10.1007/978-94-015-7975-9_21](https://doi.org/10.1007/978-94-015-7975-9_21)
28. Tiwari, K.S., Kothari, A.G.: Design and implementation of rough set algorithms on FPGA: a survey. *Int. J. Adv. Res. Artif. Intell.* **3**(9) (2014). doi:[10.14569/IJARAI.2014.030903](https://doi.org/10.14569/IJARAI.2014.030903)

Intellectualization of Sorting Processes Control on the Basis of Instrumental Determination of Analogies

A.N. Shabelnikov and N.N. Lyabakh 

Rostov State Transport University, Rostov-on-Don, Russia
shabelnikov@rfniias.ru, liabakh@rambler.ru

Abstract. An analogy represents a component of human and/or machine intellectual activity. The task of mathematical definition of the analogies has been formed and solved which allowed a transition from a traditional logical and linguistic handling of analogies to the instrumental utilization thereof, thus ensuring a possibility to apply a well-developed mathematical instrumentarium for analysis and control of the complex technical and technological and socio-economical systems. The task of sorting processes control on the basis of analogies has been actualized. The main notions related to analogies have been commented on the example of the mentioned technical and technological task. In this work, two algorithms of sorting processes control using expert information and iterative teaching of decision-making to a machine have been offered.

Keywords: Analogy: verbal and instrumental determination · Gravity hump · Retarding mechanism · Analogy-based control algorithms

1 Introduction

In his article, an analogy is regarded as one of the bases of the natural human intelligence used to solve the task of making complex decisions [1]. The research sets a task to translate this methodological mode into the artificial intelligence systems. For this purpose, an instrumentarium of mathematical description of analogies and handling thereof is being developed.

The notion of analogy is closely related to such notions as recognitions, metaphor, figure, mathematical structures, etc. [2–4]. Still, if a metaphor understands a reinterpretation of a meaning of the word based on the similarity, the analogy is an object and the subject of mental activity. Metaphor is aimed at the verbal reflection of the analogy [3].

The analogy is the main means of making mathematical statements [2, 4]. Using analogy as a basis, the classes of tasks, the structures and the types of models are being formed; it is used for elaboration of the invariant theory which generalizes the properties of objects of different nature on the level of mathematical abstractions [2–4].

In its existing interpretation, the analogy is not a strict method and may lead to false conclusions. But the analogy serves as a basis for acquiring of experience as a result of human activities. It can be viewed both as a forerunner and the result of insight [5].

The analogy is not only the tool for mental activity. It underlies our universe. All complex structures seeming chaotic at first sight (mountain clusters and ice patterns, structure of a plant leaf and a forest of plants, heart rhythm and the structure of bronchi) are built on the algorithms in which a part is similar to the whole, that is, on analogies [6]. These cannot be described by means of classical mathematics and Euclidian geometry. Theory of fractals gives the mathematical instrumentarium to describe the controlled chaos.

The above-stated makes the elaboration of models for description and computational methods of implementation of analogies [7]. This article does not give an author's definition of analogies, but only uses the existing ones. The authors see their task as formalization of the notion concerned.

For the sake of convenience of presentation, all novelties introduced will, if possible, be commented by means of a technical and technological task of management and control of cuts of cars on a gravity hump [8, 10].

2 Content of the Article

2.1 Control of Retardation of a Gravity Hump

Gravity humps of marshalling yards are meant for splitting up the trains arriving from one address into several new destinations. From the hump crest, the train that arrived is split into separate cuts of cars which roll down under the influence of the initial kinetic energy and the potential energy of position, and then roll into various directions from the points. Due to the different physical properties, the cuts have different ride characteristics; to control the cuts, these are classified in first approximation as "good" and "bad" runners. Other more detailed classification schemes are also possible. The cuts from the first group (the "good" runners) are braked harder on the hump retarders in order to prevent both a collision with the cut of cars moving ahead (which will cause a loss of the correct route), and a collision with the cuts of cars in the train forming pool at the speed exceeding the permitted value (which will cause the breakage of the cars and the cargo). By contrast, the cuts from the second group (the "bad" runners) are braked less on the hump retarders so that such cuts would not be hit by the cuts that follow and to let such cuts roll into place in the train forming pool.

The task of control of the cuts can be extended by including the properties of the environment (weather and climatic conditions, condition of the hump railways) and the control equipment properties (parameters and current state of retarding mechanisms) into the analysis.

The classification of the cuts of cars as per ride characteristics underlies the procedure of control of the cuts. Within the existing automatic systems of sorting process control, this task is solved by means of image recognition theory [4]. It is proposed hereinafter to solve the same task by method of analogies.

2.2 Analogies: Definition and Role in Decision-Making

Analogy is a sort of statement which presents a similitude of objects of phenomena in certain properties, traits or relations [1, 5]. The logic uses such terms as “reasoning by analogy”, or “inference by analogy” to determine an inductive inference (i.e., decision) on the properties of one object based on the similarity with these or other properties of the other object(s). General patterns of inference by analogy can be represented as follows:

1. If the object O_1 has the properties $S_1, S_2, \dots, S_n, S_{n+1}$, and the object O_2 has the properties S_1, S_2, \dots, S_n , there is then a certain probability that the object O_2 also possesses the property S_{n+1} . A certain class of object can act as S_{n+1} . It means that if the object O_1 belongs to a described class, the object O_2 does also belong to the same class provided the presence of the analogy between these objects.
2. The objects O_1, O_2, \dots, O_n of a certain class have a property S ; it is then probable that the object O_{n+1} of the same class also has the property S .

There is an entire range of various forms of inference behind the general schemes of reasoning by analogy; these forms can be placed ascending order of conclusion consistency which currently has no mathematical apparatus for evaluation. Among the conditions that increase the probability of a conclusion, there are such conditions as:

- increased number and diversity of the properties or objects compared (width of analogy);
- importance of the properties compared (depth of analogy);
- dependence of the transferred property on the common properties compared;
- lack of properties with the object that admittedly exclude the transferred property.

It must be nevertheless stated that:

- observation of such conditions does not guarantee the complete consistency of the inference by analogy;
- there is a lack of methods of evaluation for the depth and width of analogy, or the consistency of the properties transferred, or the structure that either promotes or inhibits the transfer of the properties.

This research offers an instrumentarium which allows a partial or a complete resolution of the above listed problems of using the analogies in the task of decision-making.

2.3 Instrumental Determination of Analogies

Correspondence of the properties to the objects is represented as a matrix structure.

For a selected group of homogenous objects, the experts define their properties as S_1, S_2, \dots . Let us find the joining of these sets for all experts. Consequently, we obtain a complete set of the properties of the objects respective of the given group of experts. In case that some properties of the object O_1 coincide with the properties of the object O_2 , we will be able to say that the object O_1 is to some extent analogous to the object

O₂. Let us define the operation of drawing an analogy as A. A formal record of this statement looks like:

$$O_1AO_2. \tag{1}$$

Analogies may have different strengths. For example, we define the analogy in one property S_i via O₁A_iO₂, and the analogy in four properties S₁, S₂, S₄, S₈ via O₁A₁₂₄₈O₂, etc. the second analogy is obviously stronger than the first one. In the absence of coinciding properties,

$$O_1A_0O_2 = 0. \tag{2}$$

If the entire range of properties n coincide, then

$$O_1A_{1\dots n}O_2 = 1. \tag{3}$$

Obviously:

$$O_1AO_2 \rightarrow O_2AO_1. \tag{4}$$

It is also obvious that if

$$O_1AO_2, \text{ and } O_2AO_3, \text{ then } O_1AO_3. \tag{5}$$

Let us assume that we have *m* objects characterized in general *n* by the properties S_{*i*}. The common formal description can be given as a table, see Table 1.

Table 1. Formal description of objects and properties thereof

	O ₁	O ₂	...	O _m
S ₁	+	-		-
S ₂	-	+		-
...				
S _n	-	+		+

In Table 1, the “plus” symbols denote which objects have which properties. For example: the object O₂ has the properties S₂ and S_n, and does not have the property S₁.

The traits which characterize the properties of the objects under consideration within our problem can be divided into a priori properties obtained prior to an experiment (in our case, the experiment means the rolling of the cuts from the hump) and a posteriori properties obtained as a result of the experiment (rolling the cuts from the hump).

Technical appliances and technologies, socio-economical objects and processes, plants or animals (including humans) and other objects of wildlife and inorganic nature can act as the objects of research. The presence of one or another degree of analogy leads to a certain class of the existing classification scheme.

Let us introduce the evaluation of importance of *i*-th property of the objects: *p_i*. This is the extent to which the objects are defined by this property. For example, the properties

of the cut on the hump slope and on a horizontal stretch are not equivalent. The cut weight value on the slope prevails over the role rolling friction resistance, and by contrast, the rolling friction plays a greater role on a horizontal stretch. It is evident, that the relation $\sum p_i = 1$ must apply.

It is now possible to carry out a quantitative evaluation of analogies.

Problem 1. Let us consider four cuts of cars characterized by three properties: S_1 – heavy cut, S_2 – cut with regular wheel base, S_3 – cut with low rolling resistance. The properties of the selected cuts are shown in the Table 2.

Table 2. Initial data of the example

	O ₁	O ₂	O ₃	O ₄
S ₁	+	+	–	–
S ₂	+	–	+	–
S ₃	+	+	+	–

Thus, for example, the cut O₂ has the properties S₁ and S₃, and does not have the property S₂. Let us consider the following two cases.

1. The structure of the properties is binary, that is the properties have only two values. For instance, a cut may be “heavy” and “not heavy”, it may have a regular or extended wheel base, and it may have a “low” rolling resistance or “not low” rolling resistance. In this case, the presence of one property means the absence of the other – opposite property.
2. The structure of the properties is multiform, that is, the properties of the cuts have more than two values. For example, the cut can be “very heavy”, “heavy”, “middle”, “light”, etc. In this case, the absence of one property does not obligatorily witness the presence of another (alternative) property with the object.

It is obvious, that the first case is characterized by a higher degree of determination which can consequently be reflected in the stronger analogies.

Let us assume that the properties of the cuts are different: S₁ has a weight of 0.5, S₂ has a weight of 0.3, and the weight of S₃ equals to 0.2. Then, for the cases 1 and 2 we obtain the following tables of the importance of analogies (Tables 3 and 4, respectively).

Table 3. Quantitative evaluation of analogies with binary properties

	O ₁	O ₂	O ₃	O ₄
O ₁	1	0,7	0,5	0
O ₂	0,7	1	0,2	0,3
O ₃	0,5	0,2	1	0,5
O ₄	0	0,3	0,5	1

Table 4. Quantitative evaluation of analogies with multi value properties

	O ₁	O ₂	O ₃	O ₄
O ₁	1	0,7	0,5	0
O ₂	0,7	1	0,2	0
O ₃	0,5	0,2	1	0
O ₄	0	0	0	1

Diagonally, the matrix contains units because the objects are one hundred percent analogous to each other ($P_{ii} = 1$). $P_{12} = P(O_1AO_2) = 0,7$ while the first and the second objects coincide as per properties 1 and 3, with the respective weights of 0.5 and 0.2. $P_{14} = 0$ while the first and the fourth objects have no coinciding properties. $P_{34} = P(O_3AO_4) = 0,7$ while the property alternative for S_1 coincides with these objects.

In the first case, disjunction is used to evaluate the strength of analogy, and in the second case, conjunction is used.

We will subdivide the properties of the objects into a priori properties obtained prior to an experiment (in our case, the experiment means the rolling of the cuts from the hump) and a posteriori properties obtained as a result of the experiment.

The objects with both a priori and a posteriori properties known form a training sequence of data. This sequence can be seen as a table of objects and the full sets of properties thereof. Based on this table, the analogies are established which are then transferred onto the objects which do not yet have a posteriori data; this means that the probability forecasting of the properties of objects under consideration takes place. Table from the problem 2 can be used as an example of such table.

Problem 2. In the Table 5, the properties S_1 – S_5 characterize the weight of the cut of cars (shown in brackets), and the properties S_6 , S_7 refer to the ride characteristics of the cuts. The properties S_1 – S_5 belong to a priori properties. These have been known prior to rolling the cut from the hump. The properties S_6 and S_7 are a posteriori properties revealed after the rolling of the cut.

Table 5. Making decisions by analogy

	O ₁	O ₂	O ₃	O ₄	O ₅	O ₆
S ₁ (20–50)	+					
S ₂ (51–100)			+			
S ₃ (101–270)					+	
S ₄ (271–350)				+		+
S ₅ (351 and further)		+				
S ₆ – “good” runner		+		+	+	?
S ₇ – “bad” runner	+		+		+	?

The cuts O_1 , O_3 having respective properties S_1 and S_2 are “bad” runners, and the cuts O_2 and O_4 having respective properties S_5 and S_4 are “good” runners. The cut O_5 having the property S_3 , also has the properties S_6 and S_7 . The last statement means that if the cut weighs within the range from 101 to 270 tons, it can be thus both a “good” and

a “bad” runner. The cut O_6 is known to have the property S_4 . Should a decision be made by analogy which if the properties, S_6 or S_7 this cut has? By applying the analogy, it can be said that the cut O_6 also has the property S_4 .

2.4 Analogy-Based Control Algorithms of Retarding Mechanism Control on Gravity Hump

Below are the two simple algorithms (linear algorithms with no conditional transfer) of decision-making on belonging of the object to a certain class. In our example, we deal with the determination of a cut to a certain runner type.

A1:

- A threshold level of the analogy importance is being set.
- Based on a priori properties, the degrees of analogies between the object under research and the objects from the training sequence are being calculated.
- All objects having the level of degree of analogy with the object under consideration not less than the set level are being selected from the training sequence.
- These objects “vote” with the consideration of the weights of analogies for the belonging to one class or another. The weights can be considered by either multiplicative or additive convolution.
- The decision is being made by means of comparison of integral votes for each class.

A2:

- Based on a priori properties, the degrees of analogies between the object under research and the objects from the training sequence are being calculated.
- The object having the highest value of the analogy degree is being determined.
- The object under research is being assigned the class of the nearest object from the training sequence.

Below are the tasks and problems requiring an additional explanation:

1. Who and in what manner is to define the threshold level of the importance of the analogies? This problem has to be solved by the expert in virtue of the security of decisions recognition. Decrease of the threshold level expands the number of objects in the training sequence taken into consideration which increases the statistical reliability of decision-making.
2. Selection of informative a priori traits of the objects. Only the traits/properties are left which have significantly different values as per classes (a posteriori properties).
3. Weight evaluation of the properties. Within the algorithms, an iterative procedure of weight correction is being formed to help increase the probability of a correct recognition of decisions based on the training sequence.

3 Conclusion

Currently, the analogy is an insufficiently formalized tool of new knowledge introduction. This fact often leads to incompleteness and ambiguity of notion about the object under research. Thus, the task of a formalized description of analogies becomes crucial,

and the solution of this task will allow a regulation and elaboration of the procedure of decision-making by analogy. This article offers a mathematical method of description for analogies which enables the handling of analogies by using the mathematical formal descriptions already known. As an exemplification, this article uses a problem of sorting processes control on the basis of analogies. Within the framework of the article, two algorithms of sorting processes control have been developed which use the expert-provided information and the iterative teaching methods of decision-making to a machine.

References

1. Kubryakova, E.S.: Analogy. In: Encyclopedic Dictionary of Linguistics, pp. 31–32, Moscow, SE (1990). [E.S. Kubryakova, Analogiya. Entsiklopedicheskiy Slovar Lingvistiki, M., 1990, pp. 31–32]
2. Krieger, M.: Doing Mathematics: Convention, Subject, Calculation, Analogy, 2nd edn. World Scientific, Singapore (2015)
3. Lyn, D.: English: Mathematical Reasoning: Analogies, Metaphors, and Images. Routledge, Oxford (2013)
4. Spitterts, B., Van Der Weegen, E.: Type classes for mathematics in type theory. *Math. Struct. Comput. Sci.* **21**(4), 795–825 (2011)
5. Gentner, D., Smith, L.: Analogical reasoning. In: Ramachandran, V.S. (ed.) *Encyclopedia of Human Behavior*, 2nd edn, pp. 130–136. Elsevier, Oxford (2012)
6. McGreggor, K., Kunda, M., Goel, A.K.: Fractal analogies: preliminary results from the Raven's test of intelligence. In: *Proceedings of the Second International Conference on Computational Creativity (ICCC)*, Mexico City, pp. 69–71 (2011)
7. Gentner, D., Forbus, K.D.: Computational models of analogy. *WIREs Cogn. Sci.* **2**, 266–276 (2011)
8. Shabelnikov, A.N.: *Intelligent Control Systems in Railway Transport: A Monograph*. All-Russian Scientific Research Institute of Automation and Communication on Railroads under the Russian Federation Ministry of Transport, RSTU, Southern-Russian Scientific Center of the Russian Academy of Sciences, Rostov-on-Don (2004). 214 pages. [Shabel'nikov A.N. *Intellektual'nyye sistemy upravleniya na zheleznodorozhnom transporte: Monografiya*. Rostov n/D: VNIAS MPS RF, RGUPS, YURNTS RAN, 2004. – 214 s.]
9. Asadurov, S.E., Gapanovich, V.A., Lyabakh, N.N., Shabelnikov, A.N.: *Railway Transport: On a Way to Intelligent Control: A Monograph*. Southern-Russian Scientific Center of the Russian Academy of Sciences, Rostov-on-Don (2009). 322 p. [Adadurov S.E., Gapanovich V.A., Lyabakh N.N., Shabel'nikov A.N. *Zheleznodorozhnyy transport: na puti k intellektual'nomu upravleniyu*. Monografiya. – Rostov-na-Donu: YUNTS RAN, 2009. – 322 s.]
10. Lyabakh, N.N., Shabelnikov, A.N.: *Technical Cybernetics in Railway Transport: A Handbook*. RSTU, North-Caucasian Scientific Center of Higher School, Rostov-on-Don (2002). 283 p. [Lyabakh, N.N., Shabel'nikov, A.N.: *Tekhnicheskaya kibernetika na zheleznodorozhnom transporte: Uchebnik* – RGUPS, SKNTs VSh (2002), 208 s.]
11. Uyemov, A.I.: *Analogy in the Practical Scientific Research*, Moscow (1970). 262 p. [Uyemov A.I. *Analogiya v praktike nauchnogo issledovaniya*. – M., 1970. – 262 s.]

Evaluation of the Intelligence Degree of Systems

M.V. Kolesnikov and Ya.M. Gibner^(✉)

Rostov State Transport University, Rostov-on-Don, Russia
Kmv-d@list.ru, Gibner88@gmail.com

Abstract. This paper is devoted to the study of approaches to the evaluation of intelligent systems. The paper proposes a technique that takes into account existing classical methods and allows to obtain an integral assessment. Approaches to optimization of complex processes are described and demonstration calculations are made.

Keywords: Intellectuality of the system · Evaluation of intellectuality · Private and integral criteria · Convolution of criteria · Pareto method · Main criterion method

1 Introduction

The development of systems of intellectual functioning (SIF) inevitably leads to the need to measure the degree of their intellectuality. At present, the question of assessing the intellectuality of systems (IS) has not been studied sufficiently. Therefore, it has a wide potential for further study and is very relevant.

Since the initial emergence of SIFs, many scientists and researchers have been trying to evaluate their intellectuality [1–6]. There are several stable trends in approaching this problem.

The first one is based on an attempt to use the same tools that are distributed and recognized in evaluating the human intelligence. These are all possible testing methods [2, 5, 7]. Thus, the difference between artificial and natural intelligence is blurred, and this approach has a number of serious limitations. The drawbacks that this method has in the context of human intellect evaluation (the assessment of intelligence is replaced by the evaluation of knowledge, subjectivity of tests, etc.) are repeatedly amplified by ignoring the specifics of artificial intelligence [8].

The second direction of the evaluation of IS is carried out in the framework of measuring the performance of the system according to some predefined, specific criterion [1]. To evaluate IS, that was designed to solve a broad range of tasks (including unplanned, arising in the course of activities), obviously, another approach is needed. Such systems should have adaptability, be self-teaching. Accordingly, their evaluation should be different and must be based on other principles.

The third direction is based on a comparison of the results of natural and artificial intelligence. The intelligence of the machine is compared to the intelligence of a person who solves similar problems [2, 5, 7, 15].

These studies do not take into account a number of features of IS estimation: the role and influence of the external environment, the properties of the SIF itself, the value of the SIF for users. The lack of systematic approach to the formulation and solution of the problem of IS assessment has determined the range of questions studied in this article.

In Sect. 2 of this article, a brief analysis of studies on the evaluation of system intelligence is presented. The third section describes in detail the original method of IS evaluation proposed by the authors. In the fourth section, some practical results of its use are presented. And in the fifth section, the result of the whole research work is summed up.

Discussions about the advantages and disadvantages of one method or another in IS estimation have no basis. Each of them describes one of the important aspects of the process under investigation: the generation and use of intelligence (natural or artificial). And this importance varies with time, and under external and internal circumstances.

2 Related Work

The authors of work [8] assume that a computer program that can successfully solve human intelligence problems has the intelligence equal to human level and vice versa.

On the one hand, speaking about the human intellect, one can mean that it is better than the average representative of the corresponding intellectually complex fields (such as mathematics, physics). That is, the SIF is subject to unrealistic demands.

On the other hand, the term “intelligence” is traditionally used to compare and compare human abilities with other species (e.g., animals). Thus, the very concept of “intelligence” is deformed.

In the context of cognitive modelling, the performance parameters of computer models (for example, the number of iterations for solving the problem) are compared [8] to the data obtained from empirical studies with human decision makers. For example, the time required for solving a problem.

The same person shows different values of IQ intelligence index for different tests since they reflect the specificity of the professional field and/or sphere of human activity. As a result, it becomes obvious that the use of human intelligence tests in IP research (and similar ones) is useful, but one should be careful about the semantic and quantitative interpretation of the results.

At the same time, special attention should be given to the development of completely new tests specifically designed for assessment of IS. As a basis, one can use algorithmic information theory [10, 11], cognition models [12], their hybridization with cognitive generalizations of the Turing test [13] or generalizations of psychometrics [14], where tests are created for any cognitive system, regardless of its type or environment.

In [1], the authors come to the conclusion that when evaluating intellectuality, not only factors such as adaptability and reliability must be taken into account, but attention should also be paid to the final impact that the SIF has on the environment. Momentary behavior can be a rich source of information that sheds a lot of light on how a certain level of performance is achieved.

Thus, in all the diversity of approaches, methods and views on the evaluation of intellectuality, there is no single point of view. In this article, we propose an assessment method based on a combination of different points of view and evaluation methods.

3 The Proposed Method

Discussions about the advantages and disadvantages of one method or another in IS estimation have no basis. Each of them describes one of the important aspects of the process under investigation: the generation and use of intelligence (natural or artificial). And this importance varies with time, and under external and internal circumstances.

It is possible to evaluate the ability of the system to transmit to the machine to the natural intelligence of the decision-making subject – u_1 , the ability to adapt to changing operating conditions – u_2 , the ability of the system to generate new knowledge – u_3 , etc.

In practice, an effective evaluation can be achieved by means of a combination of the above partial estimates. Therefore, it is further proposed to estimate the IS by a vector:

$$u = (u_1, u_2, \dots, u_n). \quad (1)$$

The implementation of a proper IS evaluation is a complex problem and therefore requires the use of the services of qualified IS evaluation experts who are able to critically analyze a variety of assessment contexts.

As a development of existing methods of IS estimation, it is suggested to use the methodology described in [4, 9] to assess the degree of innovativeness of the product (system). We adapt it to the current task - assessing the intelligence of the system.

Let's try to represent the estimate of the IS in the form of a function V (2) combining in its components all the existing partial estimates of the IS U_n and all possible states of the environment S_k in which the CIFs exist.

$$V : U_n \times S_k \rightarrow \mathbf{R}, \quad (2)$$

where \mathbf{R} is the set of real numbers.

Partial estimates of IS (1) will be represented in scaled coordinates u_i , whose values belong to the interval $[0; 1]$.

The existing environment can also be defined by a certain set of parameters the values of which evaluate its most essential features $s = (s_1, \dots, s_k)$, $s_i \in [0; 1]$. Here, for example: s_1 is the degree of demand for intellectual functioning in a given process (for reasons of quality and/or safety of the process under study), s_2 is the intellectuality of competing systems, s_3 is economic effect achieved via introduction of intellectuality, etc.

Scaling of investigated variables and parameters within the range of values from 0 to 1, can be carried out by means of the following formula (3):

$$x_i = \frac{\tilde{x}_i - \tilde{x}_{\min}}{\tilde{x}_{\max} - \tilde{x}_{\min}}, \quad (3)$$

where $x \in [0; 1]$. In formula (3) \tilde{x} is a generalizing indicator, in which both u and s can be substituted.

The exposed values of the environment will be the same for a certain number of compared objects, since most often intellectual systems of one group exists in the same environment.

Using the weighting coefficients a_{ij} that make up the characteristic matrix of the situation A (of dimension $n \times k$), we determine how large the influence of the corresponding combination of factors u_i (estimating the completeness and accuracy of the selected particular estimates) and s_j (estimating the current state of the medium) on the function V .

$$A = \begin{pmatrix} a_{11} & a_{12} & a_{13} & \dots & a_{1k} \\ a_{21} & a_{22} & a_{23} & \dots & a_{2k} \\ a_{31} & a_{32} & a_{33} & \dots & a_{2k} \\ \dots & \dots & \dots & \dots & \dots \\ a_{n1} & a_{n2} & a_{n3} & \dots & a_{nk} \end{pmatrix}. \tag{4}$$

We multiply the row matrix u with the matrix (4) of the weight coefficients A , and then with the transposed matrix row s in the order indicated in (5) [16]:

$$V = (u_1 \quad u_2 \quad u_3 \quad \dots \quad u_n) \times \begin{pmatrix} a_{11} & a_{12} & a_{13} & \dots & a_{1k} \\ a_{21} & a_{22} & a_{23} & \dots & a_{2k} \\ a_{31} & a_{32} & a_{33} & \dots & a_{3k} \\ \dots & \dots & \dots & \dots & \dots \\ a_{n1} & a_{n2} & a_{n3} & \dots & a_{nk} \end{pmatrix} \times \begin{pmatrix} s_1 \\ s_2 \\ s_3 \\ \dots \\ s_k \end{pmatrix}. \tag{5}$$

As a result, we obtain the desired formula (6).

$$V = u \times A \times s^t, \tag{6}$$

where t is the sign of transposition.

Private assessments of IS and factors characterizing the environment are evaluated with the help of experts. Experts should evaluate the given characteristics in the format of linguistic utterances, using qualitative characteristics of features.

The interval of scalable values of V will belong to the segment from 0 to the product of $n \times k$.

$$V \in [0; n \times k],$$

where

- n is the number of features in the vector u characterizing the IS;
- k is the number of features in the vector s characterizing the environment.

The value of V is scalar. With the help of formulas (5) and (6) it is possible to solve various problems of analysis:

- comparison of objects with each other (choosing the best);

- the state of the object at different times (in relation to the IS);
- management of IS.

Comparing different environments quantitatively, one can see which of them is developed more innovatively.

With an accurate and adequate IS evaluation tool, it is possible not only to exercise current control over the situation, but also to forecast further developments. It becomes possible to control the IS by adjusting the factor u_i , the level of which was not high enough.

Currently, there are several approaches to optimizing complex processes characterized by a vector of indicators (we have a vector (1)). The most well-known of them are:

1. Convolution (additive or multiplicative) of criteria. For example, for additive convolution we have:

$$\text{Max } \sum_1^n c_i u_i, \quad (7)$$

where c_i are the weighting factors of the importance of the individual intelligence indicators of the system that are set by the experts.

This method has the main drawback which is that the values of some indicators are compensated by others. The overall indicator “hides” private shortcomings.

2. The Pareto method is a method of not degrading solutions: the parameters u_i change as long as each of them, under existing constraints, has the possibility of improvement. The method requires knowledge of analytic relations between parameters, which in our problem is an independent additional problem.
3. The method of the main criterion. Out of the set of particular indicators (criteria) u_i , the main criterion u_z is chosen, which is maximized (8), and the others are constrained - thresholds u_{in} , which do not allow to “skip” a system with insufficient level of intelligence (9).

$$\text{Max } u_z, \quad (8)$$

$$u_i \geq u_{in}. \quad (9)$$

An important factor in the latter method is the definition of the purpose for which an IS valuation is carried out. This purpose determines the main criterion. One of the main difficulties with this method is the determination of threshold values (9) for nonprincipal criteria. There are special methods to solve this problem [15].

4 Experimental Results

Let us consider, as an example, the evaluation of two systems in railway transport claiming the status of intelligent functioning: the Russian Integrated Automation System for Marshalling Yard Control (IAS MYC) and its German analogue (by implemented

functions) MSR-32. Experts of the above systems - practical workers of the sorting systems in Russia - acted as experts. Let us take the criteria listed at the beginning of the article and reflect the features of the functioning of the sorting stations in Russia as the factors characterizing IS and the environment.

Let these factors be the following:

- u_1 – the ability of the system to translate the machine intelligence to the natural intelligence of the decision-making subject;
- u_2 – ability to adapt to changing operating conditions;
- u_3 – the ability of the system to generate new knowledge;
- s_1 – the degree of demand for intelligent functioning in a given process (from considerations of quality and/or safety of the process under study);
- s_2 – intellectuality of competing systems;
- s_3 – the economic effect achieved through the introduction of intellectuality.

The experts put the following estimates (taking into account the scaling procedure already carried out according to the formula (3)) on the parameters necessary for the calculation:

- IAS MYC – (0,9; 1; 0,8);
- MSR-32 – (0,7; 0,4; 0,8);
- environment – (0,9; 0,9; 1);
- weighting coefficients a_{ij} – $\begin{pmatrix} 0,9 & 1 & 0,8 \\ 0,7 & 0,8 & 1 \\ 0,6 & 1 & 0,8 \end{pmatrix}$.

Having obtained the data, we calculate the level of IS for each sorting system according to the formula (6):

$$V_1 = (0,9 \quad 1 \quad 0,8) \times \begin{pmatrix} 0,9 & 1 & 0,8 \\ 0,7 & 0,8 & 1 \\ 0,6 & 1 & 0,8 \end{pmatrix} \times \begin{pmatrix} 0,9 \\ 0,9 \\ 1 \end{pmatrix} = 6,401;$$

$$V_2 = (0,7 \quad 0,4 \quad 0,8) \times \begin{pmatrix} 0,9 & 1 & 0,8 \\ 0,7 & 0,8 & 1 \\ 0,6 & 1 & 0,8 \end{pmatrix} \times \begin{pmatrix} 0,9 \\ 0,9 \\ 1 \end{pmatrix} = 4,489,$$

where:

- V_1 is the estimate of IAS MYC;
- V_2 is the MSR-32 score.

For stronger clarity, we scale the results obtained by the use of formula (3) in the interval from 0 to 1 (where 0 is the lack of intelligence, and 1 is the maximum possible intelligence of the system):

- $V_1 = 0,711$;
- $V_2 = 0,499$.

5 Conclusion and Future Work

As it can be seen from the calculations, the level of intelligence of IAS MYC significantly exceeds the one of MSR-32. This is due to the fact that the latter system has significant restrictions of the functions of adaptation, which are quite important for intelligent systems utilized in Russia.

This example shows the operability of the described technique and with real data (and experts) it allows to obtain accurate and unbiased results on the state of the level of intelligence in each particular system chosen.

It is possible to draw the following conclusions.

1. The possibility of estimating IP by means of some function V, which combines all existing private estimates of IP in its components, is justified.
2. There was proposed:
 - IS model;
 - the method for optimizing complex processes characterized by a vector of specific indicators.
3. The operation principle of the above IS estimation model was illustrated by a practical example (the evaluation of two systems in railway transport: IAS MYC and MSR-32).

References

1. Bieger, J., Thorisson, K.R., Steunebrink, B.: Evaluation of general-purpose artificial intelligence: why, what & how. In: EGPAI 2016 - Evaluating General-Purpose AI, The Netherlands (2016)
2. Turing, A.M.: Computing machinery and intelligence. *Mind* **59**(236), 433–460 (1950)
3. Legg, S., Hutter, M.: Tests of machine intelligence. CoRR, abs/0712.3825. [arXiv:0712.3825](https://arxiv.org/abs/0712.3825) (2007)
4. Gibner, Ya.M.: The entrepreneurial environment and innovations interaction modeling. *Kybernetika*, № 6, pp. 11–14 (2011)
5. Marcus, G., Rossi, F., Veloso, M.: Beyond the turing test. In: *AI Magazine*, vol. 37, 1st edn. AAAI (2016)
6. Thorisson, K.R., Bieger, J., Schiffel, S., Garrett, D.: Towards flexible task environments for comprehensive evaluation of artificial intelligent systems & automatic learners. In: *Proceedings of AGI-15*, pp. 187–196. Springer, Berlin (2015)
7. Bringsjord, S., Schimanski, B.: What is artificial intelligence? Psychometric AI as an answer. In: *IJCAI*, pp. 887–893. Citeseerx (2003)
8. Besold, T., Hernandez-Orallo, J., Schmid, U.: Can machine intelligence be measured in the same way as human intelligence? *KI-Kunstl. Intell.* **29**, 1–7 (2015)
9. Shabelnikov, A.N., Gibner, Ya.M.: Management of the development of innovative projects. *Soc. Polit. Econ. Law* **1**, 27–30 (2016)
10. Hernandez-Orallo, J.: Beyond the turing test. *J. Logic Lang. Inf.* **9**(4), 447–466 (2000)
11. Legg, S., Hutter, M.: Universal intelligence: a definition of machine intelligence. *Mind. Mach.* **17**(4), 391–444 (2007)

12. Mueller, S.T., Jones, M., Minnery, B.S., Hiland, J.M.H.: The BICA cognitive decathlon: a test suite for biologically-inspired cognitive agents. In: Proceedings of Behavior Representation in Modeling and Simulation Conference, Norfolk (2007)
13. Besold, T.R.: Turing revisited: a cognitively-inspired decomposition. In: Muller, V.C. (ed.) Philosophy and Theory of Artificial Intelligence. SAPERE, vol. 5, pp. 121–132. Springer, Heidelberg (2013)
14. Hernandez-Orallo, J., Dowe, D.L., Hernandez-Lloreda, M.V.: Universal psychometrics: measuring cognitive abilities in the machine kingdom. *Cogn. Syst. Res.* **27**, 50–74 (2014)
15. Adadurov, S.E., Gapanovich, V.A., Lyabakh, N.N., Shabelnikov, A.N.: Railway transport: on the way to intellectual management. Monograph, Rostov-on-Don (2009)
16. Kolesnikov, M.V., Gibner, Ya.M.: Comparative analysis of the innovative potential of the leading transport industries in Russia. *Science and education; Economy and economics; Entrepreneurship; Law and management*, № 2 (21), pp. 34–39 (2012)

Transport Systems Intellectualization Based on Analytical Control Synthesis of Angular Velocities for the Axisymmetric Spacecraft

Vladimir Taran¹(✉) and Vladimir Trofimenko^{1,2}(✉)

¹ RSTU, Rostov-on-Don, Russia

vladitaran@rambler.ru, trofimvn@mail.ru

² DSTU, Rostov-on-Don, Russia

Abstract. Satellite navigation and monitoring, appearing as a component of the transport systems intellectualization, are based on spacecraft position control algorithms. The article presents a method for synthesis of optimal terminal control of angular velocities for an axisymmetric spacecraft based on the predicting model method. Analytical dependences for laws of control were also derived. The control actions and the spacecraft reactions were calculated using the derived analytical dependences. The control costs and terminal velocities values were also disclosed.

Keywords: Synthesis · Optimum control · The spacecraft · The predicting model

1 Introduction

Satellites are involved in vehicle monitoring tasks within intelligence transport systems for navigation and information purposes. Amount of computations plays an important role in knoware algorithms synthesis. Analytical methods for control algorithm synthesis in intelligence systems are widely used lately since such methods reduce required computations amount and therefore free computational compatibilities for such tasks as business intelligence, identification, forecasting and decision-making [1, 2].

Satellite navigation and monitoring, appearing as a component of the transport systems intellectualization, are based on spacecraft position control algorithms, including control algorithms for spacecraft angular velocities. In most cases a spacecraft has axial symmetry. So, angular velocities control for an axisymmetric spacecraft is one of the tasks for intelligence transport systems operation.

The predicting model method, based on generalized work functional [3], is widely used for control algorithm synthesis of various objects [4–7], due to a number of advantages comparing to Bellman dynamic programming method [8]. The most important among them are computational cost reduction and increased noise stability. Non-linear objects control algorithm synthesis based on the predicting model method allowed to derive the close-form law for non-linear objects control [6, 7]. This method usage allows deriving effective spacecraft control algorithms, spacecraft orientation task and related angular speed control task. A spacecraft may be represented as a solid

with one axis of symmetry while deriving angular speed control law in many practical applications [9].

2 Problem Definition

The angular motion of a spacecraft considered as a solid body with one axis of symmetry is described by following equations [9]:

$$\begin{cases} \dot{\omega}_1 + A\omega_2\omega_3 = u_1, & \omega_1(t) \Big|_{t=t_1} = \omega_{s1}, \\ \dot{\omega}_2 - A\omega_1\omega_3 = u_2, & \omega_2(t) \Big|_{t=t_1} = \omega_{s2}, \\ \dot{\omega}_3 = u_3, & \omega_3(t) \Big|_{t=t_1} = \omega_{s3}, \end{cases} \quad (1)$$

where A – reduced inertia moment; $\omega_1, \omega_2, \omega_3$ and u_1, u_2, u_3 – angular velocities and controls as time-dependent functions, respectively; the point over a variable designates derivation on time.

Let's make definitions for vectors of angular velocities and controls:

$$\omega = (\omega_1, \omega_2, \omega_3)^T, \quad u = (u_1, u_2, u_3)^T, \quad (2)$$

where T – a transposing symbol.

If necessary to specify some point of time we will put the time value in brackets behind the vector. For example, $\omega(t_1)$ – vector of angular velocities at the time moment t_1 .

For control quality estimation we will choose the functional

$$J = V(\omega(t), \omega(t_2)) + \int_{t_1}^{t_2} Q(\omega, t) dt + \frac{1}{2} \int_{t_1}^{t_2} (u^T k^{-1} u) dt, \quad (3)$$

being a generalized work functional.

In expression (3) $Q(\omega, t) = (\omega^T q \omega)$, $V(\omega(t), \omega(t_2))$ – target functions integral and terminal functional components. Terminal components is defined by expression.

$$V(\omega(t), \omega(t_2)) = [\omega(t_2) - \omega(t, t_2)]^T m [\omega(t_2) - \omega(t, t_2)], \quad (4)$$

where $\omega(t, t_2)$ – predicted terminal values of angular velocities for the time moment t ; k, q, m – positive definite matrixes of weight coefficients.

It is required to find such control u_0 which would transfer system (1) from a state $\omega(t_1)$ to a state $\omega(t_2)$ while minimizing the functional (3).

3 The Predicting Model Method

As proven in paper [5], for the dynamic object described by the equation

$$\dot{x} = \varphi(x, t) + u, \quad u \in \mathbf{R}^m, x \in \mathbf{R}^n, \quad (5)$$

optimum control u_0 is determined by minimizing the Krasovsky functional (generalized work functional)

$$J = V(x(t), x(t_2)) + \int_{t_1}^{t_2} Q(x, t) dt + \frac{1}{2} \int_{t_1}^{t_2} (u^T k^{-1} u + u_0^T k^{-1} u_0) dt \quad (6)$$

and is defined by the expression

$$u_0(t) = -k \left[\int_t^{t_2} (G^T(s, t) \dot{Q}_x) ds + G^T(t_2, t) \dot{V}_x \right]. \quad (7)$$

In expressions (5–7) x – object state vector, u – vector of the controls being optimized, u_0 – required optimum control vector; $V(x(t), x(t_2))$, $Q(x, t)$ – the given positively definite differentiable functions, $k = \text{diag}(k_1, k_2, \dots, k_m)$ – diagonal matrix of the given coefficients. The fundamental matrix $G(s, t)$ and vectors of partial derivatives of the corresponding functions \dot{Q}_x , \dot{V}_x are defined on solutions of the unrestricted motion of the system

$$\dot{x} = \varphi(x, s), x(s) \Big|_{s=t} = x(t), \quad s \in [t, t_2], \quad (8)$$

and, a fundamental matrix of $G(s, t)$ is defined by the solution of the following equation:

$$\frac{\partial G(s, t)}{\partial s} = F_x \cdot G(s, t), \quad G(s, t) \Big|_{s=t} = I, \quad (9)$$

where I – a unit matrix, F_x – a matrix of Jacobi for the object motion Eq. (5), and s – the parameter meaning the accelerated (predicted) time.

Therefore, the optimum control vector u_0 transferring system (1) from a state $\omega(t_1)$ to a state $\omega(t_2)$ while minimizing functional (3) is determined by the expression:

$$u_0(t) = -k \left[\int_t^{t_2} (G^T(s, t) q \omega(s, t)) ds + G^T(t_2, t) \cdot \frac{\partial V(\omega(t_2))}{\partial \omega(t_2)} \right], \quad (10)$$

where $\frac{\partial V}{\partial \omega} \Big|_{t=t_2} = \left[\frac{\partial V}{\partial \omega_{1k}}, \frac{\partial V}{\partial \omega_{2k}}, \frac{\partial V}{\partial \omega_{3k}} \right]^T$ – a terminant derivative on a terminal vector $\omega(t_2)$.

4 Terminal Control Laws

For system (1) the Jacobi matrix appears as follows:

$$F_{\omega} = \begin{bmatrix} 0 & -A\omega_3(s) & -A\omega_2(s) \\ A\omega_3(s) & 0 & A\omega_1(s) \\ 0 & 0 & 0 \end{bmatrix}. \quad (11)$$

Vector of $\omega(s) = [\omega_1(s), \omega_2(s), \omega_3(s)]^T$ is in a matrix (11) from the equations of the unrestricted motion of the system:

$$\begin{cases} \dot{\omega}_1 + A\omega_2\omega_3 = 0, & \omega_1(s) \\ \dot{\omega}_2 - A\omega_1\omega_3 = 0, & \omega_2(s) \\ \dot{\omega}_3 = 0, & \omega_3(s) \end{cases} \Bigg|_{s=t} = \begin{cases} \omega_1(t), \\ \omega_2(t), \\ \omega_3(t). \end{cases} \quad (12)$$

Matrix $G(s, t)$, being the solution of the Eq. (9) is a fundamental matrix because, first, Eq. (9) are linear, secondly, its initial conditions is the unit matrix. The analytical solution of the matrix Eq. (9) for system (1) is the matrix:

$$G(s, t) = \begin{bmatrix} \cos \beta & \sin \beta & A(t-s)(-\omega_1 \cos \beta + \omega_2 \sin \beta) \\ -\sin \beta & \cos \beta & A(t-s)(-\omega_1 \sin \beta + \omega_2 \cos \beta) \\ 0 & 0 & 1 \end{bmatrix}, \quad (13)$$

In expression (13) $\omega_1, \omega_2, \omega_3$ – variables depending on the current time t ; $\beta = A\omega_3(t)(t-s)$.

Expression for a fundamental matrix (13) allows to integrate the Eq. (10) and to find analytical expressions for components of the terminal control vector:

$$u_1(t) = -k_1 \left\{ \omega_1(q_1 + q_2)(t_2 - t) - \frac{q_1 - q_2}{2\alpha} [\omega_1 \sin 2\gamma - \omega_2(\cos 2\gamma) - 1] + \omega_1 \right. \\ \left. \times (m_1 + m_2) + (m_1 - m_2)(\omega_1 \cos 2\gamma + \omega_2 \sin 2\gamma) - 2m_1\omega_{1k} \cos \gamma + 2m_2\omega_{2k} \sin \gamma \right\}, \quad (14)$$

$$u_2(t) = -k_2 \left\{ \omega_2(q_1 + q_2)(t_2 - t) + \frac{q_1 - q_2}{2\alpha} [\omega_2 \sin 2\gamma - \omega_1(\cos 2\gamma) - 1] + \omega_2 \right. \\ \left. \times (m_1 + m_2) + (m_1 - m_2)(\omega_1 \sin 2\gamma - \omega_2 \cos 2\gamma) - 2m_1\omega_{1k} \sin \gamma - 2m_2\omega_{2k} \cos \gamma \right\}, \quad (15)$$

$$u_3(t) \\ = -k_3 \left\{ \omega_3 q_3 (t_2 - t) + \frac{q_1 - q_2}{4\alpha^2} [(\omega_2^2 - \omega_1^2)(\sin 2\gamma - 2\gamma \cos 2\gamma) - 4\omega_1\omega_2(\cos 2\gamma \right. \\ \left. + 2\gamma \sin 2\gamma - 1) + 2m_3(\omega_3 - \omega_{3k}) + A(m_1 - m_2)(t - t_2) [(\omega_2^2 - \omega_1^2) \sin 2\gamma + 2\omega_1\omega_2 \right. \\ \left. \times \cos 2\gamma] + 2A(t - t_2)[m_1\omega_{1k}(\omega_1 \sin \gamma - \omega_2 \cos \gamma) + m_2\omega_{2k}(\omega_1 \cos \gamma + \omega_2 \sin \gamma)] \right\} \quad (16)$$

In formulas (14–16) $\alpha = A\omega_3(t); \gamma = A\omega_3(t)(t - t_2)$; matrices k, q, m have a diagonal appearance. k matrix terms in expressions (14–16) stand for control system amplification coefficients.

Let’s carry out the analysis of the received expressions. When matrix m equals to zero, a terminal part of a functional (3) is nullified, therefore, formulas (14–16) become the law of zeroing of angular velocities. When matrix q equals to zero second component of a functional (3) is nullified – we receive the terminal control law for the spacecraft. At equality of matrix terms $q_1 = q_2 = q_3$ the controls are directly proportional to optimization interval and have maximal values at the initial moment of the control. At the given restrictions for controls this dependence allows to determine the necessary optimization interval.

In Fig. 1 results of calculations at $k_1 = k_2 = k_3 = 1$ (thin lines) and at $k_1 = k_2 = k_3 = 5$ (reinforced lines) are presented. Final angular velocities values and controls costs at various values of coefficients are given in Table 1.

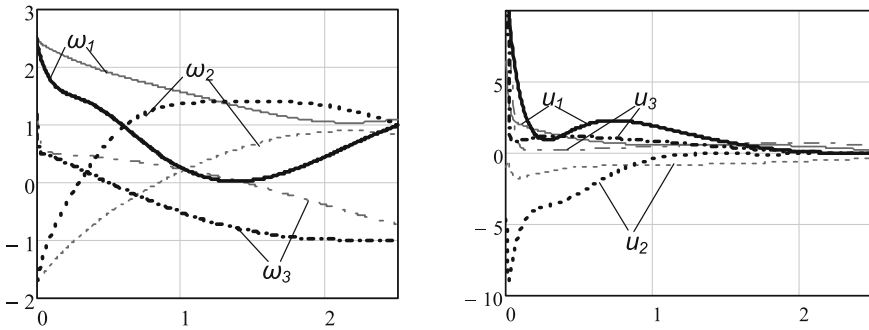


Fig. 1. Dynamics of coordinates and controls

Calculations of terminal controls were carried out for the starting conditions corresponding to an example in work [6]: $\omega_{s1} = 2.5 \text{ s}^{-1}; \omega_{s2} = -1.7 \text{ s}^{-1}; \omega_{s3} = 1.2 \text{ s}^{-1}$; the given moment of inertia – $A = 0.955$; an optimization interval – $[0, 2.5 \text{ s}]$.

Table 1. Angular velocities on the end of an interval and controls costs

Коэффициенты k	$\omega_1(t_2)$	$\omega_2(t_2)$	$\omega_3(t_2)$	$\int_{t_1}^{t_2} (\sqrt{u_1^2} + \sqrt{u_2^2} + \sqrt{u_3^2}) dt$
$k_1 = k_2 = k_3 = 1$	1.105	0.83	-0.72	6.054
$k_1 = k_2 = k_3 = 5$	1.0	1.0	-1.0	9.204

The analysis of results of calculations gives the chance to draw the following conclusions:

1. The scientific contribution of the paper is specification of the general control synthesis statements based on the semidefinite Krasovsky functional minimum to an

- important class of the controlled systems, including various purpose spacecrafts using intellectual navigation and control systems. The given solution benefit is the constructive analytics which allows practically applicable control algorithm design.
2. The derived control law allows to reach terminal angular velocities values with a high precision. The accuracy depends on controls costs (Table 1).
 3. Comparing to example reviewed in paper [6], computations amount significantly lowered due to exception of a numerical integration when determining a fundamental matrix and control.

5 Conclusion

The received analytical expressions (14–16) for angular velocities control are practically applicable since the Eq. (1) appear to be a good approximation for angular motion modeling of an axisymmetric spacecraft.

The value of the derived algorithm is its constructability, since analytical expressions are used for the controls calculation. This is the key factor for on-board computers having severe limitations on mass, memory space, computing speed and power consumption. Researching a non symmetric solid body case, e.g. manned space station, it may be considered as an axisymmetric body with corresponding controls being the initial approximation. The approximation may be corrected lately by means of the numerical methods.

References

1. Kostoglotov, A.A., Kostoglotov, A.I., Lazarenko, S.V., Tsennykh, B.M.: Method of structural-parametric identification of Lagrangian dynamic systems in the processing of measurement information. *Measur. Tech.* **57**, 153–159 (2004). doi:[10.1007/s11018-014-0422-3](https://doi.org/10.1007/s11018-014-0422-3). (in Russian)
2. Kostoglotov, A.A., Kostoglotov, A.I., Lazarenko, S.V.: Joint maximum principle in the problem of synthesizing an optimal control of nonlinear systems. *Autom. Control Comput. Sci.* **41**, 274–281 (2007). doi:[10.3103/S0146411607050069](https://doi.org/10.3103/S0146411607050069)
3. Aleksandrov, A.G., Krasovsky, A.A., et al.: *Spravochnik po teorii avtomaticheskogo upravleniya* [The reference book on the theory of automatic control] Under the editorship of A.A. Krasovsky. Nauka. Gl. Red. Phiz-math. Lit. [Science. Hl. Edition physical. mat. litas.], Moscow (1987). (in Russian)
4. Bukov, V.N.: Sintez upravlyayushchikh signalov s pomoshchyu prognoziryuyushchey modeli v adaptivnoy sisteme upravleniya [Synthesis of the operating signals by means of the predicting model in an adaptive control system] *Problemy upravleniya i teorii informatsii* [Problem of management and the theory of information]. T. 9(5), pp. 329–337 (1980). (in Russian)
5. Taran, V.N.: Maksimalno pravdopodobnaya otsenka sostoyniya optimalno upravlyayemy sistemy [Maksimalno's ram a plausible assessment of a condition of optimum operated system] *Avtomatika i telemekhanika* [Automatic equipment and Telemechanics]. N 8. pp. 101–108 (1991). (in Russian)

6. Detistov, V.A., Tatan, V.N.: Terminalnoe upravlenie uglovymi skorostyami KA na osnove prognoziryuyushchey modeli [Terminal management of angular speeds of the spacecraft on the basis of the predicting model] Kosmicheskiye issledovaniya [Space researches]. T. 31 N6, pp. 104–109 (1993). (in Russian)
7. Taran, V.N., Trofimenko.: Sintez optimalnogo algoritma uglovoy stabilizatsii metodom prognoziryuyushchey modeli [Synthesis of an optimum algorithm of angular stabilization by method of the predicting model] Avtomatika i telemekhanika [Automatic equipment and Telemechanics]. N5, pp. 82–85 (1997). (in Russian)
8. Bellman, R.: Dynamic Programming. Princeton University Press, Princeton (1957)
9. Tikhonravov, M.K., Yatsunsky, I.M., Maximov, G.Y., Bazhinov, I.K., Gurko, O.V.: Osnovy teorii poleta i elementy proyektirovaniya iskusstvennykh sputnikov Zemli [Bases of the theory of flight and elements of design of artificial Earth satellites]. M.: Mashinostroeniye, Moscow (1967). (in Russian)

Executable Logic Prototypes of Systems Engineering Complexes and Processes on Railway Transport

Alexander N. Guda, Vera V. Ilicheva^(✉), and Oleg N. Chislov

Rostov State Transport University (RSTU), Rostov-on-Don, Russia
guda@rgups.ru, vilicheva@yandex.ru, o_chislov@mail.ru

Abstract. In this paper we examine software tools and design examples of executable logic prototypes for modelling of complex systems. The prototype is set by the specification in predicate calculus language. Semantics of specification supposes effectively realized interpretation whose result is a prototype and/or diagnosis of project errors. We use rapid prototyping techniques, the specification is easily modified. The approach provides three levels of logic modelling in the same programming environment: prototyping of static structure of a system, logic of processes, dynamic behaviour. Prototyping of structure and technological processes of freight terminal “Taganrog” has been chosen as an example.

Keywords: Logic language · Logic prototype · Predicate calculus · Freight railway terminal · Error diagnosis

1 Introduction

Nowadays prototyping is an actively investigated branch of information technologies. Developing as necessary software tool of program engineering, prototyping has turned into the accumulation of research-and-development and experimental kinds of activity raising quality and speed of project development. Physical, visual, logic prototypes can be used at different stages of working out. Representing early ideas and concepts, they help people who make decisions understand a problem better, and find methods of its solution. Rapid prototyping plays a special role speeding innovations. It is widely applied in the defense industry where high speed of prototype modification is extremely important for working out of easily configured weapon systems [1]. Technologies of prototyping are being developed in designing of web-sites, electronics [2].

The special niche in this direction is occupied by logic prototyping - use of languages and methods of mathematical logic for development and analysis of logic models of software, technical systems and processes [3–7]. However, use of logic means cannot be widely applied because well-known logic languages of Prolog type are not suitable for this purpose. The models of terms that can be found semantics of these languages, do not allow working with equality, negation, or diagnosing even such logic errors as contradiction, redefinition or uncertainty of functions. Meanwhile, it is the logic device that is often the most suitable means for such problems, as the analysis of consistency of design solutions and estimation of consequences of undertaken

actions. It is absolutely essential for maintenance of correctness of performance of sophisticated systems with heterogeneous elements. Modern marshaling yards and freight railway terminals can be an example of such complexes [8].

In this paper we use the approach based on the language in calculation of first-order predicates with equality. Language possesses the computable and effectively realized semantics whose basis is represented by models from the constants coding objects of a subject field [3]. The method gives an opportunity to obtain fast the logic model of the object – its static or dynamic structure displaying all logically connected elements and interactions. Executable logic prototype is a tool of rapid modelling: it is easily supplemented with new properties and behaviour variants, easily adapts for changes in a subject field. The received specifications can be immediately executed by the interpreter. The technology was applied to prototyping of the space simulators modelling process of docking of extraterrestrial objects.

Our approach presupposes two stages. At the first stage one should make the description of investigated object in the offered logic language. The description comprises the following: a list of elements, their attributes, relations among them, axioms, inductively composing definitions of these objects, and also the axioms that restrict their structure or behaviour. They describe emergencies, and conditions when the functioning of modelled system is correct, etc. At the second stage there are interpreters of the specifications whose purpose is to construct a logic model (prototype) of the object and to check feasibility of demanded properties. In the course of interpretation one can also diagnose logic errors, such as contradictoriness and incompleteness of representation of an object or a system project. The technique can provide three levels of logic modelling in the same environment. These are prototyping of static structure of a complex, prototyping of logic of processes, and prototyping of dynamic behaviour. In this paper we consider these aspects with reference to a freight terminal “Taganrog”. We illustrate it with examples of prototyping of its structure and technological processes.

2 Logic Language and the Specification

Language of first-order predicate calculus is used for the description of modelled objects. Its basic difference from the Prolog and its analogues is possibility to use modules, negations, equalities, limited quantifiers and variables of a sort “time” in clauses.

The description – specification $S = (\Sigma, T)$ of the investigated system is composed by the signature Σ (alphabet) and the theory $T = T_{fact} \cup T_{def} \cup T_{rest}$. The signature $\Sigma = (R, F, C)$ is represented by sets R that are names of predicates (relations), F that are names of functions (attributes), and C that are constants. C is not empty, and all constants are various. Constants represent (coding) objects of a subject field (for example, fleets, ports, tracks, moorings, devices, fixed values), essential for prototype construction. The theory is a final set of axioms - logic formulas without free variables (all variables are connected by quantifiers or are presented by constants). General description T is made by three groups: T_{fact} is a set of the facts - statements about concrete objects, T_{def} is a set of definitions of relations and functions (dependences

between objects and their attributes), T_{rest} is a set of restrictions on these dependences and on values of attributes. We will agree to make the following designations for any set A : a is an element of A , \bar{a} is a vector of such elements; for an arbitrary formula ϕ : V_ϕ is a set of its variables. In practice, multi-sorted logic language is more adequate, but for simplicity of statement one-sorted signature is used further. For effective interpretation with the help of logic conclusion it is very important to formulate a class of formulas to be used. Axioms of the theory T are the following.

T_{fact} is presented by the following formulas without variables $r(\bar{c}), \neg r(\bar{c}), f(\bar{c}) = c$. For example (inverted commas limit constants):

occupied ('PORT_T', '15.30'), \neg shipped ('GroupC2'), $quantity_tracks$ ('A_FLEET') = 6.

T_{def} are formulas, such as $\forall \bar{x}(\varphi(\bar{x}) \rightarrow \psi(\bar{x}))$ or $\forall x \in \theta(\varphi(\bar{x}) \rightarrow \psi(\bar{x}))$, where \bar{x} is a vector of variables, $\varphi(\bar{x})$ is conjunction of atomic formulas, such as $r_i(\bar{t}), t_i(\bar{x}) = t_j(\bar{x})$ or their negations ($r_i \in R, t_i, t_j, \bar{t}$ are signature terms Σ); $\psi(\bar{x})$ is conjunction of atomic formulas, such as $r_k(\bar{x})$ (relation definition $r_k \in R$) or $f_k(\bar{x}) = t_k(\bar{x})$ (function definition $f_k \in F$), θ is the finite list. At each relation $\neg r(\bar{x})$ with negation from $\varphi(\bar{x})$ a conjunct should be present $q(\bar{x})$, positively entering into the same formula, playing a role of a limited quantifier for $\neg r(\bar{x})$. This restriction is connected with computability of predicates falsity domain. The equality relation is considered built-in (axioms of definition of equality are automatically added to T_{def}). Variable formulas satisfy the ratio: $V_\psi \subseteq V_\varphi$. For example, you can see here one of relation definitions – «a transit track»:

$$\forall x, y, z(\text{is_transit}(x, y) \ \& \ \text{is_transit}(y, z) \rightarrow \text{is_transit}(x, z));$$

T_{rest} are set by any first-order formulas with the limited quantifiers. The belonging of values of variables to a finite sort (domain) can be considered as quantifier restriction. For example, a condition-restriction «there should be an exit to the main track from the basic objects of station (marshalling yards and railway loading complex)»:

$$\neg \exists x, y (\text{type}(y) = \text{'Main'} \ \& \ \neg \text{is_transit}(x, y)).$$

specifications defined the concept of correctness which comprise properties of completeness of definition of functions, consistency concerning axioms of equality, and consistency concerning the use of negations [9].

Semantics of language supposes not only effective realizability, but also exact diagnosis of logic errors. There were defined logic, denotational and operational semantics of the given class of specifications, and proved their equivalence. As logic semantics we have used initial (minimal with respect to a homomorphic embedding) inductive-computable (IC-) models from constants C , possessing the property of uniqueness in the category of finitely-generated models. Such a model is designed according to the description $T_{fact} \cup T_{def}$, functions and relations are defined in the course of a direct logic derivation. There were proved unique correspondence between correctness of the specification and existence of a model of this type for the description $T_{fact} \cup T_{def}$. Constructing of the model does not require restricted recursion in definitions and introductions of any order or hierarchy in the set of axioms.

In order to represent dynamic aspects as logic formulas, time variables should be used. Variables run final sections τ of a discrete set of points, each of which can be set either by concrete time (on railway transportation it can be hours, minutes within 24 h), or an event (a name or a signal of an event).

Despite a complicated mathematical justification, practical specifications look quite clear and simple. The possibility of dynamic change of descriptions (addition or removal of the facts, or axioms) defines a convenient representation of the contingencies, emergencies and reaction adjustment during incorrect giving or reception of signals.

3 Interpretation and Diagnosis of Errors

The interpreter represents operational semantics of specifications. It realises a direct logic derivation using definitions $T_{fact} \cup T_{def}$, substituting constants instead of variables. The derivation begins with substitution of the facts in the left parts of axioms and finishes with reception of all possible logic consequences of this theory. At this stage contradictions (redefinition of functions or predicates) and uncertainty of functions can be diagnosed. If there have been no errors, the received set of consequences forms the target logic model – a prototype of the described system. The interpreter can use the constructed model to check high-quality of a prototype - satisfiability of restrictions T_{rest} .

Formally, the interpreter calculates interpreting function i of IC-model $M = (C, i)$ according to the denotational equations that set a representation of signature symbols on set of functions and relations on C . For maintenance of accuracy of diagnosis of logic errors in the capacity of data domains on which function i is constructed, full grids with the bottom – “uncertainty” (\perp), the top – “an error of redefinition” (\top) and the approximation relation \sqsubseteq are considered: for any element x of domain X the following takes place: $\perp \sqsubseteq x, x \sqsubseteq x, x \sqsubseteq \top$. Monotony provides uniqueness of a fix point of calculations that is the result of interpretation. In case of occurrence of an error of redefinition, it is possible to predetermine on value \top those functions and relations in which calculation erroneous elements took place. Thereby you can reach unambiguity of result of interpretation.

The algorithm of interpretation consists in alternate performance of two steps until the general motionless point of calculations is received. On the first step we interpret the definitions which do not contain negations. Every new fact, starting from T_{fact} initiates a derivation from an axiom containing occurrence of the corresponding relation or function in the left side of the implication. Then we search for a suitable substitution of constants, and define the validity of the left part of the rule. If the value of interpretation of this formula is true or \top , the relations and functions that are defined in the right part of this substitution are interpreted as true or equal to \top accordingly. The facts, received in this way if they are new, continue to make actions of step 1 active. If there are no new facts (the local fix point), we start to perform step 2 – interpretation of negatively entering relations. To make the result of interpretation independent from the order of choice of axioms with negation, every of them is interpreted on consequences after step 1, they are independent from each other, thus, if the predicate $r(\bar{x})$ from the formula $\neg r(\bar{x})$ in the left part of an axiom has not been

defined on step 1 as true on a suitable substitution \bar{c} , it is supposed to be false in it. The new facts $\neg r(\bar{c})$ (if they occur) initiate the repetition of step 1 if the received consequences have not led to the contradiction.

It is proved that the interpreter builds model M if it exists, does not cycling and finishes work for a final number of steps. Capacitive complexity of interpretation has order $O(n)$ where n is capacity of the model, time-complexity is estimated by product $p \times n \times k$, where p is complexity of search for suitable substitutions for one axiom, k is the quantity of axioms. An optimistic estimation of complexity $O(n \log n)$, pessimistic one is $O(n^2)$ for practical prototypes.

Result of performance is either actually a prototype – a model of the theory forming the specification, or preliminary treatment of project errors.

The errors which are found out at interpretation are divided into three classes: uncertain functions (attributes of objects), redefinition of functions or relations (contradiction) and an impracticability of restrictions. The first two concern a specification correctness $(\Sigma, T_{fact} \cup T_{def})$, the third one concerns incorrect behaviour or the structure of a modelled complex set in T_{rest} . If we assume that axioms T_{def} describe the object completely and accurately according to its technical characteristics, and the initial set of the facts T_{fact} is real, but the presence of errors means that the modelled object is designed incorrectly. It allows correcting project errors in time. If we prototype the already working object for the purpose of training, the error states that the set of the facts set on an input T_{fact} is either not enough for a reconstruction of a full picture of an investigated situation, or it is absurd, or it leads to an accident. By means of purposefully “spoil” facts it is possible to train in emergency operation. Let us consider the diagnosis in more detail.

Undefiniteness (\perp) value of some function f on arguments \bar{c} means that $f(\bar{c})$ has not received value in the course of interpretation. It should be noted that as the classical logic is used here, functions should be defined completely. The situation when a function substantially should not be defined on a set of objects, is solved by the usage of multisorted domains of definition. Therefore, undefiniteness of value for some $f(\bar{c})$ is an error which can be called by either absence of a necessary axiom or the initial fact for this function, or undefiniteness $f(\bar{c})$ of terms participating in the derivation. Actually it means that there was an attribute specified in the description of a the structure of the prototyped object f , that had not been set.

Redefinition of function f or predicate r on arguments \bar{c} means that the task of equality or the relation r is inconsistent. Discrepancy of equality corresponds to ambiguity of the function: two logic consequences $f(\bar{c}) = c_1$ and $f(\bar{c}) = c_2$ are derived at various values c_1 and c_2 . The inconsistent task of the relation r is found out only in case definitions contain formulas with negation. As long as negation for the considered type of axioms occurs only in left sides of implications, the classical formulation of the inconsistent theory is the following: both $r(\bar{c})$ and $\neg r(\bar{c})$ can be proved replaced by: $r(\bar{c})$ is derived in the valid assumption $\neg r(\bar{c})$, as syntactically $\neg r(\bar{c})$ is impossible to derivate. Thus, both $r(\bar{c})$ and $\neg r(\bar{c})$ appear to be true in a prototype, which speaks about contradiction of the description (in particular, the input T_{fact} contradicts definitions T_{def}).

The impracticability of restrictions means that for the elements of a prototype set by definitions and facts, the rule of their behaviour or the structural connection, formulated in T_{rest} cannot be executed.

Here is the result of interpretation: if the specification is correct, and entrance set of the facts do not contradict it, the set of all its atomic logic consequences representing a logic prototype will be an output. It will present all static and dynamic interrelations that are obtained on the set interval of time as well as all calculated attributes of objects.

4 Prototyping of Static Structure

The modern freight terminal represents a complicated complex of objects with different functions and devices [10]. There are the following fleets: receiving-departure yard - «B»; passenger - «A»; sorting-departure - «G»; marshalling - «E» and «C»; freight yard - «F». The complex comprises also the plants participating in cargo operations, seaport, moorings, tracks of different functions. There are the following transport objects: rolling stocks, groups of cars, locomotives.

The main mission of the station is performance of operations on receipt and shipment of cargoes by rail from commercial sea port. These operations, being dynamic processes, are analyzed in the logic model that considers time of their performance. We can refer the following to the static structure: arrangement of objects, tracks, the devices regulating traffic. A prototype includes static properties, such as quantity of tracks, moorings, locomotives, carrying capacity of stations. The most part of structural restrictions includes prohibition or possibility of direct journey from one object to another. Besides, the quantity of maintenance centers, possibility of merging of the fleets aimed at performance of homogeneous technological operations are limited. Prototyping is used at different design stages. Every new level sets modelled structure in more detail. New relations, functions, and objects are included, so interrelations become complicated.

Here you can see the fragment of the description of a prototype of static structure of station. For better understanding of the approach the description includes the objects of the first level without detailed study of separate configurations. The specification comprises the following: the description of relations and functions with stating the quantity and types (sorts) of arguments and values (for functions), the description of constants in axioms, clauses T_{def} and T_{rest} .

Sorts:

OBJECT = FLEET \cup PORT \cup PLANT \cup MAIN.

Relations:

is_way (from, to): OBJECT \times OBJECT – presence of a direct track between objects;

is_transit (from, to): OBJECT \times OBJECT – presence of a transit track between objects;

must_connect (what, with what): OBJECT \times OBJECT – necessity of creation of a new track;

cross_tracks (track, track): OBJECT \times OBJECT \times OBJECT \times OBJECT – traverse of tracks.

Functions:

type (of what): OBJECT \cup TRACK \rightarrow OBJECT \cup NUMBER \cup TRACK_NUMBER;

tracks_quantity (from, to): OBJECT \times OBJECT \rightarrow INTEGER;

moorings_quantity (whose): PORT \rightarrow INTEGER;

Avg_time (from, to): OBJECT \times OBJECT \rightarrow NUMBER.

Constants:

‘B’, ‘G’, ‘E’, ‘A’, ‘Seaport’, ‘Main’, ‘Plant’: \rightarrow OBJECT; k_1, c_1 : \rightarrow NUMBER.

Definitions:

$\forall x, y$ (must_connect (x, y) \rightarrow is_way (x, y));

$\forall x, y, z$ (is_way (x, y) & is_way (y, z) \rightarrow is_transit (x, z));

$\forall x, y, z$ (is_transit (x, y) & is_transit (y, z) \rightarrow is_transit (x, z));

$\forall x, y$ (is_way (x, y) & type (x) = ‘B’ & type (y) = ‘Seaport’ \rightarrow

tracks_quantity (x, y) = k_1 & Avg_time (x, y) = c_1);

$\forall x, y, z$ (is_way (x, y) & is_way (z, v) & type (x) = ‘E’ & type (y) = ‘B’ & type (z) = ‘G’ & type (v) = ‘Main’ \rightarrow cross_tracks (x, y, z, v));

Restrictions:

$\forall x, y$ (is_way (x, y) & type (y) = ‘Seaport’ \rightarrow tracks_quantity (x, y) \leq moorings_quantity (y));

$\exists x, y$ (type (x) = ‘G’ & type (y) = ‘Main’ & is_way (x, y));

$\exists x, y$ (type (x) = ‘G’ & type (y) = ‘Main’ & is_way (x, y));

$\exists x, y$ (type (x) = ‘B’ & type (y) = ‘Plant’ & is_transit (x, y));

$\neg \exists x, y$ (is_way (x, y) & type (x) = ‘A’ & (type (y) = ‘G’ \vee type (y) = ‘C’ \vee type (y) = ‘E’ \vee type (y) = ‘F’));

$\neg \exists x, y$ (type (y) = ‘Main’ & \neg is_transit (x, y));

$\exists x, y$ (is_way (x, y) & type (x) = ‘E’ & type (y) = ‘Plant’).

5 Prototyping of Dynamic Processes

The formulas comprise variable t of sort TIME to which numerical constant values (i_0, \dots, i_{18}, c) of duration of technological operations can be added.

Here is a description fragment:

Sorts:

DESTINATION = PORT \cup FLEET \cup TAIL_TRACK;

T_OBJECT = ROLLING STOCK \cup LOCOMOTIVE \cup CARS_GROUP;

Relations:

is_located (what, where, time_start): $T_OBJECT \times FLEET \times TIME$;
 goes_to (what, where, time_start): $T_OBJECT \times FLEET \times TIME$;
 wait_accumulation (what, time_start): $CARS_GROUP \times TIME$;
 shipped (what): T_OBJECT ;
 $\text{reception, transmission}$ (signal, track, t): $SIGNAL \times TRACK \times TIME$;
 vacant, occupied (what, time_start): $(TRACK \cup MOORING) \times TIME$;
 uncouple, couple (what, from_what/to_what, on_track, time_start):
 $(CARS_GROUP \cup LOCOMOTIVE) \times (CARS_GROUP \cup ROLLING\ STOCK) \times$
 $TRACK \times TIME$;
 $\text{maintenance checkup}$ (what, on_track, time_start): $ROLLING\ STOCK \times TRACK \times$
 $TIME$;
 train_locomotive (locomotive, what_train): $LOCOMOTIVE \times ROLLING\ STOCK$;
 cars_group (group, whose, on_track, time_start): $CARS_GROUP \times ROLLING$
 $STOCK \times TRACK \times TIME$;

Constants:

‘Main track’, ‘B’, ‘Tail track’, ‘Seaport’, ‘G’: $\rightarrow DESTINATION$;
 i_0, \dots, i_{18}, c : $\rightarrow NUMBER$;
‘vacant’, ‘occupied’, ‘MCH1_over’, ‘trailer_locomotive’: $\rightarrow SIGNAL$;

Definitions:

$\forall x, t, t_1$ (is_located (x, ‘Main track’, t) & $t_1 = t + i_1 \rightarrow \text{goes_to}$ (x, ‘B’, t_1));
 $\forall x, t$ (is_located (x, ‘B’, t) & $\neg \text{shipped}$ (x) $\rightarrow \text{goes_to}$ (x, ‘Tail track’, $t + i_2$));
 $\forall x, t, t_1$ (is_located (x, ‘Tail track’, t) & $t_1 = t + i_3 \rightarrow \text{goes_to}$ (x, ‘Seaport’, t_1));
 $\forall x, t$ (goes_to (x, ‘Seaport’, t) & vacant (‘Seaport’, $t + i_4$) \rightarrow
 is_located (x, ‘SeaPort’, $t + i_4$) & occupied (‘Seaport’, $t + i_4$));
 $\forall x, y, t, t_1$ (goes_to (x, y, t) & $t_1 = t + c \rightarrow \text{is_located}$ (x, y, t_1));
 $\forall x, t, t_1$ (is_located (x, ‘SeaPort’, t) & $t_1 = t + i_5$ & $\neg \text{wait_accumulation}$ (x, t_1) \rightarrow
 goes_to (x, ‘B’, t_1) & vacant (‘SeaPort’, t_1));
 $\forall x, t$ (is_located (x, ‘SeaPort’, t) $\rightarrow \text{shipped}$ (x));
 $\forall x, t, t_1$ (is_located (x, ‘SeaPort’, t) & $t_1 = t + i_6$ & wait_accumulation (x, t_1) \rightarrow
 goes_to (x, ‘G’, t_1) & vacant (‘SeaPort’, $t + i_7$));
 $\forall x, t$ (is_located (x, ‘B’, t) & shipped (x) $\rightarrow \text{goes_to}$ (x, ‘Main track’, $t + i_8$));
 $\forall x, y, t$ (is_located (x, ‘Main track’, t) & vacant (y, t) $\rightarrow \text{is_located}$ (x, y, $t + i_{10}$) &
 occupied (y, $t + i_{10}$));

Restrictions:

$\neg \exists x, y, t$ (goes_to (x, y, t) & is_located (x, y, t));
 $\neg \exists t, y$ (occupied (y, t) & vacant (y, t));
 $\neg \exists x, y, t$ (occupied (y, t) & goes_to (x, y, t)).

Here is the prototype detailed elaboration: addition of the new technological operations is regulated by signals. The following can be added to axioms *Definitions*:

$$\begin{aligned} &\forall x, y, l, t \text{ (is_located (x, y, t) \& train_locomotive (l, x) \rightarrow} \\ &\text{uncouple (l, x, y, t + i}_{11}\text{))}; \\ &\forall x, y, z, l, t \text{ (uncouple (l, x, y, t) \& vacant (z, t) \rightarrow} \\ &\text{is_located (l, z, t + i}_{12}\text{) \& occupied (z, t + i}_{12}\text{))}; \\ &\forall x, y, t \text{ (is_located (x, 'Main track', t) \& reception ('vacant', y, t) \rightarrow} \\ &\text{is_located (x, y, t + i}_{13}\text{) \& transmission ('occupied', y, t + i}_{13}\text{) \&} \\ &\text{transmission ('vacant', 'Main track', t + i}_{13}\text{))}; \\ &\forall x, y, z, l, t \text{ (uncouple (l, x, y, t) \& reception ('vacant', z, t) \rightarrow is_located (l, z,} \\ &\text{t + i}_{14}\text{) \& transmission ('occupied', z, t + i}_{14}\text{))}; \\ &\forall x, y, l, t \text{ (uncouple (l, x, y, t) \rightarrow maintenance_checkup (x, y, t + i}_{15}\text{))}; \\ &\forall x, y, g, t \text{ (maintenance_checkup (x, y, t) \& reception ('MCH1_over', y, t) \&} \\ &\text{cars_group (g, x, y, t) \rightarrow uncouple (g, x, y, t + i}_{16}\text{))}; \\ &\forall x, y, g, l, t \text{ (uncouple (g, x, y, t) \& is_located (l, y, t) \&} \\ &\text{reception ('trailer_locomotive', y, t) \rightarrow couple (l, g, y, t + i}_{17}\text{))}; \\ &\forall x, y, g, l, t \text{ (couple (l, g, x, t) \& reception ('vacant', y, t) \rightarrow goes_to (g, y, t));} \\ &\forall x, y, g, t \text{ (goes_to (g, x, t) \& reception ('vacant', y, t) \rightarrow is_located (g, y, t + i}_{18}\text{))}. \end{aligned}$$

For interpretation, facts must be added to the definitions - concrete statements about objects. For example (fragment):

$$\begin{aligned} &\rightarrow \text{is_located ('№ 1201-1298', 'Main track', 11.00);} \\ &\rightarrow i_1 = 0,25; \\ &\rightarrow \text{is_located ('№ 1211-1503', 'SeaPort', 12.10);} \\ &\rightarrow \text{is_located ('№ 1150-2219', 'B', 10.05);} \\ &\rightarrow \text{train_locomotive ('№ 4001-4092', '№ 1150-2219').} \end{aligned}$$

6 Conclusion

The findings of the research have confirmed utility of logic prototyping for modelling and the analysis of complicated technological complexes and processes. The chosen logic means have proved to be a good tool of fast prototyping. Specifications are easily modified, tested, replenish and integrated, forming libraries of axioms. Efficiency of the interpreter depends only on a kind of formulas. Therefore, detailed elaboration of descriptions does not influence essentially resource-intensiveness of designing of prototypes.

Predictably, the approach has perfectly proved for representation of static properties and structures and diagnosis connected with them. Test of dynamic prototypes has shown detection of emergencies for time intervals not less than a minute (time of manual input of the facts). Natural nondetermination of descriptions suits well for the representation of parallel processes, but it is of little use for problems of optimisation and accumulation of values in strict sequence.

References

1. Hencke, R.: Prototyping increasing the pace of innovation. In: Defense AT&L Magazine, pp. 10–14 (2014)
2. Spivey, G., Bhattacharyya, S.S., Nakajima, K.: Logic foundry: rapid prototyping for FPGA-based DSP systems. *EURASIP J. Appl. Sig. Process.* **6**, 565–579 (2003)
3. Ilyicheva, O.A.: Technology of logic modelling and the analysis of complex systems. In: The Engineering Bulletin of Don, vol. 2, issue 4 (2012). <http://www.ivdon.ru/ru/magazine/archive/n4p2y2012/1234>
4. Komorowski, H.J.: Logic programming and rapid prototyping. *Sci. Comput. Program.* **2**(9), 179–205 (1987)
5. Brunette, C., Taplin, J., Gamatie, A., Gautier, T.: A metamodel for the design of polychromous systems. *J. Logic Algebraic Program.* **78**(4), 233–259 (2009)
6. Kerdprasop, N., Kerdprasop, K.: Frequent pattern discovery with constraint logic programming. *Int. J. Math. Models Methods Appl. Sci.* **5**(8), 1345–1353 (2011)
7. Kerdprasop, N., Intharachatorn, K., Kerdprasop, K.: Prototyping an expert system shell with the logic-based approach. *Int. J. Smart Home* **7**(4), 161–173 (2013)
8. Chislov, O.N., Mamaev, E.A., Guda, A.N., Zubkov, V.N., Finochenko, V.A.: Algorithmic and software support of efficient design of railway transport technological systems. *Int. J. Appl. Eng. Res.* **23**(11), 11428–11438 (2016)
9. Ilyicheva, O.A.: Means of effective preliminary treatment of errors for systems of logic prototyping. *Autom. Remote Control* **9**, 185–196 (1997)
10. Chislov, O.N., Bogachyov, V.A., Zadorozhnyi, V.M., Bogachyov, T.V.: Distribution of traffic volumes of operation company in port hubs by method of economic and geographical differentiation. *News Petersburg State Transport Univ.* **3**(48), 302–313 (2016)

Intellectualization of Monitoring Vibroacoustic Characteristics of the Permanent Way and Passing Rolling Stock

O.A. Belyak, A.E. Larin, and T.V. Suvorova^(✉)

Rostov State Transport University, 344038 Rostov on Don, Russia
{o_bels, suvorova_tv111}@mail.ru

Abstract. The emergence of high-speed railways, having indisputable economic and ecological benefits, has aroused great interest in the problems of their higher operation reliability. The leading role is given to monitoring the permanent way under dynamic impact. This process is run by means and techniques of vibration diagnostics. The problem of monitoring and diagnosing modern railway trunk lines is extremely complex and requires the development of both theoretical methods of calculating the track-rolling stock interaction and field experimental studies. Mathematical modeling of the process of propagation of oscillations generated by the passing train is a necessary step to develop monitoring systems for evaluating the permanent way strains and stresses. It will also contribute to assessing the vibration impact on wayside infrastructure and environment. One of the major characteristics of the permanent way and the underlying road bed stability is known to be the movement of ballast section surface. The present work investigates the interaction between different permanent way parameters and surface displacements near it. The basis of the study is mathematical modeling the problem of generating oscillations by a passing train. The difference between the used models lies in applying the methods of continuum mechanics and mathematical theory of elasticity. These mathematical models are described by systems of partial differential equations. More complex methods of constructing problem solutions are compensated with full physical representation of multi parameter oscillation process. Under these circumstances one can examine the impact of permanent way defects and carriage operating conditions on surface displacements as well as create the reference database of system status and its admissible variations. It is the combination of theoretical methods of model problem solving and experimental methods of analyzing dynamic responses of complex technical systems that allows solving the tasks of automatic vibration-based diagnostics and monitoring systems.

Keywords: Displacement permanent way · Monitoring · Mathematical models · Geterogenues foundation

1 Problem Formulation and Analytical Solution

Creation of the mathematical model which are more precisely taking into account reaction of the foundations and allowing to study feature of wave fields in a ground, raised by a permanent way under action of moving loadings, is the actual problem and basis of permanent way monitoring.

Harmonic oscillations of a rectangular stamp on the surface of semi-bounded base being a package of viscoelastic and porous elastic liquid-saturated layers are considered to be the main model task. The front surface of the layered medium houses an M mass rectangular stamp oscillating under the applied force. Out of the stamp the front surface of the base is not loaded.

One should find the distribution of contact normal stresses under the stamp, as well as the relationship between the interacting force P and the stamp settling, displacement of the front surface of the medium outside the stamp. The problem is considered in steady state conditions of oscillations with frequency ω .

The behavior of viscoelastic layers is described by Lamaet equations [1], representing a system of three partial differential equations. These equation coefficients are complex numbers with a small imaginary component. The Biot model [2, 3], experimentally confirmed for most groundwater soils [4, 5] is adopted for describing the liquid saturated porous elastic media. The system of Biot equations contains six partial differential equations. The boundary conditions are formulated for the displacements, stresses, and depend on the type of environment components and their interaction.

The application of bivariate Fourier transform to constitutive equations and boundary conditions using algebraic recurrence transformations meets the requirements of the exactly set boundary conditions. The more detailed process description is given in [6]. The solution of the contact problem comes to a system of matched integral equations, their form for normal oscillations being:

$$\iint_{\Omega} \int_{\mathbb{R}_1} \int_{\mathbb{R}_2} K(\sqrt{\alpha^2 + \beta^2}) e^{i\alpha(x-\xi) + i\beta(y-\eta)} q(\xi, \eta) \, dx d\beta d\xi d\eta = f(x, y), \quad (x, y) \in \Omega,$$

$$\int_{-\infty}^{\infty} \int_{-\infty}^{\infty} \int_{-a}^a \int_{-1}^1 q(\xi, \eta) e^{i\alpha(x-\xi) + i\beta(y-\eta)} \, dx d\beta d\xi d\eta = 0, \quad (x, y) \notin \Omega. \tag{1}$$

$$M\omega^2 f(x, y) = P(x, y) - \iint_{\Omega} q(x, y) \, dx dy$$

Here P is the load applied to the stamp.

The integrand Green’s function $K(u)$ (1) describes the behavior of the layered base and carries information on the mechanical characteristics of each layer, water content and presence of cavity-shaped defects. The analytical view of the function $K(u)$, having very lengthy expression, is presented for different base types in [6–8]. Contact stresses are found in the series form according to Chebyshev polynomials:

$$q(x, y) = \sum_{k=0}^{\infty} \sum_{l=0}^{\infty} \frac{R_{kl} T_{2k}(x/a) T_{2l}(y)}{\sqrt{a^2 - x^2} \sqrt{1 - y^2}}, \tag{2}$$

$$T_k(x) = \cos k \arccos x$$

These representations (2) bearing in mind, the second system’s integral equation is met identically. The integral multiplicity in the first integral Eq. (1) is reduced twice

due to the analytical calculation of integrals on the basis of finite segments, Chebyshev polynomials and Bessel functions communication being taken into account. The system of integral equations is reduced to solving the infinite system of algebraic equations by means of the reduction methods.

$$\sum_{k=0}^N \sum_{l=0}^N K_{kl}(x_k, y_l) R_{kl} = P(x_k, y_l) / \vartheta_0, \quad (3)$$

$$K_{kl} = \int_{\mathfrak{R}_1} \int_{\mathfrak{R}_2} K(u) e^{i(\alpha x_k + \beta y_l)} J_{2k}(\alpha \alpha) J_{2l}(\beta) d\alpha d\beta - \vartheta_0 \delta(0, 0),$$

$$u = \sqrt{\alpha^2 + \beta^2},$$

$$\vartheta_0 = M\omega^2,$$

$$\delta(k, l) = \begin{cases} 1, & k = l, \\ 0, & k \neq l. \end{cases}$$

here, N is the number of terms left in the expansion, $J_k(ap)$ is the first kind Bessel function of order k .

While solving the latter system (3) the collocation method is used. The displacement of the front medium surface in case of plane vibrations is expressed through the solution of the latter system in the form:

$$u(x, y) = \sum_k^N \sum_l^N R_{kl} \int_{\mathfrak{R}_1} \int_{\mathfrak{R}_2} K(u) e^{i\alpha x + i\beta y} J_{2k}(\alpha \alpha) J_{2l}(\beta) d\alpha d\beta \quad (4)$$

2 Numerical Results

The analytic-numerical approach allows not only to study distribution of stress-strain fields, but also to predict behavior of mechanical system at change of characteristics, increase in speed of movement of loading.

Figure 1 shows graphs illustrating the distribution of contact stresses (2) under the square stamp at the frequency $\omega = 150$ Hz of oscillations of the porous two-layer half-space.

On the basis of the contact problem solution dealing with rectangular stamp one can come to the conclusion about the degree of adjacent sleepers' interaction under passing trains and the sleepers' impact on the permanent way. The problem statement allows considering additional real process random components, for example, track nonuniform elasticity, defects of rails or wheel flanges, etc.

The adjacent sleepers' interaction is rather small due to the structure of the ballast and its properties as a low-frequency filter. The discreteness of the contact area under

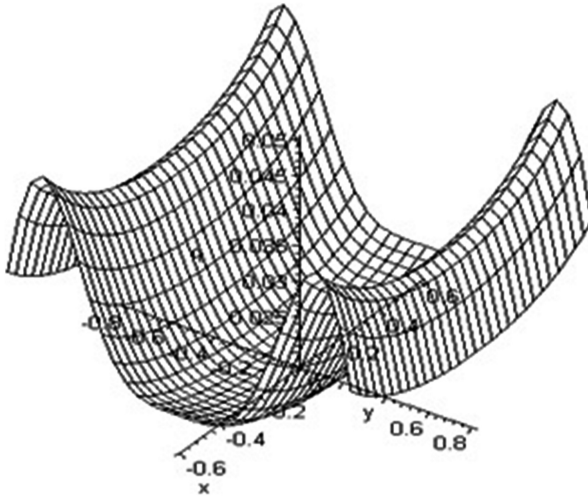


Fig. 1. Distribution of contact stresses under the square stamp at the frequency $\omega = 150$ Hz of oscillations of the porous two-layer half-space.

the train load on rails and sleepers can be traced up to 0.1–0.2 m in depth. 94% of the bogie pressure level covers the area occupied by 3 to 5 sleepers. The most significant contribution to the oscillating process is determined by the effective number of vibrating sleepers, occupying the rectangular area. By means of superposition decisions (2) and (4), mathematical model transfer function and theoretical amplitude-time and amplitude-frequency characteristics are constructed.

3 Experimental Data and Discussion

Experimental researches of wave fields and acceleration fields of the response of system a – railway track – a ballast prism – the stratified soil at passage of the train are executed. The carried out experiment allows to estimate adequacy of the suggested mechanics-mathematical model.

On Fig. 2 the amplitude-time acceleration characteristics points of the surface which is taking place on distance of 4 m from a near rail of a way a passenger train with speed of movement roughly of 56 km/h, consisting of the locomotive and fifteen cars is resulted.

The coincidence and similarity of spectral characteristics is the main criterion for identifying the dynamic processes in systems. To determine the dominant frequencies and assess the energy contribution of different harmonics, the amplitude-frequency characteristic (AFC) is graphed on the basis of amplitude-time characteristic (ATC) experimental data by means of windowed Fourier transform.

Figure 3 shows amplitude-frequency displacement characteristic, generated by first carriages. The ATC spectral analysis shows that the frequency range of 20 Hz–45 Hz is the most energy intensive and dangerous. frequency about 32 Hz is determined by a resonance of a permanent way.

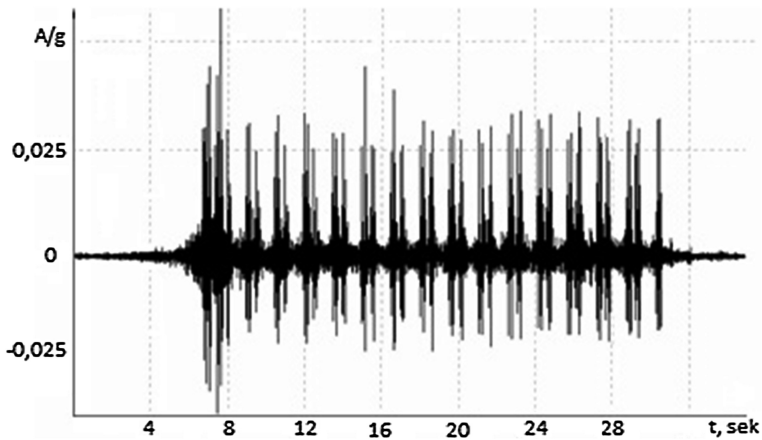


Fig. 2. Amplitude-time displacement characteristic, generated by train with 15 carriages.

The similar researches which have been carried out on a way with stacking on ferro-concrete cross ties, have shown displacement of a resonant range in area of higher.

Figure 4 shows amplitude-frequency displacement characteristic, generated by carriages two curves: the enveloping curve of the experimental amplitude-frequency displacement characteristics and the theoretical one.

Studying of the resonant phenomena in the top structure of a way is one of directions carried out in experimental researches. On resonant frequencies permanent way, the ballast prism, soil will be observed significant levels of amplitudes of oscillation.

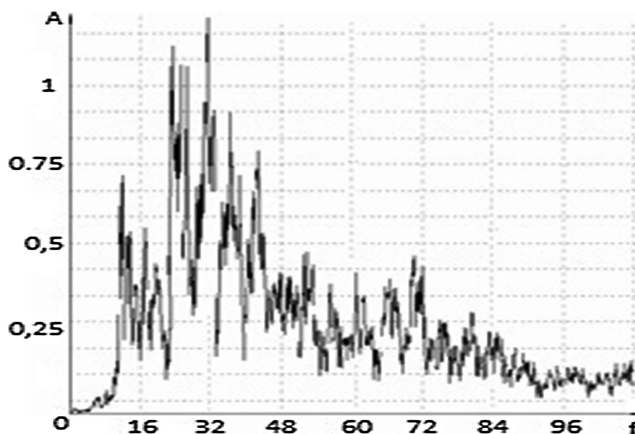


Fig. 3. Amplitude-frequency displacement characteristic, generated by first carriages

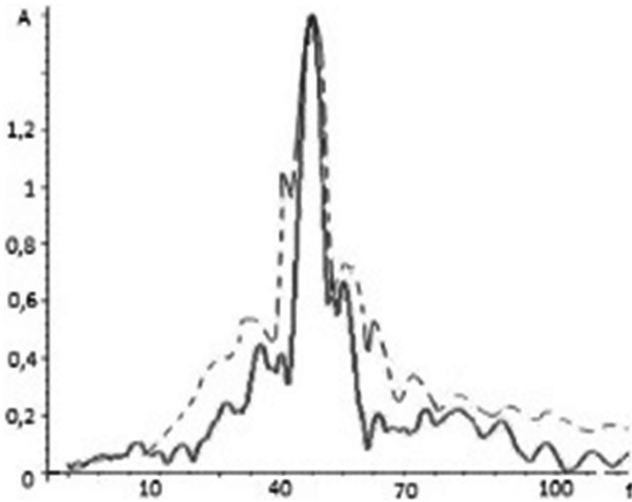


Fig. 4. Amplitude-frequency displacement characteristic, generated by carriages two curves: the enveloping curve of the experimental (dotted line) amplitude-frequency displacement characteristics and the theoretical (solid line) one.

Thickness and mechanical characteristics of soil layers, character of interaction between layers also influence its resonant properties.

Monitoring data of surface displacements of the ballast section and its spectral processing by means of fast Fourier transform contain the information about the characteristics of the passing rolling stock, the ballast properties and the permanent way condition. Besides it is possible to determine the type and technical condition of cars and their number.

Greater potential for vibration-based diagnostics is provided for account of processing and consequent analysis of experimental data by means of wavelet transforms. Unlike the classical spectral analysis, the application of the wavelet transform allows to obtain the dynamic process spectrogram and examine the evolution of all frequency fluctuation components in time. This is especially important for searching and recording all short-time transient non-ergodic signals associated with increased bogie's wear in particular.

4 Conclusion

The solution of the model problem taken as the basis, one can distinguish a number of parameters that are most important for permanent way monitoring. This is the appropriate level of displacements and accelerations that occur while train passing, their monotonic behavior while freight train passing, the stability of the most power intensive oscillation frequency range.

The above described theoretical and experimental approach to monitoring the movements of the ballast section can also be applied to the following tasks:

- to predict the permanent way deformations;
- to control the performance quality of rail and sleeper array and the subgrade;
- to assess the soil compaction;
- to estimate the quality of stiffening railroad embankments and the degree of ballast foulness.

References

1. Novacki, W.: Theory of Elasticity. Mir, Moscow (1975)
2. Bio, M.A.: Mechanics of deformation and acoustic wave propagation in a porous. *Mechanics* **6**(82), 103–134 (1963). Period Collection of Translations of Foreign Articles
3. Burridge, R., Keller, J.B.: Poroelasticity equations derived from microstructure. *J. Acoust. Soc. Amer.* **70**(4), 1140–1146 (1981)
4. Yeh, C.-L., Lo, W.-C.: An assessment of characteristics of acoustic wave propagation and attenuation through eleven different saturated soils. American Geophysical Union, Fall Meeting, December 2006
5. Hofmann, M., Hofstetter, G.: Parameter identification for partially saturated soil models. In: 2nd International Conference on Computational Methods in Tunnelling, Ruhr University Bochum, 9–11 September 2009, pp. 1–4. Aedi_catio Publishers (2009)
6. Kolesnikov, V.I., Suvorova, T.V.: Modeling the Dynamic Behavior of the System “Superstructure of the Railway Track – Layered Soil Medium”. VINITI RAS, Moscow (2003)
7. Usoshina, E.A., Suvorova, T.V.: Mathematical models of dynamical systems that include layered saturated porous elastic bases. *Vestnik of the Don State Technical University* **3**, pp. 10–15 (2016)
8. Suvorova, T.V., Novakovich, V.I.: The impact of structure and water saturation of the subgrade of the railway on its deformation during high-speed movement. *Int. J. Appl. Eng. Res.* **11**(23), 11448–11453 (2016). ISSN 0973-4562

Intelligent Security Analysis of Railway Transport Infrastructure Components on the Base of Analytical Modeling

Igor Kotenko^{1,2}, Andrey Chechulin^{1,2(✉)}, and Mikhail Bulgakov^{1,2}

¹ St. Petersburg Institute for Informatics and Automation of Russian Academy of Sciences (SPIIRAS), 14-th Liniya, 39, St. Petersburg 199178, Russia

{ivkote, chechulin, bulgakov}@comsec.spb.ru

² St. Petersburg National Research University of Information Technologies, Mechanics and Optics (ITMO University), 49, Kronverkskiy prospekt, St. Petersburg, Russia

Abstract. To increase the level of security in control systems for railway infrastructure the paper proposes to use the intelligent methods of security analysis based on analytic modeling of cyber-physical attacks. The paper suggests a technique of security evaluation based on analytical modeling, adapted for railway transport. To confirm the applicability of the proposed approach the results of experiments using models that reflect the railway transport infrastructure are provided.

Keywords: Railway transport · Security analysis · Modeling of cyber-physical attacks · Semi-full-scale models

1 Introduction

General purpose railway transport infrastructure is a sophisticated technological complex, which includes railway tracks of common use, railway stations, power supplies, communication networks, systems of alarm, centralization and blocking, information complexes, traffic control system and others buildings, structures, constructions, devices and equipment, providing functioning of this complex. The scale and popularity of railway transport is steadily increasing.

Currently various components of complex control systems of Positive Train Control (PTC) [1] are implemented. These systems have a layered architecture and are designed for automatic control of railway infrastructure, including schedule management. Failures of such systems can lead to large economic losses and even disasters. To date, management system of the railway infrastructure allow to monitor performance and provide effective management of the railway transport in real time. Such systems are equipped with the alarm and warning system which is designed to alert the operator about malfunctions in the system. However, with the increasing automation of railway connections, a growing threat are cyber-physical attacks on both physical and computer components of control systems, and problems of integral counter actions for them are now becoming increasingly relevant. In control systems of the railway transport

infrastructure it is critical to detect and eliminate faults and destabilizing factors. Therefore, speaking about cyber-physical attacks, it is advisable to use a proactive system of protection that can help to prevent security incidents before they occur. To solve this problem it is proposed to use the approach to intelligent analytical attacks modeling, allowing to perform analysis of the current situation in security, forecasting of possible ways of attacker's actions and countering them.

The main contribution of the paper is in development of an approach to the intelligent analysis of security of the railway infrastructure on the basis of analytical modeling. As a basis for the proposed approach, the paper used and refined the earlier suggested technique for security evaluation based on attack graphs [2, 3]. To ensure the possibility of its use for the railway infrastructure there was developed the analytical and semi-full-scale model of the PTC system, including both models of the elements of conventional computer networks (the control segment) and models of specialized objects, such as built-in devices, located in the rolling stock. The paper is organized as follows. The second section provides the review of related work on the subject of the paper. The third section presents the developed analytical and semi-full-scale model of control system of railway communication and its implementation. The fourth section is devoted to the technique of analytical modeling for PTC. The fifth section discusses application scenarios of proactive protection methods for control systems of railways communications and the analysis of the obtained results. The sixth section presents the conclusions and directions of future research.

2 Related Work

Currently, there are many works, describing different approaches to control systems of railway transport and its service infrastructure. So, [4] describes the principles on which modern systems of railway transport control are built, as well as the approach to modeling of such systems using Petri nets. [1] discusses the problems of providing security at control on the railway transport, as well as the review of the technology PTC (Positive Train Control), describing the architecture of systems based on this technology. [5] presents a system of railway infrastructure control ITCS implemented in Michigan using wireless radios, and the problems of the reliability of this decision are described. [6] presents the system ACSES, launched in 2002 and using fixed structure of signaling. At that, only a small number of scientific papers is devoted to the organization of protection of railway architecture from attacks. [7] describes the architecture of PTC systems as well as the analysis of the possible consequences of malicious use of the vulnerabilities in these systems. [8] discusses the vulnerabilities of modern control systems for railway service. This paper presents the classification of attacks on railway communication control systems and describes the tools of information security control for mitigation of these attacks. In the present paper for the analysis of security of the railway transport infrastructure we propose to use methods based on analytical modeling of attacks that would indicate possible attacks both at the stage of infrastructure building and during the operational phase. It is assumed that the simulation of incidents and security events, based on automatic mechanisms that use information about the history of the analyzed events and forecast of future events, as well as implementing

automatic adjustment of the parameters of the events' monitoring to the current state of the protected system, will allow to increase the level of protection of the railway infrastructure. For modeling of attack actions in this paper we propose to use attack graphs. Attack graphs are used for analysis of system security by determining how its vulnerabilities can be used by attackers within multi-stage attacks. They describe all possible ways of attacks. In addition, they can reflect system state and interstate transition in accordance with the used vulnerability. In order to take into account that vulnerabilities cannot always be used, there are limitations, depending on the skill of the attacker and the difficulty of vulnerability exploitation.

We can distinguish the following main types of attack graphs. The complete attack graph [9] involves all the ways an attacker can compromise the network. The main drawback of using such an attack graph is that the complexity $O(n!)$ too quickly grows with the network size. In the predictive attack graph [10] a node is added to the graph if no ancestor of this node uses the same vulnerability for transition to the same condition as the new node. These graphs are built much faster, but still contain excess structures. A graph with a set of preconditions [11] includes three types of nodes: state; precondition; vulnerability. Additional circular arcs are added to show the relationships with existing nodes. The advantage of this type of attack graphs is efficiency of their construction. Such a graph can be converted into a full or a predictive graph.

Basing on the constructed attack graphs using a variety of methods of analysis, e.g., [13–16], the evaluation of the current security state of the simulated object is done. At this we may take into account not only the possibilities of the attacker, but also the metrics describing the criticality of the information stored or transmitted through the analyzed elements in the protected infrastructure. The end result of methods' execution is the integrated assessment of security in the form of a qualitative assessment of potential damage. It is assumed that basing on the obtained measurements, one can assess the effectiveness of the implementation of countermeasures. In general case the proposed approach to the security analysis was suggested in [2, 3]. In this paper this approach has been adapted and improved taking into account the specifics of the railway infrastructure and the developed semi-full-scale model. It allows to experiment with different types of cyber-physical attacks.

3 Analytical and Semi-full-scale Models of PTC System

To apply the suggested approach to the security analysis we propose analytical and semi-full-scale models of perspective control systems for railway transport, such as Positive Train Control. These systems are deployed over an existing infrastructure of means for signaling, centralization and blocking and intended to improve the safety of trains' movement. In general, the Positive Train Control system is an integrated system, structural composition of which can be represented in the form of four segments (Fig. 1): Dispatch, Communication, Locomotives, and Wayside.

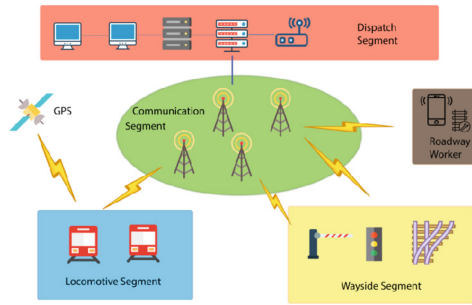


Fig. 1. Generalized structure of Positive Train Control systems

The first (dispatch) segment is the operational center, which includes the posts of dispatcher's control and centralization, coordination and matching devices, servers for storage, processing, analysis and visualization of data. In this segment the status of the objects of centralization and diagnostics of microprocessor tools of the system, current location and speed of trains, storing of temporary speed restrictions and other information are visualized. The main task of the operational center is the analysis of the current state of railway infrastructure, management of the trains' time schedule and remote control of the locomotives' speed. As a rule, the upper information layer also includes the remote monitoring stations, associated with operators' workstations through a wireless connection. In the analytical model this segment is presented as a set of computers with installed operating systems and common software and hardware. In the semi-full-scale model this segment is implemented as the system of Arduino controllers and the computer running a software intended to control models of mobile and stationary equipment.

The second (communication) segment is a wireless telecommunication network. This segment is designed to provide fast and reliable data transfer between all components of the integrated system. In the analytical model this segment is presented as a set of network telecommunication devices. In the semi-full-scale model this segment is realized as the transmission medium for commands from the control system to models of rolling stock and stationary equipment of railway transport. At that in the semi-full-scale model there are two parts of data transfer: from the computer to Arduino controllers and from controllers to equipment models. The first phase is implemented on the basis of RS232 protocol, and the second part uses the DCC Protocol to control the locomotives, which is standard for railroads models and uses the railway tracks to transmit the data.

The third (locomotives) segment includes on-board computers to control trains, brakes mechanisms, and movement controls. In this segment, the immediate control of the movement of the locomotive is done. In addition, this segment is responsible for receiving information from the satellite about the current location of the locomotive, sending operative information on the current speed and location to the operations center and receiving control commands. In the analytical model this segment is presented as a set of hardware components with vulnerabilities, specified directly by the system operator. In semi-full-scale models this segment is realized as a model of railroad under

digital control from the company PIKO. Digital control of locomotives enables to programmatically simulate the work of the train driver both as in interaction with the operator/dispatcher, and in the case where no command from the operator is received or communication with him is broken.

The fourth (wayside) segment is a set of executive and control equipment at the railway track. This equipment includes drives and interface units for switches, traffic lights, devices of track circuits, automatic barriers, as well as detectors and sensors. In the analytical model this segment is represented as a set of local stationary subnets, with standard software and hardware. In the semi-full-scale models this segment is realized in the form of switches, semaphores, and barriers with digital control according to the DCC protocol.

Thus, for experiments on the use of intelligent protection methods we developed the analytical model for the railway communication control system. This model is physical and is a computer network consisting of four zones, corresponding to the segments of the PTC (Fig. 2). A generalized model structure of the control system of railway communication corresponds to the architecture of the systems Positive Train Control and tailored to allow the modeling of security incidents. The proposed approach allows to simulate security incidents, similar to potential security incidents in real systems of railway transport.

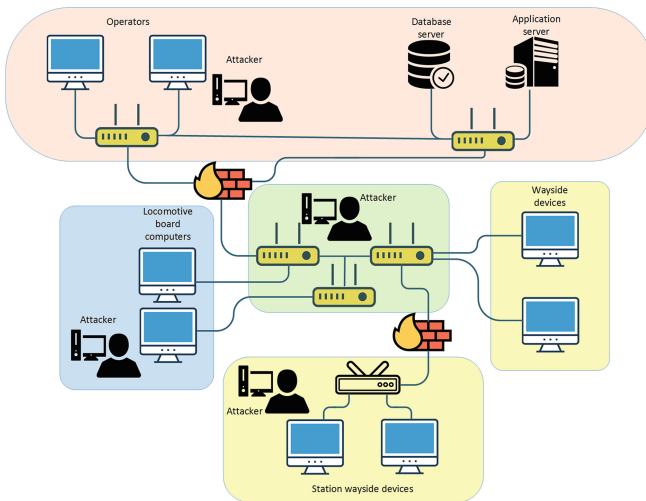


Fig. 2. Analytical model for railway communication control system

For performing visual demonstrations and experiments there was developed a semi-full-scale model that includes all the essential elements of the railway infrastructure and providing the ability to simulate locomotives movement control according to the given schedule. This model supposes the possibility of an attack by the attacker, aimed at different segments of the system. At that, the attacker can conduct the attack either directly (for example, the attack on the on-board computer of the locomotive

over a wireless connection directly from the cabin of the train), or remotely (e.g., via remote monitoring channel). Thus, the developed model allows to conduct experiments on the application of intelligent methods of protection of the railway infrastructure: the model displays the architecture of the Positive Train Control systems and allows to play all kinds of scenarios of carrying out attacks.

The proposed scheme of railway tracks is presented in Fig. 3.

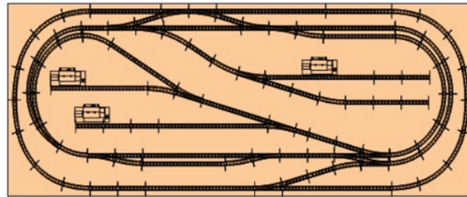


Fig. 3. The scheme of railway tracks in the semi-full-scale model

The proposed structure and composition, as well as the scheme of railway tracks, in the semi-full-scale model assumes usage of a large number of switches and traffic lights, allows to place railway crossings, to provide overtaking and downtime of trains, change of direction and route. Due to these features, this model allows to simulate attacks against infrastructure objects, that are specific to railway transport.

4 Security Analysis Technique and Its Implementation

Let us present the proposed technique for security analysis of railway infrastructure on the basis of analytical modeling. The technique assumes that for each attacker its own attacks tree is formed. Together these trees represent the attacks graph for the analyzed infrastructure and for all simulated attackers. The specificity of the PTC is presented in the form of specific infrastructure objects (locomotives, road infrastructure, etc.), including both hardware and software and possible vulnerabilities and attacks. In the preparation stage to the construction of attack trees for each object of the simulated infrastructure the 3-dimensional matrix is built for the following data: (1) class of attacks (data collection, preparatory actions, elevation of privilege, execution of the attack's target); (2) needed access type (remote source without access rights, remote user, local user, administrator); (3) the level of knowledge of the attacker (the types of vulnerabilities that the attacker can implement).

Figure 4 shows the generalized scheme of the proposed algorithm for analysis of the attack graph. The figure shows the following key steps of the algorithm: (1) formation of matrices by the databases of vulnerabilities and the configuration of software and hardware of hosts; (2) formation of the lists of the attacks available to attackers; (3) generation of attack trees based on the connectivity graph of the network and the lists of attack actions; (4) security metrics calculation.

The source data for building the attack graph are data relating to the analyzed infrastructure, and data about the vulnerabilities inherent to the software and hardware of this infrastructure. The data about the vulnerabilities for widely distributed software and hardware are downloaded from public databases such as the National Vulnerability Database (NVD) [12] and data for specific railway transport software and hardware are generated by the system operator.

For the experiments with the analytical models there was developed the software prototype. This prototype consists of several modules: (1) the database of vulnerabilities and attacking actions; (2) the model constructor for the analyzed object; (3) the security assessment system on the base of attack graphs. Adding specific to this area vulnerabilities occurs at the stage of forming the base of vulnerabilities and attacks (with the ability to update this information in the process of work) through module 1. Module 2 allows to build analytical models of individual infrastructure elements and describe the relationships between them. Module 3 enables to specify the model of attackers for the analyzed infrastructure and to conduct experiments to evaluate the current security state and evaluate possible countermeasures. Figure 5 presents the simulated infrastructure specified in module 2.

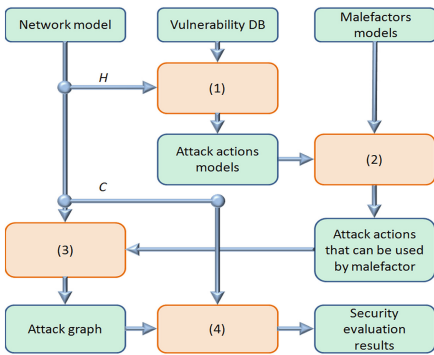


Fig. 4. The scheme of the algorithm

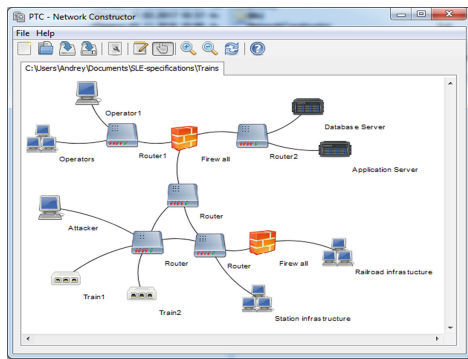


Fig. 5. Representation of the PTC infrastructure

For experiments the computer was added to the general scheme that is connected to the communication segment from which the attack is performed. For each element the information is provided about installed hardware and software that will allow to further analyze the possible attack actions.

5 Implementation of Attack Scenarios and Security Analysis

Let us consider the main attack scenarios from the point of view of the PTC system.

For attackers in the dispatch segment the target object (operator’s computer) is an address within the dispatch segment. So its attacking impacts are generally similar to attacks on workstations and servers. The attacker can eavesdrop the communication

channels, explore the remote services of the target device and search for errors in software and hardware. It is expected, but is not mandatory, that the attacker is familiar with the target system, however, the attack can be carried out without any prior knowledge. Examples of attacks that can be made by this type of attackers are: interception, modification and forgery of TCP/IP messages between the operator's computer and the servers (the attack "Man-In-The-Middle"); classical network attacks (DDoS attack, TCP SYN Flood, etc.); remote and local exploitation of vulnerabilities.

Wayside segment and the locomotive segment can also be the target of attackers. Attacks on the communication channels, analyzing and forgery of messages, attacks against controllers that are responsible for processing data from different sensors are possible. Examples of attacks that can be performed by the attacker are: attack by the third-party channel based on the remote access settings (e.g., electromagnetic radiation); attacks on availability (e.g., open lines of communication); the interception, modification and forgery of messages from the device through the connection segment, as well as cryptographic analysis of the message; remote and local exploitation of vulnerabilities; remote attacks on control modules by direct influence on their hardware components (for example, radio frequency attack).

As an example scenario of the usage of intelligent protection methods for the security analysis of railway transportation infrastructure systems we consider the case when the attacker attempts to remotely exploit the vulnerabilities of system components. As the source location for attacker we selected the segment of the wireless telecommunications network. The structure of developed model is shown in Fig. 6.

Within the framework of this model it is assumed that the purpose of the attacker is the impact on the control subsystem of the moving train, but attacker does not have sufficient knowledge for the attack, aimed directly at the locomotives. Thus, the simulated multi-stage attack consists of the following parts: (1) connection to the communication segment (due to the fact that the elements of this segment are partially located in the Internet, the potential access possibility is almost always present); (2) the attack on the firewall, protecting the dispatch segment; (3) the attack on computers of operators, engaged in the management of the moving train; (4) the attack on the application server, responsible for communication with managed railway objects; (5) the attack on the locomotive (i.e. the object which is the main target of the attack).

The overall results of analysis of the defended network are as follows: totally in the attack graph there are 5 hosts (and 3 routers, which allowed this traffic), for these hosts there were built about 100 different attack routes (routes differ from each other by the sets of vulnerabilities used). For each action of the attacker and for each route we calculated the parameters of complexity (Access Complexity (AC)) and potential mortality (Mortality (M)). Figure 7 shows the example attack tree leading from the initial position of the attacker to its target. Also possible deviations are shown from the direct route to the goal for modeling the fact that the attacker does not have in advance the exact information about the target infrastructure. In the process of building the graph we simulated three main stages of the attack – information gathering, identification of vulnerabilities, and their exploitation.

As the result there was selected the route from the initial location of the attacker to its target with minimum complexity and maximum values of mortality for each host. Based on data about the route there was calculated the level of security for the network

as a whole. The value of the security level for the analyzed network was 3 of 4, where level 1 is the maximum protection that means that the network requires urgent attention of the security specialist. The weakest point of the network (i.e. the host, through which the maximum number of attacks' routes passes) is the router through which the connection was made (which means that the main recommendation would be the protection from external connections, for example, by creating a virtual private network VPN) and host "Operator 1". Thus, the second recommendation is to increase the security level of that host. More detailed recommendations relate to correcting specific vulnerabilities and are based on data from the vulnerability data base.

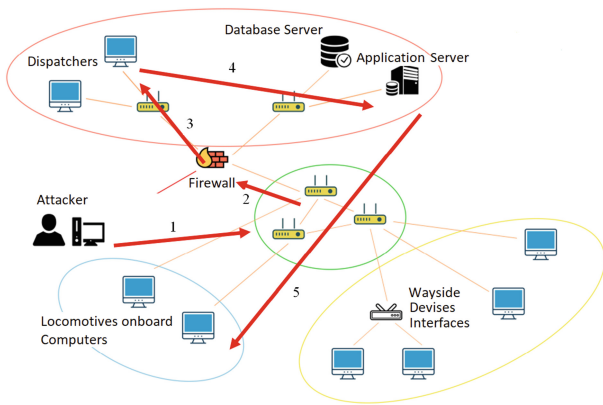


Fig. 6. The scenario of attacker's actions

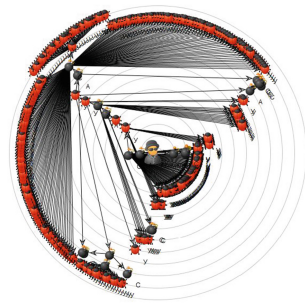


Fig. 7. Attack tree

Currently, there are many approaches to evaluation of security, including those based on attacks' simulation. In comparison with existing analogues the proposed technique allows to perform assessment of the protection of such specific object as railway transport infrastructure. This is achieved by constructing highly specialized analytical models of particular railway infrastructure's objects and through implementation of infrastructure elements in the form of semi-full-scale model.

6 Conclusion

In this paper we presented the approach to modeling of attacks to improve security of railway transport infrastructure. In addition, the paper presents analytical and semi-full-scale models of the PTC infrastructure, on which the experiments were carried out. The results of the system for modeling attacks can be as follows: (1) weaknesses in network's topology (hosts, through which the largest number of attack graphs passes); (2) selected countermeasures to reduce the probability of the maximum number of attack graphs; (3) possible consequences of implementation of countermeasures, taking into account the dependencies of the services. The solutions, discussed in the paper, can be elements of the overall system for the railway

infrastructure protection control. At present, theoretical investigations of attack graphs construction methods based on existing vulnerabilities and zero-day vulnerabilities, security policies, services dependencies, etc. are continued, and design of software prototype is performed for the system of construction and analysis of attack graphs. Further work is planned: to expand the system's functionality to include the analysis of zero-day attacks and communications services; to expand the list of security metrics for better assessment of the network security level; to clarify the model of the attacker for the railway infrastructure; to speed up the system performance through the optimization of the attack graphs constructing process; to expand the model of the railway infrastructure based on elements from the company PIKO.

Acknowledgements. This research is being supported by the grants of the RFBR (15-07-07451, 16-37-00338, 16-29-09482), partial support of budgetary subjects 0073-2015-0004 and 0073-2015-0007, and Grant 074-U01.

References

1. Peters, J.-C., Frittelli, J.: Positive Train Control (PTC): Overview and Policy Issues, Congressional Research Service Report for Congress, Washington (2012). 17 pages
2. Kotenko, I., Chechulin, A., Novikova, E.: Attack modelling and security evaluation for security information and event management. In: International Conference on Security and Cryptography (SECRYPT 2012), Rome, Italy, pp. 391–394 (2012)
3. Kotenko, I., Chechulin, A.: Attack modeling and security evaluation in SIEM systems. *Int. Trans. Sci. Appl.* **8**, 129–147 (2012)
4. Jansen, L., Meyer Zu Horste, M., Schnieder, E.: Technical issues in modelling the European Train Control System (ETCS) using coloured petri nets and the design/CPN tools. In: Workshop on Practical Use of Coloured Petri Nets and Design (1998)
5. Olson Jr., R.T.: Incremental train control system on Amtrak's Michigan Line, Presentation at AREMA Annual Conference, Chicago, IL (2007)
6. AGE's Positive Train Control Technology is Full Speed Ahead on Amtrak's Michigan Line, General Electric press release, Chicago, IL (2005)
7. Hartong, M., Goel, R., Wijesekera, D.: Securing positive train control systems. In: Goetz, E., Sheno, S. (eds.) *Critical Infrastructure Protection*. IFIP International Federation for Information Processing, vol. 253, pp. 57–72. Springer, Boston (2008)
8. Hartong, M., Goel, R., Wijesekera, D.: Communications security concerns in communications based train control. *WIT Trans. Built Environ.* **88**, 693–702 (2006)
9. Artz, M.: NetSPA: a Network Security Planning Architecture. Master's thesis, Massachusetts Institute of Technology, Cambridge, MA (2002). 96 pages
10. Lippmann, R.P., Ingols, K., Scott, C., Piwowarski, K., Kratkiewicz, K., Artz, K., Cunningham, R.: Validating and restoring defense in depth using attack graphs. In: *Proceedings of MILCOM 2006*, Washington, DC (2006). 10 pages
11. Idika, N.C.: Characterizing and aggregating attack graph-based security metric. Ph.D. thesis, Purdue University (2010). 131 pages
12. National Vulnerability Database. <https://nvd.nist.gov/>
13. Kotenko, I., Stepashkin, M.: Attack graph based evaluation of network security. In: *Proceedings of the 10th IFIP Conference on Communications and Multimedia Security (CMS 2006)*, Heraklion, Greece, pp. 216–227 (2006)

14. Poolsappasit, N., Dewri, R., Ray, I.: Dynamic security risk management using Bayesian attack graphs. *IEEE Trans. Dependable Secur. Comput.* **9**(1), 61–74 (2012)
15. Kanoun, W., Cuppens-Bouahia, N., Cuppens, F.: Automated reaction based on risk analysis and attackers skills in intrusion detection systems. In: *Proceedings of CRISIS 2008* (2008)
16. Kotenko, I., Stepashkin, M.: Analyzing vulnerabilities and measuring security level at design and exploitation stages of computer network life cycle. *LNCS*, vol. 3685, pp. 317–330. Springer (2005)

Applied Systems

Sensing Thermal Processes with Piezoelectric Film Elements

Iliya Hadzhidimov^(✉) and Emil Rosenov

Technical University of Varna, Studentska 1, 9010 Varna, Bulgaria
{i_hadzhidimov, erosenov}@tu-varna.bg

Abstract. The Piezoelectric Polymer Sensors discovered in the early 20th century, are widely used today in different technologies and applications. The high piezo-activity in polarized fluoropolymer polyvinylidene fluoride, known as PVDF - observed since 1969, is currently a fundamental effect for some of many promising sensors. In this research an attempt to use a PVDF sensor to estimate some thermal processes have been performed. The reaction of PVDF under some thermal loadings is examined. For this purpose an amplifier for Piezofilm signal conditioning is provided, some experiments performed and conclusions reported.

Keywords: Piezoelectric film elements · PVDF · Pyroelectric effect

1 Background

PVDF based sensors have very good sensitivity and low thickness in a range of 9–110 μ [1]. This makes such sensors suitable to sense different processes due to mechanical to electric conversion. Beside of the piezoelectric effect caused by pressure, when the changes of the temperature of the objects also generate electric potential - this effect is known as “pyroelectric effect” [2]. The activity of the PVDF films is determined by the coefficients of proportionality between the mechanical or thermal processes causing subsequent electrical effect [3]. PVDF strongly absorbs infrared energy in the 7–20 μ m wavelengths. New copolymers of PVDF have expanded the applications of piezoelectric polymer based sensors. These copolymers permit applications with higher temperatures (125 °C). The Piezoelectric films are widely used as pressure sensors, acoustic components, in robotics, security, medical, electrical devices and others. Since the PVDF based sensors convert signal from electrical to mechanical, mechanical to electrical and thermal to electrical, sometimes it is difficult to divide the parts of a complex signal in order to analyze a thermal process. On the other hand some processes connected with electric heaters induce large electromagnetic noise which leads to instability when measuring the reaction of PVDF based sensors. The area of implementation of these sensors can be expanded if the pyroelectric effect can be correctly estimated and analyzed. They are several examples for implementation of such sensors intended for industrial needs [4–10] and connected with thermal behavior of the objects in most of cases using different types amplifiers, signal or charge [11]. In spite of all these efforts it is sometimes very hard to obtain a strong mathematical description even nonlinear of PVDF’s

electrical reaction as a result of different thermal processes. In present paper an attempt to reveal some simple mathematical dependencies related with electrical and thermal reaction of a PVDF element based on some specific cases is performed.

2 Equipment

In order to sense thermal processes a PVDF LDT Series element (LDT0-028K) production of “MEAS” is used [12], Fig. 1. The corresponding signal amplifier [13] is produced to extract PVDF sensor thermal signal, Fig. 2. The thermal signal amplifier is realized using equivalent operational amplifiers and including the decoupling capacitors located as close as possible to the operational amplifiers.

For data recording a specialized development board – Arduino Uno is used. The board includes 8-bit μC with an integrated 10-bit ADC. In order to avoid external noise by USB cable and main source, the board has been powered by a battery and data



Fig. 1. PVDF LDT0-028K

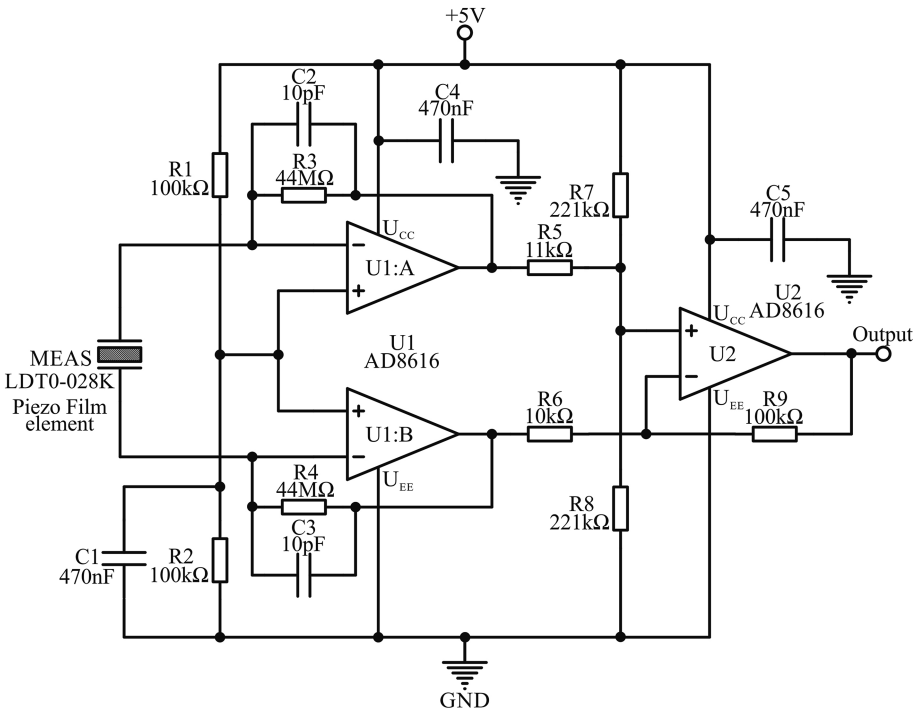


Fig. 2. PVDF thermal signal amplifier

transfer is done using 433 MHz RF communication via two APC200A RF transceivers, one to transmit and other to receive, Fig. 3.

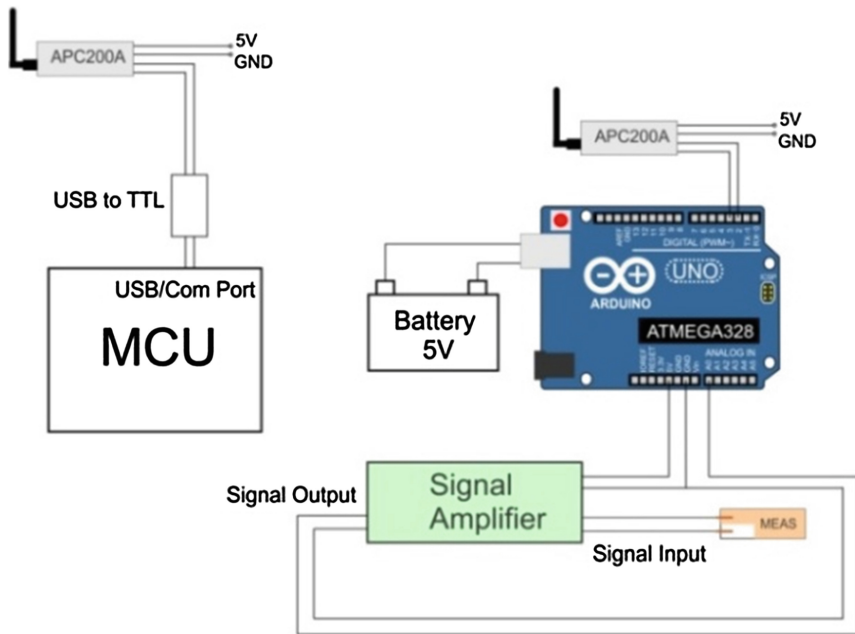


Fig. 3. Measurement equipment. Left APC200A is connected to the MCU and is functioning as a receiver. The right APC200A works as a transmitter

3 Experiments

Two types of experiments are performed with low level heat source. First is a thermal signal with less noise (human hand and a gas heater) and second with electric heater plate introducing electromagnetic interference. The PVDF is fixed vertically on a plastic plate, Fig. 4. To find dependence between PVDF voltage signal and the temperature also a wireless infrared thermometer MLX90614 has been included in the measurement setup. The infrared thermometer is closely positioned to the PVDF which is painted black for better emissivity.

All experiments are performed with connection via USB COM Port to the MCU with baud rate of 9600 bps. In order to obtain the frequency of the signal transmitted by the signal amplifier a test was carried out. After 5000 analog readings the sample time and frequency of the data transferred through the measurement equipment are calculated as follows:

$$\text{Sample time} = 5119,99 \cdot 10^{-6} \text{ s, Frequency} = 195,31 \text{ Hz.}$$

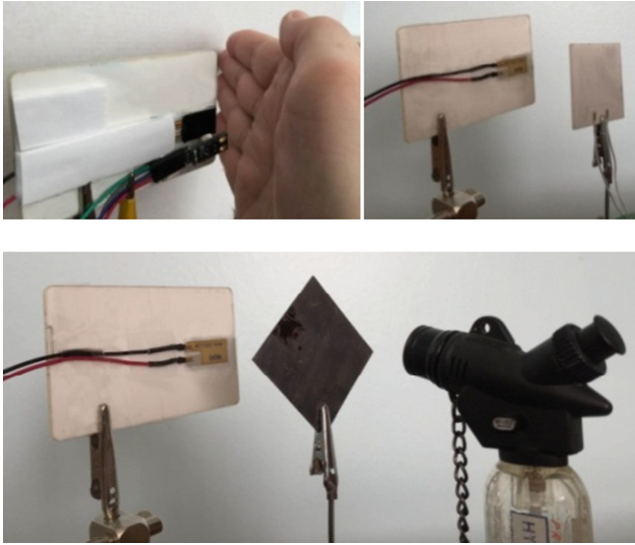


Fig. 4. PVDF, heat sources position and infrared thermometer MLX90614. Between the nozzle and PVDF a Cu plate for heat dissipation and sensor protection is provided

After analog to digital conversion a delay of 5 ms is provided. The fragment of the code in “setup part” is given below. Instead “Serial” commands “rfSerial” are used because of RF communication library.

```

long t_start, time;
int number_samples = 5000;

void setup(void)
{
  rfSerial.begin(9600);
  t_start = micros();
  for(int i=0; i < number_samples; i++)
  {
    int sample = analogRead(A0);
    delay(5);
  }
  time = micros() - t_start; // elapsed time
  rfSerial.print("Sample time > ");
  rfSerial.println((float)time/number_samples);
  rfSerial.print("Frequency : ");
  rfSerial.println((float)number_samples*1e6/time);
}

```

4 Results and Discussion

The first experiment is realized when a human hand is nearly positioned to the sensor, for a small period of time and then removed, Fig. 5. The heat source of the second experiment is a gas torch with Cu plate between the source and PVDF. The recordings consist of data in regime Off/On/Off which means starting without heat source and then the gas torch is switched on and after few times the torch has been switched off, Fig. 6. When the heat is reaching the surface of the PVDF the first reaction is increasing voltage and temperature. This process continues until the limit of the PVDF's tension is reached and it drops down still the temperature continues rising. After the heat source is switched off both voltage and temperature fall down. And after releasing the tension, voltage starts rising again parallel with decreasing of temperature, Fig. 6. The proportion between voltage and temperature can be found during the period when both voltage and temperature increase. Based on data measured the inverse problem of finding the pyroelectric coefficient also may be solved.

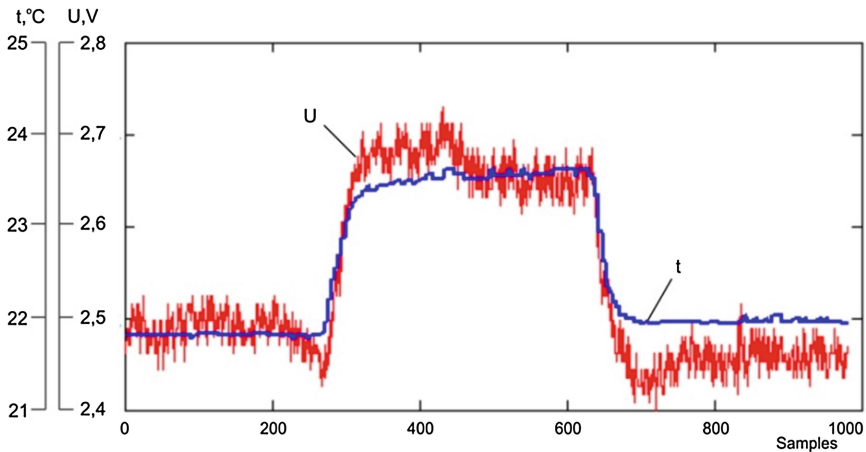


Fig. 5. PVDF voltage and temperature recorded. The heat source is a human hand

To find dependence between pyroelectric voltage and temperature the part of data shown in Fig. 5 at the beginning of voltage rising is used, samples between 280 and 315. A polynomial regression is implemented with $n = 4$ where the argument “ x ” may be the number of samples or time of recording:

$$f(x) = a_0 + a_1 \cdot x + a_2 \cdot x^2 + \dots + a_n \cdot x^n \quad (1)$$

Consecutively this function is used to smooth voltage and temperature.

The next step is to calculate the pyroelectric coefficient. The thickness of the PVDF is $\delta = 28 \cdot 10^{-6}$ m and permittivity $\epsilon = 106 \cdot 10^{-12}$ pF/m. The pyroelectric coefficient “ p ” has been expressed as follows and shown in Fig. 7 as a function of temperature:

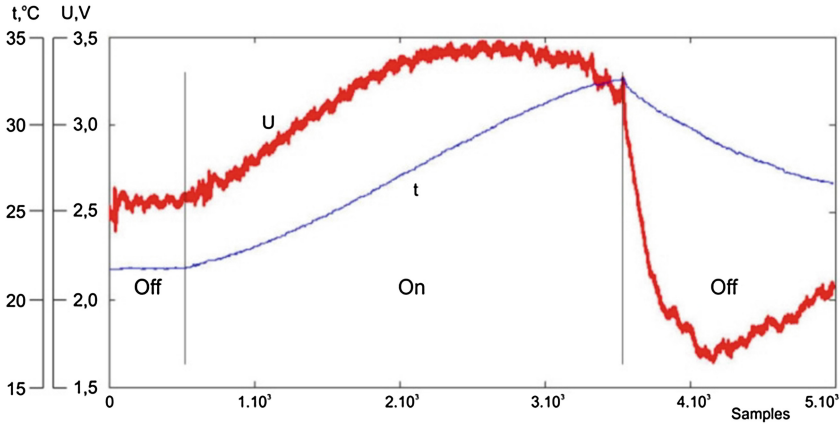


Fig. 6. PVDF voltage and temperature recorded. The heat source is a gas flow in regime Off/On/Off

$$p = \frac{V \cdot \varepsilon}{\delta \cdot t} \tag{2}$$

where

- V – Sensor voltage, V,
- t – Temperature, °C.

If the same procedure is applied to the data in sample range from 500 to 1500 in Fig. 6 the pyroelectric coefficient may be defined for higher temperatures, Fig. 8.

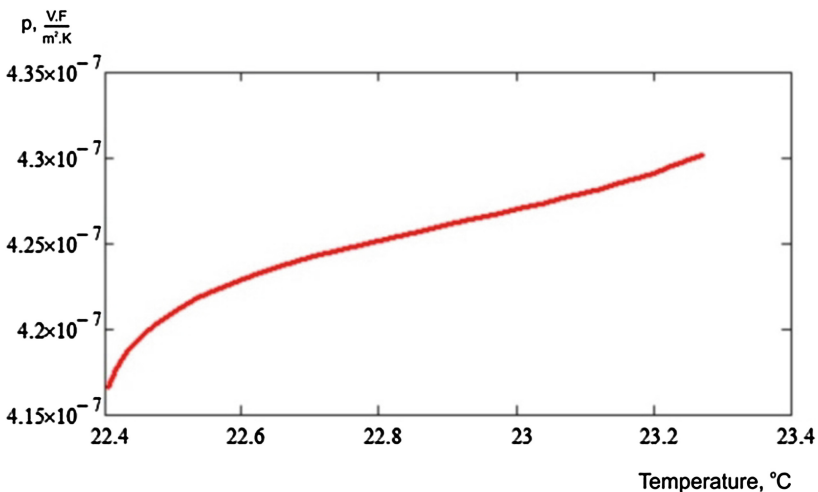


Fig. 7. Pyroelectric coefficient “p” expressed as a function of temperature, heat source is a human hand

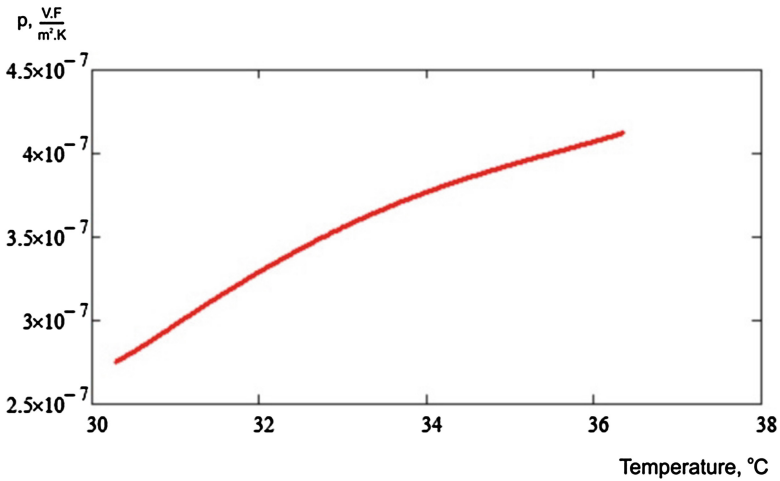


Fig. 8. Pyroelectric coefficient “p” expressed as a function of temperature, heat source is a gas flow

PVDF can be used as a temperature sensor if the temperature can be correctly expressed as a function of pyroelectric voltage within a suitable parametric range.

More complicated is to find the dependence between voltage and temperature when electric heaters are used. The distortion of the signal is significant and a data filtration is necessary. During this experiment the heat source was pushed forward to the PVDF and then moved back. A FFT procedure over 2048 raw voltage readings was performed to estimate the filtered data. In Fig. 9 the recordings and filtered data are presented.

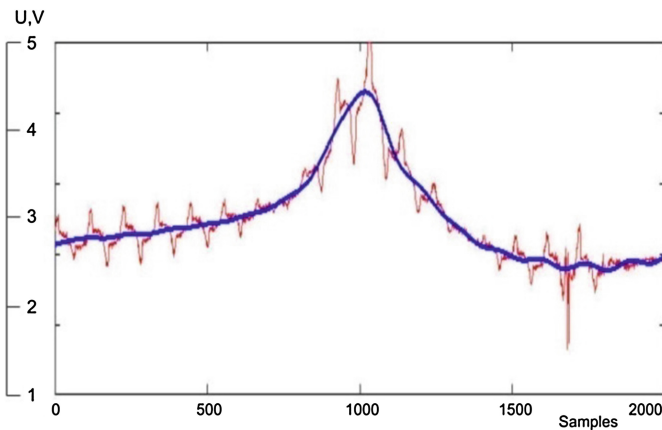


Fig. 9. Raw and filtered voltage data, frequency FFT filter implemented

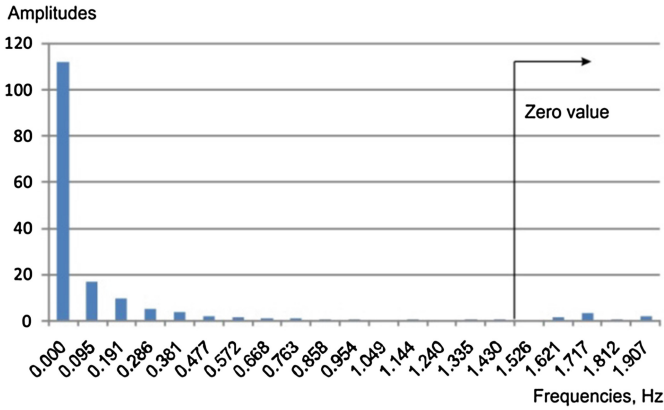


Fig. 10. Signal frequencies below 2 Hz. Frequencies greater than 1,526 Hz are assumed as noise

As seen in Fig. 10, all frequencies of the signal greater than 1,526 Hz are assumed zero and by an inverse FFT the filtered data may be calculated.

Finally both voltage and temperature signal may be seen in Fig. 11.

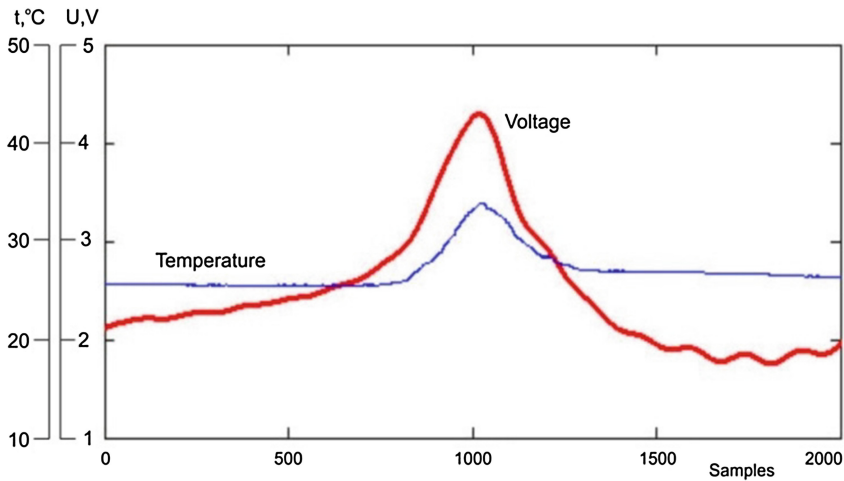


Fig. 11. Temperature and filtered voltage signal

5 Conclusion

Beside the other properties of PVDF’s sensing thermal processes is also possible. More complicated is the problem to use a Piezopolymer as a thermometer or flux sensor. Such measurements may be realized easy in processes with corresponding behavior of temperature and PVDF in a dynamic range of rising and dropping down (Fig. 11). In

other cases like this shown in Fig. 6 the increasing time of thermal load causes reaction of PVDF different than temperature of the sensor. The PVDF's are very suitable for detecting heat even of small quantities which corresponds to temperature reaction of the sensor. They are reliable, low cost and only a signal amplifier is needed. When a stable dependence between temperature and voltage measured exists simple mathematical function may be used for temperature evaluation. On the other hand if adequate measuring of heat flux can be performed also dependence between heat and sensor voltage can be found. One of the obstacles to avoid is the interface noise of measurement equipment and MCU intended for data collection. Wired transmission may cause noise (usually USB) and any wireless protocol like Wi-Fi, Bluetooth or RF is convenient in dependence of data transferred frequency required. Also a battery to power the measurement equipment is suitable by the same reason.

References

1. PIEZOELECTRIC FILMS TECHNICAL INFORMATION, PIÉZOTECH S.A.S.: Polymères pyro- et piézoélectriques. www.piezotech.fr
2. Malmonge, L., Malmonge, J., Sakamoto, W.: Study of pyroelectric activity of PZT/PVDF-HFP composite. *Mater. Res.* **6**(4), 469–473 (2003)
3. Piezo Film Sensors Technical Manual. Measurement Specialties, Inc., Sensor Product Division. www.msiusa.com
4. Marinov, A., Stanchev, O., Bekov, E.: Application of charge amplifiers with Polyvinylidene Fluoride materials. In: 2014 37th International Convention on Information and Communication Technology, Electronics and Microelectronics, MIPRO 2014 (2014)
5. Bekov, E., Marinov, A., Valchev, V.: PVDF based rain sensor for weather assessment relevant to renewable energy sources. In: PCIM Europe Conference Proceedings, pp. 1658–1661 (2012)
6. Marinov, A., Bekov, E., Valchev, V.: PVDF based wind direction and speed sensor for weather assessment relevant to renewable energy generation. In: 15th International Power Electronics and Motion Control Conference and Exposition, EPE-PEMC 2012, pp. DS1d.41–DS1d.44. ECCE Europe (2012). Art. no. 6397236
7. Manju, A.: Thermal diffusivity measurement of polymers, metals, superconductors and a semiconductor by combined piezoelectric and pyroelectric detection. Ph.D. thesis, University of Hong Kong, October 1999
8. Gusarov, B.: PVDF piezoelectric polymers: characterization and application to thermal energy harvesting. THÈSE Pour obtenir le grade de DOCTEUR DE L'UNIVERSITÉ GRENOBLE ALPES, HAL archives-ouvertes.fr, December 2015
9. Odon, A.: Voltage response of pyroelectric PVDF detector to pulse source of optical radiation. *Measur. Sci. Rev.* **5** (2005). Section 3
10. Dimitrov, B., Nenov, H., Marinov, A.: Comparative analysis between methodologies and their software realizations applied to modeling and simulation of industrial thermal processes. In: 2013 36th International Convention on Information and Communication Technology, Electronics and Microelectronics, MIPRO 2013 (2013)

11. Marinov, A., Stanchev, O., Bekov, E.: Application of charge amplifiers with polyvinylidene fluoride materials. In: 37th International Convention on Information and Communication Technology, Electronics and Microelectronics - MiPro 2014, Opatija, Croatia, MiPro Proceedings, pp. 91–95 (2014). ISBN 978-953-233-078-6
12. LDT with Crimps Vibration Sensor, MEASUREMENT SPECIALTIES. www.meas-spec.com
13. Amplifier Provides Signal Conditioning for Piezofilm Sensor, Maxim Integrated, Application Note 1127

Reliability Estimation of Electricity Distribution Substation Surge Protection System Composed by Surge Arresters with Different Operational Parameters

Nikolay Nikolov^{1(✉)}, Neli Dimitrova², Anton Georgiev¹,
and Margreta Vasileva²

¹ Department of Electronic Engineering and Microelectronics,
Technical University of Varna, Varna, Bulgaria
nikolay.nikolov@tu-varna.bg

² Department Electric Power Engineering, Technical University of Varna,
Varna, Bulgaria

Abstract. The aim of this article is to suggest an approach to obtaining estimation values regarding reliability of electricity distribution substation surge protection system in cases when it is composed by surge arresters characterized by different operational parameters. A benchmarking is performed in order to select a set of surge arresters providing the surge protection system with a high reliability. Based on it some practical recommendations are given to be considered applying the approach suggested regarding surge protection system in operation.

Keywords: Reliability · Surge protection · Overvoltage

1 Introduction

A very important part of the electricity distribution middle voltage and high voltage systems are the surge protection systems (SPS) [1]. These are intended to protect the substation equipment against overvoltages resulting from lightning strokes on the substation area and particularly on the incoming/outgoing overhead lines (OHL). The present study concerns only this part of a surge protection system which is composed by surge protection devices, such as surge arresters (SA). Within the study below this is called SPS. Most often the basic and auxiliary substation equipment is protected against overvoltages of atmospheric origin by metal-oxide SA and the SPS system is a set of such. A very important task standing in front of operational engineers is to perform the right selection of a proper set of SA so that to ensure as high as possible equipment protection level [5]. A key role in fulfilment of this play the overvoltages values expected, as well as the technical characteristics of SA [8]. The usual approach to selection of suitable SA set is to consider data collected during the substation operation and the operational experience of the engineers as a basis of this, taking also into account the referential data of the SA types at the disposal.

Such approach does not always guarantee a high SPS reliability as this is not based on SPS reliability assessment. As it is known from the reliability theory [6] the first

precondition for to provide a system with a high reliability is this to be composed by reliable components. For an SPS these are metal-oxide SA and their respective groundings. It is also important the system reliability to be assessed considering its components interconnection and interaction in terms of reliability.

Following a classical approach to reliability assessment of an SPS there is developed and presented in [3] a mathematical model of substation SPS reliability there. This is chosen as a basis for the current study, which object is to determine a well-grounded approach to a proper SA set selection, based on SPS reliability assessment.

The SPS reliability model cited is derived based on assumptions in regard to the system elements as follows:

- their failures are random and independent events;
- their failure rate does not depend on time, hence the uptime distribution can be described by the exponential random variables distribution;
- they are characterized by rated values of their parameters and operate within the limits of their operational mode, specified in the technical documentation.

2 Reliability Estimation of SPS

In order to make the study more perspicuous, a particular case is analyzed below.

Consider an electricity distribution substation presented by its single-line diagram, shown on Fig. 1. The substation is supplied by three 110 kV incoming overhead lines (OHL). It is composed in line of single bus system with bus sectionalizer and includes two 110/20 kV, 25 MVA power transformers.

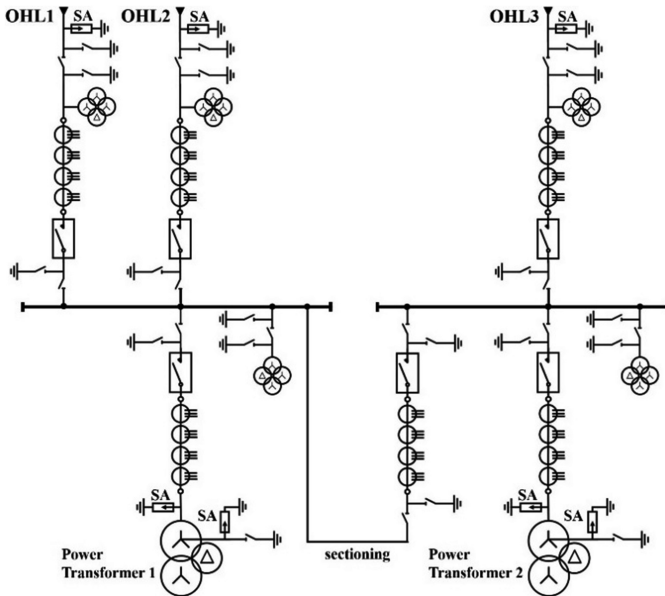


Fig. 1. Single-line diagram of a 110/20 kV substation under analysis

Usually SA are installed in groups of three at each of OHL, connected respectively one by one between each of the phase lines and each of the groundings. Such groups of SA are installed also at the power supply side of the power transformers. Another pairs of one SA and one grounding are connected to the neutral at the power supply side of each of power transformers. Let denote the SA installation points as follows: at an incoming OHL as *Position 1*, at a power transformer as *Position 2* and at a power transformer neutral as *Position 3*. These positions reflect some hierarchy in the surge protection of the substation equipment.

From structural point of view the SA, which the SPS system is composed of, are power semiconductor components, designed as metal-oxide varistors intended to work under high voltages. In terms of reliability they are considered as non-repairable electronic devices. The SA reliability indices would take different values for the SA from different groups, depending both on the installation point and the degree of the voltage, power and temperature stress. Thus the failure rate estimations of SA in separate groups take different values.

Typically the SA in a group are of the same type and have identical operational characteristics. For the purpose of this analysis and for to simplify the mathematical model chosen and easily to derive the most specific dependences, emphasizing at the same time the role of the SA characteristics and SA positioning, it is assumed that:

- All SA within groups installed at *Position 1* are of a same type, are characterized by identical operational parameters and also by equal values of reliability indices;
- All SA within groups installed at *Position 2* are of a same type, are characterized by identical operational parameters and also by equal values of reliability indices;
- The SA connected at the *Position 3* are of a same type, are characterized by identical operational parameters and also by equal values of reliability indices;
- All groundings have equal values of its reliability indices at certain operational regime of the SPS;
- The voltage stress as well as the temperature stress of the SA of same type at same positions are equal at certain operational regime of the SPS.

Applying the mathematical model describing the substation SPS reliability presented in [3] in the case when the number of OHL $n = 3$, the number of power transformers $m = 2$, and taking into consideration the assumptions above, it becomes possible this model to be simplified and it takes the form below

$$P(t) = e^{-\lambda_B \cdot \pi_\varphi \cdot t} \left(9 \cdot \pi_{T_1} \cdot \pi_{S_1} + 6 \cdot \pi_{T_2} \cdot \pi_{S_2} + 2 \cdot \pi_{T_3} \cdot \pi_{S_3} + \frac{17 \cdot \lambda_G}{\lambda_B \cdot \pi_\varphi} \right) \quad (1)$$

where $P(t)$ is the probability of SPS reliable operation for a certain period of time t , i.e. the SPS reliability function; λ_B denotes the basic failure rate of a metal-oxide SA, and its value is the same for all metal-oxide SA; λ_G denotes the failure rate of a grounding connection; π_{T_1} , π_{T_2} and π_{T_3} are coefficients, reflecting the temperature stress of the SA at *Positions 1*, *2* and *3* respectively; π_{S_1} , π_{S_2} and π_{S_3} are coefficients reflecting the voltage stress of the SA at *Positions 1*, *2* and *3* respectively; π_φ is a complex coefficient, which is equal to $\pi_\varphi = \pi_C \cdot \pi_Q \cdot \pi_E$ [2], where π_C is a coefficient reflecting the design peculiarity of SA; π_Q is a coefficient reflecting the production quality level

satisfied by SA; π_E is a coefficient reflecting the environmental conditions during SA operation; t denotes the period of time for which the SPS reliability function is estimated.

Let the substation equipment surge protection is performed by three SA types, e.g. *Type 1*, *Type 2* and *Type 3*, different in their rated and operational characteristics, produced by same producer. Each of these SA types can be installed at the three possible positions identified above (see Fig. 1). The task laid is the SPS reliability to be assessed for different variants of positioning the SA of the three types, and based on benchmarking of all possible variants an approach to selection of variants ensuring the highest level of substation equipment protection to be suggested.

The number of possible variants is determined by the formula for the number of variations with repetition as below

$$\bar{V}_p^k = k^p \quad (2)$$

where p denotes the number of positions; k denotes the number of SA types.

In this case $p = 3$ and $k = 3$. Hence the total number of possible variants of the SPS composition is $\bar{V}_3^3 = 27$.

Let the basic characteristics of the three types of SA are as follows:

- The rated operational voltage U_C is this, which a SA can endure long enough time without any damages, keeping its operational characteristics within the standard. Let the root mean square (*rms*) values of this, valid for the SA in the example are: $U_C = 84$ kV for SA *Type 1*, $U_C = 77$ kV for SA *Type 2*, and $U_C = 58$ kV for SA *Type 3*;
- The protection level at which SA perform overvoltage limitation U_P for the SA in the example its values are: $U_P = 240$ kV for SA *Type 1*, $U_P = 226$ kV for SA *Type 2*, and $U_P = 212$ kV for SA *Type 3*.

For the SPS reliability assessment is chosen the methodology presented in MIL-HDBK-217F [2] as it is the most applied reliability prediction methodology for systems composed by electronic components [7]. According to this as well as to the *Part stress analysis* approach also presented in [2], the SPS reliability function for a certain time $P(t)$, which is the basic reliability index of the SPS system, is determined by the reliability indices of the system components, i.e. the SA. The operational environmental conditions are specified in [2] as 14 types, depending on the location of the operation, climatic conditions, factors of the operating conditions severity, etc. There are presented there also initial reliability data regarding electronic components, necessary to perform a reliability estimation of system composed by such.

Two different operational regimes are typical for an SPS. The first of it is the normal operational one. This is the case when the SPS and its components are put under normal stress in regard to operational conditions such as voltage, temperature, power dissipated etc. The SPS and its components can endure such operational conditions for a long enough time, i.e. for its lifetime.

The second operational regime is this when the SPS is put under extreme stress. This is occurred during a lightning stroke on an OHL followed by occurrence of an overvoltage wave. The duration of this regime is very short and usually lasts microseconds.

In order to find out an applicable approach to proper SA set selection it is necessary the SPS reliability to be assessed during these two operational regimes.

The reliability estimation is performed considering the respective reliability data regarding power electronic components presented in [2]. The indices and coefficient, valid for both of the regimes, take the values as follows: λ_B is equal to $0,0013 \cdot 10^{-6} \text{ [h}^{-1}\text{]}$ as for transient suppressors/varistors; π_C takes the value 1,0 corresponding to metallurgically bounded SA contact construction; π_Q takes the value of 0,7 which corresponds to the highest quality level; π_E takes the value of 8,0, which corresponds to the outdoor operational condition.

2.1 SPS Reliability Function Estimation During a Normal Operation

For SPS reliability estimation during a normal operation (*Regime 1*) it is appropriate to choose the SPS reliability function for a certain period of time as SPS reliability index for to estimate. Its estimation value can be used as a basis for benchmarking of different SPS compositions. The initial reliability data corresponding to this SPS operational regime are as follows: λ_G takes the value of $0,001 \cdot 10^{-6} \text{ [h}^{-1}\text{]}$; t is assessed as equal to 4320 h, which corresponds to the time between two consecutive periodic inspections and preventive maintenance, which typically is six months; The voltage stress is assessed as in [2], for operational linear voltage of 110 kV.

The respective data regarding coefficients π_T and π_S are presented in the Table 1.

Table 1. Values of π_T and π_S for the three SA types at the three positions, in *Regime 1*

SA type	π_{T_1}	π_{S_1}	π_{T_2}	π_{S_2}	π_{T_3}	π_{S_3}
1	1,643920	0,506767	1,643920	0,506767	1,400415	0,035108
2	1,696444	0,626239	1,696444	0,626239	1,446645	0,043409
3	1,805500	1,246741	1,805500	1,246741	1,542765	0,086372

2.2 SPS Reliability Function Estimation During a Lightning Stroke

As this operational regime is a specific one, the SPS reliability analysis during this requires additional particularization. For this purpose a hypothesis is adopted. This is that an eventual lightning stroke hits an incoming OHL in close proximity to the substation. Practically this is the worst case of impact and this must provoke activation of the protective function of the entire SPS in regard to the basic facilities, such as the power transformers. This is called below *Regime 2*.

As the duration of this SPS operational regime is extremely short, there are not any studies regarding uptime distribution of the SA at this. For to overcome this obstacle it is additionally assumed, that SA uptime distribution during this regime also can be described by the exponential random variables distribution and it can be applied the same mathematical model as above. The difference here is that during the operational regime which is characterized by extreme stress is more sufficient to choose the probability of failure $Q(t)$ of the SPS system as a basic reliability index for to estimate.

At this SPS operational regime λ_G takes the value of $0,015 \cdot 10^{-6} \text{ [h}^{-1}\text{]}$.

The processes during a lightning stroke are analyzed by a computer simulation, presented in [4]. This is performed considering the conditions as follows:

- A lightning hits an OHL up to about 100 m far from the substation;
- The lightning stroke lasts 10 μs . This is the value of t ;
- The substation is equipped with SA installed as it is already shown (see Fig. 1).

As a result of the analysis it is ascertained that the peak voltage value at the *Position 1* is equal to 260 kV, at the *Position 2* it is 201 kV and at the *Position 3* its value is equal to 196 kV. Considering the respective voltage stress at each position, as well as the fact that the maximal junction temperature of SA in case of their activation is up to 80 °C [9, 10], the coefficient values of π_T and π_S for this SPS operational regime are determined as it is shown on Table 2.

Table 2. Values of π_T and π_S for the three SA types at the three positions, in *Regime 2*

SA type	π_{T_1}	π_{S_1}	π_{T_2}	π_{S_2}	π_{T_3}	π_{S_3}
1	4,438424	1,2147	4,216297	0,64991	3,231927	0,611381
2	4,669512	1,4044	4,438424	0,75215	3,412731	0,706946
3	5,033468	1,6420	4,788491	0,87830	3,698647	0,826331

The probability of failure of SPS is expressed as $Q(t) = 1 - P(t)$.

3 Results Obtained

The estimations of SPS reliability function P in *Regime 1* and also the estimations of SPS probability of failure Q in *Regime 2* for all 27 variants (Var. No) of SPS composition, are presented in Table 3. The variant type (V. type) is shown in the form x, x, x , where the numbers denote the SA type at the first, second and third position respectively. The dependence of SPS reliability function estimation P in *Regime 1* and also the dependence of SPS probability of failure estimation Q in *Regime 2* on the variants of SPS composition are presented graphically on Figs. 2 and 3 respectively.

Table 3. Estimations of P and Q of SPS for 27 variants of compositions

Var. No	V. type	Regime 1 P	Regime 2 $Q \cdot 10^{-14}$	Var. No	V. type	Regime 1 P	Regime 2 $Q \cdot 10^{-14}$
1	1,1,1	0,99953058	0,199840	15	2,2,3	0,99941718	0,244249
2	1,1,2	0,99952972	0,222045	16	2,3,1	0,99919833	0,244249
3	1,1,3	0,99952529	0,222045	17	2,3,2	0,99919747	0,244249
4	1,2,1	0,99948733	0,222045	18	2,3,3	0,99919305	0,244249
5	1,2,2	0,99948647	0,222045	19	3,1,1	0,99912951	0,266454
6	1,2,3	0,99948204	0,222045	20	3,1,2	0,99912865	0,266454
7	1,3,1	0,99926318	0,222045	21	3,1,3	0,99912423	0,266454
8	1,3,2	0,99926232	0,222045	22	3,2,1	0,99908628	0,266454
9	1,3,3	0,99925790	0,222045	23	3,2,2	0,99908543	0,266454
10	2,1,1	0,99946571	0,222045	24	3,2,3	0,99908100	0,266454
11	2,1,2	0,99946485	0,244249	25	3,3,1	0,99886222	0,288658
12	2,1,3	0,99946042	0,244249	26	3,3,2	0,99886137	0,288658
13	2,2,1	0,99942246	0,244249	27	3,3,3	0,99885694	0,288658
14	2,2,2	0,99942161	0,244249				

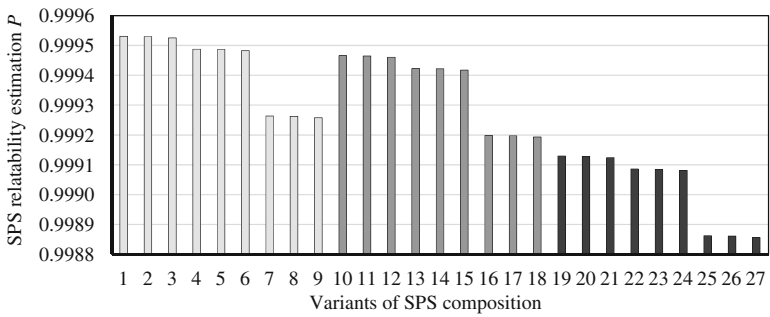


Fig. 2. Dependence of P of SPS in *Regime 1* on the variants of composition.

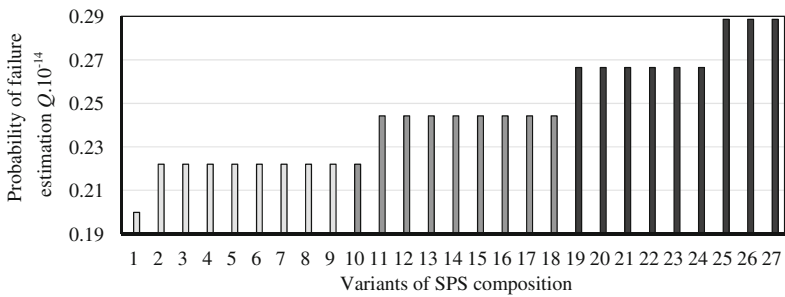


Fig. 3. Dependence of Q of the SPS in *Regime 2* on the variants of composition.

4 Conclusions and Final Remarks

The data resulting from this study, presented above, cannot be used as highly accurate SPS reliability estimations. Their value is that they allow to be performed a benchmarking of all possible variants of SPS composition by SA with different characteristics. The results display that there are variants of SPS composition which provide the system with higher reliability than others. These are variants 1 to 6 from Fig. 2 and 1 to 10 from Fig. 3. These variants are characterized by roughly equal estimations of the SPS reliability function, and of the probability of failure respectively.

Selecting a proper set of metal-oxide SA the maintenance engineers can apply the approach presented, in regard to a substation with certain n and m , considering SPS reliability and its estimations, valid for all variants of SPS composition, taking also into consideration the technical and operational requirements regarding the basic substation equipment. During this process it is advisable the next steps to be followed:

1. Preparation of a list of all generally suitable metal-oxide SA on stock and/or available by request. Review of their referent characteristics;
2. Determination of the coefficients values and reliability indices values regarding each type of SA at each possible position, at each of the two operational regimes of SPS, considering SA referent and operational characteristics;
3. Reliability estimations of all variants of the SPS composition resulting from all possible variations in positioning of the SA of different types already listed. Benchmarking of all variants, based on estimations obtained. The current step is executed twice, i.e. once per each of the SPS regimes analyzed above. Selection of the SPS composition variants, providing the system with highest reliability;
4. Final choice of the SPS composition of metal-oxide SA on the basis of additional considerations, such as financial, operational etc. It is also advisable to be taken into consideration the maintenance experience of the personnel.

References

1. Holtzhausen, J.P., Vosloo, W.L.: High Voltage Engineering Practice and Theory (2014). ISBN 978-0-620-3767-7
2. Handbook, M.: Reliability Prediction of Electronic Equipment, MIL-HDBK-217F. US Department of Defence, USA (1995)
3. Nikolov, N., Dimitrova, N., Georgiev, A., Vasileva, M.: Reliability assessment of electricity distribution substation surge protection system. In: Jubilee 40th International Spring Seminar on Electronics Technology, Sofia, Bulgaria, pp. 134–135 (2017). ISBN 978-619-7066-15-9
4. Velikova, N., Dimitrova, R., Vasileva, M., Yordanova, M.: Model research of the protection against arriving atmospheric surges in the substation 110 kV. In: International Scientific conference in Electro Energy, p. 78 (2016). ISBN 978-954-20-0762-3
5. Daman-Khorshid, H., Ajri, F., Shariatinasab, R.: Probabilistic evaluation of failure risk of transmission line surge arresters caused by lightning flash. IET Gener. Transm. Distrib. **8**(2), 193–202 (2014)
6. Rausand, M.: System reliability theory. Wiley, New Jersey (2004). ISBN 0-471-47133-X

7. Nikolov, N., Papanchev, T., Georgiev, A.: Reliability assessment of electronic units included in complex electronic systems. In: Jubilee 40th International Spring Seminar on Electronics Technology, Sofia, Bulgaria, pp. 132–133 (2017). ISBN 978-619-7066-15-9
8. Bayadi, A., Harid, N., Zehar, K., Belkhiat, S.: Simulation of metal oxide surge arrester dynamic behavior under fast transients. In: International Conference on Power Systems Transients, IPST 2003, New Orleans, USA (2003)
9. Christodoulou, C.A., Assimakopoulou, F.A., Gonos, I.A., Stathopoulos, I.A.: Simulation of metal oxide surge arresters behavior. In: IEEE Power Electronics Specialists Conference - PESC 2008, Rhodes, Greece, pp. 1862–1866 (2008)
10. Miyakawa, Y., et al.: Influence of temperature variation on characteristics of ZnO elements. In: International Symposium on Electrical Insulating Materials - ISEIM 2008, pp. 119–122 (2008)

Approximate Solutions of Timoshenko's Differential Equation for the Free Transverse Vibration of Stubby Beams

Victor A. Chirikov^(✉)

Department of Mechanics and Machine Elements,
Technical University of Varna, Studentska St. 1, 9010 Varna, Bulgaria
chirikov@tu-varna.bg

Abstract. To obtain the analytical formula for the natural frequencies of the transverse vibration of stubby beams from Timoshenko's differential equation is an age-long dream of many mathematicians. Although advances in this direction have been achieved, room for new progress still remains. This paper comprehensively presents an innovative attempt to obtain successive approximate solutions of Timoshenko's differential equation. An accuracy analysis is undertaken by comparing the model fit of the suggested approximate solutions to experimental data. The results of the analysis show that the second approximation significantly improves the model fit compared to previous approximations as well as other relationships used in standard practice, including those for very short stubby beams. Therefore, the suggested analytical formula accurately meets the requirements for real stubby beams transverse vibration analysis.

Keywords: Timoshenko beam · Transverse vibration · Approximate solution

1 Introduction

This research work further extends the analytical methods for calculation of natural frequencies of the free transverse vibration of stubby beams. Previous scientific work [4, 5] dealing with obtaining the analytical solution of the Timoshenko differential equation for the transverse vibration of stubby beams experimentally establishes that when one omits the last term in the equation because of its small effect of second order, one can obtain a relationship that is rather close to various experimental measurements performed in different laboratories. Given the universal nature of the Timoshenko differential equation, that initial approximate solution is also called universal.

This paper presents successive approximations for the solution of the full Timoshenko differential equation for beams' transverse vibration without dropping the last term mentioned above. Accuracy analysis is conducted by comparing the derived analytical approximations to how they fit experimental data. The final approximate solution that satisfies the measurement accuracy of beams transverse vibration is presented.

The relationships obtained in this research work give an opportunity for more precise vibration modeling of structural elements, buildings, machine parts, etc. and for

control algorithms simplification of modern automatic manipulators, components of which often are short massive bodies subjected to oscillations. The analytical formulation further enables determination of the elastic characteristics of different materials by impulse excitation of sample vibration, without destroying the sample, which often occurs in tests conducted by tension. Such non-destructive approach allows for keeping the sample safe and to use it as a mechanical standard in a follow-up study. This approach is also particularly successful when studying the elastic characteristics of a wide variety of advanced composite materials of various mechanical properties.

2 Differential Equations for the Free Transverse Vibration of Beams

To determine the analytical relationships for the natural frequencies of the transverse vibration of stubby beams that account for the effects of rotary inertia and shear deformation, let us first present the differential equation by Timoshenko S.P. [1] as follows:

$$\rho A \frac{\partial^2 y}{\partial t^2} - \rho I \left(1 + \kappa \frac{E}{G} \right) \frac{\partial^4 y}{\partial t^2 \partial x^2} + EI \frac{\partial^4 y}{\partial x^4} + \kappa \frac{\rho^2 I}{G} \frac{\partial^4 y}{\partial t^4} = 0 \tag{1}$$

where: y is transverse displacement of the beam axis, x is longitudinal coordinate along the beam axis, t is time parameter, A is cross section area, $I = Ar^2$ is the second moment of cross section area, where r is the radius of gyration of the cross section about z -axis, ρ is mass density, E is Young's modulus, $G = \frac{E}{2(1+\nu)}$ is shear modulus, κ is cross section shape factor (contrary to the shape factor presented in [2], the reciprocal value is introduced here), ν is Poisson's ratio.

If the last term in the Eq. (1) is omitted due to its small size of second order [2], then (1) simplifies to:

$$\rho A \frac{\partial^2 y}{\partial t^2} - \rho I \left(1 + \kappa \frac{E}{G} \right) \frac{\partial^4 y}{\partial t^2 \partial x^2} + EI \frac{\partial^4 y}{\partial x^4} = 0 \tag{2}$$

If the second term, which accounts for the effects of rotary inertia and shear deformation, is also omitted then we obtain the well-known differential equation of the Bernoulli-Euler's beam free transverse vibration that holds true for slender beams with small cross-sectional dimensions with respect to the beam's length L :

$$\rho A \frac{\partial^2 y}{\partial t^2} + EI \frac{\partial^4 y}{\partial x^4} = 0 \tag{3}$$

It is well known that the natural angular frequencies of vibration ω_n for a slender simply supported beam can be derived from Eq. (3) as follows:

$$\omega_n = \frac{n^2 \pi^2}{L^2} \cdot \sqrt{\frac{EI}{\rho A}} \tag{4}$$

It is worth remembering that for frequencies presented in hertz, the following relationship holds:

$$f_n = \frac{\omega_n}{2\pi}.$$

In the search for natural frequencies of vibration of beams with different type of supports at their ends, it is necessary to use the full expression for the normal mode shapes of vibration [2]:

$$X_n = C_{n1} \sin(p_n x) + C_{n2} \cos(p_n x) + C_{n3} sh(p_n x) + C_{n4} ch(p_n x) \tag{5}$$

where: $C_{n1}, C_{n2}, C_{n3}, C_{n4}$ are the constants obtained from the conditions at the beam's ends in each particular case; parameter p_n is introduced by the following expression:

$$p_n = \frac{n_c \pi}{L}, \tag{6}$$

where: n_c is a so called frequency-correlated number that can be obtained from the solution of transcendental frequency equation arising from the boundary conditions imposed at the beam's ends, explained in more detail below.

In obtaining relationship (4), the first term in expression (5) is used. It can be shown that utilization of the other terms in (5) for different end conditions for the beam does not change the structure of Eq. (4). The general expression for the natural frequencies of transverse vibration of beams with arbitrary end conditions can be written as follows:

$$\omega_n = \frac{n_c^2 \pi^2}{L^2} \cdot \sqrt{\frac{EI}{\rho A}} \tag{7}$$

where the frequency-correlated number n_c takes the following values at the specific end conditions of beams.

For a simply supported beam, the successive frequency-correlated numbers n_c are equal to the serial frequency numbers n , i.e. $n_c = n$. For clamped-clamped and free-free beams, the successive frequency-correlated numbers are as follows: 1.505619, 2.499753, 3.50001, 4.5, etc. For clamped-pinned or one-end-pinned beams they are: 1.249876, 2.249999, 3.25, 4.25, etc. For cantilever beams they are as follows: 0.5996864, 1.494176, 2.500247, 3.5, 4.5, etc. A general term for the higher frequencies of these series could be easily deduced. For clamped-clamped or free-free beams it is $n_c = n + 0.5$. For pinned-fix or pinned-free beams it is $n_c = n + 0.25$. For cantilever beams it is $n_c = n - 0.5$. Zero values for the frequency-correlated numbers related to the rigid body motions are not taken into account.

For the convenience of presenting the analytical solution of the frequency equations obtained from differential equations (3), (2) or (1), let's introduce the dimensionless parameter s , representing geometrical and inertial beam characteristics, type of end supports, and the serial frequency number and defined as:

$$s = \frac{L}{n_c r} \tag{8}$$

Note that the ratio $\frac{L}{n_c}$ occurring in expression (8) is the generalized equivalent of the parameter that Timoshenko S.P. denoted as half the length of the waves a simply supported beam is divided into during vibration.

Thanks to the introduced parameter s , the classical natural transverse frequency (7) of every slender beam subjected to typical constraints can be presented as follows:

$$\omega_n = \frac{c}{r} \left(\frac{\pi}{s}\right)^2, \tag{9}$$

where the following notation is introduced $c = \sqrt{\frac{E}{\rho}}$, representing the speed of sound in the beam. It is apparent that relationship (9) is the equation for quadratic hyperbola. Again, for the convenience of results presentation, let us introduce another dimensionless parameter z :

$$z = \left(\frac{\pi}{s}\right)^2, \tag{10}$$

which is a small quantity relative to the unit for beams.

Taking into account Eqs. (6) and (8), the following expression can be additionally derived

$$z = p_n^2 r^2 \tag{11}$$

By applying parameter z from (10), the natural frequencies of vibration ω_n in (7) acquire the form:

$$\omega_n = \frac{c}{r} \cdot z \tag{12}$$

It is evident that the general formula (7) and its analytic simplification (12) are true for beams with arbitrary end conditions. That means that all transverse frequencies of beams made from the same material and having the same cross-section would lie on the same curve, with it being a quadratic hyperbola in the reference frame with parameter s along the horizontal axis and ω_n on the vertical axis [3].

3 First Approximation

Let us now turn to the solution of Eq. (2) using the introduced variables. For this purpose, let us substitute in (2) the formula representing the first term from the general relationship for the deflection curve of beam vibration with arbitrary end conditions:

$$y = C_{n1} \cdot \sin(p_n x) \cdot \sin(\omega_n t) \quad (13)$$

It must be particularly emphasized that this term always occurs in the general solution for the beam deflection curve, irrelevant of end conditions, as all normal mode shapes of beam transverse vibration contain the first term in the expression (5). After simplifications, we can get the following equation for the determination of the frequencies:

$$-\rho A \omega_n^2 - \rho I(1 + 2\kappa(1 + \nu))p_n^2 \omega_n^2 + E I p_n^4 = 0 \quad (14)$$

from where, after transformations, we obtain:

$$\omega_n = \sqrt{\frac{EI}{\rho A}} \cdot \frac{p_n^2}{\sqrt{1 + (1 + 2\kappa(1 + \nu))p_n^2 r^2}} \quad (15)$$

Substituting in (15) relationships (11) and $I = Ar^2$, and executing evident transformations, we can obtain the following:

$$\omega_n = \frac{c}{r} \cdot \frac{z}{\sqrt{1 + (1 + 2\kappa(1 + \nu))z}} \quad (16)$$

It may be shown that utilization in (13) of the second term or the sum of first and second terms from the normal modes of vibration in (5) would result in the same Eq. (16). It is reasonable to expect that the third and fourth terms in (5) can be omitted when deriving the analytical solutions for frequencies from the differential equation of beam vibration, similar to the way it is done for the general expression for frequencies in (7) from Eq. (3), as they do not contribute to vibration. Therefore, it is important to notice that the obtained solution (16) for the differential Eq. (2) for stubby beam vibration extends to beams with any boundary conditions and across all their natural frequencies of transverse vibration.

Comparing formulas (12) and (16), it can be noted that because of the division of the right hand side of formula (12) by the square root in (16), which is greater than one, the natural frequencies of transverse vibration for the same beams subject to rotary inertia and shear deformation effects are lower than frequencies not accounting for those effects. This difference becomes greater with an increase in the value of parameter z presented by relationship (10). In turn, this implies lowering the value of parameter s defined in (8), i.e. whether by diminishing the beam length to depth ratio or by increasing the serial frequency number. Considering the presented above values for the frequency-correlated numbers n_c , it can be observed that the fundamental frequencies

of cantilever and simply supported beams are exposed to lower influence of rotary inertia and shear deformation effects, compared to beams with different boundary conditions. The same is true for the subsequent number frequencies. Beams most influenced by those effects are the clamped-clamped and free-free beams, for which identical natural frequencies of transverse vibration get obtained, as their frequency-correlated numbers n_c are identical. This fact seems to be rather strange in view of the increasing strength of beams when constraining.

To verify these statements and to determine the accuracy of the obtained formulas, it is necessary to test them in a series of experiments. In articles [4–6] the results of several tests are presented that confirm the high accuracy of formula (16) for sets of steel beams with free ends. The relative divergence between formula (16) and the experimental data does not exceed 3%, and the bigger parameter s is (in those experiments $s > 6$), the less the discrepancy. Paper [6] pursues the similarity between formula (16) and the standard relationship given in [7]. An example of the relationship of the abovementioned dependencies as tested against experimental data is presented in Fig. 1.

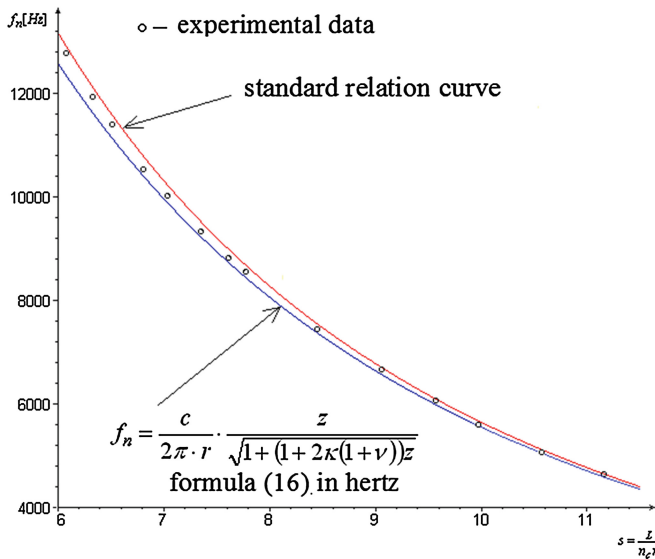


Fig. 1. Comparison between formula (16), experimental results and standard relation [7]

In Fig. 1, it is clearly seen that the standard relationship [7] over-estimates, while formula (16) under-estimates the natural frequencies of transverse vibration for stubby beams relative to experimental data beginning with some value of parameter s . It must be said that in [7] the standard relationship yields high accuracy when the beam length to depth ratio is no lower than 5, which for the tested set of specimens corresponds to parameter $s > 11$ range. For considered test specimens with s ranges up to 6, it is

evident that results with formula (16) are going beyond the high accuracy range of the standard relation. The difference between frequency values based on formula (16) and the standard relationship [7] at $s = 6$, relative to (16), come up to 4.6%. The same conclusion can be made for beams of other materials, for instance for beams made of aluminum [8].

The work fulfilled to date experimentally confirms the validity of formula (16) for stubby beams with free ends, which gives the opportunity to propose a methodology for the calculation of Young’s modulus of materials by impulse excitation of beam transverse vibration [6]. Unfortunately, attempts to confirm experimentally the validity of formula (16) for stubby beams with different end conditions, other than free ends, have not been successful. Thus, it is established that the “Timoshenko beam” is certainly a stubby beam with free ends, in contrast to the conventional assumption to it being a simply supported stubby beam.

4 Second Approximation

Despite the high accuracy of formula (16), it is instructive to extend the analytical approximations in order to obtain more accurate solutions of the full differential equation for the free transverse vibration of stubby beams (1). For this purpose, let us substitute general relation (13) into Timoshenko Eq. (1). After obvious simplifications, the following equation for the frequency determination can be obtained:

$$-\rho A \omega_n^2 - \rho I(1 + 2\kappa(1 + \nu))p_n^2 \omega_n^2 + EI p_n^4 + \kappa \frac{\rho^2 I}{G} \omega_n^4 = 0 \tag{17}$$

Taking advantage of the fact that formula (16) approximates with high accuracy the experimental data for natural frequencies of stubby beams vibration, the last term in Eq. (17), after substitution of formula (16) and relation (11), takes the form:

$$\begin{aligned} \kappa \frac{\rho^2 I}{G} \omega_n^4 &= \kappa \frac{\rho^2 I}{G} \cdot \frac{c^4}{r^4} \frac{z^4}{(1 + (1 + 2\kappa(1 + \nu))z)^2} \\ &= \kappa \frac{\rho^2 I}{G} \cdot \frac{E^2}{\rho^2} \cdot \frac{p_n^4 r^4 z^2}{r^4 \cdot (1 + (1 + 2\kappa(1 + \nu))z)^2} \\ &= \kappa \frac{E}{G} \cdot EI p_n^4 \cdot \frac{z^2}{(1 + (1 + 2\kappa(1 + \nu))z)^2} \\ &= 2\kappa(1 + \nu) \cdot EI p_n^4 \cdot \frac{z^2}{(1 + (1 + 2\kappa(1 + \nu))z)^2} \end{aligned} \tag{18}$$

From the first line in (18), it becomes clear that the last term in the equation for frequency determination (17) is a small quantity of second order compared to another small quantity z , as stated by Timoshenko S.P. in [2]. After substitution of (11) and (18) into (17), and execution of trivial transformations, the solution for ω_n is:

$$\begin{aligned} \omega_n &= \sqrt{\frac{EI}{\rho A}} \cdot P_n^2 \cdot \sqrt{\frac{1 + 2\kappa(1 + \nu) \cdot \frac{z^2}{(1 + (1 + 2\kappa(1 + \nu))z)^2}}{1 + (1 + 2\kappa(1 + \nu))z}} \\ &= \frac{c}{r} \cdot z \cdot \sqrt{\frac{(1 + (1 + 2\kappa(1 + \nu))z)^2 + 2\kappa(1 + \nu)z^2}{(1 + (1 + 2\kappa(1 + \nu))z)^3}} \end{aligned} \tag{19}$$

or, in more concise form:

$$\omega_n = \frac{c}{r} \cdot \frac{z}{\sqrt{1 + (1 + 2\kappa(1 + \nu))z}} \cdot \lambda \tag{20}$$

where the following correlation factor is added to formula (16):

$$\lambda = \frac{\sqrt{1 + 2(1 + 2\kappa(1 + \nu))z + (1 + 6\kappa(1 + \nu) + 4\kappa^2(1 + \nu)^2)z^2}}{1 + (1 + 2\kappa(1 + \nu))z} \tag{21}$$

which is obtained after expansion and simplifications made in the numerator of expression (19). The accuracy of the first approximation can be estimated by utilizing factor λ , which accounts for the last term in Timoshenko's Eq. (1). Before proceeding to the next approximation, it is desirable first to assess the increase in accuracy of formula (19) compared to formula (16).

5 Accuracy of the Second Approximation

Assessment of the accuracy of formula (19) (or respectively formulas (20) and (21)) can be carried out with comparison to experimental data or available standard relationships. In our case, the accuracy assessment of the second approximation formula can be easily executed by comparing formulas (16) and (19) using a ratio error Δ . The ratio error is calculated by subtracting the initial formula (16) from the new formula (19) and dividing the obtained difference by (16). It yields the following:

$$\Delta = \lambda - 1 \tag{22}$$

Expressed as a percentage, this result at $s = 6$ is roughly 2.5% into the upward bias of frequencies. Furthermore, the ratio error diminishes as parameter s increases (i.e. as the length to depth ratio of a beam increases and/or the serial number of a beam frequency decreases). From Fig. 2, one can visually ascertain that the curve of formula (19) more precisely approximates the experimental data.

The maximum ratio error between the values of formula (19) and the test results for precisely manufactured specimens made of steel does not exceed 0.7%, i.e. the accuracy increases more than four times. The experimental measurements in this study were of the same precision. Therefore, the obtained approximation formula (19) could be

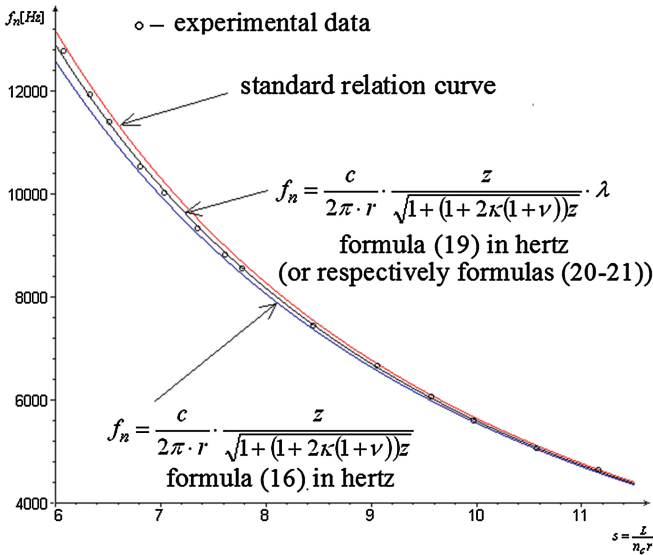


Fig. 2. Formula (19) curve lies between the curve of formula (16) and the standard relationship

assumed to be final, given the four-fold increased accuracy of formula (19) relative to the experimental data.

The suggested approach can be used further to obtain more precise approximate solutions of Timoshenko’s differential equation by substituting a new approximation formula into the last term of Eq. (17). As it was proved in previous research [6], this procedure does not contribute significantly to the further enhance of the accuracy. However, if someone needs of more accurate solution, he/she can make calculations by himself/herself in the same manner, as it is presented above.

6 Conclusion

One can find a variety of solutions for the Timoshenko’s differential equation in the vast amount of literature accumulated on the topic during the last roughly hundred years. Many of the solutions are given as approximations of the solution of Timoshenko’s equation, like in [9], although there are also many attempts to obtain an exact solution, like in [10]. Any new solutions are usually compared to those previously derived via other analytical or computational means. Unfortunately, the literature does not provide enough evidence to date of attempts to compare obtained analytical solutions to experimental data.

The present paper establishes a real high accuracy formula for transverse beam vibration and advances the literature by providing an analytical solution that is tested by a set of experiments and that is compared against standard relationships based on a large body of experimental research. The experimental confirmation established for stubby beams with free ends gives an opportunity to develop a new method for test

determination of the elastic constants for different materials based on the impulse excitation of free beam transverse vibration. Attempts to obtain experimental confirmation of the theoretical formula for stubby beam vibration with different end conditions than free ends have not yet been successful and research is ongoing.

References

1. Timoshenko, S.P.: On the correction for shear of the differential equation for transverse vibration of prismatic bars. *Philos. Mag.* **41**(6), 744–746 (1921)
2. Timoshenko, S., Young, D.H.: *Vibration Problems in Engineering*. D. Van Nostrand Company Inc., Toronto, New York, London (1955)
3. Chirikov, V.A.: On the range of rotary inertia and shear effects for beams. In: *Applied Mechanics in the Americas, Proceedings of PACAM VII in Temuco, Chile*, vol. 9, pp. 9–12 (2002)
4. Victor, A.C., Ozaki, K.: Experimental formula for transverse vibrations of stubby free-free beams. In: *International Conference "Tehnonav 2004"*, Constanta, Romania, pp. 25–28 (2004). ISSN-1223-7221
5. Chirikov, V.A., Dimitrov, D.M., Kostov, K.P.: Universal experimental relation for natural frequencies of transverse vibration of stubby free-free beams. In: *Diagnostics, Resource and Mechanics of materials and structures. Open Access J. RAS*, (4), 42–54 (2015). ISSN 2410-9908
6. Chirikov, V.A.: Analysis of universal relation for natural frequencies of stubby free-free beams transverse vibration. In: *Scientific Proceedings "NDT days 2015"*, Sozopol, Bulgaria, pp. 349–352 (2015). ISSN 1310-3946
7. ASTM E1876 - 09 Standard Test Method for Dynamic Young's Modulus, Shear Modulus, and Poisson's Ratio by Impulse Excitation of Vibration. In: *ASTM-International, USA* (2012)
8. Chirikov, V.A., Dimitrov, D.M.: Experimental verification of the universal relation for determination of transverse natural frequencies of vibration of free beams from aluminum. In: *National Conference on ACCOUSTICS*, Sofia, Bulgaria, pp. 192–194 (2015). ISSN 1312-4897
9. Van Rensburg, N.F.J., van der Merve, A.J.: Natural frequencies and modes of a Timoshenko beam. *Wave Motion* **44**, 58–69 (2006)
10. Senjanović, I., Vladimir, N.: Physical insight into Timoshenko beam theory and its modification with extension. *Struct. Eng. Mech.* **4**(48), 519–545 (2013)

A Computing Approach to Risk Assessment Related to Electromagnetic Field Exposure from Overhead Power Lines

Marinela Yordanova^(✉) and Mediha Mehmed-Hamza

Technical University, Varna, Bulgaria
m.yordanova@tu-varna.bg, mediha.hamza@mail.bg

Abstract. The paper presents a computing approach to risk assessment of the occupational exposure of persons to electromagnetic fields from overhead power lines. With a computer program, created by the authors, data for the electric field intensity at a point on arbitrary height from the ground, transversely from the center of the tower of the transmission lines 110 kV, 220 kV and 400 kV, are presented. The current flowing through the person, located in the area of the point, and the power absorbed by the body are also obtained. The calculations are done for different types of electrical power line towers as a construction and as an arrangement of the phase conductors. The employers may assess the risks of exposure to electromagnetic fields at the workplaces based on the data presented in the paper for many typical towers of the transmission lines.

Keywords: Electromagnetic fields · Risk assessment · Electrical field intensity · Overhead power lines

1 Introduction

Directive 2013/35/EC of the European Parliament and of the Council of 26 June 2013 [1] defines the health and safety requirements regarding the exposure of the workers to the risks arising from physical agents - electromagnetic fields (EMF) [1]. The directive defines the effects of the EMF as “direct” and “indirect” biophysical effects. “Direct biophysical effects” [1, 2] means effects in the human body directly caused by its presence in EMF. “Indirect effects” [1, 2] means effects, caused by the presence of an object in EMF, which may become the cause of a safety or health hazard.

The calculations, measurements or data provided by the manufacturers or the distributors of the equipment must prove that the exposure does not exceed the respective evaluation parameters for assessment introduced by documents [1, 2]: exposure limit values (ELVs); health effects exposure limit values (HEELVs); sensory effects exposure limit values (SEELVs); action levels (ALs).

The EMF with frequency 50 Hz in the context of the Directive [1] are within the low frequency range from 1 Hz to 10 MHz. The health effects and the effects of the sensitivity used to limit the exposures in this frequency range are respectively: phosphenes, minor changes in brain and function; nerve stimulation resulting in tingling sensations or pain, muscle contraction, heart arrhythmia.

In this frequency range the electric field intensity E , V/m, the magnetic flux density B , T, and the contact current I_c , A, are normed (Table 1).

Table 1. Evaluation parameters for electric field [2].

Parameter	Frequency range	Value for $f = 50$ Hz	
HEELVs – electric stimulation of all peripheral and central nervous system tissues in the body, including the head	1 Hz ÷ 3 kHz	$E_{HEELVs} = 1,1$ V/m peak value Internal electric field	
SEELVs – on the central nervous system in the head, i.e. retinal phosphenes and minor transient changes in some brain functions	25 Hz ÷ 400 Hz	$E_{SEELVs} = 0,14$ V/m peak value	
ALs for exposure to electric fields	50 Hz ÷ 1,64 kHz	low 10 kV/m	high 20 V/m
ALs for contact current I_c	2,5 Hz ÷ 100 kHz	0,02 mA	

The paper presents a computing approach to risk assessment of the occupational exposure of the staff to EMF from overhead power lines (OHPLs). With a computer program, created by the authors, some results for the electric field intensity in the area under OHPLs 110 kV, 220 kV and 400 kV are obtained. Data for the current flowing through a human body, standing in this area, are also presented. The calculations are done for different types of the power line towers as a construction and as an arrangement of the phase conductors.

2 Description of Related Work

The employers can assess risks and they can determine EMF exposure at the workplace based on calculations or measurements [1, 2]. Other approaches to risk assessment of EMF at the workplaces are [1, 2]: the use of practical guides and other relevant standards; the use of data provided by the manufacturer or distributor of the equipment.

Mathematical approaches to determine the electric field intensity have been developed [3–6]. Most of them provide a solution for the horizontal arrangement of the phase conductors on the tower. There are also measurement results of the EMF intensity for different voltages of OHPLs [5, 7]. For practical purpose to assess EMF exposure risk and to check up the requirements of the European Directive [1], employers may define the electric field intensity for the arbitrary construction of the tower and arbitrary arrangement of the phase conductors on the tower using a computer program.

3 Proposed Method

A calculation approach [3], based on the mirror images, is used for determining of the electric field intensity under overhead power lines without a lightning protection wire (a ground wire) only in the case of horizontal arrangement of the phase conductors on the tower. It is assumed that the phase conductors are infinitely long and rectilinearly

located close to a flat surface of a conductive medium (the ground). Here the field is caused not only by the charges of the conductors but also by the charges of the underground mirror images. The vector of the electric field intensity is determined by a geometrical sum of the vectors of the electric field intensity of all conductors. Based on these assumptions, the equation of the electric field intensity E , V/m is as follows [3]:

$$E = \frac{CU}{2\pi\epsilon_0} \cdot \sqrt{(2k_1 - k_3 - k_5)^2 + 3(k_3 - k_5)^2 + (2k_2 - k_4 - k_6)^2 + 3(k_4 - k_6)^2}, \quad (1)$$

where C is the capacitance of the phase conductors towards the ground, F/m; U is the voltage of the phase conductors towards the ground, kV; $k_1 \div k_6$ are coefficients, depending on the distance between the points, where the phase conductors are installed on the tower and the surface of the ground, the distance from the ground to the point P where the electric field intensity is determined, the distance from this point P to the power line tower and the distance between the phase conductors. All equations of the coefficients are presented in [3].

The current that flows through the person I_h , A standing in area with electric field intensity E , is determined by the dimensions of the person's body, the body shape, the condition of the insulation between the person and the ground [3].

The following assumptions have been accepted in order to determine the current I_h , [3]:

1. The human body is replaced by equal in height and volume half-ellipsoid with first semi-axis a , m - corresponding to the height of the person and located perpendicularly to the surface of the ground and second semi-axis b , m - respectively corresponding to the equivalent diameter. For a given weight of the human G , kg and height a , m and considering that the average density of the human body is $\rho_b = 1,05 \text{ g/cm}^3$, b may be defined as:

$$b = \sqrt{\frac{3 \cdot G}{2 \cdot \pi \cdot a \cdot \rho_b}}. \quad (2)$$

2. The material of the half-ellipsoid is assumed to be uniform having resistivity equal to the average human's body $\rho_v = 10 \text{ }\Omega\text{m}$. However, at the starting point it is considered that the half-ellipsoid is non-conductive, having average conductivity σ and corresponding relative permittivity ϵ_r .
3. It is assumed that the electric field is uniform before and after the placement of the half-ellipsoid in it. The vector of the electric field intensity is considered directed along the semi-axis a . The electric field intensity in the half-ellipsoid is as follows [3]:

$$E_r = \frac{E}{1 + N_a \cdot (\epsilon_r - 1)}, \quad (3)$$

where E is electric field intensity, V/m, ϵ_r is relative permittivity of the half-ellipsoid. The coefficient of depolarization N_a of the half-ellipsoid on the axis of rotation, i.e. along the axis a can be given by an approximate formula [3]:

$$N_a \approx \frac{b^2}{a^2} \cdot \left(\ln \frac{2 \cdot a}{b} - 1 \right). \quad (4)$$

where a , m and b , m are semi-axis of the of the half-ellipsoid.

The current flowing through the person is [3]:

$$I_h = E \cdot \varepsilon_0 \cdot \frac{\pi \cdot b^2 \cdot \omega}{N_a}, \quad (5)$$

where $\varepsilon_0 = 8, 85 \cdot 10^{-12}$ F/m and $\omega = 314$ rad/s.

Thereafter, the absorbed by the body power [3] is:

$$P_h = I_h^2 \cdot \frac{2 \cdot a \cdot \rho_v}{3 \cdot \pi \cdot b^2}. \quad (6)$$

where ρ_v , Ωm is the average human's body resistivity.

4 Calculation Data for Risk Assessment of the Occupational Exposure of the Staff to Electromagnetic Fields of EPLs

A computer program has been developed on the base of the aforementioned dependencies. The authors have developed further the approach [3] to arbitrary arrangement of the phase conductors on the tower. The program calculates the intensity of the electric field E at a point on arbitrary height from the ground, transversely from the center of the tower of the transmission lines 110 kV, 220 kV and 400 kV, the current flowing through the person I_h , located in the area of the point and the power absorbed by the body P_h .

4.1 Overhead Power Lines 400 kV

The parameters of the investigated overhead power line 400 kV are:

- Steel-aluminum conductors with cross-section 500 mm²;
- The tower with a horizontal placement of the conductors;
- Horizontal separation between phase conductors – 5,5 m;
- The distance between the conductors and the surface of the ground – 24 m.

According to [8] in urban area the maximum permitted phase conductor sag is 9 m for the overhead power lines 400 kV. The results for one of the investigated towers are given in Figs. 1 and 2. The tower has a phase conductor suspension 24 m, conductor sag – 11,5 m and a horizontal separation between the phases – 5,5 m. The curve 1 corresponds to the values under the conductor sag, curve 3 - under the tower and curve 2 - under the power conductor at a point between them.

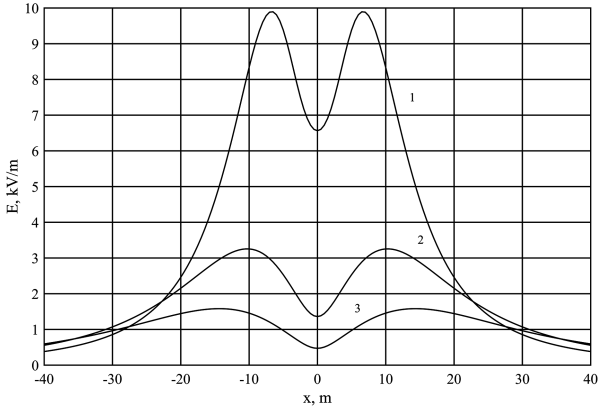


Fig. 1. The electric field intensity under 400 kV OHPLs, x - distance from the center of the tower

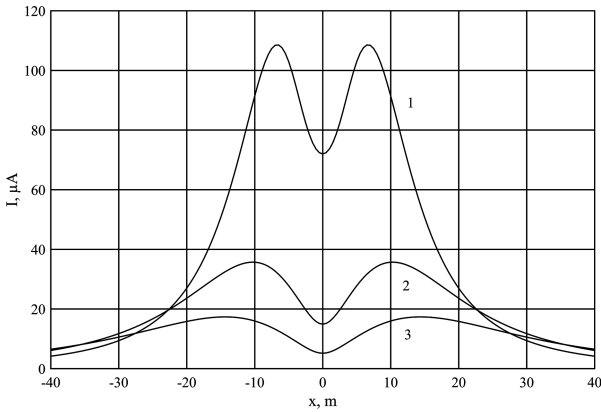


Fig. 2. The current flowing through the human body around 400 kV OHPLs – for electric field intensity at 1,8 m height from the surface of the ground, x - distance from the center of the tower

Values of the current through the human body have been obtained by Eq. (5) with the field intensity in points at different heights from the ground surface 1,8 m, 1,5 m, 1,2 m and 0,9 m. The alteration is not significant – the increasing of the height two times leads to increasing the current from 102,5 μA to 110 μA . These values are safe according to the electrical safety standards.

Figure 3 presents the internal electric field intensity in the human body at 1,8 m (curve with the biggest values), 1,5 m, 1,2 m and 0,9 m (the smallest values) heights from the surface of the ground. The alteration of the values is significant compared to that of the current flowing through the human body.

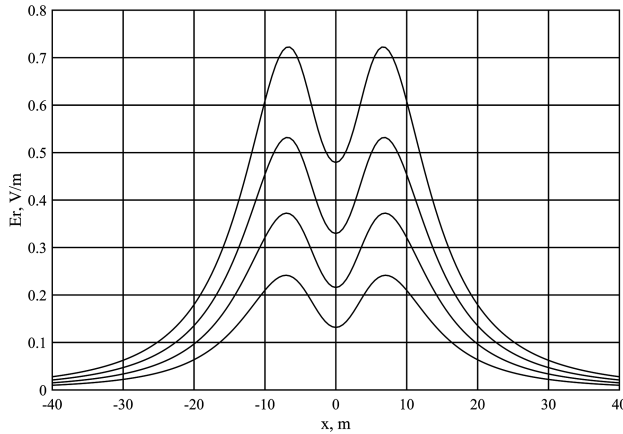


Fig. 3. The internal electric field intensity in the human body – at 1,8 m (the curve with the biggest values), 1,5 m, 1,2 m and 0,9 m (the smallest values) height from the surface of the ground, x- distance from the center of the tower

4.2 Overhead Power Lines 110 kV and 220 kV

Table 2 presents the data for the towers’ geometrical parameters of the investigated OHPLs according to Fig. 4. The phase conductors of 110 kV OHPLs are aluminum-steel with cross-section 185 mm², for 220 kV - aluminum-steel with cross-section 400 mm².

Table 2. Tower construction parameters.

Case	Un, kV	xa, mm	ya, mm	xb, mm	yb, mm	xc, mm	yc, mm	H, mm	Lins., mm
1	110	-2200	3500	2200	1750	-3200	0	10500	1500
2	110	-4000	0	0	0	4000	0	10500	1500
3	220	-3500	6000	3500	3000	-7000	0	20500	2500
4	220	-7000	0	0	0	7000	0	20500	2500

The electric field intensity of OHPLs 220 kV for case 3 in Table 3 is presented in Fig. 5. It is seen, that the alteration is not symmetrical because of the arrangement of the phase conductors on the tower (Fig. 4) and the bigger values are under the tower side with two phases. The results of the maximum electric field intensity *E* and the current through the person *I_h* for all cases are presented in Table 3.

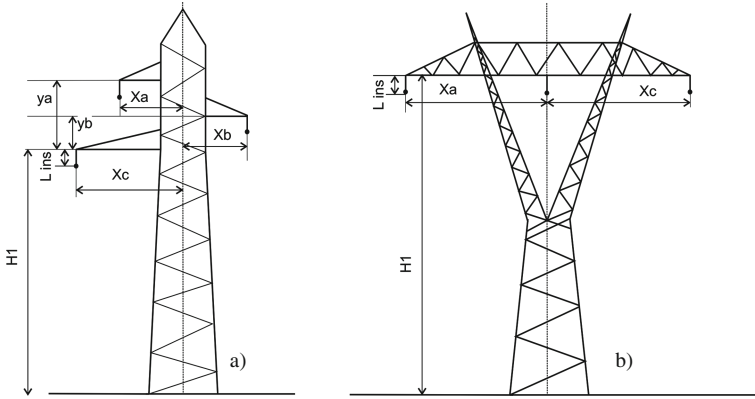


Fig. 4. Towers for overhead power line 110 kV and 220 kV

Table 3. The maximum electric field intensity E and the current through the person I_h .

U_n , kV	The arrangement of the phase conductors on the tower	E_{max} , kV/m	I_h , μA
110	Triangular – Case 1	2.79	30.69
	Horizontal – Case 2	3.47	38.06
220	Triangular – Case 3	6.27	68.77
	Horizontal – Case 4	7.27	79.72

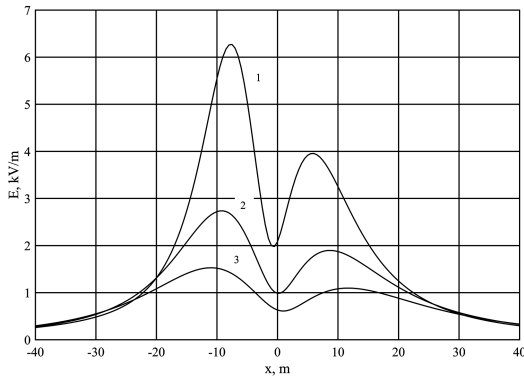


Fig. 5. The electric field intensity of OHPLs 220 kV (Case 3) under the tower – curve 3, under the conductor sag – 1 and under the power conductor at a point between them - 2, x - distance from the center of the tower

5 Conclusions

- A comparison between the results from the program, developed by the authors of the paper and the experimental measurements, published in [4–7], has been done.
- The type of the tower’s construction and the phase conductors’ arrangement affects the values of E .

- The obtained results for ALs and HEELVs for all investigated OHPLs 110 kV, 220 kV and 400 kV meet the requirements of documents [1, 2].
- The obtained results for the action levels for the contact current and SEELVs meet the requirements of documents [1, 2] only for OHPLs 110 kV, except the values under the lowest conductor sag at triangular arrangement.

Acknowledgment. This research is realized within the frame of project “Computer modelling, programming, visualization and development of laboratory complex education” NP1/2017 in Technical University of Varna, Bulgaria.

References

1. Directive 2013/35/EU of the European parliament and of the Council of 26 June 2013 on the minimum health and safety requirements regarding the exposure of workers to the risks arising from physical agents (electromagnetic fields). <http://eur-lex.europa.eu>
2. Ordinance № RD-07-5 of 15 November 2016 on the minimum requirements to ensure the health and safety of workers from the risks related to exposure to electromagnetic fields. <https://www.mh.government.bg>
3. Dolin, P.A., Medvedev, V.T., Korochkov, V.V.: Electrical Safety, A Book of Problem. Gardarika, Moskva (2003)
4. Valchev, M.: Labor Safety. Tehnika, Sofia (1990)
5. Milutinov, M., Juhas, A., Prša, M.: Electromagnetic field underneath overhead high voltage power line. In: 4th International Conference on Engineering Technologies ICET 2009, Novi Sad, Serbia (2009). www.ktet.ftn.uns.ac.rs/download.php?id=391
6. Anev, G.: Harmful Effects from Electricity and Protection. Tehnika, Sofia (1987)
7. Lesov, A., Pehlivanova, V., Kirchev, V., Angelov, A.: Analysis of electromagnetic emanations with industrial frequency of overhead high voltage transmission lines. J. Tech. Univ. Plovdiv Fundam. Sci. Appl. **13**, 71–92 (2006)
8. Ordinance № 3 regarding the construction of electrical switchyards, switch-gears and power lines, State Gazette, issue 90 and 91/2004, issue 108/2007 and 92/2013 (amendment and supplement). <http://www.nspbzn.mvr.bg>

Modified Scheduler for Traffic Prioritization in LTE Networks

Veneta Aleksieva^(✉) and Aydan Haka

Technical University of Varna, Str. Studentska 1, 9010 Varna, Bulgaria
valeksieva@tu-varna.bg, aydin.mehmed@abv.bg

Abstract. LTE is widely used 4G technology, which provides simultaneously voice, data and video (with different priority) on networks. The major concept of the LTE network uses the QoS bearers technique that provides high performance in packet delivery based on prioritization of the traffic. In this paper is proposed a simulation framework for LTE technology, which realized an efficient method for QoS for LTE service classes, which reorders packets, based on classification mechanism and the associated scheduler, based on priority. Simulation's results show that the proposed mechanism improves QoS, but the observed parameters degrade when the use of more subscribers is related to the priority implemented scheduler, in which less priority queues may not be served in the case of network overload or congestion.

Keywords: LTE · QoS · Optimization of QoS in LTE

1 Introduction

According to published from Ericsson paper [12], suggests that by 2020 it is expected a growth of LTE subscriptions up to 3.7 billion. In February 2015 Cisco System published, in turn, prognosis for the period 2014–2019 [7], where the Global mobile data traffic will grow three times faster than global fixed IP traffic from 2014 to 2019. The Mobile data traffic will grow 10-fold from 2014 to 2019, a compound annual growth rate of 57%, and it will reach an annual run rate of 291.8 Exabytes by 2019, up from 30.3 Exabytes in 2014. In the middle of 2016 the European Commission in [13] presents coordinated designation and authorization of the 700 MHz band for wireless broadband by 2020 and coordinated designation of the sub-700 MHz band for flexible use which safeguards the provision of audiovisual media services to mass audience, as well as investments into more efficient technologies, which are needed in order to vacate the current use of the 700 MHz band by digital terrestrial television. The prognosis of these estimates require the search of optimal 4G solutions in terms of QoS offered by telecom providers.

Requirements of IMT-Advanced [6] for 1 Gbit/s speeds for fixed and 100 Mbit/s for mobile users present two challenges for providers of wireless services:

- Optimization of the dynamic selection of the best interfaces of multi-interface devices according to user requirements and limitations in the models of devices

such as power consumption, user fees, and application specific requirements for QoS (delay, latency and throughput);

- Scalability of the work of billions of devices on the wireless network.

Up to 2016 under these requirements, providers of 4G services choose between two advanced wireless technologies - LTE [9] or WiMAX [11], but since 2016 widely used 4G technology is LTE and many vendors implement only this technology in their end devices. The beginning of hybrid schemes supporting WiMAX/LTE is placed in 2010 from companies such as Huawei, Vodafone, KDDI, UQ Communication and others. But in nowadays companies such as Vodafone, Verizon, China Mobile, AT & T, Nokia and Ericsson stake in their equipment of LTE.

Solutions are needed to improve QoS in terms of delays in larger loads and any packet loss. For communications to be successful, it is also essential to focus on network traffic prioritizes for different types of communication streams.

2 Essence of Traffic Management by Priority in LTE Networks

Even with the developing of LTE technology the QoS for uplink is discussed by many authors [3–5, 8, 10]. After the first implementations of LTE the focus in the allocation of resources is shifting towards to the profit maximization and user satisfaction [2].

In 3GPP, the QoS Class Indicator (QCI) consist of basic classes, which are defined as “default”, “expedited forwarding”, and “assured forwarding”. It means: expedited forwarding is used for ‘strict’ priority (video and voice), and ‘assured forwarding’ is used for business differentiation (e.g., weighted-fair priority).

In LTE network QoS is between end-user devices and Packet Data Network (PDN) Gateway applying the ‘bearers’. ‘Bearers’ is a set of network configurations to provide a special handling of traffic to its set prioritization. Their hierarchy is presented in Table 1. Default bearer is established when the user equipment (UE) connects to the LTE network, while Dedicated bearer is established whenever must be set QoS for a specific traffic type (service) as VoIP, video and etc.

Table 1. Hierarchy of LTE QoS

LTE QoS		
Dedicated bearer		Default bearer
Non-GBR	GBR	Non GBR
QCI 5-9	QCI 1-4	QCI 5-9
APN-AMBR	GBR	APN-AMBR
UE-AMBR	MBR	UE-AMBR
TFT	TFT	APN
ARP	ARP	IP address
L-EBI	L-EBI	ARP

GBR (Guaranteed Bit Rate) provides guaranteed bandwidth and monitors two parameters in directions uplink and downlink:

- GBR- minimum GBR for EPS (Evolved Packet switched System) bearer,
- MBR- maximum GBR for EPS bearer,
- Non-GBR bearer does not provide guaranteed bandwidth and also monitors two parameters in directions uplink and downlink: A-AMBR-general maximum speed permitted for the entire non-GBR throughput for specific APN (Access Point Name) and UE -AMBR- overall maximum speed permitted for the entire non-GBR throughput for all of APN particularly UE.

ARP (Allocation and Retention Priority) is used to decide whether the distribution of resources is to be modified according to the new bearer or to maintain the current distribution of the resource.

TFT (Traffic Flow Template) is associated with Dedicated bearer, while Default bearer may or may not have TFT. TFT defines rules based on the source or destination address or protocol used, so that the UE and the network know which IP packets to send over the individual Dedicated bearer.

L-EBI (Linked EPS bearer ID). Each dedicated bearer is always connected to one of the default bearers and L-EBI notifies the Dedicated bearer to which default bearer is connected.

In LTE networks for differentiation of QoS same as in WiMAX are applicable classes which here are called QoS Class of Identifier (QCI). They define the basic characteristics of the IP packet level, as presented in Table 2.

Table 2. QCI classes in LTE

QCI	Bearer type	Priority	Delay of the packet (ms)	Packets loss	Example of traffic type
1	GBR	2	100	10^{-2}	VoIP
2		4	150	10^{-3}	Video call
3		3	50	10^{-3}	Real time games
4		5	300	10^{-6}	Video stream
5	Non-GBR	1	100	10^{-6}	IMS signaling
6, 8, 9		6, 8, 9	300	10^{-6}	TCP based services – chat, ftp...
7		7	100	10^{-3}	Voice, video, interactive games

Then in the cell is applied a preemption algorithm, which allows high priority requesting bearers to displace low priority connected bearers in order to reduce the cell load. This algorithm coupled with a priority-based admission control can achieve low dropping and blocking probabilities.

3 Proposed Algorithm for Prioritization of UEs in the LTE

The Functions for management of QoS in access networks are responsible for the efficient allocation of resources in a wireless interface. They are generally defined as the control algorithms of radio resources (Radio Resource Management) and incorporate power management (Power Control), control of the transfer connection (Handover Control), access control (Admission Control), managing load (Load Control) and the management packet (PS), but directly related to QoS level cell are the last three. They are used to ensure a maximum throughput for individual services. The aim is to achieve keeping the network throughput as high as possible at a small price of only a bit more handovers.

LTE uses multiple access technology (OFDMA) and the total bandwidth is divided into Resource Blocks (RBs) in the frequency domain. The Data is transmitted in the Transport Blocks (TB) in one transmission time interval (TTI) for 1 ms. Each RB consists from 12 subcarriers (each of them is 15 kHz). The frame is 10 ms and divides into 10 equal subframes. Each subframe contains 2 slots * 0.5 ms. Each RB is related to one slot in time. One TB is related to 1 subframe and it is the minimum unit to schedule. The serve rule is to find first space that can fit the TB. If there are not enough RBs in the current TTI, the scheduler tries to find resources in the next TTI. This strategy minimizes the response latency, which is the best practice for delay sensitive traffic.

In wireless radio networks, the base station should allow access of as many users as possible to increase revenue. On the other hand, the quality of service should be guaranteed in order to provide satisfactory service. The maximum number of users a base station can support is bound by the system bandwidth. Under the restriction of QoS, if the maximum bandwidth is achieved, new connection requests should be rejected.

Let capacity of cell is C . Then the load L of cell at time slot t is

$$L = \sum_{i=1}^n L_i(t) \quad (1)$$

where

$$L_i(t) = \frac{b_i^u}{b_i(t)} \quad (2)$$

and

$$L \leq C \quad (3)$$

If bearer j want to use the same cell in the same time slot t , this will be possible if

$$L + L_j(t) \leq C \quad (4)$$

If this condition is not executed, this means that the resources in the current TTI are not enough and scheduler must reorder resources in the whole TTI window and must allocate resources in reserved bandwidth. In this case a task is to find spaces big enough for the new request. If there are not enough resources in the current TTI, the scheduler

tries to find resources in the next TTI. This strategy minimizes the response latency, and thus is useful for delay sensitive traffic.

But this procedure is not applicable for beacon transmissions (it is sent among devices each 100 ms), because of emergency information it conveys, therefore the reserved resource blocks exist to accommodate the temporary overload.

This means, that important factors for QoS are: the Modulation and Coding Scheme (MCS) which be used, the MAC Transport Block (TB) size, the allocation bitmap which identifies which RBs will contain the data transmitted by the eNB to each user, number of users and prioritization of users.

The drop ratio is defined as the number of the rejected beacons to the number of the accepted beacons. For non-prioritization scheme, the beacons are rejected due to the cell overload. New arrival beacons can only be accepted after some users move out the service region, resulting in load reduction. For prioritization scheme, the rejected beacons are the ones that are removed by the congestion control algorithm.

The present paper offers an algorithm for UEs service in the distribution of resources in the uplink of LTE network as composed of two modules - by a control mechanism for admission (admission control) and Scheduler. According to the network load, the admission control for the reception of orders manages the number of UEs, which can enter into the Scheduler, in order to avoid overloading the system with too many UEs. The Scheduler allocates RBs among UEs according to UEs needs. In order to actuate the control mechanism of the base station (eNodeB), UE has to be connected with it. For this purpose, when the UE is in the range of several base stations and it wants to start data transfer, follows the next steps:

1. UE initiates a search of the nearest of the base stations.
2. UE decodes the system information, which the base station sent to it (This is the base station to which UE will try to connect).
3. In case of successful synchronization with the base station, UE starts the process of authentication.
4. If the authentication is successful, UE sends a request to connect to the eNodeB:
 - (a) If UE did not get the identifier from eNodeB, it does not receive any allocated resource for the transfer of user data and could only look the service channel. In this state UE falls and when it made connection to the eNodeB, it has received allocated resources (it sent/received RBs), but for some time periods it is inactive for data transmission.
 - (b) If UE get the identifier from eNodeB, the base station is calculated which resource (number of RB) can allocate to it, based on prioritization. After that UE synchronizes with eNodeB for sending/receiving data. This decision is made from second module - Scheduler.
 - (c) If UE received the identifier from eNodeB, but it lost synchronization with eNodeB due to temporary inactivity, it can only receives data, but not send (uplink connection is inactive).

After successful authentication of the UE with the base station the Scheduler starts, as its first module - the allocation control generally operates in the following steps:

1. It is determined the total number of UEs (BR), which will be serviced by Sheduler for this moment (t):

If in the previous time (t-1) are satisfied all UEs will be (5), otherwise (6).

$$BR_t = BR_{t-1} + 1 \tag{5}$$

$$BR_t = BR_{t-1} - 1 \tag{6}$$

2. It is determined whether a new UE may enter for treatment in the Scheduler: If it reaches the maximum number of UE to serve at one timeslot, the request from this UE is rejected, or the UE is included in the system and the Scheduler starts to serve it.

Resource allocation in the Scheduler is based on the priority, which is presented on the Fig. 1 (right).

4 Designed Simulation Framework of LTE Scheduler

In this approach a simulation environment was established for implementation and exploration of the proposed algorithm. Used software tool is Visual Basic 2010. The architecture of the simulator is presented on the Fig. 1 (left). The modules “Topology Maintenance” and “Topology Modification” are realized with classes “Form1” and “Form2”. The classes contain methods for adding parameters of eNodeB and related UEs. A database for storing data from individual experiments for each eNodeB and its connected UEs is created. The tables from database with parameters for eNodeB and related UEs are presented on the Fig. 2 (left). The module “Traffic Management” is realized with class “Form3”. It loads data into the ‘UserEquipment’ table and visualizes the chart of the timing diagram.

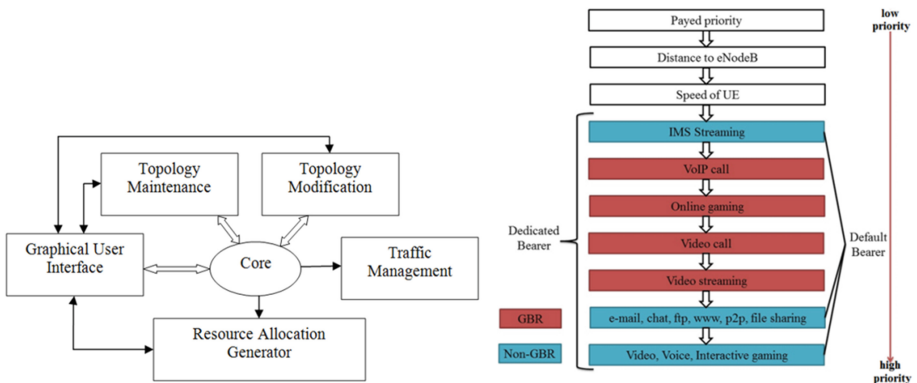


Fig. 1. The architecture of the LTE simulator and traffic prioritization in the scheduler

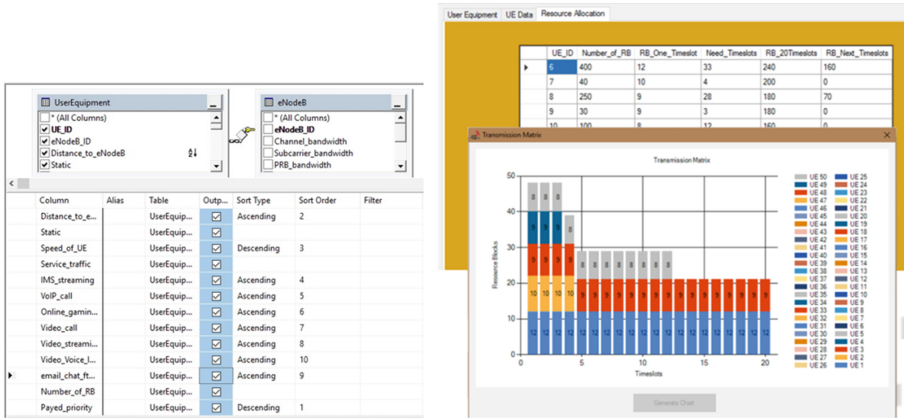


Fig. 2. Database of LTE prioritization in the eNodeB (left) and resource allocation and transmission matrix (right)

The module “resource Allocation Generator”, based on class “eNodeBdata”, realizes the proposed algorithm for priority. The class contains methods for sorting UEs, adding it’s data in array and arranging them. On Fig. 2 (right) is presented one example of resource allocation and transmission matrix. The data from different experiments are send in .xls format to the next estimation.

5 Experimental Estimation of the Algorithm and Results

In this approach it is used Rapid Miner 6.0 to create a model of influence of multi-factors on QoS parameters in LTE network such as real throughput and drop ratio. The test data is obtained according to the values of TB size reported in [1], considering an equal distribution of the physical resource blocked among the users using Resource Allocation Type 0 as defined in Sect. 7.1.6.1 of [1]. Estimated data is obtained from the presented simulation framework. The acceptable relative tolerance (standard deviation) is

$$\sigma = 0.05 \tag{7}$$

This tolerance is needed to take an account for the transient behavior at the beginning of the simulation. The main part of DataSet is presented in the Table 3.

Table 3. Data for model of QoS in LTE network

Number of users	Throughput [Mbps] with MCS = 22	Throughput [Mbps] with MCS = 12	Drop ratio with prioritization by distance	Drop ratio without prioritization
2	8.978	8.328	0.020	0.100
4	6.933	6.283	0.013	0.100
6	4.889	4.239	0.010	0.040
8	2.844	2.194	0.004	0.024
10	0.800	0.150	0.003	0.023

The input DataSet is partitioned into 10 subsets of equal size. Of the 10 subsets, a single subset is retained as the testing DataSet, and the remaining 9 subsets are used as training data set. The cross-validation process is then repeated 10 times, with each of the 10 subsets used exactly once as the testing data. Then results can be averaged to produce a single estimation. The learning processes usually optimize the model to make it fit the training data as well as possible. The Cross-Validation operator predicts the fit of a model to a testing data. This can be especially useful when separate testing data is not present. The model is presented on the Fig. 3.

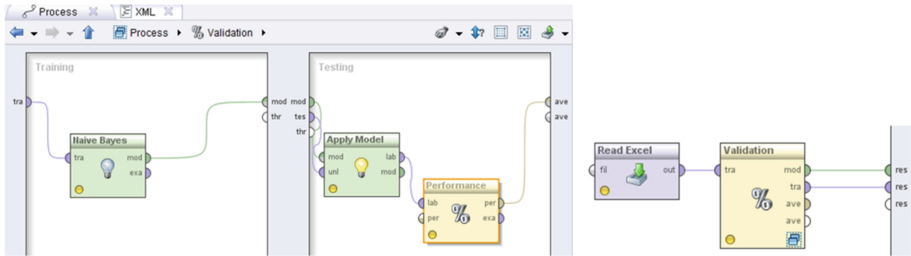


Fig. 3. Validation of the model of QoS in the LTE network

The Fig. 4 presented throughput in Mbps with different MCS- 22 (left) and 12 respectively. In each case when number of users grows up, the throughput decreases. When comparing values among these figures, it is possible to see that for the equal number of users when MCS is more, throughput is more too. When the MCS decreases, the scatter of measured data for throughput increases.

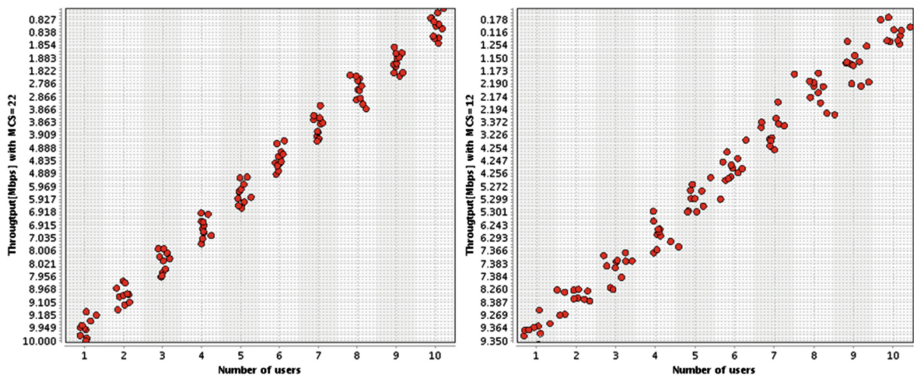


Fig. 4. Throughput with MCS = 22 (left) and MCS = 12 (right)

On Fig. 5 is presented the Drop ratio. It is possible to compare the number of drops when it is applied with prioritization, based on distance between the user and Base station and drops without prioritization. When the number of users grows up, the

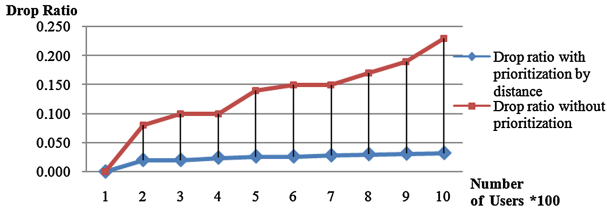


Fig. 5. Drop Ratio

numbers of rejected beacons grow up too. This is the reason to increase the drop ratio when the number of the users is increased. The observed parameters degradation when connecting more users is related to the priority implemented scheduler, in which case the less priority queues may not be served in the case of network overload or congestion.

In assessing the performance of admission control of Scheduler it also is assumed that UEs are evenly distributed within the range of the cell according to Sect. 7.1.6.1 of [1]. Each UE sends a signal periodically to know the channel condition of the UE for each TTI period of 1 ms. In the Fig. 6 (left) is presented the dependence of the average time to establish a connection from the UE to eNodeB depending on the number of the UE, which are within the scope of the eNodeB for three different values of intensity of applications - 10%, 50% and 100%. It is easy to see a trend of increase in the time for establishing connection with an increase in the number of UE within the eNodeB, such as at a higher intensity time is significantly larger. If number of UEs is 200 and 100% intensity is reached 92 ms, while number of UEs is 200 and 10% intensity the average time is 3 times less - 32 ms.

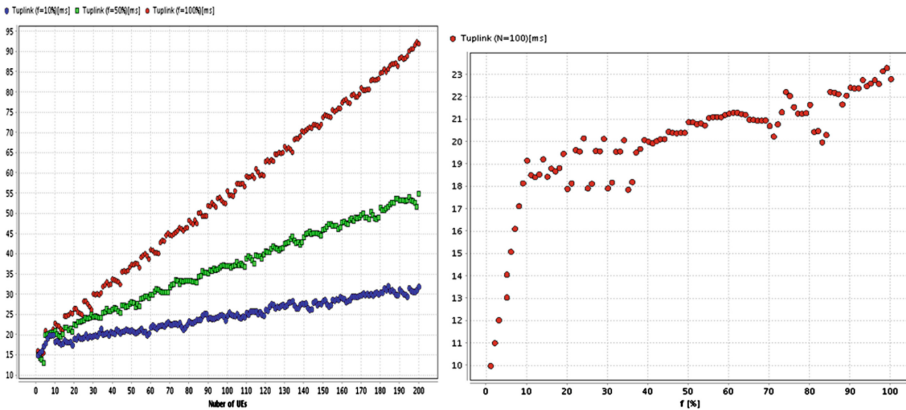


Fig. 6. Average time for connection establishment with requests intensity of 10%, 50% and 100% (left) and Average time for connection establishment with 100 UEs (right)

Figure 6 (right) shows the dependence of the average time to establish a connection from UE to the eNodeB at different average intensity of applications when under area of the eNodeB are 100 UEs. An increase of the time for establishing a connection from the UE to eNodeB when the intensity of the requests is increased, as for the first 10% of the increase is from 10 ms to 17 ms, then the increase is significantly smoother and it is amended in the range of 18 ms to 23 ms.

The results give reason to conclude that the presented algorithm for the Scheduler for LTE network can be applied successfully in the number of UEs under 100, because regardless of the intensity of the requests of the active UEs the average connection time is under 25 ms - time, fully satisfying the requirements of [1].

6 Conclusion

The main goal of researchers is creating a smart network which is flexible, robust and cost effective. Due to this reason QoS stays in focus in each network- wired, wireless or hybrid. In this paper is proposed an algorithm for Scheduler to prioritize users in order to fit the bandwidth requirement, while satisfying the application needs, based on analytical data for many factors as MCS which be used, the TB size, the number of users and the prioritization of users. In this paper is proposed a simulation framework for LTE technology, which realized an efficient method for QoS for LTE service classes. Simulation's results show that the proposed mechanism improves QoS, but the observed parameters degrade when the use of more subscribers is related to the priority implemented Scheduler, in which less priority queues may not be served in the case of network overload or congestion. There are presented two QoS parameters – throughput and drop ratio with prioritization and without prioritization. It was always assured a minimum transmission for all the service classes, although with different performances due to prioritization.

References

1. 3GPP, Technical Specification Group Radio Access Network; Physical layer procedures, 3GPP TS36.213, ver.12.4 (2015)
2. Abu-Ali, N., Taha, A.-E.M., Salah, M., Hassanein, H.: Uplink scheduling in LTE and LTE-advanced: tutorial, survey and evaluation framework. *IEEE Commun. Surv. Tutorials* **6** (3), 1239–1265 (2014)
3. Ahmed, R.E., Al Muhallabi, H.M.: Throughput-fairness tradeoff in LTE uplink scheduling algorithms. In: *International Conference on Industrial Informatics and Computer Systems* (2016)
4. Ameigeiras, P., Navarro-Ortiz, J., Andres-Maldonado, P., et al.: 3GPP QoS-based scheduling framework for LTE. *EURASIP J. Wirel. Commun. Networking* **2016**(1), 78 (2016)
5. Chaudhuri, S., Baig, I., Das, D.: Utility based QoS aware uplink scheduler scheme for LTE small cell network. In: *2015 IEEE International Conference on Communications* (2015)
6. Document IMT-ADV/I-E: Background on IMT-Advanced, ITU Radiocommunication Study Groups, ps. 3 (2008)

7. Global - 2019 Forecast Highlights, 2019 Mobile Data Traffic (2015). http://www.cisco.com/c/dam/assets/sol/sp/vni/forecast_highlights_mobile/index.html#~Region
8. Kanagasabai, A., Nayak, A.: Channel aware scheduling algorithm for lte uplink and downlink. *Network Protoc. Algorithms*. 7(3), 111–139 (2015)
9. LTE: Capacity and cell-edge performance improvements (2014). <http://www.3gpp.org/>
10. Ragaleux, A., Baey, S., Karaca, M.: Standard-compliant LTE-A uplink scheduling scheme with quality of service. *IEEE Trans. Veh. Technol.*, 1 (2017)
11. Ramadas, K., Jain, R.: WiMAX System Evaluation Methodology v2.1, WiMAX Forum (2008)
12. Cerwall, P., et al.: Ericsson Mobility Report - On the Pulse of the Networked Society (2015). <http://www.ericsson.com/res/docs/2015/ericsson-mobility-report-june-2015.pdf>
13. Use of the 470-790 MHz frequency band in the Union (2016). <http://eur-lex.europa.eu/legal-content/EN/TXT/?qid=1454410061980&uri=COM%3A2016%3A43%3AFIN>

Multithreaded Hybrid Library

Hristo Valchanov^(✉) and Simeon Andreev

Technical University of Varna, Varna, Bulgaria
hristo@tu-varna.bg

Abstract. The multi-thread programming is a widely used approach to build high performance parallel and distributed applications. The massive spreading in recent years of processors containing multiple independent cores that can operate independently is a prerequisite for the development of multi-threaded model. The software developer must be able to choose different functionality of multi-threaded libraries depending on the specifics of the various tasks to solve. The paper presents the features of the implementation of general-purpose hybrid multi-threaded library under Linux, which allows running both in user and kernel-space mode. A comparative analysis of performance with Linux library *pthread*s is performed. The results indicate that the presented library has reached identical, and in certain cases - high performance.

Keywords: Threads · Multithreaded library · User-space · Kernel-space

1 Introduction

Multithreading programming is widely used modern approach to increase computing performance by introducing parallelism of the programs [1, 2]. This approach has several advantages over the use of multiple processes. The threads require less system overhead than the processes, while the communication between the threads is considerably more efficient in comparison with inter-process communication. Massive use in recent years of processors with multiple separate cores (up to 12 in some high-performance desktop machines) which can operate independently of one another, boosts the use and development of the multithreaded model for building distributed applications [3, 4]. A number of widely used and effective programming languages such as C++, Java and others include multithreaded libraries as its core part.

The availability of different specific architectures makes the development of parallel and distributed applications difficult and some time even impossible for effective implementation. Because of this they are developed many individual libraries optimized for a specific architecture and operating system. Currently, there are multiple implementations of multithreaded libraries with different functions. The library GNU Portable Threads (Pth) [5] has been created with the idea of portability for a wide range of UNIX systems. The library Next Generation POSIX Threading (NGPT) [6] has been developed by IBM for compatibility with POSIX standard for Symmetric Multi-Processing (SMP) machine. The Linux Threads [7, 8] is an implementation of IEEE POSIX 1003.1c standard for Linux platforms. It is based on the model one-to-one and operates in user mode (user-space) only. The new implementation of threads in

Linux - Native Posix Thread Library (NPTL) [9] is also compatible with the POSIX standard, but it is based on a kernel-space model.

The implementations are optimized for different architectures - uniprocessor, multiprocessor with shared memory, multiprocessor with distributed memory. At the same time must take into account the fact that not every class of algorithms is subject to parallelism. There are some algorithms for which there is not yet found an effective multi-threading implementation, or even proven inability to create one. On the other hand, there are numerous tasks for which the improvement in execution speed is great and justifies the additional difficulties that arise in multiprocessor operation. The developer of software should have a choice of different functionality of multithreaded libraries depending on the specifics of the various tasks of solving [10]. It is also necessary to take into account the programming model in the development of parallel applications. The POSIX library is widely used for general-purpose multithreaded programming (multithreaded Internet servers). The OpenMP library [11] is an open source and widely supported but it is specialized mainly in computational algebra/applications. In other side, it is optimized according to a model of single threaded main process, most of which work is made in loops. The Intel Threading Building Blocks [12] provides tools for task-level parallelism such as loops and pipes, but is not suitable for applications with blocking IO operations.

This paper presents some aspects of the implementation of the general-purpose hybrid multi-threading library under Linux, which allows for operation both in user (user-space) and the system (kernel-space) mode. The library provides application user interface that is maximum identical in both modes. The results from experimental studies of its performance compared with the multi-threading library POSIX *threads* are presented.

2 Implementation in User-Space Mode

2.1 Threads Switching

The way of organizing of threads switching from the dispatcher is essential to the effectiveness of multi-threaded library. One option for detaching the processor from the user thread and making it available to the next ready thread is using an interrupt. In Linux the signals are convenient system for the realization of such user software interruptions. The actual interruption may be taken by a timer. However, there are several problems making such a decision not very effective. First, the great advantage of the design of the library entirely in user-space, is the ability to quickly switch between threads. Using signals and timers, however, requires switching to the kernel, which slows down this usually fast operation. Secondly, keeping the user context that is interrupted by the timer is difficult. This is because when an interrupt function is executed, for some library functions there is no guarantee to function correctly. Another possible approach is the dispatcher to run in a separate thread visible to the operating system, but this leads to other difficulties in the implementation without providing the required efficiency. In the proposed implementation of user-space library is used non-preemptive dispatching scheme, allowing avoid those problems.

2.2 Threads States

Each thread is represented by a special structure (Thread Control Block - TCB), containing the necessary information for its management. This information is used by the dispatcher for planning and switching the context of threads. It takes care of the management of the events, which is very important for proper operation of the library. The dispatcher is invoked whenever a thread processor is reassigned to another thread or when it is blocked automatically to an event.

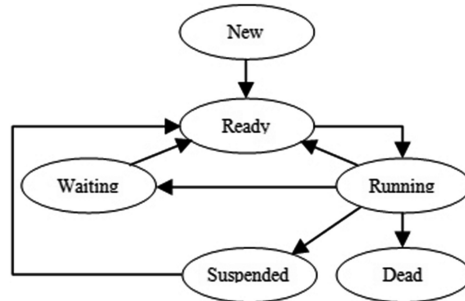


Fig. 1. Graph of threads states in user-space mode

On Fig. 1 is shown a graph of thread states during its existence. Each of the states except *Running*, is implemented as a priority queue of TCB of threads in it. On creating a thread it first falls in *New* state. From there as soon as the dispatcher can move it the *Ready* queue. On every dispatch operation the dispatcher chooses from *Ready* queue the most priority task which becomes *Running*. From *Running* state a thread can go in any of the following states: *Dead* - if it completes its execution, *Waiting* - if it is blocked at the event or in *Ready* state otherwise. On each dispatching the threads in the *Waiting* queue are checked and moved to the *Ready* queue if the appropriated event is occurred. In the *Suspended* state each thread can be moved if it must be put in the sleeping state for a given period of time.

The unblocking read/write operations, the thread sleeping for a specified time, the operations with synchronization primitives and functionality for connecting a thread to another are entirely based on events system of Linux.

3 Implementation in Kernel-Space Mode

3.1 Threads States

In this mode for the scheduling and dispatching of threads are used system resources available to the operating system level. This allows for much better planning and use of resources of the entire system, but the downside is that there are more slowly switching between threads because of invoked system calls. The realization of the threads is based on a system call *clone()*. In Linux the information for a given thread is stored in

the same structure in which information is stored for a separate process. The basic information is stored in the system structures of the operating system, but it is needed to maintain information about the thread and user context (for example, the initial function of the application). This allows simpler realization of certain library functions. Figure 2 shows a graph of the threads states in this mode.

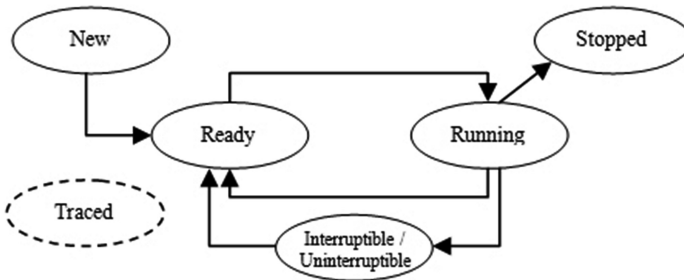


Fig. 2. Graph of threads states in kernel-space mode

The thread may be in one of following states:

- **Running** - The thread is executed.
- **Interruptible** - The thread is temporarily suspended while awaiting the fulfillment of some condition. It wakes up at the event or on receipt of a signal.
- **Uninterruptible** - The state is identical to the previous, the only difference is that the signals have no effect on the thread.
- **Traced** - The state when a thread is traced in the system (on debugging).
- **Stopped** - The execution of the thread is terminated. This state is reached when it receives certain signals.

3.2 Synchronization

In the current library implementation are developed two types of synchronization primitives - *spinlocks* and *mutexes*. For spinlocks the synchronization is based on the active waiting - CPU cycles are used. In terms of efficiency, this approach is not desirable, but the implementation is very simple.

The second type of primitives is based on the passive waiting. When there is a need of waiting the occurrence of a specific event (for example, completion of the input-output operation), the thread releases the CPU and goes to standby mode. This type of primitives is more complicated to implement because it requires the use of a system call to the kernel. This is necessary to enable the dispatcher to suspend execution of the thread and to choose another thread to continue its work.

In the current implementation the synchronization primitives - *mutexes* are realized by a mixed approach, which aims to achieve greater efficiency. Initially it is made an attempt to short actively waiting. If after this waiting the *mutex* is still locked, the kernel blocks the thread. For this purpose is used a Linux tool for base lock access - Fast User-Space Mutex (*futex*) [13]. In general, for the correct operation of a *futex* it is

needed to allocate a system semaphore. In the current implementation is used a special versions of *futex*, which are local to the process. Thus is eliminating the need of checking the semaphore internally in the kernel. This implies the implementation to be faster than that provided by the NPTL library, where *mutexes* have a much more complex structure, delaying their use.

4 Experimental Study and Results

The experimental study of the multi-threaded library is made with respect to the two main types of system loading:

- With processes limited by CPU time. These are processes that perform huge calculations.
- With processes, limited by input-output operations. These are processes that perform intensive system calls to the operating system. For example, a write in the files, waiting for user input or using network communications.

The fastest performance for processes limited by processing time is expected to be achieved when the dispatcher uses maximum long period between two threads switching. This allows retention of the information and maximum use of CPU caches. These processes almost always work without disrupting using their entire time given them by the dispatcher. Optimal policy for them is to be allowed to work long time, while it is not necessary their frequent starting.

On the other hand, the processes limited by IO operations do not require long periods to be provided with the processor. This is because they rarely use it thoroughly and often they are blocked alone. Optimal policy for them is the dispatcher to run them as much as possible more often for work.

Comparisons were made with the most common multithreading *pthread*s library and in particular with its most recent implementation in Linux – NPTL.

The experimental platform is based on Intel i7 2600K, running at 4.0 GHz clock speed. The processor uses the Hyper Threading technology and can execute 8 threads simultaneously. Each core has its own cache memory: L1 - 64 KB, L2 - 256 KB and shared L3 cache size 8 MB. Memory DDR3 SDRAM size 8 GB, 1600 MHz, dual channel mode. The OS is 64-bit distribution Arch Linux with kernel version 3.8 compiler gcc 4.8.1 and glibc 2.17.

The first test involves classical multiplication of matrices, as an example of a task comprising a plurality of calculation (Fig. 3). There are created 5 separate threads, each of which multiplied by 20 times the square matrices of size 100×100 elements.

As is expected the *pthread*s and kernel-space implementations cope best with the test. The results are close, but the advantage is for *pthread*s library. From this test is shown the great disadvantage of the user-space libraries - they can work on only on one processor. The remaining two libraries take advantage of the available eight cores in the processor. The test does not involve blocking threads.

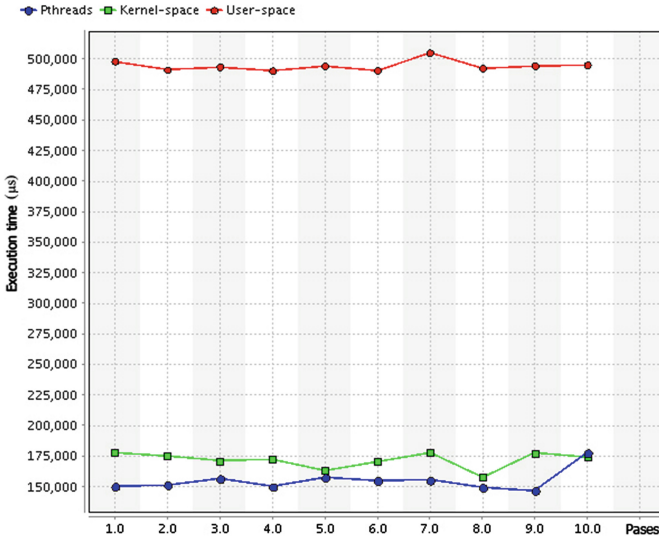


Fig. 3. Results of test with matrices multiplication

The second test uses operating with an input output operations. There are created two threads, one of which reads from a file and other writes in it. The couples operations read/write are performed 1000000 times. It is expected that some of the operations to occur and blocks. On Fig. 4 are shown the obtained experimental results.

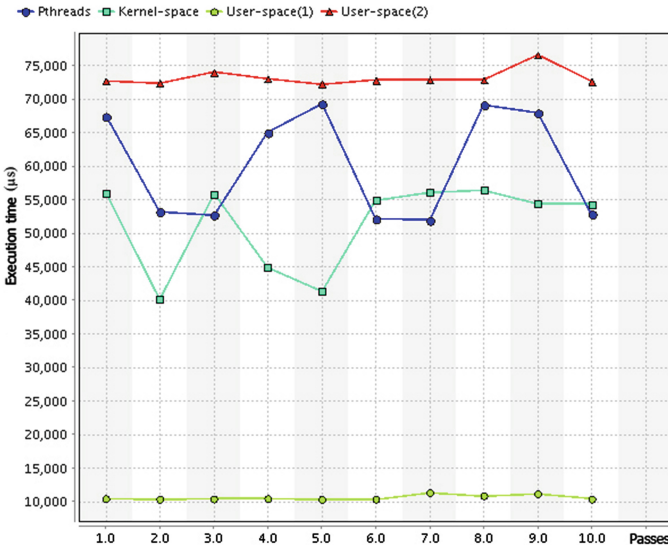


Fig. 4. Results of test with IO operations

The user-space library is used in two ways. With “1” is indicated the use of non-blocking primitives provided by the current implementation and with “2” - when they are replaced with the standard functions *write()* and *read()*. It is shown the better performance of the developed tools in comparison to the standard ones for Linux.

The *pthread*s and kernel-space libraries show the same performance with a slight preponderance of the kernel-space implementation. In the test are observed greater fluctuations between different starts due to unpredictable cases in input-output operations.

The goal of the third test is to evaluate the effectiveness of the synchronization primitives for accessing a shared resource. In a cycle of 1000000 iterations a *mutex* is locked and unlocked. There are created 5 separate threads, each of which performs the described action. On Fig. 5 are shown the obtained results.

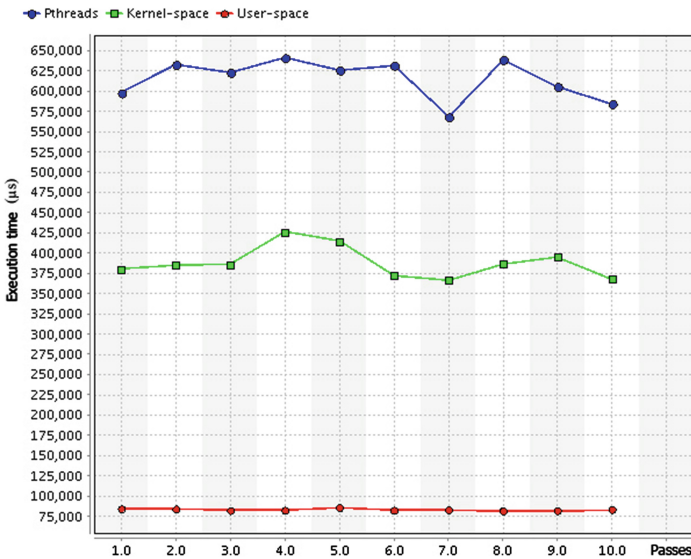


Fig. 5. The results of test with synchronization primitives

It is clear that implementation of *mutex* in *pthread*s library is slower and requires an average time of 615154 μ s.

The kernel-space library is approximately 1.5 times faster, thanks to a simple and efficient structure of the organization of the threads. Also the advantage is due to the fact that it is used a short active waiting rather than to break immediately the thread operations.

Quite expectedly the user-space implementation is fastest with an average time of 82875 μ s. This is due to the fact that it is not reached the use of slow system call, which is typical for kernel-space implementation.

5 Conclusions

This paper presents the implementation of a hybrid multi-threaded library under Linux, allowing operation as well in user-space and in kernel-space mode. Some features of the implementation are given. Experimental comparisons and evaluations are made with famous *pthread*s library at various CPU loads. The results show that is achieved identical and in certain cases and high performance of existing implementations. The developed library is relatively small, which results in fast compilation. The code is written in a simple way, allowing the use of the library in teaching of multi-threaded programming.

As guidelines for future work are the improvement of signal processing in user-space mode, as well as developing additional synchronization primitives such as conditional variables and monitors.

References

1. Carver, R., Tai, K.: Modern Multithreading. Wiley Inc., Hoboken (2008)
2. Haldar, S., Aravind, A.: Operating Systems. Dorling Kindersley Ltd., New Delhi (2010)
3. Rauber, T., Runger, G.: Parallel Programming for Multicore and Cluster Systems. Springer, Heidelberg (2013)
4. Sandem, B.: Design of Multithreaded Software. Wiley Inc., Chichester (2010)
5. Engelschall, R.: Portable multithreading. The signal stack trick for user-space thread creation. In: Proceedings of 2000 USENIX Annual Technical Conference, pp. 18–23 (2000)
6. IBM Corporation. Next Generation POSIX Threading, November 2002
7. Love, R.: Linux System Programming. O'Reilly, Sebastopol (2013)
8. Leroy, X.: The Linux Threads Library (2017). <http://pauillac.inria.fr/~xleroy/>
9. Native Posix Thread Library. <http://people.redhat.com/drepper/nptl-design.pdf>
10. Ljumovic, M.: C ++ Multithreading Cookbook. Packt Publishing, Birmingham (2014)
11. OpenMP (2017). <http://www.openmp.org/>
12. Intel Threading Building Blocks (2017). <https://www.threadingbuildingblocks.org/>
13. Futex Semantics and Usage (2017). <http://man7.org/linux/man-pages/man7/futex.7.html>

Opportunities for Application of TCSC in Low Voltage Power Supply Systems as Technical Solution for Improving of Power Quality

Valentin Gyurov^(✉) and Yuliyana Yordanov

Technical University of Varna, Varna, Bulgaria
valentin.gyurov@tu-varna.bg, ypyordanov4@gmail.com

Abstract. Thyristor controlled series compensator (TCSC) is well-known technical solution which is used in transmission systems on High voltage (HV) and Extra-high voltage (EHV). The main application of TCSC is a power flow control in terms of energy system sustainability. The schematic of TCSC is characterized by the relative simplicity of the power scheme and lack of mechanical switching elements. The study focuses on the ability to use basic properties of TSCS - simultaneous control of regimes of reactive power compensation and voltage regulation by examining the application of the scheme on low voltage. The paper shows possibilities design and construction of physical laboratory model of TCSC. The results from simulation study in Matlab and experimental study with scaled physical model presents the opportunities for application of TCSC in low voltage networks as an solution for improvement of power quality in LV distribution networks.

Keywords: Electric power quality · Voltage regulation · TCSC · Electric power supply networks · Power factor improvement

1 Introduction

Thyristor-controlled series compensation (TCSC) is a useful tool for power flow control. A TCSC is a device consisting of capacitor and parallel thyristor controlled inductor that can provide continuous control of power on the AC line over a wide range [1, 2]. The change of impedance of TCSC is performed by thyristor switched reactor connected in parallel to capacitor. Inductive reactance is defined by firing angle of thyristors. The fast electronics control and proven reliability of the thyristors lead to maximum controllability of the transmission system [3, 4]. Control is fast, efficient and increase limits of transmitted power. Some of the positive effects of series compensation on a long power line are increased power transmission capability by a decreased total circuit reactance, improved voltage, decreased circuit losses, reduced voltage fluctuations and voltage imbalance [5, 6]. That means using TCSC it is possible to operate stably at higher power levels than the system was designed. This report presents a TCSC model that operates both as a series compensator and voltage reducer.

2 Developing a Software Application with Matlab Simulink for Research and Analysis of the Physical Model

The principal scheme of thyristor serial adjustable compensator (TSCS) and its characteristics depending on the angle of opening of thyristors α are shown in Fig. 1 [1].

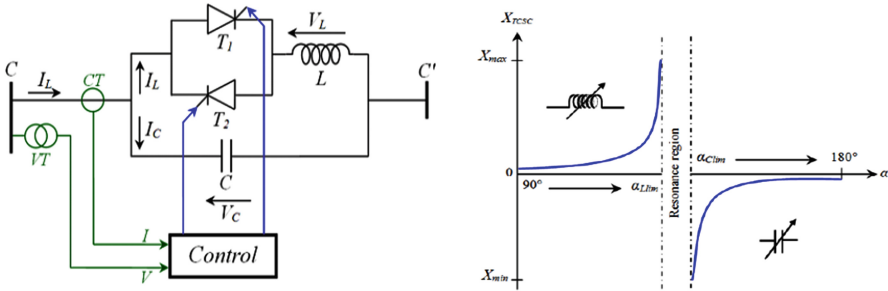


Fig. 1. Principal scheme and characteristic of TCSC.

A given characteristic is described by formulas:

$$X_{TCSC}(\alpha) = \frac{X_C \cdot X_L(\alpha)}{X_L(\alpha) - X_C} \tag{1}$$

$$X_L(\alpha) = X_L \cdot \frac{\pi}{\pi - 2\alpha - \sin \alpha} \tag{2}$$

$$X_L = \omega \cdot L \tag{3}$$

The graph is characterized by its zone of resonance, the width can be different depending on the used capacitances and inductances. The preliminary calculation and the possibility of realizing the model, determine the initial selection of the following elements $L = 187 \text{ mH}$, $C = 66 \text{ }\mu\text{F}$. The values correspond to the parameters of the scaled physical model.

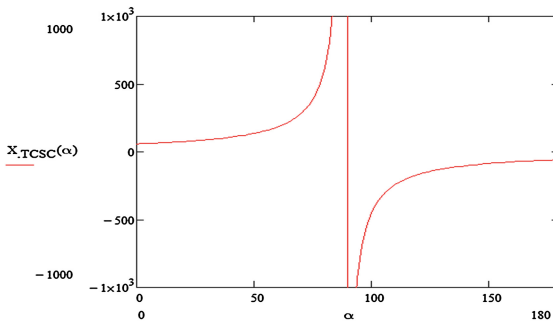


Fig. 2. Experimental characteristic of TCSC laboratory model.

The characteristic for these values was built using software MathCAD and it is shown in Fig. 2.

3 Simulation Researches in Matlab SimPower Systems in Three-Phase and Single-Phase Series Compensator of the Type TSCS

3.1 Simulation Model of Three-Phase Series Compensator TSCS is Represented in Fig. 3

An application developed software for MatLab Sim Power Systems reproduce compensator under various operating modes. The choice of parameters determined capacitive mode of operation only (compensator of inductive reactive power) and allows reports to the zone of parallel resonance. In a purely resistive load was taken regulatory characteristic in terms of voltage. The model visualizes a deep voltage downward regulation.

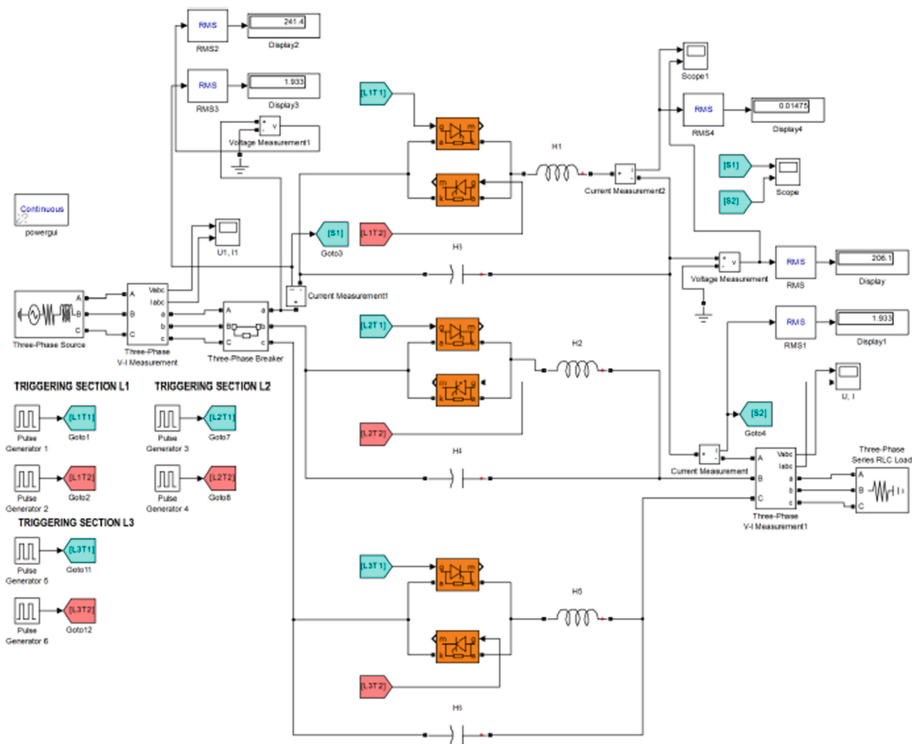


Fig. 3. MatLab Sim Power System simulation of TCSC laboratory model.

3.2 Data from the Simulation Experiment

Table 1 shows change of the voltage depending on the thyristors firing angle varying from 90 to 180°.

Table 1. Simulation results for TCSC laboratory model.

Firing angle [°]	U_1 [V]	U_2 [V]	U_C [V]	I_1 [A]	I_2 [A]	I_L [A]
90	229.3	85.9	216.2	0.812	0.811	3.183
100	229.3	83.41	212.4	0.788	0.788	3.613
110	229.3	83.39	212.4	0.788	0.788	3.613
120	229.3	94.85	206.7	0.896	0.896	3.39
130	229.3	122.1	190.4	1.154	1.154	2.8
140	229.3	147.4	172.6	1.393	1.393	2.207
150	229.3	161.9	160.4	1.531	1.531	1.829
160	229.3	172.4	149.3	1.629	1.629	1.513
170	229.3	184.4	134.5	1.743	1.743	1.105
180	229.3	192.8	122.8	1.822	1.822	0.793
180	229.3	264.2	260.4	3.196	3.196	2.306

The waveform shape of the voltage on the load U_2 and current have a character close to a pure sine wave. The serial compensator does not disturb the supply voltage and does not deform current curve. The simulation shows the possibility of increasing the voltage in condition close to the serial resonance with inductive impedance of the load. At load ratio $P = 500$ W and $Q = 400$ VAR leads to increasing voltage 265 V at input 230 V or +15%.

This corresponds to the load with $\cos \varphi = 0.78$ which is a possible situation in industrial power supply systems. Using negative phenomena serial resonance can be useful for regulating the voltage at values above the nominal in skillfully controlling of TCSC and load parameters.

The waveforms of U_1 , U_2 , I_1 , I_2 and I_L for firing angle $\alpha = 180^\circ$ are shown in Fig. 4. The shape of the current I_2 is sinusoidal, indicating that TCSC not cause harmonic disturbances in network. The phase angle between U_1 and U_2 is related to reactive power compensation of the scheme.

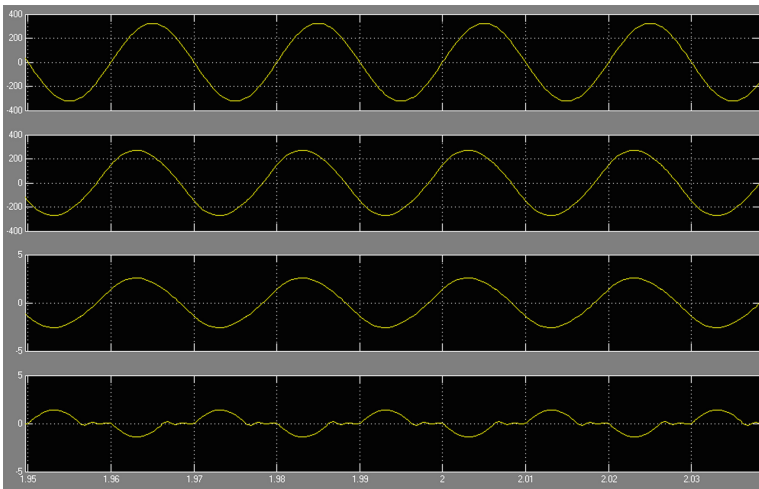


Fig. 4. Waveforms U_1 [V], U_2 [V], $I_2(I_1)$ [A] и I_L [A] angle $\alpha = 180^\circ$

4 Realization of a Physical Model of Serial Compensator

4.1 Used Element Base for Realization

The model is based on serial produced components – capacitors, inductors and thyristor controlled voltage regulator (opposite connected thyristors). The rated power of TCSC is 3 kVA and the components are designed for transmission of 2 kW trough the capacitor banks. The variable inductance is realized with conventional ballast for high-pressure mercury lamp with nominal wattage 400 W and parameters - $L = 187 \text{ mH}$ and $I_n = 2.5 \text{ A}$. The capacitor bank of $\mu\text{F}/400 \text{ V}$ is designed for 10 A rated current. The voltage regulator is triac dimmer for incandescent lamps with rated current $I = 3 \text{ A}$. In three-phase configuration are used 3 identical single-phase modules. The measurement device is Velleman PC500 oscilloscope connected to PC and PCS 2000 software platform.

4.2 Obtained Experimental Data from the Research of Physical Model of TCSC

With the use of physical model and related equipment was taken experimental regulating characteristic of TCSC. The results are shown in Table 2 and Fig. 5.

Table 2. Experimental results for TCSC laboratory model.

Firing angle [°]	U_1 [V]	U_2 [V]	I_1 [A]	I_2 [A]	P_2 [W]
110	225	106	0.88	0.88	93.28
120	224	135	1.22	1.22	164.7
130	223	165	1.56	1.56	257.4
140	224	185	1.78	1.78	329.3
150	223	199	1.98	1.98	394.02
160	223	199	1.98	1.98	394.02
170	223	199	1.98	1.98	394.02
180	223	199	1.98	1.98	394.02

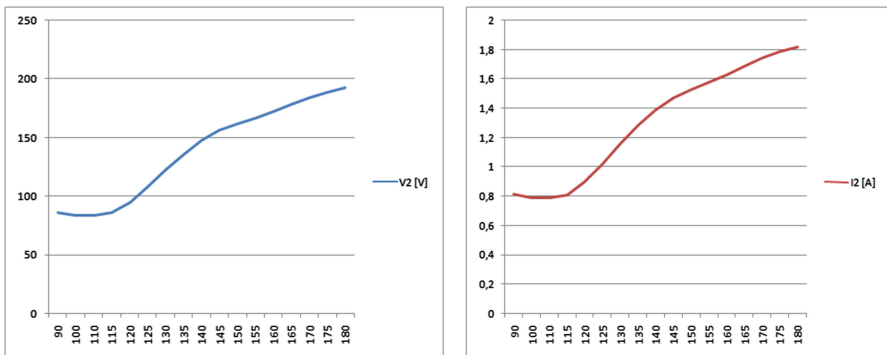


Fig. 5. U_2 and I_2 characteristics of TCSC laboratory model

The experimental regulating characteristics are presented in capacitive mode of TCSC. Operating mode for $\alpha = 90 \div 115$ is a zone of parallel resonance. For $\alpha = 120 \div 180$ the characteristics are close to linear and represent the real regulating capabilities for voltage control (Fig. 5). In Fig. 6 are shown experimental oscillograms for current I_1 and I_L (Fig. 6 - left) and current I_1 and voltage U_2 (Fig. 6 - right). The results are similar to expected from the Matlab simulation study. The developed physical model is applicable for study and demonstration of TCSC principles in a laboratory environment on low voltage.

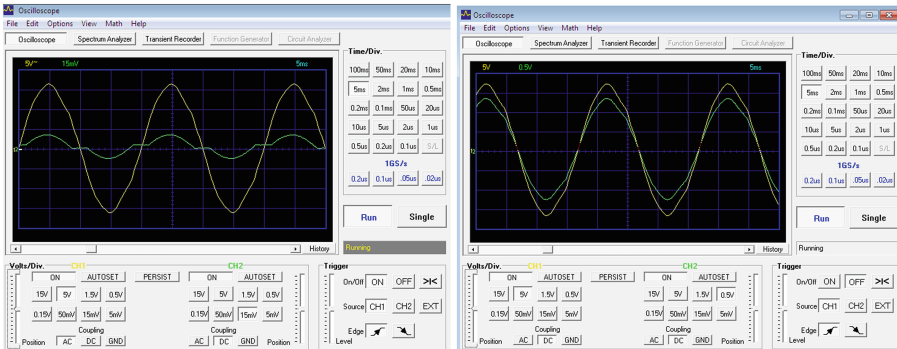


Fig. 6. I_1 , I_L and I_1 , U_2 characteristics of TCSC laboratory model

5 Conclusion

The study presents realization of laboratory physical model of TCSC. The obtained experimental regulating characteristic shows the functional relation between voltage and firing angle. The resulting waveforms represent the sinusoidal condition voltage and current. The developed physical model is suitable for process visualization of the application of TCSC in power supply systems.

References

1. Hluben, D., Bena, L., Kolcun, M.: Use of TCSC for active power flow control in the electric power system. *Przegląd Elektrotechniczny (Electrical Review)*, ISSN 0033-2097, R. 88 NR 8/2012
2. Kathal, P., Bhandakkar, A.: Power flow control in power system device Thyristor Controlled Series Capacitor (TCSC). *Int. J. Sci. Res. (IJSR)*. India Online ISSN: 2319-7064
3. Sangheetha, A.P., Padma, S.: Study of thyristor controlled series compensator for the enhancement of power flow and stability. *Int. J. Sci. Eng. Res.* 5(4), April 2014. ISSN 2229-5518

4. Noroozian, M., Ghandhari, M., Andersson, G., Hiskens, I.: A robust control strategy for shunt and series reactive compensators to damp. Electromechanical Oscillations. IEEE (2001)
5. Huang, G., Zhu, T.: TCSC as a Transient Voltage Stabilizing Controller. Texas A&M University College Station, TX 77840, USA (2001)
6. Кабышев, М.А.: Компенсация реактивной мощности в электроустановках промышленных предприятий (2012)

Simulation Modeling of Stormwater Sewage Discharge and Dispersion in the Bulgarian Black Sea Coastal Waters

Tatyana Zhekova^{1(✉)}, Anna Simeonova², and Nikolay Nikov¹

¹ Department of Navigation, Transport Management and Protection of Waterways,
Technical University, Varna, Bulgaria
tatianazhekova@gmail.com

² Department of Ecology and Environmental Protection, Technical University, Varna, Bulgaria

Abstract. Simulation modeling was used to assess the impact of the stormwater sewage discharges of “Sveti Vlas” resort complex on the Bulgarian Black Sea coastal water quality. For the simulation model a software product ArcGIS was applied. The model was developed by geo-referencing of raster images; digitizing part of the information for spatial database; organizing the information in thematic layers as well as creating wind rose, 3D model of the seasonal variation of currents and GIS data base. Input data was used to create the following thematic layers: location of the study area and the sewerage system discharge; shoreline specifics; bathymetry, hydrology and sediments of the coastal waters; bathing waters location in the area of discharge. Simulation modeling was carried out, taking into consideration different hydrological and meteorological characteristics of the investigated area. The results showed that the discharge and distribution of the stormwater sewage didn't reach the bathing waters, situated nearby, thus avoiding water quality deterioration.

Keywords: ArcGIS modeling · Sewage system · Coastal waters · Bulgarian Black Sea

1 Introduction

The Bulgarian Black Sea coastal waters are the most significant national resource with social, economic and ecological importance. The prevention and protection of marine environment from deterioration and biodiversity conservation are one of the priorities of the Bulgarian environmental policy in line with the requirements of the EU water directives [1, 2].

Over the last years the Bulgarian Black sea coastal waters are subject to strong anthropogenic pressure due to different activities - port operations, shipbuilding and ship repair, chemical industry and agriculture, tourism. Moreover, the coastal waters are the main receiver of substantial quantities of rivers inflows, treated and untreated municipal wastewater discharges and polluted stormwater runoff [3–5].

The stormwater runoff is one of the primary degrader of coastal waters especially after heavy rains and flooding [6, 7]. Some of the stormwater runoff drains into sanitary

sewage systems or separate storm sanitary systems and is discharged in the marine environment as a point source of pollution. Great quantities of heavily contaminated surface runoff are entering the coastal waters as nonpoint sources of contamination. The composition of stormwater is considerably different and depends on variety of factors: precipitation amounts; air contamination; surface structure and its pollution; intensity and storm duration, etc. which makes the assessment of the pollution loads very difficult [8]. Therefore, models that predict runoff and pollutants' loads are required to estimate the impact of urbanization and anthropogenic activities on the water receivers.

Remote Sensing and GIS techniques are being increasingly used for planning, development, management, prevention of natural resources and solving different environmental problems [9, 10]. GIS has been a powerful tool for the marine impact assessment because it integrates many kinds of data (marine geology, marine biology, chemistry, currents, sediments, etc.) in order to see the larger picture. It can turn the numbers that data represents into interpretations to create new information and to understand more effectively the processes in the marine environment [11].

The objective of the present study was to investigate the impact of stormwater sewage discharges of "Sveti Vlas" resort on the northern Bulgarian Black Sea coastal waters, using simulation modeling which has not been created and applied until now.

2 Study Area

The object concerned was the "St. Vlas" resort complex, Nessebar municipality, Burgas region, Southeastern Bulgaria (Fig. 1). The "St. Vlas" resort is situated in the area of the Big Burgas Bay (a water body of the Bulgarian Black Sea) along the coastline of two bathing zones, subject to intense recreational activities during the summer period.



Fig. 1. Location of the "St. Vlas" resort at the Bulgarian Black Sea coastal waters

The entire southern border of the complex is located along the bathing zone - “St. Vlas - the Hospital” and the western border near the “Sunny Beach” bathing zone (Fig. 2).

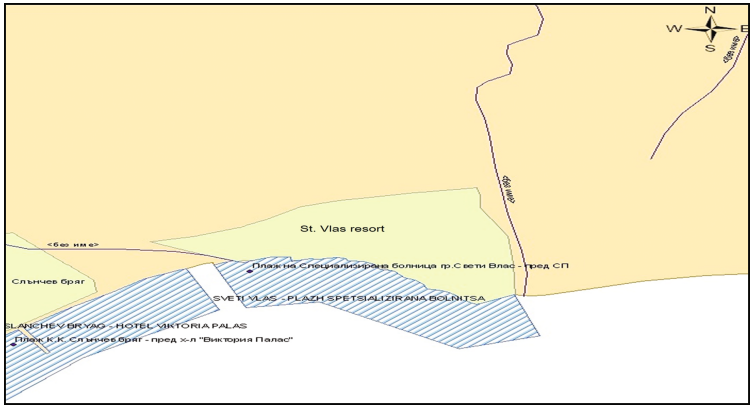


Fig. 2. Location of the “St. Vlas” resort toward the bathing zones

The “St. Vlas” waste waters are discharged through an existing sewerage system to the waste water treatment plant of the nearest resort “Ravda - Sunny Beach”. In order to prevent the bathing water pollution of the beaches nearby new underground storm-water sewage system was designed and constructed, discharging the stormwater to the eastern and western site of the bathing zone “St. Vlas - the Hospital”.

3 Methodology

Simulation modeling was applied to predict the area of discharge and dispersion of stormwater from the newly constructed sewage system of “St. Vlas” resort into the bathing waters of the Big Burgas Bay. Software product ArcGIS was used for the simulation, including input data for the basic factors, influencing the system: storm water - sewage system - coastal waters. The model involves geo - referencing of raster images; digitizing part of the information for creating spatial database; organizing the information in thematic layers for development of GIS based maps and finally assessment of the distribution of stormwater discharge in the coastal waters of the study area. The following input data was used to create thematic layers (files) for the simulation modeling: resort attributes - latitude, longitude and location; bathing zones characteristic in the area of discharge; bathymetry, sediments, shoreline, hydrological and meteorological characteristics of the water body; design characteristics of the storm water sewage system. All these data was used to create the following thematic 3D vector layers:

- Landscape, shoreline and sediments of “St. Vlas” coastal waters;
- Bathymetry of the coastal waters;
- Bathing waters location in the area of stormwater sewage system discharge;

- Hydrological characteristics of the coastal waters - currents in the study area;
- Hydro meteorological characteristics of “St. Vlas” coastal waters;
- Sewerage system discharge;
- Stormwater sewage dispersion in the area of “St. Vlas” coastal waters.

Simulation model of the impact of the hydrological and hydro meteorological factors on the coastal waters of the study area was created from the 3D vector layers.

3.1 Input Data and Creation of Landscape, Shoreline and Sediments Thematic 3D Layer

Burgas water body is characterized with the longest coastline in the country - 113 km. The coast is highly indented, with numerous bays and heavily modified as a result of different anthropogenic activities, related to numerous ports for multi-ton vessels, fishing, etc. The shoreline has a complex configuration. The marine sediments are predominantly multicomponent belonging to two basic groups - sandy (silicates sediments) and silty (clay minerals). Regarding the “St. Vlas - the Hospital” bathing zone in the eastern part of the beach the bottom is steep, and in the western - sloping. The bottom is covered with sand (60%) and gravel (30%). The data of the landscape, shoreline and sediments was visualized and presented in Fig. 3.

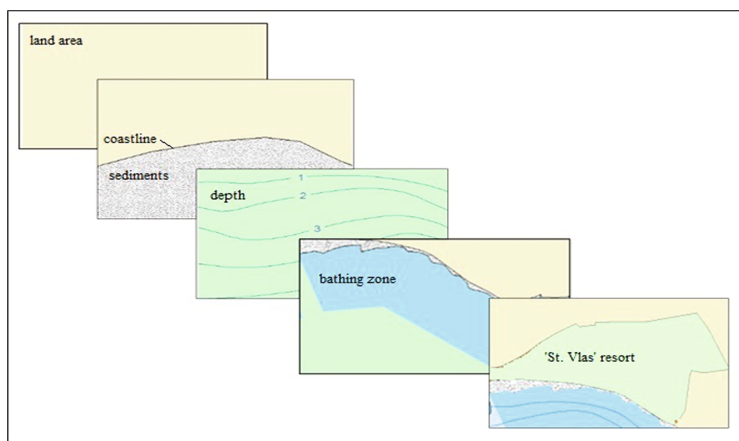


Fig. 3. Thematic layers of the study area

3.2 Input Data and Creation of Bathymetry Thematic 3D Layer

Part of the Big Burgas bay - the Small Burgas Bay is deeply recessed inland bay and represents a submerged river valley. The biggest depths of the Big Burgas Bay are located in the northeastern part of the water body. The aquatory with depth of 10 meters occupies 20% of the water body. Depths ranging between 11 and 20 m occupy 42% of the total area of this water body and depths between 26 and 30 m -16% of the area. Only 1% of the water area > 30 m depth.

On the basis of the input data and the Big Burgas Bay bathymetry map [12] a thematic layer of the land and bathymetry of the investigated area was generated. The isobaths were depicted in 1 m and presented in Fig. 3.

3.3 Input Data and Creation of Thematic Layer of the Bathing Waters Allocation Towards the Study Area

The bathing zone “St. Vlas - the Hospital” is situated in the central part of the Bulgarian Black sea coastal waters, about 9 km north of Nessebar city and about 3 km southwest of the center of St. Vlas town. The total area of the bathing zone is 168,676 m² with length of the coastline 801 m and an average width of the sea beach - 19 m. GPS coordinates of the bathing zone are E 27° 44' 0" N 42° 42' 0"–E 27° 45' 0" N 42° 42' 0" [13]. The GPS data and attributes concerning the bathing zone and study area boundaries were integrated in ArcGIS. A thematic layer of the bathing zone allocation towards the area of the resort complex was created and visualized in Fig. 3.

3.4 Input Data and Creation of Thematic 3D Layer of the Study Area

To create thematic layer of the study area location a map of the bathing zone “St. Vlas - the Hospital” was used, prepared by the Regional Health Inspection, Burgas [13]. The thematic layer was generated from the hard copy of the map, which was scanned, geo-referenced and digitized to create the spatial database. ArcGIS software and relevant data for the study area attributes were used for the generation of the thematic layer (Fig. 3).

Compiled map of the investigated region was developed using the different thematic layers and presented in Fig. 4.

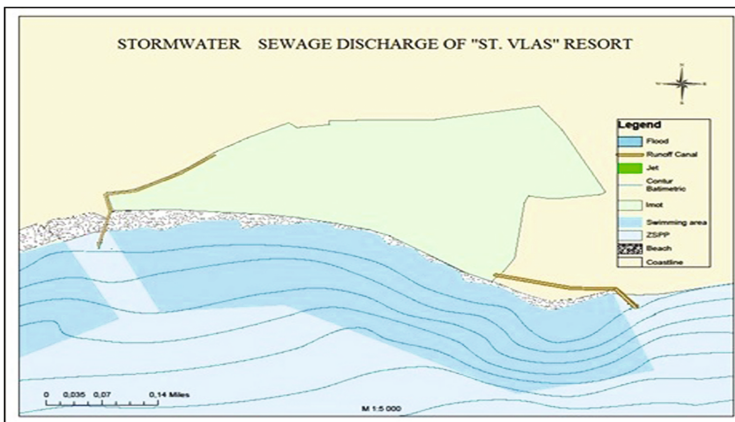


Fig. 4. Map of the “St. Vlas” resort complex and the stormwater sewage system, developed by compiling the different thematic layers

3.5 Hydrological and Hydro Meteorological Data of the Water Body and Mapping

The Big Burgas Bay refers to a type of shallow, moderately open water body with mixed bottom substrate. Surface currents reach speeds of up to 0,10–0,15 m/s under calm winds and under stormy winds the pulsations reach 0,40–0,50 m/s. The currents movement is more intensive in the north than in the south. In the region of the water body north-western winds are prevailing with annual frequency of 24%, followed by western and eastern winds with 14,5% frequency. The southern winds are only 6,8%. During the worm period - April, May, June and August prevailing are the eastern winds, related to the daily sea breeze [14].

The wind characteristics for one year ago during the summer period were used to create a wind rose of the “St. Vlas” study area. The prevailing wind directions during the summer period are mainly eastern, followed by northern, north - eastern and north - western. For the simulation modelling the eastern and northern winds were taken into consideration. The maximum speed of the eastern winds is 14 m/s and the maximum speed of the northern winds is 16 m/s [15].

3.6 3D Simulation Model of the Currents

The meteorological data and the compiled land, shoreline, bathymetric and sediments thematic layers (Fig. 4) were used to create 3D simulation model of the currents. 3D model of the seasonal variability of the currents in the north - western coastline of the Big Burgas Bay under calm weather and the vectors of the currents in different depths (from 0 to 15,5 m) and periods was created. The currents circulation was determined by numerical simulation applying data for the climate, obtained from Burgas and Sozopol meteorological stations [15].

3.7 Sewage System Characteristics

The storm water sewage system is composed of two branches - branch 1 and branch 2 (Fig. 4).

Branch 1-2 pipes with diameter $\Phi 800$ and $\Phi 1000$ mm, the point of inclusion of branch 1 is at a distance of about 37 m west of the bathing zone - the “St. Vlas - the Hospital”;

Branch 2-2 pipes with diameter $\Phi 800$ and $\Phi 1000$ mm, the point of inclusion of branch 2 is at a distance of 24 m east of the bathing zone - the “St. Vlas - the Hospital”

For the assessment of the hydrodynamic characteristics of the stormwater flow through the sewage system the following parameters were calculated: the maximum volume of the flow discharge - V (m^3) and the maximum speed - v (m^2/s). The values of the maximum flow - Q (m^3/s) and the depth of the discharge according to the project documentation was used.

4 Results and Discussions

In order to predict the stormwater discharge and dispersion in the coastal waters of the “St. Vlas” the input data was integrated in a simulation model and applied in ArcGIS. The stormwater discharge in the marine coastal waters includes two stages [16]:

- *Initial dilution.* Discharge of the effluent from the end of the pipe as a jet in the form of a funnel. This gives rise to strong velocity gradients which cause mixing between the sewage and the receiving water. The buoyant jet (because of the density difference between the jet and the marine water) bends towards the vertical and rises to the surface. The region in which this occurs is called the near field, and the dilution between the discharge port and the surface is known as an initial dilution.
- *Secondary dilution.* When the effluent reaches the surface, it begins to spread away from the outfall site, as a buoyant surface plume. The plume will travel in the general direction of the prevailing surface current and further dilution will occur because of turbulent diffusion.

For the simulation modelling and assessment of the hydrodynamic characteristics of the sewage jet, the calculated parameters of the jet were used in ArcGIS. Priority was given to the parameters during the summer period due to the low intensity of self-purification processes in the coastal waters and the high intensity of the recreational activities.

Using these database and parameters a simulation models were developed for the most typical situations, including two scenarios:

- Simulation model, applying the maximum stormwater flow which could be discharged by the two branches of the sewage system without taking into consideration the influence of the hydrological and meteorological parameters. In this case only the characteristics of the effluent jet will influence the spreading.
- Simulation model, applying the maximum stormwater flow taking into account the impact of hydro - meteorological parameters - the wind and the currents.

The first and second simulation model is presented in Fig. 5 for branch 1 and Fig. 6 for branch 2. The second simulation model was created taking into account the typical currents and the strongest winds during the summer period - *the northern winds*, presented in the segment on the bottom right of Figs. 5 and 6 and the *eastern winds*, presented in the segment on the top left of the figures. The results of the analyses for the first and the second model are presented in Tables 1 and 2.

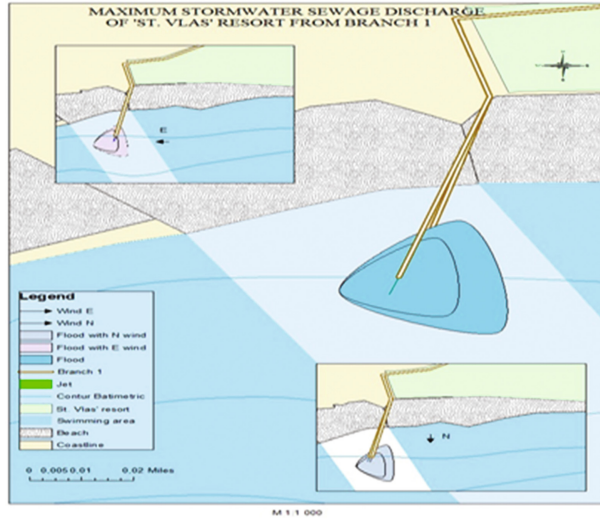


Fig. 5. Simulation of the maximum stormwater sewage discharge and dispersion of the “St. Vlas” resort from branch 1 for both scenarios

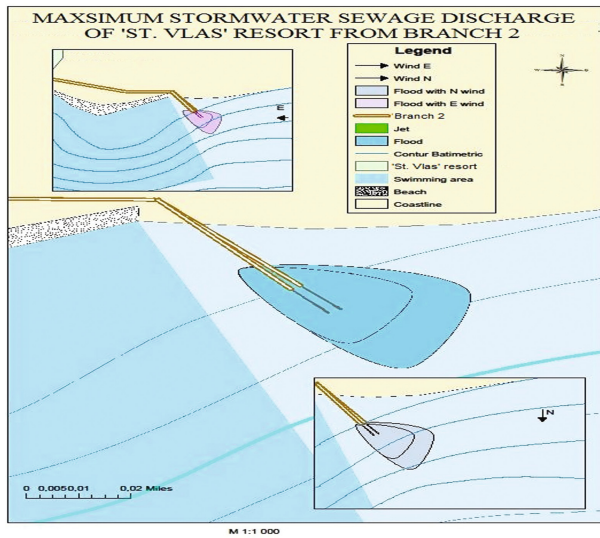


Fig. 6. Simulation of the maximum stormwater sewage discharge and dispersion of the “St. Vlas” resort from branch 2 for both scenarios

Table 1. Characteristics of stormwater sewage dispersion in the coastal waters without taking into consideration the influence of the hydrological and meteorological parameters

Stormwater sewage dispersion characteristics	Branch 1	Branch 2
Depth of the area of stormwater and coastal water mixing, m	0,5–1,2	0,7–2,0
Depth of the field of spreading of both water masses before the full mixing, m	0,4–1,3	0,7–2,8
Maximum distance of the field of spreading from the discharge point, m	37	39

Table 2. Characteristics of stormwater sewage dispersion in the coastal waters taking into consideration the influence of the hydrological and meteorological parameters at northern and eastern winds

Stormwater sewage dispersion characteristics	Northern winds		Eastern winds	
	Branch 1	Branch 2	Branch 1	Branch 2
Depth of the area of stormwater and coastal water mixing, m	0,9–1,4	1,0–2,4	0,8–1,4	0,9–2,1
Depth of the spreading field of both water masses before the full mixing, m	0,7–1,6	1,0–3,1	0,5–1,4	0,8–2,9
Maximum distance of the field of spreading from the discharge point, m	37	85	40	75

Concerning the first simulation the minimum distance of branch 1 stormwater distribution is 11 m from the “St. Vlas - the Hospital” and 22 m from the “Sunny Beach” and of branch 2–16,5 m east of the “St. Vlas - the Hospital”, not entering the aquatory of the bathing zones. With reference to the second simulation model at *northern winds* the minimum distance of branch 1 stormwater distribution is 18 m from the “St. Vlas - the Hospital” and 12,5 m from the “Sunny Beach” bathing zones. The field of dispersion of branch 2 stormwater is 25 m minimum distance east of the bathing zone the “St. Vlas - the Hospital”. Regarding *eastern winds* the minimum distance of branch 1 stormwater distribution is 22 m from the “St. Vlas - the Hospital” and 9,0 m from the “Sunny Beach” bathing zones. Branch 2 stormwater field dispersion is 11 m east of the bathing zone the “St. Vlas - the Hospital”. In both cases the stormwater field is not entering the aquatory of the bathing zones.

5 Conclusion

The simulation modeling of the hydrodynamic characteristics in the mixing zone of both water masses - the stormwater sewage discharge and the coastal waters of “St. Vlas” resort indicates that there is no influx of stormwater from branch 1 and 2 into the bathing zones - “St. Vlas - the Hospital” and the “Sunny Beach” under different hydro - meteorological conditions. The stormwater sewage system design is consistent with the specifics of the coastal zone and favors the preservation of its integrity.

Acknowledgements. The authors would like to acknowledge all specialists who helped with the provision of data for the model from: Burgas and Sozopol meteorological stations, Regional Health Inspection - Burgas, Institute of Oceanography - BAS and the designers of “St. Vlas” stormwater sewage system.

References

1. EC: Directive 2000/60/EC of the European Parliament and of the Council of 23 October 2000 establishing a framework for Community action in the field of water policy. Official Journal of the European Communities L 327/1, 22 December 2000, pp. 1–71 (2000)
2. EC: Marine Strategy Framework Directive 2008/56EC of the European Parliament and of the Council of 17 June 2008 establishing a framework for community action in the field of marine environmental policy. Official Journal of the European Union L 164/19, 25 June 2008, pp. 19–40 (2008)
3. Simeonova, A., Chuturkova, R., Bojilova, V.: Bathing water quality monitoring of Varna Black Sea Coastal Zone, Bulgaria. *Water Resour.* **37**(4), 520–527 (2010)
4. Simeonova, A.: Ecological status of the coastal water of Burgas bay. *J. Sustain. Dev.* **4**, 63–67 (2012)
5. Simeonova, A., Nikov, N., Toneva, D., Jekova, T.: Quality of the coastal water in the region of Sozopol and Chernomorets towns. In: Proceedings of the III International Congress - 50 Years of TU, vol. 7, pp. 70–75 (2012). (in Bulgarian)
6. Walsh, C.J.: Urban impacts on the ecology of receiving waters: a framework for assessment, conservation and restoration. *Hydrobiologia* **431**, 107–114 (2000)
7. Walsh, C.J., Papas, P.J., Crowther, D., Sim, P.T., Yoo, J.: Stormwater drainage pipes as a threat to a streamdwelling amphipod of conservation significance. *Austrogammaurus australis*, in south-eastern Australia. *Biodivers. Conserv.* **13**, 781–793 (2003)
8. Rozkošny, M., Kriška, M., Šalek, J., Bodik, I., Istenič, D.: Natural technologies of waste water treatment. In: Global Water Partnership, Central and Eastern Europe, GWP CEE, p. 138 (2014)
9. Nagraj, S.P., Gosain, A.K.: Geographical Information System (GIS) for water resources management. *Int. J. Res. Eng. Technol.* 417–422 (2013). IC-RICE Conference Issue
10. Avinash, K., Dubey, O.P., Ghosh, S.K.: GIS based irrigation water management. *Int. J. Res. Eng. Technol.* **3**(14), 62–65 (2014)
11. Wright, D.J., Blongewicz, M.J., Nalpin, P.N., Breman, J.: Arc Marine, GIS for a Blue Planet, p. 202. ESRI Press, Redland (2007)
12. IO: Assessment of the ecological status of the marine waters - 2013. Report, Varna, pp. 13–40 (2014)
13. RHI Burgas: Profiles of the bathing zones. <http://www.rzi-burgas.com/Vodi/profil%20na%20vodite%20za%20kapane.htm>. Accessed 22 November 2016
14. BAS: National Institute of Meteorology and Hydrology, Sea state. <http://www.meteo.bg/en/node/59>. Accessed 22 November 2016
15. Zhekova, T.: Simulation model of the hydrodynamic parameters north - west Burgas Bay. In: Conference Proceedings of the Fourth National Conference with International Participation and Youth Scientific Session on Ecological Engineering and Environment Protection (EEEEP 2015), Burgas, 3–6 June 2015, pp. 46–55 (2015)
16. Sharp, J., Joseph, L.: Hydraulic and sustainable waste water disposal in rural coastal communities. Hydraulic structures, equipment and water data acquisition systems, encyclopedia of life supporting systems, vol. 3, pp. 127–138 (2009)

A Computing Approach for Determination of the Magnetic Flux Density Under Transmission Power Lines

Emil Panov^(✉), Mediha Mehmed-Hamza, and Marinela Yordanova

Technical University, Varna, Bulgaria
eipanov@yahoo.com, mediha.hamza@mail.bg,
m.yordanova@tu-varna.bg

Abstract. The assessment of the risks from an exposure to electromagnetic fields with frequency 50 Hz at places under transmission power lines includes the determination of the magnetic flux density. It may be ensured by measurements or calculations.

The paper presents a computing approach for determination of the magnetic flux density under overhead electrical power lines. By the help of a specialized computer program created by the authors, the data for the magnetic flux density at points at an arbitrary height from the ground, transversely from the center of the tower of the transmission lines of 220 kV and 400 kV, are presented.

The calculation approach is based on the condition that the phase conductors are infinitely long and rectilinear, located close to a flat surface of a conductive medium (the ground). Then the total magnetic field can be considered as a superposition of the magnetic fields of the line conductors and their mirror images. So, the vector of the total magnetic flux density can be determined by a vector sum of the vectors of the magnetic flux densities of all the conductors.

The presented results are extracted for different constructions of electrical power line towers and horizontal arrangements of the phase conductors. The results describe the field characteristics around some typical constructions of transmission power lines of 220 kV and 400 kV.

Keywords: Computing approach · Electromagnetic fields · Magnetic flux density · Electrical power lines

1 Introduction

The Directive 2013/35/EC of the European Parliament and of the Council of 26 June 2013 and also Ordinance № RD-07-5 of 15 November 2016 on the minimum requirements to ensure the health and safety of workers from the risks related to exposure to electromagnetic fields defines the health and safety requirements regarding the exposure of people to the risks arising from electromagnetic fields (EMF) [1, 2]. EMF with frequency 50 Hz are within the low frequency fields with a frequency range from 1 Hz to 10 MHz. For that range the Directive gives the norms of the electric field intensity E [V/m] and the magnetic flux density B [T]. The value of the first quantity is thought to be more dangerous compared with the second one. However, it is always

important to determine the magnetic flux density in the various situations, which occur in practice. The Directive defines limits for the root-mean-square (RMS) values of the magnetic flux density for low B_{LAL} , high B_{HAL} action levels (LAL and HAL) and the maximum safe value of the magnetic flux density for exposure of limbs to a localized magnetic field B_{EL} . These values for 50 Hz are as follows: $B_{LAL} = 1.10^3 \mu\text{T}$; $B_{HAL} = 6.10^3 \mu\text{T}$; $B_{EL} = 18.10^3 \mu\text{T}$.

The paper presents a computing approach for determination of the magnitude of the magnetic flux density B under overhead electrical power lines (OHPL). By the help of a specialized computer program the data for the magnetic flux density B at points at arbitrary height from the ground, transversely from the center of the tower of the transmission lines of 220 kV and 400 kV can be calculated. It is well-known that the magnetic field is difficult to shield and it easily penetrates most materials, including building materials, vegetation and people.

2 Description of Related Work

The calculation of the magnetic field density B can be made by the help of the image and superposition theorems [3, 4]. Here, the earth is considered as a nonmagnetic conductive medium with a conductivity σ with typical of the usual types of soil values $\sigma = 10^{-12} \div 0,1 \text{ S/m}$ and a relative permeability μ_{ground} in the range between $1,00001 \div 14$ [5, 6]. The magnetic field around OHPL can be taken for quasi-static because of the low frequency of 50 Hz. The magnetic permeability over the ground is equal to the magnetic permeability of air, where its relative permeability is $\mu_{air} = 1,000038$.

The power lines are mounted on towers of height H_n [m]; the sag of the phase conductors is H_0 [m]; the distance between two towers is l ; x [m] is the distance between a given tower and the position of a standing person; h [m] is the height of that person. Except that, the radius of the phase conductor is r_0 [m]; the RMS value of the current flowing through the first phase of the three-phase power line is denoted by I_1 [A]; d [m] is the distance between two neighboring conductors. Then, the height H of the phase conductors above a standing person will be [7, 8]:

$$H = H_n - \frac{4 \cdot f \cdot x}{l} \left(1 - \frac{x}{l}\right) \tag{1}$$

where $f = H_n - H_0$ is the conductor sag and $0 \leq x \leq l$.

The image currents are negative of the line currents and they are situated in the ground below the power line at depth equal to H . The distances from the air conductors to the point P , where the head of the person is situated are denoted by m_a , m_b and m_c :

$$m_A = \sqrt{(x + d)^2 + (H - h)^2} \tag{2}$$

$$m_B = \sqrt{(x)^2 + (H - h)^2} \tag{3}$$

$$m_C = \sqrt{(x - d)^2 + (H - h)^2} \tag{4}$$

The distances from the image currents in the ground to the same point P are n_a , n_b and n_c :

$$n_A = \sqrt{(x + d)^2 + (H + h)^2} \tag{5}$$

$$n_B = \sqrt{(x)^2 + (H + h)^2} \tag{6}$$

$$n_C = \sqrt{(x - d)^2 + (H + h)^2} \tag{7}$$

3 Proposed Method

The method for description of the RMS values of the magnetic flux density B comprises several steps. First, the RMS value of the first image current I_{i1} can be expressed in the following form:

$$I_{i1} = \frac{(\mu_{ground} - \mu_{air}) \cdot \ln\left(\frac{H}{r_0}\right)}{[(\mu_{air} + \mu_{ground}) \cdot \ln\left(\frac{H}{r_0}\right) + \mu_{cond}]} \cdot I_1 \tag{8}$$

Here, the relative permeability of the aluminum cables is taken to be $\mu_{rAl} = 1,00002$.

The RMS values of the phasors of the currents flowing through the air conductors and the corresponding image currents in the ground are:

$$\dot{I}_1 = I_1 \tag{9}$$

$$\dot{I}_2 = a^2 \cdot I_1 \tag{10}$$

$$\dot{I}_3 = a \cdot I_1 \tag{11}$$

$$\dot{I}_{i1} = I_{i1} \tag{12}$$

$$\dot{I}_{i2} = a^2 \cdot I_{i1} \tag{13}$$

$$\dot{I}_{i3} = a \cdot I_{i1} \tag{14}$$

where $a = \left(-\frac{1}{2} + j\frac{\sqrt{3}}{2}\right)$ and this is the operator of the phasor calculations.

The RMS values of the phasors of the corresponding magnetic flux densities, caused by these currents at point P along the x -axis and y -axis of the Cartesian coordinate system with an origin situated on the ground level below the central air cable are:

$$\dot{B}_{1x} = \frac{\mu_{air}}{2\pi} \left[\frac{I_1 \cdot (H - h)}{m_A^2} - \frac{I_{i1} \cdot (H + h)}{n_A^2} \right] = \frac{\mu_{air}}{2\pi} (\dot{K}_1 - \dot{K}_2) \quad (15)$$

$$\dot{B}_{1y} = \frac{\mu_{air}}{2\pi} \left[\frac{I_1 \cdot (x + d)}{m_A^2} + \frac{I_{i1} \cdot (x + d)}{n_A^2} \right] = \frac{\mu_{air}}{2\pi} (a_1 \dot{K}_3 + b_1 \dot{K}_4) \quad (16)$$

$$\dot{B}_{2x} = \frac{\mu_{air}}{2\pi} \left[\frac{a^2 I_1 \cdot (H - h)}{m_B^2} - \frac{a^2 I_{i1} \cdot (H + h)}{n_B^2} \right] = \frac{\mu_{air}}{2\pi} (\dot{K}_5 - \dot{K}_6) \quad (17)$$

$$\dot{B}_{2y} = \frac{\mu_{air}}{2\pi} \left[\frac{a^2 I_1 \cdot x}{m_B^2} + \frac{a^2 I_{i1} \cdot x}{n_B^2} \right] = \frac{\mu_{air}}{2\pi} (c_1 \dot{K}_7 + d_1 \dot{K}_8) \quad (18)$$

$$\dot{B}_{3x} = \frac{\mu_{air}}{2\pi} \left[\frac{a I_1 \cdot (H - h)}{m_C^2} - \frac{a I_{i1} \cdot (H + h)}{n_C^2} \right] = \frac{\mu_{air}}{2\pi} (\dot{K}_9 - \dot{K}_{10}) \quad (19)$$

$$\dot{B}_{3y} = \frac{\mu_{air}}{2\pi} \left[\frac{a I_1 \cdot (x - d)}{m_C^2} + \frac{a I_{i1} \cdot (x - d)}{n_C^2} \right] = \frac{\mu_{air}}{2\pi} (e_1 \dot{K}_{11} + f_1 \dot{K}_{12}) \quad (20)$$

Here, if $x > 0$ and $x > d$, then $a_1 = b_1 = c_1 = d_1 = e_1 = f_1 = +1$; if $x > 0$ and $x < d$, then $a_1 = b_1 = c_1 = d_1 = +1$ and $e_1 = f_1 = -1$; if $x < 0$ and $x > -d$, then $a_1 = b_1 = +1$ and $c_1 = d_1 = e_1 = f_1 = -1$; if $x < 0$ and $x < -d$, then $a_1 = b_1 = c_1 = d_1 = e_1 = f_1 = -1$.

Then, the x -component and the y -components of the RMS values of the phasors of the magnetic flux densities have the following forms:

$$\dot{B}_x = \dot{B}_{1x} + \dot{B}_{2x} + \dot{B}_{3x} \quad (21)$$

$$\dot{B}_y = \dot{B}_{1y} + \dot{B}_{2y} + \dot{B}_{3y} \quad (22)$$

Therefore, the RMS values of the magnitudes of the phasors of the magnetic flux densities along the x -axis and y -axis are:

$$B_x = |\dot{B}_x| \quad (23)$$

$$B_y = |\dot{B}_y| \quad (24)$$

The RMS value of the magnitude of the vector of the magnetic flux density B at point P is as follows:

$$B = \sqrt{B_x^2 + B_y^2} \quad (25)$$

4 Experiments

The algorithm which was presented above was implemented in a specialized computer program by the help of Matlab and several explorations of different OHPL were conducted for different types of soils and different distances of point P towards the origin of the coordinating system. The program calculates the RMS value of the module of the vector of the magnetic flux density B at point P transversely from the center of the tower of the transmission line. The parameters and the peculiarities of one of the investigated OHPL tower for 400 kV are:

- Steel-aluminum conductors with cross-section 500 mm^2 ;
- Towers with a horizontal placement of the conductors;
- Horizontal separation between the phase conductors – 5,5 m;
- Phase conductor suspension – 24 m.

For the OHPL 400 kV in urban area the maximum permitted phase conductor sag is 9 m. The results for one of the investigated towers are given in Fig. 1. Curve 3 corresponds to the values under the conductor sag ($H_0 = 9 \text{ m}$), curve 1 - under the tower ($H_n = 24 \text{ m}$) and curve 2 - under the power conductor at a point between them (at height $H = 12,75 \text{ m}$). The current in the feeder is 100 A.

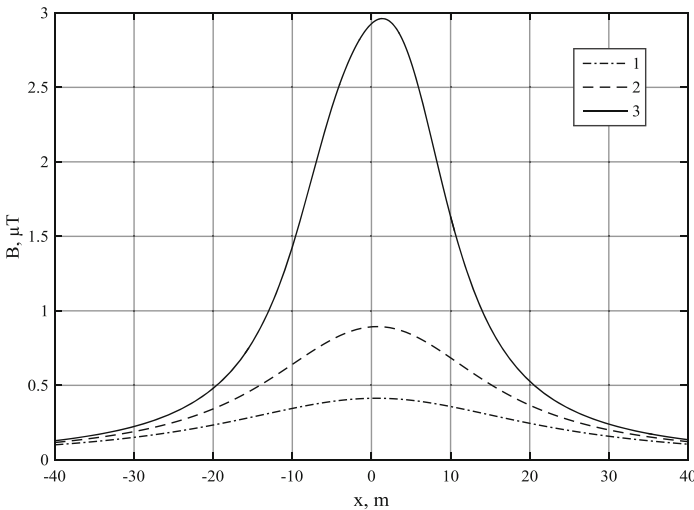


Fig. 1. The magnetic flux density under OHPL 440 kV versus x – the distance from the center of the tower

The results for one of the investigated towers of OHPL 220 kV are given in Fig. 2. Curve 3 corresponds to the values under the conductor sag ($H_0 = 8$ m), curve 1 - under the tower ($H_n = 18$ m) and curve 2 - under the power conductor at a point between them (at height $H = 11, 25$ m). The current in the feeder is 100 A.

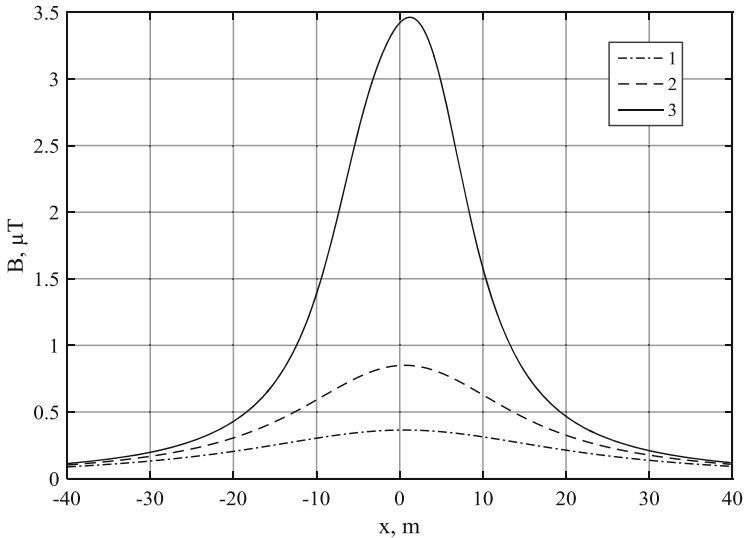


Fig. 2. The magnetic flux density under OHPL 220 kV versus x – the distance from the center of the tower

These results are received for OHPL with towers with a horizontal placement of the conductors. That's why the next researches can be focused on the development of the expressions for other types of arrangements of the phase conductors of the OHPL.

5 Conclusions

1. The presented computing approach can be used by employers to evaluate the risk from magnetic field exposure determining the magnitude of the magnetic flux density B under OHPL for each real case of practice.
2. The obtained results for the magnitude of the magnetic flux density B meet the requirements of [1, 2] for the investigated OHPL 220 kV and 440 kV.
3. The computer simulations gave results, which show that the different types of soil do not influence on the magnitudes of magnetic flux density.
4. The researches gave no real evidence of any substantial influence of the conductivity of the ground over the values of the magnetic flux density B under the explored OHPL.

References

1. Directive 2013/35/EU of the European Parliament and of the Council of 26 June 2013 on the Minimum Health and Safety Requirements Regarding the Exposure of Workers to the Risks Arising from Physical Agents (electromagnetic fields) (2013)
2. Ordinance № RD-07-5 of 15 November 2016 on the Minimum Requirements to Ensure the Health and Safety of Workers from the Risks Related to Exposure to Electromagnetic Fields (2016). (in Bulgarian)
3. Govorkov, V.A.: Electrical and magnetic fields. Energia, Moscow (1968). (in Russian)
4. Milutinov, M., Juhas, A., Prša, M.: Electromagnetic field underneath overhead high voltage power line. In: 4th International Conference on Engineering Technologies ICET 2009, Novi Sad, Serbia (2009). www.ktet.ftn.uns.ac.rs/download.php?id=391
5. Patitz, W.E., Brock, B.C., Powell, E.G.: Measurement of Dielectric and Magnetic Properties of Soil. Sandia Report, SAND95-2419.UC-706 (1995)
6. Scott, J.H.: Electric and Magnetic Properties of Rock and Soil. Open-File Report 83-915, US Department of the Interior Geological Survey (1983)
7. Dolin, P.A., Medvedev, V.T., Korochkov, V.V.: Electrical Safety. A Book of Problem. Gardarika, Moskva (2003). (in Russian)
8. Valchev, M.: Labor Safety. Tehnika, Sofia (1990). (in Bulgarian)

An Approach for Monitoring Transport and Delivery Chain of Liquid Fuels in Bulgaria

Todorka Georgieva¹, Siyka Demirova²(✉), and Penka Zlateva³

¹ Department of Communication Engineering and Technologies,
Faculty of Computing and Automation, Studentska Str. 1, 9010 Varna, Bulgaria

t_georgieva@tu-varna.bg

² Department of Industrial Management,
Faculty of Machine Technology, Studentska Str. 1, 9010 Varna, Bulgaria

s_demirova@tu-varna.bg

³ Department of Thermal Engineering, Shipbuilding Faculty,
Technical University of Varna, Studentska Str. 1, 9010 Varna, Bulgaria

pzlateva@tu-varna.bg

Abstract. In recent years in the field of transport services becomes more pervasive requirements to ensure the monitoring, evaluation and control of the transported liquid fuels. The aim of this publication is to offer an optimal solution for monitoring and control of the supply chain for the transport of liquid fuels in Bulgaria. Proposed is a one approach and algorithm to ensure the safety of supply of liquid fuels through logistics solutions and monitoring system for traffic.

Keywords: Supply chain · Algorithm · Specialized software · Transportation of liquid fuels · Risk in the supply chain

1 Introduction

The trends of globalization in recent decades significantly affect the logistics processes and their importance. A key element in the logistics process are freight. Without a well-developed and clearly defined transport system logistics process can not be competitive and can not give customers efficient and quality service. Well structured freight ensure reliability of supply, increasing the speed of the process and reduce costs. About 1/3 to 2/3 of the cost in the logistics process are precisely transport.

This publication presents an approach to monitor and control the transport chain and the supply of liquid fuels in Bulgaria for this purpose is represented algorithm selection system for transport of liquid fuels. Attention is paid to security in the logistics chain of supply of liquid fuels and addresses the main risks in the transportation of liquid fuels.

2 Management Aspects Influencing the Control of the Supply Chain for the Production and Supply of Liquid Fuels

The production, transport and delivery of materials and products play an integrating role in the logistics process, helping to transform resources into goods. Planning and optimizing freight minimize costs while making maximum service fast, reliable and quality [1, 2]. Well structured and managed supply chain logistics makes possible reliable, builds strong relationships between producers and consumers and business organization becomes easy and efficient (see Fig. 1).

BASIC ACTIVITIES	LOGISTICS COMPANY			EXTERNAL LOGISTICS		
	INCOMING LOGISTICS	MANUFACTURING LOGISTICS	OUTPUT LOGISTICS	PLACEMENT / DISTRIBUTION	WHOLESALE CUSTOMERS	RETAIL CUSTOMERS
KEY ACTIVITIES	1.Management of procurement and supply of raw materials 2.Loading and unloading operations 3.Transport	1. Management of production processes	1.Management of finished products 2. Loading and unloading operations 3. Transport 4. Stock management 5.Management of requests	1. Loading and unloading operations 2. Transport 3. Distribution	1. Loading and unloading operations 2. Stock management 3. Management of requests 4. Sales management	1.Unloading operations
SUPPORTING ACTIVITIES	COMPANY TECHNOLOGICAL DEVELOPMENT			MANAGEMENT OF HUMAN RESOURCES		
	INFRASTRUCTURE OF THE COMPANY					
	TOTAL LOGISTICS COSTS					

Fig. 1. Logistics chain for production, transport and delivery of liquid fuels.

3 Security in the Supply Chain

The increased interest in security in the supply chain (SC) is an important trend that is reflected in the number of international, regional and national initiatives and practices applied by enterprises in the management of the supply chain (MSC). The security chain is focused on protecting its assets (products, facilities, equipment, information and personnel) of any kind of damage and malicious acts [3]. This includes the application of policies, procedures and technologies for asset protection not only from theft, but also from terrorism, piracy, sabotage, and prevent the involvement of smuggled goods, persons or weapons of mass destruction in SC [4].

So security in SC becomes an essential part of the MSC and as such has different dimensions: security of material, information, financial flows, knowledge flows, and security of nodes in logistics systems (plants, terminals, warehouses, stores) [5].

3.1 Major Risks in the Transportation of Liquid Fuels

The transport of liquid fuels is a specific activity that is performed with special vehicles and drivers who have undergone training. In the European Agreement concerning the International Carriage of Dangerous Goods by Road (ADR) specified any details about this activity [6]. The main risks facing the transport of liquid fuels are: the impact of

cargo on the stability of the moving vehicle influence of tires on the stability of the moving vehicle leak of flammable liquids, fire or explosion, traffic accidents, violence and assaulting drivers operating voltage due respect for the principle Just in Time etc. In connection with improving customer service in Logistics Center - Varna done a survey presented below.

Survey of the attitudes of owners/managers of companies operating in the transport of liquid fuels. In connection with the study between March 2016–February 2017. Is a survey of owners/managers of 12 companies involved in the transport of liquid fuels in Bulgaria. The questionnaire contains 13 questions, such semantics would undermine the view of the owners/managers of transport companies on the risks and need for a global positioning system (GPS) to monitor and control the transport of liquid fuels (see Figs. 2, 3, 4, 5, 6, 7, 8, 9, 10, 11, 12 and 13). Synchronization of open and closed questions provide respondents more freedom of expression and the ability to identify specific proposals (Fig. 14).

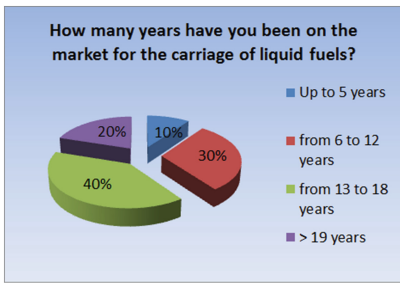


Fig. 2. Market presence

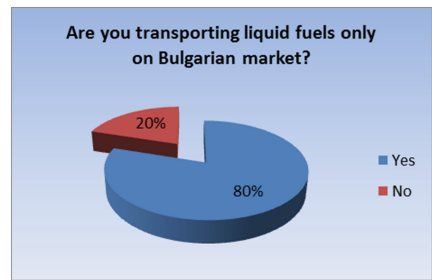


Fig. 3. Bulgarian market

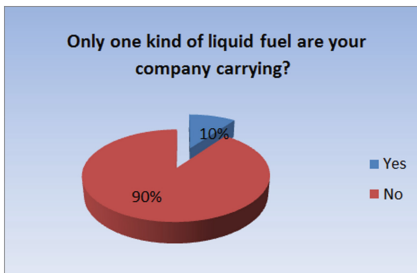


Fig. 4. Assortment

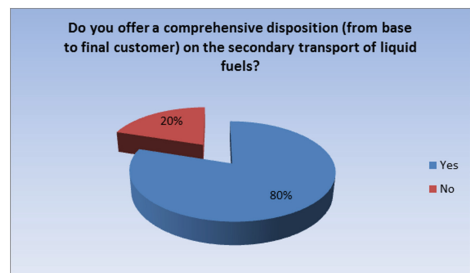


Fig. 5. Disposition

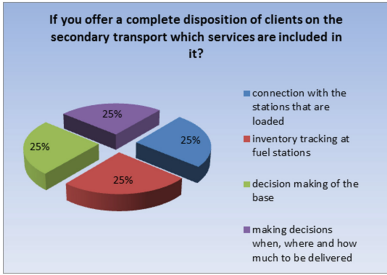


Fig. 6. Services

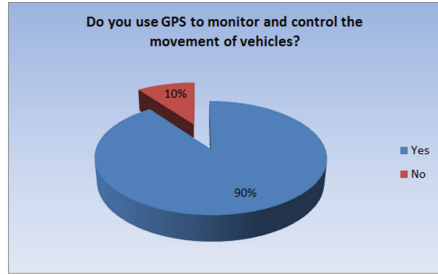


Fig. 7. Use of GPS in vehicles

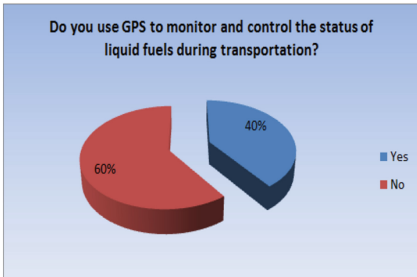


Fig. 8. Use GPS during transportation

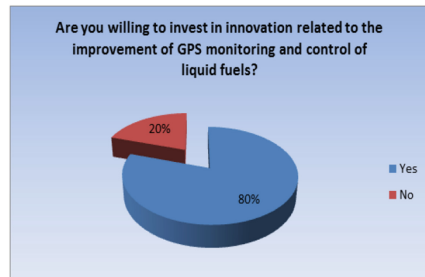


Fig. 9. Innovations in GPS

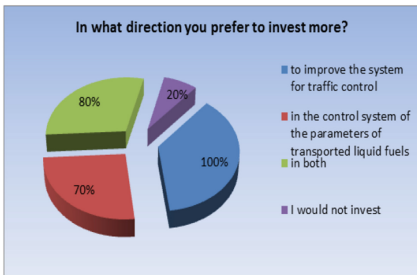


Fig. 10. Invest in GPS

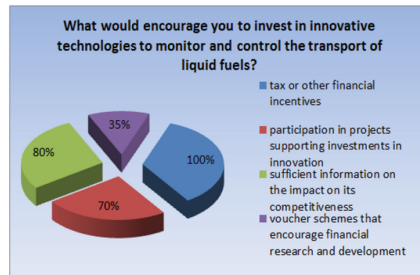


Fig. 11. Investment directions

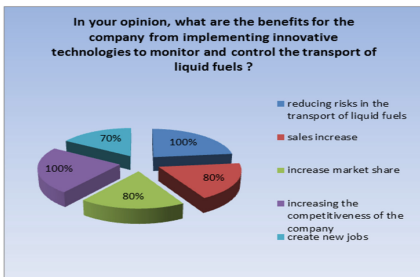


Fig. 12. Reasons to invest

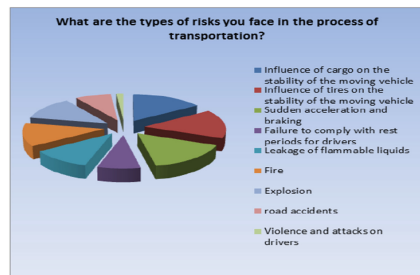


Fig. 13. Types of risks

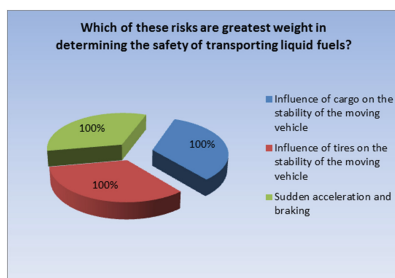


Fig. 14. Impact of the risks

Conclusions of the survey

The survey was processed with special software in the middle of a software product. Opinion on the questions raised a total of 22 owners/managers of 12 companies involved in the transport of liquid fuels in the Republic of Bulgaria.

What conclusions can be formulated after analyzing the information from the survey?

1. Bulgarian companies dealing with transportation of liquid fuels are active in the Bulgarian and international market an average of 10 years. A large percentage of them offer a complete disposition of clients on the secondary transport, which includes a link to stations that load, tracking stocks in them, deciding when, where and how much to be delivered.
2. Companies are willing to invest in innovative solutions related to monitoring and control of the supply chain for the transport of liquid fuels. Some of the reasons are tax or other financial incentives, increase their competitiveness, participation in various projects supporting investments in innovation and more.
3. Almost all Bulgarian companies use GPS to monitor and control the transport of liquid fuels. Moreover, many companies are investing in monitoring the status of the fuels themselves during their transportation. In order to reduce the risks of transportation companies are working to improve the system for traffic monitoring and control system parameters transported liquid fuels.
4. The main risks to the transport of liquid fuels in Bulgaria have been the influence of cargo on the stability of the moving vehicle influence of tires on the stability of the moving vehicle, sudden acceleration and braking, failure breaks the driver leaks flammable liquids, fire, explosion and others. With the weight of them influence of cargo on the stability of the moving vehicle influence of tires on the stability of the moving vehicle, sudden acceleration and braking.

4 Algorithm for the Selection of a Reliable System for the Carriage of Liquid Fuels

In connection with the logistics chain for the supply of liquid fuels and safe transportation is proposed algorithm selection system for transport of liquid fuels (see Fig. 15). It includes the following information: request for transport, type of cargo, contractor selection, route selection, expected risk, implementation of the transport service, current inspection and delivery to the end customer.

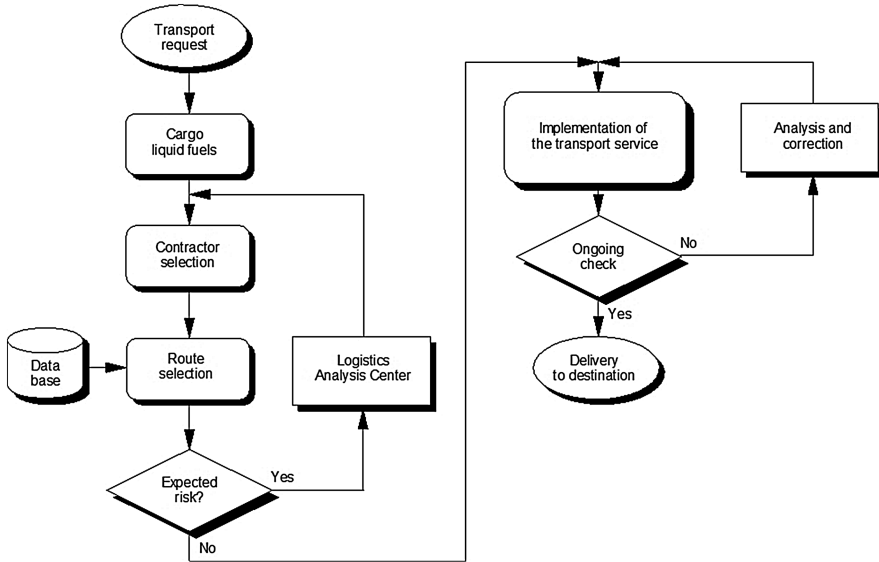


Fig. 15. Algorithm selection system for the transport and delivery of liquid fuels.

Presented above algorithm would lead both to a correct choice of transport system delivery and storage of liquid fuels and to their safe transportation. This leads to further improvement of the logistics chain to transport liquid fuels.

5 Control and Monitoring the Transportation of Liquid Fuels

In connection with the conclusions drawn from the survey on the use of GPS-systems and risks in the transportation of liquid fuels offers an approach to monitor and control the supply chain for transport of liquid fuels in the Republic of Bulgaria.

Use FleetBoard Logistics Management. The right choice of hardware components allows fully satisfying customers in tracking their fleet. In most cases, the various spheres of business have very different requirements in terms of priorities for the use of such systems [7]. All this suggests that the proper implementation of a project is

essential at the outset to be clear criteria for what is expected from the GPS system. Only in this way can be selected right components through which to fully implement the preliminary draft [8, 9].

Higher efficiency through better transparency. Thanks to FleetBoard, the new Actros meets the requirements for higher profitability on the road. Fleet management of FleetBoard reduces fuel costs and physical wear of equipment extended service periods of up to 150,000 km and shorter periods of downtime.

More efficient logistics processes. Management FleetBoard transport contributes to increased efficiency in logistics processes. The basis for this is DispoPilot.guide. The system includes a fixed bracket in the cabin and a monitor measuring 185 × 120 × 25.5 mm (W × H × D). It allows data requests to be sent to the vehicle in real time, addresses to be forwarded directly to the navigation system and the courses of the truck to be managed as efficiently as possible. At any one time there is complete information on the status of the car, courses and applications. DispoPilot.mobile provides another method of optimizing the logistic processes. Unlike DispoPilot.guide, this system can be used outside the vehicle to scan the data on cargo/goods or to introduce electronic signatures. FleetBoard transport management can be integrated safely into the reporting system of material and technical resources (MRP), the system of managing commercial operations and planning system business resources (ERP) company. This allows coordinators to continue working with their familiar software to integrate all data from FleetBoard. The chosen system processes and stores the data obtained from navigation devices located in the vehicle in a variety of communication channels. Performed optimizing workflow in the company, reducing the cost of communication and management of vehicles at home and abroad, improve control of transport, reducing costs and maintenance time and documentation analysis [10, 11].

FleetBoard Logistics has the following advantages: accurate monitoring of the individual logistics processes of the company; optimized communication; security for the driver. Based on the data obtained an analysis and evaluation by selected criteria - total mileage, excessive revving, braking, stops and average fuel consumption. During the break time and the truck is constantly monitored by GPS control. Dispatchers monitor any deviation from the route. Through GPS monitoring to determine the location of each vehicle in real time. Observed while driving daily, weekly and monthly charges gives security logistics. Using the system for logistics management FleetBoard leads to: Control and monitoring in real time through mobile application for iOS and Android for the communication between dispatcher and driver record information and more; Reduce economic costs; Increase the efficiency and economy of the system; Reducing fuel consumption through the introduction of the system Predictive Powertrain Control (PPC) - cruise control with GPS control; Reduction of risks during transport; Monitor the parameters of cargo - liquid fuel.

6 Conclusion and Final Analysis

Based on the above studies and the results obtained can be made the following conclusions:

1. An approach to monitor and control the logistics chain for the production and supply of liquid fuels. This leads to better structured supply chain optimization of all activities in it and creating stable relationships between producers and consumers.
2. An algorithm helps to correct choice of system for transport and storage of liquid fuels, which would have further improved the logistics chain for transportation.
3. In the environment of the product with specialized software has done a survey in the logistics center of the attitudes of owners/managers of companies operating in the transport of liquid fuels.
4. Made survey shows that: a large percentage of Bulgarian companies offer complete disposition of clients on the secondary transport; They are willing to invest in innovative solutions related to monitoring and control of the supply chain for the transport of liquid fuels, using GPS-systems; invest in monitoring the status of the fuels themselves during their transportation. In order to reduce the risks of transportation companies are working to improve the system for traffic monitoring and control system parameters transported liquid fuels.

The above conclusions are grounds to assert that the proposed logistics chain and supplementing algorithm and survey will contribute to further improvement of the presented approach to monitor and control the supply chain for the transport of liquid fuels in Bulgaria.

References

1. Maruchek, A., Greis, N., Mena, C., Cai, L.: Product safety and security in the global supply chain. *J. Oper. Manag.* **29**, 707–720 (2011)
2. Peck, H.: Reconciling supply chain vulnerability, risk and supply chain management. *Int. J. Logistics Res. Appl. Lead. J. Supply Chain Manag.* **9**, 127–142 (2006)
3. Wagner, S.M., Bode, C.: Risk and security – a logistics service industry perspective. In: Wagner, S.M., Bode, C. (eds.) *Managing Risk and Security: The Safeguard of Long-term Success for Logistics Service Providers*, p. 20. Haupt, Berne (2009)
4. Williams, Z., Lueg, J.E., LeMay, S.A.: Supply chain security: an overview and research agenda. *Int. J. Logistics Manag.* **19**(2), 254–281 (2008)
5. Rakovska, M.: Management of the supply chain in Bulgaria in the context of global trends. In: Dimitrov, P., Rakovska, M. (ed.) *IBIS 2011, Logistics Present and Future*, Sofia, pp. 35–46 (2011)
6. European Agreement concerning the International Carriage of Dangerous Goods by Road, ADR applicable as from 1 January 2017
7. <https://www.fleetboard.info/products/products/logistics-management.html>. Accessed 12 Apr 2017

8. Georgiev, A., Nikolai, N., Toncho, P.: Maintenance process efficiency when conduct reliability-centered maintenance of complex electronic systems. In: XIX-th International Symposium on Electrical Apparatus and Technologies SIELA 2016 (IEEE Conference and IEEE holds the Copyright of the Symposium Proceedings), Bourgas, Bulgaria (2016). doi:[10.1109/SIELA.2016.7543002](https://doi.org/10.1109/SIELA.2016.7543002)
9. Hristov, R., Dimitrov, R.: Opportunities to use the software for remote reading of vehicle parameters for Android based tablets and smart phones. In: Scientific and Technical Conference with International Participation, vol. XIX, pp. 24–28. ECO Varna (2012)
10. Milicic, M., Atanaskovic, P., Savkovic, T., Dejanovic, B.: Fleet management using the fleetboard system. *Suvremeni Promet - Modern Traffic*, vol. 35, no. 3–4, pp. 168–173. Hrvatsko Znanstveno Društvo za Promet (2015). ISSN: 0351-1898
11. Schlott, S.: Vehicle systems for logistics 4.0. *ATZ Worldwide* **119**(2), 8–13 (2017). doi:[10.1007/s38311-017-0002-7](https://doi.org/10.1007/s38311-017-0002-7)

On the Electrodynamics of Moving Bodies According to the Rotary Theory

Emil Panov^(✉)

Technical University, Varna, Bulgaria
eipanov@yahoo.com

Abstract. The paper is dedicated to one of the greatest breakthroughs in the classical electromagnetic theory connected with the creation of the system of basic equations of Maxwell-Hertz-Einstein of the electromagnetic field according to the special theory of relativity. In 1998 the rotary theory appeared, trying to explain the electromagnetic phenomena from another point of view and to answer to series of questions connected with the basic electromagnetic laws, reaching the same results but giving simpler and direct answers. The present paper is concerned with the complement (the correction) of the Maxwell-Hertz-Einstein system of equations for moving objects with arbitrary speed less than that of light or even equal to it according to the rotary theory. In it the vector of the magnetic field intensity \vec{H} and the vector of the magnetic flux density \vec{B} are presented as moments of the vector of the current density of the tangential displacement current \vec{j}_{D_t} , claiming in this way that the magnetic field is a form of a rotating electric field. The final result is a set of electromagnetic equations in fully electrical form, depicting all the electromagnetic phenomena connected with moving objects with arbitrary speeds less or equal to that of light. From these equations the relative transformations of the vector of the current density of the tangential displacement current \vec{j}_{D_t} and the effective radius-vector \vec{R}_{eff} are extracted. In this way rotary theory becomes a part of the realistic theories, which are dedicated to the explanation of the electromagnetic phenomena.

Keywords: Electromagnetic field · Maxwell-Hertz-Einstein system of equations · Rotary theory of the electromagnetic field · Special theory of relativity

1 Introduction

The set of Maxwell's equations appeared in the period between 1861 and 1873 [1–3]. In 1890 they were corrected by Hertz for moving objects with speeds smaller than the speed of light [4]. Today they are well-known as Maxwell-Hertz equations. In 1904 Lorentz made an attempt to present them for moving media [5]. In 1905, in his first paper on special theory of relativity (STR) Einstein made the next complement to these equations for two different cases – for displacement currents and for displacement and convection currents [6]. In 1908 Einstein and Laub presented the same equations in more concise form [7]. Today that set is known as Maxwell-Hertz-Einstein system of basic equations of the electromagnetic field. It is concerned with moving objects with arbitrary velocities less than the speed of light c or even equal to it.

2 Description of Related Work

In 1998 the rotary theory (RT) appeared trying to explain the electromagnetic phenomena from another point of view connected with the relative rotation of the electric field of the moving charges towards a static observer [8–10]. In that way RT could answer to series of questions connected with the basic electromagnetic laws, reaching the same results but giving simpler and direct answers starting from the basic terms of the basic magnetic quantities – the vector of the magnetic field intensity \vec{H} , the vector of the magnetic flux density \vec{B} and some others, reaching a new model of propagation of the electromagnetic wave in free space. RT is based on 10 physical theorems. It introduces 2 new principles and leads to rearrangement of the Maxwell’s set of equations, showing that it contains equations similar to the current and voltage equations according to the Kirchhoff’s laws of the electric circuits.

Today, Maxwell-Hertz-Einstein system of basic equations of the electromagnetic field is a substantial part of many basic scientific sources giving the bases of the modern electromagnetic field theory [11–13]. The last researches on the base of RT gave an additional impact over the development of that very important branch of the modern science [14, 15].

3 Proposed Method

The Maxwell’s set of equations in differential form for a static coordinating system S has the following form:

$$\text{rot } \vec{H} = \vec{j} + \frac{\partial \vec{D}}{\partial t} \tag{1}$$

$$\text{rot } \vec{E} = - \frac{\partial \vec{B}}{\partial t} \tag{2}$$

$$\text{div } \vec{D} = \rho \tag{3}$$

$$\text{div } \vec{B} = 0 \tag{4}$$

The Maxwell’s set of equations in differential form for any moving coordinate system S' (in which the direction of the x' -axis coincides with the x -axis of the static coordinate system S) with a uniform speed \vec{v} for high frequencies preserves its form (i.e. it is invariant):

$$\text{rot } \vec{H}' = \vec{j}' + \frac{\partial \vec{D}'}{\partial t'} \tag{5}$$

$$\text{rot } \vec{E}' = - \frac{\partial \vec{B}'}{\partial t'} \tag{6}$$

$$\operatorname{div} \vec{D}' = \rho' \tag{7}$$

$$\operatorname{div} \vec{B}' = 0 \tag{8}$$

In more detailed form the same set consists of 8 partial differential equations:

$$\frac{\partial H'_{z'}}{\partial y'} - \frac{\partial H'_{y'}}{\partial z'} = j'_{x'} + \frac{\partial D'_{x'}}{\partial t'} \tag{9}$$

$$\frac{\partial H'_{x'}}{\partial z'} - \frac{\partial H'_{z'}}{\partial x'} = j'_{y'} + \frac{\partial D'_{y'}}{\partial t'} \tag{10}$$

$$\frac{\partial H'_{y'}}{\partial x'} - \frac{\partial H'_{x'}}{\partial y'} = j'_{z'} + \frac{\partial D'_{z'}}{\partial t'} \tag{11}$$

$$\frac{\partial D'_{x'}}{\partial x'} + \frac{\partial D'_{y'}}{\partial y'} + \frac{\partial D'_{z'}}{\partial z'} = \rho' \tag{12}$$

$$\frac{\partial E'_{z'}}{\partial y'} - \frac{\partial E'_{y'}}{\partial z'} = -\frac{\partial B'_{x'}}{\partial t'} \tag{13}$$

$$\frac{\partial E'_{x'}}{\partial z'} - \frac{\partial E'_{z'}}{\partial x'} = -\frac{\partial B'_{y'}}{\partial t'} \tag{14}$$

$$\frac{\partial E'_{y'}}{\partial x'} - \frac{\partial E'_{x'}}{\partial y'} = -\frac{\partial B'_{z'}}{\partial t'} \tag{15}$$

$$\frac{\partial B'_{x'}}{\partial x'} + \frac{\partial B'_{y'}}{\partial y'} + \frac{\partial B'_{z'}}{\partial z'} = 0 \tag{16}$$

The components of the electromagnetic quantities of the electromagnetic field towards the coordinates of the moving coordinate system S' expressed by the components of the same quantities towards the coordinates of the static coordinate system S according to the STR are as follows [6, 11–13]:

$$E'_{x'} = E_x \tag{17}$$

$$E'_{y'} = \gamma(E_y - v \cdot B_z) \tag{18}$$

$$E'_{z'} = \gamma(E_z + v \cdot B_y) \tag{19}$$

$$D'_{x'} = D_x \tag{20}$$

$$D'_{y'} = \gamma\left(D_y - \frac{v}{c^2} \cdot H_z\right) \tag{21}$$

$$D'_z = \gamma \left(D_z + \frac{v}{c^2} \cdot H_y \right) \tag{22}$$

$$H'_{x'} = H_x \tag{23}$$

$$H'_{y'} = \gamma (H_y + v \cdot D_z) \tag{24}$$

$$H'_{z'} = \gamma (H_z - v \cdot D_y) \tag{25}$$

$$B'_{x'} = B_x \tag{26}$$

$$B'_{y'} = \gamma \left(B_y + \frac{v}{c^2} \cdot E_z \right) \tag{27}$$

$$B'_{z'} = \gamma \left(B_z - \frac{v}{c^2} \cdot E_y \right) \tag{28}$$

$$j'_{x'} = \gamma (j_x - \rho \cdot v) \tag{29}$$

$$j'_{y'} = j_y \tag{30}$$

$$j'_{z'} = j_z \tag{31}$$

$$\rho' = \gamma \left(\rho - \frac{v}{c^2} \cdot j_x \right) \tag{32}$$

where

$$\gamma = \frac{1}{\sqrt{1 - \frac{v^2}{c^2}}} \tag{33}$$

Therefore, these formulas express the Lorentz transformations of the components of the electromagnetic quantities, where $0 \leq v \leq c$.

The same results may be presented by the transverse and the longitudinal components of the electromagnetic quantities according to the notations of Einstein-Laub as follows [7]:

$$\vec{E}'_{||} = \vec{E}_{||} \tag{34}$$

$$\vec{E}'_{\perp} = \gamma (\vec{E}_{\perp} + \vec{v} \times \vec{B}_{\perp}) \tag{35}$$

$$\vec{D}'_{||} = \vec{D}_{||} \tag{36}$$

$$\vec{D}'_{\perp} = \gamma \left(\vec{D}_{\perp} + \frac{\vec{v} \times \vec{H}_{\perp}}{c^2} \right) \tag{37}$$

$$\vec{H}'_{||} = \vec{H}_{||} \tag{38}$$

$$\vec{H}'_{\perp} = \gamma(\vec{H}_{\perp} - \vec{v} \times \vec{D}_{\perp}) \tag{39}$$

$$\vec{B}'_{||} = \vec{B}_{||} \tag{40}$$

$$\vec{B}'_{\perp} = \gamma\left(\vec{B}_{\perp} - \frac{\vec{v} \times \vec{E}_{\perp}}{c^2}\right) \tag{41}$$

$$\vec{J}'_{||} = \gamma(\vec{J}_{||} - \rho \cdot \vec{v}) \tag{42}$$

$$\vec{J}'_{\perp} = \vec{J}_{\perp} \tag{43}$$

$$\rho' = \gamma\left(\rho - \frac{v}{c^2} \cdot j_{||}\right) \tag{44}$$

Maxwell's set of equations in differential and fully electric form for a static coordinating system according to the RT has the following form:

$$\text{rot}(\vec{R}_{\text{eff}} \times \vec{j}_{D_i}) = \vec{j} + \frac{\partial \vec{D}}{\partial t} \tag{45}$$

$$\text{rot} \vec{E} = -\frac{\epsilon_r \mu_r}{c^2} \cdot \frac{\partial}{\partial t} \left(\vec{R}_{\text{eff}} \times \frac{\vec{E}_{\tau}}{\partial t} \right) = -\frac{\epsilon_r \mu_r}{c^2} \cdot \left(\vec{R}_{\text{eff}} \times \frac{\partial \vec{E}_{\tau}}{\partial t^2} \right) \tag{46}$$

$$\text{div} \vec{D} = \rho \tag{47}$$

$$\text{div} \left[\frac{\epsilon_r \mu_r}{c^2} \cdot \left(\vec{R}_{\text{eff}} \times \frac{\vec{E}_{\tau}}{dt} \right) \right] = \mu \cdot \text{div}(\vec{R}_{\text{eff}} \times \vec{j}_{D_i}) = 0 \tag{48}$$

where \vec{E}_{τ} is a differential quantity. The vector of the magnetic field intensity \vec{H}_M and the vector of the magnetic flux density \vec{B}_M at a given point M in space have the following form:

$$\vec{H}_M = \int_{(L)} d\vec{H}_M = \int_{(L)} \vec{R} \times \vec{j}_{dD_i} = \sum_{p=1}^{S \rightarrow \infty} (\vec{R}_p \times d\vec{j}_{dD_i, p}) = R_{\text{eff}} \cdot j_{D_i} \cdot \vec{n} = \vec{R}_{\text{eff}} \times \vec{j}_{D_i} \tag{49}$$

$$\begin{aligned} \vec{B}_M &= \int_{(L)} d\vec{B}_M = \int_{(L)} \frac{\epsilon_r \mu_r}{c^2} \cdot \left(\vec{r}_A \times \frac{d\vec{E}_{\tau}}{dt} \right) = \mu \cdot \vec{H}_M = \mu \cdot (\vec{R}_{\text{eff}} \times \vec{j}_{D_i}) \\ &= \frac{\mu_r}{c^2 \cdot \epsilon_0} \cdot \left(\vec{R}_{\text{eff}} \times \frac{\vec{D}_{\tau}}{dt} \right) = \frac{\epsilon_r \mu_r}{c^2} \cdot \left(\vec{R}_{\text{eff}} \times \frac{\vec{E}_{\tau}}{dt} \right) \end{aligned} \tag{50}$$

where \vec{D}_{τ} is a differential quantity, too.

Thereafter, having in mind that the vectors \vec{R}_{eff} and \vec{j}_{D_t} , presented in a static Cartesian coordinate system S , have the following form:

$$\vec{R}_{eff} = R_{eff_x} \cdot \vec{i} + R_{eff_y} \cdot \vec{j} + R_{eff_z} \cdot \vec{k} \quad (51)$$

$$\vec{j}_{D_t} = j_{D_{t_x}} \cdot \vec{i} + j_{D_{t_y}} \cdot \vec{j} + j_{D_{t_z}} \cdot \vec{k} \quad (52)$$

and they can be substituted in the next vector product

$$\vec{H} = \vec{R}_{eff} \times \vec{j}_{D_t} = \begin{bmatrix} \vec{i} & \vec{j} & \vec{k} \\ R_{eff_x} & R_{eff_y} & R_{eff_z} \\ j_{D_{t_x}} & j_{D_{t_y}} & j_{D_{t_z}} \end{bmatrix} \quad (53)$$

That results in the following expressions of the components of the vector \vec{H} :

$$H_x = R_{eff_y} \cdot j_{D_{t_z}} - R_{eff_z} \cdot j_{D_{t_y}} \quad (54)$$

$$H_y = R_{eff_z} \cdot j_{D_{t_x}} - R_{eff_x} \cdot j_{D_{t_z}} \quad (55)$$

$$H_z = R_{eff_x} \cdot j_{D_{t_y}} - R_{eff_y} \cdot j_{D_{t_x}} \quad (56)$$

Then, using these results, the system of Eqs. (17)–(32) can be rearranged as follows:

$$E'_{x'} = E_x \quad (57)$$

$$E'_{y'} = \gamma(E_y - v \cdot B_z) = \gamma[E_y - \mu \cdot v \cdot (R_{eff_x} \cdot j_{D_{t_y}} - R_{eff_y} \cdot j_{D_{t_x}})] \quad (58)$$

$$E'_{z'} = \gamma(E_z + v \cdot B_y) = \gamma[E_z + \mu \cdot v \cdot (R_{eff_z} \cdot j_{D_{t_x}} - R_{eff_x} \cdot j_{D_{t_z}})] \quad (59)$$

$$D'_{x'} = D_x \quad (60)$$

$$D'_{y'} = \gamma\left(D_y - \frac{v}{c^2} \cdot H_z\right) = \gamma\left[D_y - \frac{v}{c^2} \cdot (R_{eff_x} \cdot j_{D_{t_y}} - R_{eff_y} \cdot j_{D_{t_x}})\right] \quad (61)$$

$$D'_{z'} = \gamma\left(D_z + \frac{v}{c^2} \cdot H_y\right) = \gamma\left[D_z + \frac{v}{c^2} \cdot (R_{eff_z} \cdot j_{D_{t_x}} - R_{eff_x} \cdot j_{D_{t_z}})\right] \quad (62)$$

$$H'_{x'} = H_x = R_{eff_y} \cdot j_{D_{t_z}} - R_{eff_z} \cdot j_{D_{t_y}} \quad (63)$$

$$H'_{y'} = \gamma(H_y + v \cdot D_z) = \gamma[(R_{eff_z} \cdot j_{D_{t_x}} - R_{eff_x} \cdot j_{D_{t_z}}) + v \cdot D_z] \quad (64)$$

$$H'_{z'} = \gamma(H_z - v \cdot D_y) = \gamma[(R_{eff_x} \cdot j_{D_{t_y}} - R_{eff_y} \cdot j_{D_{t_x}}) - v \cdot D_y] \quad (65)$$

$$B'_{x'} = B_x = \mu \cdot (R_{eff_y} \cdot j_{D_{tz}} - R_{eff_z} \cdot j_{D_{ty}}) \tag{66}$$

$$B'_{y'} = \gamma \left(B_y + \frac{v}{c^2} \cdot E_z \right) = \gamma \left[\mu (R_{eff_z} \cdot j_{D_{tx}} - R_{eff_x} \cdot j_{D_{tz}}) + \frac{v}{c^2} \cdot E_z \right] \tag{67}$$

$$B'_{z'} = \gamma \left(B_z - \frac{v}{c^2} \cdot E_y \right) = \gamma \left[\mu (R_{eff_x} \cdot j_{D_{ty}} - R_{eff_y} \cdot j_{D_{tx}}) - \frac{v}{c^2} \cdot E_y \right] \tag{68}$$

$$j'_{x'} = \gamma (j_x - \rho \cdot v) \tag{69}$$

$$j'_{y'} = j_y \tag{70}$$

$$j'_{z'} = j_z \tag{71}$$

$$\rho' = \gamma \left(\rho - \frac{v}{c^2} \cdot j_x \right) \tag{72}$$

If we substitute Eqs. (57)–(72) into the system of Eqs. (9)–(16) we shall receive the set of Maxwell-Hertz-Einstein equations for the electromagnetic field in a moving media with the complements (the corrections) made according to the RT of the electromagnetic field. The new system will be in a fully electric form, proving that the magnetic field is a form of a rotating electric field.

The Lorentz transformations of the components of vector \vec{H} can be extracted from Eqs. (57)–(68):

$$R'_{eff_{x'}} = \gamma \cdot R_{eff_x} \tag{73}$$

$$R'_{eff_{y'}} = R_{eff_y} \tag{74}$$

$$R'_{eff_{z'}} = R_{eff_z} \tag{75}$$

$$j'_{D_{\tau_{x'}}} = \gamma \cdot j_{D_{\tau_x}} \tag{76}$$

$$j'_{D_{\tau_{y'}}} = j_{D_{\tau_y}} \tag{77}$$

$$j'_{D_{\tau_{z'}}} = j_{D_{\tau_z}} \tag{78}$$

Therein, if we use the notations of Einstein-Laub [7], we can rewrite Eqs. (73)–(78) in more concise form:

$$R'_{eff_{||}} = \gamma \cdot R_{eff_{||}} \tag{79}$$

$$R'_{eff_{\perp}} = R_{eff_{\perp}} \tag{80}$$

$$j'_{D_{\parallel}} = \gamma \cdot j_{D_{\parallel}} \quad (81)$$

$$j'_{D_{\perp}} = j_{D_{\perp}} \quad (82)$$

So, RT becomes an indivisible part of the electromagnetic theory. Its main goal is to support the existing theory of Maxwell and to introduce some improvements towards the basic terms, connected with the basic electromagnetic quantities.

The solution of the Maxwell's set of equations with retarded potentials is known for a long time [12, 13], but RT makes some corrections in the expressions of the magnetic flux density \vec{B} and the vector magnetic potential \vec{A}_μ . And that doesn't contradict to the principle of the close action [14, 15]:

$$\vec{E} = -gradV - \frac{\partial \vec{A}_\mu}{\partial t} = -gradV - \frac{\partial(\vec{R}_{eff} \times \vec{B}_\tau)}{\partial t} = -gradV + \left(\frac{\vec{B}_\tau}{\partial t} \times \vec{R}_{eff} \right) \quad (83)$$

$$\vec{B} = \mu \cdot (\vec{R}_{eff} \times \vec{j}_{D\tau}) = rot \vec{A}_\mu = rot(\vec{R}_{eff} \times \vec{B}_\tau) \quad (84)$$

$$V(1, t) = \iiint_{(V)} \frac{\rho(2, t - \frac{r_{12}}{c})}{4\pi\epsilon r_{12}} \cdot dv \quad (85)$$

$$\vec{A}_\mu(1, t) = \iiint_{(V)} \frac{\mu \cdot \vec{j}(2, t - \frac{r_{12}}{c})}{4\pi \cdot r_{12}} \cdot dv = \vec{R}_{eff} \times \vec{B}_\tau \left(1, t - \frac{r_{12}}{c} \right) \quad (86)$$

where

$$B_\tau = \frac{E\tau}{v_1} \quad (87)$$

Here, vector \vec{B}_τ is a differential quantity and the vectors \vec{B}_τ and \vec{E}_τ are perpendicular.

In RT the system of Maxwell's equations is rearranged and the first law in it is the continuity principle of the total current (the law of Kirchhoff-Lenz), which is as global as the rest of the four equations of the Maxwell's set [9, 10, 14, 15]:

$$\oiint_{(S)} \vec{j}_{total} \cdot d\vec{s} == \iint_{(S)} \vec{j} \cdot d\vec{s} + \iint_{(S)} \frac{\partial \vec{D}}{\partial t} \cdot d\vec{s} = i_{cond.} + i_{displ.} \quad (88)$$

RT can illustrate and such a complicated process as the propagation of the electromagnetic wave [9, 10]. In its propagation, the tangential rotary displacement currents, the moments of their densities and the displacement currents of the electric flux density take part. This means, that the propagation of the electromagnetic wave in space is a very complex whirling-translational flowing of displacement currents.

The propagation of the electromagnetic wave in space is accompanied by the spread (movement) of electric whirls ahead in space – a phenomenon that is linked to the manifestation of complex electric processes.

4 Experiments

The RT of the electromagnetic field is supported by several practical proofs for its reality, within which there are some of the well-known results from experiments with rotating charged objects [9, 10]. Except them there is an enormous variety of results from different experiments, connected with different electromagnetic phenomena, effects and experimental settings, which prove the validity of Maxwell-Hertz-Einstein system of equations [11–13]. It is possible to organize additional experiments to detect directly the electric whirls and to measure directly their parameters and this is one of the possible directions of development of the RT.

5 Conclusions

The main objective of the present paper is to make a complement (correction) to the systems of equations of Maxwell-Hertz-Einstein for moving media, introducing the components of the basic electromagnetic quantities – the vector of the magnetic field intensity \vec{H} and the vector of the magnetic flux density \vec{B} , i.e. the vector of the current density of the tangential displacement current \vec{j}_{D_t} and the effective radius-vector \vec{R}_{eff} . In this way that system of equations can be presented in a fully electric form showing that all types of electromagnetic processes have electrical origin. Except that, the Lorentz transformations towards the newly introduced components of vector \vec{H} - the vectors \vec{j}_{D_t} and \vec{R}_{eff} , are extracted and in this way a complement to the STR is provided. All these details are indivisible part of the process of confirmation of the RT as a part of the two big modern theories – the electromagnetic theory of Maxwell and the STR of Albert Einstein. In such a form RT is with open way out. It can be useful to every thinking person, who doesn't want to think about the magnetic field as for one vector \vec{H} and another vector \vec{B} , which are associated with any coefficient μ , as the mass technical literature - type confection, tries to imply. The primary purpose of RT was not to show new techniques for calculation of the electromagnetic quantities in various technical tasks in a faster way or with a less efforts. The main task was to create a model of the electromagnetic field, which can be useful for the clear presentation of the complex mechanisms of the electromagnetic phenomena. In this way it can be useful for “visualization” of the invisible electromagnetic processes, for prediction and explanation of new electromagnetic processes, phenomena and effects.

References

1. Maxwell, J.C.: On physical lines of force. *Phil. Mag. J. Sci.*, Part I, 161–175, Part II, 281–291, 338–347 (March), Part III, 12–24 (April, May), Part IV, 85–95 (1861). London
2. Maxwell, J.C.: A dynamical theory of the electromagnetic field. *Phil. Trans. Roy. Soc. Lond.* **155**, 459–512 (1865). London
3. Maxwell, J.C.: A Treatise on Electricity and Magnetism, vol. I, II. Macmillan and co., London (1873)
4. Hertz, H.: Ueber die Grundgleichungen der Electrodyamik für ruhende Körper. *Wied. Ann.* **41**, 106–149 (1890). (in German)
5. Lorentz, H.A.: Electromagnetic phenomena in a system moving with any velocity less than that of light. *Proc. Royal Acad. Amsterdam* **6**, 809–831 (1904)
6. Einstein, A.: Zur Elektrodynamik bewegter Körper. *Ann. Phys.* **17**, 891–921 (1905). (in German)
7. Einstein, A., Laub, J.: Über die elektromagnetischen Grundgleichungen für bewegte Körper. *Ann. Phys.* **331**(8), 532–540 (1908). (in German)
8. Panov, E.I.: Rotary Theory of the Magnetic Field. Reports of the Union of Scientists – Varna, 2'98, 1'99, pp. 77–84. Varna, Bulgaria (1998, 1999). (in Bulgarian), ISSN 1310-5833
9. Panov, E.I.: Rotary Theory of the Magnetic Field. (Monograph, 148 p.), Publishing House of the Technical University of Varna, Varna, Bulgaria (2014). (in Bulgarian), ISBN 978-954-20-0609-1
10. Panov, E.I.: Rotary Theory of the Magnetic Field, Basics, Concepts, Methods and Models (Monograph, 148 p.), LAP Lambert Academic Publishing, Germany, 29 September 2015. ISBN 978-3-659-78098-1
11. Smythe, W.R.: Static and Dynamic Electricity, 3rd edn. Hemisphere Publishing Corporation, New York (1989)
12. Feynmann, R., Leighton, R., Sands, M.: The Feynmann Lectures on Physics, vol. 2. Addison Wesley Publishing House Inc., Reading (1964)
13. Purcell, E.M.: Electricity and Magnetism, Berkeley Physics Course, vol. II. McGraw-Hill Book Co., New York (1965)
14. Panov, E.P.: Rotary theory of the electromagnetic field. In: Annual of the Technical University – Varna, pp. 46–53. Publishing House of the Technical University of Varna, Varna, Bulgaria (2015). (in Bulgarian), ISSN 1311-896X
15. Panov, E.P.: Rotary theory of the electromagnetic field. In: Proceedings of the XIX-th International Symposium on Electrical Apparatus and Technologies, SIELA 2016, pp. 244–247. Bourgas, Bulgaria (2016). IEEE Catalog Number: CFP1628Z-PRT, ISBN 978-1-4673-9521-2

On the Electromagnetic Radiation from a Short Electric Dipole According to the Rotary Theory

Emil Panov^(✉)

Technical University, Varna, Bulgaria
eipanov@yahoo.com

Abstract. The paper is dedicated to a basic question, connected with the Maxwell's classical electromagnetic theory, concerning the electromagnetic wave equations and their meaning. Rotary theory appeared after 1998 and it introduced new terms about the basic quantities of the electromagnetic field - the vector of the magnetic field intensity \vec{H} , the vector of the magnetic flux density \vec{B} and some others, presenting them as moments of the vector of the current density of the tangential displacement current \vec{j}_{D_t} , claiming in this way that the magnetic field is a form of a rotating electric field around the moving charges. The final result is a set of electromagnetic equations in a fully electrical form, reaching a new model of propagation of the electromagnetic wave in free space, different from the classical one. In this way rotary theory gives a new possibility to explain what kind of object is the electromagnetic wave. The concrete investigation is concerned with the electromagnetic wave, which is radiated from elementary electric dipole antenna (taken as an example for simplicity of the extraction of the new equation of the electromagnetic wave). By the help of the method of moments, the \vec{H} -wave equation is turned into a wave equation of the vector \vec{j}_{D_t} , which also obeys to Ohm's law in differential (point) form, proving the fact that the propagation of the electromagnetic wave is really a process of flowing of the displacement current in space. That confirms the statement, that the electromagnetic processes in nature have only electrical origin.

Keywords: Electromagnetic field · Wave equations · Plane electromagnetic wave · Rotary theory of the electromagnetic field · Elementary electric dipole antenna

1 Introduction

The creation of the Maxwell's set of equations of the electromagnetic field gave the possibility for extraction of the electromagnetic wave equations and their solutions [1–3]. In 1998 the rotary theory (RT) has appeared trying to explain the electromagnetic phenomena from another point of view introducing the idea of the relative rotation of the electric field of the moving charges towards a static observer [4–6]. In that way RT could answer to series of questions connected with the basic electromagnetic laws, reaching the

same results but giving simpler and direct answers starting from the basic terms of the basic magnetic quantities – the vector of the magnetic field intensity \vec{H} , the vector of the magnetic flux density \vec{B} and some others, reaching a new model of propagation of the electromagnetic wave in free space. RT is based on 10 physical theorems. It introduces 2 new principles and leads to a rearrangement of the Maxwell's set of equations, showing that it contains equations similar to the current and voltage equations according to the Kirchhoff's laws of the electric circuits.

2 Description of Related Work

The last researches in that direction are connected with the extraction of the solutions of the Maxwell's set of equations with retarded potentials [7–9]. A substantial part of these solutions is connected with the introduction of the method of moments, which gives the possibility to express the vectors \vec{H} and \vec{B} as moments of the current density of the tangential displacement current \vec{j}_{D_τ} , where a new parameter appears - the effective radius-vector \vec{R}_{eff} . The Maxwell's set of equations in differential and a fully electric form for a static coordinating system according to the RT [4–6] has the following form:

$$rot(\vec{R}_{eff} \times \vec{j}_{D_\tau}) = \vec{j} + \frac{\partial \vec{D}}{\partial t} \quad (1)$$

$$rot \vec{E} = -\frac{\epsilon_r \mu_r}{c^2} \cdot \frac{\partial}{\partial t} \left(\vec{R}_{eff} \times \frac{\vec{E}_\tau}{\partial t} \right) = -\frac{\epsilon_r \mu_r}{c^2} \cdot \left(\vec{R}_{eff} \times \frac{\partial \vec{E}_\tau}{\partial t^2} \right) \quad (2)$$

$$div \vec{D} = \rho \quad (3)$$

$$div \left[\frac{\epsilon_r \mu_r}{c^2} \cdot \left(\vec{R}_{eff} \times \frac{\vec{E}_\tau}{dt} \right) \right] = \mu \cdot div(\vec{R}_{eff} \times \vec{j}_{D_\tau}) = 0 \quad (4)$$

where \vec{E}_τ is a differential quantity. The vector of the magnetic field intensity \vec{H}_M and the vector of the magnetic flux density \vec{B}_M at a given point M in space have the following form:

$$\vec{H}_M = \int_{(L)} d\vec{H}_M = \int_{(L)} \vec{R} \times \vec{j}_{dD_\tau} = \sum_{p=1}^{S \rightarrow \infty} (\vec{R}_p \times d\vec{j}_{dD_\tau, p}) = R_{eff} \cdot j_{D_\tau} \cdot \vec{n} = \vec{R}_{eff} \times \vec{j}_{D_\tau} \quad (5)$$

$$\begin{aligned} \vec{B}_M &= \int_{(L)} d\vec{B}_M = \int_{(L)} \frac{\varepsilon_r \mu_r}{c^2} \cdot \left(\vec{r}_A \times \frac{d\vec{E}_\tau}{dt} \right) = \mu \cdot \vec{H}_M = \mu \cdot (\vec{R}_{eff} \times \vec{j}_{D_\tau}) \\ &= \frac{\mu_r}{c^2 \cdot \varepsilon_0} \cdot \left(\vec{R}_{eff} \times \frac{d\vec{D}_\tau}{dt} \right) = \frac{\varepsilon_r \mu_r}{c^2} \cdot \left(\vec{R}_{eff} \times \frac{\vec{E}_\tau}{dt} \right) \end{aligned} \tag{6}$$

where \vec{D}_τ is a differential quantity, as well. Here, the vectors \vec{R}_{eff} and \vec{j}_{D_τ} can be presented in Cartesian coordinate system as follows:

$$\vec{R}_{eff} = R_{eff_x} \cdot \vec{i} + R_{eff_y} \cdot \vec{j} + R_{eff_z} \cdot \vec{k} \tag{7}$$

$$\vec{j}_{D_\tau} = j_{D_{\tau_x}} \cdot \vec{i} + j_{D_{\tau_y}} \cdot \vec{j} + j_{D_{\tau_z}} \cdot \vec{k} \tag{8}$$

They can be substituted in the next vector product:

$$\vec{H} = \vec{R}_{eff} \times \vec{j}_{D_\tau} = \begin{bmatrix} \vec{i} & \vec{j} & \vec{k} \\ R_{eff_x} & R_{eff_y} & R_{eff_z} \\ j_{D_{\tau_x}} & j_{D_{\tau_y}} & j_{D_{\tau_z}} \end{bmatrix} \tag{9}$$

Therefore, the following expressions of the components of vector \vec{H} can be received:

$$H_x = R_{eff_y} \cdot j_{D_{\tau_z}} - R_{eff_z} \cdot j_{D_{\tau_y}} \tag{10}$$

$$H_y = R_{eff_z} \cdot j_{D_{\tau_x}} - R_{eff_x} \cdot j_{D_{\tau_z}} \tag{11}$$

$$H_z = R_{eff_x} \cdot j_{D_{\tau_y}} - R_{eff_y} \cdot j_{D_{\tau_x}} \tag{12}$$

The solution of the Maxwell’s set of equations with retarded potentials is well-known for a long time, but RT makes some corrections in the expressions of the magnetic flux density \vec{B} and the vector magnetic potential \vec{A}_μ and it doesn’t contradict to the principle of the close action [7–9]:

$$\vec{E} = -gradV - \frac{\partial \vec{A}_\mu}{\partial t} = -gradV - \frac{\partial (\vec{R}_{eff} \times \vec{B}_\tau)}{\partial t} \tag{13}$$

$$\vec{B} = \mu \cdot (\vec{R}_{eff} \times \vec{j}_{D_\tau}) = rot \vec{A}_\mu = rot (\vec{R}_{eff} \times \vec{B}_\tau) \tag{14}$$

$$V(1, t) = \iiint_{(V)} \frac{\rho(2, t - \frac{r_{12}}{c})}{4\pi \varepsilon r_{12}} \cdot dv \tag{15}$$

$$\vec{A}_\mu(1, t) = \iiint_{(V)} \frac{\mu \cdot \vec{j}(2, t - \frac{r_{12}}{c})}{4\pi \cdot r_{12}} \cdot dv = \vec{R}_{eff} \times \vec{B}_\tau \left(1, t - \frac{r_{12}}{c} \right) \tag{16}$$

where \vec{B}_τ is a differential quantity.

The solutions of the Maxwell’s set of equations can be used for investigations, connected with a big variety of electromagnetic devices, among which one is very interesting for the electronic engineers – the researches about the propagation of the electromagnetic field from different types of antennas. Equation (15) is a solution of the homogeneous wave equation in regard to the scalar potential V :

$$\Delta V = \varepsilon \cdot \mu \cdot \frac{\partial^2 V}{\partial t^2} \tag{17}$$

and Eq. (16) is a solution of the homogeneous wave equation in regard to the vector magnetic potential \vec{A}_μ

$$\Delta \vec{A}_\mu = \varepsilon \cdot \mu \cdot \frac{\partial^2 \vec{A}_\mu}{\partial t^2} \tag{18}$$

which can be extracted from the first two equations of the Maxwell’s set. These two equations do not reveal all aspects of the propagation of the electromagnetic field. And RT can be used to illustrate such a complicated process and to extract new forms of the wave equations [5, 6].

3 Proposed Method

The extraction of one of the new forms of the wave equations of the electromagnetic field can be done by using a simple object – an elementary short dipole antenna, taken because of its simplicity. Let us consider such a short dipole in free space with a length ℓ , in which an alternating sinusoidal current is flowing:

$$i(t) = i_m \cdot \sin \omega \cdot t \tag{19}$$

where ω is the angular frequency, and the corresponding frequency f has a value, for which the following inequality is valid

$$\lambda = \frac{c}{f} \gg \ell \tag{20}$$

Here, λ is the wavelength and c is the speed of light in vacuum. The orientation of the antenna is chosen to be perpendicular towards the equatorial plane, which contains the x - and y -axes of a Cartesian coordinate system, i.e. it is orientated along the z -axis, divided into two equal parts by the same plain. A spherical coordinate system is also introduced, in order to support the complicated calculations which follow. The unit vectors of the Cartesian coordinate system are denoted by $\vec{i}, \vec{j}, \vec{k}$ and the unit vectors of the spherical coordinate system with the same origin as that of the previous one are $\vec{I}_r, \vec{I}_\phi, \vec{I}_\theta$.

The phasor of the retarded vector magnetic potential \vec{A}_μ at any point M in the space around the antenna is as follows [10–12]:

$$\vec{A}_\mu(r,t) = \iiint_V \frac{\mu_0 \cdot \vec{J}_m \left(r, t - \frac{r}{c} \right)}{r \cdot 4\pi} \cdot dv = \frac{\mu_0 \cdot i_m \cdot \ell}{4\pi \cdot r} \cdot e^{-j \frac{2\pi \cdot r}{\lambda}} \cdot (\cos \theta \cdot \vec{1}_r - \sin \theta \cdot \vec{1}_\theta) \quad (21)$$

where the phasor of the vector of the magnetic field intensity \vec{H} is

$$\vec{H}(r,t) = \frac{1}{\mu_0} \cdot rot \left[\vec{A}_\mu(r,t) \right] = \left[\frac{i_m \cdot \ell \cdot \sin \theta}{4\pi \cdot r^2} \cdot \left(1 + j \frac{2\pi \cdot r}{\lambda} \right) \cdot e^{-j \frac{2\pi \cdot r}{\lambda}} \right] \cdot \vec{1}_\Phi \quad (22)$$

This result is received after the change of the Cartesian coordinate system by a spherical coordinate system, in order to use the symmetry of the electromagnetic field. It contains two components – the first one is for the near zone and the second is for the far zone.

$$\vec{H}(r,t)_{near-zone} = \left[\frac{i_m \cdot \ell \cdot \sin \theta}{4\pi \cdot r^2} \cdot e^{-j \frac{2\pi \cdot r}{\lambda}} \right] \cdot \vec{1}_\Phi \quad (23)$$

$$\vec{H}(r,t)_{far-zone} = \left[\frac{i_m \cdot \ell \cdot \sin \theta}{4\pi \cdot r^2} \cdot \left(j \frac{2\pi \cdot r}{\lambda} \right) \cdot e^{-j \frac{2\pi \cdot r}{\lambda}} \right] \cdot \vec{1}_\Phi = \left(j \cdot \frac{i_m \cdot \ell \cdot \sin \theta}{2\lambda \cdot r} \cdot e^{-j \frac{2\pi \cdot r}{\lambda}} \right) \cdot \vec{1}_\Phi \quad (24)$$

The last two equations can be presented also in rotary form in the time domain, expressed by Eqs. (5, 6, 9 and 14):

$$\begin{aligned} \vec{H}_{near-zone} \left[\omega \left(t - \frac{r}{c} \right) \right] &= \vec{R}_{eff} \times \vec{j}_{D_{near-zone}} \left[\omega \left(t - \frac{r}{c} \right) \right] = \vec{r} \times \vec{j}_{D_{near-zone}} \left[\omega \left(t - \frac{r}{c} \right) \right] \\ &= r \cdot \vec{1}_r \times j_{D_{near-zone}} \left[\omega \left(t - \frac{r}{c} \right) \right] \cdot \vec{1}_\theta = r \cdot \vec{1}_r \times \frac{i_m \cdot \sin \theta \cdot d\theta}{4\pi \cdot r^2} \cdot \sin \left[\omega \left(t - \frac{r}{c} \right) \right] \cdot \vec{1}_\theta \\ &= r \cdot \vec{1}_r \times \frac{i_m \cdot \sin \theta \cdot d\theta}{4\pi \cdot r^2} \cdot \sin \left(\omega \cdot t - \frac{2\pi \cdot r}{\lambda} \right) \cdot \vec{1}_\theta = \frac{i_m \cdot \ell \cdot \sin \theta}{4\pi \cdot r} \cdot \sin \left(\omega \cdot t - \frac{2\pi \cdot r}{\lambda} \right) \cdot \vec{1}_\Phi \end{aligned} \quad (25)$$

$$\begin{aligned} \vec{H}_{far-zone} \left[\omega \left(t - \frac{r}{c} \right) \right] &= \vec{R}_{eff} \times \vec{j}_{D_{far-zone}} \left[\omega \left(t - \frac{r}{c} \right) \right] = \vec{r} \times \vec{j}_{D_{far-zone}} \left[\omega \left(t - \frac{r}{c} \right) \right] \\ &= r \cdot \vec{1}_r \times j_{D_{far-zone}} \left[\omega \left(t - \frac{r}{c} \right) \right] \cdot \vec{1}_\theta = r \cdot \vec{1}_r \times \frac{i_m \cdot \ell \cdot \sin \theta}{2\lambda \cdot r^2} \cdot \cos \left[\omega \left(t - \frac{r}{c} \right) \right] \cdot \vec{1}_\theta \\ &= r \cdot \vec{1}_r \times \frac{i_m \cdot \ell \cdot \sin \theta}{2\lambda \cdot r^2} \cdot \cos \left[\omega \cdot t - \frac{2\pi \cdot r}{\lambda} \right] \cdot \vec{1}_\theta = \frac{i_m \cdot \ell \cdot \sin \theta}{2\lambda \cdot r} \cdot \cos \left[\omega \cdot t - \frac{2\pi \cdot r}{\lambda} \right] \cdot \vec{1}_\Phi \end{aligned} \quad (26)$$

The electromagnetic field in the near zone is quasi-static and it is not of great interest for the following researches. So, the following relations exist towards the current density of the tangential displacement current \vec{j}_{D_t} and the effective radius-vector \vec{R}_{eff} in the far zone:

$$\begin{aligned} \vec{j}_{D_{\text{far-zone}}} \left[\omega \left(t - \frac{r}{c} \right) \right] &= j_{D_{\text{far-zone}}} \left[\omega \left(t - \frac{r}{c} \right) \right] \cdot \vec{1}_\theta \\ &= \frac{i_m \cdot \ell \cdot \sin \theta}{2\lambda \cdot r^2} \cdot \cos \left[\omega \left(t - \frac{r}{c} \right) \right] \cdot \vec{1}_\theta = \frac{i_m \cdot \ell \cdot \sin \theta}{2\lambda \cdot r^2} \cdot \cos \left[\omega \cdot t - \frac{2\pi \cdot r}{\lambda} \right] \cdot \vec{1}_\theta \end{aligned} \quad (27)$$

$$\vec{R}_{\text{eff}} = \vec{r} = r \cdot \vec{1}_r \quad (28)$$

The \vec{H} -wave equation of a spherical electromagnetic wave in free space has the following form:

$$\begin{aligned} \frac{\partial^2 \vec{H}(x, y, z, t)}{\partial x^2} + \frac{\partial^2 \vec{H}(x, y, z, t)}{\partial y^2} + \frac{\partial^2 \vec{H}(x, y, z, t)}{\partial z^2} \\ = \varepsilon_0 \cdot \mu_0 \cdot \frac{\partial^2 \vec{H}(x, y, z, t)}{\partial t^2} = \frac{1}{c^2} \cdot \frac{\partial^2 \vec{H}(x, y, z, t)}{\partial t^2} \end{aligned} \quad (29)$$

In the far zone along the y-axis of the Cartesian coordinate system, the \vec{H} -wave equation can be accepted as a wave equation of a plane electromagnetic wave:

$$\frac{\partial^2 \vec{H}_x(y, t)}{\partial y^2} = \frac{1}{c^2} \cdot \frac{\partial^2 \vec{H}_x(y, t)}{\partial t^2} \quad (30)$$

where

$$\begin{aligned} \vec{H}_{\text{far-zone}} \left[\omega \left(t - \frac{r}{c} \right) \right] &= H_{\text{far-zone}} \left[\omega \left(t - \frac{r}{c} \right) \right] \cdot \vec{1}_\Phi = H_{\text{far-zone}} \left[\omega \left(t - \frac{y}{c} \right) \right] \cdot (-\vec{i}) \\ &= \vec{H}_{x_{\text{far-zone}}} \left[\omega \left(t - \frac{y}{c} \right) \right] = \vec{H}_{x_{\text{far-zone}}} (\omega \cdot t - \beta \cdot y) = \vec{R}_{\text{eff}} \times \vec{j}_{D_{\text{far-zone}}} (\omega \cdot t - \beta \cdot y) \\ &= (y \cdot \vec{j}) \times \left[\vec{j}_{D_{\text{far-zone}}} (\omega \cdot t - \beta \cdot y) \right] = (y \cdot \vec{j}) \times \left[j_{D_{\text{far-zone}}} (\omega \cdot t - \beta \cdot y) \right] \cdot (-\vec{k}) \\ &= (y \cdot \vec{j}) \times \frac{i_m \cdot \ell \cdot \sin \theta}{2\lambda \cdot y^2} \cdot \cos \left[\omega \cdot t - \frac{2\pi \cdot y}{\lambda} \right] \cdot (-\vec{k}) = \frac{i_m \cdot \ell \cdot \sin \theta}{2\lambda \cdot y} \cdot \cos \left[\omega \cdot t - \frac{2\pi \cdot y}{\lambda} \right] \cdot (-\vec{i}) \end{aligned} \quad (31)$$

The vectors $\vec{j}_{D_{\text{far-zone}}}$ and \vec{R}_{eff} in the vector product of the last equation are orientated at angle 90° and that's why it disappears finally. Then, Eq. (30) can be presented in the following form:

$$\begin{aligned} \frac{\partial^2 \vec{H}_x(y, t)}{\partial y^2} &= \frac{\partial^2 \left[\vec{R}_{\text{eff}} \times \vec{j}_{D_{\text{far-zone}}} (\omega \cdot t - \beta \cdot y) \right]}{\partial y^2} \\ &= \frac{1}{c^2} \cdot \frac{\partial^2 \vec{H}_x(y, t)}{\partial t^2} = \frac{1}{c^2} \cdot \frac{\partial^2 \left[\vec{R}_{\text{eff}} \times \vec{j}_{D_{\text{far-zone}}} (\omega \cdot t - \beta \cdot y) \right]}{\partial t^2} \end{aligned} \quad (32)$$

Here:

$$\begin{aligned} \frac{\partial^2 \vec{H}_x(y, t)}{\partial y^2} &= \frac{\partial^2 \left[\vec{R}_{eff} \times \vec{j}_{D_{\text{far-zone}}}(\omega.t - \beta.y) \right]}{\partial y^2} = 2 \left[1.\vec{j} \times \frac{\partial \left[\vec{j}_{D_{\text{far-zone}}}(\omega.t - \beta.y) \right]}{\partial y} \right] \\ &+ \vec{R}_{eff} \times \frac{\partial^2 \left[\vec{j}_{D_{\text{far-zone}}}(\omega.t - \beta.y) \right]}{\partial y^2} \approx \vec{R}_{eff} \times \frac{\partial^2 \left[\vec{j}_{D_{\text{far-zone}}}(\omega.t - \beta.y) \right]}{\partial y^2} \end{aligned} \tag{33}$$

having in mind that

$$\vec{R}_{eff} = \vec{r} = r.\vec{1}_r = y.\vec{j} \rangle 1.\vec{j} \tag{34}$$

Except that:

$$\begin{aligned} \frac{1}{c^2} \cdot \frac{\partial^2 \vec{H}_x(y, t)}{\partial t^2} &= \frac{1}{c^2} \cdot \frac{\partial^2 \left[\vec{R}_{eff} \times \vec{j}_{D_{\text{far-zone}}}(\omega.t - \beta.y) \right]}{\partial t^2} \\ &= \frac{1}{c^2} \cdot \left\{ \vec{R}_{eff} \times \frac{\partial^2 \left[\vec{j}_{D_{\text{far-zone}}}(\omega.t - \beta.y) \right]}{\partial t^2} \right\} = \vec{R}_{eff} \times \left\{ \frac{1}{c^2} \cdot \frac{\partial^2 \left[\vec{j}_{D_{\text{far-zone}}}(\omega.t - \beta.y) \right]}{\partial t^2} \right\} \end{aligned} \tag{35}$$

That's why, taking into account the results from Eqs. (33) and (35), the equation of the plain electromagnetic wave (32) can be presented in the following form:

$$\vec{R}_{eff} \times \frac{\partial^2 \left[\vec{j}_{D_{\text{far-zone}}}(\omega.t - \beta.y) \right]}{\partial y^2} = \vec{R}_{eff} \times \left\{ \frac{1}{c^2} \cdot \frac{\partial^2 \left[\vec{j}_{D_{\text{far-zone}}}(\omega.t - \beta.y) \right]}{\partial t^2} \right\} \tag{36}$$

i.e. from it we can extract a new wave equation of the plain electromagnetic wave towards the current density of the tangential displacement current \vec{j}_{D_t} . And this is the \vec{j}_{D_t} -wave equation:

$$\frac{\partial^2 \left[\vec{j}_{D_{\text{far-zone}}}(\omega.t - \beta.y) \right]}{\partial y^2} = \frac{1}{c^2} \cdot \frac{\partial^2 \left[\vec{j}_{D_{\text{far-zone}}}(\omega.t - \beta.y) \right]}{\partial t^2} \tag{37}$$

Equation (37) shows that in the propagation process of the plain electromagnetic wave the component of the displacement current \vec{j}_{D_t} takes a substantial part. And it is a component of the electric whirl, which is propagating in the free space from the antenna to the infinity.

If we take the result of \vec{j}_{D_t} for the far zone from Eq. (31) and if we find its partial derivatives of second order, we shall see, that if we put them into Eq. (37) it will be turned into identity:

$$\begin{aligned} \frac{\partial^2 \left[\vec{J}_{D_{far-zone}}(\omega.t - \beta.y) \right]}{\partial y^2} &= \frac{\partial^2 \left\{ \frac{i_m \cdot \ell \cdot \sin\theta}{2\lambda \cdot y^2} \cdot \cos \left[\omega.t - \frac{2\pi \cdot y}{\lambda} \right] \cdot (-\vec{k}) \right\}}{\partial y^2} \\ &= O_1 \left(\frac{1}{y^4} \right) + O_2 \left(\frac{1}{y^3} \right) - \left(\frac{2\pi}{\lambda} \right)^2 \cdot \frac{i_m \cdot \ell \cdot \sin\theta}{2\lambda \cdot y^2} \cdot \cos \left[\omega.t - \frac{2\pi \cdot y}{\lambda} \right] \cdot (-\vec{k}) \end{aligned} \quad (38)$$

$$\approx - \left(\frac{2\pi}{\lambda} \right)^2 \cdot \frac{i_m \cdot \ell \cdot \sin\theta}{2\lambda \cdot y^2} \cdot \cos \left[\omega.t - \frac{2\pi \cdot y}{\lambda} \right] \cdot (-\vec{k}) = - \left(\frac{\omega}{c} \right)^2 \cdot \frac{i_m \cdot \ell \cdot \sin\theta}{2\lambda \cdot y^2} \cdot \cos \left[\omega.t - \frac{2\pi \cdot y}{\lambda} \right] \cdot (-\vec{k})$$

$$\begin{aligned} \frac{1}{c^2} \cdot \frac{\partial^2 \left[\vec{J}_{D_{far-zone}}(\omega.t - \beta.y) \right]}{\partial t^2} &= \frac{1}{c^2} \cdot \frac{\partial^2 \left\{ \frac{i_m \cdot \ell \cdot \sin\theta}{2\lambda \cdot y^2} \cdot \cos \left[\omega.t - \frac{2\pi \cdot y}{\lambda} \right] \cdot (-\vec{k}) \right\}}{\partial t^2} \\ &= - \left(\frac{\omega}{c} \right)^2 \cdot \frac{i_m \cdot \ell \cdot \sin\theta}{2\lambda \cdot y^2} \cdot \cos \left[\omega.t - \frac{2\pi \cdot y}{\lambda} \right] \cdot (-\vec{k}) \end{aligned} \quad (39)$$

For free space in the far zone of the dipole, the phasor of the vector of the electric field intensity \vec{E} is:

$$\vec{E}(r,t)_{far-zone} = -j \cdot \frac{1}{\omega \cdot \epsilon_0} \cdot \text{rot} \left(\vec{H}(r,t)_{far-zone} \right) = \left[\frac{i_m \cdot \ell}{\omega \cdot \epsilon_0 \cdot \lambda \cdot r} \left(\frac{\cos\theta}{r} \cdot \vec{1}_r + j \frac{\pi \cdot \sin\theta}{\lambda} \cdot \vec{1}_\theta \right) \cdot e^{-j \frac{2\pi \cdot r}{\lambda}} \right] \quad (40)$$

For large values of the angle θ , i.e. close to the equatorial plane, the expression of vector \vec{E} becomes equal to the next one:

$$\vec{E}(r,t)_{far-zone} = \left(j \cdot \sqrt{\frac{\mu_0}{\epsilon_0}} \cdot \frac{i_m \cdot \ell \cdot \sin\theta}{2\lambda \cdot r} \cdot e^{-j \frac{2\pi \cdot r}{\lambda}} \right) \cdot \vec{1}_\theta \quad (41)$$

In the time domain vector \vec{E} has the following form:

$$\begin{aligned} \vec{E}_{far-zone} \left[\omega \left(t - \frac{r}{c} \right) \right] &= \sqrt{\frac{\mu_0}{\epsilon_0}} \cdot \frac{i_m \cdot \ell \cdot \sin\theta}{2\lambda \cdot r} \cdot \cos \left[\omega \left(t - \frac{r}{c} \right) \right] \cdot \vec{1}_\theta \\ &= Z_c \cdot \frac{i_m \cdot \ell \cdot \sin\theta}{2\lambda \cdot r} \cdot \cos \left[\omega \left(t - \frac{r}{c} \right) \right] \cdot \vec{1}_\theta = Z_c \cdot \frac{i_m \cdot \ell \cdot \sin\theta}{2\lambda \cdot r} \cdot \cos \left(\omega.t - \frac{2\pi \cdot r}{\lambda} \right) \cdot \vec{1}_\theta \end{aligned} \quad (42)$$

where Z_c is the intrinsic impedance of the free space. Having in mind the result from Eq. (26), the magnitude of vector \vec{H} is:

$$H_{far-zone} \left[\omega \left(t - \frac{r}{c} \right) \right] = \left| \vec{R}_{eff} \times \vec{J}_{D_{far-zone}} \left[\omega \left(t - \frac{r}{c} \right) \right] \right| = \frac{i_m \cdot \ell \cdot \sin\theta}{2\lambda \cdot r} \cdot \cos \left[\omega.t - \frac{2\pi \cdot r}{\lambda} \right] \quad (43)$$

and if we substitute it into Eq. (42), that will result in the following relation

$$\begin{aligned}
 E_{far-zone} \left[\omega \left(t - \frac{r}{c} \right) \right] &= Z_c \cdot H_{far-zone} \left[\omega \left(t - \frac{r}{c} \right) \right] = Z_c \cdot \left| \vec{R}_{eff} \times \vec{j}_{D_{far-zone}} \left[\omega \left(t - \frac{r}{c} \right) \right] \right| \\
 &= Z_c \cdot R_{eff} \cdot j_{D_{far-zone}} \left[\omega \left(t - \frac{r}{c} \right) \right] = \frac{1}{\sigma} \cdot j_{D_{far-zone}} \left[\omega \left(t - \frac{r}{c} \right) \right]
 \end{aligned}
 \tag{44}$$

And this is Ohm’s law in differential (point) form, where:

$$\sigma = \frac{1}{R_{eff} \cdot Z_c} = \frac{1}{r \cdot Z_c} = \frac{1}{r} \cdot \sqrt{\frac{\epsilon_0}{\mu_0}}
 \tag{45}$$

Here, σ is the conductivity of the free space. Ohm’s law in differential vector form may be introduced on the base of Eqs. (27) and (42) as follows:

$$\begin{aligned}
 \vec{j}_{D_{far-zone}} \left[\omega \left(t - \frac{r}{c} \right) \right] &= \frac{i_m \cdot \ell \cdot \sin \theta}{2 \lambda \cdot r^2} \cdot \cos \left[\omega \cdot t - \frac{2 \pi \cdot r}{\lambda} \right] \cdot \vec{1}_\theta \\
 &= \sigma \cdot \vec{E}_{far-zone} \left[\omega \left(t - \frac{r}{c} \right) \right] = \frac{1}{r \cdot Z_c} \cdot \sqrt{\frac{\mu_0}{\epsilon_0}} \cdot \frac{i_m \cdot \ell \cdot \sin \theta}{2 \lambda \cdot r} \cdot \cos \left(\omega \cdot t - \frac{2 \pi \cdot r}{\lambda} \right) \cdot \vec{1}_\theta
 \end{aligned}
 \tag{46}$$

i.e. Ohm’s law in differential form is valid for the far zone of the dipole, giving the connection between the vectors \vec{j}_{D_i} and \vec{E} :

$$\vec{j}_{D_{far-zone}} \left[\omega \left(t - \frac{r}{c} \right) \right] = \sigma \cdot \vec{E}_{far-zone} \left[\omega \left(t - \frac{r}{c} \right) \right]
 \tag{47}$$

And this is the second proof, that the propagation of the electromagnetic wave is a flowing of $\sigma \cdot \vec{E}$ the tangential rotary displacement currents in the free space.

4 Experiments

There are too many experimental proofs of the validity of the wave equations of the electromagnetic field and the existence of the retarded potentials [10–12]. The RT presents a new form of presentation of the same dependencies, its results do not contradict to these experimental proofs and it can be a base for future experimental work.

5 Conclusions

The main objective of the present paper is to introduce a complement (correction) of the notion about the processes accompanying the propagation of the electromagnetic wave in free space. It became possible after the introduction of the method of moments towards the basic quantities of the electromagnetic field – the vector of the magnetic field intensity \vec{H} and the vector of the magnetic flux density \vec{B} . They were presented as

moments of the vector of the current density of the tangential displacement current \vec{j}_{D_t} and the effective radius-vector \vec{R}_{eff} . In this way these “magnetic quantities” were presented in a fully electric form showing that all types of electromagnetic processes have electrical origin. The introduction of a new \vec{j}_{D_t} -wave equation of the plain electromagnetic wave and the Ohm’s law in differential form for the vectors \vec{j}_{D_t} and \vec{E} is a direct proof that its propagation is directly connected with a flowing of tangential rotary displacement currents in the free space. This process is connected with very complex whirling-translational flowing of displacement currents. The propagation of the electromagnetic wave in space is accompanied by the spread (movement) of electric whirls ahead in space – a phenomenon that is linked to the manifestation of complex electric processes.

Another main task of that paper is to support the process of creation of a new model of the electromagnetic field, which can be useful for the clear presentation of the complex mechanisms of the electromagnetic phenomena. In this way it can be useful for “visualization” of the invisible electromagnetic processes, for prediction and explanation of new electromagnetic processes, phenomena and effects.

References

1. Maxwell, J.C.: On physical lines of force. *Phil. Mag. J. Sci. London* (1861). Part I, 161–175, Part II, 281–291, 338–347 (March), Part III, 12–24 (April, May), Part IV, 85–95
2. Maxwell, J.C.: A dynamical theory of the electromagnetic field. *Phil. Trans. R. Soc. Lond.* **155**, 459–512 (1865)
3. Maxwell, J.C.: A Treatise on Electricity and Magnetism, vol. I–II. Macmillan and Co., London (1873)
4. Panov, E.I.: Rotary theory of the magnetic field. Reports of the Union of Scientists – Varna, 2’98, 1’99, 77–84 Varna, Bulgaria (1998, 1999). (in Bulgarian). ISSN 1310-5833
5. Panov, E.I.: Rotary Theory of the Magnetic Field. Publishing House of the Technical University of Varna, Varna, Bulgaria (2014). Monograph, 148 pages. (in Bulgarian). ISBN 978-954-20-0609-1
6. Panov, E.I.: Rotary Theory of the Magnetic Field, Basics, Concepts, Methods and Models. LAP Lambert Academic Publishing, Germany, 29 September 2015. Monograph, 148 pages. ISBN 978-3-659-78098-1
7. Panov, E.P.: Rotary theory of the electromagnetic field. In: Annual of the Technical University, Varna, pp. 46–53. Publishing House of the Technical University of Varna, Varna (2015). (in Bulgarian). ISSN 1311-896X
8. Panov, E.P.: Rotary theory of the electromagnetic field. In: Proceedings of Digests, XIX-th International Symposium on Electrical Apparatus and Technologies, SIELA 2016, pp. 149–150. Publishing House Avangard Prima, Bourgas (2016). ISBN 978-619-160-648-1
9. Panov, E.P.: Rotary theory of the electromagnetic field. In: Proceedings of the XIX-th International Symposium on Electrical Apparatus and Technologies, SIELA 2016, Bourgas, Bulgaria, pp. 244–247 (2016). IEEE Catalog Number: CFP1628Z-PRT. ISBN 978-1-4673-9521-2

10. Kraus, J.D., Carver, K.R.: Electromagnetics, 2nd edn. McGraw-Hill International Book Company, New York (1981)
11. Cheng, D.K.: Field and Wave Electromagnetics, 2nd edn. Addison-Wesley Publishing Company, Inc., Reading (1989)
12. Govorkov, V.A.: Electrical and Magnetic Fields. Energia, Moscow (1968). (in Russian)

Verification of SVD Based Algorithm for Voltage Stability Assessment Against Other Methods

Nikolay Nikolaev^(✉)

Department “Electric Power Engineering”,
Technical University of Varna, Varna, Bulgaria
n.nikolaev@tu-varna.bg

Abstract. A novel algorithm for fast computation of the nearest operating point, where the power flow equations collapse was developed, based on singular value decomposition (SVD). It is claimed to be fast and capable to predict the loading direction to approach the maximum loading point of electric power systems, which requires introduction of minimum power. This algorithm still needs to be verified against other established algorithms from the literature. This paper compares the SVD based algorithm against two other ones: (i) direct approach based on the second order Newton method and (ii) reference algorithm based on Monte-Carlo method. Several test systems are used as benchmark. The results confirm the robustness of the SVD based algorithm and its possibility for practical application.

Keywords: Singular value decomposition · Voltage stability · Saddle-node bifurcation · Newton-Raphson method · Monte-Carlo method

1 Introduction

A novel algorithm for fast computation of the nearest operating point, where the power flow equations collapse was developed, based on singular value decomposition (SVD) [1]. It is claimed to be fast and capable to predict the loading direction to approach the maximum loading point of electric power systems, which requires introduction of minimum power. This algorithm still needs to be verified against other established algorithms from the literature. This paper compares the SVD based algorithm against two other ones: (i) direct approach based on the second order Newton method [3–5] and (ii) reference algorithm based on Monte-Carlo method [2]. Two test systems are used as benchmark.

1.1 SVD Based Algorithm

This algorithm, originally developed in [1], is based on SVD, applied to evaluate the sensitivity of voltage magnitudes and angles (system outputs) to real and reactive power nodal injections (system inputs). Let's consider the linearized power flow equations:

$$\begin{bmatrix} \Delta\theta \\ \Delta V \end{bmatrix} = \mathbf{J}^{-1} \begin{bmatrix} \Delta P \\ \Delta Q \end{bmatrix} \quad (1)$$

where \mathbf{J} is the Jacobian matrix.

The singular value decomposition is applied to the inversed Jacobian matrix to find suitable loading direction to the nearest voltage instability point. The algorithm has been tested for a simple two-bus system. In the text below, this algorithm will be referred to as singular value decomposition based algorithm (SVDA).

1.2 Algorithm Based on Second Order Newton Method

This algorithm utilizes the second order Newton method (SONM) for optimization to solve the following objective:

$$f(\theta, V) = \mathbf{g}^T(\theta, V) \cdot \mathbf{g}(\theta, V) \quad (2)$$

where $\mathbf{g}(\theta, V)$ is the set of power flow equations, as function of the voltage angles and magnitudes. This algorithm is designed to be able to directly find the nearest saddle-node bifurcation point.

The SONM relies on an iterative process. Important feature of its implementation is the control on the maximum deviation of the variable on every iteration:

$$\forall \Delta\theta \text{ and } \forall \Delta V \leq \Delta_{\max} \quad (3)$$

If on a particular iteration inequality (4) is not satisfied, all variable deviations are scaled down by a factor calculated as the ratio between the greatest variable deviation and Δ_{\max} . This is basically a control on the maximum step size of the iterations. Later it will be shown that the step size has significant influence on the convergence properties of the SONM.

1.3 Reference Monte Carlo Algorithm

An algorithm for voltage stability boundary assessment based on Monte Carlo method is developed in [2]. It is capable to generate many random paths/directions, which are used to load the network until a bifurcation point is reached. This algorithm is used here as a reference for the other algorithms to compare results in terms of minimal distance to collapse. In this paper this algorithm will be referred to as Monte Carlo Method (MCM).

1.4 Contributions and Structure of the Paper

The contributions of the paper are:

- Providing strong evidence that the SVDA is capable to find loading direction to the nearest saddle-node bifurcation.
- Issues with the application of the SONM are found and solutions are proposed.

The paper is organized as follows. The following two chapters present test cases with a two-bus and a three-bus test systems.

2 Test Case – Two Bus System

The two-bus test system is adopted from [2] and its data is according the reference. The system is shown in Fig. 1a. The base case operating point is $P_L + jQ_L = 0.3 + j0.2$ pu.

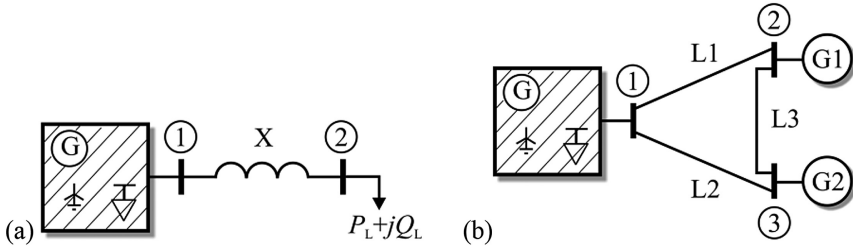


Fig. 1. (a) Two-bus test system; (b) three-bus test system

This section compares the SONM, MCM and SVDA for different initial operating points of the power system. This is released as the power injection in bus 2 is varied to have different combinations of positive and negative signs. This is clarified in Table 1. The active and reactive power magnitude is the same as the base case, only the signs are subject to variation. The identified weaknesses of the SONM are resolved. The final chapter draws the conclusions.

Table 1. Combinations of power injections for the two-bus test system

$+P_L$	$+P_L$
$+Q_L$	$-Q_L$
$-P_L$	$-P_L$
$+Q_L$	$-Q_L$

The calculations are made with the following assumptions:

- 5000 random loading directions are generated with the MCM for every combination in Table 1.
- The random loading directions allow for both increasing and decreasing the real power. The reactive power consumption in the node is restricted to only increase, since its reduction increases the voltage magnitudes and thus leads to points in space where the saddle-node bifurcation is too far away from the initial operating point. Such distant bifurcations are not of interest to the present study.
- The power step used in the SVDA is 0.001 pu.
- The solution tolerance of the MCM is 2×10^{-5} pu.

The aim of this test is to verify that with the change of the initial operating point the SVDA performs robustly and points to the nearest saddle-node bifurcation. Numerical results from the computations are presented in Table 2.

Table 2. Comparison of the calculated Euclidean distances with the different algorithms

Case	$+P_L$	$+P_L$	$-P_L$	$-P_L$
	$+Q_L$	$-Q_L$	$+Q_L$	$-Q_L$
Distance by SONM, pu	0.5443	0.9224	0.5443	0.9224
Distance by MCM, pu	0.5471	0.9230	0.5670	0.9442
Distance by SVDA, pu	0.5566	0.9714	0.5566	0.9714
Error of MCM, %	0.5237	0.0661	4.1766	2.3738
Error of SVDA, %	2.2699	5.3170	2.2699	5.3170

The data shows that in all cases the SONM finds the instability point, which is nearest to the initial operating point. For the latter reason, the SONM is used as reference for the calculation of the relative distance error of SVDA and MCM. The table shows that the two of them provide distances, which are no longer than few percent compared to SONM. This can be considered as a very good accuracy.

Although the MCM tests 5000 different directions, none of them leads to saddle-node bifurcation, which is closer than the point obtained with the SONM. This proves that the SONM is capable to find the nearest instability point in terms of Euclidean distance from the initial operating point of the system.

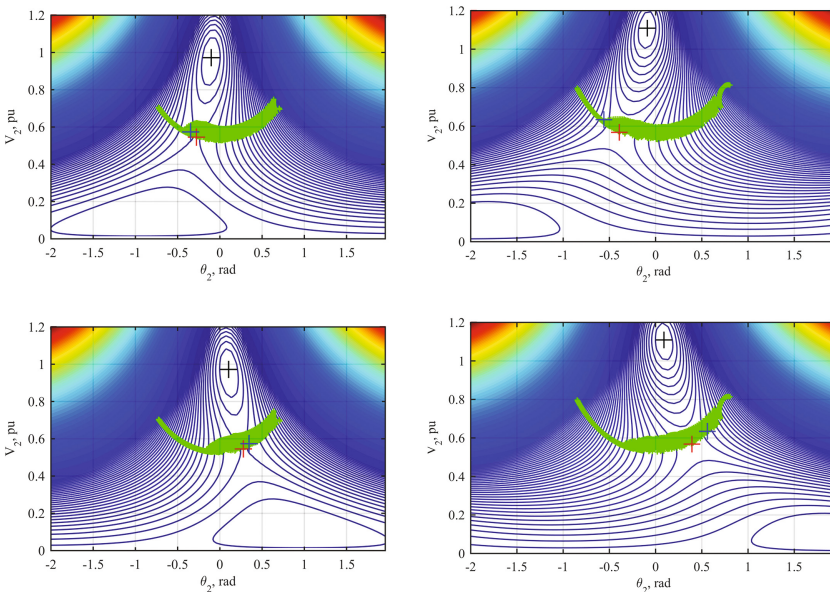


Fig. 2. Solutions from the SONM, MCM and SVDA depicted on the objective function for the cases from Table 1

The results are also presented onto the contour plot of the SONM objective function (see Fig. 2). The following convention is assumed for the graphical representation of the results:

- Black “+” denotes the initial operating point.
- Red “+” denotes the SONM solution.
- Blue “+” denotes the SVDA solution.
- Green “+” denotes the MCM solution.

The plots in Fig. 2 confirm that the SVDA is able to predict correctly the loading direction to the nearest instability point, which is almost identical to the results from the SONM.

On the next Fig. 3 the same test case results are depicted on the P-Q axis of bus 2 of the test system. The MCM forms and depicts the voltage instability boundary line. Its inner region corresponds to the physically possible and stable operating points. Figure 3 clearly indicates that both the SONM and the SVDA successfully find the nearest bifurcation.

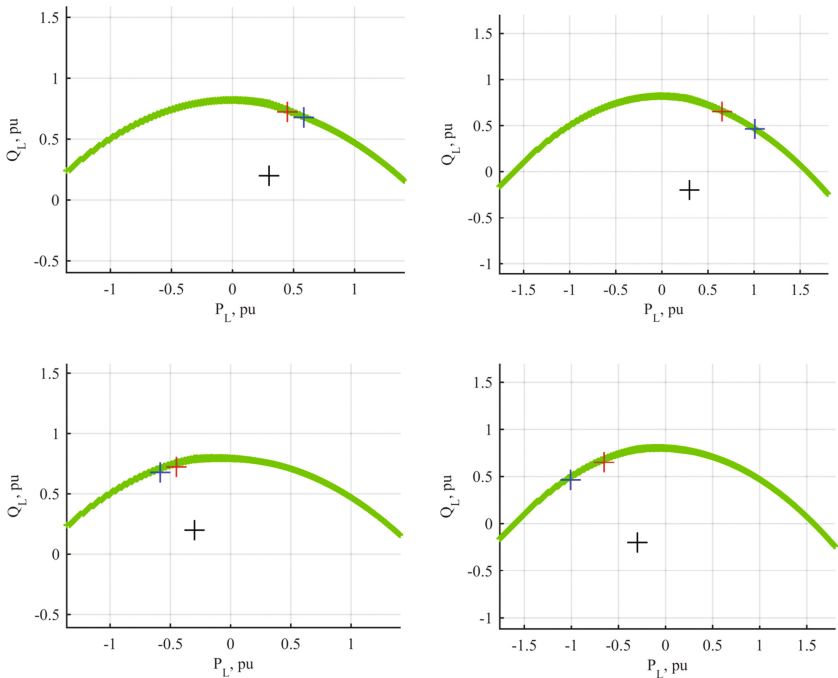


Fig. 3. Solution with the SONM, MCM and SVDA in terms of injected power depicted on the objective function for the cases from Table 1

3 Test Case – Three Bus System

Figure 1b presents the three-bus test system. It is adopted from [2] and its data is as in the original paper. It consists of three lines, two P-V generators and a slack bus. The variable parameters are real power injections of the two generators and the power flow solution variables are the voltage angles θ_2 и θ_3 .

This section once again presents a comparison between the SONM, MCM and the SVDA. The computations are performed with the following assumptions:

- The MCM simulates 1000 random loading directions for the two generators. No power sign limitations were imposed, meaning that the generation power may increase or reduce.
- The solution tolerance of the MCM is 3×10^{-4} pu.
- The solution tolerance of the SONM is 1×10^{-5} .
- The maximum deviation of the variables in the SONM is 0.05 pu per iteration.
- The initial perturbation of the solution variables θ_2 and θ_3 in the SONM is +0.01 pu from the initial power flow solution. The perturbation predetermines the convergence direction onto the surface of the objective function.
- The power step of the SVDA is 1×10^{-4} .

The green dashed circle on the figures below denotes the radius measured between the initial power flow solution and the nearest instability point, which was indicated by the MCM.

Numerical results from the computations are presented in Table 3, for four different initial power flow cases. It should be noted that this time for a reference algorithm to be used for distance error calculation is used the MCM, as the SONM appeared not to be robust. This is explained later in the text.

The results are also depicted in Fig. 4. The closed voltage stability boundary is obtained with the MCM and is denoted with green “+”. The green dashed circle shows the distance to the nearest instability point indicated by the same algorithm.

Table 3. Comparison of the three algorithms for the three-bust test system

Case (position in figs.)	Initial point $P_{G1}; P_{G2}$ p.u.	Distance by MCM, p.u.	Distance by SONM, p.u.	Distance by SVDA, p.u.	Error of SONM, %	Error of SVDA, %
1 (up, left)	0.7; 0.7	3.5762	3.5762	3.7424	0.0010	4.6475
2 (up, right)	0.7; 2.0	2.2808	4.2092	2.3921	84.5525	4.8834
3 (down, left)	2.0; 0.7	3.4197	3.4198	3.5002	0.0019	2.3549
4 (down, right)	2.0; 2.0	2.1349	2.9497	2.2023	38.1630	3.1577

From both the table and the figure, it is obvious that the SVDA provides robust results for all four cases and the distance error is acceptable – within few percent of the referent MCM.

The SONM provides non-relevant results for cases 2 and 4, which appear to be far from the nearest instability point. This fact can be explained with Fig. 5. The latter

tracks the iteration process of SONM onto its objective function. One can see that for the particular cases 2 and 4 the solution trajectory passes over the nearest saddle-node bifurcation and converges to a further one. A detailed look on Fig. 5 reveals that the surface of the objective is different for every test case. It turns out that the surface shape significantly affects the algorithm convergence. One can see that for equal perturbations applied to the variables θ_2 and θ_3 leads to non-robust results for the different initial power flow cases. The variable perturbation is expressed in the following mathematical terms:

$$\begin{bmatrix} \theta_2 \\ \theta_3 \end{bmatrix} = \begin{bmatrix} \theta_2 \\ \theta_3 \end{bmatrix} + \begin{bmatrix} p_2 \\ p_3 \end{bmatrix} \tag{4}$$

In the beginning of the section it was clarified that for all four initial power flow cases it was assumed that $p_2 = p_3 = 0.01$ pu. One possible solution to overcome the bad convergence of the SONM could be to vary perturbations in terms of their magnitude and sign. This hypothesis will be tested with several subcases of case 4. They are explained in Table 4.

The convergence trajectories are depicted in Fig. 6. From the figure it is concluded that the proper choice of perturbations is crucial for the relevance of the solution provided by the SONM. With other words, the sign and magnitudes of the perturbations may push the solution outside the attraction zone of the nearest bifurcation point.

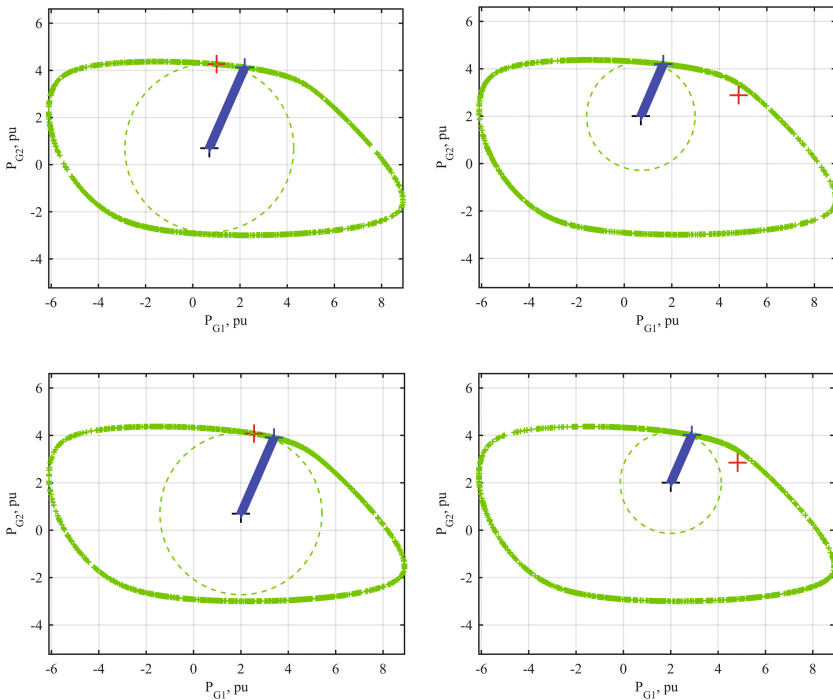


Fig. 4. Comparison of the three algorithms on the P_{G1} - P_{G2} axis for the three-bus test system

Case 4d seems interesting to study in more details. The SONM does not seem to converge to a saddle point as one can see from Fig. 6. Although, the determinant of the Jacobian matrix is zero, i.e. meaning that this is a point of collapse for the power flow equations. Also, the Hessian matrix of the SONM objective appears to have both negative and positive eigenvalues, which is a sufficient condition for an indefinite matrix and therefore for the presence of a saddle point. The solution of case 4d on the P_{G1} - P_{G2} axis is also drawn on Fig. 7. The figure shows that the SONM solution is positioned outside the circle of the nearest instability point, indicated by the MCM. The SONM solution also stands within the green stability boundary and it is far from it.

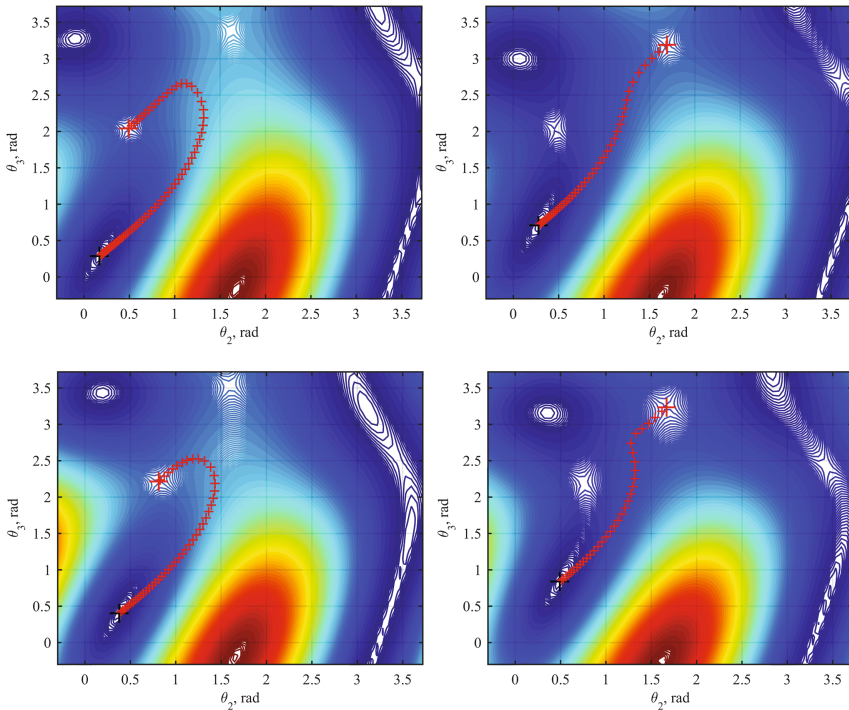


Fig. 5. Iteration process of the SONM for the three-bus test system

Table 4. Cases used to study SONM convergence properties

Case	Position on Fig. 6	p_2 p.u.	p_3 p.u.
4a	Up – left	0.01	0.01
4b	Up – right	-0.01	0.01
4c	Middle – left	0.01	-0.01
4d	Middle – right	-0.01	-0.01
4e	Down – left	0.01	0.02
4e - zoom	Down – right	0.01	0.02

It is worth noting that the stability boundary line is obtained by 30 000 random directions with the MCM and the trajectory of none of them finds the point of the SONM solution. Moreover, feeding the SONM solution to the power flow program does provide a normal solution, even when the system load was increased by 0.1 pu a

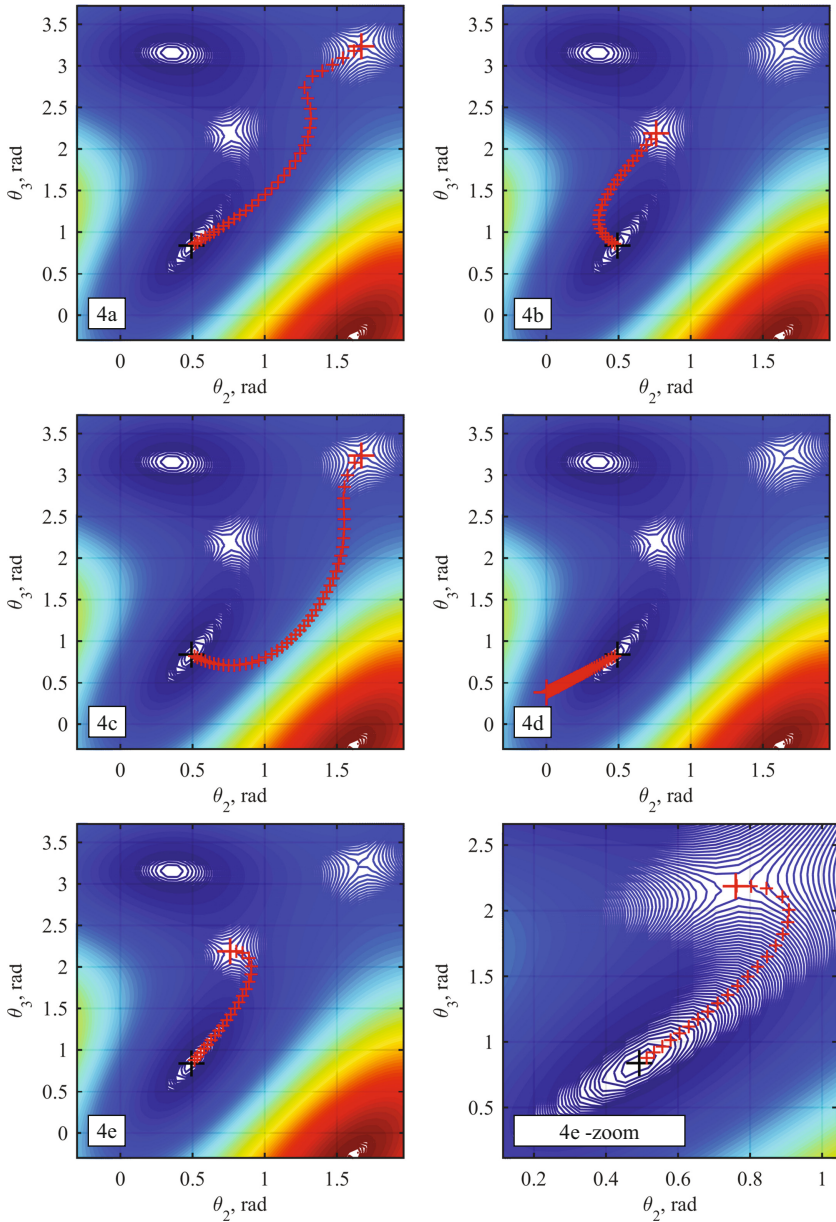


Fig. 6. Graphical results from the study of the SONM convergence properties

divergence was not observed. From this observation it is concluded that the solution of case 4d, provided by the SONM does not make any practical sense.

Detailed study of Fig. 6 reveals that the most optimal in terms of fastest convergence to the saddle point is case 4e. In this case the SONM converges to the nearest visible saddle point. When the contour plot of case 4e is zoomed in it becomes clear that the surface round the initial power flow solution is concave and elliptical. It is concluded that choosing the slope with the smallest incline is the most suitable direction for initiation of the iteration process. Therefore, an add-on to the SONM, which makes a proper choice for initial perturbation and beginning of the iteration process is developed based on algorithm for scanning the nearby surface of the objective.

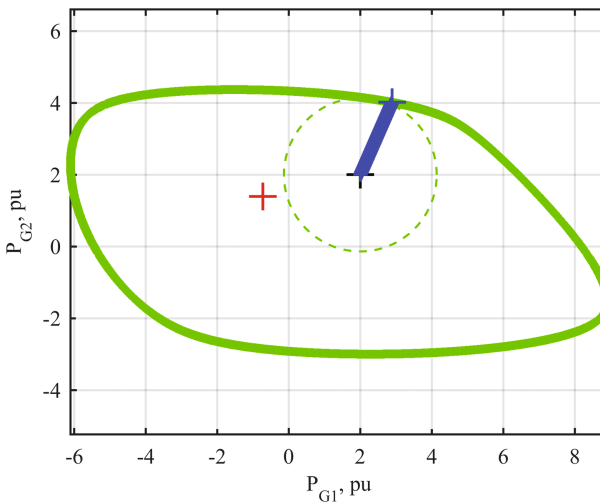


Fig. 7. Solution of case 4d on the P_{G1} - P_{G2} axis

4 Conclusions

The conducted comparative study proves the ability of the SVDA to very quickly, accurately and robustly find the nearest voltage instability point. Although for some of the cases the SONM provides the best results, for many other cases it indicates weaknesses and incapability to produce relevant and meaningful results. To overcome some of these issues and add-on was proposed which significantly improves the algorithm's robustness of the iteration process to the nearest bifurcation point. The MCM appeared to be a very useful tool for comparison and validation of the other two algorithms. With its help it was possible to perform qualitative and quantitative evaluation.

Acknowledgements. This paper is a results from project “Study of the electric power system stability and frequency control at a predominant share of renewable energy generation” grant ДН07/27/15.12.2016 from the Bulgarian National Science Fund.

References

1. Nikolaev, N.: An algorithm for fast determining the point of collapse of power flow equations based on singular value decomposition. In: XV-th International Conference on Electrical Machines, Drives and Power Systems ELMA2017, 1–3 June 2017
2. Nikolaev, N.: A Monte Carlo algorithm for determining the point of collapse of power flow equations. In: XV-th International Conference on Electrical Machines, Drives and Power Systems ELMA2017, 1–3 June 2017
3. Chusovitin, P., Pazderin, A., Shabalin, G., Tashchilin, V., Bannykh, P.: Voltage stability analysis using Newton method. In: PowerTech, 2015 IEEE Eindhoven, 29 June–2 July 2015
4. Shabalin, G., Pazderin, A., Bannykh, P., Balakh, E.: Voltage stability analysis using quadratic objective function taking into account equality constraints. In: IEEE International Conference on the Science of Electrical Engineering (ICSEE), 16–18 November 2016
5. Torelli, F., Vaccaro, A.: A second order dynamic power flow model. *Electr. Power Syst. Res.* **126**, 12–20 (2015)

Application of Principal Component Analysis for Fault Detection of DC Motor Parameters

Nasko Atanasov, Zhivko Zhekov, Ivan Grigorov^(✉),
and Mariela Alexandrova

Department of Automation, Technical University of Varna, Studentska Str. 1,
9010 Varna, Bulgaria

{nratanasov, m_alexandrova}@tu-varna.bg,
{fitter, mad_doc}@abv.bg

Abstract. The aim of technical processes supervision is to reveal the actual system state and also undesired states to be indicated. The deviations from normal process behavior are usually results of faults. They might cause malfunctions or failures that must be prevented. The monitoring of a technical process in normal operation state is a part of the supervision process. This is usually performed by a limit-checking of some measurable output variables. Certain alarms rise if the variables values are found outside of the tolerance zone set.

The main purpose of the principal component analysis (PCA) is to reduce the dimensionality of a data set containing a large number of interrelated variables, retaining at the same time as much as possible of the variations presented in the initial data set. This reduction is achieved by transformation to a new set of the uncorrelated variables called principal components. They are arranged so that the first few of them retain the most of the variations of all of the original variables presented.

This paper presents an application of the principal component analysis for real time fault detection of DC motor parameters.

Keywords: DC motor parameters · Fault detection · Limit-checking · Monitoring · Principal component analysis

1 Introduction

The supervision aims to present the current process status showing undesirable and unpermitted values of state variables, and to take appropriate action to avoid hazards and accidents. Deviations from normal behavior of the process are usually due to faults as a result of numerous possible reasons. If appropriate counteractions are not taken, after a shorter or longer period of time faults lead to failures or malfunctions. The main goal of the supervision is to avoid them [2, 7].

The process supervision is implemented by monitoring and automatic protection. By monitoring it is verified whether values of measurable variables are in a permitted limits (limit-checking) and if not an alarm sounds. The human operator must take appropriate counteractions. In the event of too dangerous conditions an appropriate

counteractions are automatically taken respectively. Typically, the process is directed to a safe condition, which is most often an emergency shutdown [7].

The goal of this paper is to investigate the applicability of the PCA for fault detections which lead to a change of DC motor parameters [3, 9].

2 Fault, Failure and Malfunction

A fault is an impermissible deviation of at least one system feature from the acceptable, normal, standard condition.

The fault is a state of the system and the unpermitted deviation is the difference between the measured value of a given parameter and the exceeded threshold of the permitted measured value area. The fault is a precondition for a failure or a malfunction.

A failure is constant system disability to perform a desired function under certain operating conditions, and the malfunction is a selfremovable irregularity in the implementation of the desired system function.

The failure and the malfunction are events that result from one or more faults, and usually occur after system start or load increase [4, 7].

Figure 1 shows the relation between fault, failure and malfunction. The fault can occur suddenly or gradually. It is assumed that the corresponding fault of the system feature is proportional to the development of the fault. Exceeding the normal feature values indicates a fault at the moment t_1 . Depending on its size follows a failure or a malfunction at time $t_2 \geq t_1$ [7].

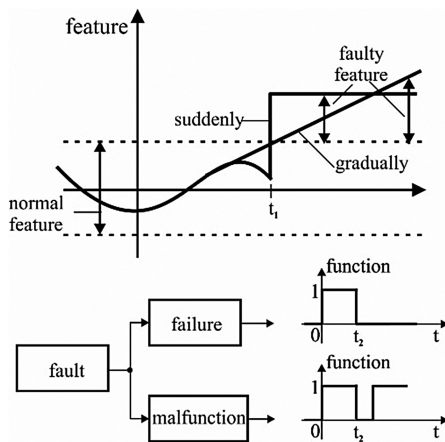


Fig. 1. Relation between fault, failure and malfunction

3 Principal Component Analysis

The main idea of PCA is reducing the dimensionality of the data set which contains a large number of interrelated variables, while preserving as much as possible of the variation presented in this array. This is achieved by transforming the measured data into a new array of uncorrelated principal components. They are arranged so that the first few of them contain most of the variations presented by all initial data [8, 10].

The main task is based on a transformation of the data $(N \times m)$ matrix $\mathbf{X} = [\mathbf{x}_1 \mathbf{x}_2 \dots \mathbf{x}_m]$ that contains N measurements of m variables $\mathbf{x}_i(k)$; $i = 1, \dots, m$; $k = 1, \dots, N$ into a new $(N \times r)$ matrix, where $r < m$. This can be obtained by transformation matrix \mathbf{P}

$$\mathbf{T}_{[N \times r]} = \mathbf{X}_{[N \times m]} \mathbf{P}_{[m \times r]} \Leftrightarrow \mathbf{P} = [p_1, p_2 \dots p_r] \quad (1)$$

This transformation is done by an orthonormal matrix \mathbf{P} , for which

$$\mathbf{P}^T \mathbf{P} = \mathbf{I} \quad (2)$$

and

$$\mathbf{X} = \mathbf{T} \mathbf{P}^T \quad (3)$$

In accordance with multivariable statistical terminology \mathbf{T} is named the score matrix and \mathbf{P} the loading matrix [7]. The matrix \mathbf{X} can be expressed as follows

$$\mathbf{X} = \mathbf{t}_1 \mathbf{p}_1^T + \mathbf{t}_2 \mathbf{p}_2^T + \dots + \mathbf{t}_r \mathbf{p}_r^T = \sum_{j=1}^r \mathbf{t}_j \mathbf{p}_j^T \quad (4)$$

In order to find the elements \mathbf{p}_j of the transformation matrix \mathbf{P} which leads to maximum variance a stepwise optimization must be taken. For each optimization procedure j step in accordance with

$$\mathbf{t}_j = \mathbf{X} \mathbf{p}_j \quad (5)$$

the maximum variance is determined by the relationship

$$\max \mathbf{t}_j^T \mathbf{t}_j = \max (\mathbf{X} \mathbf{p}_j)^T (\mathbf{X} \mathbf{p}_j) = \max \mathbf{p}_j^T \mathbf{X}^T \mathbf{X} \mathbf{p}_j \quad (6)$$

under the restriction of the orthonormal components $\mathbf{p}_j^T \mathbf{p}_j = 1$.

This optimization problem can be solved by the method of Lagrange multipliers. If the maximum of the function $f(\mathbf{p}_j)$ is sought under the condition $g = \mathbf{p}_j^T \mathbf{p}_j - 1 = 0$, the loss function can be obtained by the equation

$$V = f(\mathbf{p}_j) - \lambda_j g(\mathbf{p}_j) \tag{7}$$

where λ_j are Lagrange multipliers. This leads to the following expressions:

$$V = \mathbf{p}_j^T \mathbf{X}^T \mathbf{X} \mathbf{p}_j - \lambda_j (\mathbf{p}_j^T \mathbf{p}_j - 1) \tag{8}$$

$$\frac{dV}{d\mathbf{p}_j} = 2\mathbf{X}^T \mathbf{X} \mathbf{p}_j - 2\lambda_j \mathbf{p}_j = 0 \tag{9}$$

$$[\mathbf{X}^T \mathbf{X} - \lambda_j \mathbf{I}] \mathbf{p}_j = 0 \Leftrightarrow \mathbf{A} = \mathbf{X}^T \mathbf{X} \Leftrightarrow [\mathbf{A} - \lambda_j \mathbf{I}] \mathbf{p}_j = 0 \tag{10}$$

Therefore, this is a classic problem for eigenvalues. The matrix \mathbf{A} is proportional to the correlation matrix. Equations (6) and (10) result in

$$\max \mathbf{t}_j^T \mathbf{t}_j = \max \mathbf{p}_j^T \mathbf{A} \mathbf{p}_j = \max \mathbf{p}_j^T \lambda_j \mathbf{p}_j = \max \lambda_j \tag{11}$$

Thus, the maximum eigenvalues determine maximum variance of the coordinates \mathbf{t}_j .

The algorithm for determining the loading matrix \mathbf{P} and the new score matrix \mathbf{T} is as follows (see Fig. 2) [7]:

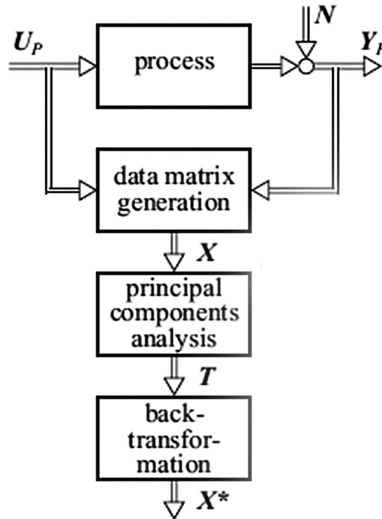


Fig. 2. Generating an array \mathbf{T} from a reduced number of variables and back-transformation

1. Calculation of the correlation matrix $\mathbf{A} = \mathbf{X}^T \mathbf{X}$.
2. Calculation of eigenvalues λ_j and eigenvectors \mathbf{p}_j of matrix \mathbf{A}

$$[\mathbf{A} - \lambda_j \mathbf{I}] \mathbf{p}_j = 0, j = 1, \dots, m$$

3. Selection of the largest (most significant) eigenvalues λ_j and eigenvectors $\mathbf{p}_j, j = 1, \dots, r$
4. Defining the transformation matrix \mathbf{P}

$$\mathbf{P} = [p_1, p_2 \dots p_r]$$

5. Calculation of the new data matrix

$$\mathbf{T} = \mathbf{XP} = [t_1 t_2 \dots t_r] \Leftrightarrow t_j = \mathbf{Xp}_j$$

A new matrix T is obtained with all of the original data but with a reduced number $r < m$ of the variable - the principal components. The matrix of the principal components of the data T gives approximately the same information for the variable variances such as the original matrix X.

4 Fault Detection with PCA

In literature are suggested various block diagrams for fault detection with PCA [7]. Methods for change detection of mean and variance of the transformed t_j and back-transformed x_i^* variables can be applied directly. Another approach is related to the usage of the residuals between the original and back-transformed variables (see Fig. 3).

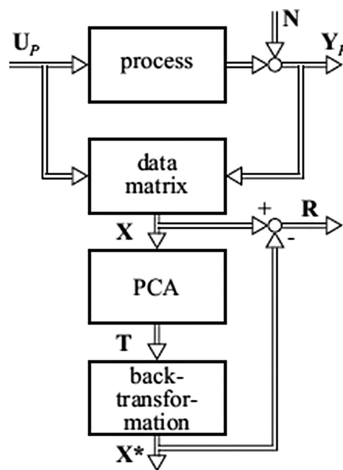


Fig. 3. Fault detection with PCA

Discussed PCA procedure is described for batch data processing. It is applicable to time windowed data. In this paper is examined PCA applicability for real time fault detection.

The variables $\mathbf{X} = [\mathbf{x}_1 \mathbf{x}_2 \dots \mathbf{x}_m]$ can be sampled with sampling time that is determined in accordance with the specific physical nature of the investigated system and the measurement equipment capabilities.

The process starts and during a specified time period (phase of study) all measurement data $\mathbf{x}^T(k) = [x_1(k), x_2(k), \dots, x_m(k)]$ are collected. According to the described algorithm the transformation matrix \mathbf{P} is calculated. It defines the principal components. Further \mathbf{PP}^T is determined for the back-transformation.

For real time fault detection into the process of normal system operation a back-transformation is calculated for each new batch of data $\mathbf{x}^T(k) = [x_1(k), x_2(k), \dots, x_m(k)]$

$$\mathbf{x}^{*T}(k) = \mathbf{x}^T(k)\mathbf{PP}^T \Leftrightarrow \mathbf{x}^{*T}(k) = [x_1^*(k), x_2^*(k), \dots, x_m^*(k)] \quad (12)$$

After that residual vector

$$\mathbf{r}^T(k) = \mathbf{x}^T(k) - \mathbf{x}^{*T}(k) \quad (13)$$

and it's scalar product

$$r'(k) = \mathbf{r}^T(k)\mathbf{r}(k) = \sum_{i=1}^m r_i^2(k) \quad (14)$$

are determined.

If some fault occurs the variables $\mathbf{x}^T(k)$ change accordingly. The PCA transformed $\mathbf{x}^{*T}(k)$ are less sensitive to the fault and significant deviations of residuals $\mathbf{r}(k)$ and $r'(k)$ appear [6].

5 Simulation Research

PCA presents an opportunity for plant fault detection. The technological plants include electric machines and PCA can be applied for fault detection in DC motors.

Mathematical description of a brushed permanent magnet DC motor is represented by following equations:

$$\begin{aligned} Ua &= Ra(La/Ra.p + 1)ia + c\Phi\omega r \\ Me &= c\Phi ia \\ Me - Mc &= Jp\omega r \end{aligned} \quad (15)$$

where: Ua – armature voltage, ia – armature current, Ra – armature winding active resistance, La – armature induction, ωr – angular velocity, Me – electromagnetic torque, Mc – load torque, Φ – magnetic flux, c – armature constant, J – moment of inertia, $p = d/dt$ [5].

At fault presence in the DC motor or the driven mechanism (with one-mass mechanical part) variation is possible in the motor physical parameters and variables R_a , L_a , J and M_c .

The following block diagram made in Matlab/Simulink can be used to simulate changes in these physical parameters (Fig. 4).

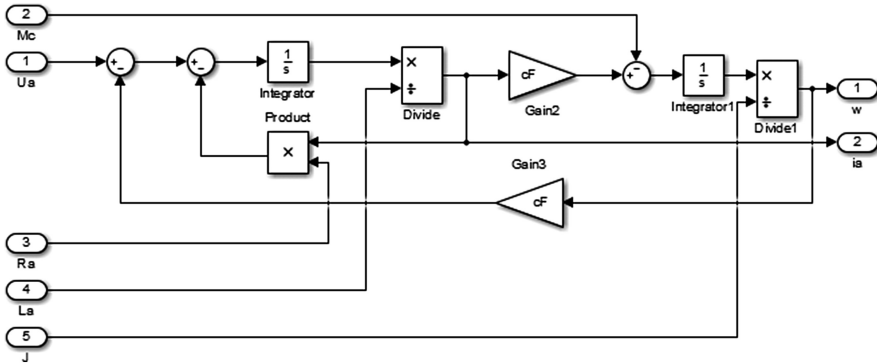


Fig. 4. The DC motor block diagram

The physical parameters define the motor model parameters: $K_d = 1/c\Phi$ – voltage gain; $K_{mc} = Ra/c^2\Phi^2$ – load gain; $T_a = La/Ra$ – rotor time constant; $T_m = JRa/c^2\Phi^2$ – mechanical time constant.

The motor model block diagram is shown in Fig. 5.

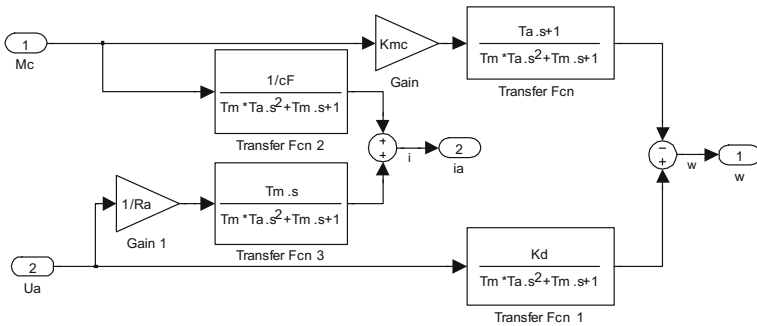


Fig. 5. The DC motor model block diagram

The block diagram from Fig. 5 forms the subsystem DC-motor for further research.

The simulation model is based on a PIVT 6-25/3A DC motor with the following parameters:

$U_a = 30\text{ V}$ (rated voltage); $R_a = 5.25\ \Omega$, $L_a = 0.0105\text{ H}$, $c\Phi = 0.072\text{ Nm/A}$, $J = 25 \cdot 10^{-6}\text{ kg.m}^2$; $Me = 0.11\text{ Nm}$ (rated torque).

During the phase of study of 2 s a sine input signal with magnitude 10, bias 20 and frequency 8π is applied (see Fig. 6). The variables $\mathbf{X} = [U_a\ i_a\ w]$ are sampled with sampling time 10^{-4} s and all measurement data $\mathbf{x}^T(k) = [U_a(k)\ i_a(k)\ w(k)]$ are collected. According to the algorithm described in Sect. 3 the transformation matrix \mathbf{P} is calculated

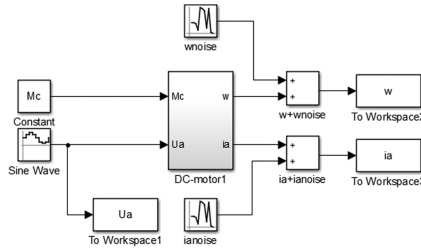


Fig. 6. Block diagram for the phase of study

$$P = \begin{bmatrix} -0.9804 & 0.0676 \\ -0.1857 & -0.0003 \\ 0.0664 & 0.9977 \end{bmatrix}$$

It defines the principal components and matrix \mathbf{PP}^T for the back-transformation. The block diagram shown in Fig. 7 can be used to detect changes in the physical parameters of the motor.

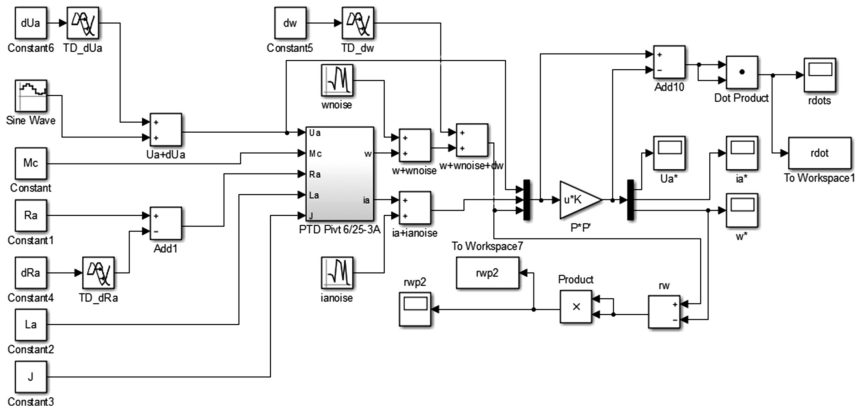


Fig. 7. Block diagram for change detections of physical motor parameters

Additive faults of the input, output and parameters (in this case it is Ra) are simulated with 3 pairs of blocks **Constant** and **Transport Delay**. Noise is added to the outputs w and ia . The matrix PP^T is a parameter of the matrix gain block ($u * K$). Real-time fault detection is based on analysis of squared residuals quantities $rdot$ and $rwp2$ by change detection methods.

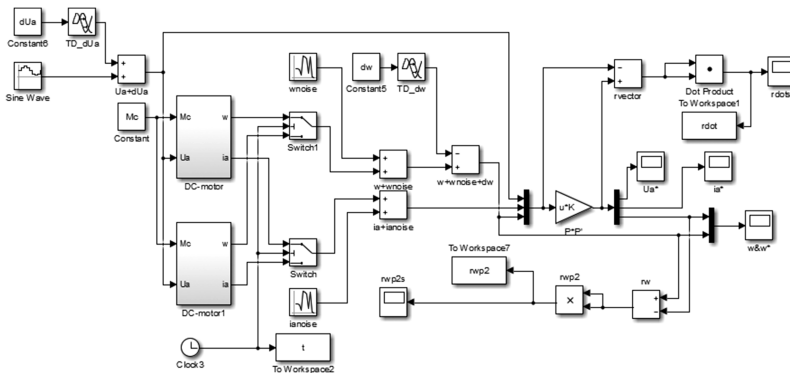


Fig. 8. Block diagram for change detections of motor model parameters

The block diagram shown in Fig. 8 can be used to detect changes in the model parameters of the motor.

Faults of the model parameters are simulated with 2 pairs of blocks **DC-motor** and **Switch**. For real time fault detection change detection methods of the mean and variance of squared residuals quantities $rdot$ and $rwp2$ can be used. According with the known relations

$$\bar{r} = E\{r(t)\} = \lim_{T \rightarrow \infty} \frac{1}{T} \int_0^T r(t) dt; \quad \sigma_r^2 = E\{[r(t) - \bar{r}]^2\} = \lim_{T \rightarrow \infty} \frac{1}{T} \int_0^T [r(t) - \bar{r}]^2 dt \quad (16)$$

the mean and variance are calculated respectively by the block diagrams shown in Figs. 9 and 10. Two block diagrams are presented as subsystems **M** and **D**.

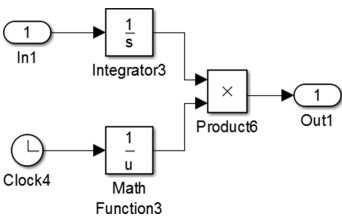


Fig. 9. Block diagram - mean

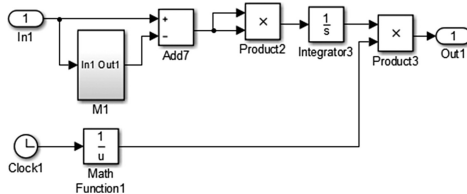


Fig. 10. Block diagram - variance

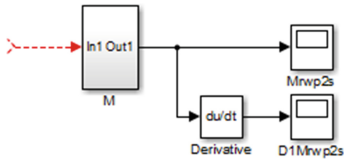


Fig. 11. Derivative of the mean

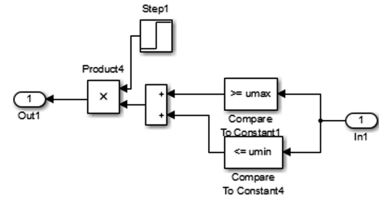


Fig. 12. Limit checking

The derivative of the mean allows its changes to be detected faster (see Fig. 11). These changes can be detected by limit or threshold checking (see Fig. 12) [6, 7].

Simulation experiments are made for the duration of 4 s. Faults of parameters and variables Kmc , Kd , Tmc , Ta , Ua , w are simulated during the time period from 2 s to 4 s.

A part of the results from simulation research about twofold change of Kmc are presented with Figs. 13, 14, 15, 16, 17 and 18. Respectively they represent: scalar product of vector residuals \mathbf{rdot} (Fig. 13); mean of \mathbf{rdot} (Fig. 14); variance of \mathbf{rdot} (Fig. 15); angular velocity residual $\mathbf{rwp2}$ (Fig. 16); mean of $\mathbf{rwp2}$ (Fig. 17); limit checking of the mean of $\mathbf{rwp2}$ (Fig. 18).

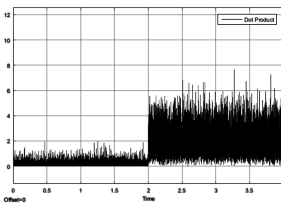


Fig. 13. Rdot

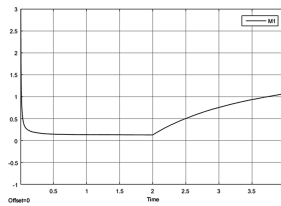


Fig. 14. Mrdot

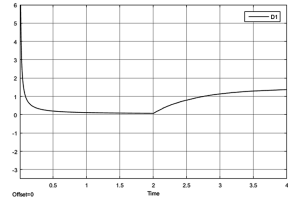


Fig. 15. Drdot

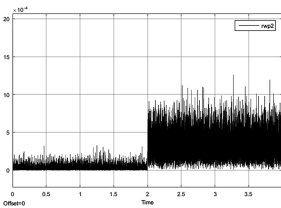


Fig. 16. $\mathbf{rwp2}$

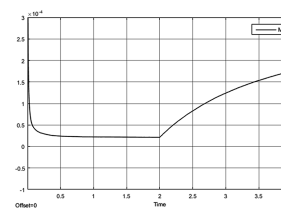


Fig. 17. $\mathbf{Mrwp2}$

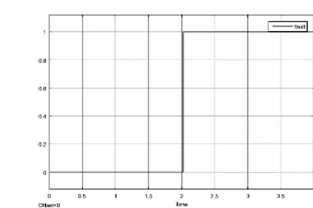


Fig. 18. Fault- $\mathbf{Mrwp2}$

6 Conclusion

The demonstrated simulation results verify the application possibility of the PCA method for real-time fault detection in DC motor parameters. Additive faults of the input and output signals are more easily detected compared to changes in the model parameters. On the other hand the gain model parameters are more efficiently detected in contrast to the time constant parameters. A weak point of the proposed method is the lack of fault isolation capabilities which will be a subject of further reasearch.

Acknowledgments. The scientific research, the results of which are presented in the present publication have been carried out under a project №PD1 within the inherent research activity of TU-Varna, target financed from the state budget.

References

1. Blanke, M., Kinnaert, M., Lunze, J., Staroswiecki, M.: *Diagnosis and Fault-Tolerant Control*, 2nd edn. Springer, Heidelberg (2006). ISBN-10: 3-540-35652-5
2. Chiang, L.H., Russell, E.L., Braatz, R.D.: *Fault Detection and Diagnosis in Industrial Systems*. Springer, London (2001). ISBN: 1-85233-327-8
3. Crowder, R.: *Electric Drives and Electromechanical Systems*. Elsevier Inc., Oxford (2006)
4. Ding, S.X.: *Model-based Fault Diagnosis Techniques Design Schemes, Algorithms, and Tools*. Springer, Heidelberg (2008). ISBN: 978-3-540-76303-1
5. Drury, B.: *The Control Techniques Drives and Controls Handbook*. The Institution of Engineering and Technology, London (2009)
6. Ichetv, A., Atanosov, N., Petrov, M.: Parameter estimation for fault diagnostic of a servo system, *Sozopol* (2009). ISSN: 1313-9487, стр 87-93
7. Isermann, R.: *Fault-Diagnosis Systems: An Introduction from Fault Detection to Fault Tolerance*. Springer, Heidelberg (2006). ISBN-10: 3-540-24112-4, ISBN-13: 978-3-540-2412-6
8. Jolliffe, I.T.: *Principal Component Analysis*, 2nd edn. Springer, New York (2002)
9. Leonhard, W.: *Control of Electrical Drives*. Springer, Heidelberg (2001)
10. Smith, L.I.: *A Tutorial on Principal Components Analysis*. Cornell University (2002)

Automated Stress Level Monitoring in Mobile Setup

Valentina Markova^(✉), Kalin Kalinkov, Petar Stanev, and Todor Ganchev

Technical University of Varna, 1 Studentska Str., 9010 Varna, Bulgaria
{vim,tganchev}@ieee.org, kalin.kalinkov@gmail.com,
petar.stanev@gmail.com

Abstract. We present the design of a mobile system for real-time stress-level assessment. The system combines wearable sensors, wireless data acquisition, and Cloud computing in order to collect and analyze physiological signals, such as, Galvanic Skin Response (GSR) and skin temperature. We report on the implementation of a specific use case, which incorporates functionality for real-time data logging and analysis. Experimental results demonstrate excellent recognition accuracy of affective arousal and decent accuracy for binary detection of valence. In addition, we also evaluate the feasibility for detection of high arousal/negative valence (HANV) events, which in specific setups can be connected to stress.

Keywords: Stress detection · Cloud computing · Galvanic skin response · Skin temperature

1 Introduction

Stress is an indispensable part of our lives and can have both positive and negative impact on the human body. Chronic exposure to stress-causing factors brings long-term negative effects to cognitive abilities and work performance, and may increase the risk of mental and cardiovascular diseases, immune system disturbances, and degenerative neurological disorders. In this regard, stress management plays an important role for efficient work and wellness.

Unobtrusive continuous stress monitoring during daily activities requires the use of mobile technological tools and services, such as Cloud-based services, IoT technology etc. [1, 2]. In this regard, the advance of wearable sensing technology, wireless networks, smart mobile devices, and cloud computing enabled the real-time measuring of stress-indicative physiological parameters. In the same time, stress monitoring in mobile setup, e.g. during work and everyday activities, imposes restrictions on the sensor set which could be used. Sensors need to be non-obtrusive, easy to wear and have to provide reliable readings despite body movements and interferences from the environment.

To this end, various technological solutions for stress monitoring have been researched. In brief, two main groups of methods have been used to this end. The first one measures self-reported stress levels based on questionnaires and the second one is directly acquiring physiological signals of the human body. Here we focus on the later one and the corresponding technological solutions.

Various wearable sensors, often organized in body area networks, typically measure physiological signals, behavioral patterns, and sociometric clues tuned to specific application scenario. For instance, in [3] it was reported a wearable device for arousal measurement, which is considered evidence of stress. Physiological measurements of GSR, PPG, and HRV and sociometric activity sensor were used for stress detection [4]. Other studies [5, 6], take advantage of ECG, GSR and respiration activity for indirect biomarkers for stress, which are later used to measure stress-related driving behaviors [7]. Wearable sensors and smart phone-based solutions [8, 9] were used to recognize stress level in real-world environment. Real-time mental stress detection during work was studied in [10, 11]. Evidence derived from camera, mouse, and biosensor data streams were combined in order to monitor stress in driving scenario [12].

In the present work, we report on a technological advance towards the development of a real-time system for stress monitoring in mobile setup. It makes use of wearable smart sensors that upload psychological readings to a cloud-based service. Data processing and analysis are performed using cloud computing resources and outcomes are then accessible for visualization on various platforms (mobile devices, PCs etc.). The overall concept relies on the assessment of binary arousal clues based on physiological signals, such as GSR, ECG, and skin temperature. Here, the particular focus is on the estimation of affective arousal derived from GSR and body temperature. In addition we also aim to estimate the valence of emotion, which opens the opportunity for the binary detection of high arousal/negative valence (HANV) conditions. In a specific context, the HANV condition may be interpreted as acute stress. In the following sections, we present the overall concept of real-time stress monitoring system and some experimental results obtained to this end. Specifically, in Sect. 2, we discuss the overall concept of real-time stress monitoring and outline the technological solutions, on which our system builds in order to implement such a conceptual design. Next, in Sect. 3, we provide a comprehensive description of the arousal detection method employed here, and in Sect. 4 present empirical results for automated binary detection of affective arousal based on GSR signals and skin temperature, as well as results for binary valence detection and the recognition of HANV events. Finally, in Sect. 5 we conclude this work and provide outlook for future research activities.

2 Overall Concept

Real-time stress monitoring, based on the objective evaluation of physiological signals, imposes tough requirements to the sensors used for data acquisition. In this regard, technological solutions are usually restricted to the use of a small set of unobtrusive wearable sensors, with robust attachment, fulfilling the requirements for reliable operation during work duties, intense activities, and daily routine. From this perspective, we present the overall concept of real-time stress monitoring (Fig. 1) and discuss certain technological solutions, on which we built in our efforts to implement such a concept.

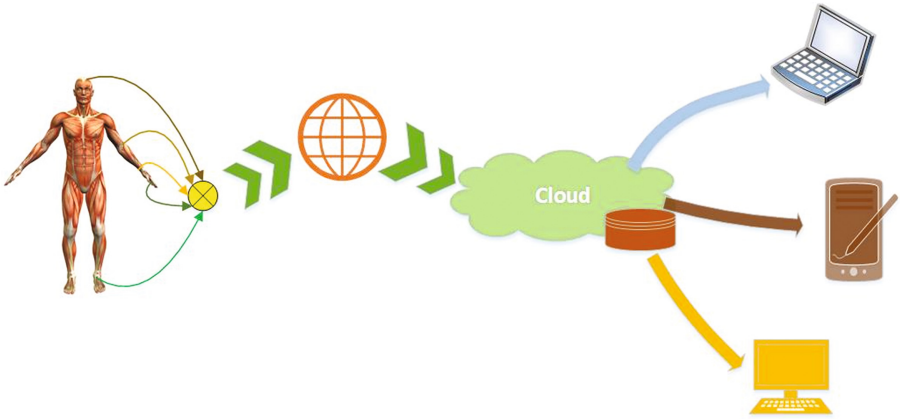


Fig. 1. Overall concept of real-time stress level monitoring

In brief, the conceptual design presented in Fig. 1 depends on the development of method, which makes use of a small set of easy to attach wearable sensors that are known to provide reliable indications about stress. Specifically, we rely on custom-built smart sensors for the acquisition of skin temperature and GSR signals, and electrodes attached on the internal side of a fingerless glove or directly stick on the fingers. The use of smart sensors allows the physiological signals collected to be transmitted wirelessly to the Cloud for further storage and processing. Furthermore, a straightforward implementation of such a concept could be based on the now ubiquitous smart phones. Alternatively, an independent gateway to the Cloud could provide extended operational time and provide consistent planning of the available battery resources, and enhance the overall reliability of service. Physiological signals and the results of data processing are made accessible to the potential end-users through services, which provide appropriate interface to various platforms, such as mobile devices, laptop computer, desktop PC etc. The last allows operative information about the suspected onset of stress to be provided to the user or medical staff, and hypothetically to provide guidance on how to manage stress, smoothly implement transition or mission adaptation according to some fallback strategy, obtain feedback about the perceived challenge, effort etc.

In Fig. 2, we present the overall architecture of a system for real-time stress monitoring which follows the abovementioned conceptual design (Fig. 1). In particular, due to the specific requirements of mobile stress monitoring setups, the real-time system described here relies only on GSR and skin temperature readings. The data acquisition is carried out with sticky silver/silver-chloride (Ag/AgCl) electrodes, attached on the left-hand. The GSR signal is measured between the index and ring fingers, and the skin temperature is measured on the middle finger. The data acquisition is implemented with a Node MCU with integrated on-board ADC (http://nodemcu.com/index_en.html). Next, data are sent wirelessly to a Cloud service or alternatively directly to a remote server of the customer. For that purpose, we make use of an ESP8266 WiFi module, available on the Node MCU board. In the current design, data are transported via TCP/IP and HTTP. Upon receive data are stored in a

Cloud-based storage repository and are next subject to Cloud-based processing (cf. Sect. 3).

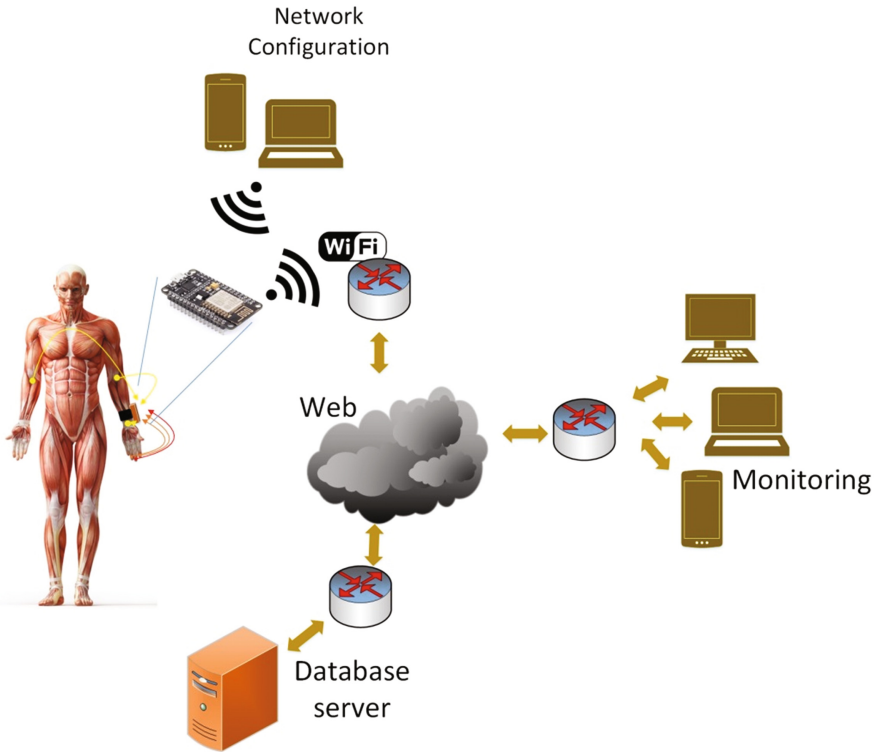


Fig. 2. Architecture of the real-time stress monitoring system in mobile setup

Following that, we evaluated various functionalities of the Google Drive service: establishing connection, sending data, and implementing real-time statistical analysis. In particular, once data are sent to google drive, we create a Google sheet form where real-time computing of the GSR descriptors is implemented. We also kept track on the load of the Google service, based on the latency, and compared these with a custom-made server.

Finally, prospective users of the stress monitoring system can also take advantage of a graphic interface, available for various client devices, in order to visualize history graphs, results of analyses in previous periods, history of alerts etc.

3 Automated Arousal Detection

Depending on the context, affective arousal can be used as an indicator of whether a person is stressed at a certain moment in time or not. At present, the most precise methods for measuring the level of affective arousal are based on an analysis of Galvanic Skin Response (GSR) of skin, because GSR is directly influenced by the discharges of sweat

glands secretion. Stress is among the main factors, which condition such secretion. In particular, the GSR signal (cf. Fig. 3) consists of two informative components: skin conductance level (SCL) and skin conductance response (SCR). The SCL component is the slowly varying tonic level, which changes slightly within tens of seconds to minutes, and usually differs among people. The SCR component, aka GSR peaks, is the elicited reaction to specific stimuli and is considered informative for the assessment of acute stress levels.

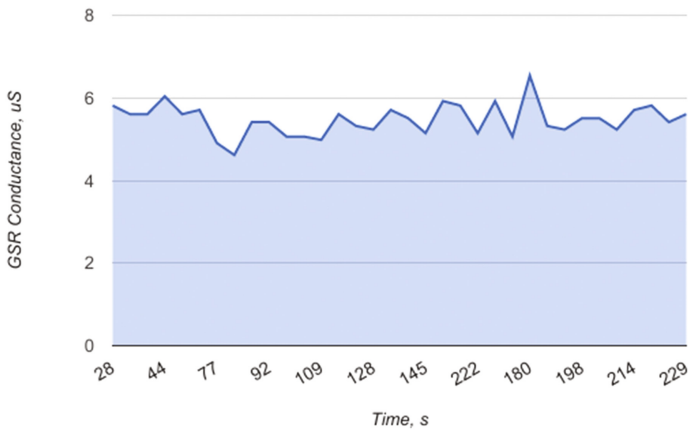


Fig. 3. Plot of a GSR recording obtained with the proposed system (stored on the Cloud in a Google sheet form)

In Fig. 4, we present the signal processing flow, which leads to the extraction of various GSR signal features. In particular, the GSR values are first normalized, converted to conductivity units, and then filtered with a moving average filter. The filtered signal is then subtracted from the raw signal, and the GSR peaks signal is obtained and the GSR peaks are counted. For that purpose, we made use of a reference threshold value equal to $0.01 \mu\text{S}$ (cf. Fig. 5). In the following paragraphs, we will make use of the denotation GSR peaks not for the signal itself but for the number of GSR peaks, which exceed the predefined threshold value, in that segment. Neighboring peaks, whose amplitude valleys do not reach negative values, were counted as one instance. The descriptors SCL mean and SCL standard deviation were computed directly from the tonic component of the GSR signal.

In addition to the GSR-based descriptors, we also measured the momentous skin temperature, which was smoothed by a moving average filter.

The binary arousal detection method proposed here is based on the on-line evaluation of these features with a decision tree C4.5 based detector, which operates on short overlapping segments of the signal. In addition to the binary detection of affective arousal, we also investigated the applicability of these descriptors {GSR peaks, SCL mean, SCL std, and average temperature} to the needs of positive/negative valence detection. Reliable classification of valence would permit the detection of high arousal/negative valence (HANV) events.

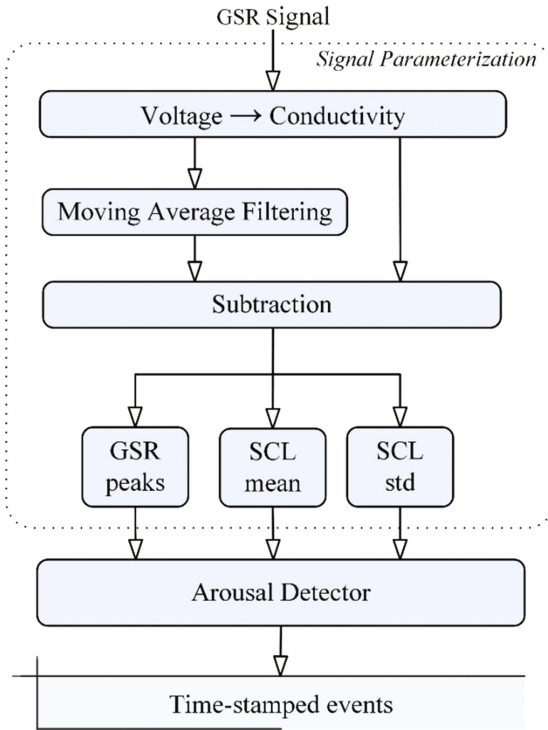


Fig. 4. Diagram of the GSR signal processing flow

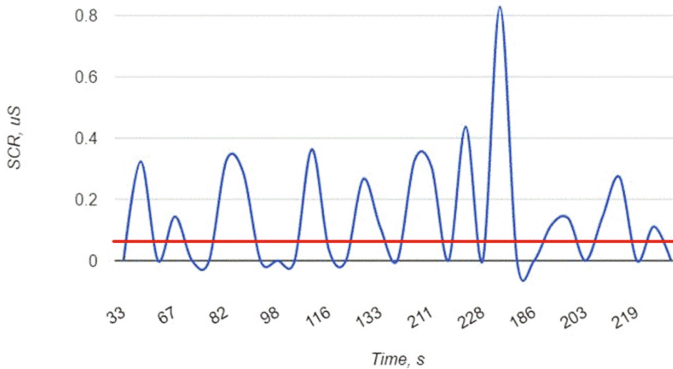


Fig. 5. Illustration of the SCR component of the GSR signal and the predefined threshold used in the estimation of the number of *GSR peaks*

Once some HANV events are detected, an HANV indication flag is set and the particular person can be contacted through a purposely designed and personalized Cloud-based monitoring service. We deem that depending on the specific context, the HANV events can be associated with episodes where a person experiences acute stress.

4 Experimental Results

In the present work, we present an experimental evaluation of the automated binary detection of affective arousal, valence, and the recognition of HANV events based on GSR and temperature readings. These results were obtained in off-line mode as we made use of annotated recordings, with known ground truth tags, which facilitated the assessment and comparison of the recognition accuracy for all binary detectors.

In all experiments, we followed a common experimental protocol, based on a dataset of 42 prerecorded and tagged GSR and temperature measurements for a single person. Each recording has a duration of 1 min and was processed following to the workflow discussed in Sect. 3. In Table 1, we show the number of instances in the dataset for the affective arousal, valence, and high arousal/negative valence events.

Table 1. Quantitative overview of the dataset used in the experimental evaluation.

	Category 1	Category 2	Total instances
Affective arousal	19 Low	23 High	42
Valence	18 Negative	24 Positive	42
High arousal/negative valence	8 Target	34 Other	42

In Table 2, we present an experimental evaluation of the relevance of the individual signal descriptors discussed in Sect. 3, and namely the GSR peaks, SCL mean, SCL std, and the average temperature.

Table 2. Recognition accuracy for the individual signal descriptors considered here: GSR peaks, SCL mean, SCL std, and average temperature.

Exp. #	Feature set	Accuracy [%] bin. Arousal	Accuracy [%] bin. Valence	Accuracy [%] HANV
1	Average temperature	100	83.3	81.0
2	GSR peaks	76.2	69.0	81.0
3	SCL mean	71.4	88.1	85.7
4	SCL std	90.5	78.6	92.9

The experimental result support the high relevance of skin temperature readings with affective arousal events, but also to a certain degree with the positive/negative valence condition, which motivated us to evaluate the recognition rate for the high arousal/negative valence (HANV) events.

In order to evaluate whether these descriptors are complementary and whether their joint use would improve the overall detection accuracy of affective arousal, valence and HANV events, we carried out two additional experiments with different sets of descriptors:

- (i) Set consisting of all GSR signal-based descriptors, and
- (ii) Set combining all GSR signal-based descriptors with the average temperature.

In Table 3, we present the results of an experimental evaluation of the recognition accuracy observed for the binary detection of affective arousal and valence, as well as for the detection of the high arousal/negative valence (HANV) condition.

Table 3. Recognition accuracy for the binary detection of affective arousal and valence, as well as for the recognition of the *high arousal/negative valence* (HANV) condition.

Exp.#	Feature set	Accuracy [%] bin. Arousal	Accuracy [%] bin. Valence	Accuracy [%] HANV
1	{GSR peaks, SCL mean, SCL std}	71.4	95.2	85.7
2	{GSR peaks, SCL mean, SCL std, averaged temperature}	100	92.9	85.7

Based on the experimental results we can conclude that the joint use of signal descriptors computed from GSR and temperature readings allows excellent recognition of affective arousal events, and to a lesser degree the classification of valence to negative/positive condition. This opens opportunities for the detection of high arousal/negative valence (HANV) events. We deem that further improvement of the recognition accuracy for the HANV condition is possible if extra descriptors, based on ECG readings, are added to the current set of descriptors.

5 Conclusion

In the present work, we presented the overall design and the implementation of a system for real-time stress monitoring in mobile setup. The stress monitoring is based on readings of GSR and skin temperature on the left hand. The experimental evaluation of recognition accuracy reported here support the hypothesis that binary assessment of affective arousal, based on descriptors computed from GSR and skin temperature readings is feasible. Such a functionality facilitates the development of technology for real-time monitoring of stress in a mobile setup. In addition, we evaluated the possibility to detect positive/negative valence condition based on the same set of signal descriptors. Although the observed recognition accuracy of valence does not meet the requirements of real-life applications, we consider the experimental results quite interesting as these demonstrated the feasibility to detect specific instances of the high affective arousal/negative valence condition. In specific situations and context, the automated detection of high arousal/negative valence events can be interpret as the onset of stress condition. Depending on the application area, a team supervisor (or an operator) can immediately contact the person in order to instruct her/him on how to proceed further with her/his mission. Hypothetically, the last could be useful to enhance stress management in high-risk professions, in support of teams involved in medical assistance, and in the rehabilitation of patients who recover of severe trauma, such as injuries of the spinal cord, lower limbs etc.

Acknowledgement. The authors acknowledge with sincere thanks the support received through the research project NP5/2017 entitled “Study of Methods and Apparatus for the Acquisition of Biomedical Data in Mobile Setup”, financed by the National Science Fund of Bulgaria and Technical University of Varna.

References

1. Islam, S.M.R., Kwak, D., Kabir, M.H., Hossain, M., Kwak, K.S.: The internet of things for health care: a comprehensive survey. *IEEE Access* **3**, 678–708 (2015). doi:[10.1109/ACCESS.2015.2437951](https://doi.org/10.1109/ACCESS.2015.2437951)
2. Alamri, A., Ansari, W.S., Hassan, M.M., Hossain, M.S., Alelaiwi, A., Hossain, M.: A survey on sensor-cloud: architecture, applications, and approaches. *Int. J. Distrib. Sens. Netw.* **9**(2), 917923 (2013)
3. Mozos, O.M., Sandulescu, V., Andrews, S., Ellis, D., Bellotto, N., Dobrescu, R., Ferrandez, J.M.: Stress detection using wearable physiological and sociometric sensors. *Int. J. Neural Syst.* **0**, 1–17 (2005)
4. Fletcher, R.R., Dobson, K., Wilder-Smith, O., Goodwin, M., et al.: iCalm: wearable sensor and network architecture for wirelessly communicating and logging autonomic activity. *IEEE Trans. Inf. Technol. Biomed.* **14**(2), 215–223 (2010). doi:[10.1109/TITB.2009.2038692](https://doi.org/10.1109/TITB.2009.2038692)
5. Valenza, G., Allegrini, P., Lanatà, A., Scilingo, E.P.: Dominant Lyapunov exponent and approximate entropy in heart rate variability during emotional visual elicitation. *Frontiers Neuroeng.* **5**(3), 7 (2012)
6. Acharya, U.R., Joseph, K.P., Kannathal, N., Lim, C.M., Suri, J.S.: Heart rate variability: a review. *Med. Biol. Eng. Comput.* **44**(12), 1031–1051 (2006)
7. Lanatà, A., et al.: How the autonomic nervous system and driving style change with incremental stressing conditions during simulated driving. *IEEE Trans. Intell. Transp. Syst.* **16**(3), 1505–1517 (2015). doi:[10.1109/TITS.2014.2365681](https://doi.org/10.1109/TITS.2014.2365681)
8. Sano, A., Picard, R.W.: Stress recognition using wearable sensors and mobile phones. In: 2013 Humaine Association Conference on Affective Computing and Intelligent Interaction, Geneva, pp. 671–676 (2013). doi:[10.1109/ACII.2013.117](https://doi.org/10.1109/ACII.2013.117)
9. Garcia-Ceja, E., Osmani, V., Mayora, O.: Automatic stress detection in working environments from smartphones’ accelerometer data: a first step. *IEEE J. Biomed. Health Inform.* **20**(4), 1053–1060 (2016). doi:[10.1109/ICDMW.2011.17](https://doi.org/10.1109/ICDMW.2011.17)
10. Bakker, J., Pechenizkiy, M., Sidorova, N.: What’s your current stress level? detection of stress patterns from gsr sensor data. In: 2011 IEEE 11th International Conference on Data Mining Workshops, Vancouver, BC, pp. 573–580 (2011). doi:[10.1109/ICDMW.2011.17](https://doi.org/10.1109/ICDMW.2011.17)
11. Wijsman, J., Grundlehner, B., Liu, H., Hermens, H., Penders, J.: Towards mental stress detection using wearable physiological sensors. In: 2011 Annual International Conference of the IEEE Engineering in Medicine and Biology Society, Boston, MA, pp. 1798–1801 (2011). doi:[10.1109/IEMBS.2011.6090512](https://doi.org/10.1109/IEMBS.2011.6090512)
12. Liao, W., Zhang, W., Zhu, Z., Ji, Q.: A real-time human stress monitoring system using dynamic bayesian network. In: 2005 IEEE Computer Society Conference on Computer Vision and Pattern Recognition (CVPR’05) - Workshops, San Diego, CA, USA, p. 70 (2005). doi:[10.1109/CVPR.2005.394](https://doi.org/10.1109/CVPR.2005.394)

Evaluation of Sandstone Internal Structure with Application of Micro-CT and FOTOM System

Lačezar Ličev¹(✉), Jakub Hendrych¹, Radim Kunčický¹,
Kateřina Kovářová²(✉), and Ivana Kumpová³

¹ VŠB-TU Ostrava, 708 33 Poruba, Ostrava, Czech Republic
{lacezar.licev,jakub.hendrych,radim.kuncicky}@vsb.cz

² ČVUT Praha, 166 29 Praha 6, Czech Republic
katerina.kovarova@fsv.cvut.cz

³ Centrum Excellence Telč, 588 56 Telč, Czech Republic
kumpova@itam.cas.cz

Abstract. The sandstone internal structure is one of the most important factors controlling mechanical properties of this stone. There are many methods enabling study of the properties and character of the internal structure. The known methods are based on the penetration of a chosen medium of a detected volume into the pores or they are based on image analysis of rock slices, where fluorescent colouring highlights the pores. Unfortunately, these methods have a destructive character and, therefore, it is not possible to use the stone samples again. The possibility to re-use the samples makes the micro-CT a very useful tool. Interpretation of the micro-CT results in combination with the results of other methods may enable more detailed view into the internal structure. We studied widely used Czech sandstones using the micro-CT in the course of our experiment. Next, the acquired data was evaluated in commercial software VGStudio MAX 2.2 and also in our FOTOM^{NG} system. We implemented new specialized module in this system for evaluating of such data. For a measurement we prepared several image preprocessing methods. This preprocessing is consisted for example from image binary thresholding for a better diversity between inner porosity and sandstone itself or colour inversion. As addition we implemented function for cropping the samples, due to depreciation of the sample borders caused by repeated measurement. We are able to calculate the value of porosity, for whole series a volume of porespace of sandstone samples or other statistical values. Results and limitations of interpretability are discussed in this article.

Keywords: Porosity · Sandstones · Micro-CT · FOTOM

1 Introduction

Weathering of stones is a natural process, during which stones, which originated under specific physical conditions (above all temperature and pressure), are adapting to the new environment. The processes include physical degradation and chemical changes [1].

The character of the internal structure is the most important factor influencing and controlling the stones' mechanical properties and also their durability.

In case of stones, the internal structure is generally understood as the spatial arrangement of rock forming minerals [2–4]. Pore space is the characteristic part of the stone internal structure, and building materials generally and it is significantly modified during weathering processes. Pores may have a different shape, size and rate of inter-connection. Pore space is usually quantified by one parameter – porosity, which expresses the ratio of the pore volume to the volume of the solid phase [5, 6]. We can generally distinguish two porosity types – effective porosity and ineffective porosity. The effective porosity, also called open porosity, is defined as the ratio of the part of the pore volume where the water can circulate to the total volume of a representative sample of the medium. The ineffective porosity, also called closed porosity, is created by such pores in which fluids or gases may be present but in which fluid flow cannot effectively take place and include the closed pores. The sum of effective porosity and ineffective porosity is called total porosity. Porosity influences many mechanical-physical properties, such as uniaxial compressive strength, deformation characteristics, water absorption and permeability [e.g. 5, 7]. According to Zdravkov et al. [8], the determination of pore space properties, such as pore size, their geometry and interconnection, may contribute to clarification of physical properties changes of given porous material.

There are many methods enabling study of properties and character of the internal structure. Determination of pore size is possible using the two-dimensional measurements with optical microscopy with color-highlighted pores [9], image analysis [10], electron microscopy [11], X-Ray microtomography [12] or using indirect measurement methods such as high-pressure mercury porosimetry [13] or velocity of ultrasonic waves assessment [14]. Most of these methods, unfortunately, have a destructive character and, therefore, it is not possible to use the stone samples again. This is the main reason why we created image processing method by using non-destructive micro-CT. Now we are able to repeat measurement and observed the changes of sandstone samples.

The use of Micro-CT method for the purposes of stone porosity study is discussed in many research works. For example, Cnudde et al. [15] used this method to characterize porosity and microstructure of building stone (sandstone and limestone) and concrete. They used the 3D-software “ μ CTanalySIS” for the evaluation of pore space properties. Kovářová et al. [12] compared the porosity data obtained by mercury porosimetry and micro-CT. The use of these two methods enables the detailed description of pore space and enables the better evaluation of initiated internal structure changes due to stone weathering.

2 Material and Procedure

In the course of our research, the mobile experimental stonewalls were built. For these purposes, we used more Czech sandstone types with different kind of processing. We carried out the accelerated climatic treatment, which was composed of 58 freeze/thaw cycles. Each of the freeze/thaw cycle consisted of twenty hours lasting freezing in the large capacity freezer within the temperature range from $-13\text{ }^{\circ}\text{C}$ to $-20\text{ }^{\circ}\text{C}$ with

following five hours sunlight thawing. The walls were manually wetted before every placement in to the freezer.

We studied the internal structure changes of Božanov sandstone, which was processed using double point hammer. To be able to evaluate the changes of internal structure we studied the same stone samples before and after the climatic treatment using the Micro-CT analysis. We tried to achieve the most similar behaviour of the sample internal structure as in the real conditions. For these purposes, the cylindrical samples of untreated sandstones were inserted back into the ashlars after their primal Micro-CT analysis (Fig. 1). The cylindrical samples had the size of ca. 2 cm diameter and 2,5 cm height.



Fig. 1. (a) First from the left – The inserted cylindrical sample of Božanov sandstone after its primal Micro-CT analysis, (b) second from the left – experimental stone walls

The sample was measured with one pair X-Ray tube – detector. For CT scanning, a microfocus X-Ray tube (XWT-240-SE, X-Ray WorX, Germany) operating at micro-focus mode (spot size 4.0 μm) with a voltage of 80 kV, current of 210 μA and power output of 16.8 W was used. As a detector, flat panel (XRD-1622-AP-14, Perkin Elmer, USA) with dimensions 40 \times 40 cm, pixel matrix 2048 \times 2048 and 200 μm pixel pitch was used.

By geometry adjustment to the focus-detector distance of 1325 mm and focus-object distance of 125 mm, the projection magnification factor 10.6 was obtained, leading to the resolution of 18.87 μm per pixel in projections and 18.67 μm per voxel in 3D reconstruction. Geometrical parameters were chosen in order to obtain the best possible resolution with regard to the size of the sample and the detector area.

For image correction in projection images, standard “dark field” and “open beam” correction, along with a “beam hardening” correction (BHC), were used. Data for BHC was taken for a set of aluminium filters with thicknesses of 0, 0.2, 0.4, 0.6, 1.0, 2.0, 4.0, 6.0, 10.0 and 20.0 mm, the correction image for each filter was averaged out of one hundred images with the acquisition time of 999 ms. For the tomography, 800 projections were taken, each averaged from two images acquired with the exposure time of 999 ms.

To processed Micro-CT data we implemented new module for FOTOM^{NG} system. This module is consisted from two parts. The first part is focused on image pre-processing and the second part is for sample measurement.

The image pre-processing has several steps:

1. Object cropping – We are able to crop the sample by circle – it is important, because sandstone samples (mainly samples after the climatic treatment) has devaluated borders caused by repeated measurement (Fig. 2a).

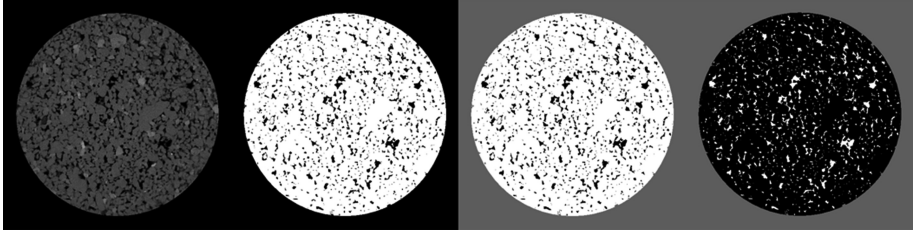


Fig. 2. (a) First from the left – Object cropping, (b) second from the left – Image binary thresholding, (c) third from the left – Sample and background distinction, (d) fourth from the left – Colour inversion

2. Binary thresholding - The principle is based on the brightness evaluation of each pixel of the image. Then we need to select a brightness value (threshold), for which it is true that all pixels with lower brightness than the threshold value belong to background – pores and background of the image. Otherwise, pixels with higher brightness than the threshold value belong to foreground (assuming an object of interest is brighter than its background) – solid material of sandstone sample (Fig. 2b).
3. Distinction between pores and background of the image – At this phase the background is assigned to grey color, pores to black color and solid material to white color (Fig. 2c).
4. Color inversion – This step is important mainly for voxel 3D modeling. It depends if we want the internal pores colored by white or black color (Fig. 2d).

The sample measurement process – We need to define ratio R between pixels value and metric units. It is done by setting of two control points and their real distance in metric units, the process is described in [16]. Now we are able to count pixels that represent the pores and solid material. Then by application of ratio R we can calculate the area of porosity from one image or volume from the whole image series. As output from measurement we can create image series for voxel 3D model or a result data set.

3 Results and Discussion

After the climatic treatment, the increase of total porosity was detected using VGStudio MAX 2.2., whereas the decrease of total porosity was detected using FOTOM^{NG}, which is shown in the following Table 1. In both cases of data processing, the central parts of sample were analysed, especially regarding to the need of clear-cut definition of the outer surface of the analysed volume.

Table 1. Porosity of Božanov sandstone determined using VGStudio MAX 2.2. and FOTOM^{NG} before and after the climatic treatment.

Data processing method	Porosity (%)		Relative change (%)
	Before	After	
VGStudio MAX 2.2	8,88	10,22	15,1
FOTOM ^{NG}	8,38	8,20	-2,07

The most important differences between the values determined using both methods of data processing are most likely caused by the analysis of a different central part of sandstone sample.

It was proven that detected pores are frequently open and interconnected; these pores are labelled by the pink colour in Figs. 3 and 4. Relatively small amount of pores are closed and separated, such pores are labelled by the green and blue colours. Unfortunately, we were not able to compute their volume separately using both ways of data processing. One can see that interconnected individual pores have similar dimensions as the separated ones. Based on this type of data processing, we were able to detect the change of open porosity, which was not significant in this case.

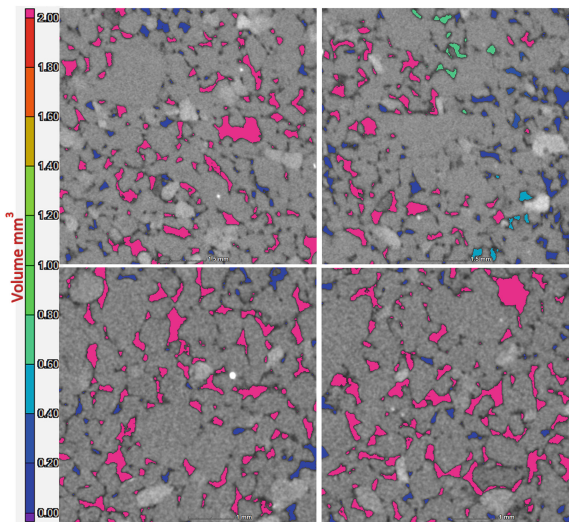


Fig. 3. The micro-CT cross sections of Božanov sandstone with coloured highlighted pores; the untreated sample above, the treated sample below (VGStudio MAX 2.2. screenshot)

Porosity increasing from 8.88% (untreated sample) to 10.22% (treated sample) was evaluated for pores with volume larger than $26.88 \times 10^{-6} \text{ mm}^3$ (diameter $\sim 30 \mu\text{m}$). Note that pores are not spherical, therefore pore description by its diameter is not too adequate.

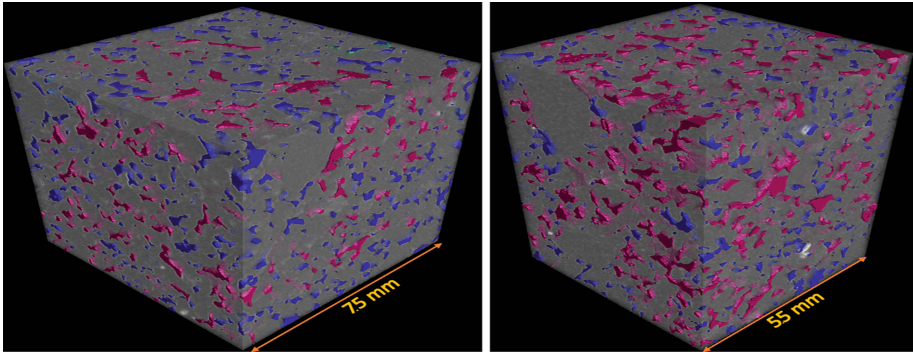


Fig. 4. The micro-CT brick 3D reconstruction of Božanov cylindrical sandstone sample with coloured highlighted pores; the untreated sample on the left side, the treated sample on the right side (VGStudio MAX 2.2. screenshot)

A sample has to be much smaller to be able to evaluate pores with micrometric scale volume. Technical limit of the smallest pore detection is approximately $6 \mu\text{m}^3$ for such heterogeneous material, however related measurement and data processing is much more demanding task in comparison with the sample reported.

Using the FOTOM^{NG} system we were able to calculate the total volume of solid matrix, total volume of pores and therefore we were able to calculate the total porosity. The comparison of pore area before and after the climatic treatment is shown in following figure (Fig. 5).

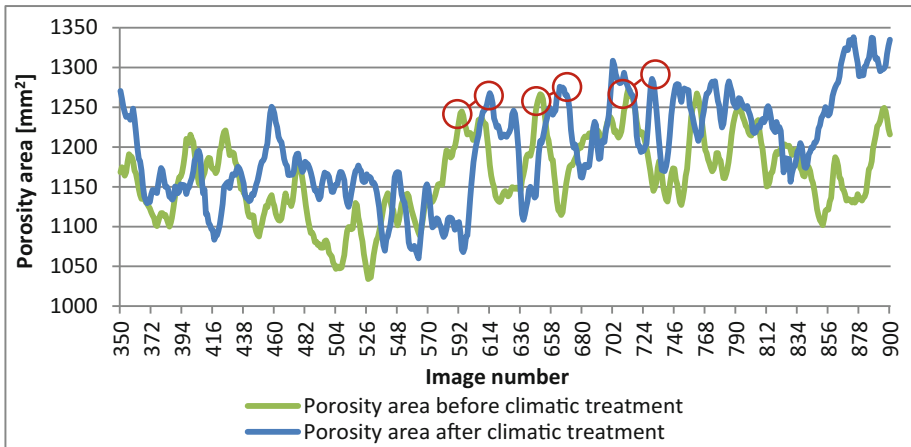


Fig. 5. Comparison between porosity area before and after climatic treatment

It is necessary to emphasize, that the internal structure of sandstone is strongly heterogeneous. Therefore it is fundamental to compare the identical part of the stone

sample, which is often very difficult because of the large number of analysed images. The process of the selection of the same image is quite time demanding. As it is obvious from circled parts of curves (Fig. 5), we will have to “shift” the inscribed volume and compare the same pictures one another. Therefore the result of porosity from the Table 1 will be different. Also a large error occurred by the material for sample attachment in the micro-CT scanning. That is why we use images from series number 350. Previous images were depreciated by attachment material. Also by repeatable measurement the sandstone samples was no longer 100% cylindrical shape.

4 Conclusion

In conclusion, use of the micro-CT method is very helpful for the purposes of internal structure description and also for the evaluation of its changes after the climatic treatment. As any other method, it has its own limitations. First of all, it is necessary to compare the identical parts of stone sample. Secondly, the correctness of results depends on the way of pore/grain boundary setting. Usually, it is manually determined and therefore it depends on the personal experience of the operator. From that point of view, it is appropriate to perform the analysis by the same person. Finally, the same micro-CT arrangement has to be kept.

We would like to focus our next research on the influence of internal structure changes on strength properties of building stone. Furthermore, we would like to use the micro-CT method for the evaluation of the suitability and effectiveness of stone consolidant in the relationship to the stone degradation. However, we have to find out the best way how to evaluate the same sample volume before and after climatic treatment.

Acknowledgements. The following grants are acknowledged for the financial support provided for this research: Grant Agency of the Czech Republic – GACR P103/15/06700S, Grant of SGS No. SGS 2017/134, VSB-Technical University of Ostrava, The Ministry of Education, Youth and Sports from the National Programme of Sustainability (NPU II) project “IT4Innovations excellence in science - LQ1602”.

References

1. Ollier, C., et al.: *Weathering*. Longman Group, London (1984)
2. Winkler, E.: *Stone in Architecture: Properties. Durability*. Springer Science & Business Media, New York (2013)
3. Lama, R.D., Vutukuri, V.S.: *Handbook on Mechanical Properties of Rocks-Testing Techniques and Results*, vol. iii (1978)
4. Wenk, H.R. (ed.): *Preferred Orientation in Deformed Metal and Rocks: An Introduction to Modern Texture Analysis*. Elsevier (2016)
5. Schön, J.H.: *Physical Properties of Rocks: Fundamentals and Principles of Petrophysics*. Elsevier, Amsterdam (2015)
6. Prentice, J.E.: *Geology of Construction Materials*. Springer Science & Business Media, New York (1990)
7. Goodman, R.E.: *Introduction to Rock Mechanics*. Wiley, New York (1989)

8. Zdravkov, B., et al.: Pore classification in the characterization of porous materials: a perspective. *Open Chem.* **5**(2), 385–395 (2007)
9. Nishiyama, T., Kusuda, H.: Identification of pore spaces and microcracks using fluorescent resins. *Int. J. Rock Mech. Min. Sci. Geomech. Abstr.* **31**, 369–375 (1994)
10. Ruzyla, K., et al.: Characterization of pore space by quantitative image analysis. *SPE Formation Eval.* **1**(04), 389–398 (1986)
11. Nadeau, P.H., Hurst, A.: Application of back-scattered electron microscopy to the quantification of clay mineral microporosity in sandstones. *J. Sed. Res.* **61**(6) (1991)
12. Kovářová, K., Ševčík, R., Weishauptova, Z.: Comparison of mercury porosimetry and X-ray microtomography for porosity study of sandstones. *Acta Geodynamica et Geomaterialia* **9**(4), 541–550 (2012)
13. Cerepi, A., Burlot, R., Humbert, L.: Caractérisation de la complexité du réseau poreux des grès et calcaires par porosimétrie mercure. *Comptes rendus de l'Académie des sciences. Série 2. Sciences de la terre et des planètes* **324**(7), 563–571 (1997)
14. Carrara, E., et al.: Evaluation of porosity and saturation degree by laboratory joint measurements of velocity and resistivity: a model improvement. *Pure Appl. Geophys.* **154**(2), 211–255 (1999)
15. Cnudde, V., et al.: Porosity and microstructure characterization of building stones and concretes. *Eng. Geol.* **103**(3), 76–83 (2009)
16. Ličev, L.: Systém FOTOMNG: architektura, funkce a použití. BEN - technická literatura, Praha (2015). ISBN 978-80-7300-521-4

Operational Reliability Assessment of Systems Containing Electronic Elements

Julia Garipova^(✉), Anton Georgiev, Toncho Papanchev,
Nikolay Nikolov, and Dimitar Zlatev

Technical University of Varna, Varna, Bulgaria
juliq.garipova@tu-varna.bg

Abstract. This paper analyzes the operational reliability assessment of systems containing electronic element supplied in medicine. The analysis is based on the probability modeling through a Markov process. The identification of the system states is conducted from the system workability point of view. The possibilities for transitions from one system state to another are also analyzed. The analysis performed is illustrated by a case study of operational reliability indices estimation in regard to a type of semi-automatic blood pressure monitor. The basis of the case study are statistical data obtained regarding operational events occurred during the system operation. As a result of the analysis and the case study some prescriptions are suggested to be considered for to increase the operational system reliability.

Keywords: Reliability · Operational reliability · Reliability estimation · Markov chain

1 Introduction

The aim of this article is to seek suitable means for reliability research, evaluation and analysis of the electronic equipment used for medicine purposes and also for purposes of medical research [1–6]. In order to achieve accurate and precise results from medical tests it is necessary to have at the disposal as a high precision [7] and reliability of equipment [8–10], and suitable methods for processing of the medical statistical data as well [11].

Among activities ensuring the electronic devices reliability the acquisition, procession and analysis of data regarding these items behavior under real operational conditions play an important role. The significance of these activities in resolving reliability problems is considered in two aspects: determination, normalization and control of reliability indices for availability, reparability, and effectiveness performing function intended; predictable function; improvement of all reliability indices through detection and elimination of failures and identification of causes for their occurrence due to errors in their design, technology, operation, maintenance. The subject of a study in this paper is the analysis of the operational reliability of electronic devices composed in line with a serial reliability block diagram, referring to information collected by real data service from maintenance and repair of specific kind electronic items. The analysis of operational reliability assessment of such electronic devices is based on probability

modeling Markov processes. This provides with an opportunity for development of an algorithm of isomorphic stochastic mathematical models which consider maintenance data [12]. The possible states in terms of their workability are described.

2 Reliability Block Diagram

Consider a serial reliability block diagram [13] of a system given in Fig. 1. Here a failure of any element results in a failure of the entire system. A process in the system studied is continuous-time and owns finite state spaces. The failures distribution in the system is ordinary¹, simple, no-effect² and non-shift.

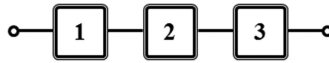


Fig. 1. Serial reliability block diagram

The parameter of failure intensity $\omega(t)$ is a major index of repairable electronic systems reliability evaluation. In its physical nature it is close to the index of failure rate used in the assessment of non-repairable items. It is defined by the limit of the probability ratio of occurrence of even just one failure during a considered period of time, to the size of this time Δt , under condition that the time period is extremely small ($\Delta t \rightarrow 0$)

$$\omega(t) = \lim_{\Delta t \rightarrow 0} \frac{P(t, t + \Delta t)}{\Delta t} \quad (1)$$

The parameter of failure intensity is a reliability index that changes its value over time. At any point in time it has a specific value, reflecting the reliability current state of the repairable items under test. Instantaneous values of $\omega(t)$ can be written in a table or can be used for a function graphical form to be drawn.

In statistics, point estimation of the failure intensity $\omega^*(t)$ is a ratio of failures per unit of time $n(\Delta t)/\Delta t$ to the number of the devices tested during a specified time interval Δt . During of a repairable electronic systems normal operation, the parameters of both failure intensity and repair rate take constant values along the time ($\omega = const, \mu = const$). The distribution of time between failures and also the distribution of time for repairs are described by an exponential law. Listed operational characteristics of the system permit its reliability modeling over time to be achieved by Markov processes.

¹ In ordinary flow appearance at the same time of two or more failures, it is considered impossible.

² The absence of in-effect in the flow means that failures at any previous time interval do not impact on the number of failures in later time intervals.

3 Markov Process

A Markov decision process is defined by a plurality of determiners $[S; X; \Gamma; q_0; Q; \pi; \delta]$, where: S is a nonempty and finite set of states; X is a nonempty and finite set of actions; $\Gamma : S \rightarrow 2^X$ is a non-empty constraint correspondence; $q_0 \in \Delta(S)$ is a probability distribution of the initial state; $Q : G_r(\Gamma) \rightarrow \Delta(S)$ is a transition probability function (for a correspondence $\Gamma : S \rightarrow 2^X$, its graph is defined by $G_r(\Gamma) \equiv \{(s, x) \in S \times X : x \in \Gamma(s)\}$); $\pi : G_r(\Gamma) \times S \rightarrow R$ is a per-period pay-off function; $\delta \in [0;1)$ is a discount factor [14]. Or loosely defined, a Markov process is stochastic process (sequence) without after-effect, i.e. such process for which the knowledge of the present state uniquely determines its future stochastic behavior, and this behavior does not depend on the past time of the process [15], i.e. satisfying the Markov property. The presentation of serial reliability block diagram by Markov process is realized using a geometric interpretation of the possible system transitions from one state to another in the graphic form describing the various system states. The possible system states described by Fig. 2 are given in Table 1:

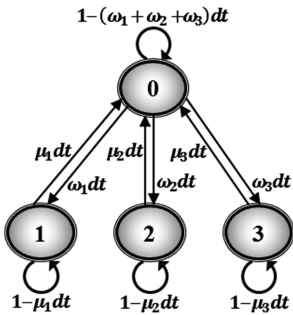


Table 1. Possible states of a system of two elements

State	Block 1	Block 2	Block 3
0	1	1	1
1	0	1	1
2	1	0	1
3	1	1	0

Fig. 2. State transition diagram of tree-elements serial system

With respect to continuous-time Markov process, the Kolmogorov equations are system of differential equations that describe the time-evolution of the transition probabilities $\{P_{ij}(t) = P(t), t \geq 0\}$ in their dependence on the initial point i .

$$\dot{P}^n(t) = \frac{dP^n}{dt} = A^n P^n(t) \tag{2}$$

where A is the transition matrix or stochastic matrix of a Markov chain. The derivation of (2) is given in [16]. The solution of these differential equations represents the transition probability from each state to another as a function of time. The probability that the chain is in the state i after n steps is the i -th entry in the vector, and its solution has the form

$$P^n(t) = e^{A^n t} P^n(0) \quad (3)$$

where $P^n(0)$ denotes probability vector which represents the starting distribution (initial distribution).

For the state transition diagram from Fig. 2 the following transition rate matrix is built

$$A = \begin{pmatrix} -(\omega_1 + \omega_2 + \omega_3) & \omega_1 & \omega_2 & \omega_3 \\ -\omega_1 & \omega_1 & 0 & 0 \\ -\omega_2 & 0 & \omega_2 & 0 \\ -\omega_3 & 0 & 0 & \omega_3 \end{pmatrix} \quad (4)$$

For state transition diagram given in Fig. 2 the following differential equations where the unknowns correspond to probability of system presence in a particular state are presented below

$$\begin{cases} P'_0(t) = -(\omega_1 + \omega_2 + \omega_3)P_0(t) + \mu_1 P_1(t) + \mu_2 P_2(t) + \mu_3 P_3(t) \\ P'_1(t) = -\mu_1 P_1(t) + \omega_1 P_0(t) \\ P'_2(t) = -\mu_2 P_2(t) + \omega_2 P_0(t) \\ P'_3(t) = -\mu_3 P_3(t) + \omega_3 P_0(t) \end{cases} \quad (5)$$

Through $P_0(t)$, $P_1(t)$, $P_2(t)$, and $P_3(t)$ are denoted the state transition probabilities of the system presence in each of its four states. If the mean time between failures $MTTF$ vastly exceeds the mean downtime MDT for any of system states, then the stationary values of the availability and unavailability of the system studied are:

$$A = P_0 \quad (6)$$

$$\bar{A} = 1 - A = 1 - P_0 = P_1 + P_2 + P_3 \quad (7)$$

where

$$\begin{cases} P_0 = \frac{\mu_1 \mu_2 \mu_3}{(\omega_1 + \mu_1)(\omega_2 + \mu_2)(\omega_3 + \mu_3)} = \frac{MTTF_I}{MTTF_I + MDT_I} \frac{MTTF_{II}}{MTTF_{II} + MDT_{II}} \frac{MTTF_{III}}{MTTF_{III} + MDT_{III}} = A_I \cdot A_{II} \cdot A_{III} \\ P_1 = \frac{\omega_1}{(\omega_1 + \mu_1)} = \frac{MDT_I}{MTTF_I + MDT_I} = \bar{A}_{nI} \\ P_2 = \frac{\omega_2}{(\omega_2 + \mu_2)} = \frac{MDT_{II}}{MTTF_{II} + MDT_{II}} = \bar{A}_{nII} \\ P_3 = \frac{\omega_3}{(\omega_3 + \mu_3)} = \frac{MDT_{III}}{MTTF_{III} + MDT_{III}} = \bar{A}_{nIII} \end{cases} \quad (8)$$

4 Case Study

As it is known, there exist two fundamental statistical approaches there for data analysis: descriptive statistics, which summarizes data from a sample using indices such as the mean or standard deviation, and inferential statistics, which draws conclusions from data that are subject of random variation (e.g., observational errors, sampling variation) [17]. For the research case it is suitable to be chosen the first of these two approaches.

Consider the Table 2 representing statistical data regarding a number of 30 pieces of semi-automatic blood pressure monitors (*SABPMs*) of identical models. Among 30 pieces *SABPMs*, an amount of approximately 43% demonstrates a failure, approximately 15% of which are due to failure in the electronic module.

Let present one *SABPM* by a serial reliability block diagram where the failure of any *SABPM* modules results in the entire *SABPM* failure. If the Markov model shown in Fig. 2 is applied to one *SABPM*, the probability states are described as follows:

- P_0 – *SABPM* is functioning;
- P_1 – a failure occurred in the electronic module;
- P_2 – a failure occurred in the automatic pressure release valve (*APRV*);
- P_3 – a failure occurred in the arm cuff.

By means of (5) can be calculated the probability states of the system in each of its four states $P_0(t)$, $P_1(t)$, $P_2(t)$, and $P_3(t)$. It is assumed that at the beginning of the study all *SABPMs* are functioning. Hence, the differential equations solution is under initial conditions as $P_0(0) = 1$, $P_1(0) = 0$, $P_2(0) = 0$, $P_3(0) = 0$ and $P_4(0) = 0$. Based on statistical data shown in Table 2, it is calculated that the study time is the average time to first failure of the *SABPMs* with duration $t = 9212,8$ h. According to informal data (statistics summarized from customers relationship), the mean downtime *MDT* including the *SABPM* downtime, repair and/or prevention time, and time spent in transit to and from the service, is $MDT = 25,9$ h. The failure intensity ω for any transition state is given by the well-known formula

$$\omega^*(t) = \frac{n(\Delta t)}{N \cdot \Delta t} \quad (9)$$

where N is the total number of *SABPMs*, and $n(t)$ is the number of failures per time unit t . Hence:

$$P_0(t) = 0.998783$$

$$P_1(t) = 0.000281$$

$$P_2(t) = 0.000842$$

$$P_3(t) = 0.000094$$

Table 2. Statistical data regarding semi-automatic blood pressure monitor

№	Product	Model	Serial number	Adoption date	Transmission date	Guarantee	Status	Comment
1	Microlife	BPA50	241301***	26.01.2015	26.01.2015	13.01.2014	Prevention	Cleaning of PRV, testing - without deviation
2	Microlife	BPA50	421301***	03.06.2015	03.06.2015	17.09.2014	Test	Testing - without deviation
3	Microlife	BPA50	241301***	03.06.2015	03.06.2015	13.01.2014	Prevention	Cleaning of PRV, testing - without deviation
4	Microlife	BPA50	491302***	04.06.2015	04.06.2015	12.06.2014	Prevention	Operating instructions testing - without deviation
5	Microlife	BPA50	511200***	03.07.2015	03.07.2015	20.09.2013	Repair	Cleaning ribbon cable, testing -without deviation
6	Microlife	BPA50	301404***	31.08.2015	31.08.2015	12.05.2015	Prevention	Operating instructions, cleaning of PRV, testing - without deviation
7	Microlife	BPA50	511200***	31.08.2015	31.08.2015	20.09.2013	Repair	Replacement crystal oscillator testing – without deviation
8	Microlife	BPA50	391401***	30.10.2015	30.10.2015	20.10.2015	Repair	Adjusting the PRV, testing - without deviation
9	Microlife	BPA50	191406***	30.10.2015	30.10.2015	13.01.2015	Test	Testing - without deviation
10	Microlife	BPA50	351302***	08.12.2015	08.12.2015	06.03.2014	Prevention	Cleaning of PRV, testing - without deviation
11	Microlife	BPA50	241301***	23.12.2015	23.12.2015	21.11.2014	Test	Unfounded claims, testing - without deviation
12	Microlife	BPA50	301403***	07.01.2016	07.01.2016	15.05.2015	Prevention	Cleaning of PRV, testing - without deviation
13	Microlife	BPA50	391400***	07.01.2016	07.01.2016	22.12.2015	Test	Testing – without deviation
14	Microlife	BPA50	391400***	07.01.2016	07.01.2016	21.12.2015	Test	Testing - without deviation
15	Microlife	BPA50	481402***	12.01.2016	12.01.2016	24.12.2015	Test	Testing - without deviation
16	Microlife	BPA50	491302***	27.01.2016	27.01.2016	12.06.2014	Prevention	Cleaning of PRV, testing – without deviation
17	Microlife	BPA50	161302***	25.02.2016	25.02.2016	21.11.2013	Repair	Soldering the battery terminals testing - without deviation
18	Microlife	BPA50	491303***	14.03.2016	14.03.2016	15.01.2016	Test	Testing - without deviation
19	Microlife	BPA50	391400***	14.03.2016	14.03.2016	17.02.2016	Test	Testing – without deviation
20	Microlife	BPA50	161505***	25.04.2016	25.04.2016	18.01.2014	Test	Testing – without deviation
21	Microlife	BPA50	301402***	27.05.2016	27.05.2016	12.06.2015	Test	Testing – without deviation
22	Microlife	BPA50	341400***	20.06.2016	20.06.2016	13.12.2015	Test	Testing - without deviation
23	Microlife	BPA50	191406***	20.06.2016	20.06.2016	13.01.2015	Test	Testing - without deviation
24	Microlife	BPA50	101400***	20.06.2016	20.06.2016	29.06.2014	Prevention	Cleaning of ADV, testing – without deviation
25	Microlife	BPA50	191403***	20.06.2016	20.06.2016	03.12.2014	Prevention	Cleaning of ADV, testing - without deviation
26	Microlife	BPA50	341400***	20.06.2016	20.06.2016	27.08.2015	Test	Testing - without deviation
27	Microlife	BPA50	481403***	20.06.2016	20.06.2016	01.04.2016	Test	Testing - without deviation
28	Microlife	BPA50	421301***	25.08.2016	25.08.2016	01.04.2014	Repair	Replacement arm cuff, testing - without deviation
29	Microlife	BPA50	241301***	31.08.2016	31.08.2016	23.01.2014	Test	Testing - without deviation
30	Microlife	BPA50	391400***	15.12.2016	15.12.2016	22.12.2015	Test	Testing - without deviation

The stationary probability of system states of the *SABPMs* for each of the four states P_0, P_1, P_2 , and P_3 can be evaluated by (8) as follows:

$$P_0 = 0,998797$$

$$P_1 = 0,000278$$

$$P_2 = 0,000833$$

$$P_3 = 0,000092$$

The availability and unavailability given by (6) and (7) is evaluated as:

$$A = P_0 = 0,998797$$

$$\bar{A} = 1 - P_0 = 0,001203$$

5 Conclusions and Final Remarks

The results and conclusions of the study conducted are based on both the data service processing and the technical characteristics of blood pressure monitors (*BPM*). As a result from the reliability analysis, it is found that the highest failure state probability value is P_2 (a failure occurred in the *APRV*), which is significantly higher in comparison with the others failure states. The lowest *SABPM* failure state probability value is the probability of a failure in the arm cuff P_3 occurred, followed by the probability of a failure occurred in the electronic module P_1 . According to preliminary empirical data collected during maintenance process, the most frequently failures ascertained are demonstrated by the arm cuff or by the inflation bulb, caused by wear and/or the rubber sheet stock degradation. The statistical data from the case studied show that from a number of 30 pieces *SABPM*, failure of such a nature arises only in one of the *SABPM* arm cuffs.

As a result of this reliability research case, the availability established is relatively higher in comparison with other electronic devices [11, 13]. It is due to the low mean downtime MDT of the *SABPMs*.

During the test procedure conducted in the service center, the electronic module accuracy of the *SABPMs* model studied does not exceed the deviation permissible value (static accuracy: pressure within ± 3 mmHg; pulse accuracy: $+ 5\%$ of the readout value).

The most frequently ascertained failures in this *SABPM* model occur in the *APRV*. The main reasons for this are: occlusion (by house dust, cloth, pet hair, etc.) of the *APRV* rubber valve, repair attempts by users or a misuse.

The measurement precision depends not only on the accuracy of the medical item, but also on the correct manner the user handles it, as well as on the user's condition. The experts suggest special recommendations related to blood pressure measuring that directly affects the measured values accuracy. In some types of cardiovascular disease

(CVD), non-specially designed medical items demonstrate an error in measurement values. Therefore, for people with such problems, specialized electronic *BPM* (different technologies as *AFIB*, *MAM*, *PAD* or *Risk Classification*) [18] or manual *BPM* is necessary. On the other hand, a number of factors affect the measurement accuracy with a manual *BPM*, especially the subjective decision factor regarding to determination of systolic and diastolic blood pressure.

Acknowledgements. The scientific research and the presented results are developed under the financial support of National Research Fund, in the frame of Technical University of Varna, named “Development of design capabilities and hardware implementation of monolithic integrated circuits and electronic systems with programmable analog matrices”, 2017.

References

1. Georgiev, T., Ivanova, M., Stoilov, R.: Recent trends in the pathogenic mechanism of osteoarthritis. *J. Rheumatol.* **3**, 2275–2276 (2013). Sofia
2. Georgiev, T., Stoilov, R., Boyadzhieva, V.L., Ivanova, M.: Hyaluronic acid—historical data, classification, mechanism of action and recommendations. *J. Rheumatol.* **2**, 1143–1149 (2014). Sofia
3. Georgiev, T., Stoilov, R., Ivanova, M.: Biomarkers in Osteoarthritis. *J. Rheumatol.* **4**, 859 (2014). Sofia
4. Georgiev, T.: A mathematical method for integration of information, which is similar in nature, for the purpose of medical research. *J. Comput. Sci. Commun.* **5**(1), 51–59 (2016). (in Bulgarian)
5. Georgiev, T., Georgiev, A.: Statistical method for the purpose of medical research based on involvement of a priori data interpretation of running experimental results. *Hi Tech J. / HiTech Agency* **1**(1), 2–9 (2017). (in Bulgarian)
6. Georgiev, T., Georgiev, A., Nikolov, N., Papanchev, T.: New opportunities for accelerated extraction of reliable and accurate information for the purpose of medical-diagnostic research. In: 2nd Scientific Forum “Innovation and Business”, Technical University of Varna, Bulgaria (2016)
7. Vasilev, R., Chikov, V.L., Gyurov, V., Nedelchev, I., Tashev, S., Krastilev, A., Nikolova, N.: System for intelligent measuring, registering and control in electrical substation. *J. E+E* **50**(5–6), 18–24 (2015)
8. Nikolov, N., Georgiev, A., Papanchev, T., Zlatev, D., Georgiev, T.S.: Reliability assessment of sensor networks. In: 2nd Scientific Forum “Innovation and Business”, Technical University of Varna, Bulgaria (2016)
9. Papanchev, T., Georgiev, A., Todorinov, G.: Analysis of parameter estimation methods for weibull distribution and interval data. *Int. J. Eng. Innovative Technol. IJEIT* **3**(9), 230–235 (2014)
10. Georgiev, A., Nikolov, N., Papanchev, T., Marinov, A., Garipova, J., Zlatev, D.: Overview of scientific researches related to practical aspects of electronic items operation reliability. In: 12th International Conference “Strategy of Quality in Industry and Education”, Varna, Bulgaria
11. Georgiev, A., Georgieva, N.: Estimation of the failureless work of micro-electronic devices via non-homogeneous priori Data’. In: Annual School Lectures Special Issue II. 21st International “Spring” Seminar on Semiconductor and Hybrid Technologies, vol. 21, issue 2, pp. 15–20. Sofia (1999)

12. Georgiev, A., Nikolov, N., Papanchev, T.: Maintenance process efficiency when conduct reliability-centered maintenance of complex electronic systems. In: 19th IEEE International Symposium on Electrical Apparatus and Technologies SIELA 2016, pp. 123–126 (2016)
13. Georgiev, A., Papanchev, T., Nikolov, N.: Reliability assessment of power semiconductor devices. In: 19th IEEE International Symposium on Electrical Apparatus and Technologies SIELA 2016, pp. 123–126 (2016)
14. Esponda, I., Pouzo, D.: Equilibrium in Misspecified Markov Decision Processes. Elsevier, SSRN 2783805 (2016)
15. Takacs, L.: Stochastic Processes Problems and Solutions. Methuen & Co Ltd., 11, New Fetter Lane, London (1960)
16. Rausand, M., Høyland, A.: System Reliability Theory: Models, Statistical Methods, and Applications, 2nd edn. Wiley, Hoboken (2005)
17. Laerd Statistics. <https://statistics.laerd.com/statistical-guides/descriptive-inferential-statistics.php>
18. Microlife Technologies. http://www.mldevelope.ch/index.php?id=hyp_technologies_ee

Sensorless Control of the High-Speed Switched-Reluctance Generator for the Steam Turbine

Pavel G. Kolpakhchyan^(✉), Alexey R. Shaikhiev,
and Alexander E. Kochin

Rostov State Transport University, Rostov-on-Don, Russian Federation
kolpahchyan@mail.ru

Abstract. The article deals with the control of switched-reluctance electrical machine acting as a generator in combination with the steam turbine. Particularities of the rotor's position sensorless control use are identified for the high-speed switched-reluctance electrical machines. The cases of work with high rotation velocity, in starting and acceleration conditions are considered. The results of electromechanical process' simulation in the considered system are set out.

Keywords: Switched-reluctance electrical machine · Electric generator · Sensorless control

1 Introduction

The use of distributed and autonomous energy generation systems on basis of the renewable power sources is one of the modern tendency of the energy engineering development. The use of the low-powered generation sets in these systems is efficient; the power should not exceed 100–200 kW. Their particularity is the combined use of different energy sources such as sunlight, wind, geothermal heat, elimination of waste etc. In this case, the efficient use of appropriate energy sources is one of the most important problems. The heat energy must be converted into electrical power. It complicates the use of the heat energy in the distributed and autonomous energy generation systems. The use of steam microturbine is efficient in these systems when the electrical generator converts the wet vapour or superheated steam into electrical power. The turbine must have the high revolutions to reduce its dimension and improve its efficiency. In this case, the generator must also have the high frequency. In this case the use of switched-reluctance electrical machine without winding and permanent magnets on the rotor as an electrical generator combined with steam microturbine is rational.

The switched-reluctance electrical machine control requires the information about rotor position. Generally, the rotor position sensor is used for this purpose. However, under the high temperature and velocity conditions its use is not advised. The maintenance of comfortable conditions of transducer performance complicates the generator's design. There are different methods to define the position of sensorless switched-reluctance electrical machine's rotor. However, there use for the high-speed generator

requires the considering of series of peculiarities. This article deals with the use of sensorless control of the high-speed switched-reluctance generator for the steam turbine.

2 Known Research in the Field of Sensorless Control of Swithed-Reluctace Electrical Machines

There are different principles of rotating switched-reluctance electrical machines sensorless control, which use different informative characteristics of rotor position determination [1–6]. They are mostly intended on the traction mode and they can not be used for high speed generator.

Essentially all ways of sensorless rotor position determination is based on the phase inductance dependence upon the rotor position. The inductance is maximum when the rotor tooth is under the stator tooth (aligned position) and it is minimum when the rotor tooth is between the stator teeth (unaligned position). The magnetic saturation influences the difference between the maximum and minimum of the inductance but it does not change the type of the dependence. Consequently, we can use the indirect measurement of the switched-reluctance electrical machine phase inductance to determinate the moving element position.

Different realizations of this method estimate by different ways the inductance of one phase or several ones of the switched-reluctance electrical machine work [7–10]. This method is based on the electrical machine inactive phase exploration and the current's determining in this phase. The exploration is made by fast pulses of equal duration. The amplitude of the current pulse is inversely proportional to its inductance when the voltage pulse duration is much less than the phase time constant. Hence, we can determine the rotor passes an unaligned position for the exploration phase by the registration of the maximum amplitude of the current pulse.

They feed test pulse during all the time when the rotor passes the unaligned position. The rotor position accuracy depends on the test pulse frequency.

The use of the master pulse as a test pulse is one of the variety of this method. The realization of this method is possible in a traction and generator mode.

The use of this method is limited. The test pulse time depends on the current amplitude. The current amplitude must be sufficient for the precise rotor position determination. At low speeds, the necessary pulse time is insignificant with due regard to the time of all measurements. As the frequency increases, the number of monitoring pulses decreases. Their number decrease reduces the rotor position accuracy. Therefore, at high speed the use of this method is limited. It needs the use of additional methods of rotor position verification. In this case, we can use two accuracy-improving methods. The first method measures the current rate of rise on the voltage pulse supplying. The second one measures the frequency of voltage pulses that forms the phase current before the passage in the single-pulse mode of control.

3 Design of the High-Speed Switched-Reluctance Generator for the Steam Turbine

We have designed the laboratory bench for the purpose of the determining the technical feasibility of the SRM sensorless control methods. The laboratory bench consists of high-speed SRM and steam microturbine. The microturbine is designed for rated speed of 12 000 rev./min. and rated power of 35 kW. Figure 1 shows the sketch of electrical machine magnet system. The main dimensions and proportions of the generator are following:

Teeth number on the stator/rotor	6/4
Stator outside diameter	$D_{1out} = 200$ mm
Stator tooth axis inside diameter	$D_1 = 100.4$ mm
Air gap diameter (rotor outside diameter)	$D_2 = 100$ mm
Air gap	$\delta = 0.2$ mm
Rotor inside diameter	$D_{2in} = 40$ mm
Magnetic circuit active length	$l_\delta = 200$ mm
Stator wind turns number (per one coil)	15
Stator winding peak current	$I_{f\max} = 100$ A

Stator and rotor stacked magnetic circuits are made from the electrotechnical steel 0.35 mm in thickness. Air gap increases of 0.1 mm to the stator teeth edges to decrease the saturation influence when the rotor tooth edge passes the stator tooth edge. For this purpose, the stator teeth edges are rounded.

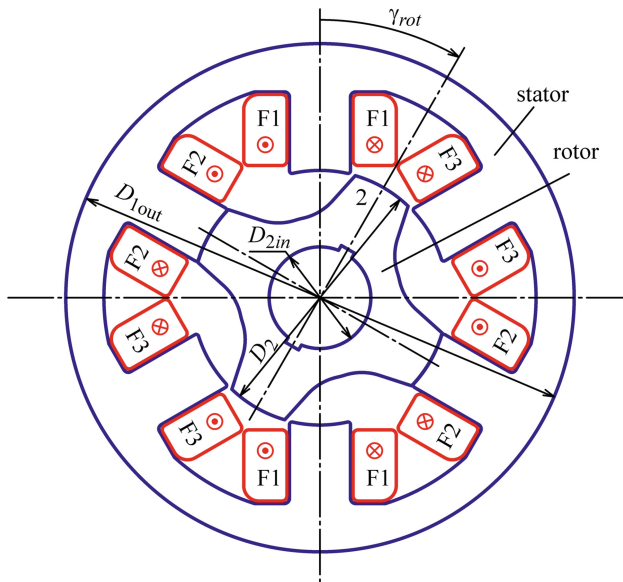


Fig. 1. Magnetic system of high-speed switched-reluctance electrical generator

The field theory methods have allowed to calculate the Weber-Ampere characteristics of the electrical machine stator phases and the air gap torque at different rotor and stator relative positions. We used software package FEMM (Finite Element Method Magnetic © David Meeker) for calculations. We solved series of magnetostatic problems. Figure 2 shows the stator phase flux linkage and powering torque dependence on the current and rotor angle to turn.

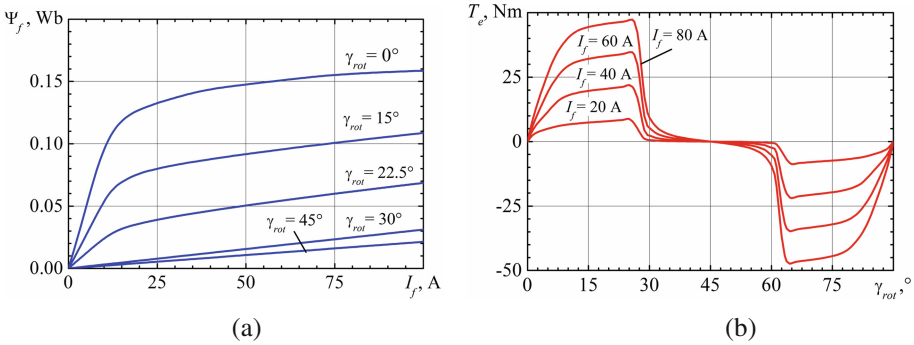
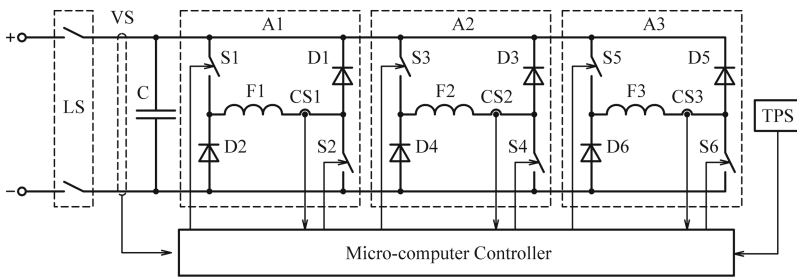


Fig. 2. The stator phase flux (a) and powering electromagnetic torque (b) dependence

The electronic voltage inverter converts the electric energy of the electric generator. Each SRM phase is connected to individual autonomous half bridge voltage inverter.

Each inverter consists of two IGBT transistors and two diodes. The converter powers DC link. Each phase has current sensor. The voltage sensor is installed in the DC link because the generator mode is the main SRM mode. The control of each phase is independent. The control computer receives information from the current and voltage sensors and it determines on-off power switches. Figure 3 shows structure and function scheme of the SRM control system.



SRM – switched-reluctance motor; TPS – rotor position sensor; A1, A2, A3 – phase modules of asymmetric half-bridge converter; S1 ... S6 – power switches (IGBT); D1...D6 – power diodes; VS – voltage sensor; CS1, CS2, CS3 – phase current sensors; LS - load switch

Fig. 3. Structural and functional scheme of switched-reluctance electric machine control system

4 Sensorless Control of the High-Speed Switched-Reluctance Generator Problem Formulation

The SRM constructive peculiarity is phase inductance direct relation to the rotor and stator collocation. This effect can be used for the rotor position indirect determination. This method of rotor position determination is the most accepted. The significant influence of the magnet system saturation on the inductance must be considered. The under study electric generator is EM having a high-level inductance saturation. It is provoked by the necessity of minifying the rotor dimension for decrease the rotor moment of inertia and improve its strength. In aligned position when the stator current is maximum, the inductance decreases by a factor of 3 over the inductance in unsaturated state. Figure 4 shows phase inductance dependence on the rotor angle to turn with different current values.

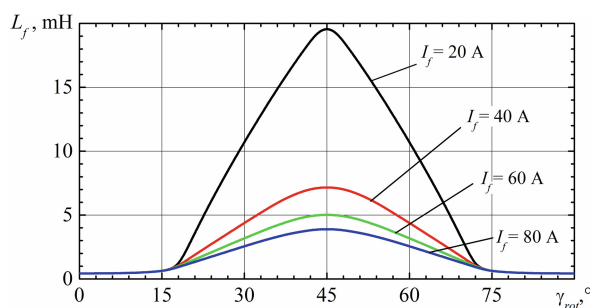


Fig. 4. Phase inductance dependence on the rotor angle to turn with different current values

The type of applying analog-to-digital converter determines the frequency of test pulses that are used to analyze the phase inductance. The conversion time is about 2–3 ms is typical. The phase current pulse frequency with used correlation of stator and rotor teeth must account for 800 Hz when the revolution rate is 12 000 rpm.

The test pulsing is realizing in the absence of phase current. The measurement performance can be realized only in pulse repetition quarter-period [2, 9–11]. Another condition of pulsing is the inductance change depending on the rotor position. Figure 5 shows that the phase inductance change takes place when the rotor angle to turn is between 20° and 45°.

For the case under consideration the time period of test pulses is about 300 ms. During this period of time the analog-to-digital converter can make 100 to 120 measurements. In this case, their number will not exceed 6 or 8 test impulse on the measurement interval. It lets to determine the rotor position when the angle to turn is 4 to 6°. This rotor position accuracy is not sufficient for the control.

When the power pulse is used to determine the position of the rotor, the position determination accuracy is 0.5 to 1°. This method of rotor position measurement is preferable on high rotation speed.

5 Mathematical Model of the Switched-Reluctance Electrical Machine

We worked out the mathematical model (MM) to estimate the accuracy of elaborated high speed SRM control method. MM comprises the SRM method, electric energy converter and control system. We took into account the particularities of solvable problem [8, 12, 13] and we admitted following assumption:

- SRM phases has disintegrated magnetic circuits;
- each phase processes are accounted separately.

With admitted account, the following equation governs the SRM phase electro-magnetic processes [14–16]:

$$\frac{d\Psi_{f1,2,3}}{dt} = U_{f1,2,3} - I_{f1,2,3}(\Psi_{f1,2,3}, \gamma_{rot})R_{f1,2,3}, \quad (1)$$

where, $\Psi_{f1,2,3}$, $U_{f1,2,3}$ and $R_{f1,2,3}$ are flux linkage, voltage and phases resistance respectively; $I_{f1,2,3}(\Psi_{f1,2,3}, \gamma_{rot})$ is phase current, it depends on phase flux linkage and rotor position.

For the SRM under consideration we determinate the phase flux linkage dependences on the flowing current.

With admitted account, the equations describing processes in the DC link can be written as follows:

$$\begin{aligned} \frac{dI_0}{dt} &= \frac{1}{L_0}(E_0 - R_0I_0 - U_c); \\ \frac{dU_c}{dt} &= \frac{1}{C}(I_0 - (I_{d1} + I_{d2})), \end{aligned} \quad (2)$$

where E_0 , L_0 , R_0 are voltage, inductance and DC linkage active resistance respectively; C , U_c are DC linkage capacity at the converter input and voltage.

The phase voltage is formed by the way to ensure the forming of current pulse with specified value and time.

The start and end angles α_0 and α_1 which are count off from phase coincidence defines current phase time and phase of squared shape with assigned amplitude

Equations (1) and (2) are MM describing processes in SRM under consideration. We have designed the SRM processes with the use of sensorless control. We also used the following values:

- active resistance and DC link inductance are $R_0 = 0,1 \text{ Om}$; $L_0 = 0,001 \text{ H}$;
- DC link condenser capacitance $C = 5000 \text{ uF}$;
- DC link voltage $E_0 = 595 \text{ V}$;

6 Simulation Results and Analysis

The nominal speed mode is important for research of variants of sensorless SRM rotor position determination. The moments of on-off power keys can be determined by the rotor position. The most efficient operational phase energy output is the specified current supply in phase when rotor is in the position corresponding to the generation interval beginning of this phase (see Fig. 4). For this purpose, the positive voltage pulse (excitation pulse) is applied to the phase in some advance. For this purpose, the both power keys are closed (for example, for phases A - S1, S2). When rotor is in the position of the generation beginning, the power keys are closed and the generation process begins. To limit the uncontrolled current increasing when it reaches the specified value one of power keys is opened. In this moment the phase closed-circuit fault contour takes place through the closed power key and diode. In this mode, EM control is performed in a single-pulse mode.

Figure 5 shows the modeling results of SRM electromagnet process with nominal rate of rotation. Pulses parameters of feed voltage are calculated in such a way as phase current reaches the value of 100 A to the generation beginning. In this case there are not the pause between the actuating pulse and generation beginning when phase is in the closed-circuit fault mode. Figure 6 shows the voltage, current, inductance and electromagnet moment dependences.

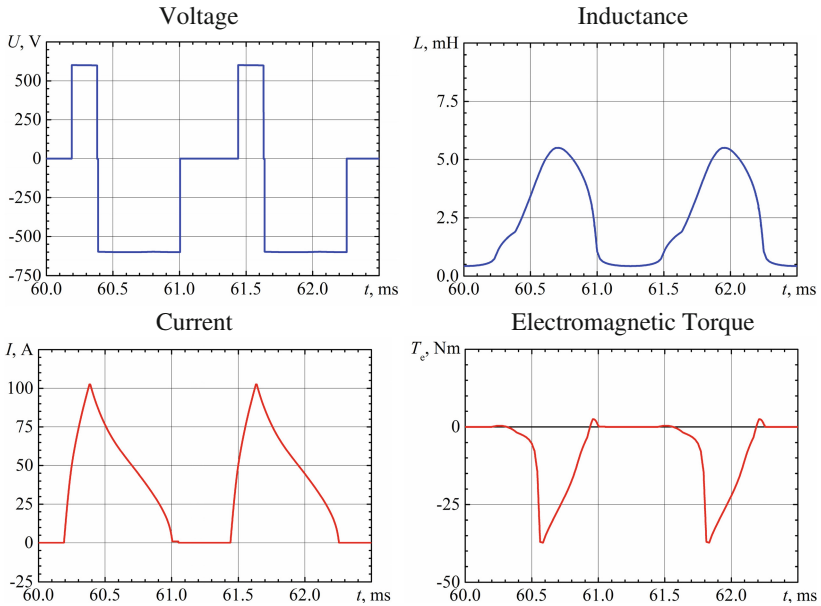


Fig. 5. Mathematical modeling results of processes in a switched-reluctance-flux generator at a nominal rotation speed

In single-pulse mode the generation it not controlled. SRM control is carried out by changing the parameters of the excitation pulse. Its on-off moments depend on rotor position. Therefore, the accuracy of position determination is important for the effective EM operation. If the excitation pulse is early, it displaces towards the phase inductance decreasing. In such a case, the phase current increases with greater intensity, the phase places in the closed circuit fault mode. The pause between the excitation pulse end and the generation beginning depends on discrepancies between estimated and real rotor position. The pause value can be used for the correction of rotor position determination.

If the excitation pulse is early is retarding about the estimated time, it displaces towards bigger inductance and the pulse time is not sufficient for the current rise to the design value. Therefore, the current decreasing in the moment of excitation pulse end shows that the rotor position determination is made with a time lag from the real value. Figure 6 shows the dependences of phase current for the cases of coincidence, advance and lag of rotor position determination.

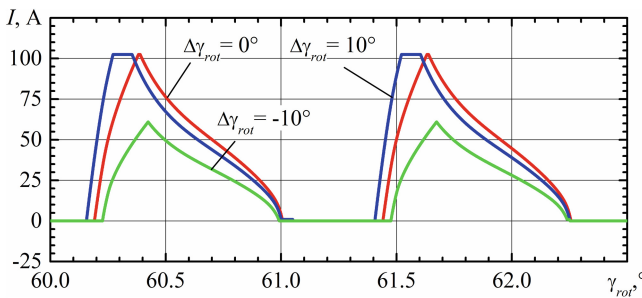


Fig. 6. SRM phase current dependences for the cases of coincidence, advance and lag of rotor position determination

The dependences on the Fig. 6 confirm the possibility of using the elicited characteristics for the purpose of error estimation of rotor position determination. The obtained curves comparison reveals the following feature. The phase current curve in the generator mode has knee point that corresponds to phase inductance maximum. When the phase current amplitude is constant, as Fig. 6 shows, it corresponds to aligned rotor and stator position. When the current decreases the magnet system saturation decreases, the phase inductance reaches its maximum on the bigger angle to turn of rotor.

Use of the described feature requires current control its first and second derivative. When using common types of ADC, the measurement data will have error of 5 to 10%. Therefore, we propose to use the third order Kalman filter for filtering the current signal in the high speed SRM control system.

The dependence that uses phase current model is based on the equation [13–15]:

$$\frac{dI_f}{dt} = \frac{1}{L_f(\gamma_{rot}, I_f)} \left(U_f - R_f I_f - I_f \omega_{rot} \frac{\partial L_f(\gamma_{rot}, I_f)}{\partial \gamma_{rot}} \Big|_{I_f = \text{const}} \right).$$

Figure 7 shows the SRM process analysis results when using the sensorless control realizing rotor position determination principles described above. The calculations were carried out under the following conditions. EM rotates at rated speed. The excitation pulse has the same parameters as for the case considered earlier. Stator phase currents are measured by an ADC for 5 μs and have an error of 10% distributed according to the normal law. At the initial moment, rotor position determination differ by 5° from the real position. The process of the rotor position determination correction is shown. The analysis of the obtained results showed the effectiveness of the proposed filtering method for measuring the phase currents. The proposed algorithm shows the correction effectiveness of rotor position determination in SRM single-pulse mode.

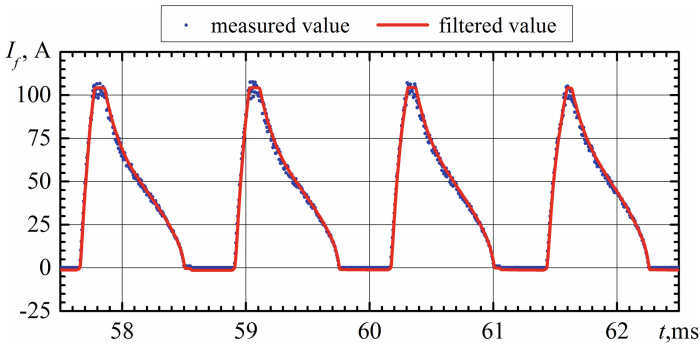


Fig. 7. Correction of rotor position evaluation in single-pulse operation mode of the switched-reluctance electrical machine

7 Conclusions

On the high rate of rotation speed without a rotor position sensor the use of methods based on the test pulse delivery in inactive phase is not rational, as method resolution is not sufficient for the effective generator control. In this case, the parameters control of the current main pulse is rational.

The SRM control in the generation mode is performed by changing the delivery time and the voltage pulse (excitation pulse) time. The excitation pulse produces current by the generation beginning. The delivery moment and the excitation pulse time are determined by the rotor position. Therefore, the effective generation control is possible only with the accurate rotor position determination.

To correct the rotor position, such features can be used: the pause between the excitation pulse and the beginning of the generation (the determination outrips the

real rotor position); the current decreasing by the generation beginning (the determination lags the real rotor position). The current knee of curve on the generation interval can be used to specify the rotor position determination. The knee of curve corresponds to the phase inductance maximum. It is observed at the same rotor position. The use of these features lets create an effective algorithm of the rotor position sensorless determination of high-speed SRM.

References

1. Mvungi, N.H., Stephenson, J.M.: Accurate sensorless rotor position detection in an SR motor. In: Proceedings European Power Electronics Conference, vol. 1, pp. 390–393 (1992)
2. Borges, T.T., de Andrade, D.A., de Azevedo, H.R., Luciano, M.: Switched reluctance motor drive at high speeds, with control of current. In: IEEE International Electric Machines and Drives Conference Record, Milwaukee, WI, pp. TB1/12.1–TB1/12.3 (1997)
3. Ye, J., Bilgin, B., Emadi, A.: An extended-speed low-ripple torque control of switched reluctance motor drives. *IEEE Trans. Power Electron.* **30**(3), 1457–1470 (2015)
4. Ye, J., Bilgin, B., Emadi, A.: An offline torque sharing function for torque ripple reduction in switched reluctance motor drives. *IEEE Trans. Energy Convers.* **30**(2), 726–735 (2015)
5. Torrey, D.A.: Switched reluctance generators and their control. *IEEE Trans. Ind. Electron.* **49**(1), 3–14 (2002)
6. Shao, B., Emadi, A.: A digital PWM control for switched reluctance motor drives. In: IEEE Vehicle Power and Propulsion Conference, Lille, pp. 1–6 (2010)
7. Uygun, D., Bal, G., Sefa, I.: Linear model of a novel 5 - phase segment type switched reluctance motor. *Elektronika ir Elektrotechnika* **20**(1), 3–7 (2014)
8. Do, V.L., Minh, C.T.: Modeling, simulation and control of reluctance motor drives for high speed operation. In: Proceedings of Energy Conversion Congress and Exposition, ECCE 2009, pp. 1–6. IEEE, San Jose (2009)
9. Cai, J., Deng, Z.: A position sensorless control of switched reluctance motors based on phase inductance slope. *J. Power Electron.* **13**(2), 264–274 (2013)
10. Kai, X., Qionghua, Z., Jianwu, L.: A new simple sensorless control method for switched reluctance motor drives. In: Proceedings of the Eighth International Conference on Electrical Machines and Systems, ICEMS 2005, vol. 1, pp. 594–598 (2005)
11. Kolpakhchyan, P., Kochin, A., Shaikhiev, A.: Emergency generator design for the maritime transport based on the free- piston combustion engine. *OUR SEA* **62**(2), 78–84 (2015)
12. Chi, H.-P., Lin, R.-L., Chen, J.-F.: Simplified flux-linkage model for switched reluctance motors. *IEE Proc. Electr. Power Appl.* **152**(3), 577 (2005)
13. Fahimi, B., Suresh, G., Mahdavi, J., Ehsami, M.: A new approach to model switched reluctance motor drive application to dynamic performance prediction, control and design. In: 29th Annual IEEE Power Electronics Specialists Conference, Fukuoka, vol. 2, pp. 2097–2102 (1998)
14. Krna, P.: Sensorless control of the SRM using nonlinear observer. Ph.D. thesis, 115 p., VSB Technical University of Ostrava (2013)
15. Kolpakhchyan, P.: Sensorless control of the linear switched-reluctance motor of emergency power generator. In: Kolpakhchyan, P., Shaikhiev, A., Kochin, A. (eds.) Book of Abstracts VII International Scientific Conference “Transport Problems 2015”, Proceedings, Katowice, Poland, 23–26 June 2015 (CD). Faculty of Transport, Silesian University of Technology, Katowice (2015)

Design and Implementation of High Speed AES on a RISC Microcontroller

Plamen Stoianov^(✉)

Department of Communication Engineering and Technologies,
Technical University of Varna, Varna, Bulgaria
pl_stoianov@tu-varna.bg

Abstract. Advanced Encryption Standard (AES) symmetric block cipher is widely used in cryptographic applications. It is extremely efficient on many different platforms, ranging from 8-bit microcontrollers to 64-bit processors. This paper presents fast software implementation to an 8-bit RISC microcontroller, typical for Smart Cards, sensor nodes etc. Their performance, including memory size and encryption time, was measured through simulation and the results are presented and compared to results obtained in other implementations.

Keywords: AES · Microcontroller · Fast software · Embedded security

1 Introduction

Plenty of real problems of software technologies are solved by using cryptographic methods. Task of cryptography is transformation from plaintext to ciphertext by using the cryptographic algorithm and unique recovery of the original text. The process of transformation into ciphertext is called encryption while inverse process of recovery - decryption. In both the processes a key for encryption and a key for decryption are used. If these two keys are matched, the algorithm is called symmetric or an algorithm with a secret key. If both the keys are different, the algorithm is asymmetric or an algorithm with a public key [1]. The most widely used symmetric algorithm is DES (Data Encryption Standard). The algorithm transforms 64-bit plaintext to 64-bit ciphertext. The key is 64-bit where 56 bits are used directly in the algorithm, and every 8th bit is recommended for verification on parity at storage and exchange.

Due to the low dimensionality of key and conducted successful attacks against DES, in 1997, NIST (National Institute of Standards and Technology) initiated an exchange of this standard.

Further DES used permutations and rotations, which suggests better realization of hardware. In 2000, the algorithm Rijndael was chosen, developed by Belgian cryptographers. The next year it was standardized like AES (Advanced Encryption Standard) by FIPS PUB 197 [3]. This algorithm has an effective structure of transformation using basic arithmetical operations and is suitable for software implementation of wide range of processors. Equally comfortable for realization as 8-bit and the 64-bit processors. It is able to encrypt data of different capacity and use keys of different dimensionality as well. It easily increases the dimensionality of the input block of data

(Increase of number of columns) and the number of stages without changing the actual algorithm. The difference between Rijndael and AES, is only in the class of the block of data processed. The algorithm Rijndael enables processing of 16, 24 or 32 bytes while the standard AES determines input block of only 16 bytes (128 bits). Until now no successful attacks against AES have been reported. An exception is the use of redundant options, i.e. in fewer steps than those provided in the standard [4]. The purpose of all software implementations is to accelerate the process of encryption and decryption, with a possible reduction of the program size. For the realization of AES, a PIC18 microcontroller company MICROCHIP is selected.

2 AES Algorithm

The mathematical basis of AES is field theory. Actions with polynomials in Galois Field $GF(2^8)$ are carried out. Part of the operations are performed with bytes, while the rest use 4-byte words. Data are presented as polynomials of grade less than 8 and coefficients in $GF(2)$. The intermediate results of processing are called states and are presented like a square matrix of 4 rows and 4 columns.

Every byte of a state is marked as $s_{r,c}$, where r is a row and c is a column from 0 to 3. The data are processed in 10, 12 or 14 uniform rounds - N as number depends on the class of the key - 128, 192 or 256 bits. Depending on the key, the standard identifies three options: AES-128, AES-192 and AES-256. Each round includes four transformations - SubBytes, ShiftRows, MixColumns, AddRoundKey and further for the preparation of subkeys for each step – ExpandKey.

The algorithm is implemented in the following sequence:

```

Input = State , Key
      AddRoundKey(State, Key)
      ExpandKey(Key)
For round = 1 to  $N_r - 1$ 
      SubBytes(State)
      ShiftRows(State)
      MixColumns(State)
      AddRoundKey(State,Key)
      ExpandKey(Key)
End for
      SubBytes(State)
      ShiftRows(State)
      AddRoundKey(State,Key)
Output = State

```

The final stage is carried out separately as it does not perform mixing columns. Within the individual steps and by getting subkeys the following actions are implemented:

- **SubBytes** – to obtain the output value two separate calculations are carried out: multiplicative inverse and affine transformation. If $a(x)$ is an input polynomial, it

multiplicative inverse $a(x)^{-1}$ it is through $a(x).a(x)^{-1} \equiv 1 \pmod{m(x)}$. Use irreducible binary polynomial of degree 8: $m(x) = x^8 + x^4 + x^3 + x + 1$.

The dimensionality in the field (2^8) elements pre-calculation of values and memory storage is appropriately given as a table with dimensions of 256 bytes. This leads to a higher speed of implementation and less volume of storage used. By the execution of the related transformation every bit of the output value is determined by the amount mod2 between certain bits of the input value and a previously set constant. At multiplicative inverse, a table is used, therefore its values can be recalculated under the terms of the affine transformation. Thus both operations are executed through a single indexing table. For a process of decryption an additional table is required. For the process of retrieval of a table a preliminary entry register TBLPTR is necessary, therefore the replacement of one byte takes 6 cycles of the microcontroller. For one row or column it takes 24 cycles, and for the entire matrix - 96 cycles.

- **ShiftRows** – performed rotation of words in different rows of the matrix. The zero row of each stage remains unchanged, while the first, second and third row of the matrix are rotated to the left at 1, 2 and 3 bytes. The steps SubBytes and ShiftRows can unite, wherein abbreviated instructions for re-reading and writing. As a result, the overall turnaround time requires 96 cycles as in SubBytes.
- **MixColumns** – each column of the matrix is represented as a 4 membered polynomial $s(x)$ with coefficients which are elements of the field GF(2). The new values $s'(x)$ are obtained after multiplying the $s(x)$ by the polynomial specified in the standard:

$$a(x) = \{03\}x^3 + \{01\}x^2 + \{01\}x + \{02\} \tag{1}$$

The piece is reduced modulo $(x + 1)$ i.e.:

$$s'(x) = a(x).s(x) \pmod{x^4 + 1} \tag{2}$$

In the process of decryption (InvMixColumns) are used inversed polynomial:

$$a^{-1}(x) = \{0B\}x^3 + \{0D\}x^2 + \{09\}x + \{0E\} \tag{3}$$

defined by $a^{-1}(x).a(x) \equiv 1 \pmod{x^4 + 1}$

The operations in (2), with known values of $a(x)$ (1) can express matrix:

$$\begin{bmatrix} s'_{0,c} \\ s'_{1,c} \\ s'_{2,c} \\ s'_{3,c} \end{bmatrix} = \begin{bmatrix} 2 & 3 & 1 & 1 \\ 1 & 2 & 3 & 1 \\ 1 & 1 & 2 & 3 \\ 3 & 1 & 1 & 2 \end{bmatrix} \cdot \begin{bmatrix} s_{0,c} \\ s_{1,c} \\ s_{2,c} \\ s_{3,c} \end{bmatrix} \text{ where } c = 0 \div 3 \text{ are columns} \tag{4}$$

After multiplication, the new values of column are:

$$\begin{aligned}
 s'_{0,c} &= 2.s_{0,c} \oplus 3.s_{1,c} \oplus s_{2,c} \oplus s_{3,c} \\
 s'_{1,c} &= s_{0,c} \oplus 2.s_{1,c} \oplus 3.s_{2,c} \oplus s_{3,c} \\
 s'_{2,c} &= s_{0,c} \oplus s_{1,c} \oplus 2.s_{2,c} \oplus 3.s_{3,c} \\
 s'_{3,c} &= 3.s_{0,c} \oplus s_{1,c} \oplus s_{2,c} \oplus 2.s_{3,c}
 \end{aligned} \tag{5}$$

Coefficients of used polynomial are different by only 1, and therefore dependence could be used: $c.s_i \oplus (c + 1).s_j = c.(s_i \oplus s_j) \oplus s_j$. If pre-calculate the amount $\text{Temp} = s_{0,c} \oplus s_{1,c} \oplus s_{2,c} \oplus s_{3,c}$ then the value of the first byte from column can be represented by $s'_{0,c} = (s_{0,c} \oplus s_{1,c}).2 \oplus s_{0,c} \oplus \text{Temp}$. Multiplication operations are reduced while maintaining the number of summation on mod2.

For finding the four bytes of the column 32 cycles are needed, consequently for all 16 bytes of the matrix 128 cycles are needed.

- **AddRoundKey** – each byte of matrix sums in mod2 with the corresponding byte of the current subkey to obtain the new state. Reading and summation in mod2, which takes 32 cycles for all 16 bytes, is required. In the loop body, the execution of AddRoundKey immediately after MixColumns and therefore the two steps can be combined. After receiving the new value of mixing columns, it is summed with the corresponding byte of the key and recorded in the matrix as a new state. As a result of unification of the two steps are cut instructions for reading, and overall execution time from $128 + 32$ cycles is reduced to $128 + 16 = 144$ cycles.
- **ExpandKey** – for each stage a different key is used derived from the primary through conversions. As by the data, the area of the key as a matrix of 4 rows and 4 columns is presented. After each execution of the AddRoundKey (except for the last stage), the 4th row is rotated by one byte into left, and SubBytes in the same table is carried out, the same as for the data. The first byte is summed with a constant, which is different for the different stages. It sums on mod2 4th to 1st, 1st to 2nd, 2nd to 3rd and 3rd to 4th line. Thus subkeys for each subsequent stage are obtained. The time required each step to implement is 53 cycles. They could be reduced if the replacement of the bytes is performed by a table in the data memory, instead of the program memory. Another way to accelerate is by removal of ExpandKey out of data processing. By any change of the user key, a calculation of all subkeys is made in advance. The values are stored in the RAM and by the process of encrypting are only read, and not calculated. Many blocks are encrypted with the same key, whereby the total execution time is being reduced. The disadvantage is occupying additional 160 bytes of RAM for all subkeys.

Decryption is performed in a reverse order. First, the rotation of the lines to the right is done (when the encryption is left), then replacing the bytes according to an inverse table is carried out. It is possible to use the same table, but this would increase the decryption time. The matching search is slower and depends on the time of the input data. A high level of performance is achieved by the addition of a new table and

an increase in the program memory further by 256 bytes. Another difference is the use of an inverse polynomial with coefficients other than the coefficients of the polynomial in encryption.

3 Experimental Results

The results (E) of a software implementation of the encryption algorithm AES-128 are shown in Table 1. The number of cycles required for the execution of certain decisions is compared. The third and sixth columns show the number of cycles required to perform the encryption and decryption process. This is a key indicator because it determines the speed of data processing. There are variants with pre-calculation of the subkeys, and then the encryption is performed at a higher speed. This pre-calculation is performed only when changing the user key, and then many blocks are encrypted with the calculated subkey. A disadvantage is lending additional 160 B of data memory. At the 4th and 7th columns an amount of memory is required to accommodate the program. Proposal (A) is the creator of the algorithm AES, developed on the basis of a microcontroller INTEL. The first option is optimized for faster implementation of encryption. Suggestions (B), (C) and (D) are based on AVR microcontrollers company ATMEL. Within (C) three versions have been developed depending on the number of cycles and the dimensionality of the program. In the first version, less decryption cycles are required, with a greater program volume. The program features four tables of multiplication of the coefficients of the polynomial used, which are employed by **MixColumns**. The table is presented with the option Shut up cycles. Suggestion (E) is based on the PIC18 Microcontrollers Company MICROCHIP. The program (E) developed performs the encryption of 16 byte block in less cycles, mainly due to the faster calculation of polynomials in step MixColumns. Another reason for the high level of performance is not using subroutines. They reduce the volume of the program, but require additional 4 cycles of execution. Opportunity to reduce the required number of cycles is by transferring the replacement table in a data memory. Feature of the microcontroller used is that extracting byte of program memory requires 5 cycles, while

Table 1. Comparative results for the implementation AES-128

	Encryption			Decryption		
	Precompute [cycles]	Encrypt [cycles]	Code [bytes]	Precompute [cycles]	Decrypt [cycles]	Code [bytes]
(A) Daemen Rijmen [5]	–	3168	1016	–	–	–
	–	4065	768	–	–	–
(B) Rinne [6]	–	3766	–	–	4558	–
(C)Poettering [7]	756	2474	1102	4977	3441	2352
	756	2739	1100	756	3579	1490
	–	4059	–	–	4675	–
(D) Plos [8]	–	3084	2158	–	4505	–
(E) This work	782	2341	1159	824	3502	1697
	–	2866	1185	–	–	–

index reading of a data memory runs for 3 cycles. Replacement table is being used 16 times in SubByte, suggesting 320 cycles less at options to pre calculations. The achieved reduction of cycles of encryption is at the expense of increased program memory with 768B in the provisional calculations and 512 cycles.

4 Conclusion

The article examines the widely used symmetric algorithm AES. Different steps in encryption are analyzed to find opportunities for faster execution. The main indicator is the number of cycles required for the microcontroller to implement the encryption and decryption. A variant with prior calculation of the required subkeys is developed, with the number of cycles for execution reduced by 10%. It is particularly efficient for encrypting block data with the same key. An additional reduction of 320 cycles is possible if within the preliminary calculations, the substitution table is saved in the RAM. The software solution proposed is compared to other popular programs. Simulations prove the efficiency of the program and the required number of cycles of the microcontroller.

References

1. Rankl, W., Effing, W.: Smart Card Handbook. Wiley, New York (2010)
2. Daemen, J., Rijmen, V.: AES Proposal: Rijndael, AES Algorithm Submission (1999). <http://csrc.nist.gov>
3. FIPS PUB 197: Advanced Encryption Standard (AES), Federal Information Processing Standards (FIPS), NIST, US Department of Commerce (2001)
4. Biryukov, A., Dunkelman, O., Keller, N., Khovratovich, D., Shamir, A.: Key recovery attacks of practical complexity on AES-256 variants with up to 10 rounds. In: Gilbert, H. (ed.) EUROCRYPT 2010. LNCS, vol. 6110, pp. 299–319. Springer, Heidelberg (2010). doi:10.1007/978-3-642-13190-5_15
5. Daemen, J., Rijmen, V.: The block cipher rijndael. In: Quisquater, J.-J., Schneier, B. (eds.) CARDIS 1998. LNCS, vol. 1820, pp. 277–284. Springer, Heidelberg (2000). doi:10.1007/10721064_26
6. Rinne, S., Eisenbarth, T., Paar, C.: Performance analysis of contemporary light-weight block ciphers on 8-bit microcontrollers. In: Software Performance Enhancement for Encryption and Decryption (SPEED 2007), pp. 33–42. Amsterdam (2007)
7. Poettering, B.: AVRAES: The AES block cipher on AVR controller. <http://point-at-infinity.org/avraes/>
8. Plos, T., Groß, H., Feldhofer, M.: Implementation of symmetric algorithms on a synthesizable 8-bit microcontroller targeting passive RFID tags. In: Biryukov, A., Gong, G., Stinson, Douglas R. (eds.) SAC 2010. LNCS, vol. 6544, pp. 114–129. Springer, Heidelberg (2011). doi:10.1007/978-3-642-19574-7_8

An Algorithm for Generating Optimal Toolpaths for CNC Based Ball-Burnishing Process of Planar Surfaces

Stoyan Slavov^(✉)

Technical University of Varna, Varna, Bulgaria
sdslavov@tu-varna.bg

Abstract. This paper presents an algorithm for generating optimal toolpaths for CNC based ball-burnishing process of planar workpieces having burnished areas with rectangular or circular shape. The proposed algorithm firstly calculates the 2D coordinates of the points from a polyline, which describes the needed complex toolpath of the ball-tool to obtain a regular shaped roughness on burnished areas. Then Boolean constraints conditions are used to restrict the generated sub-toolpaths only within ball-burnishing area of the workpiece. Finally, all trajectories are connected in one single continuous curve (i.e. polyline in DXF file format) which represents the optimal toolpath, depending on the shape and the dimensions of the burnishing area. The obtained toolpath from proposed generation strategy most resembles the toolpath, obtained from the classical setup for planar vibrations-assisted ball-burnishing method, using milling machines without CNC control. The purposed algorithm has comparatively simple implementation, minimizes the blank movements of the ball tool, and provides high accuracy of the burnished planar surfaces.

Keywords: Ball-burnishing process · Toolpath · Manufacturing · Generation · CAD-CAM · CNC · Milling machines

1 Introduction

It is well known that the cold-forming processes such as ball-burnishing [1–4, 6, 7, 10] most often applies for improvement of physical and mechanical characteristics in the surface layer of the functional surfaces of different types of workpieces such as shafts, slid-guides, heavily loaded sliding contact pairs, rollers, etc. Depending on the properties of the material from which the workpiece has been made and regime parameters of the process, some significant improvements in the operational characteristics of burnished details can be obtained, such as increasing the wear resistance, fatigue life, corrosion resistance etc. In certain cases, vibrations-assisted ball-burnishing process applies to obtain some specific textures of roughness, which under certain values of the regime parameters may have different patterns [2, 7]. These patterns can consist of abutting or mutually intersecting grooves (i.e. plastically deformed traces that remains after passing the ball tool), as can be seen in Fig. 1a, b, c, textures of cells with a regular shape (see Fig. 1d, e), or textures with completely overlapping grooves (see Fig. 1f). For obtaining such patterns, it is necessary the ball-tool to follow a near to

sinusoidal trajectory (see Fig. 2c) and to provide its overlay within the ball burnishing surface (face) of the workpiece.

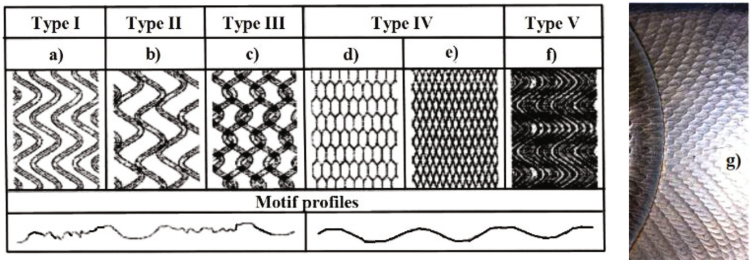


Fig. 1. a–f, Different types of traces overlays after vibrations-assisted ball-burnishing process with different regime parameters; (g) An image of regular microshape roughness from Type IV.

Figure 2a shows a technological setup for vibrations-assisted ball-burnishing process of 2D surfaces from planar workpieces, by which it is possible to obtain all of types of the patterns shown in Fig. 1 [8]. A simplified equivalent kinematical chart of the setup from Fig. 2a, and the regime parameters of this type of vibrational ball-burnishing process are shown in Fig. 2b. The setup includes manual controlled milling machine equipped with an additional vibrational ball-burnishing device, which has its own driving motor. By using stepped V-belt pulleys, driving power from the motor transmits to the shaft which can be rotated with five different values of angular velocity ω_1 , rad/sec. At the other end of the shaft is mounted an eccentric mechanism. This mechanism through a connecting rod transforms the rotational movement of the shaft into reciprocating motion of the ball tool with a certain amplitude $2.e$, mm. Additionally, the ball-tool spinning around the spindle axis with angular velocity ω_0 ,

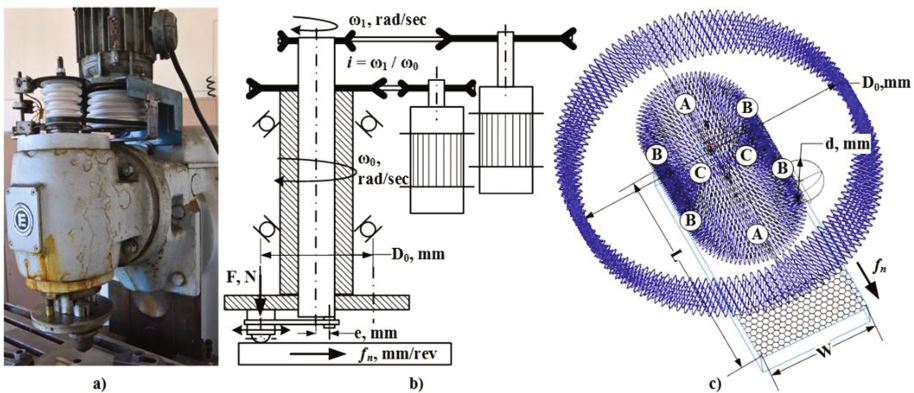


Fig. 2. (a) Setup for vibrations-assisted ball-burnishing process of planar surfaces; (b) Simplified kinematical chart of the setup and regime parameters of the process [8]; (c) Resulting toolpath of the ball-tool, which indicates how the traces superimpose each other.

rad/sec along with the device, describing a circle with a diameter D_0 , mm,. Depending on D_0 , the ratio between the angular velocities ω_0 and ω_I can be adjusted so that, the ball tool to perform i - number of reciprocating movements per revolution of the spindle.

The burnished prismatic workpiece moves linearly together with the table of the milling machine at a specific feed rate - f_n , mm/rev.

In order to perform plastic deformation in the surface layer of the workpiece's face, the ball-tool is pressed with a certain force F , N into it, depending on his diameter d , mm and on the hardness of the workpiece material [7].

In Fig. 2c is shown the superimposition of the toolpath trajectory of the ball-tool, related with application of the kinematic scheme (see Fig. 2b) for vibrations-assisted ball-burnishing on flat surfaces. As can be seen from this figure, if the diameter D_0 is less or equal than the width W of the burnished surface, areas A and B with different types of overlapping of traces are obtained. For instance, in areas of type A the toolpath overlays properly to produce the textures of Type IV (see Fig. 1d, e), while in the areas of type B the patterns of Type V are rather be obtained. If the length L of the burnished surface is greater than the diameter D_0 , sections of the type C will also be obtained, due to re-passing the ball-tool over already burnished area. These effects are undesirable, because of them is obtained heterogeneous texture roughness and differing physical and mechanical characteristics in the surface layer of the sections A, B and C. To avoid these negative effects some changes in the original scheme for vibrations-assisted ball burnishing have been made [8]. The diameter D_0 is increased to be larger than the width W of the workpiece (see Fig. 2c), which avoids obtaining the sections of type B on the burnished surface. In order to avoid obtaining the C-type sections, the vertical milling head of the milling machine is tilted at a small angle ($1-2^\circ$) relative to the table of the machine, thereby ball-tool does not contact with the burnished surface in half of the circle with diameter D_0 . Above described changes in the ball burnishing scheme, showed in Fig. 2 seemingly solve the problem with different roughness textures areas, but also lead to some other significant drawbacks, which are as follows:

- The contact between the ball-tool and burnished surface cyclically interrupted. Therefore, there will be possibilities to arise some shock loads at the beginning and at the end of the contact between the ball tool and the processed surface. In addition, the reciprocating movement performed by the eccentric mechanism generates vibrations with a frequency depending on the values of the angular velocity ω_I ;
- The reduction of the width of contact between ball-tool and burnished surface in addition to the inclination of the axis of the spindle of milling machine will result in low productivity of the process, because more than 50% of the tool movement in its circular toolpath will be performed "in the air";
- Not always be possible to satisfying the condition D_0 to be greater enough than W (in cases of workpieces with larger width). This restricts the maximum width of the workpiece that can be burnished by using that approach.

Using this kinematic scheme for vibrational ball-burnishing process is also related to some additional constraints, as follows:

- The manual controlled milling machine and additional vibrational device, driven by stepped V-belt pulleys, do not allows stepless control of the speeds and feed rates, or smooth adjustment of the parameter $i = (\omega_1/\omega_0)$ over a wide range. This restricts the opportunities for obtaining more diverse textures with regular roughness;
- Because the angular velocities ω_0 and ω_1 are provided by two different and not synchronized with each other kinematic drive chains (see Fig. 2a, b) and due to the relative slip between the belt and pulleys, the parameter i may be amended during the process, which can lead to undesirable changes in the shape and dimensions of the cells within the burnished surface;

All above-mentioned disadvantages of the vibrational burnishing process using the kinematic scheme from Fig. 2a, b makes it ineffective according to the requirements for manufacturability and productivity in contemporary production processes. Therefore, it is necessary to explore new approaches to implementation of the ball burnishing process to avoid or minimize the existing deficiencies of the conventional schemes for its implementation. In line with this, the main objective of the current work is to create an appropriate algorithm for generating optimal toolpaths suitable for ball-burnishing process implementation, using modern CAD-CAM based approaches and CNC equipment to achieve better productivity and repeatability of the resulting roughness textures.

2 Optimal Tool-Path Generation Approach

2.1 Opportunities for Improvement of the Ball-Burnishing Process

Significant improvements of the ball-burnishing process can be achieved if instead of manually controlled milling machines and vibrations-assisted burnishing devices move to application of more automated processing equipment controlled by CNC [6]. Thus, the required trajectories of the ball-tool can be set by an appropriate NC-code as a toolpath rather than being determined by the instantaneous values of the regime parameter $i = (\omega_1/\omega_0)$, which (as explained above) is not firmly constant over time. Using machines with CNC control ensures elimination of some drawbacks and fundamental hardware limitations of the setup, shown in Fig. 2a, b. For instance, the diameter of rotation of the ball-burnishing device D_0 can be virtually increased so much more than in reality, the regime parameter - i can be adjusted infinitely variable, etc., which will result in many more opportunities for fine-adjustment the shape and dimensions of the cells of the ball-burnished surfaces.

Because burnished surfaces is considered to be planar, it can be used even 2,5D (also called a two-and-a-half-axis) CNC milling machines. This means that it is enough that they be able to perform the cutting operation only in two of the three axes at a time (usually these axes are X and Y) due to hardware or software limitations, or a machine that has a solenoid instead of a true, linear Z-axis.

The required trajectory of the ball-tool needed for NC-code programming can be obtained using a sufficient number of points from a planar polyline, which coincides

with it (see Fig. 2c). The distances between adjacent points of the polyline are connected to each other by straight lines. As the number of points is greater, the lengths of these segments will be smaller and approximation of the toolpath will be closer to the actual trajectory. From the number of points of polyline depends what will be the size (number of rows) of the resulting NC-code. In order to create a smooth and well-fitted toolpaths, the number of points of the polyline can reach several hundred thousand in case of burnishing surfaces with bigger dimensions. Therefore, the NC code will also reach such a number of lines, which will require using the CNC milling machine in DNC (Direct Numerical Control) mode. Because it is practically impossible writing “by hand” such a NC-control program, it will be necessary to use an appropriate CAM software for its automated compilation. In order to do this it is necessary to draw up an appropriate mathematical model, which will describe the tool path of the ball tool.

2.2 Mathematical Description of the Needed Toolpath

The toolpath trajectory of the ball-tool (see Fig. 2c) mathematically describes with following system of equations:

$$\begin{cases} x(t) = \left(e \cdot \cos(\omega_1 \cdot t) + \frac{1}{2} \cdot \sqrt{D_0^2 + 4 \cdot e^2 \cdot \cos^2(\omega_1 \cdot t)} \right) \cdot \sin(\omega_0 \cdot t) + f_n \cdot t \\ y(t) = \left(e \cdot \cos(\omega_1 \cdot t) + \frac{1}{2} \cdot \sqrt{D_0^2 + 4 \cdot e^2 \cdot \cos^2(\omega_1 \cdot t)} \right) \cdot \cos(\omega_0 \cdot t) \end{cases} \quad (1)$$

where (see Fig. 2b): t , min is the time for which the ball-burnishing setup works, $\omega_1 = 2 \cdot \pi \cdot n_1$, rad/min is the angular velocity of the eccentric mechanism, which depends on the speed of rotation n_1 , rev/min, $\omega_0 = 2 \cdot \pi \cdot n_0$, rad/min is the angular velocity of the spindle of milling machine, which depends on the speed of rotation n_0 , rev/min, f_n , mm/min is a feed per revolution, i.e. the value indicating how far the ball-tool moves during one complete rotation of the ball-burnishing device, along X axis, D_0 , mm is the diameter of rotation of the ball-burnishing device, and e , mm is the half of the amplitude of the reciprocating motion of the eccentric.

Setting specific values of the regime parameters of the process and dimensional parameters of the device in the system of Eq. (1), the coordinates $x(t)$ and $y(t)$ of the successive locations of the center point of the ball-tool can be computed (in the coordinate plane XY) as a function of the operating time t of the ball-burnishing device.

The system of Eq. (1) can be used for initial adjustments of the regime parameters of the ball-burnishing process, but they are continuous functions of the parameter time and this does not make them convenient for establishing the NC-program. In order to be used for creating operative NC-code, the Eq. (1) are transformed from continuous into discrete form, and they acquire the following type:

$$\begin{cases} X_{m,n} = \left(e \cdot \cos\left(\frac{2 \cdot \pi \cdot n}{P}\right)_m + \frac{1}{2} \cdot \sqrt{D_0^2 + 4 \cdot e^2 \cdot \cos^2\left(\frac{2 \cdot \pi \cdot n}{P}\right)_m} \right) \cdot \sin\left(\frac{2 \cdot \pi \cdot n}{P} + i_p \cdot m\right) + d_{fn} \cdot m \\ Y_{m,n} = \left(e \cdot \cos\left(\frac{2 \cdot \pi \cdot n}{P}\right)_m + \frac{1}{2} \cdot \sqrt{D_0^2 + 4 \cdot e^2 \cdot \cos^2\left(\frac{2 \cdot \pi \cdot n}{P}\right)_m} \right) \cdot \cos\left(\frac{2 \cdot \pi \cdot n}{P} + i_p \cdot m\right) \end{cases} \quad (2)$$

where: p is the preset number of points from the polyline, n is the index of the current point from polyline ($n = 0, 1, 2, \dots, p$), m is the index of current complete turnover of the ball-burnishing device ($m = 0, 1, 2, \dots, q$), q is the number of the needed turnovers (calculated using formula (3)), and i_p is only fractional part of the ratio $i = (\omega_f/\omega_0)$. The i_p determines the phase shift of the trajectories after each complete revolution of the ball-burnishing device. The fractional part of the parameter i can be changed within a range from 0 to 0.5. In the source [8] experimentally has been established that when $i_p \approx 0.15$ the patterns have a cells with near to the hexagonal shape, and when $i_p \approx 0.45$ the cells have a near to the rectangular shape.

The other parameters in Eq. (2) have the same meanings as in Eq. (1). However, in Eq. (2) instead of the feed per revolution parameter f_n , mm/rev, the linear distance d_{fn} , mm between every two successive circular trajectories of the ball-tool is used. This parameter can be set as an arbitrary value because it is not tied to gear ratios of the main and the feeding actuators, as is the case when using manual controlled milling machines. The number of the needed complete turnovers can be calculate, using the following formula:

$$q = L(D)/d_{fn} \quad (3)$$

where: $L(D)$, mm is the length (or the diameter) of the ball-burnished area from workpiece, and d_{fn} , mm is the linear distance between successive circular trajectories of the ball-tool.

If q is obtained as fractions, it must be rounded to the next highest integer value. Using the system of Eq. (2) it is possible to calculate the X and Y coordinates of all points from the polyline that represents the toolpath of the ball-tool. However, this still does not solve the problem of finding the optimal length of the toolpath to the dimensions of the treated area. At this stage, the toolpath of the ball-tool still has the form shown in Fig. 2c, i.e. most of it is outside the boundaries of the burnished area.

2.3 Determining the Restrictive Terms

To obtain an optimal toolpath should be used additional restrictions in order to limit generation of toolpaths only within the boundaries of the ball-burnished area. The parts with planar functional surfaces, most often have a rectangular or circular shape of their cross section. Hence, some Boolean comparison operators can be used in “For–Do and While–Do” loop termination conditions and conditional expression such as “If–Then–Else” for “cut off” those parts of the toolpath, which fall outside of the rectangular or circular ball-burnished area.

In the case of rectangular shape (see Fig. 3a), the constraints are determinates by the length L , mm and width W , mm of the rectangular ball-burnished area. Using them, it can be calculated the coordinates X_{\min} and X_{\max} along to X-axis, and Y_{\min} and Y_{\max} along to Y-axis of the area, using following formulas:

$$L = X_{\max} - X_{\min}, \text{ mm, and } W = Y_{\max} - Y_{\min}, \text{ mm} \quad (4)$$

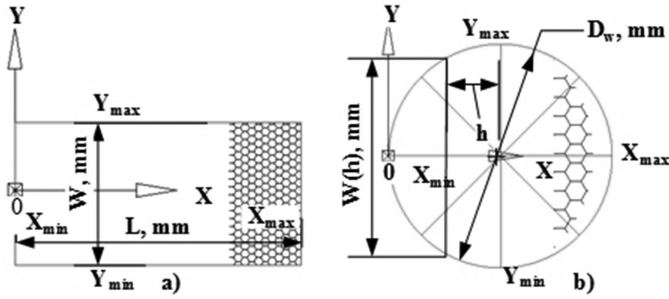


Fig. 3. Determination of the boundaries of the ball-burnished area in cases of: (a) an area with rectangular shape; (b) an area with round shape.

The signs of the coordinates Y_{\min} and Y_{\max} , and the location of the origin of the coordinate system XY (see Fig. 3a, b) should be taken into consideration.

When the ball-burnished area has a round shape with a certain diameter D_w , mm (see Fig. 3b), the determination of the coordinates X_{\min} and X_{\max} along to X -axis is analogous to the Eq. (3). Here the length L coincides with the diameter D_w , but as can be seen from Fig. 3b, the width W in this case is not constant.

The instantaneous width of the chord $W(h)$ depends on the distance h from the center of the circle, and can be determined by the following equation [9]:

$$W(h) = 2 \cdot \sqrt{(0.5 \cdot D_w)^2 - h^2} \quad (5)$$

As can be seen from Fig. 3b, when the coordinate X increases from $X_{\min} = 0$ to $X_{\max} = D_w$, the width $W(h)$ starts from zero when $X = 0$, then reaches to D_w when $X = 0.5 \cdot D_w$, and finally decreases again to zero, when $X = D_w$.

2.4 Overall Algorithm for Generating Optimal Toolpaths

The overall algorithm for generating continues polylines, which can then be used as toolpaths with optimal length within the ball-burnished area, is shown in Fig. 4. Proposed algorithm has three major steps, which are explained below.

After the initial setting of the input parameters at Stage A using Eqs. (2), (4) or (5), the coordinates of all points from the polyline are calculated. Those points that do not fall within the boundaries of the rectangular (or circular) burnished area are assigned a corresponding combination of values of their coordinates: X_{\min} or X_{\max} and Y_{\min} or Y_{\max} . Thus, the “unnecessary” points from the trajectory (see Fig. 2c) are superimposed on the borders of the area (see Fig. 4). If they are included as elements of the polyline, the overall length of the toolpath will not be optimal, i.e. the ball-burnishing operation will be unnecessarily extended in time. Furthermore, the ball-tool will pass repeatedly at the borders of the burnished area that can result in greater than the permissible hardening of the surface layer and deterioration of its physical and mechanical properties. Therefore, they must be removed from the other points of the polyline.

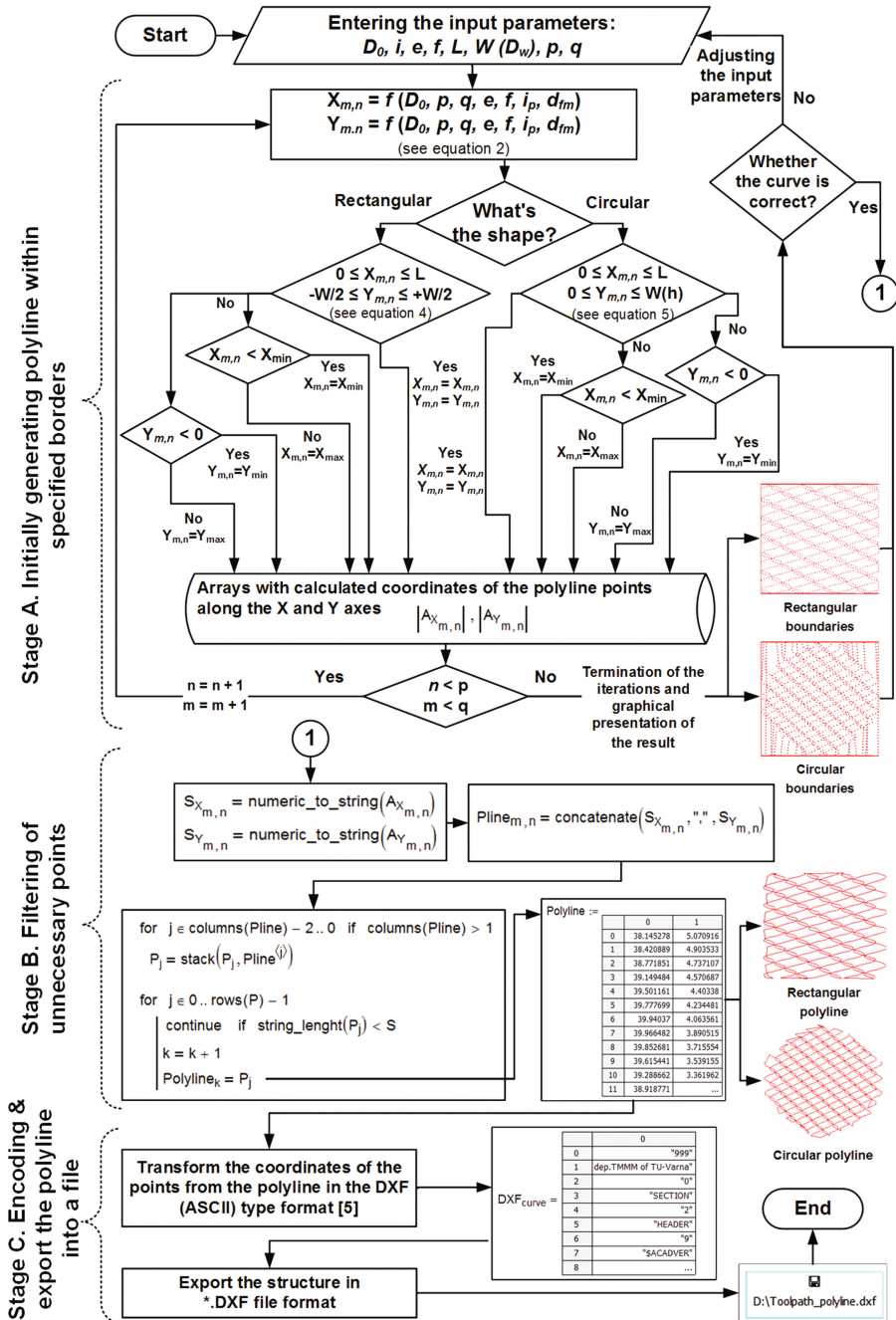


Fig. 4. Overall algorithm for generating continues polylines, which can be used like optimal toolpaths within the ball-burnished area with a rectangular or circular shape.

At Stage B of the algorithm (see Fig. 4), unnecessary points from the trajectory of the tool are removed and the remaining within the area individual trajectories are connected to each other with straight lines to obtain one single continuous polyline as a result. For that purpose, initially the coordinates in the two-dimensional arrays S_X and S_Y (having dimensions $p \times q$) are converted from scalar into strings. Then in two-dimensional array *Pline* the strings concatenated, and take the format (“ $\pm X$ coordinate value “+”, “+” $\pm Y$ coordinate value”) for all points from the polyline.

Then the rows of all columns of the matrix (called *Pline*) are rearranged into one under another, eliminating those of them where the strings have a smaller length than 31 symbols. Essential to filtering of the unnecessary points of the polyline is the difference in the length of strings representing the coordinates of the points that are inside of the area and those that are located in its borders. After transformation into strings and concatenation of the coordinates, the smallest length of the string of the points, which are inside of the burnished area, is not less than 31 symbols (including the comma, decimal points and signs before the numbers). For comparison, the length of the strings with the coordinates of points that lie on the boundaries of burnished area does not exceed 9–10 symbols. The difference in the lengths of both types of strings due to the fact that those of them which lies along the borders of the area, are set manually. In this case the number of decimal places rarely exceeds more than 3 characters, while other strings contains calculated by Eq. (2) coordinates and the number of decimal point for them is fixed by default to 15 symbols. After removing the unnecessary items, the resulting polyline has an optimal length (see the tool path graphics in Stage B shown in Fig. 4).

Because DXF file format is possibly the most widespread CAD exchange format in use by CAD-CAM packages, in Stage C of the algorithm (see Fig. 4) the coordinates of the points from the optimal polyline are converted into DXF syntactic structure [5], and then exported as a computer file. After that, DXF file containing a polyline can be loaded into a suitable CAM software for modeling the toolpath and generating NC code for execution of that operation by appropriate CNC machine. Some examples of ball-burnished planar surfaces by using polylines as toolpaths, generated by the described algorithm are shown in Fig. 5a, b, c.

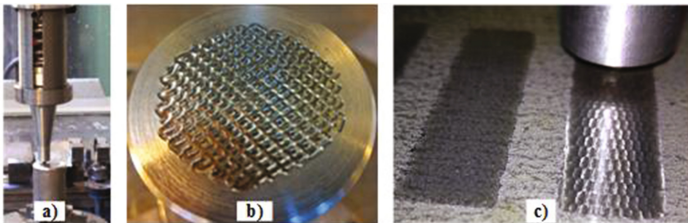


Fig. 5. (a) CNC milling machine based setup for ball-burnishing process of flat surfaces; Ball-burnished textures on areas with: (b) circular cross section; (c) rectangular cross section.

3 Results and Discussion

The proposed algorithm can be used to creating polylines with unrestricted overall length within the ball-burnished area and provides a much better control of the overlapping roughness patterns, rather than the setup shown in Fig. 2a, b. In the CNC milling based setup, there are no coerced oscillations of the ball-tool because the needed ball-tool trajectory is calculated mathematically and then execute programmatically by the machine, which significantly improves the uniformity of dimensions and shape of the cells from the roughness with a regular shape. This also leads to simplification of the instrument for ball-burnishing operations (see Fig. 5a) because there is no need to use any belt drives or other type of transmissions or additional electric motors.

The rear part of the tool is constructed so that standardized CNC instrumental holders can be used. Thus, the ball-burnishing instrument can easily be added to the tool magazine of the CNC machine and manipulated by the tool changer by instructions from the NC code. This allows the ball burnishing operations to be added directly after the remaining technological operations for shape forming of the workpiece. Thus, all operations can be performed on a single workpiece setup and on the same CNC milling machine, which leads to increased productivity.

4 Conclusion

The algorithm for generating polylines in DXF file format, proposed in this work can be implemented both by using various mathematical software products, such as Mathcad, S-Math, Matlab, etc., but also as a programming language code (such as macros written in Visual Basic for Applications for example) because such resources are integrated into many of today's CAD-CAM software products. This makes it easily applicable for different types of software used by the developers of NC programs.

The future work will be oriented towards the development and improvement of the presented algorithm so that it can be used to generate polylines for burnished areas with free form of the cross section and for creating tool paths for burnishing of non-planar surfaces.

References

1. Bourebia, M., Laouar, L., Hamadache, H., Dominiak, S.: Improvement of surface finish by ball burnishing: approach by fractal dimension. *Surface Eng.* **33**(4), 255–262 (2017). doi:[10.1080/02670844.2016.1232778](https://doi.org/10.1080/02670844.2016.1232778)
2. Gomez-Gras, G., Travieso-Rodriguez, J.A., Jerez-Mesa, R., et al.: *Int. J. Adv. Manuf. Technol.* **87**, 363 (2016). doi:[10.1007/s00170-016-8490-y](https://doi.org/10.1007/s00170-016-8490-y)
3. Revankar, G., Shetty, R., Rao, S., Gaitonde, V.: Wear resistance enhancement of titanium alloy (Ti–6Al–4 V) by ball burnishing process. *J. Mater. Res. Technol.* **6**(1), 13–32 (2017). ISSN 2238-7854. <http://doi.org/10.1016/j.jmrt.2016.03.007>

4. Ibrahim, A.A., Khalil, T., Tawfeek, T.: Study the influence of a new ball burnishing technique on the surface roughness of AISI1018 low carbon steel. *Int. J. Eng. Technol.* **4**(1), 227–232 (2015). ISSN 2227-524X
5. Bourke, P.: Minimum Requirements for Creating a DXF File of a 3D Model (1993). <http://paulbourke.net/dataformats/dxf/min3d.html>
6. Shiou, F.J., Banh, Q.N.: *Int. J. Adv. Manuf. Technol.* (2016). doi:[10.1007/s00170-016-8413-y](https://doi.org/10.1007/s00170-016-8413-y)
7. Schneider, Yu. G.: *Operational Properties of Parts with Regular Microrelief*. Publishing IVA, St. Petersburg (2001). 261 p. ISBN 5-7577-0166-8
8. Slavov, S. D.: A device for processing regularly distributed roughness on planar surfaces by using flat vibratory ball burnishing process. In: *Proceedings from AMTECH, Sozopol, Bulgaria*, vol. 2, pp. 51–56 (2001). ISBN 954-438-303-0
9. Weisstein, E.W.: Circular Segment. From MathWorld—A Wolfram Web Resource. <http://mathworld.wolfram.com/CircularSegment.html>
10. García-Granada, A.A., et al.: Ball-burnishing effect on deep residual stress on AISI 1038 and AA2017-T4. *Taylor & Francis* (2017). doi:[10.1080/10426914.2017.1317351](https://doi.org/10.1080/10426914.2017.1317351)

Improvement Aspects in Teaching Analog Electronics

Ekaterina Dimitrova^(✉), Dimitar Kovachev, and Vencislav Valchev

Technical University of Varna, Varna, Bulgaria
edimitrova55@gmail.com, dmkt@tu-varna.bg,
vencivalchev@hotmail.com

Abstract. Information technologies are an excellent opportunity for Active Learning and Project Based Learning in Electronics. The paper emphasizes on some improvements in teaching Analog Electronics in TU-Varna's four year Electronics Engineering Bachelor course. A short research on Active Learning approaches is presented. Curriculum construction approach based on Spiral Learning Theme model is highlighted. An accent on FPAA/dpASPs as an effective tool in Analog Electronics education is commented. The **Predict-Observe-Discuss-Synthesize** teaching methodology is presented as a learning approach which provides highly interactive and at the same time productive lectures. An emphasis on student's skills for successfully solving simulation tasks in a case study and design of analog circuits is performed. An example for PODS interactive lecture is developed.

Keywords: Active learning · Analog circuits · Analog electronics · Field Programmable Analog Arrays · Interactive lectures · Spiral learning

1 Introduction

Electronics provides the bases for development of computers, communication systems, control and measurement instrumentation, medical equipment etc. With the increasing complexity of digital design, it moves away from the gate level descriptions to hardware description languages (HDL) such as Verilog and VHDL. In addition the advances in the computer-aided synthesis tools have moved the digital design process to much higher level of abstractions. Following that trend in the industry there is no emphasis placed on analog electronics in computer engineering curricula.

The continued miniaturization of transistors, shrinking of interconnect dimensions, higher frequencies of operation brought back a host of signal integrity related issues in digital circuits [1–5]. Current high-end circuit design and board-level designs face a number of design challenges such as crosstalk, interconnect parasitics, substrate noise, etc., that need to be addressed. At the same time the increased demand of portable applications that operate on energy constrained resources present a need to consider alternate design methodologies. Analog signal processing can provide energy conserving solutions for a number of portable applications [6].

IEEE Computer Society and ACM published a report on curriculum guidelines for undergraduate degree programs in computer engineering [7]. *Electronics, including*

analog electronics, is a core component of the recommendation. This is a clear sight for putting an emphasis on **Analog Electronic Education (AEE)** in Computer and Electrical Engineering. There are publications for modifications of the computer engineering curricula to accommodate these recommendations. Literature [8] presents with details the changes in the curriculum at the Ohio Northern University. Two courses sequence is recommended -Analog Electronics 1, taken by both electrical engineering and computer engineering majors and Analog Electronics 2, a required course for electrical engineering majors. They also suggest the pedagogical approaches considered and used in the development of these courses. Spiraling and spacing learning concepts are extensively used in the course sequence to enhance student learning.

The actualization of the curriculum in Electronics in the **TU of Varna (TUV)** is almost every year activity and it is dictate not only by the rapid development in the microelectronics and computer areas, but also by the increasing demand of the high level technical staff at different industrial, medical, educational institutions etc., and in the same time by the reality that the number of applying students is decreasing. For example, the number of applying students in Electronics at TUV is reduced 3 times for last 10 years. The average score of mathematics at the input is also about 25% reduced. It is obvious that the curriculum and teaching approaches have to be adjusted for achieving relevant results at the end of the Bachelor degree education.

2 A Short Research on Active Learning Approaches in AEE

It is a common opinion that students have difficulties in understanding **Analog Circuits (ACs)** and there are a high number of publications describing alternative approaches which can be used to improve its teaching methodology. Computer-Aided Analog Electronics Teaching is well presented in [9]. A project-based learning (PBL) is a student-centered strategy that fosters student initiative and focuses the student on real-world, open-ended projects that can increase the motivation for most of them. These projects foster a wide range of abilities, not only those related to content knowledge or technical issues, but also practical skills [10]. A good example for PBL approach to Design Electronic Systems Curricula is presented in [11].

It has been shown that excellent results may be achieved with active forms of learning performed not only during labs but also during lectures. Active learning approach in technical colleges and universities is up to date and there are proven results for better understanding of the studied material. Interactive lectures, including demonstrations of real problems in the lecture hall, in addition to the theoretical presentation of the subject, are effective for learning the basic concepts and principles in electronics. The blended approach on giving lectures includes a mixture of traditional lectures and some interactive lectures. More specifically, the concept of conducting interactively lectures with demonstrations by applying the **Predict-Observe-Discuss-Synthesize (PODS)** approach to increase conceptual understanding of students is well demonstrated in [12–14]. The main steps of PODS interactive lectures can be described as follows:

- The lecturer explains by words the experiment that will be realized. It is over the topic which has been presented in conventional lecture (for example: the frequency

band of a given AC amplifier will be measured). Students have to discuss in small groups the expected result and they **predict** their group's answer.

- There is a discussion in the hall and the common answer will be **predicted** and written on the board.
- The experiment is demonstrating in front of all students and everyone is writing his/her **observations**.
- When there are differences between predictions and observations, then lecturer takes a part in the small group **discussions** to provoke right understanding of the experimental result.
- The lecturer helps, if necessary, for **synthesizing** student's explanations for understanding the conceptions which are related with the observations.

The real experiment can be replaced by computer simulations. Nowadays, students are well adapted to the present computer technologies and these are powerful instruments to increase the student interest and active participation during lectures.

Programmable logic, especially **Field Programmable Gate Arrays (FPGAs)**, has significant impact on prototyping and implementation of digital circuits. FPGAs allow implementation of complex systems-on-chip (SoC) with a very short development time. Thus it is possible to study different design tradeoffs at higher level of abstraction and on a physical implementation. In the recent years, the synthesis automation of circuits has made progress in analog domain with invention of **Field Programmable Analog Arrays (FPAAs)** and their application for implementation [15, 16]. FPAAs provide a quick and automatic means of prototyping low to medium frequency range analog applications. Typical FPAAs are uncommitted arrays of components – operational amplifiers and switched-capacitors necessary for assembling the analog signal processing circuits. The purpose of programming in the FPAAs is to set circuit parameters, as well as to quickly study different circuit topologies and their implementation. FPAAs are used in the laboratory to study different filter topologies and understand the design tradeoffs of one topology to other. It is much recommended to arrange lectures and laboratory classes on introducing the basic concepts of switched capacitor circuits and FPAAs, and a concomitant software suite in analog electronics education. FPAA's are an excellent tool for active learning in general, and to easy unify conceptual knowledge, programming and implementation of electronic devices and systems. This hardware allows for higher complexity designs during laboratory sessions and can reduce the troubleshooting and frustrations in realizing circuits with discrete components, clearly focusing on course learning objectives. Very good works for FPAAs in laboratory exercises are presented in [17].

This article presents the experience of applying a novel method in teaching ACs as an approach to increase its efficiency in Electronics specialty at TUV.

3 Organization of Study in AEE in Bachelor Degree

3.1 Curriculum Construction Approach

Students that enlist in TU-Varna's four year Electronics Engineering Bachelor course can gain knowledge and expertise in the general field of electronics including: Analog and Digital Circuit design; Embedded Systems; Power electronics; CAD systems in Electronics. In addition there are specialization courses available in: Biomedical Electronics, Industrial Electronics, Electronics in Renewable Energy Systems, Microelectronics. In this paper the focus is on the course subjects that concern analog circuits. The development of the curriculum in Electronics Engineering Bachelor course in TUV is based on spiraling and spacing conceptual learning to enhance student knowledge. The spiraling and spacing concepts result in back and forth coverage of topics. This approach is demonstrated on Fig. 1. Spacing refers to the presentation of material spaced out over a longer period of time rather than as one continuous presentation over a shorter period of time [18]. Spiraling refers to revisiting previously learned topics and expanding them to a higher knowledge level. Both of these techniques have shown very effective in increasing effectiveness of student learning.

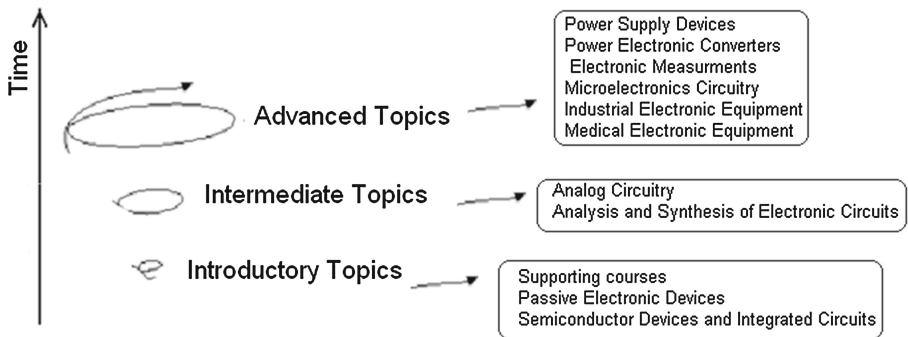


Fig. 1. Spiral learning themes based model

During their studies through balanced program of lectures, seminar and laboratory exercises students obtain both practical and theoretical experience that encompasses not only the hardware aspects of electronics but also the software ones where: Various programming languages are studied, such as: C++ for embedded controllers; C# for application development; and VHDL for programmable digital circuits. Various professional software products such as: MATLAB and Cadence are introduced.

In this paper the focus is on the subjects that concern analog circuits. The main disciplines, starting from the first semester are: Passive electronic components (1 semester), Semiconductor devices and Integrated circuits (3 semester), Analysis and synthesis of Electronic Circuits (4 semester), Analog Circuitry (5 semester), Analysis and synthesis of Electronic Circuits – Project (5 semester), Power Supply Devices (5 semester), Power Electronic Converters (6 semester), Electronic Measurements (6 semester), Analog Circuitry – Project (6 semester), Microelectronics Circuitry (7 semester), Sensors (7

semester), Industrial Electronics (7 semester), Power Electronic Converters – Project (7 semester), Medical Electronic Equipment (8 semester).

The spiraling and spacing approach is well seen. Coverage of topics in Solid State Electronic Devices and Integrated Circuits (1 and 3 semester) provides a breadth in analog electronics. The supportive subjects of Mathematics and Circuit theory have to be mention also. The courses present a number of applications based on the material learned in earlier part of the course to improve knowledge retention. In 4 semester Analysis and Synthesis of Electronic Circuits subject presents intermediate topics of spiraling approach, to increase depths of comprehension of modeling of electronic devices (BJTs, MOSFETs, and Operational Amplifiers), special techniques for analysis of Electronic Circuits, Transfer functions and Classical approach of Filters' Synthesis. The depth of comprehension of Analog Circuits is increasing in Analog Circuitry course. The biasing of Amplifiers and its Frequency response is well covered; many Linear Operational Amplifier applications are presented, Oscillators are covered, too. Under the instructor management students develop an analog module as an individual (or group) assignment, which enhances their understanding and design skills. Starting from the 6 semester the mentioned above special courses, which cross the analog and the digital electronics topics, are higher in time and at space, giving advanced, and industry orientated knowledge to students.

As the topics are covered at a later point of time, they reinforce students' prior knowledge and expand them to engage at a higher intellectual level. Some examples of spiraling learning are given below:

Operational Amplifiers: Ideal **Operational Amplifier** (OpAmp) concepts are introduced in Semiconductor Devices and Integrated Circuits. In Analysis and Synthesis of Electronic Circuits, different behavioral models are taught as a prerequisite to Analog Circuitry. These models help in analyses and understanding of circuit applications that use op amps - amplifiers, comparators, timing circuits. OpAmps with positive feedback is used in Oscillators circuits. In Electronic Measurements course OpAmp non-idealities that affect the errors in Measuring Converters and Measuring Amplifiers and limit its range and scope are covered, also data converter circuits that use OpAmps are thought. In addition special applications for sensor conditioning circuits, medical equipment etc., are taught in advanced topic disciplines.

Filters: In Analysis and Synthesis of Electronic Circuits subject filter specifications and transfer functions are introduced. The active filter design principles to build first and second order filter circuits are taught. The basic topological filter structures are reinforced in Analog Circuitry. Filter realizations are implemented using automated analog synthesis tools using FPAAs. This knowledge is used to build a filter with given specifications and verify it in the laboratory. In Advanced Topics disciplines filters are building blocks in different Electronic Measuring Converters, Medical or Industrial Systems.

FPAAs are an excellent tool in analog circuit courses. They can be used in early circuits' courses to provide students with hands - on experience learning measurement techniques, characterizing basic components, and even designing simple analog

systems. In later courses, FPAA can be used to experiment with concepts in analog system design, integrated circuit (IC) design, and signal processing. With the proper mix of different computational elements with each CAB (Configurable Analog Block), specialized CABs, and peripheral blocks such as A/D and D/A converters, analog multiplexers, and analog shift registers, a single FPAA can be used in a wide variety of courses and experiments [27].

There are a number of excellent textbooks available for analog electronics [19–22]. Typical coverage in these books addresses most of topics in the course sequence except for FPAA and switch-mode power supplies. However, the material in the textbooks is organized for traditional course offering of analog electronics. The spiraling and spacing concepts result in back and forth coverage of topics. An excellent book for rapidly teaching electronic concepts using computer based design tools including National Instruments Multisim and the Anadigm based Programmable Analog Module is [23]. It is additionally accompanied by the laboratory exercises manual [24].

4 An Example for PODS Interactive Lecture

The course of Analog Circuitry is given as an Intermediate topic as per Spiral learning themes based model on Fig. 1. Lectures are given in blended approach - part of them is conventional and others are interactive. In 5th semester of 15 weeks, 30 h lectures are scheduled (24 h conventional lectures and 6 h PODS lectures). Practical laboratory exercises are developed on specifically constructed PCBs with Measuring Digital Devices and different signal sources for student’s experiments. Textbooks written by well-established teachers and specialists in the field of analog electronics in Bulgarian and English are provided [25, 26].

Detailed presentations in electronic form have been developed, which are available to the students for their exam preparation as well as taking notes during the theoretical discussions on various subjects discussed in the lecture hall. This results in saving time for presentation of the theoretical material, while allowing more time for showing of more demonstrations by the lecturer.

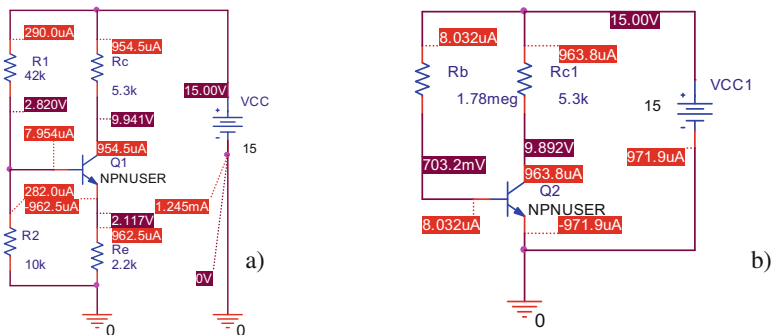


Fig. 2. Single stage BJT amplifier – (a) Four resistor topology; (b) Base topology

Theory is given preliminary, before the PODS classes. Students are well trained to do and to understand the process of main PSpice analyses.

The topic of the demonstration is a single stage BJT amplifier in common emitter configuration. The example here is only over DC operating point biasing and negative current feedback by resistor R_e between emitter and ground. Two circuits will be compared. They are shown on Fig. 2 with node voltages and branch currents over.

Given: Power supply voltage $V_{CC} = 15$ V, collector current $I_C = 1$ mA, NPN transistor current gain $\beta = 100$ to 300.

Design rules for circuit with BJT and four resistors, Fig. 2a:

1. Maximum swing of the output voltage without distortions requires

$$V_{CE} = 0.5 V_{CC}$$

2. Voltage drops on R_c and R_e are equal, or $3V_{R_e} = V_{R_c}$, $V_{R_e} + V_{R_c} = 0.5 V_{CC}$
3. V_B has to be independent on β ! $V_B = V_{R2}$, so $R2$ is in parallel with the resistance looking in Base node - R_b , $R_b = (V_{BE} + V_{R_c})/I_B$;

h_{ie} - input resistance of BJT;

$$R_b = (I_B * h_{ie} + I_E * R_e)/I_B = (I_B * h_{ie} + (1 + \beta) * I_B * R_e)/I_B = h_{ie} + (1 + \beta) * R_e \approx (1 + \beta) * R_e$$

As $R2$ is in parallel with R_b , and R_b depends on β , $V_{R2} = V_B$ will not depend on β if $R2 \ll R_b$.

Calculations:

1. $V_{CE} = 7.5$ V
2. $V_{R_e} = 7.5/4 \approx 2$ V; $R_e = 2.2$ k; $R_c = 5.3$ k
3. $R2 \ll 100 * R_e$; $R_e \ll 220$ k; One possible value is $R_e = 10$ k
4. $I_{R2} = V_B/R2 = (2.2 + 0.7)/10$ k = 290 μ A.
5. $I_B = I_C/\beta = 1$ mA/100 = 10 μ A or $I_B = 1$ ma/300 ≈ 3 μ A
6. $I_{R1} = I_{R2} + I_B = 290$ μ A + 10 μ A. $I_B \ll I_{R2}$ and $I_{R1} \approx I_{R2}$
7. $R1 = (V_{CC} - V_B)/I_{R2} = (15 - 2.9)/290$ μ A ≈ 42 k

Calculations for the circuit without resistor in emitter branch, Fig. 2b:

1. R_c has the same value: $R_c = 5.3$ k
2. $I_{R_b} = I_b$; $R_b = 14.3/8$ μ A = 1.78 M Ω

During the PODS lecture students are divided in small groups (2–4 students). The parts of such lecture are:

PREDICT:

Every one receives a *predict sheet of paper* with circuits on Fig. 1 (without simulation results for voltages and currents) and input data ($V_{CC} = 15$ V and $I_C = 1$ ma, NPN transistor current gain $\beta = 100$ to 300) and several questions to answer:

1. Predict the value of V_{CE} .
2. If $V_{Re} = V_{Rc}/3$, predict the values of Rc and Re
3. If $V_{BE} = 0.7$, predict the value of V_B
4. Predict the value of I_B, I_E
5. Predict the value of $R1$ and $R2$
6. Predict: Will I_C and V_C change when β is changing for both circuits?
7. Predict which of the two circuits has a stable DC operating point and why?

Discussions in the group are to be wished!

OBSERVE:

Lecturer demonstrates the simulation using Multimedia and students observe the process and the results. For this example:

Both BJT transistor amplifiers on Fig. 2 are preliminary drawn in OrCAD Capture. The impact of Bf – the current gain of the transistors Q1 and Q2 is observed.

Using the model editor program, the model parameter denoted by Bf (*current gain*) is specified as a parameter, like it is shown on Fig. 3.

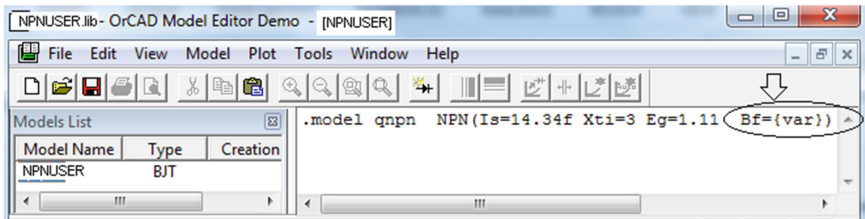


Fig. 3. User defined parameterized model of Q1 and Q2

DC Sweep analysis is specified. The parameter of this analysis is Bf . After the simulation, the results for the DC voltages and currents are directly visible on the circuits, Fig. 2. Students may check their answers immediately. Small differences are possible because of the free choice of $R2$. $R2$ may be changed very easy for every group and simulations are very fast.

The results about DC operating point stability are shown on Fig. 4. It is well seen that the collector current and collector voltage of the circuit with emitter resistor as a negative current feedback is stable. The collector current and collector voltage of the circuit, without emitter resistor is not stable.

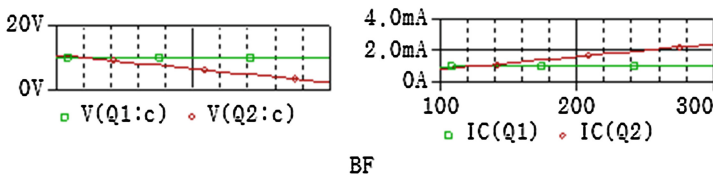


Fig. 4. Collector voltages and currents of Q1 and Q2 (BJTs) when Bf is changing

DISCUSSION:

Every group discusses the results comparing them to the simulated quantities.

SYNTHESIS:

Every student in the group synthesizes for himself over the *synthesis sheet of paper*, his/her understanding for every question. The instructor and assistant in help (who is providing the practical labs) checks and helps if the writing is not correct.

This is just a small example. In this manner different POST problems may be demonstrated.

5 Conclusion

The authors are satisfied with the increasing attendance of students during POST lectures. Students are positively influenced not only with better understanding of the content of the topics, but also they like to work in team, they practice more to present their results and to formulate their observations.

Assessment and evaluation of student learning from these modified course has to be made and will be presented at a later time.

Acknowledgements. The scientific research and the presented results are developed under the financial support of National Research Fund, in the frame of TUV, Project HPI7/2017, named “Development of design capabilities and hardware implementation of monolithic integrated circuits and electronic systems with programmable analog matrices”.

References

1. Blyler, J.: Analog issues confront digital designers. *Chip Design Magazine* (2005)
2. McConaghy, T.: Forget digital, think analog. *Design Strategies*, Electronic News, 28 October 2002
3. Beccara, J., Friedman, E. (eds.): *Analog Design Issues in Digital VLSI Circuits and Systems*. Springer, New York (1997). Special Issue in *Analog Integrated Circuits and Signal Processing Journal*
4. Caignet, F., Delmas-Bendhia, S., Sicard, E.: The challenge of signal integrity in deep submicron CMOS technology. *Proc. IEEE* **89**(4), 556–573 (2001)
5. Nourani, M., Attarha, A.: Detecting signal-overshoots for reliability analysis for high-speed systems-on-chips. *IEEE Trans. Reliab.* **51**(4), 494–504 (2002)
6. Hasler, P.: Is analog VLSI becoming a reality, keynote speech. In: *IEEE Midwest Symposium on Circuits and Systems*, Knoxville, TN (2008)
7. *Computer Engineering 2004: Curriculum guidelines for undergraduate programs in computer engineering*. A Report by IEEE CS/ACM Joint Task Force on Computer Engineering Curricula. http://www.acm.org/education/education/curric_vols/CE-Final-Report.pdf. Accessed 12 Apr 2017
8. Vemuru S.: Work in progress: modified analog electronics sequence for computer and electrical engineers. In: *ASEE North Central Sectional Conference, Session 2A*, Pittsburgh, PA, 26–27 March 2010, 2A-1 to 5 (2010)

9. Hemanshu, P.: Computer-aided analog electronics teaching. *IEEE Trans. Educ.* **40**(1), 22–35 (1997)
10. San-Segundo, J., Montero, M., Macías-Guarasa, J., Ferreiros, J., Córdoba, R.: Towards the acquisition of soft and systemic skills: a project based learning experience in massive laboratories on electronics. Presented at the international conference on engineering computer education 2005, ICECE 2005, Madrid, Spain, November 2005
11. Macías-Guarasa, J., Montero, J., San-Segundo, R., Araujo, Á., Nieto-Taladriz, O.: A project-based learning approach to design electronic systems curricula. *IEEE Trans. Educ.* **49**(3), 389–397 (2006)
12. Sokoloff, D., Thornton, R.: *Interactive Lecture Demonstrations*. Wiley, New York (2006). ISBN 0-471-48774-0
13. Mazzolini, A., et al.: Using interactive lecture demonstrations to enhance student learning in electronics. In: *Proceedings of the 21st Annual Conference for the Australasian Association for Engineering Education*, Sydney, Australia, p. 417 (2010)
14. Mazzolini, A., Daniel, S., Edwards, T.: Using interactive lecture demonstrations to improve conceptual understanding of resonance in an electronics course. *Australas. J. Eng. Educ.* **18**(1), 69–88 (2012)
15. Abramson, D.: A mite based translinear FPAA and its practical implementation, Ph.D. thesis, Georgia Institute of Technology (2008)
16. Dong, P., Bilbro, G., Chow, M.: Implementation of artificial neural networks for real time applications using Field Programmable Analog Arrays. In: *Proceedings of the International Joint Conference on Neural Networks*, pp. 1518–1524 (2006)
17. Todd, J., Maundy, B.: Incorporating FPAAs into laboratory exercises for analogue filter design. *Int. J. Elect. Eng. Educ.* **50**(2) 188–200 (2013). ©Manchester University Pres
18. DiBiasio, D., Clark, W., Dixon, A.: Evaluation of a spiral curriculum for engineering, Session12d1. In: *Proceedings of the Frontiers in Education Conference*, pp. 15–18 (1999)
19. Sedra, A., Smith, K.: *Microelectronic Circuits*, 6th edn. Oxford University Press, Oxford (2009)
20. Razavi, B.: *Fundamentals of Microelectronics*. Wiley, Hoboken (2008)
21. Jaeger, R., Blalock, T.: *Microelectronic Circuit Design*, 3rd edn. McGraw Hill, New York (2007)
22. Hambley, A.: *Electronics*. Prentice Hall, Upper Saddle River (2000)
23. Floyd, T.: *Electronic Devices*, 8th edn. Pearson/Prentice Hall. ISBN 0-13242973-X
24. Buchla, D., Wetterling S.P.: *Laboratory Exercises for Electronic Devices*, 8th edn. Pearson/Prentice Hall. ISBN 0-13-242971-3
25. Pandiev, I., Donevska, L., Stamenov, D: *Analog Circuits I*. TU - Sofia (2011). ISBN 978-954-438-693-1 (in Bulgarian)
26. Pandiev, I., Donevska, L., Stamenov, D: *Analog Circuits II*. TU - Sofia (2010, 2011). ISBN 978-954-438-694-8 (in Bulgarian)
27. Tyson, S., Hasler, P.: *Field-Programmable Analog Arrays Enable Analog Signal Processing Education*. <https://pdfs.semanticscholar.org/910e/8a962cce98405a4bb316afe0307be200f4a4.pdf>. Accessed 13 Apr 20107

Increasing the Education Quality by Means of Computer-Aided Visualization of the Processes in Electric Power Systems

Mediha Mehmed-Hamza^(✉), Margreta Vasileva, and Plamen Stanchev

Technical University, Varna, Bulgaria

mediha.hamza@mail.bg, m.vasileva@tu-varna.bg, stanchev_p@abv.bg

Abstract. This paper presents the possibility for increasing the education quality by computer-aided visualization of the processes in electric power systems. For a 20 kV electrical distribution grid operational parameters, such as currents and voltages, are computed to study the behavior of the relay protection and auto-reclosing devices, the protective properties and energy sustainability of metal-oxide surge arresters in the visual programming environment of Matlab Simulink. Standard library blocks as well as user-defined ones are utilized during the simulations. The created blocks encompass the following functionalities of modern numerical relay protection devices: overcurrent protection, short-circuit current protection, earth-fault protection, auto reclosing, tripping and closing coils of a circuit-breaker, metal-oxide surge arrester (MOSA). The assessment of the risks from an exposure to electromagnetic fields with frequency 50 Hz at places under transmission power lines includes the determination of the magnetic flux density. It may be ensured by measurements or calculations.

Keywords: Numerical relay protection simulation models metal-oxide surge arrester

1 Introduction

Improving the quality of students' education and the classification of specialties is a continuous task of modern society. The purpose of this paper is to develop simulation models of relay protections with Auto Reclose and metal-oxide surge arresters (MOSA), used in medium voltage electric power systems.

Numerical relay protections are in widespread use for protection of facilities in electric power grids.

To enhance the qualification and training of the staff in charge and to check the correctness of the selected settings using simulation models is appropriate. This paper presents one of the developed simulation models for numerical relay protection encompassing (51) time overcurrent relay, (50) instantaneous overcurrent relay, (51 N) Neutral Time Overcurrent and Auto Reclose. The simulation model is developed in Matlab Simulink programming environment using the advantages of the product enabling visualization of the mode parameters by means of an open and easy to operate system with

quick and effective expansion of the models provided with the available libraries, models and programs thus excluding the necessity to develop any other further program tools.

Computer-aided modeling and visualization of the operation of the relay protections and protective devices enables specialists to appropriately analyze the selected settings and operation of the specified devices.

The simulation model presented herein uses standard blocks of the software product such as transformer, line, relay, but also models developed by the authors for block with an algorithm for relay protection of medium voltage electric power grids with protective functionalities and Auto Reclosing that displays signaling for its operation.

2 Description of the Simulation Models

2.1 Model Scheme of a Digital Relay Protection and Electric Power Grids 20 KV

The model scheme of the considered electric power grids 20 kV is presented in Fig. 1. The model includes the following blocks: electric power supply system 110 kV (S), power transformer 110/20 kV (PT) with grounded neutral at medium voltage through active resistance 40 Ω, model of a powerline, (W1, W2, W3), load (B), block for modeling of a short circuit (3-Phase Fault) and subsystem for numerical relay protection (Relay Protection).

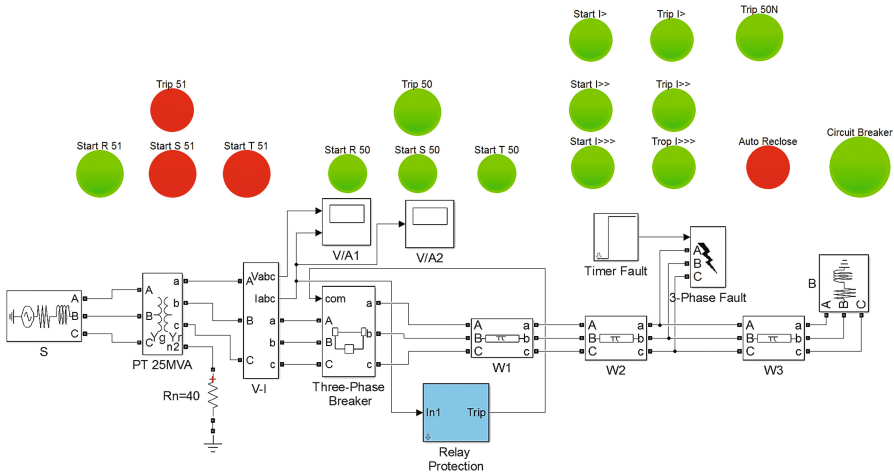


Fig. 1. Model scheme of a block for relay protection and signalization of electric power grid 20 kV

Special attention in the simulation model is paid to the lamp-like signalization in the development of the protections, automatic auto reclosing (79) and the condition of the circuit breaker (switched on/off 52 circuit breaker) [1–4].

In Fig. 2 a created subsystem of digital relay protection with the necessary input parameters is presented [5–7].

Relay Protection block (mask)

Parameters

SampleTime	I1 current transformer, A	I2 current transformer, A
0.25	200	5

Overcurrent (51)

On/Off 51

I 51 (от 0.2 до 40).In t 51 (от 0 до 10 s)

2 0.06

Speed-up 51 Before 79 After 79

Overcurrent (50)

On/Off 50

I 50(от 0.2 до 40).In t 50 (от 0 до 10 s)

8 0.01

Earth fault (51N)

On/Off (Earth fault (51N))

I> Earth fault (51N)	I>> Earth fault (51N)	I>>> Earth fault (51N)
<input type="checkbox"/> On/Off I> Earth fault (51N)	<input type="checkbox"/> On/Off I>> Earth fault (51N)	<input type="checkbox"/> On/Of I>>>
I> (от 0.02 до 20).I0n	I>> (от 0.02 до 20).I0n	I>>> (от 0.02 до 20).I0n
0.2	0.3	0.5
t I> (от 0 до 10 s)	t I>> (от 0 до 10 s)	t I>>> (от 0 до 10 s)
0.04	0.05	0.08

Auto Reclose (79)

On/Off Auto Reclose (79)

Auto Reclose time, s	Number of cycles Auto Reclose (79)
0.05	1

Fig. 2. Block for entering of the digital relay protection input parameters of a powerline 20 kV

The simulation model of the digital relay protection includes:

- Overcurrent protection (51 time overcurrent relay) – with possibility for putting in and out of operation of the protection, possibility of putting in and out of operation of protection acceleration for two variants – before and after auto-reclosing;
- Overcurrent protection (50 instantaneous overcurrent relay) – possibility for switching in and out of operation of the protection;
- Overcurrent earth protection (51 N Neutral Time Overcurrent) – possibility for switching in and out of operation of the protection, possibility of putting in and out of operation of the separate steps;
- auto reclose (79 Auto Reclose) – possibility for switching in and out of operation, setting the time and number of cycles of the auto reclose.

The displayed signaling for the operation of the simulation model includes:

- Trip from 51 time overcurrent relay;
- Trip from 50 instantaneous overcurrent relay;
- Trip from 51 N Neutral Time Overcurrent from I, II and III stage;
- Starting the operation of the current relays in Overcurrent protection and instantaneous overcurrent relay and Neutral Time Overcurrent;
- Starting Auto Reclosing.

The activation of the respective protections and of respective relays is marked with red. The condition of the circuit-breaker of the protected equipment is closed circuit breaker (red signaling) and open circuit-breaker (green signaling).

The subsystem for the relay protections and the created circuit breaker model with tripping and closing coil is presented in Fig. 3 [8].

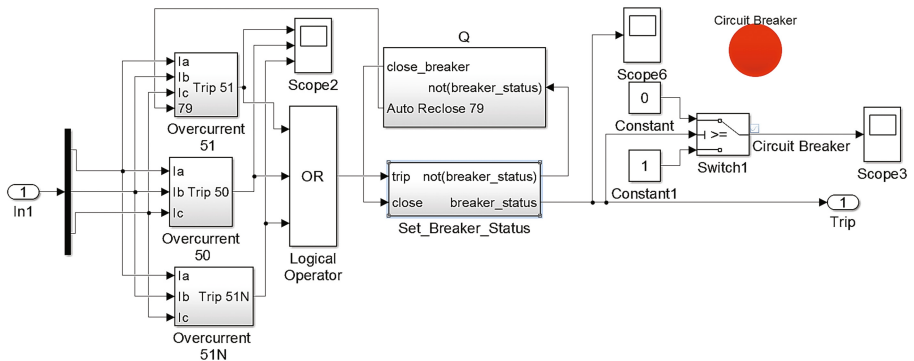


Fig. 3. Subsystem for relay protections and model of a circuit breaker

2.2 Study of the Protective Action and Energy Sustainability of Devices for Surge Protection Against Lightning Stroke of a Phase Conductor of the Overhead Powerline (OHL)

The processes in the electric power grid under the effect of a single lightning stroke on phase A in the first interpole of OHL with current amplitude $I_m = 80$ kA and shape $1/10 \mu s$ are studied. The shown parameters correspond to lightning current higher than the level of lightning protection for OHL 20 kV, i.e. in the model for investigation the impulse breakdown is considered which leads to cutting of the overvoltage wave. The voltages in the other two phases (UB and UC) are sinusoidal with frequency 50 Hz and amplitude equal to the maximum phase voltage of the power grid.

The structure elements in the studied electric power grid are with the following parameters:

- Power transformer 110/20 kV, 63 MVA (T1);
- Overhead power line (W1), constructed with conductors AC 95, concrete or steel towers with isolating elements NS20 or VHD20 and length 2,5 km;
- Cable powerline (W2), constructed with single-phase cables type XLPE 120 (W3) and length 30 m;

- MOSA (Metal-Oxide Surge Arresters) with continuous operating voltage 19 kV [10];
- Power transformer 20/0,4 kV, 630 kVA (T2)
- Voltage instrument transformers TV1 and TV2, presented as a capacitance of 200 pF.

Controlled quantities for assessment of the processes are the voltage, which the overvoltage protection device (OVPD) limits the overvoltage to, the current through OVPD, the energy dissipated in MOSA and the voltage in the non-protected end of the cable line [9].

For comparison of the calculated results is used controlled measurement of the voltages at the beginning of the OHL, at the end of the OHL and at the end of cable line without connected MOSA (Fig. 4).

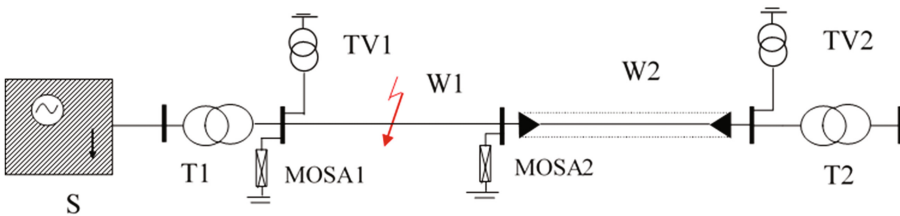


Fig. 4. Single line scheme of electric power grid 20 kV with cable connection of a transformer substation (W1-OHL; W2-Cable line)

3 Practical Results

The work of the relay protection simulation model and visualization of the change of the regime parameters are presented in Fig. 5. Two-phase short circuit at 20 km from the beginning of the powerline, which arises at a moment 0.02 s is simulated. The fault is permanent. Overcurrent relay (51) is introduced with acceleration before auto-reclosing, instantaneous overcurrent relay (50) and overcurrent neutral relay (51 N). The auto-reclosing is with single action. It can be seen from the Fig. 5 the fault trip at 0.062 s, auto reclose action and second trip by 51 time overcurrent relay. The time for trip from time overcurrent relay for the first time is with smaller delay because acceleration of the protection is introduced.

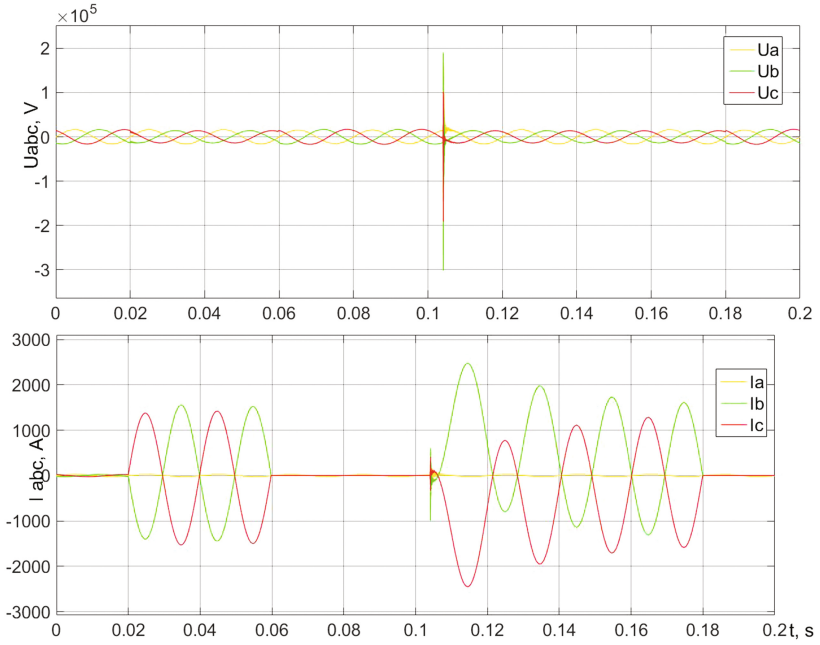


Fig. 5. Change of the regime parameters for two-phase short-circuit and tripping time overcurrent relay

The three-phase currents (I_a , I_b , I_c) for single-phase fault and single auto-reclosing action is shown in Fig. 6.

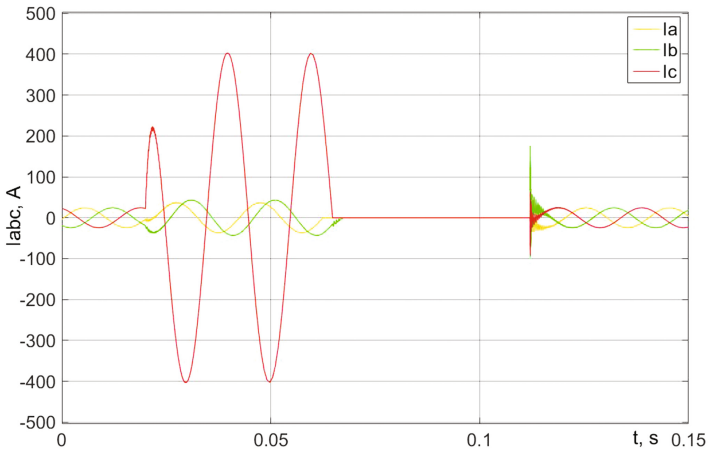


Fig. 6. Currents at single-phase fault and single auto-reclosing

The simulation model allows one to change:

- the supply power transformer;
- the type of powerline and its length;
- the load;
- location and type of the fault;
- the used relay protections;
- On/Off of the acceleration of time overcurrent relay;
- On/Off of the auto reclose.

In Fig. 7 are presented the current and voltage in the phase conductors of OHL at the place of a lightning stroke under the impact of a lightning over a phase conductor of a OHL. Currents and voltages of the phase A are given in green, in red - phase B and in blue - of the phase C.

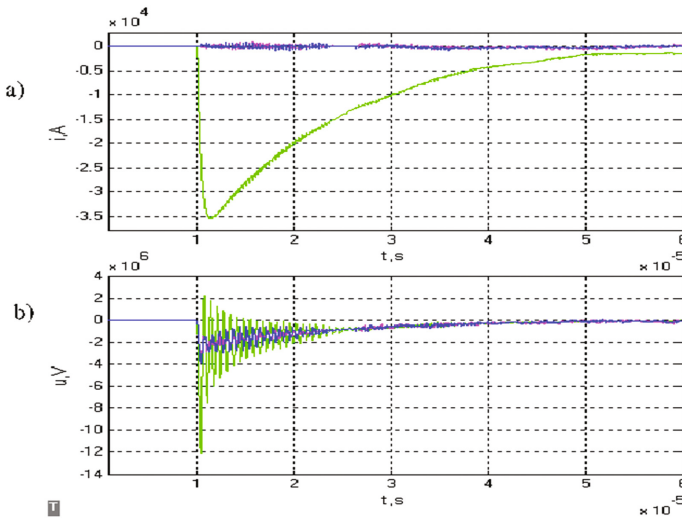


Fig. 7. Current (a) and voltage (b) in the phase conductors of OHL at the place of a lightning stroke

The results for the voltage of the three phases at the beginning and at the end of the OHL and at the end of cable line without switch on MOSA are presented in Fig. 8.

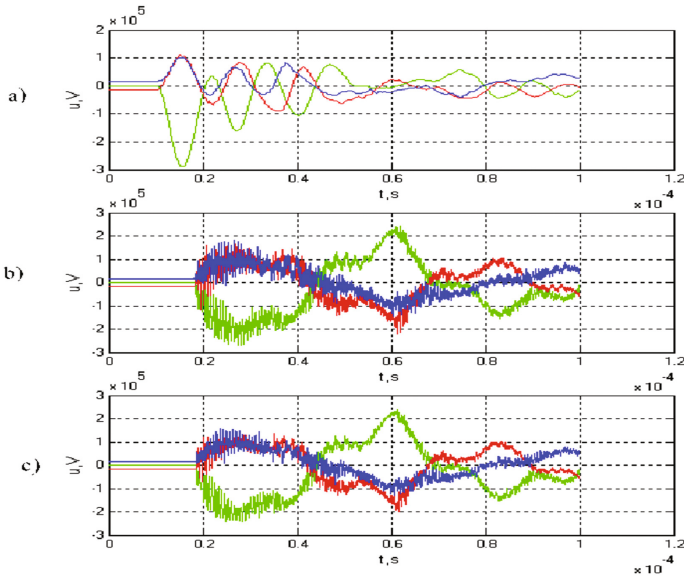


Fig. 8. Voltage at the beginning OHL, (a) at the end of OHL (b) at the end of cable line (c) without MOSA

Common regularity in the received time dependencies of the voltages is that they develop as inharmonic attenuating oscillations, which in established mode go to the shape of the operating voltages.

The overvoltage in phase A at the beginning of OHL is with amplitude 14,7 p.u and induces in other two phases overvoltage with amplitude 5,9 p.u. (Fig. 8).

In Fig. 9 are shown the results with MOSA for the voltages, currents and energy dissipated in MOSA1. The MOSA of all phases limit the overvoltage to the respective protection level (Fig. 9). The time for which MOSA remain in conductive state can also be reported from these figures.

The energy, dissipated in MOSA1 and MOSA2 of the affected phase A, under the impact of atmospheric overvoltage with set parameters of the lightning current is less than the acceptable for the investigated type MOSA. The energy dissipated in MOSA of the other two phases are even smaller.

The voltage in the unprotected end of the cable line can exceed the standard isolation level for equipment with $U_n = 20$ kV at certain conditions.

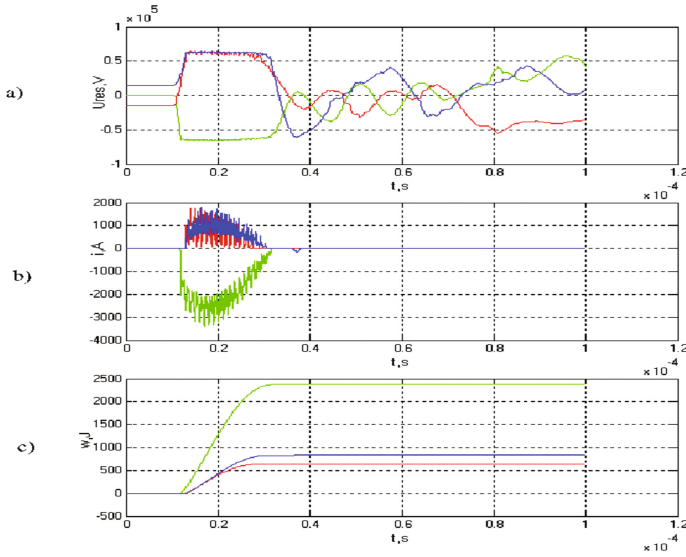


Fig. 9. Residual stresses (a), currents (b) and energy (c) separated in MOSA 1

4 Conclusions

The Matlab Simulink programming environment described in this study is used to develop simulation models of numerical relay protections and Auto Reclose, used in medium voltage electric power grids.

The advantages of the developed models are as follows:

- Easy input of set-up parameters for the numerical relay protections with Auto Reclose for advanced protection of power systems by means of the developed block for data input;
- The developed lamp signaling for the operation of the separate functional protections and Auto Reclose visualizes the work of the simulation model of the numerical relay protection and the state of the circuit-breaker of the protected facilities;
- Visualization of the variation of the mode parameters in the values when the relay protection and the operation of the Auto Reclose trip the short circuit;
- To provide an option for input and output of the separate blocks according to the instantaneous values of the numerical relay protections and Auto-Reclose, as well as an option to set the operation parameters of the Auto Reclose;
- The simulation model of a 20 kV electric power grid with a numerical relay protection can be used for training and advanced qualification of electrical engineers as well as for analysis and verification of selected settings of the numerical relay protections.

The developed models for investigation of MOSA in electric power grids can be used for their more precise choice as the configuration of the scheme and the elements in it under the impact of overvoltage with different shape and duration are considered.

Acknowledgment. This research is realized within the frame of project “Computer modelling, programming, visualization and development of laboratory complex education” NP1/2017 in Technical University of Varna, Bulgaria.

References

1. Andreev, S: Relay protection. TU-Varna, Varna (2005)
2. Paul, A.M.: Power System Protection. IEEE Press, New York (1998)
3. Kezunovic, M., Ren, J., Lotfifard, S.: Design, Modeling and Evaluation of Protective Relays for Power Systems. Springer, Cham (2016). doi:[10.1007/978-3-319-20919-7](https://doi.org/10.1007/978-3-319-20919-7)
4. Idris, H., Hardi, S., Hasan, Z., Hasan, S., Nisja, I., Baharudin, H.: Modelling and simulation of transmission line auto-reclose scheme using matlab/Simulink. In: International Conference on Power, Energy and Communication Systems - IPECS 2015, Perlis, Malaysia (2015)
5. Siemens 7SJ64 Manual
6. <http://www.abb.com/>
7. <http://www.roconbg.com/bg>
8. <http://www.mathworks.com>
9. Bayad, A., Harid, N., Zehar, K., Belkhiat, S.: Simulation of metal oxide surge arrester dynamic behavior under fast transients. In: The International Conference on Power Systems Transients - IPST 2003, New Orleans, USA (2003)
10. Overvoltage protection Metal oxide surge arresters in medium voltage systems, Application guidelines, ABB, May 2011

Project of Experimental Complex for Power System Stability Studies

Yulian Rangelov, Nikolay Nikolaev^(✉), Yoncho Kamenov, and Krum Gerasimov

Department “Electric Power Engineering”, Technical University of Varna, Varna, Bulgaria
{y.rangelov,n.nikolaev,j.kamenov,k.gerasimov}@tu-varna.bg

Abstract. The goal of the publication is to present a project for an experimental complex of a small-scale electric power systems that would allow real-time small-signal and dynamic stability analysis. The model of the power system would allow for simulation of different ratio between renewable and conventional generation. The physical model will be three-phase and will include all main components the electric power systems usually comprise – conventional synchronous units, generators based on renewables (wind and solar), power transmission grid (lines and transformers) and controllable loads. All generation units will be able to control the voltage magnitude and frequency. The system operational parameters will be measured and logged in real-time by using very accurate DAQ system with high sampling rate. The system will allow manual and automatic control of the processes.

Keywords: Experimental complex · Power system · Physical model · Synchronous generator · Wind generator · Photovoltaic generator

1 Introduction

Power system analysis is a process based on solid mathematical foundation, relying on many factors, which guarantee adequate results. Nowadays, the computer technologies have provided very big processing power and software platforms to model interconnected power systems and study the power flows, transient and small-signal stability without major difficulties. Similar to any other scientific field, it is desirable to confirm the mathematical models with real-life experiments. Such experiments in the real power system are almost impossible to conduct due to significant risk for violating its secure operation. From that perspective, it is preferable to perform experiments in a laboratory environment meaning that a physical model of a power system is built [1–5]. Such lab model should be capable to adequately reproduce the studied phenomena in the real world. This paper presents a project for the development of such power system laboratory model, which will be used to confirm results regarding the impact of renewable generation on the load-frequency control and power system stability issues. The general concept of the model is presented. It includes a transmission grid, generation and load power units, DAQ measurement and control systems [6].

2 Power System Model

Every power system consists of three main interconnected components – generation units, transmission system and electrical energy consumers. The concept for power system physical model includes all three components combined and connected to external grid. Figure 1 depicts the single-line diagram of the model, although it is going to be three-phase. The system includes four types of generation – conventional (three synchronous generators) and two generators based on renewable energy (wind and solar). The transmission grid consists of eight buses and has meshed topology, which allows switching to many different configurations. Every node will have its own load, either constant impedance or motor load. The transmission branches will be modelled with inductors to represent both power lines and transformers. The power system model will be modular and will thus allow easy upgrades and reconfiguration to meet future

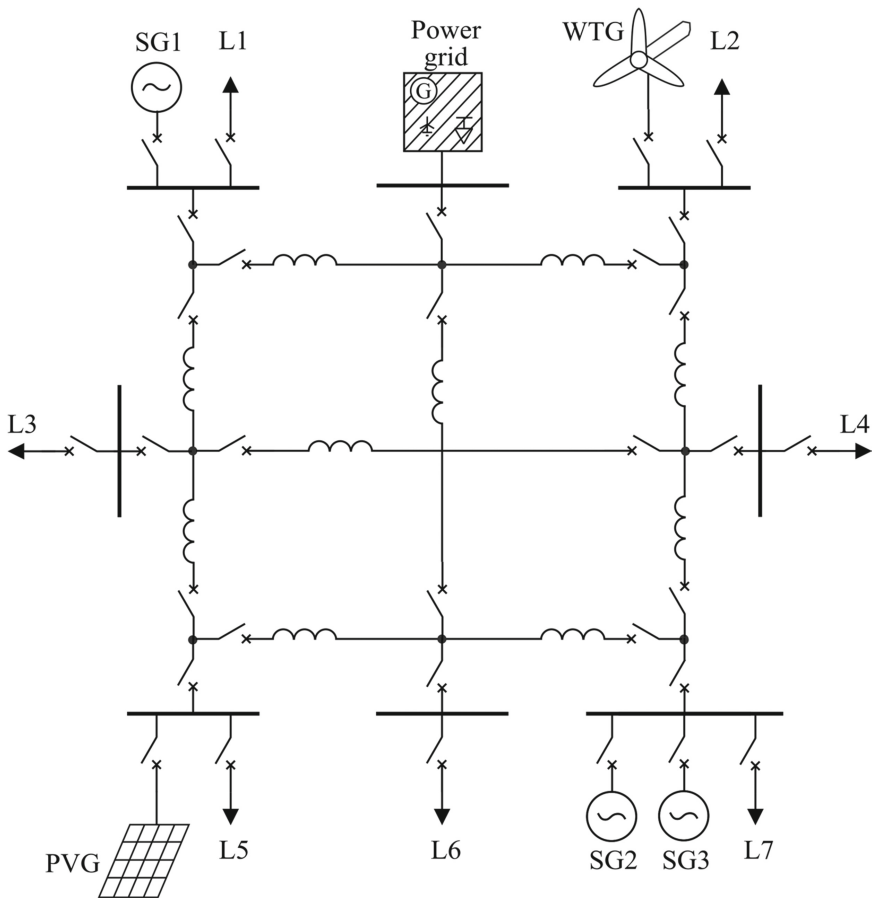


Fig. 1. Single line diagram of the power system lab complex

needs. The control of the model will be performed in two ways: (i) with pushbuttons and indicators on an electrical cubicle and (ii) via web based SCADA system.

3 Description of the Power Units

The subsections below briefly explains the main components and functionality of the system components depicted in Fig. 1. Every generator and load will be further referred to as a power unit.

3.1 Synchronous Generator

The block diagram of the power unit “synchronous generator” is depicted on Fig. 2. Instead of real steam/hydro turbine the generator is coupled to a DC motor with either shunt or compound excitation. The torque of the motor (turbine) is controlled by means of pulse-width modulation (PWM). The excitation of the synchronous machine is released with a DC power source, whose current is controlled by electronic switch (IGBT transistor¹) via PWM.

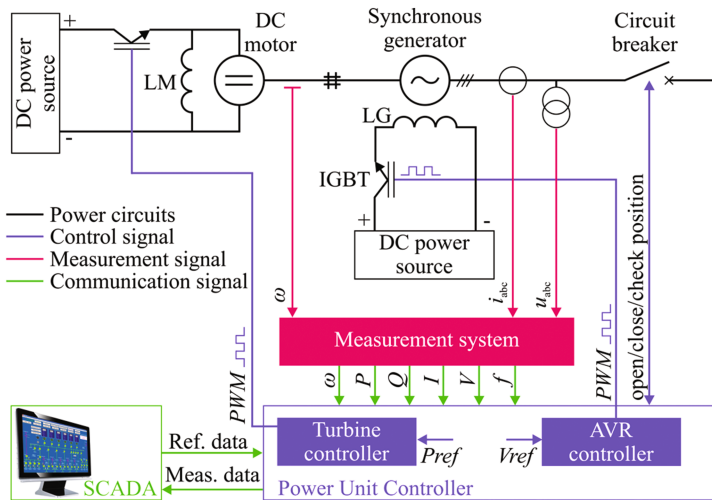


Fig. 2. Synchronous generator

The generator and the motor are controlled by a Power Unit Controller (PUC). The PWM signal for the DC motor is regulated to maintain a real power output of the generator equal to the reference value P_{ref} (turbine controller). In a similar way, the generator output voltage is controlled by a PID regulator (Automatic Voltage Regulator) which produces PWM signal with a value that guarantees an output equal to V_{ref} .

¹ The protective collector-emitter diode is not depicted on the schematic.

The position of the circuit-breaker, as well as the open/close operations are also managed by the PUC.

The measurement system comprises the following sensors: current transformer, voltage transformer and speed transducer. Based on their input, the measurement system computes the operating parameters (power, voltage, current, frequency, rotor speed) and communicates them to the PUC. The measurement data is used as feedback within the PUC and is also transferred to the SCADA system of the laboratory complex. The reference values for the controlled parameters are either passed by the user via the SCADA or via the local interface of the PUC.

3.2 Photovoltaic Generator

The photovoltaic (PV) generators usually comprise PV modules connected into strings and a power inverter to interface the modules to the electrical grid. The idea of the lab complex is to be capable of performing experiments in any time of the day and throughout the entire year. For that reason, mounting PV modules on the rooftop of the faculty building would impose one to rely on the weather conditions, meaning that the experiment cannot be conducted at arbitrary time. Other possible solution is to install the modules inside the building and power them with controlled light source. The peak power of the PV power unit will be about 5 kW. This amount of power requires approximately 20 panels, which would take a lot of space in the lab. Considering that the lighting source should be many times more powerful than the modules and a lot of heat should be dissipated, one should classify such a solution as non-feasible.

A more feasible and flexible solution is to use a controlled current source instead of real PV modules (see Fig. 3). This source can be programmed to have an arbitrary V-A characteristics and arbitrary power output at any time desired. Suitable electronic circuit is proposed by [7].

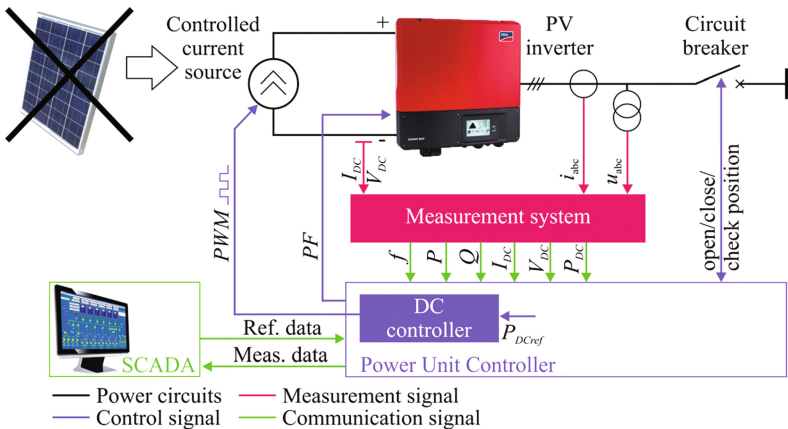


Fig. 3. Photovoltaic generator

The measurement system and the PUC has similar functionality. This time the controller regulates the DC power injected into the PV inverter.

3.3 Wind Generator

The wind turbine model to be implemented is full-converter type [8]. Permanent magnet synchronous generator (PMSG) will be used, as it does not need AVR (see Fig. 4). DC motor, possibly brushless, will be used to imitate the wind turbine. Its power output will be controlled via PWM and the turbine characteristics will be modelled in the PUC. The power of the unit should be few kilowatts.

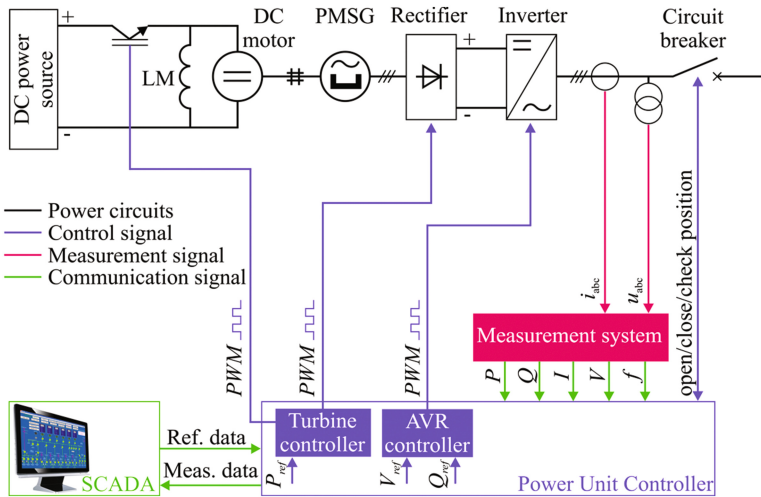


Fig. 4. Wind turbine generator

Since the rotor speed will vary with the power output, the PMSG will produce voltage with variable frequency. Therefore, the AC voltage will be rectified and then inverted into AC, to interface the grid.

3.4 Motor Load

Big part of the power system demand accounts for induction motors [9]. Hence, a realistic power system model should possess such type of load. The proposed motor load model is presented in Fig. 5. To control the power consumption, an electromagnetic (EM) break will be coupled to the rotor [10]. The break will create variable loading torque, which will be controlled by the PUC, respecting a reference power output P_{ref} .

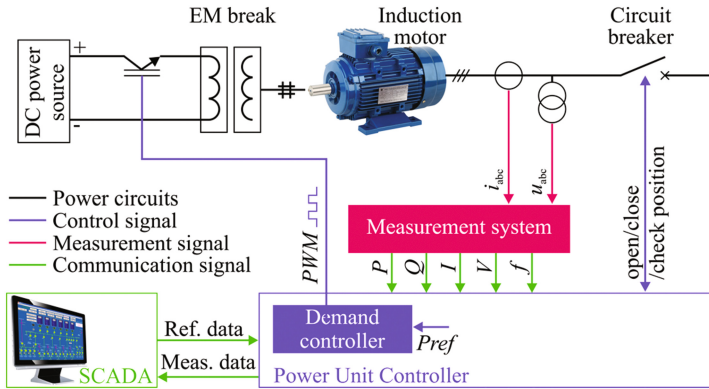


Fig. 5. Motor load unit

3.5 Resistive Load

Another significant part in the system demand is the constant impedance load. Therefore, this type of consumption will also be implemented in the laboratory complex. Its diagram is presented in Fig. 6. To minimize the construction of this power unit we propose to use a rectifier and an IGBT transistor, controlled with PWM, to power a resistive element.

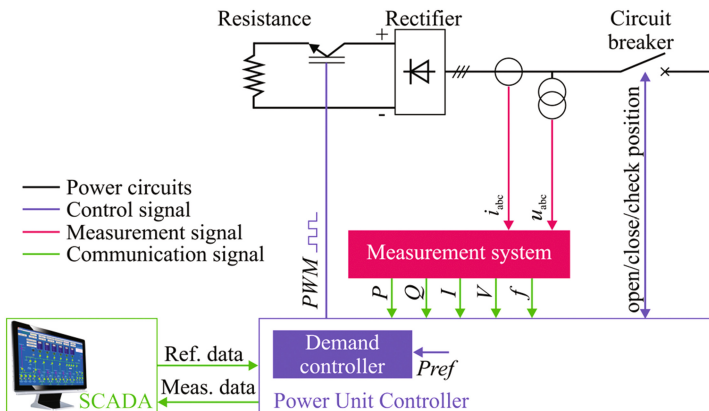


Fig. 6. Resistive load unit

4 Measurement and SCADA System

It has become clear that the function of all power unit controllers is to collect data from the measurement system. This data is used for two main purposes: (i) feedback for the regulators and (ii) to communicate it to the SCADA system. The SCADA will visualize the measurements and the circuit-breakers position on the display. The most convenient

from for programming the user interface is in the form of web server which will be assessable from the local area network. Another important functionality of the SCADA will allow the user to specify reference parameters directly from the web interface and therefore control the operating point of the power system in real-time.

5 Conclusions

The laboratory complex will be suitable to study the effects of significant share from renewable generation on the power system stability and load-frequency control. It is designed in a modular way and allows for easy reconfiguration in many different states. The presented power unit controllers, measurement systems and SCADA system will ensure maximum controllability and observability of the power system. In such a set up the data can be easily stored, processed and analyzed after the experiments. Besides stability studies, the experimental complex can be used to educate students in many other different operational aspects of power system operation.

Acknowledgements. This paper is a results from project “*Study of the electric power system stability and frequency control at a predominant share of renewable energy generation*” grant ДН07/27/15.12.2016 from the Bulgarian National Science Fund.

References

1. Balamurugan, S., Nambiar, T.N.P., Janarthanan, N., Vijaya Chandrakala, K.R.M.: Laboratory model to teach power system stability. In: IEEE International Conference on MOOC, Innovation and Technology in Education (MITE) (2014)
2. Meliopoulos, A.P.S., Cokkinides, G.J.: Virtual Power System Laboratories: Is the Technology Ready? Web document (2002)
3. <http://electricalelectronicsindia.com/educational-motors-machines>. Accessed Apr 2017
4. Karady, G., Heydt, G., Iwamoto, S.: Role of laboratory education in power engineering: is the virtual laboratory feasible? Part I. In: Power Engineering Society Meeting, IEEE (2000)
5. Tamura, Y., Dan, E., Horie, I., Nakanishi, Y., Yokokawa, S.: Development of power system simulator for research and education. IEEE Trans. Power Syst. 5(2), 492–498 (1990)
6. Rangelov, Y., Avramov A., Nikolaev, N.: Design and construction of a laboratory SCADA system. In: Proceedings of Papers on ICEST 2015, Sofia, Bulgaria, 24–26 June 2015, pp. 300–303 (2015). ISBN 978-619-167-182-3
7. Romeo, G., Urbini, G.: “Unstable” Power Supply Simulates Solar Panel Behavior. Web document (2009)
8. Standard IEC 61400-27-1:2015, Wind turbines - Part 27-1: Electrical simulation models - Wind turbines
9. Navarro, I.: Dynamic load models for power systems. Ph.D. thesis, Lund University (2002). ISBN 91-88934-26-8
10. <http://www.magnetictech.com/current-controlled-electric-hysteresis-brakes/>. Accessed Apr 2017

Determination of the Temperature of Cathode Unit of Indirect Plasma Burner Through a Computer Simulation Model

Krastin Yordanov^(✉), Tatyana Mechkarova, Aneliya Stoyanova, and Penka Zlateva

Technical University of Varna, Studentska Str.1, 9010 Varna, Bulgaria
krystinkr@gmail.com, {tatqna13,tatuna10,pzlateva1}@abv.bg

Abstract. The article is developed computer simulation analysis of the spread heat flows in indirect torch for gas nitriding, using the software Autodesk CFD. Different methods of using a stream of ionized plasma as a source of energy are applied early 50 s of last century, but only in recent years, they are widely used in chemical heat metal processing. The process is based on the ionization of different gases by an electric arc and plasma jet Focus on the product developed through a special nozzle design of the torch indirect.

During recent years research in the area of application of low-temperature plasma in chemical engineering, metallurgy, machine-building and a number of other branches of industry is underway in the technically developed countries. The use of the research results allows substantially intensifying the existing technological processes and creating entirely new materials, technologies and equipment in production.

One of the new highly productive methods for hardening a titanium surface is the plasma nitriding with indirect plasma torch.

Analysis of the factors influencing the spatial stabilization of the arc and the erosion of the nozzle node in indirect Plasma torch for chemical and thermal treatment shows that significant influence, unless the technological parameters of the regime, has the type and geometry of the nozzle node. In order to reduce the volume and the amplitude of a large-scale shunt create a computer simulation model describing the thermal load on the main nodes of indirect plasma torch in plasma nitriding of titanium alloys.

Keywords: An indirect plasma torch · A computer model · Temperature fields · Cathode node

1 Introduction

As a result of the rapid development of the technologies for treatment of titanium and titanium alloys over the last 10 years, the production of various components and parts has expanded. Although the titanium alloys operating in the conditions of friction and contact load have some disadvantages, such as low surface hardness and low wear resistance, they remain a preferred product by many industries [1–4].

The existing conventional methods of surface strengthening require costly equipment, long action time and highly qualified staff. New methods are sought to reduce the action time and improve the efficiency of existing equipment. A new method in this regard is thermo chemical treatment (nitriding) using an indirect plasma torch.

This paper studies the results obtained from a computer model created for defining the temperature effect on a cathode node of an indirect plasma torch for the surface plasma gas nitriding.

2 Content

The topicality of the proposed paper is determined by the necessity to improve the efficiency of operation of the nodes with the highest heat load in a PTN50 indirect plasma torch [1, 5–7].

Figure 1 shows the section view of the plasma torch PTN50 [7–9].

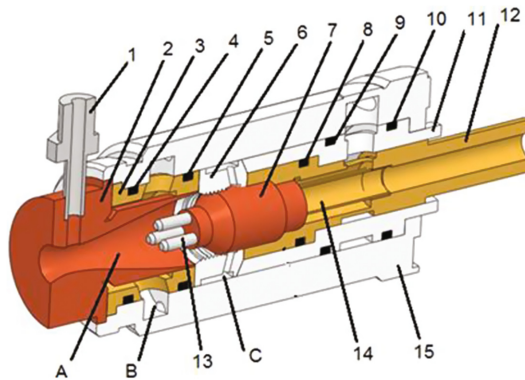


Fig. 1. Schematic view of a PTN50 plasma torch with three electrodes: 1-an inlet fitting; 2- a copper nozzle (anode); 3- cooling water inlet and distribution bush; 4, 5, 8, 9 and 10-gasketed ring; 6-a teflon gas distribution bush; 7- a copper cathode holder; 11- a polyamide electrical insulation bush; 12- an inner brass body; 13- three tungstic cathodes; 14- cooling water outflow; 15- brass body; A- ionization chamber; B- damping chamber; C- compensation chamber

2.1 Model of Torch PTN50 with Three Electrodes

The plasma torch is made up of an outer body 15 to which the nozzle/anode/2 is fitted and an inner body 12 to which the cathode holder 7 is fitted. The cathode holder is designed as a central body made up of a copper water cooling body and tungstic electrodes 13. The inner body is electrically insulated from the outer one by bush 11. The gas distribution bush 6 by its compensation chamber C provides a plasma-forming gas feed with permanent pressure and debt in the ionization chamber A. Thus steadiness of arc burning is ensured. The nozzle anode is designed as a central body. It ensures a steady arc length and axial leak of the plasma-generating gas, directing the plasma jet to the area of treatment with sufficient quantity of atomic /N/ and /N+/ ionized nitrogen.

It is well known that the steadiness of operation of plasma torches is determined by the ability of the cathode and anode nodes to retain their original geometric shape for a maximum period of time. Even minimal loss of electrode material that in certain cases is deposited on the treated surface may fail the process of nitriding.

Our experience using a PTN50 proves that often the turbulent pulsations of the plasma-forming gas and the vertical pulsations of the electric arc create erosion pits on the nozzle and the tungstic cathode due to local overheating and melting of the metal.

The analyses have shown that the geometry of the tungstic electrode and the regime parameters have a significant effect on the arc stabilization [8, 10–12].

The author's previous studies examined the possibility of using a composite cathode node with one, three and five tungstic electrodes. It was established that in different technological parameters, used in titan and titan alloys nitriding, a composite cathode node with three tungstic cathodes has the highest service life rate [8, 13, 14].

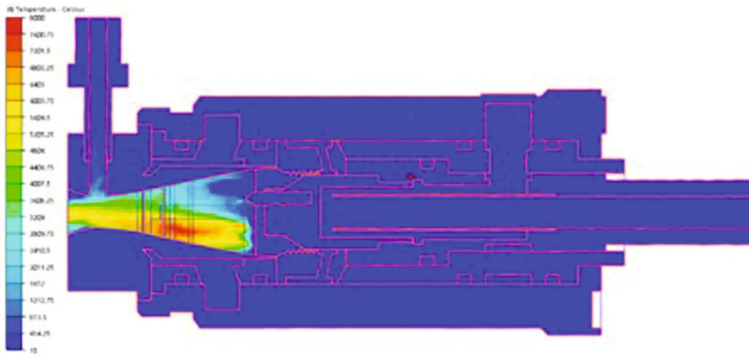
From a theoretical point of view, the heat streams being formed on the surface of the cathode are immediately associated with the physical processes taking place in the area near to the electrode and the arc core. In a composite cathode node with three tungstic electrodes, their front surface is heated up by the electric arc mainly due to its heat action. The heat exchange between the tungstic electrodes and the cathode holder that is made of electrolytic copper is determined by the microgeometry of the contacting surfaces for each of the electrodes [7, 11].

2.2 Thermal Analysis of the Torch PTN50 with Three Electrodes

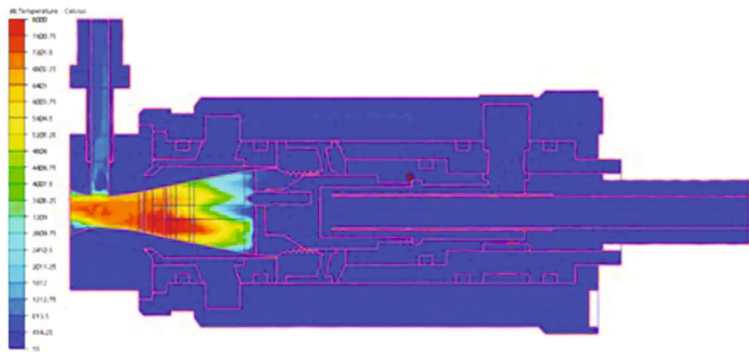
To determine the effect of temperature on the cathode node, a computer simulation is developed and a thermal analysis is conducted by entering input data in the Autodesk Simulation CFD Program. To achieve a better reliability of the obtained results in the program, real regime parameters using plasma-forming gas - Ar/N₂ are entered and the basic criteria for geometric similarity [9, 14]:

- Operating current – I , 500 A;
- Electric power – P , 35 kW;
- Type of plasma-forming gas – Ar/N₂;
- Gas flow rate of plasma-forming gas – Q , 50 nlpm;
- Length of the electrode – l , 14 mm;
- The arc discharge is carried out in geometrically similar plasma torches;
- The temperature of the gas in the inlet to the electric arc chamber is not significantly different from that of the ambient medium;
- Direct current with straight polarity is used;
- The density of the heat stream on the surface of the cathode is equal along its entire vertical section;
- Current density is equal along the vertical section of the cathode;
- The process is stationary. In fact, it is a quasistationary one.

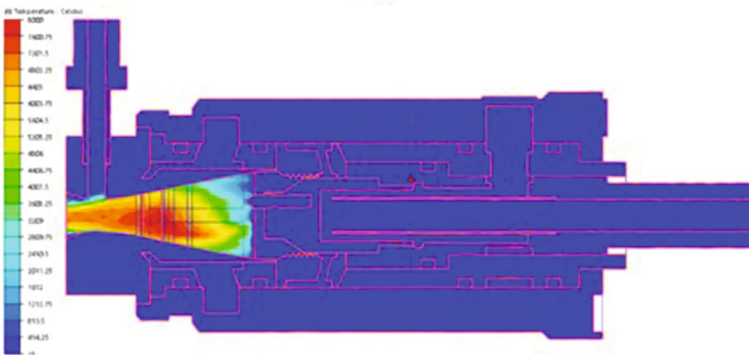
After entering the initial and border-line conditions in the model, a thermal analysis (Fig. 2) of temperature distribution in the cathode node is conducted (Fig. 3) [15].



a)



b)



c)

Fig. 2. The distribution of temperature fields from the Autodesk Simulation CFD program at a power of 35 kW to the indirect plasma engine: (a) 30 s, (b) 60 s, (c) 120 s

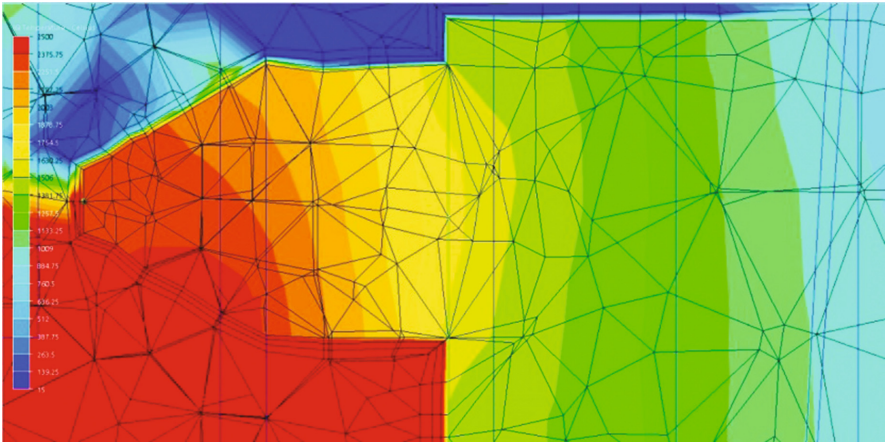


Fig. 3. The distribution of temperature fields of the cathode node at 120 s

The computer simulation is performed for a period of 8 h. In the assigned computer simulation program, the maximum temperature of the front surface is established in 10-th sec and is within the limits from 2170 °C to 2200 °C (Figs. 2 and 5). After 60-th sec, the temperature settles down to a constant value and is within the limits between 1150 °C and 1000 °C for the entire period of 8 h. This is an indication of a lower temperature load of the electrodes, and respectively of a higher service life rate of the plasma torch. After the 8th hour, a sharp increase in temperature is observed and it reaches up to the overcritical value (Fig. 4).

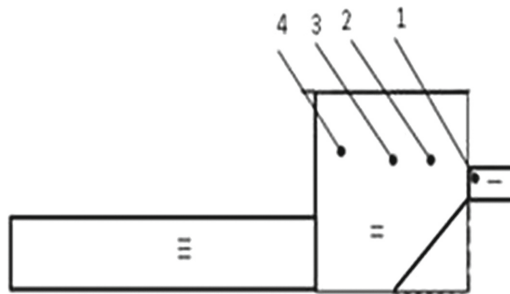


Fig. 4. Positions of the thermocouples in the cathode

The obtained experimental results for the temperature in the four characteristic points of the cathode are illustrated in Table 1.

To compare the theoretical and experimental results, they are both shown graphically in Fig. 5, with the ordinate being the temperature distribution in °C, and the abscissa is the temperature impact time in sec.

Table 1. Results from the thermocouples in the cathode

Time, τ , sec	Temperature, t °C			
	t1	t2	t3	t4
5	1600	600	300	40
10	2100	1000	500	42
20	2000	1200	600	22
40	1150	1100	570	19
60	1200	800	400	18
80	1100	650	320	16
120	1000	430	300	15

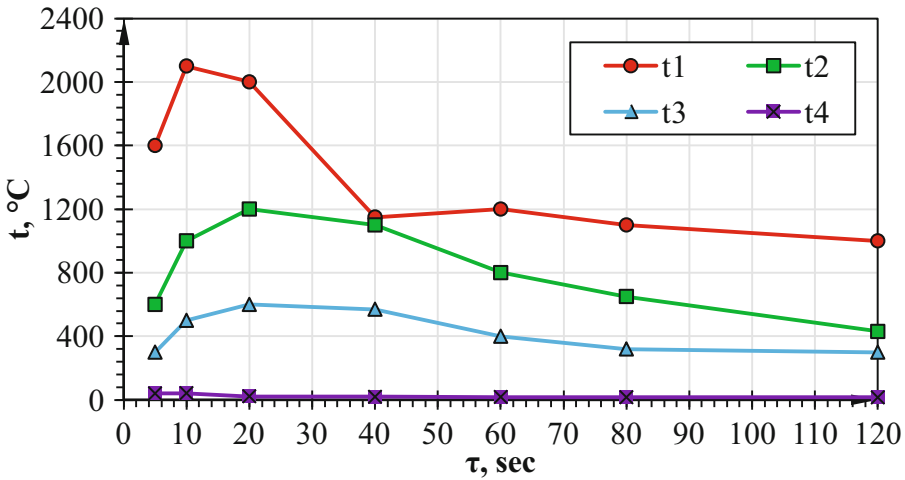


Fig. 5. Time – temperature curves in the cathode of the indirect plasma torch at 35 kW

From the graph, it is seen that the highest cathode temperature recorded by sensor 3 obtained in 45 s, and from Fig. 3 the maximum reading at the tip of the electrodes is about 2350 °C.

3 Summary

On the grounds of the conducted analysis of the obtained results the following conclusions are drawn:

1. A computer simulation model of the temperature field distribution in the cathode node of an indirect plasma torch with the aid of the Autodesk Simulation CFD program product is proposed.
2. The maximum temperature detected by the computer simulation model is in 10-th sec and within the range between 2170 °C and 2200 °C. It was established that the temperature parameters remain constant after 60-th sec; they are within the range

between 1150 °C and 1000 °C and remain unchanged for the whole 8-hour duration of the action.

3. It has been found that the results obtained from the computer simulation model adequately reproduce the heat field distribution processes in depth of the cathode.

References

1. Annual Book of ASTM Standards, 03.01 (Standard E384), pp. 406–429. ASTM, Philadelphia, PA (2000)
2. Annual Book of ASTM Standards, 03.01 (Standard E92), pp. 218–226. ASTM, Philadelphia, PA (2000)
3. Bajic, D., Jozic, S., Podrug, S.: Design of experiment's application, Prispjeb (2009)
4. Clarke, R.D.: *Int. J. Adhes. Adhes.* **19**, 205–207 (1999)
5. Badini, C., Bianco, M., Guo, B.: *Applied Surfaces Science* (2002)
6. Guo, Z.: Modelling of phase transformations and mechanical properties of titanium alloys during processing. Ph.D. thesis, The Queen's University of Belfast, UK (2000)
7. Skulev, H., Manov, M.: Surface hardening methods of titanium and titanium alloys. *Microsc. Anal.* **13**(7), 23–29 (2010)
8. Skulev, H., Georgiev, B., Iordanova, I., Sprecher, C.M., Wahl, D., Hristova, A.: Bond order potentials for atomistic studies of dislocations and other extended defects in TiAlN. *J. Optoelectron. Adv. Mater.* **11**(9), 69–83 (2009)
9. Skulev, H.: Examination of formed nitride layer during gas nitriding of titanium. In: *International Scientific Conference UNITECH 2008*, No. 2, pp. 181–186 (2008)
10. *ASM Hand Book, Alloy Phase Diagrams*, vol. 3 (1995). 512 pages
11. DIN 2310-87, Teil 1. Termisches Schneiden. Allgemeine Begriffe und Benennungen
12. Ivanova, R., Sha, W., Malinov, S., Zhecheva, A.: *Conference Proceedings of 15th International Corrosion Congress*, Grenada, Spain (2002)
13. *ASM Hand Book, Heat Treating*, vol. 4 (1995). 534 p
14. Boyer, R., Welsch, G., Collings, E.W. (eds.): *Materials Properties Handbook: Titanium Alloys*. ASM International, Materials Park, OH (1994)
15. Kleijnen, J.P.C.: An overview of the design and analysis of simulation experiments for sensitivity analysis, Tilburg (2003)

Modeling, Measurement and Management of Business Processes in Organization

Krasimira Dimitrova^(✉)

Technical University of Varna, Varna, Bulgaria
krasimira.dimitrova@tu-varna.bg

Abstract. Creating value in each company is based on business processes in it. Their rational organization is a key factor in their transformation into a competitive advantage for the company. In order to achieve this it is necessary the business processes to be analyzed in detail, continuously optimized and effectively managed by means of combining of management methods and techniques with tools of information technology.

This study is focused in particular on business models and business modeling as a formalized and understandable to all stakeholders' activities of the organization and their interaction through material, financial and information flows. The main issues in it are monitoring and control of business processes as well as reengineering of the business processes as a fundamental rethinking and a complete redesign of business processes to achieve radical improvements in the key indicators of the company. For management of processes it is necessary to be realized full cycle of the process - planning, implementation, monitoring and improvement.

Keywords: Business processes · Business process modeling · Material flows · Information flows · Information technology

1 Introduction

In a competitive environment, companies must constantly respond to the changes in the market, to seek for innovative solutions and to achieve a competitive advantage over their competitors. The idea of process-oriented company structure begins to apply by the end of the 80s in order to increase the efficiency of business through the application of Business Process Re-engineering or management of internal business processes (Business Process Management).

Business process is a special process that serves the implementation of the main goals of the enterprise and describes the whole range of activities in the organization.

Effective management of processes, especially in big companies today is practically impossible without adequate IT support. But the introduction of information systems is not sufficient. Companies' long-term success can be achieved mainly through the efficiency and coherence of implemented business processes and their proper organization within the company and it becomes one of the key factors for competitive advantage on

the market. Modeling of processes is often an integral precondition for their effective implementation and improvement of management processes. Business process model transforms innovation into an economic value for the business. Business model describes how the business organization positions its products on the free competitive market and how on that basis it participates in the value chain creation.

2 Business Process Modeling

Business process model includes everything that is related to the effective and efficient management of processes in the organization.

The quality of information models has long been a subject of scientific debate, especially in models for the transfer of data and process models. However, until now are not formed standardized criteria for quality of information models. The information models are associated with economic risks. This requires focusing on factors such as time, cost and quality.

The quality of the models is not associated only with their internal properties but also with the acceptance by their users. Experience shows that good results are obtained in adapting the concept of quality in terms of Total Quality Management (TQM) for industrial products. Product quality is determined not only by objectively measurable characteristics of the product, but also on its ability to meet the requirements, expectations and needs of consumers. TQM concept binds the quality of products to the processes that create them and all these processes are interrelated in a functional system (Fig. 1).

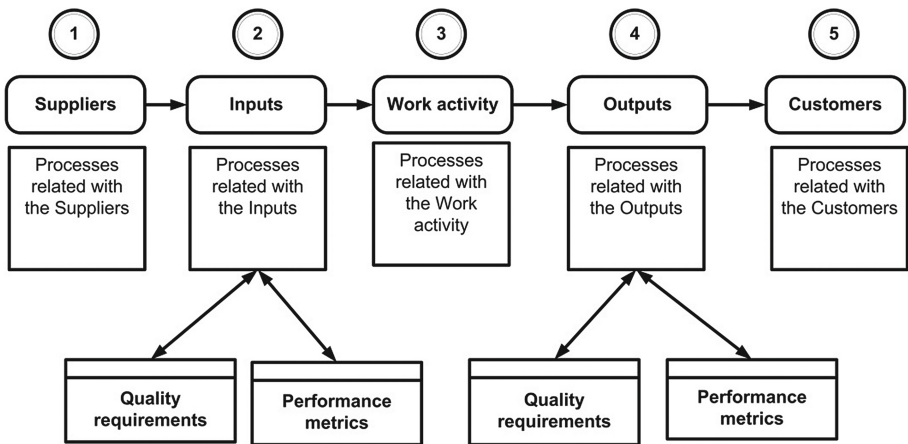


Fig. 1. Business process model on the base on TQM concept

Regarding to the models of processes in order to evaluate their suitability should be taken into account the existing consumer preferences and how they can be associated with the models. In this way developers of software based on the model will take into account the general scheme of interaction and will implement other requirements of the

employees of organizational departments, using the same model to form the organizational structure. Thus the model will be used from the viewpoint of its users, and it follows that subjectively perceived quality of process models depends on:

- the objective pursued;
- the role of the user in the organization;
- the individual preferences graphical or conceptual layout [1].

3 Choice of Corporate IT Systems

The business process model analyses the process flow, all key activities, involves the executors of each activity, order of activities, and results generated by each activity. The importance of business process modeling consists in providing of verifiable insight into underlying business processes in order to design complex software systems such as Enterprise Information Systems [2].

Corporate planning and resource management (ERP - Enterprise Resources Planning) - this is the standard for adoption and use of integrated software for organizational and economic solutions for both the main processes and the supporting processes by using integrated database. The system can integrate different but closely related functional areas of the enterprise as a control of material flows, production planning, accounting or personnel management. In this case, the configuration of such systems

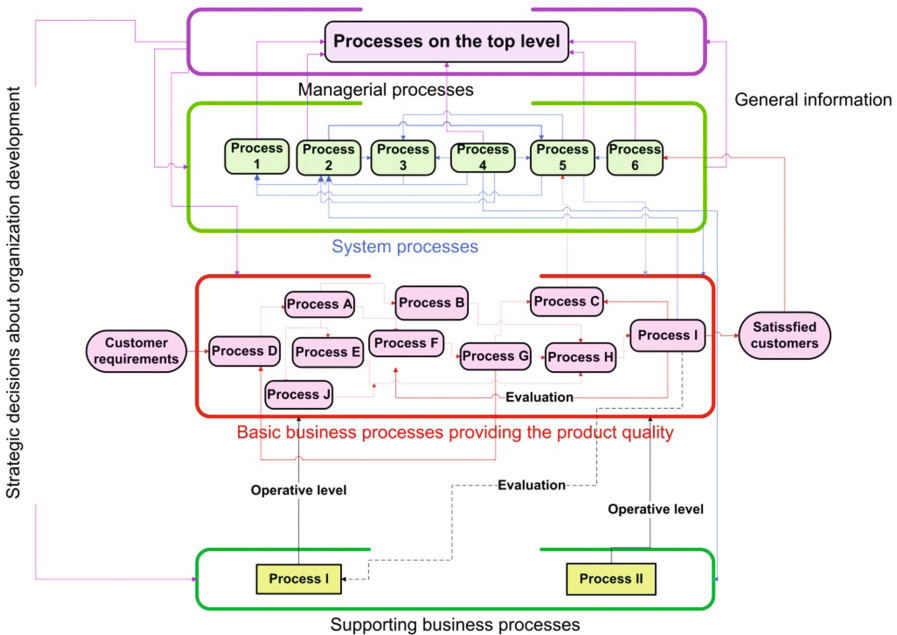


Fig. 2. Process oriented model of organization

based on the specificity of the enterprise is based on the built mechanisms. An example of a process oriented model of organization is shown on the Fig. 2.

The range of functionality of these systems is usually documented in the form of standard models of the processes. Therefore, in the choice of software it is possible to compare models of business processes with reference models of different information systems. The degree of similarity is one of the main criteria for the selection of the information system, according to the specifics of the corresponding company. The advantage of this process approach is that it is taken into account not only the presence of various features of the software but also the sequence of operations. On the Fig. 3 is shown a model of a process of negotiating with customers.

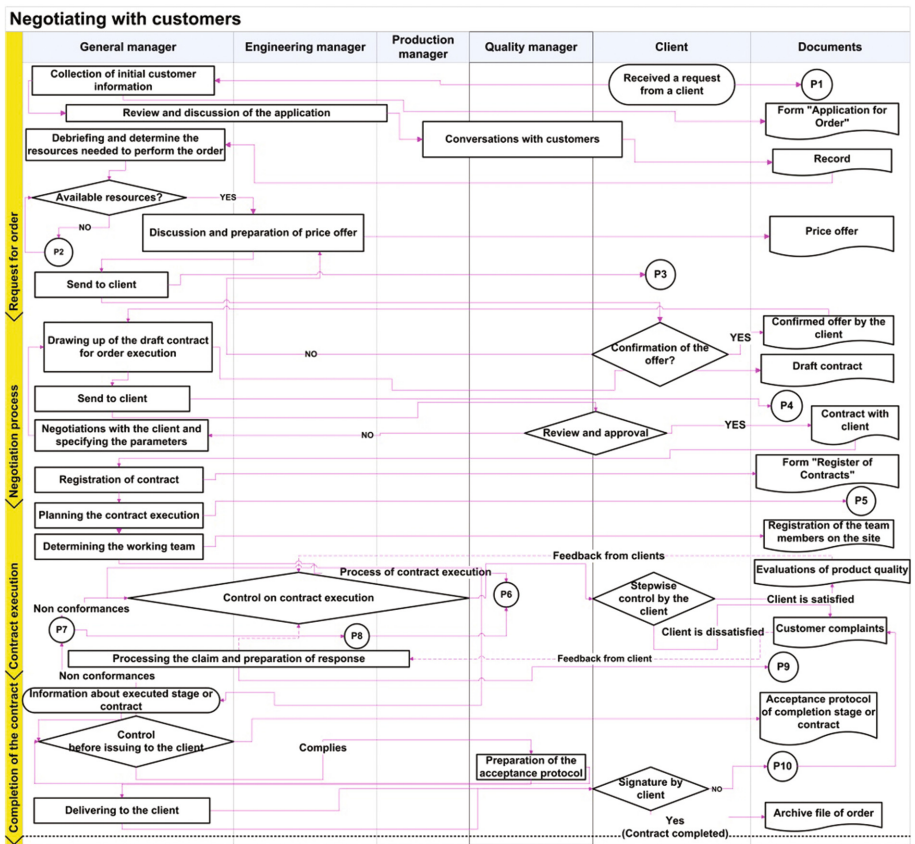


Fig. 3. Negotiating with customers process

The adequate supporting processes through information and communication systems and the availability of the necessary technical infrastructure is an important precondition for process optimization. In analyzing the situation to build the model and its compatibility with the capabilities of the software applications it should be paid an attention to these sources of problems:

- Lack of the necessary functionality into existing applied systems;
- Low productivity of the systems;
- Lack of interaction between the applicant and the user, and other inconveniences;
- Use of different systems performing the same tasks in different departments of the enterprise;
- Unnecessary data storage in the systems associated with the risk of incompatibility with different sets of data;
- Multiple inputs of the same data as a result of missing or incompatible interfaces;
- Lack of an opportunity for fast administration of data;
- Lack of electronic data exchange between the units of the company or with business partners;
- It is not used technology to facilitate the integration of data, such as planning and management of operations, resources, flow management, document management, internet sales etc.

4 Efficiency of the Model

Efficiency of the process is assessed by quantitative criteria as indicators of process the time value of the process and quality of process implementation. An important feature of process efficiency is the amount of organizational interfaces. Optimizing the use of production factors, such as personnel, equipment etc. is measured by the criteria of effectiveness. The aim is to achieve the maximum load of existing production factors. Effective use of resources, as a rule, decreases if some organizational units do not use the information system.

Taking into account the specifics of the companies, ERP system can be modeled according to the specific needs of companies and their specific processes and functions. ERP system is a central element with extensions specific to the enterprise (Collaborative Business Solutions), for internal company and external processes, such as supply chain management (SCM - Supply Chain Management) or customer relationships management (CRM - Client Relationship Management). In contrast to the system MRP – Material Requirements Planning or MRP II – Material Resources Planning, at the base of ERP is not a general theoretical concept. ERP is characterized by some similar solutions offered by big corporate IT developers of systems such as SAP, IBM or Microsoft. As the basic principle is ERP system fully to integrate production and economic data, the introduction of such systems enables to control the business processes of the company.

Business process modeling (BPM) may be viewed as a set of methods, techniques and tools in support of the analysis and improvement of business processes. In order to achieve greater efficiency in BPM, it is extremely important to understand the matter of business processes. Every business process may be viewed from different angles - as competitive deterministic machine, complex dynamic system, interacting feedback loop, as well as social structure [3].

Figure 4 shows an amendment of the elements of the business object for adjusting the standard business object in accordance with the requirements and needs of specific users [4].

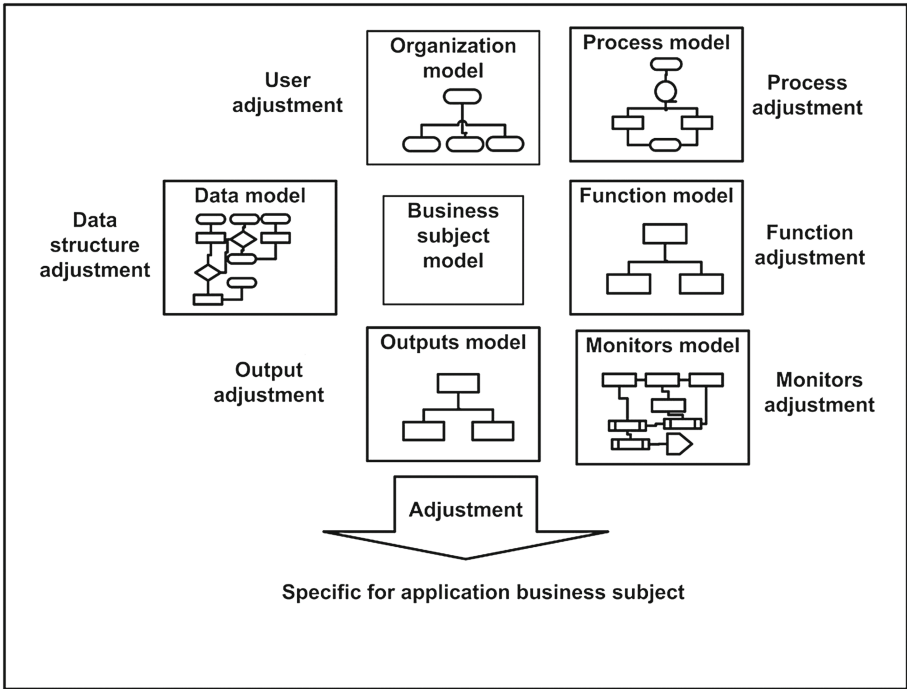


Fig. 4. Amendment of the elements of the business object for adjusting the standard business subject to the requirements and needs of specific users [4]

5 Economic Efficiency of IT

The economic efficiency is a fundamental principle of economic activities of enterprises. All business activities are related to both desirable and undesirable consequences. The aim is to achieve a balance between the costs incurred and the results obtained. IT resources perform different operations in the processes. Improvement of the process efficiency is expressed in increasing of their productivity, which in turn leads to increased productivity of the company as a whole [5]. Mechanism of impact of the IT system on the company's success is shown on the Fig. 5.

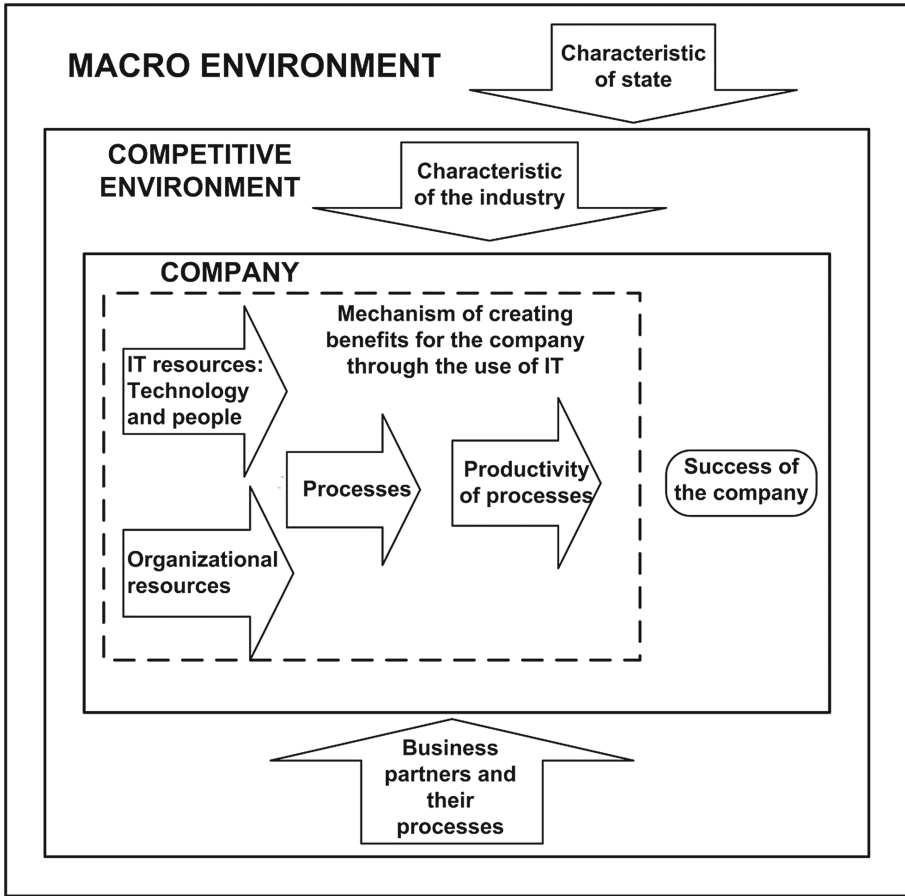


Fig. 5. Mechanism of impact of the IT system of the company's success

6 Effects from the Introduction of IT Systems

Through process improvement the company aims to increase its productivity, reduce the execution time and use other resources of the enterprise, as well as reducing the cost of implementation process. The effects of the impact may be quantitative (monetary and non-monetary) and qualitative (nonmonetary). The manifestation of the effects on the processes results in [5]:

- Effect of automation: results from the replacement of human labor in the IT area, especially within the operational processes;
- Effect of information: it is the result of the ability effectively to collect, store, process and distribute information, often as part of the management and administrative processes;

- Effect of transformation: it stems from the possibility for innovation and results in the substitution of old processes with new.

7 Technological and Organizational Effects

Probably the most important aspect of the application of information systems is the availability of the above mentioned effects. As these systems, by their nature, are a collection of people and technology (Fig. 4), the advantages of the implementation of IT systems is expressed in the targeted interaction of these components.

Technological effects are associated with the accelerated product introduction by automatic design and production)

Organizational effects are associated with the acceleration of acceptance and moving of goods due to changes in the order of arrangement of stocks, as well as the optimization of the roles and professional responsibilities of staff.

Therefore, these companies should first focus on the effectiveness of their organizational structure. The technological effect, and with it the benefits are smaller than the organizational effect. Advanced companies in terms of their organization, economic activity may increase the efficiency of their processes by means of using the innovative technologies [5].

8 Process Analysis and Improvement Network (PAIN)

There are several reasons to use the process analysis and improvement of network (PAIN). Every time when a process shows undesirable handling properties, the owner of the process, stakeholders of the process, team members of the process improvement and all other stakeholders should take timely and appropriate remedial action to eliminate or at least reduce the presence or influence of negative properties. Most often these negative qualities are [1]:

- Processes are very long (excessive length of the cycle);
- Processes are very inconsistent (excessive deviation);
- Processes are complicated (too many steps);
- Processes are expensive (excessive costs for cycle);
- Too many errors (poor quality of the transactional process);
- Too many defects (poor quality of production process);
- Insufficient documentation for the process (for training or benchmarking).

On the Fig. 6 is presented the main model of Process analysis and improvement navigator (PAIN). The basic steps of PAIN model are [1]:

- Full definition of the work activities;
- Description of all outputs of the work activities;
- Identification of the users of the work activities, i.e. those who receive the outputs;
- Description of the quality requirements associated with the outputs of the work activities;

- Creation a list of performance metrics used to evaluate the quality requirements of the outputs;
- Description of all inputs of the work activities;
- Description of the quality requirements associated with the inputs of the work activities;
- Creation a list of performance metrics used to evaluate the quality requirements of the inputs and outputs;

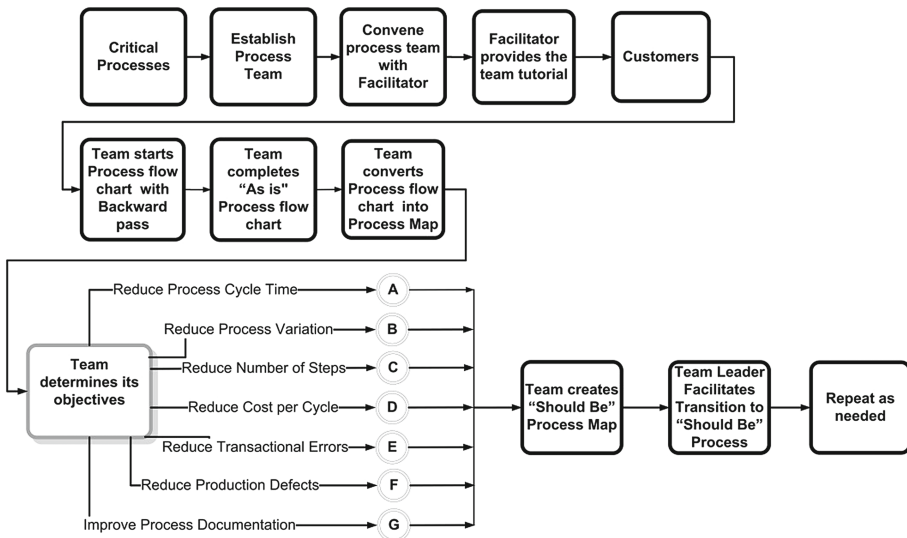


Fig. 6. Main model of process analysis and improvement navigator (PAIN) [1]

9 Conclusion

Based on the analysis may be concluded that a major factor in providing of sustainable achievements in the organization is the business process management, which inevitably requires continuous measurement of their efficiency. The implementation of initiatives for management of business processes usually passes through the following main stages:

- Modeling and documentation of processes in order to increase their understanding and to identify opportunities for optimization;
- Redesigning and transforming of the business processes implemented on paper into electronic processes, in order to eliminate paper forms, records and other documents, and inefficiency associated with them;
- Complete automation of process steps by integrating them into corporate information systems;
- Adding intelligent automatic checks of data into electronic forms in order to avoid gaps or errors - for example, by choice of products from the nomenclature instead of manually filling its item number;

- Implementation of procedures for automatic control in order to provide the continuity of the processes and to provide the functionality in case of technical problems or human error;
- Providing visibility of process status in real time;
- Analysis of the efficiency of processes in order to facilitate their subsequent improvement.

Continuous optimization of business processes is a key factor for achievement of competitive advantage for many organizations. These of them which are actually process oriented operate faster, operate more predictable and consistent, are proud with the employees who understand better their roles and the roles of others stakeholders, perform fewer projects for reengineering of information systems, adapt to new business expectations much easier than other competing organizations.

This survey provides a basic framework for future more detailed and extensive research in the field of modeling, measurement and management of business processes in organization and the achieved practical results will be a subject of next publications.

References

1. Melão, N., Pidd, M.: Business processes: four perspectives. In: Grover, V., Markus, M.L. (eds.) Business Process Transformation. *Advances in Management Information Systems*, vol. 9, pp. 41–66. M.E. Sharpe, Armonk (2008). ISBN 978-0-7656-1191-8, ISSN 1554-6152
2. Becker, J., Vilkov, L., Taratuchin, V., Kuegel, M., Rozemann, M.: Process Management. Publishing house “Exmo”, Tambov (2007)
3. ReVelle, J.B.: Manufacturing handbook of best practices: an innovation, productivity, and quality focus p. cm. APICS Series on Resource Management. St. Lucie Press (2002). ISBN 1-57444-300-3
4. Barjis, J.: The importance of business process modeling in software systems design. *Sci. Comput. Program.* **71**(1), 73–87 (2008)
5. Scheer, A.-W.: Modeling of Business Processes, 2nd edn. News-MetaTechnology, Moscow (2000)

Application of Recursive Methods for Parameter Estimation in Adaptive Control of DC Motor

Ivan V. Grigorov^(✉), Nasko R. Atanasov, Zhivko Zhekov,
and Mariela Alexandrova

Department of Automation, Technical University of Varna,
Studentska Str. 1, 9010 Varna, Bulgaria
{mad_doc, fitter}@abv.bg,
{nratanasov, m_alexandrova}@tu-varna.bg

Abstract. The adaptive control uses a number of methods which provide a systematic approach for real-time automatic control. The recursive parameter estimation methods in particular are best applicable if simple parameter estimates are obtainable using real-time identification algorithms. This is imposed by the fact that model adjustments after submission of new data from monitoring, require generation of adequate (adjusted) control signal within the sample time. The present article investigates an application of those methods for parameter estimation and their influence on the quality of adaptive control process of DC motor.

Keywords: Adaptive system · Instrumental variable method · Least squares method · Recursive methods for parameter estimation · DC motor

1 Introduction

System control by default requires deep understanding the dynamic features of the processes [3]. Recursive methods for parameter estimation are only used for real-time system identification. The real dynamics of the system should be reflected in the dynamic of the control signal synthesis and in the model in accordance with the new data received. This is of crucial importance especially when the parameters are estimated for time variant systems. These changes are analyzed in terms of values of input and output variables for the purpose of synthesis of control signal for adaptive systems. Those recursive methods are often used in transmission and of signal processing as independent real time control instrument [1, 2, 7, 8].

2 Recursive Versions of Least Squares Method for Parameter Estimation

Short description of the methods used in the present paper will be presented below.

2.1 Recursive Weighted Least Squares (RWLS)

Recursive estimates using weighted least squares method can be obtained with:

$$\hat{\theta}_{N+1} = \hat{\theta}_N + \frac{C_N f_{N+1}}{\frac{1}{w_{N+1}} - f_{N+1}^T C_N f_{N+1}} \left(y_{N+1} - f_{N+1}^T \hat{\theta}_N \right) \quad (1)$$

According to (1) the previous value $\hat{\theta}_N$ is adjusted proportionally to the difference $y_{N+1} - \hat{y}_{N+1}$ with a vector coefficient of proportionality:

$$\Gamma_{N+1} = \frac{C_N f_{N+1}}{\frac{1}{w_{N+1}} - f_{N+1}^T C_N f_{N+1}} \quad (2)$$

Where: $\hat{y}_{N+1} = f_{N+1}^T \hat{\theta}_N$ is predicted value for y_{N+1} , where $\hat{\theta}_N$ is the vector of the coefficients estimated in the previous iteration.

Instead of using prediction errors it is possible residuals to be used as follows:

The prediction error included in formula (1) can be written also:

$$e_{N+1} = y_{N+1} - \hat{y}_{N+1} \left(\hat{\theta}_N \right) = y_{N+1} - f_{N+1}^T \hat{\theta}_N \quad (3)$$

for improvement of the accuracy of prediction instead of e_{N+1} is used the residual:

$$r_{N+1} = y_{N+1} - f_{N+1}^T \hat{\theta}_{N+1} \quad (4)$$

combining (2) and (3) gives:

$$r_{N+1} - e_{N+1} = -f_{N+1}^T (\hat{\theta}_{N+1} - \hat{\theta}_N) \quad (5)$$

If difference $(\hat{\theta}_{N+1} - \hat{\theta}_N)$ is derived using (2) and substituted in (5) it follows:

$$r_{N+1} = \frac{\frac{1}{w_{N+1}} e_{N+1}}{\frac{1}{w_{N+1}} - f_{N+1}^T C_N f_{N+1}} \quad (6)$$

Calculation Procedure Requirement.

In order to obtain parameter estimates using the method of weighted least squares initial estimates of $\hat{\theta}_N$ and C_N should be available. This is only possible if $N \geq k$ observations for $\hat{\theta}_N$ and C_N are obtained with non-recursive method of weighted

least-squares. Then the procedure continues following the calculation procedure described with (1) and (7).

$$C_{N+1} = C_N - \frac{C_N f_{N+1} f_{N+1}^T C_{N+1}}{\frac{1}{w_{N+1}} - f_{N+1}^T C_N f_{N+1}} \tag{7}$$

The algorithm of the recursive weighted least squares method is the corner stone for many other recursive procedures. It could be shortly presented by steps 1 to 4:

1. $N \geq k$ observations are collected and processed with non-recursive method of weighted least-squares and the initial estimates $\hat{\theta}_N$ and C_N are obtained.
2. The new estimates are calculated by the formula

$$\hat{\theta}_{N+1} = \hat{\theta}_N + \frac{C_N f_{N+1}}{\frac{1}{w_{N+1}} - f_{N+1}^T C_N f_{N+1}} \left(y_{N+1} - f_{N+1}^T \hat{\theta}_N \right)$$

3. Recalculation of matrix C_{N+1} to be submitted for next iteration

$$C_{N+1} = C_N - \frac{C_N f_{N+1} f_{N+1}^T C_{N+1}}{\frac{1}{w_{N+1}} - f_{N+1}^T C_N f_{N+1}}$$

4. The new estimates $\hat{\theta}_{N+1}$ and C_{N+1} start the next iteration from point 2 of the algorithm presented above [2-4].

2.2 Recursive Ordinary Least Squares

Recursive least squares is also a special case of RWLS when $W = I$. This means that all weights are significant and unbiased estimates when equal values are assigned (1), which is only possible if $\rho = 1$. subsequently, the recursive least squares method (RLS) can be applied using the same procedure, as described in paragraph 1.1. to substitute $\rho = 1$ where possible [3-5].

3 Recursive Method of Instrumental Variables

Obtaining estimates by the method of the instrumental variables is using similar procedure to the one used for the least squares method.

The Instrumental vector v_{N+1} is chosen from (8), or (9)

$$v_i^T == [-\hat{y}_{i-1} \quad -\hat{y}_{i-2} \dots -\hat{y}_{i-n} \quad u_{i-1} \quad u_{i-2} \dots u_{i-m}] \tag{8}$$

$$v_i^T = [u_{i-1} \quad u_{i-2} \dots u_{i-m}] \tag{9}$$

The Recursive Algorithm used When the Method of Instrumental Variable is Applied is:

1. The calculations start with RWLS. The higher is the number of iterations the higher is the accuracy of the initial estimates. Once a certain number $N > k$ observations is obtained the calculations continue using the recursive method of instrumental variable (RIV). N is usually chosen to satisfy the following condition – to be equal to 3 to 5 times the number of coefficients.
2. The estimated coefficients of $N + 1$ -st iteration are calculated by the formula:

$$\hat{\theta}_{N+1} = \hat{\theta}_N + \frac{C_N v_{N+1}}{\rho + f_{N+1}^T C_N v_{N+1}} (y_{N+1} - f_{N+1}^T \hat{\theta}_N) \tag{10}$$

3. Recalculation of matrix C_{N+1} to be submitted for the next iteration by the formula:

$$C_{N+1} = \frac{1}{\rho} \left(C_N - \frac{C_N v_{N+1} f_{N+1}^T C_N}{\rho + f_{N+1}^T C_N v_{N+1}} \right) \tag{11}$$

4. The calculation procedure continues with repetition of step 2 with the new estimates obtained. If weighing of observations (10) and (11) is not needed then it is simply substituted $\rho = 1$ [4–6].

4 DC Motor Control System

DC motors are widely used in terms of automation, robotics and various control systems. They are suitable where a precise regulation of torque and velocity is needed, while maintaining the torque at low and zero velocity [1, 6, 7].

4.1 DC Motor

The dynamics of the DC motor may be expressed by the following equation:

$$\begin{cases} U_a = R_a(T_a p + 1)i_a + c\Phi\omega \\ M_e = c\Phi i_a \\ M_e - M_c = Jp\omega \end{cases} \tag{12}$$

where: $T_a = L_a/R_a$ and U_a – armature voltage, i_a – armature current, R_a – armature winding active resistance, L_a – armature induction ω – angular velocity, M_e – electromagnetic torque, M_c – load torque, Φ – magnetic flux, c – armature constant, J – moment of inertia. The block diagram of the DC motor used in the present study is shown in Figs. 1, 6, and 7:

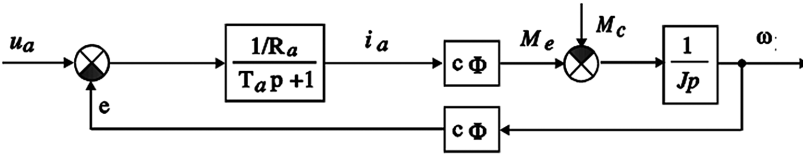


Fig. 1. Block diagram of the DC motor

4.2 DC Motor Control Using Pulse-Width Modulation

Modern DC motor control systems use pulse-width modulation, which is found to be characterized with better energetic parameters, smaller current and velocity pulsations, which in turn leads to reduction of energetic losses and expansion of the control span.

In Fig. 2 is presented block diagram of DC motor control with PWM, where: TWG- Triangle Wave Generator, C – comparator, TDB – time delay block, IS– Impulse shaper, UR – uncontrolled rectifier, PTC – power transistor commutator, M– DC motor [1, 6, 7].

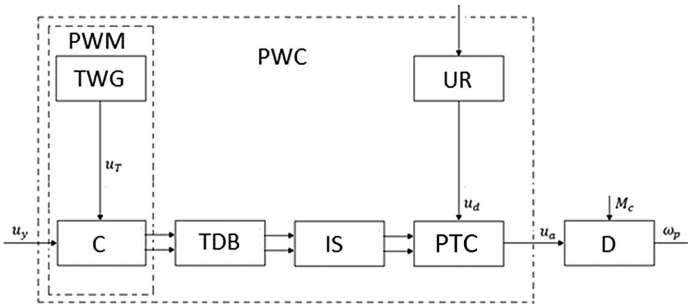


Fig. 2. Block diagram of PWM - DC motor

5 Self-tuning Controller

Self-tuning controllers (STC) use a combination of recursive process identification based on selected model process and controller synthesis based on apriory knowledge for control process system features, parameters estimates and ranges of variability.

Block diagram of STC (with direct identification) is shown in Fig. 3.

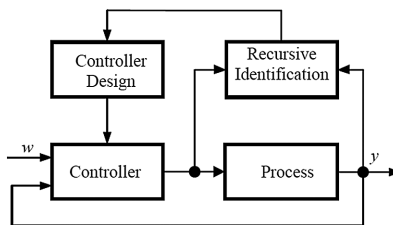


Fig. 3. Block diagram of STC

Self-tuning control (STC) is one of the control methods which have been developed considerably over the past years. Self-tuning control is focused on discrete or sampled models of processes. Computation of appropriate control algorithms is then realized using discrete model of representation of the system.

STC has three main elements (Fig. 3). The first element presents classic feedback system. The second shows implementation of identification block. The third realizes the algorithm of parameters adjustment of controller, based on estimates of the process parameters. This block diagram can be used in both stationary systems with unknown parameters and is also applicable for systems with distributed parameters which are expected to vary within certain limits. The present study investigates application of direct STC with minimal variance (STC-MV) [1, 8, 9].

Algorithm for Direct STC - MV.

1. Based on input/output data for the process at a given k -th time sample, the estimates $f_i(k)$ and $g_i(k)$ of the polynomials $F(z^{-1})$ and $G(z^{-1})$ are obtained using one of the methods described in paragraphs 2 and 3
2. The estimates derived at step 1 form the control signal $u(k)$:

$$u(k) = -\frac{1}{g_0} [f_0 y(k) + f_1 y(k-1) + \dots + f_{n-1} y(k-n+1) + g_1 u(k-1) + g_2 u(k-2) + \dots + g_{m+d-1} u(k-m-d+1)] \quad (13)$$

3. Once the new data is received and processed the procedure is repeated from steps 1 to 2.

It is clear that when the direct method of estimation of $F(z^{-1})$ and $G(z^{-1})$ is applied, the use of more complicated algorithms as well as solving the Diophantine equation is not needed and could be skipped [1, 8, 9].

6 Experimental Research and Results

The present research is mostly focused on the performance capabilities of the described recursive methods for parameter estimation used in real time adaptive control of DC motor. For this purpose the study is completed using random input signal which is simulating noise at the input of the system under investigation.

The research has been done using the System Identification Toolbox in Matlab \Simulink. For simulation purposes custom blocks in Simulink are developed each one corresponding to a certain recursive parameter estimation algorithm as follows: recursive least squares (RLS), recursive least squares with using the residuals modification instead of the prediction errors (RLSr) and recursive instrumental variable method (IVu). (Figs. 4, 5 and 8)

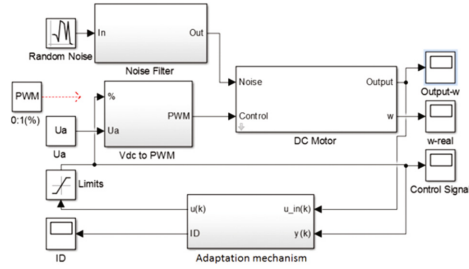


Fig. 4. Block diagram of adaptive DC motor control with STC-MV in Simulink

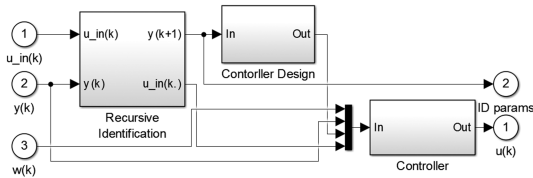


Fig. 5. Block diagram of the subsystem “Adaptation mechanism”

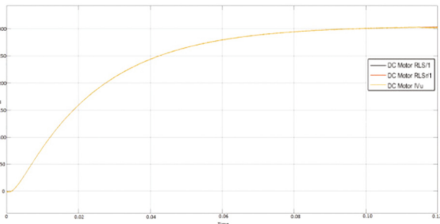


Fig. 6. Output with $\omega = 304,7$ rad/s

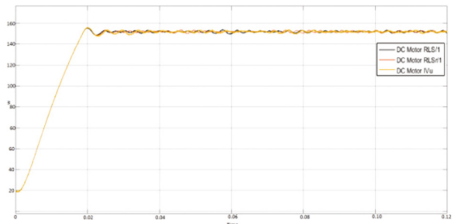


Fig. 7. Output with $\omega = 152,35$ rad/s

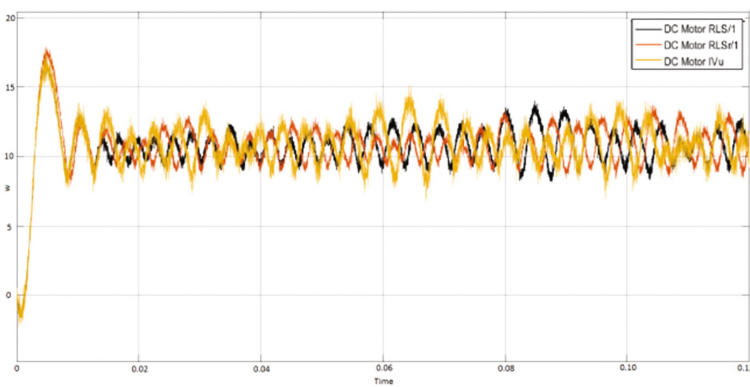


Fig. 8. Output with $\omega = 10,1567$ rad/s

7 Conclusions

The simulation results prove the applicability of described recursive methods for parameter estimation in adaptive control of DC motor. The results show that in the low speed interval the variation of the signal from the reference is the highest even if it still belongs to acceptable limits. As it was formulated the recursive instrumental variable method require a second (external) noise signal in the output of the object for the purpose of better estimates of parameters however it strongly affects the quality of the control process. The described methods for parameter estimation can be further modified for better performance and process quality in other adaptive control systems. If there is an option for direct selection of the estimates weights the algorithms described can be used to facilitate a variety of robust estimates that can be noise resistant. Future research will be focused on this issue.

Acknowledgments. The scientific research, the results of which are presented in the present publication have been carried out under a project №PD1 within the inherent research activity of TU-Varna, target financed from the state budget.

References

1. Agustin, O., Oscar, L., Francisco, Q.: Identification of DC motor with parametric methods and artificial neural networks (2012)
2. Andonov, A., Hubenova, Z.: Robust methods for control under undetermined criteria (2008)
3. Nielsen, A.A.: Least squares adjustment: linear and nonlinear weighted regression analysis (2013)
4. Bobál, V., Chalupa, P., Kubalčík, M., Dostál, P.: Identification and Self-tuning Control of Time-delay Systems, 2012
5. Angrist, J.D., Krueger, A.B.: Instrumental variables and the search for identification (2001)
6. Kama, O., Mahanijah, K., Nasirah, M., Norhayati, H.: System identification of discrete model for DC motor positioning
7. Krneta, R., Antić, S., Stojanović, D.: Recursive least squares method in parameters identification of DC motors models (2005)
8. Landau, I.D., Lozano, R., M'Saad, H., Kariirri, A.: Adaptive control algorithms, analysis and applications (2011)
9. Hassan, L.H.: Unknown input observers design for a class of nonlinear time-delay systems (2011)
10. Hovakimyan, N., Cao, C.: Adaptive control theory guaranteed robustness with fast adaptation (2010)

Electronic Differentials with Active Torque Distribution for IWD Vehicles

Petr Simonik^(✉), Tomas Mrovec, and Samuel Przeczek

Department of Electronics, VSB – Technical University of Ostrava,
17. listopadu 15, 708 33 Ostrava, Czech Republic
{petr.simonik,tomas.mrovec,samuel.przeczek.st}@vsb.cz

Abstract. This paper concerns proposal the simulation model of Individual-Wheel Drive (IWD) with electronic differentials. The MATLAB/Simulink environment is used for simulation model of the electronic differential and electronic centre differential for real IWD vehicle called “Democar”. One of the components that affect the resulting behaviour of the vehicle is a mechanical differential. The work is the first part based on the description of the behaviour of vehicles in terms of driving performance. Based on the analysis of the requirements on stability of the vehicle was developed his mathematical description. From the mathematical description, there is also a general simulation model vehicles with separate all-wheel drive. This model allows to simulate a variety of driving situations and compare the influence of torque control on individual wheels resulting behaviour of the vehicle. The results of the simulations it is possible to create an optimal control algorithm high-level control system to separate all-wheel drive IWD. The work is focused on the management of electronic differential and electronic centre differential with active torque distribution.

Keywords: IWD vehicle · Electronic differential · Electronic centre differential · Torque distribution · MATLAB/simulink · PMSM · Democar · Active torque management

1 Introduction

Traditional four-wheel drive improves handling characteristics of the vehicle, but the vehicle has only one engine and torque is elaborated through gearboxes, clutches and axle to the driven wheels. In these conventional systems is very difficult to control the torque on each wheel individually, due to the mechanical linkages and a single source of torque moment [3]. Differential serve for improved handling with Ackerman chassis control. Purely electronic differentials are based on the principle that when turning lane changes, which must pass through the wheel. Therefore, assesses the steering angle. From this angle is calculated turning radius and adjusts the speed of each wheel. When using, differential improves vehicle handling. This reduces stress on the chassis frame, wheels of wear tires due to a slight slip of the tires during cornering, further reducing the loading of drive motors. Also, reduces power consumption when cornering, because there is no wrestling of motors on the axle. Before assembling the vehicle have been created mathematical models for IWD management in MATLAB / Simulink and these were verified. Model of IWD management is described in the paper.

2 Behavior of IWD Vehicle

The simulation model of the vehicle is made up of three subsystems which are connected into the overall model. The subsystems are structured systematically with respect to functional components of the electric drive. The vehicle model is therefore formed by the following subsystems: Central control unit for management of torque to each wheel; Drive unit with four independent electric machines; Mechanical part of the chassis realizing the driveability of the vehicle. Inputs into the model are torque request by an accelerator pedal and steering angle.

2.1 Vehicle Mathematical Model

To build a mathematical model, it is important specify coordinate systems. All coordinate systems are defined in the plane of the road shown in Fig. 1, the axes x, y, z are the axes of the coordinate system center of gravity of the vehicle. Axes x_0 and y_0 axes are the starting point position of the center of gravity in this coordinate system is drawn trajectory of the vehicle. Axes x_k to the y_k and then indicate the coordinate system of the individual wheels.

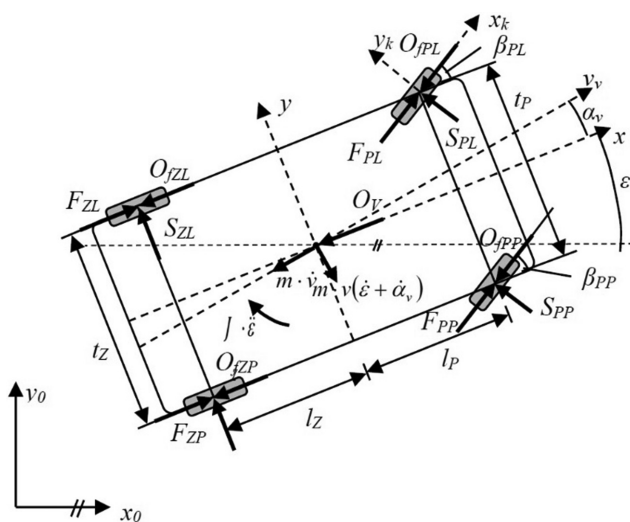


Fig. 1. Forces acting on vehicle in the transverse and longitudinal direction

On the basis of Fig. 1 is derived equations for forces acting in individual directions, based on the balance of forces and moments to the centre of gravity. In the direction of the x axis Eq. (1) and in the y axis Eq. (2) are valid.

$$\begin{aligned}
 & -m \cdot \dot{v}_v \cdot \cos(\alpha_v) + m \cdot v_v \cdot (\dot{\epsilon} + \dot{\alpha}_v) \sin \alpha_v - S_{PL} \cdot \sin \beta_{PL} + T_{ZL} + T_{ZP} \\
 & - S_{PP} \cdot \sin \beta_{PP} - \frac{1}{2} \cdot S_x c_x \cdot \rho \cdot (v + v_0)^2 + T_{PL} \cdot \cos \beta_{PL} + T_{PP} \cdot \cos \beta_{PP} = 0
 \end{aligned} \tag{1}$$

$$\begin{aligned}
 & -m \cdot \dot{v}_v \cdot \sin \alpha_v - m \cdot v_v \cdot (\dot{\epsilon} + \dot{\alpha}_v) \cos \alpha_v + S_{PL} \cdot \cos \beta_{PL} + S_{ZL} + T_{PL} \cdot \sin \beta_{PL} \\
 & + T_{PP} \cdot \sin \beta_{PP} + S_{PP} \cdot \cos \beta_{PP} + S_{ZP} = 0
 \end{aligned} \tag{2}$$

From the moment balance around the vertical axis z is obtained in Eq. (3).

$$\begin{aligned}
 & -\frac{\ddot{\epsilon}}{J_z} + (S_{PL} \cdot \cos \beta_{PL} + S_{PP} \cdot \cos \beta_{PP}) \cdot l_P - (S_{ZL} + S_{ZP}) \cdot l_Z + (S_{PL} \cdot \sin \beta_{PL} \\
 & - S_{PP} \cdot \sin \beta_{PP}) \cdot \frac{t_p}{2} + T_{PL} \cdot l_P \cdot \sin \beta_{PL} + T_{PP} \cdot l_P \cdot \sin \beta_{PP} - T_{PL} \cdot \frac{t_p}{2} \cdot \cos \beta_{PL} \\
 & + T_{PP} \cdot \frac{t_p}{2} \cdot \cos \beta_{PP} - T_{ZL} \cdot \frac{t_z}{2} + T_{ZP} \cdot \frac{t_z}{2} = 0
 \end{aligned} \tag{3}$$

Vertical load of each wheel is balanced by the center of gravity at a standstill. However, when driving the individual wheel load changes due to inertial forces that operate in the center of gravity of the vehicle when changing a longitudinal or transverse velocity. These forces generate additional moments due to non-zero height of the center of gravity of the vehicle.

When considering an ideal rigid body and chassis can be vertically acting force calculated. For this calculation, it is important to consider the acceleration oriented in a coordinate system of the vehicle centre of gravity, i.e. in the direction axes x and y .

$$a_x = \dot{v}_v \cdot \cos \alpha_v + v_v \cdot (\dot{\epsilon} + \dot{\alpha}_v) \sin \alpha_v \quad [ms^{-2}, ms^{-2}, \circ, ms^{-1}, rads^{-1}, rads^{-1}, \circ] \tag{4}$$

Acceleration applied in a direction of the x axis is given by the Eq. (4) and in the y axis is given by the Eq. (5).

$$a_y = -\dot{v}_v \cdot \sin \alpha_v + v_v \cdot (\dot{\epsilon} + \dot{\alpha}_v) \cos \alpha_v \quad [ms^{-2}, ms^{-2}, \circ, ms^{-1}, rads^{-1}, rads^{-1}, \circ] \tag{5}$$

At zero lateral acceleration is obtained by vertical forces split 50/50 for each wheel axles. If a non-zero lateral acceleration and vertical forces are distributed according to Eqs. (6) to (9).

$$Z_{PP} = \frac{Z_{PN}}{2} + Z_{PN} \cdot \frac{a_y}{g} \cdot \frac{h_t}{t_p} \quad [N, N, ms^{-2}, ms^{-2}, m, m] \tag{6}$$

$$Z_{PL} = \frac{Z_{PN}}{2} - Z_{PN} \cdot \frac{a_y}{g} \cdot \frac{h_t}{t_p} \quad [N, N, ms^{-2}, ms^{-2}, m, m] \tag{7}$$

$$Z_{ZP} = \frac{Z_{ZN}}{2} + Z_{ZN} \cdot \frac{a_y}{g} \cdot \frac{h_t}{t_z} \quad [N, N, ms^{-2}, ms^{-2}, m, m] \tag{8}$$

$$Z_{ZL} = \frac{Z_{ZN}}{2} - Z_{ZN} \cdot \frac{a_y}{g} \cdot \frac{h_t}{t_z} \quad [N, N, ms^{-2}, ms^{-2}, m, m] \tag{9}$$

2.2 Wheel Mathematical Model

It is important to know the speed of movement of the wheel centre to build a model of the vehicle wheel. This speed is different from the circumferential speed of the wheel caused by slip of the tire. Its calculation will be described below. Velocity of the wheel centre can be expressed by means of gravity of the vehicle speed v_v and the sum of the speed of rotation from the vehicle velocity vector $\dot{\alpha}_v$ with the yaw rate of the vehicle $\dot{\epsilon}$. Geometric superposition according to Fig. 2 is obtained movement speed of individual wheel centres. By dividing the components in the x -axis and y -axis get relations (10) to (13).

$$v_{PL} = (v_v \cdot \cos \alpha_v - \dot{\epsilon} \cdot r_{PL} \cdot \sin \vartheta_{PL}) \cdot \bar{e}_x + (v_v \cdot \sin \alpha_v - \dot{\epsilon} \cdot r_{PL} \cdot \cos \vartheta_{PL}) \cdot \bar{e}_y \quad (10)$$

$$v_{PP} = (v_v \cdot \cos \alpha_v - \dot{\epsilon} \cdot r_{PP} \cdot \sin \vartheta_{PP}) \cdot \bar{e}_x + (v_v \cdot \sin \alpha_v - \dot{\epsilon} \cdot r_{PP} \cdot \cos \vartheta_{PP}) \cdot \bar{e}_y \quad (11)$$

$$v_{ZL} = (v_v \cdot \cos \alpha_v - \dot{\epsilon} \cdot r_{ZL} \cdot \sin \vartheta_{ZL}) \cdot \bar{e}_x + (v_v \cdot \sin \alpha_v - \dot{\epsilon} \cdot r_{ZL} \cdot \cos \vartheta_{ZL}) \cdot \bar{e}_y \quad (12)$$

$$v_{ZP} = (v_v \cdot \cos \alpha_v - \dot{\epsilon} \cdot r_{ZP} \cdot \sin \vartheta_{ZP}) \cdot \bar{e}_x + (v_v \cdot \sin \alpha_v - \dot{\epsilon} \cdot r_{ZP} \cdot \cos \vartheta_{ZP}) \cdot \bar{e}_y \quad (13)$$

Equations (14) to (17) are the basis for determining the lateral deviations of wheels. This deviation is defined as the angle between the x_k -axis to the relevant wheel and the velocity vector of centre of the same wheel. This deviation is formed as a result of partial wheel skidding, and also due to its lateral flexibility [4].

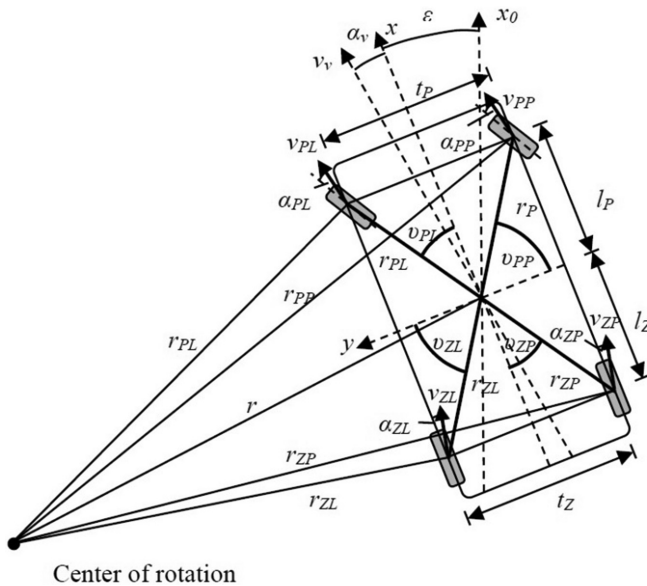


Fig. 2. The layout of parametres for calculating the wheel centre speed

$$\alpha_{PL} = \beta_{PL} - \tan^{-1} \left(\frac{v_v \cdot \sin \alpha_v - \dot{e} \cdot r_{PL} \cdot \cos \vartheta_{PL}}{v_v \cdot \cos \alpha_v - \dot{e} \cdot r_{PL} \cdot \sin \vartheta_{PL}} \right) \tag{14}$$

$$\alpha_{PP} = \beta_{PP} - \tan^{-1} \left(\frac{v_v \cdot \sin \alpha_v - \dot{e} \cdot r_{PP} \cdot \cos \vartheta_{PP}}{v_v \cdot \cos \alpha_v - \dot{e} \cdot r_{PP} \cdot \sin \vartheta_{PP}} \right) \tag{15}$$

$$\alpha_{ZL} = - \tan^{-1} \left(\frac{v_v \cdot \sin \alpha_v - \dot{e} \cdot r_{ZL} \cdot \cos \vartheta_{ZL}}{v_v \cdot \cos \alpha_v - \dot{e} \cdot r_{ZL} \cdot \sin \vartheta_{ZL}} \right) \tag{16}$$

$$\alpha_{ZP} = - \tan^{-1} \left(\frac{v_v \cdot \sin \alpha_v - \dot{e} \cdot r_{ZP} \cdot \cos \vartheta_{ZP}}{v_v \cdot \cos \alpha_v - \dot{e} \cdot r_{ZP} \cdot \sin \vartheta_{ZP}} \right) \tag{17}$$

Equation (18) of motion rotary wheel is

$$J_K \omega_{ij} = M_{ij} - O_{fij} r_d - T_{ij} r_d [kgm^2, rads^{-1}, Nm, N, m] \tag{18}$$

Rolling resistance is the energy that is lost when the tire is rolling and the main reason for loss of energy is the constant deformation of the tire. The rolling resistance is approximately constant up to 80 km/h, and above hardly depends on vehicle speed. Tire pressure, tire diameter, tire construction, tire tread and other factors all have an effect on rolling resistance. The coefficient of rolling resistance is a number that has been empirically determined for different materials [1]. (Table 1)

Table 1. Coefficient of rolling resistance for various surface

Surface	μ_R	Surface	μ_R
Asphalt	0.01 – 0.02	Grass	0.08 – 0.15
Concrete	0.015 – 0.025	Sand	0.15 – 0.3
Pavement	0.02 – 0.03	Snow	0.2 – 0.3

Longitudinal tire slip is calculated from the peripheral speed of the wheel and speed of the wheel centre. Lateral tire slip of the wheel is determined as tangent of the lateral deviations of wheels α_{ij} . Wheel slippage is defined separately for the case of braking, when the peripheral speed less than the speed of the wheel centre, and the case of acceleration when the wheel peripheral speed greater than the speed of the wheel centre. Longitudinal slippage will always lie in the interval from -1 to 1. The slip is then given by the geometric sum according to (19).

$$s_c = \sqrt{s_x^2 + s_y^2} [-, -] \tag{19}$$

The coefficient of friction μ is dependent on the direction of slip. This fact indicates the so called Kamm adhesive circle

$$\mu_x = \mu_c \frac{S_x}{S_c} [-,-] \quad \mu_y = k_y \mu_c \frac{S_y}{S_c} [-,-] \quad (20)$$

where k_y expresses the reduction factor for different type of tire. The reaction forces T_{ij} acting between the tire and the road in the direction of x_k -axis and the reaction force S_{ij} acting in the y_k -axis is obtained by multiplying force Z_{ij} from acting vertically to the tire and the relevant coefficients of friction are then given by relations (21) and (22).

$$T_{ij} = \mu_x Z_{ij} [N, -, N] \quad (21)$$

$$S_{ij} = \mu_y Z_{ij} [N, -, N] \quad (22)$$

3 Model of Electronic Differential

This capture presents a simulation model of the electronic differential ED. The input value to the system is total required torque on the axles, whose value is determined by the higher-level control system based on the position of the control lever and the feedback of the actual speed of the left and right wheel.

3.1 Primary Function of the ED

ED block of the electronic differential splits the total torque according to Eq. (23) at the required torque of each engine M_{RR} , M_{RL} .

$$M_{RL} = M_{RR} = \frac{M_{RA}}{2} [Nm, Nm] \quad (23)$$

3.2 Lock Function of the ED

Model of electronic differential lock is based on equality of wheel speed at each end of the axle.

$$\omega_{WL} = \omega_{WR} [rads^{-1}, rads^{-1}] \quad (24)$$

According to Eq. (24) are constantly evaluated and compared the current wheels speed. When one of the wheels loses adhesion, increases its speed because of excessive torque, which is very undesirable in terms of the driving stability of the vehicle. The input values to the electronic differential lock are actual wheels speed and required motors torque per axle. The deviation flowing from the wheels speed difference enters to block PI controller, output of this controller is a correction moment for the wheel. Power correction runs separately for each wheel in blocks $CM_{L,P}$ whose output has been corrected torque demand for regulation of the frequency converters. If the wheels speed are the same ED lock is disabled and electronic differential performs its primary function. (Fig. 3)

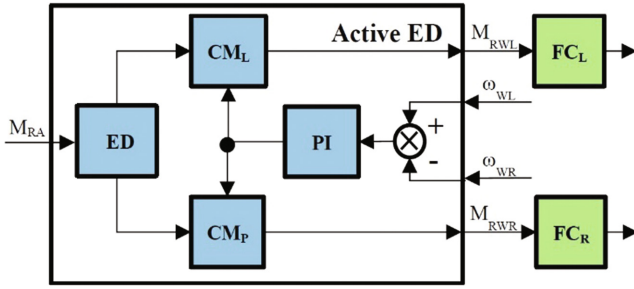


Fig. 3. Block diagram of the ED with active function

The advantage of active electronic differential lock is its automatic closure according to the current driving situation [1]. In the Fig. 4 is a comparison of the course of the wheel speed obtained from the simulation results. If the ED lock is active, and during wheel slip, torque of the wheel is reduced due to decreased adhesion. This solution allows to keep the same speed of the wheels on one axle. If the electronic drive lock is not active, wheel speed are increasing due to the surplus of torque on wheel. Solution to the active distribution of the torque on the axle would be undesirable due to driving stability. This will cause to an increase torque wheels with high adhesion, i.e., that would increase the traction force on one side of the axle and the vehicle began to turn due to the imbalance of forces and could get into a skid.

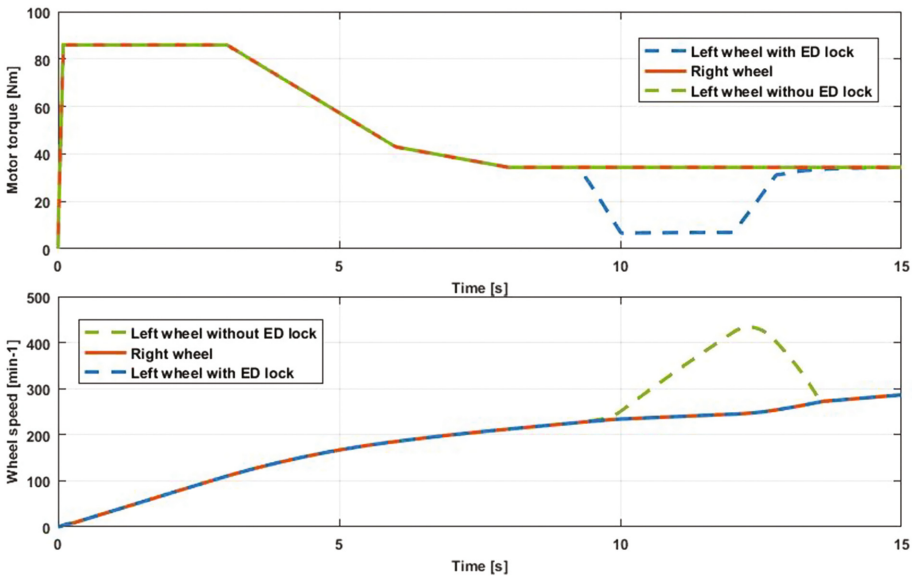


Fig. 4. Simulation results of ED lock

4 Model of Electronic Centre Differential

This capture presents a simulation model of the electronic centre differential ECD. The input value to the system is total required torque of the vehicle M_{RT} , whose value is determined by the higher-level control system based on the position of the control lever and the feedback of the actual speed of the left and right wheel.

4.1 Primary Function of the ECD

CED block of the electronic centre differential splits the total required torque according to Eq. (25) at the required torque of front and rear axle M_{RFA} , M_{RRA} .

$$M_{RFA} = M_{RRA} = \frac{M_{RT}}{2} [Nm, Nm] \quad (25)$$

These moment torque are inputs to the blocks ED_{FA} , ED_{RA} represent a model of electronic differential on front and rear axle.

4.2 Lock Function of the ECD

Model of electronic center differential lock is based on equality of wheels speed on front and rear axle. According to Eq. (26) are constantly evaluated and compared the current average wheels speed of each axle.

$$\bar{\omega}_{WFA} = \bar{\omega}_{WRA} [rads^{-1}, rads^{-1}] \quad (26)$$

When one of the axels loses adhesion, increases its speed because of excessive torque, which is very undesirable in terms of the driving stability of the vehicle. The input values to the electronic differential lock are actual average wheels speed of each axle and total required torque of the vehicle. The deviation flowing from the average wheels speed difference enters to block PI controller, output of this controller is a correction moment for front and rear axle. Power correction runs separately for each wheel in blocks $CM_{RA,FA}$ whose output has been corrected torque demand for electronic differential of each axle. If the average wheels speed are the same ECD lock is disabled and electronic centre differential performs its primary function. (Fig. 5)

In Fig. 6 shows a simulation results of the ECD lock. After the acceleration of the vehicle then front wheels lose adhesion and must be activated ECD lock function. Which results in a reduction torque attributable to the front axle. This reduction is inappropriately reflected in the total vehicle torque and speed increase will slacken slightly. Once the front wheels have again a sufficient adhesion, resulting in loss of adhesion of the rear axle. This time, without activating the differential lock. Will increase the speed of the rear axle due to slippage, because there is no limited torque at rear axle.

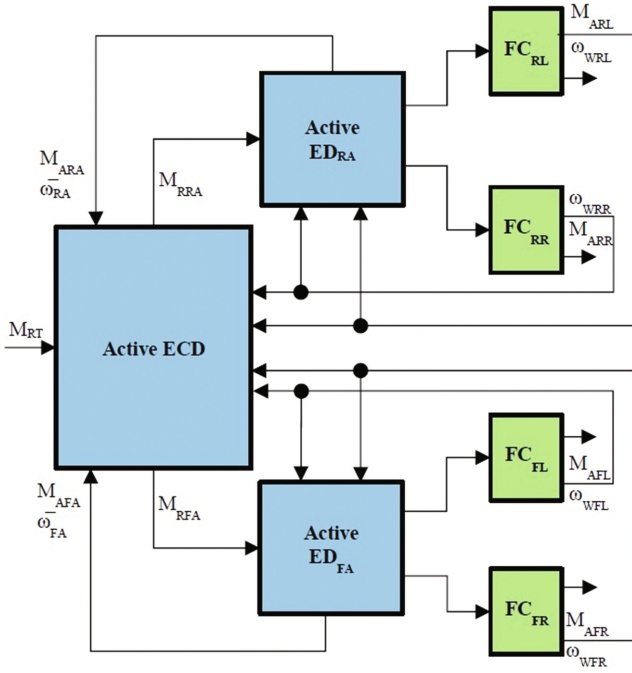


Fig. 5. Block diagram of the ECD with active function

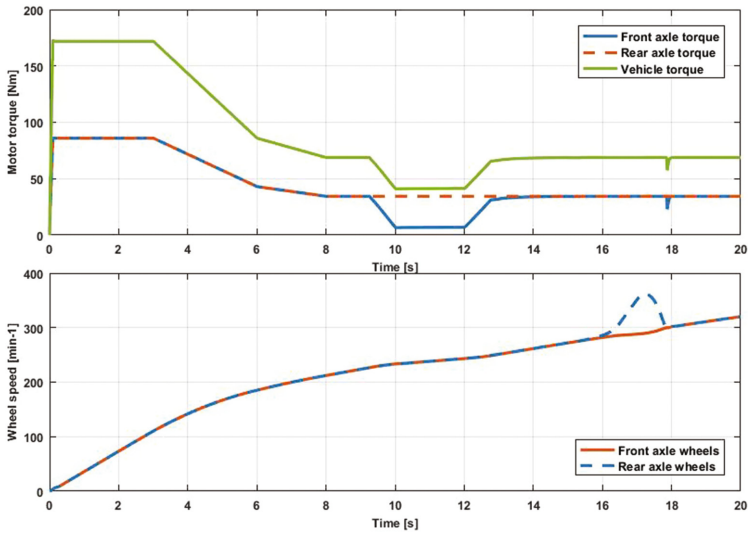


Fig. 6. Simulation results of ECD lock

4.3 Active Torque Distribution Function of the ECD

Function of active torque distribution is an appropriate complement to the electronic centre differential lock [2]. Its mathematical model is based on requirement for the total torque of the vehicle. (Fig. 7)

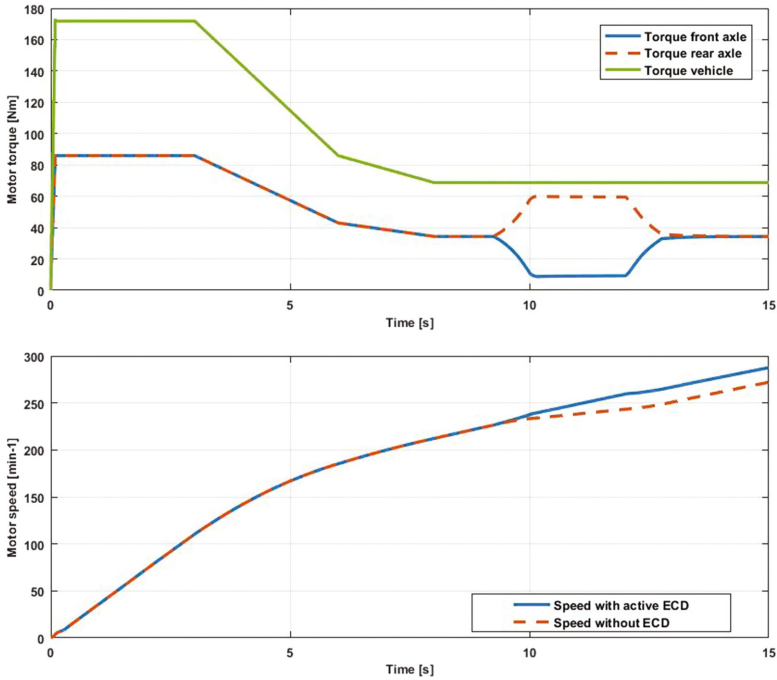


Fig. 7. Simulation results of ECD with active torque distribution

If the wheel of one of the axles slips, it is activated electronical lock and torque supplied to the wheels of the axle is lowered due to adhesion.. This effect is indeed desired in terms of driving stability, but also undesirable in terms of vehicle performance - reduces the total torque of the vehicle.

$$M_{RT} - M_{RRA} - M_{RFA} = \Delta M_{RA} [Nm, Nm] \tag{27}$$

Function of active torque distribution between the individual axles constantly compares total required torque for the vehicle with torque moments attributable to the individual axle. If on one axle decreases torque, then the second axle torque will be increased by this value, as is evident from Eq. (27). It must also comply with the condition by Eq. (28). The maximum torque of the motors are the main limiting factor [4].

$$M_{RiA} + \Delta M_{RA} \leq 2M_M \ \&\& \ M_{RRA} + M_{RFA} = M_{RT} [Nm] \tag{28}$$

From the simulation results is evident function of the active distribution of the torque to each axle. As soon as the front wheels slip, responds ECD lock and torque fed to the front wheels is limited. At the same time responds function of active torque distribution and supply torque to the rear wheels is increased by a part subservient to decreased torque on the front axle.

5 Conclusion

At present is the results of simulation applied for design of control unit of the vehicle. Based on this model is also created another version of the simulation model including all wheel steering. All applications are realized within the research activity in the branch of automotive electronics in the Department of Electronics, VSB – Technical University of Ostrava.

Acknowledgment. Work is partially supported by Grant of SGS No. SP2017/130, VŠB - Technical University of Ostrava, Czech Republic, for which author express their sincere gratitude.

References

1. Neborak, I., Simonik, P., Odlevak, P.: Electric vehicle modelling and simulation. In: 14th International Scientific Conference on Electric Power Engineering 2013, pp. 693–696 (2013)
2. Palacky, P., Slivka, D., Hudecek, P., Sobek, M.: Synerga of control units in electric vehicle. In: International Scientific Conference EPE 2011, Kouty nad Desnou, vol. 12 (2011). ISBN 978-80-248-2393-5
3. Brandstetter, P., Krecek, T.: Sensorless control of permanent magnet synchronous motor using voltage signal injection. *Elektronika ir Elektrotechnika* **19**(6), 19–24 (2013)
4. Rajamani, R.: *Vehicle Dynamics and Control*, p. 492. Springer, London, New York, Dordrecht, Heidelberg (2012). e-ISBN 978-1-4616-1433-9

EMG as Objective Method for Revealed Mistakes in Sport Shooting

Lucie Svecova, David Vala, and Zdenek Slanina^(✉)

Department of Cybernetics and Biomedical Engineering, VSB - Technical University of Ostrava, 17. listopadu 15, 70833 Ostrava, Czech Republic
{lucie.svecova,zdenek.slanina}@vsb.cz

Abstract. The article describes using electromyography as an objective method for identification of wrong muscles work during aimed shooting focused on sport shooting, especially standing position. The measurement was focused on upper limbs, especially of tension of biceps brachii during aiming and its effect on rifle movements. For this task were used SCATT Shooter Training system and SOMNOScreen device with two channels EMG. Several shooters with different shooting skill participated on measurement. There is presumption dependence between increased tension in muscles and rifle trajectory. Also shooters errors which were hard to find were detect with electromyography.

1 Introduction

Sport shooting is a sport which is focused on details [4]. Proper muscle tension affecting stability of shooter - gun system and thus affects the accuracy of hits. In normal practicing with a constant repeating of shooting each shot muscles “learn” to be at a certain tension according to the load, so that the position of the shooter, being the most stable and comfortable. This tension should be the same, not only at each shot, but also throughout the time aiming and firing. Despite all the efforts of the shooter and coach, situations occur when accuracy of hits does not improve or may be worse. If excluded the possibility of defectiveness of the shooting material, it is necessary to focus on the position of the shooter. If even the position of the shooter looks good, there will probably be a suboptimal muscle tension that undermines the stability of the position.

Checking the steadiness of position is currently possible by using commercially available shooting simulators. Simulators record the movement of the end of the barrel compared to the target. Mostly, they work on the optoelectronic principle. The trajectory of the end of the barrel and the hit on target is displayed on the computer screen in real-time. These simulators give us the opportunity to verify the stability of the shooter and to reveal some errors. But if the shooter apparently done everything right, and yet its performance does not improve, it is possible that the changed muscle tension in some muscles appeared and disrupts stability. It can also be caused by several factors, e.g.: poor balance of weapons,

effect of injury, overload of certain muscles or change the proportions, whether it concerns weight change or growth of young shooters. Reveal a problem in this case is not at all easy, see [5–7]. In addition to changing the balance of guns, all other changes are progressive and the shooter would not have to notice them. The very perception of muscular tension requires long-term training and, moreover, it is a subjective feeling. The way, how to control muscle tension objectively, is using electromyography (EMG).

The goal is to create a map of optimal muscle tension during shooting. This would be possible to detect bugs, which is still hidden and thereby more effective workout. In the research shooters of all skill levels participate - very experienced shooters at international level, Intermediate young shooters, beginners and hobby shooters.

2 EMG Measurement During Shooting

Measuring muscle activity is carried by SOMNOScreen device, which is equipped with two channels for surface EMG. First, there was tested the functionality of the method. To verify certain assumptions, SCATT shooters training system was used (see [10]), where the trajectory of the end of the barrel and the point of impact were recorded (Fig. 1).

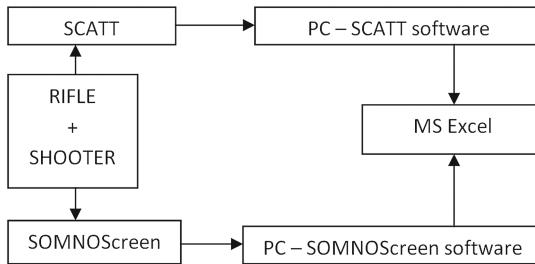


Fig. 1. Block diagram of the measurement.

The first measurements [8,9] were performed on young shooters who still make mistakes that are usually easy to detect. For measurements were initially selected muscles of the upper limbs, especially left and right biceps brachii and muscles of forearm [1–3]. These muscles are muscles of surface layer - m. flexor carpi radialis and m. palmaris longus, second layer muscle m. flexor digitorum superficialis and third layer muscle m. flexor digitorum profundus. Tension in them will vary depending on whether the left or right arm, while these muscles are more “susceptible” to error than the other muscle groups (Figs. 2 and 3).

The first is investigated standing position with an air rifle at a distance of 10 m. Standing position (see Fig. 4) is in terms of shooting skills the simplest.

Shooting is a sport with static loads. Most muscles are in varying degrees in slight tension, which have to be unchanged during aiming and triggering.

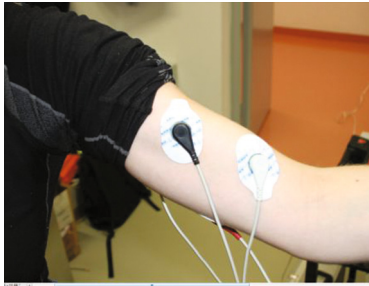


Fig. 2. EMG electrode attached on left biceps brachii.

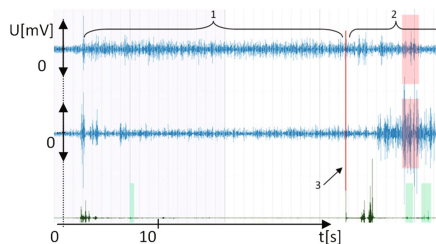


Fig. 3. Tension of right biceps brachii (upper graph) and muscles of right forearm: 1 aiming, 2 interval after shot, 3 moment of shot.

Value of optimal tension in the muscle, respectively a group of muscles beneath the electrode varies according to the load while shooting. E.g. tension in the right biceps brachii is different than the tension in the left biceps brachii. Also, there is different tension magnitude of the same muscle groups between various shooters, however, the tension ratio between the muscle groups should be similar, i.e. greater tension is always in the left biceps brachii than in the right one.

The value of the tension between shooters varies according to their fitness, somatotype, subcutaneous fat, skin conductance, etc. Optimal muscle tone will be derived from measurements of muscle tension mainly very experienced and advanced shooters and compared with impeccable shots of unexperienced shooters.

3 Revealed Mistakes

The process how to make precise shot consists of several parts. First, there is preparing and quieting down the shooters position after loading weapon. Next part is aiming followed by pulling trigger. At the end, there is interval of continuous aiming after trigger is pulled. Time interval of each part is individual for each shooter. Only in the first part may be some fluctuation in muscle tension.

During aiming, triggering and interval after trigger is pulled the muscle tension would be steady, as is shown on Fig. 3. There is electromyogram of right biceps brachii and muscle of right forearms of elite shooter. There is not any



Fig. 4. Preparing of measurement in laboratory – shooter in standing position with air rifle. Sensor of SCATT system is attached on the end of the barrel.

marked amplitude in muscle tension since aiming began. This is precise work on a shot.

Also on next picture is precise shot (Fig. 5). There are record of electromyogram of right and left biceps brachii and record from SCATT shooters training system of young shooter with three years of experiences. Workflow of muscle tension is unchanged. On the other hand, on Fig. 6 is another shot of the same shooter from the same session. There is increased activity of left biceps brachii (1) together with deflection of the rifle from center of the target. There was the shooters effort to get the rifle back to the target, which resulted in additional impetus (2).

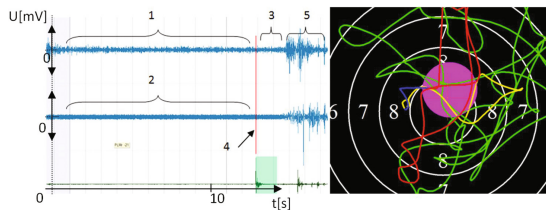


Fig. 5. Left: Electromyogram of left and right biceps brachii, right: SCATT record. 1 aiming, tension in left biceps brachii, 2 aiming, tension in right biceps brachii, 2 time interval after shot, before putting rifle aside, 4 moment of shot, 5 putting rifle aside.

Although the weapon approached the center, shooters position was bad since the start of this shot, with a tendency to “stretch” to the left, the rifle deflected again (3); SCATT record: yellow line shows one second before firing. At this moment the shot was fired (4), and it missed the center. Also tension of right biceps brachii slightly increased (5), which is the result of efforts to regain stability.

On the Fig. 6 there is EMG record of right and left biceps brachii of another young shooter. The shooter participated in several measurements, and therefore

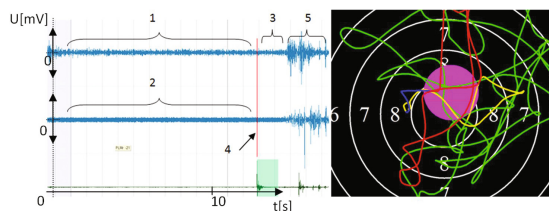


Fig. 6. Left: Electromyogram of left and right biceps brachii, right: SCATT record. 1 increased activity of left biceps brachii during aiming, 2 another impetus of left biceps brachii, 3 yellow line recorded 1s before shot, 4 moment of shot, 5 slightly increased tension of right biceps brachii.

it is possible to eliminate measuring errors caused by wrong attaching electrodes or other artefacts. This measurement was also made in the same condition as previous one. The record shows that the left biceps brachii had a similar tension (2) as on the Fig. 5. Right biceps brachii, which should be more relaxed, is in bigger tension. This means that the shooter holds the rifle with his right hand too tightly, which affects on triggering. In this case, it was obvious that shots not always correspond with shooters performance. Also his preparation for the shot was atypical, when he raised and putted down his rifle with his right hand instead of the left. This is the case, that work on shot seemed properly, but EMG revealed that shooter made mistakes.

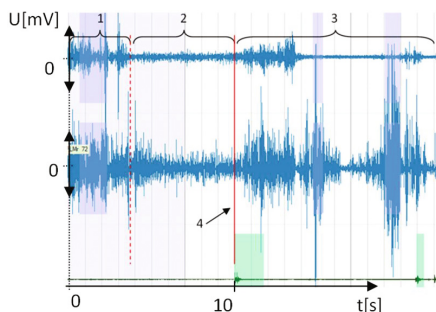


Fig. 7. Tension of left (upper graph) and right biceps brachii: 1 preparation for aiming, 2 aiming, 3 interval after shot, putting rifle aside and relaxing before next shot, 4 moment of shot.

4 Rifle Balance Setting

The previous measurement examined usability of surface EMG in sport shooting. There was demonstrated influence of muscle tension on rifle movements and compared with electronic training system for revealed hidden mistakes. In another

measurement, muscles tension in left biceps brachii and muscles of left forearm under different load were investigated. Measurement was performed with elite shooter in standing position with two different rifles during one training session. One of them was the same air rifle with weight of 5.2 kg, the second one was sport rifle (smallbore rifle) with weight of 6.0 kg. Each rifle was balanced differently, so support point for left hand is not in the same distance of vertical axis of rifle center of gravity (Fig. 8).



Fig. 8. Rifle setting. Above: sport rifle. Middel and bottom: air rifle. T – vertical axis of rifle center of gravity, S – support point, Z – additional weight.

Shooters standing position is the same for both rifles and varies slightly just due to another load of shooters body. If the shooter position seems almost the same, will be similar also tensions in muscles? In case of this participating shooter, the muscle tension was surprisingly different. Tensions in forearm and in biceps brachii were significantly smaller with heavier sport rifle (Fig. 9).

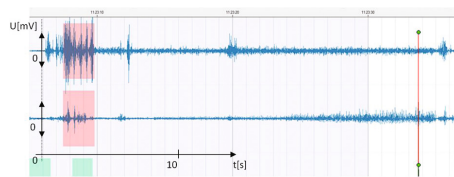


Fig. 9. Electromyogram of left biceps brachii (upper curve) and muscles of forearm (bottom curve) during shooting with sport rifle. Red line – moment of shot.

It means that the sport rifle was balanced better for this particular shooter. According to measurement result, additional weight on air rifle was moved closer to center of gravity to reduce distance between support point and center of gravity (Figs. 8, 9, 10 and 11).

Repeated measurement showed decrease of muscle tensions, especially in biceps brachii as showed Figs. 10 and 11. When muscle tension decreased, shooter would have theoretical achieve better score, unfortunately results are not available yet.

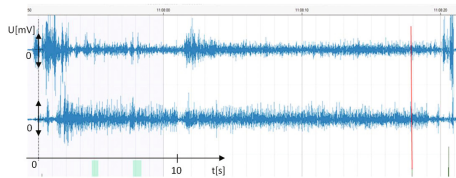


Fig. 10. Electromyogram of left biceps brachii (upper curve) and muscles of forearm (bottom curve) during shooting with air rifle. Red line – moment of shot.

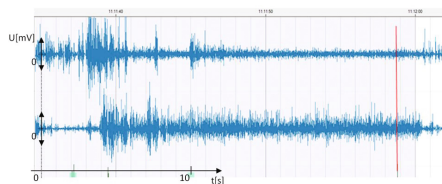


Fig. 11. Electromyogram of left biceps brachii (upper curve) and muscles of forearm (bottom curve) during shooting with air rifle after moving additional weight. Red line – moment of shot.

5 Limits of Surface EMG in Sport Shooting

The only motion in an otherwise static rifle shooting is the motion of the finger on the trigger. With the proper work, this movement should not be seen with the naked eye. Therefore, it was very interesting to see whether it will be seen on the electromyogram. *M. digitorum superficialis* and *m. flexor digitorum profundus* muscles are located in the second, respectively in the third layer of forearm muscles, and thus they are covered by *m. flexor carpi radialis*, *m. palmaris longus* and *m. flexor pollicis longus*. As a summation of all potentials, the record shows a certain tension in the muscles of the forearm.

Unfortunately, the motion of the finger on the trigger is not visible on the record. First, triggering was done properly - slow, smooth motion. But the main reason, why the motion is not visible is very small trigger weight, only about 100 g, which is common setting of trigger in sport shooting with air rifle or small

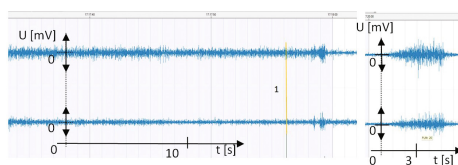


Fig. 12. Electromyographs of flexor digitorum superficialis upper graph – muscle belly for fore-finger, lower graph – muscle belly for other fingers, 1 – moment of shot; Left: trigger weight – 100 g, Right: trigger weight – 5000 g.

bore rifle. By repeated the same action with bigger trigger load of 5000 g, muscle tension increased markedly (Fig. 12). (Notice: Trigger weight is a term from sport shooting rules, its value is determined in kilograms or grams. It is load, which trigger must hold at least. For example, sport pistol trigger has to hold weight of 1.5 kg).

6 Map of Optimal Muscle Tension During Shooting

It seems that EMG during shooting really may help show shooters errors. Electromyogram corresponds with SCATT record. But which muscles have main affect on shooting? For this purpose, a map of muscle tension is needed to create. First step, muscle of right upper limb was inspected. Muscles of arms which involved shooting position are flexors, so m. biceps brachii, m. flexor carpi radialis, m. flexor carpi ulnaris are inspected. These flexors may show some mistakes by increasing their tension as is showed in Fig. 7. Also muscles of shoulders, dorsum and thorax move with arm. Bigger tensions were record in acromial and clavicular part of deltoid, cranial part of trapezoid and m. latissimus dorsi. Rest of measured muscle was relaxed and didn't affect shooting position. The basis for creating a muscle tension map is a kinesiological analysis (Fig. 13) of the shooting positions.

7 Post-processing

Main goal of processing of measurements is to compare measured results with a model muscle tension. This model will be created by measure muscle tension

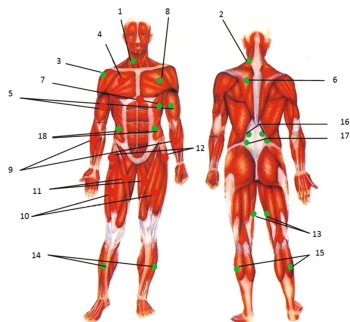


Fig. 13. Muscles chosen for measurement based od kynesiology analysis: 1 - m. sternocleidomastoideus, 2 - m. splenius capitis, 3 - m. deltoideus, 4 - m. pectoralis major, 5 - m. biceps brachii, m. brachialis, 6 - m. trapezius, m. rhobmoideus, 7 - m. serratus anterior, 8 - m. pectoralis major, m. pectoralis minor, 9 - m. flexor carpi radialis, m. flexor digitorum superficialis, 10 - m. rectus femoris, 11 - m. sartorius, 12 - m. tensor fasciae latae, 13 - m. gracilis, 14 - m. tibialis anterior, 15 - m. triceps surae (caput longum), 16 - m. spinalis, 17 - m. quadratus lumborum, 18 - m. obliquus externus abdominis, m. obliquus internus abdominis. Green – muscles, which are in tension during shooting. Red – muscles, which are relaxed during shooting.

of shooters of all skill levels - very experienced shooters at international level, Intermediate young shooters, beginners and hobby shooters. There is also possibility to correlate objective data from SCATT, specifically speed of aiming point, which can be export to MS Excel, with measured voltage from muscles. According to presumption that muscle tension influences stability of position, comparison with SCATT gets the objective view on shooters skill and conditions.

8 Conclusions

One part of measurements was documented presumption dependence of increased muscle tension in m. biceps brachii and rifle movements. Also influence of rifle setting was demonstrated on muscle tension measurement of left arm with two rifles. The experiments were supported with SCATT shooter training systems. The research is now limited with only 2 channels EMG of SOMNOScreen device, which makes possible to measure only two muscles together. Therefore, the multichannel EMG is preparing. It will be create for build into shooters equipment, which enable to measure more muscle groups at once and is more comfortable for shooter. One of main goals is to create a map of muscle tension during rifle shooting. For this part of work right upper limb was investigated. There was found also limit of surface EMG in sport shooting. Using EMG in sport shooting may improve shooting training. It shows also shooters condition and influence of muscle fatigue on shooting performance. These parameters are not possible to monitor with any of optoelectronic shooting training systems which are commonly used.

Acknowledgement. This work was supported by the project SP2017/158, “Development of algorithms and systems for control, measurement and safety applications III” of Student Grant System, VSB-TU Ostrava.

References

1. Cihak, R.: Anatomie. Grada, Praha (2016). ISBN 978-80-247-3817-8
2. Kadanka, Z., Bednarik, J., Vohanka, S.: Prakticka elektromyografie. Brno (1994). ISBN 80-7013-181-0
3. Kittnar, O.: Prakticka elektromyografie. Grada, Praha (2011). ISBN 978-80-247-3068-4
4. Horneber, R.: Wettkampfsport Gewehrschießen. Technik, Taktik, Training, 139 stran. ASIN B001UKT85M
5. Thongpanja, S., Phinyomark, A., Phukpattaranont, P., Limsakul, C.: Mean and median frequency of EMG signal to determine muscle force based on time dependent power spectrum. *Elektronika ir Elektrotechnika* **19**(3), 51–56 (2013)
6. Sawicki, A., Walendziuk, W.: Analysis of the thermal effect influence on the MEMS accelerometer sensors measurement results. In: Proceedings of SPIE, vol. 10031, no. 1003120. The International Society for Optical Engineering (2016)
7. Walendziuk, W., Wysk, L., Skoczylas, M.: The use of strain gauge platform and virtual reality tool for patient stability examination. In: Proceedings of SPIE, vol. 10031, no. 100312. The International Society for Optical Engineering (2016)

8. Martinek, R., Kahankova, R., Nazeran, H., Konecny, J., Jezewski, J., Janku, P., Bilik, P., Zidek, J., Nedoma, J., Fajkus, M.: Non-invasive fetal monitoring: a maternal surface ECG electrode placement-based novel approach for optimization of adaptive filter control parameters using the LMS and RLS algorithms. *Sensors* **17**(5), 1154 (2017). doi:[10.3390/s17051154](https://doi.org/10.3390/s17051154)
9. Martinek, R., Nedoma, J., Fajkus, M., Kahankova, R., Konecny, J., Janku, P., Nazeran, H.: Phonocardiographic-based fiber-optic sensor and adaptive filtering system for noninvasive continuous fetal heart rate monitoring. *Sensors* **17**(4), 890 (2017). doi:[10.3390/s17040890](https://doi.org/10.3390/s17040890)
10. SCATT homepage. <http://www.scatt.com>. Accessed 10 July 2017

Compensation of Nonlinear Distortions in Telecommunication Systems with the Use of Functional Series of Volterra

N.D. Pirogova^(✉) and I.O. Neches

Rostov State Transport University, Build. 2, Rostovskogo Strelkovogo Polka
Narodnogo Opolcheniya sq., 344038 Rostov-on-Don, Russian Federation
{nd-pirogova, neches-io}@yandex. ru

Abstract. The paper proposes a method for compensating for nonlinear distortions in telecommunication systems by linearizing their characteristics. It is shown that compensation of nonlinear distortions is possible when using Volterra functional series. To formalize the approach, the apparatus of differential-Taylor transformations is used. Nonlinear and correcting circuits are described by Fourier-images of the Volterra kernels. By using differential-Taylor conversions found an analytical expression for the images of the nuclei of the cascade connections of nonlinear and corrective chains. This formula is recursive and allows to define the Fourier images of Volterra kernels of the higher order via the lowest ones. With the help of this formulae are determined by the image of the Volterra kernels of a corrective circuit according to the known kernels of a nonlinear circuit and required cores of the combined blok. This allows you to compensate for the higher-order Volterra kernel of a nonlinear chain. The example of compensating of images of kernels of 3 and 5 orders is given.

Keywords: Functional modeling of nonlinear radio feedback · Volterra series · Kernel Volterra series · Nonlinear transfer function · Many-dimensional Maclaurin series · Taylor-differential conversion · Differential-Taylor function · Differentially taylor spectrum

1 Introduction

At present, in the development of telecommunication systems, the problem of increasing the data transfer rates is topical. The use of modern multi-input and multiple-output (MIMO) communication systems, modulation techniques such as orthogonal frequency division multiplexing (OFDM), provides a significant increase in the bandwidth of the radio channel by improving spectral efficiency. The use of OFDM allows to increase the transmission rate without increasing the occupied bandwidth or the modulation level. These systems are very sensitive to the nonlinear distortions introduced by the analogue part of the telecommunication system, especially on the transmitter side. Compensation of nonlinear distortions is one of the aspects of the task of increasing the linearity of radio engineering devices. In addition to compensation, there are other methods to increase the linearity of systems, such as the use of negative feedback, the optimization

of the operating mode of nonlinear elements by direct current, the use of additional corrective circuits, etc.

Many linearisation techniques have been developed recently [1]. They can be classified into three major categories: feedback methods; feedforward linearisation; predistortion techniques. The feedback methods incorporate Radio frequencies (RF) feedback techniques, divided into passive and active RF feedback, and envelope or modulation feedback techniques, including polar and Cartesian loops. The predistortion methods are divided into analogue predistortion and Digital Predistortion (DPD). The latter includes Look-Up-Table (LUT), polynomial and baseband-components injection DPD techniques. The first one uses Look-Up Tables to store coefficients for all values of the input signal and provides sample-by-sample multiplication of the input signal by these coefficients. Adaptation of LUT DPD circuits is usually accomplished by minimising the square error between the fed-back reference and fed-forward signals. Polynomial DPD is another well-developed type of digital predistortion. It uses a polynomial function in place of LUT to create the predistortion characteristic. The polynomial function is an inverse characteristic of the Power amplifier (PA) distortion, approximated by a polynomial nonlinearity. The baseband components injection technique is a new DPD technique proposed in 2005 [1] and significantly developed in this thesis with the aim of eliminating the drawbacks of the conventional DPD methods. Identifying digital predistorters with direct and indirect learning architecture of RF transmitters are considered in the paper [2]. This architecture commonly utilizes iterative optimization procedures for the parameter of the DPD to minimize the error. In book [3] an overview of digital predistortion is provided without discussing the details of the algorithms used. Digital predistortion and the challenges faced when implementing it are summarized. Adaptive systems, where the performance is optimized by measuring the output signal and adjusting DPD coefficients iteratively to reduce the residual nonlinearities, are presented. Learning structures are discussed that augment adaptive systems to improve the rate of convergence. In paper [4], are propose an efficient open-loop DPD to compensate for static distortion and memory effects induced by a PA using the recently proposed dynamic deviation reduction based Volterra series. By employing this pruned form of Volterra series, the model structure can be significantly simplified without impact on system performance.

To increase the linearity of communication systems, both analogue and digital linearization methods are widely used [5]. Among these methods, pre-distortion linearizers are very popular because they have a wide bandwidth and can be easily incorporated as separate stand-alone instruments into existing amplifiers. Linearization methods based on post-distortions [6] are also used, for constructing models in the systems with memory. The apparatus of the Volterra functional series (VFS) can be used.

The compensation problem in nonlinear systems with the use of the VFS is solved in [6] by constructing the inverse series to the original one, the synthesis of the compensator circuit, which corresponds to the constructed series and the inclusion of this scheme in a cascade with the original nonlinear circuit. However, the procedure for reversing the series is very labor-intensive computationally, it is poorly formalizable, and the complexity of the computation during the inversion substantially increases with the increase in the number of terms of the series.

2 The Method of Compensating for Nonlinear Distortions

In this paper, we propose a formalized approach to compensate for nonlinear distortions in systems with memory. Each functional block entering the system is supposed to be represented as a set of nonlinear transfer functions (NTF). From the equations compiled for the cascade connection of the nonlinear and compensating circuit, the NTF of the compensating device is determined using the apparatus of differential Taylor transformations. (Fig. 1)

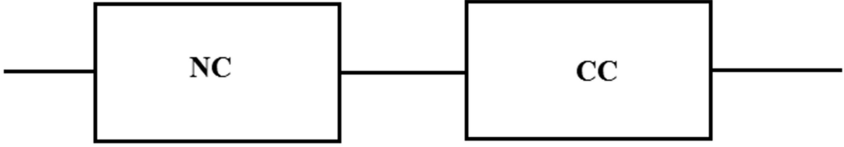


Fig. 1. Structural scheme of compensation of nonlinear distortions

Let NC be the original nonlinear circuit, CC block corrects the nonlinear distortions. Both blocks admit a description of the response of the convergent Volterra series.

Complex amplitudes and combinational response components at the output of NC and CC units can be defined as [7]

$$\begin{aligned} \dot{y}_s^{nc} &= \sum_{\gamma=1}^{\infty} \frac{\gamma!}{2^{\gamma-1} \prod_{j=-\vartheta}^{\vartheta} \eta_j!} H_{\gamma}^{nc}(\omega_1, \dots, \omega_{-\vartheta}) \prod_{r=-\vartheta}^{\vartheta} (e_r)^{\eta_r}, \\ \dot{y}_s^{cc} &= \sum_{\gamma=1}^{\infty} \frac{\gamma!}{2^{\gamma-1} \prod_{j=-l_{nc}}^{l_{nc}} \eta_j!} H_{\gamma}^{cc}(\omega_1, \dots, \omega_{-l_{nc}}) \prod_{r=-l_{nc}}^{l_{nc}} (\dot{y}_s^{nc})^{\eta_r}, \end{aligned} \quad (1)$$

where $y_s^{nc} = \dot{y}_s^{nc} \exp(j\omega_s t)$, $y_s^{cc} = \dot{y}_s^{cc} \exp(j\omega_s t)$, $s = (s^{(1)}, s^{(2)}, \dots, s^{(\vartheta)})$ – integer vector of dimension ϑ , determining the frequency of the s -th combination harmonic, ϑ – number of external influences, $s = -l_{cc}, \dots, l_{cc}$, $\omega_s = \sum_{j=1}^{\vartheta} s^{(j)} \omega_j$ – frequency of a combinative harmonica, ω_j – frequencies of external influences, e_r – complex amplitudes of external influences; $H_{\gamma}^{cc}(\omega_1, \dots, \omega_{-l_{nc}})$ – NTF block CC order γ ; η_j – the number of frequency repetitions of the external signal and the response frequencies of the NC block respectively in $H_{\gamma}^{nc}(\cdot)$; \dot{y}_r^{nc} – the combination components of the response of the NC block, respectively, $-\vartheta$ and $-l_{nc}$ under the signs of products mean that complex-conjugate quantities are also taken into account \dot{y}_s^{nc} .

In [7, 8], the principal possibility of applying differential Taylor transformations [9] is shown to obtain a mathematical model of a nonlinear inertial system in the form of a

Volterra series in mathematical models of constituent blocks. The set of NTF values is a differential-Taylor spectrum of the functional describing the given system:

$$\begin{aligned}
 Y_s^{nc}(\eta_1, \eta_{-1}, \dots, \eta_9, \eta_{-9}) &= \frac{\gamma!}{2^{\gamma-1} \prod_{j=-9}^9 \eta_j!} H_\gamma^{nc}(\omega_1, \dots, \omega_{-l_9}), \\
 Y_s^{cc}(\eta_1, \eta_{-1}, \dots, \eta_{l_{nc}}, \eta_{-l_{nc}}) &= \frac{\gamma!}{2^{\gamma-1} \prod_{j=-l_{nc}}^{l_{nc}} \eta_j!} H_\gamma^{cc}(\omega_1, \dots, \omega_{-l_{nc}}),
 \end{aligned} \tag{2}$$

where $Y_s^{nc}(\cdot)$, $Y_s^{cc}(\cdot)$ – Taylor functions of many variables.

The values $Y_s^{nc}(\cdot)$ and $Y_s^{cc}(\cdot)$ are the differential-Taylor spectra (DTS) of the s-th components of the vectors of the components of the response of NC and CC, respectively.

It follows from (2) that $H_\gamma^{cc}(\omega_1, \dots, \omega_{l_{nc}}) = H_s^{cc}(\eta_1, \eta_{-1}, \dots, \eta_{l_{nc}}, \eta_{-l_{nc}})$ as well as $Y_s^{cc}(\dots, \eta_r, \dots)$ is a Taylor function of several variables, and the values $H_s^{cc}(\dots, \eta_r, \dots)$ – T-spectrum of the combination component y_s^{cc} of the block response CC. In addition, a record $H_s^{cc}(\dots, \eta_r, \dots)$ is more compact, which is especially important for multifrequency input action.

We apply the apparatus of differential-Taylor transformations to obtain the NTF cascade connection of NC and CC blocks [7]. To do this, we obtain the T-image of expression (1):

$$\begin{aligned}
 &y_s^{cc} \div Y_s^{(cc,nc)}(\dots, \mu_r, \dots) \\
 &= \sum_{\gamma=1}^{\infty} \frac{\gamma!}{2^{\gamma-1} \prod_{j=-l_{nc}}^{l_{nc}} \eta_j!} H_s^{cc}(\dots, \eta_r, \dots) \prod_{j=-l_{nc}}^{l_{nc}} \left[Y_j^{nc}(\dots, \mu_r, \dots) \right] \eta_j,
 \end{aligned}$$

where \prod – character of Taylor multiplication of many ($2l_{nc}$) functions, η_j – character of Taylor exponentiation.

Then NTF of the combined block

$$\begin{aligned}
 H_s^{(cc,nc)}(\dots, \mu_r, \dots) &= \frac{1}{W_\gamma^{(cc,nc)}} \sum_{\gamma=1}^{\infty} W_\gamma^{cc} \\
 &\times H_s^{cc}(\dots, \eta_r, \dots) \prod_{j=-l_{nc}}^{l_{nc}} \left[W_\gamma^{nc} H_j^{nc}(\dots, \mu_r, \dots) \right] \eta_j,
 \end{aligned} \tag{3}$$

where $W_\gamma^{(cc,nc)} = W_\gamma^{nc} = \frac{\gamma!}{2^{\gamma-1} \prod_{r=-9}^9 \mu_r!}$.

To compensate for the nonlinear distortions, we require that the higher-order transfer functions of the combined block are equal to zero, the 1st order NTF of the combined (NC, CC) block is equal to the transmission coefficient \mathbf{K} , i.e.,

$$H_s^{(cc,nc)}(\dots, \mu_r, \dots) = H_s^{cc}(\dots, \eta_r, \dots) H_s^{nc}(\dots, \mu_r, \dots) = \mathbf{K}, \sum_{r=1}^{\vartheta} \mu_r = 1, \eta_r = \mu_r;$$

then $H_s^{cc}(\dots, \eta_r, \dots) = \frac{\mathbf{K}}{H_s^{nc}(\dots, \mu_r, \dots)}$.

For higher orders of NTF, we require

$$H_s^{(cc,nc)}(\dots, \mu_r, \dots) = 0, \sum_{r=1}^{\vartheta} \mu_r > 1.$$

Then, taking (3) into account, we write the equation:

$$\frac{1}{W_\gamma^{(cc,nc)}} \sum_{\gamma=2}^{\gamma_{\max}} W_\gamma^{cc} H_s^{cc}(\dots, \eta_r, \dots) \times \prod_{j=-l_{nc}}^{l_{nc}} \left[W_\gamma^{nc} H_j^{nc}(\dots, \mu_r, \dots) \right]^{\eta_j} = 0, \quad (4)$$

where γ_{\max} – the order of the desired NTF compensator.

According to the rules of differential-Taylor multiplication and the exponentiation:

$$\begin{aligned} \left[W_\gamma^{nc} H_j^{nc}(\dots, \mu_r, \dots) \right]^{\eta_j} &= W_\gamma^{nc} H_j^{nc}(\dots, \mu_r, \dots) * \left[W_\gamma^{nc} H_j^{nc}(\dots, \mu_r, \dots) \right]^{\eta_j - 1}, \\ H_s^{nc}(\dots, \mu_r, \dots) * H_s^{nc}(\dots, \mu_r, \dots) &= \sum_{s=1}^{\gamma} \sum_{2\vartheta} Y_s^{nc}(\delta_1, \delta_{-1}, \dots, \delta_r, \delta_{-r}, \dots) \\ &\times Y_s^{nc}(\mu_1 - \delta_1, \mu_{-1} - \delta_{-1}, \dots, \mu_r - \delta_r, \mu_{-r} - \delta_{-r}, \dots), \end{aligned}$$

where $\sum_{r=1}^{2\vartheta} \delta_r = s$, δ_{-r} – frequency repetition of complex-conjugate input actions;

* – character of Taylor multiplication of two functions.

Solving Eq. (4), we find $H_s^{cc}(\dots, \eta_r, \dots)$, starting with the smallest order. So the third-order nonlinearity for complex amplitude y_s^{cc} response frequency ω_s at a single-frequency input signal ($\vartheta = 1$) is determined from the assumption that the third-order kernel of the NC and CC blocks is equal to zero:

$$H_s^{(cc,nc)}(2, 1) = 0,$$

$$H_s^{(cc,nc)}(2, 1) = \sum_{m+n=1}^3 H_s^{cc}(m, n) \{ H_s^{nc}(2, 1)^m * H_{-s}^{nc}(2, 1)^n \} = 0,$$

where $H_{-s}(\cdot)$ is a complex conjugate quantity $H_s(\cdot)$.

Since with single-frequency input action $s = 1$, then we omit the subscript below $H_s(\cdot)$.

$$H^{cc}(1, 0)H^{nc}(2, 1) + H^{nc}(2, 1)H^{nc}(2, 1)^2 * H_-^{nc}(2, 1) = 0,$$

where $H_-(\cdot)$ is a complex conjugate quantity $H(\cdot)$,

$$\begin{aligned} H^{nc}(2, 1)^2 * H_-^{nc}(2, 1) &= H^{nc}(1, 0)H^{nc}(1, 0)H_-^{nc}(0, 1), \\ H^{cc}(1, 0)H^{nc}(2, 1) + H^{cc}(2, 1)(H^{nc}(1, 0))^2 H_-^{nc}(0, 1) &= 0. \end{aligned} \tag{5}$$

From (5) we will receive NTF of the third order of the adjusting quadripole taking into account that

$$H^{cc}(1, 0) = \frac{K}{H^{nc}(1, 0)}, \tag{6}$$

$$H^{cc}(2, 1) = \frac{-H^{nc}(2, 1)K}{H^{nc}(1, 0)(H^{nc}(1, 0))^2 H_-^{nc}(0, 1)}. \tag{7}$$

We find the NTF of the 5th order CC from the condition that the fifth-order kernel of the NC and CC blocks is equal to zero:

$$H^{(cc.nc)}(3, 2) = 0.$$

$$\sum_{m+n=1}^5 H^{cc}(m, n) \{H^{nc}(3, 2)^m * H_-^{nc}(3, 2)^n\} = 0.$$

$$\begin{aligned} H_1^{cc}(1, 0)H^{nc}(3, 2) + H^{cc}(2, 1) \{H^{nc}(3, 2)^2 * H_-^{nc}(3, 2)\} \\ + H^{cc}(3, 2) \{H^{nc}(3, 2)^3 * H_-^{nc}(3, 2)^2\} = 0 \end{aligned} \tag{8}$$

$$\begin{aligned} H^{nc}(3, 2)^2 * H_-^{nc}(3, 2) &= H^{nc}(1, 0)H^{nc}(2, 1)H_-^{nc}(0, 1) \\ &+ H^{nc}(2, 1)H^{nc}(1, 0)H_-^{nc}(0, 1) + H^{nc}(1, 0)H^{nc}(1, 0)H_-^{nc}(1, 2), \\ H^{nc}(3, 2)^2 * H_-^{nc}(3, 2) &= 2H^{nc}(1, 0)H^{nc}(2, 1)H_-^{nc}(0, 1) \\ &+ H^{nc}(1, 0)H^{nc}(1, 0)H_-^{nc}(1, 2) \end{aligned} \tag{9}$$

$$H^{nc}(3, 2)^3 * H_-^{nc}(3, 2)^2 = H^{nc}(1, 0)H^{nc}(1, 0)H^{nc}(1, 0)H_-^{nc}(0, 1)H_-^{nc}(0, 1). \tag{10}$$

Substituting (9), (10) into the expression (8), we obtain

$$\begin{aligned} H^{cc}(1, 0)H^{nc}(3, 2) + H^{cc}(2, 1) \{2H^{nc}(1, 0)H^{nc}(2, 1)H_-^{nc}(0, 1) \\ + H^{nc}(1, 0)H^{nc}(1, 0)H_-^{nc}(1, 2)\} + H^{cc}(3, 2)(H^{nc}(1, 0))^3 (H_-^{nc}(0, 1))^2 = 0, \end{aligned} \tag{11}$$

$$H^{cc}(3,2)(H^{nc}(1,0))^3(H_-^{nc}(0,1))^2 = -(H^{cc}(1,0)H^{nc}(3,2) + H^{cc}(2,1)\{2H^{nc}(1,0)H^{nc}(2,1)H_-^{nc}(0,1) + H^{nc}(1,0)H^{nc}(1,0)H_-^{nc}(1,2)\}).$$

From Eq. (11) we obtain the fifth-order NTF of the distortion corrector

$$H^{cc}(3,2) = -(H^{cc}(1,0)H^{nc}(3,2) + H^{cc}(2,1)(2H^{nc}(1,0)H^{nc}(2,1)H_-^{nc}(0,1) + \frac{H^{nc}(1,0)H^{nc}(1,0)H_-^{nc}(1,2))}{(H^{nc}(1,0))^3(H_-^{nc}(0,1))^2})). \quad (12)$$

3 Example Calculation

Consider an amplifier of high frequency [10].

At the input of the high-frequency amplifier (HFA) unit, a monoharmonic signal ($\vartheta = 1$) with an amplitude e_1 and the frequency f_1 . At the HFA output, the dependence of the complex response amplitude on the complex amplitude of the input signal is determined by (1)

$$y_1^{nc} = \sum_{\gamma=1}^{\infty} \frac{\gamma!}{2^{\gamma-1}\eta_1!\eta_{-1}!} H_{\gamma}^{nc}(\omega_1, \dots, \omega_{-1})(e_1)^{\eta_1}(e_{-1})^{\eta_{-1}},$$

where $H_{\gamma}^{nc}(\omega_1, \dots, \omega_{-1}) = \frac{\gamma!}{\gamma!} \left(\frac{\partial^{\gamma} y_1^{nc}}{\partial e_1^{\eta_1} \partial e_{-1}^{\eta_{-1}}} \right)_0$ – Fourier image of the Volterra nucleus of order $\gamma = \eta_1 + \eta_{-1}$.

The components of the differential-Taylor spectrum (DTS) with a single-frequency input are of the form (2):

$$Y_1^{nc}(\eta_1, \eta_{-1}) = \frac{\gamma!}{2^{\gamma-1}\eta_1!\eta_{-1}!} H_{\gamma}^{nc} \left(\underbrace{\omega_1, \dots, \omega_1}_{\eta_1}, \underbrace{\omega_{-1}, \dots, \omega_{-1}}_{\eta_{-1}} \right).$$

For HFA at the frequency of 10.5 MHz, the values of the DTS for the constituent y_1^{nc} up to the 5th order inclusive:

$$\begin{aligned} Y_1^{nc}(1,0) &= -1,0083 + j1,4111, \\ Y_1^{nc}(2,1) &= -0,5635 + j0,5837, \\ Y_1^{nc}(3,2) &= -5,5350 + j5,2176. \end{aligned}$$

The complex amplitude at the output of the HFA in the form of a segment of the Maclaurin series can be represented in the form:

$$\begin{aligned} \dot{y}_1^{nc} &= (-1, 0083 + j1, 4111)\dot{e}_1 + (-0, 5635 + j0, 5837) \\ &\times \dot{e}_1^2 \dot{e}_{-1} + (-5, 5350 + j5, 2176)\dot{e}_1^3 \dot{e}_{-1}^2. \end{aligned} \tag{13}$$

To estimate the error and the convergence of the segment of the series (13), we define the approximate radius of convergence R_γ according to [11]. To calculate R_5^{nc} let us take the 5th order component of the DTS:

$$R_5^{nc} = \frac{1}{\sqrt[5]{|Y_1^{nc}(3, 2)|}} = \frac{1}{\sqrt[5]{|-5, 5350 + j5, 2176|}} = 1, 501, \text{ B.}$$

Then, the amplitude of the input action should not exceed the value 1,501 B, i.e. $|e_1| < R_5^{nc}$.

According to (2) NTF of NC block is equal:

$$\begin{aligned} H^{nc}(1, 0) &= Y_1^{nc}(1, 0) = -1, 0083 + j1, 4111; \\ H^{nc}(2, 1) &= \frac{4}{3} Y_1^{nc}(2, 1) = -0, 7513 + j0, 7783; \\ H^{nc}(3, 2) &= \frac{8}{5} Y_1^{nc}(3, 2) = -8, 8560 + j8, 3482. \end{aligned}$$

Define NTF for the compensator (block 2) using formulas (6), (7), (12) for $K = 1$.

$$\begin{aligned} H^{cc}(1, 0) &= -0, 335 - j0, 469; H^{cc}(2, 1) = 0, 0545 - j0, 1065; \\ H^{cc}(3, 2) &= 0, 1576 - j0, 3472. \end{aligned}$$

According to (2) the coefficients of the Maclaurin series of CC block is equal:

$$\begin{aligned} Y_1^{cc}(1, 0) &= -0, 335 - j0, 469; Y_1^{cc}(2, 1) = 0, 0409 + j0, 0799; \\ Y_1^{cc}(3, 2) &= 0, 0985 + j0, 2170. \end{aligned}$$

Complex amplitude of a response with a frequency of 10.5 MHz at the output of the compensator will have an appearance:

$$\begin{aligned} \dot{y}_1^{cc} &= (-0, 335 - j0, 469)\dot{y}_1^{nc} + (0, 0409 + j0, 0799) \\ &\times (\dot{y}_1^{nc})^2 \dot{y}_{-1}^{nc} + (0, 0985 + j0, 2170)(\dot{y}_1^{nc})^3 (\dot{y}_{-1}^{nc})^2. \end{aligned} \tag{14}$$

Estimate the convergence of the resulting segment of the series (14) by means of an approximate radius of convergence R_γ [11]. To calculate R_5^{cc} Take the component of the 5th order DTS:

$$R_5^{cc} = \frac{1}{\sqrt[5]{|Y_1^{cc}(3, 2)|}} = \frac{1}{\sqrt[5]{|0,0985 + j0,2170|}} = 0,7506, \text{ B.}$$

The amplitude of the input action on the corrector (response from the previous block) should not exceed the value 0,7506 B, i.e. $|y_1^{nc}| < R_5^{cc}$.

The obtained values of the coefficients of the series segment (14) can be verified by formula (3) for combining the NC and CC blocks:

$$H^{cc,nc}(1, 0) = 1, H^{cc,nc}(2, 1) = 0, H^{cc,nc}(3, 2) = 0.$$

Thus, the Volterra kernels characterizing the nonlinearities of the third and fifth order system were compensated. Since the NC response is the input action for the compensator, then to check the results we can substitute the segment of the series (13) into expression (14). Restricting ourselves to the fifth order of nonlinearity, and carrying out simple calculations, the result was confirmed.

4 Conclusion

The resulting formula (4) is recurrent and allows to sequentially find the NTF of the correcting chain of the required order for an arbitrary (limited) number of input actions. In addition, the proposed algorithm allows to obtain the coefficients of the inverse Volterra series in the frequency domain, allowing to selectively suppress the desired harmonic.

References

1. Bondar, D.: Advanced digital predistortion of power amplifiers for mobile and wireless communications. School of Electronics and Computer Science. This is an electronic version of a Ph.D. thesis awarded by the University of Westminster. The Author (2009)
2. Soltani Tehrani, A.: Behavioral Modeling of Wireless Transmitters for Distortion Mitigation. Chalmers University of Technology, Gothenburg (2012)
3. Digital Front-End in Wireless Communications and Broadcasting: Circuits and Signal Processing / edited by Fa-Long Luo. Cambridge University Press, (2011)
4. Zhu, A., Draxler, P.J., Yan, J.J., Brazil, T.J.: Open-loop digital predistorter for RF power amplifiers using dynamic deviation reduction-based volterra series. IEEE Trans. Microw. Theory Tech. **56**(7), 1524–1534 (2008)
5. Hashmi, M.S., Rogojan, Z.S., Nazi, S.R., Ghannouchi, F.M.: A broadband dual-inflection point RF predistortion linearizer using backward reflection topology. Prog. Electromagnet. Res. C **13**, 121–134 (2010)
6. Tsimbinos, J.: Identification and compensation of nonlinear distortion. The Levels, South Australia (1995)
7. Pirogova, N.D.: Definition of transfer functions of nonlinear system on transfer functions of making blocks. J. Radioeng. (10), 51–56 (2009)

8. Pirogova, N.D.: Numerical analytical simulation technique for nonlinear feedback systems. *J. Radioelectron. Commun. Syst.* **56**(5), 251–259 (2013)
9. Pukhov, G.E.: *Differential Transformations of Functions and Equations*. Naukova Dumka, Kiev (1980)
10. Pirogova, N.D.: Application of the method of function modeling based on the use of differential-Taylor transformations. *Vestn. RGUPS* **22**(2), 99–104 (2006)
11. Neches, I.O., Pirogova, N.D.: *Methods for Analysis of Nonlinear Radio Devices Using the Apparatus of Functional Series: Monograph*. Rostov State Transport University, Rostov-on-Don (2013)

Improving the Reliability of Busbar Protection System with IEC 61850 GOOSE Based Communication

Dimitar Bogdanov¹(✉), Georgi Dimitrov²,
and Francisco Gonzalez-Longatt³

¹ Technical University of Sofia, Sofia, Bulgaria
dbogdanov@tu-sofia.bg

² TriEI Ltd. Company, Sofia, Bulgaria
georgi.st.dimitrov@gmail.com

³ Loughborough University, Loughborough, UK
F.Gonzalez-Longatt@lboro.ac.uk

Abstract. The main task of the “relay” protection system is to provide trip commands in case of faults and to prevent the operation of the electrical equipment in dangerous modes. The set of the protection functions and the system structure have an impact on the reliability and respectively dependability of the protected structure. In some smaller node-point electrical facilities like step-up substations for PVPPs and wind-farms, the set of protection functions required by the respective regulations can be limited. The multifunctional features of new generations of *Intelligent Electronic Devices* (IEDs) and the options to use IEC 61850 based communication, protection and automation, provide opportunities for improvement of the busbar protection system.

Keywords: Relay protection · Busbars · Reliability · IED · IEC 61850

1 Introduction

The contemporary grid protection and automation schemes are becoming more and closer as structure and communication topology to data exchange in computer networks. The exchange of information is widely made via Ethernet based networks, in some cases using WEB interfaces. The optical links are based also practically on the hardware and software common for the data exchange in computer networks. This utilizes the implementation of universal hardware and software, but imposes questions related to cyber security, vulnerability to unauthorized access, software “bugs”, etc.

The implementation of IEC 61850 features for substation automation provides many opportunities to improve the functionality of the respective protection system. For the particular study, experiments were made to implement a function for busbar protection utilizing the functionality of the outgoing power lines protections.

2 Improving the Relay Protection System Functionality

The contemporary operated electrical grids are challenged by the high penetration of renewable sources of electrical power generation [1, 2]. The node points for connection of renewables – typically Photo Voltaic Power Plants (PVPPs) and wind farms are sometimes regarded as non-vital for the integrity of the grid. With the increase of the concentrated capacity of such generating facilities, and their general share in the total electrical power generation mix, the importance of the reliability of the protection schemes for such node points increases. For the particular study, a model was made for a simple HV busbar system with simulated internal (on the busbar system) fault and external one – in the outgoing power lines. By utilization of IEC 61850 GOOSE (Generic Object Oriented System Event) message, the directional ground fault over-current protection was used for busbar protection logic for accelerated tripping of faults recognized “inside” the substation zone [9–11]. In such manner the classical bus differential function (ANSI 87) can be realized not with dedicated central unit and distributed measurement points at the bus connected feeders, but with data exchange between the feeder protection devices. Definitely, the proposed solution is not regarded as replacement of the bus differential protection, but as option to realize additional protection of node point. The proposed approach is to have instantaneous response.

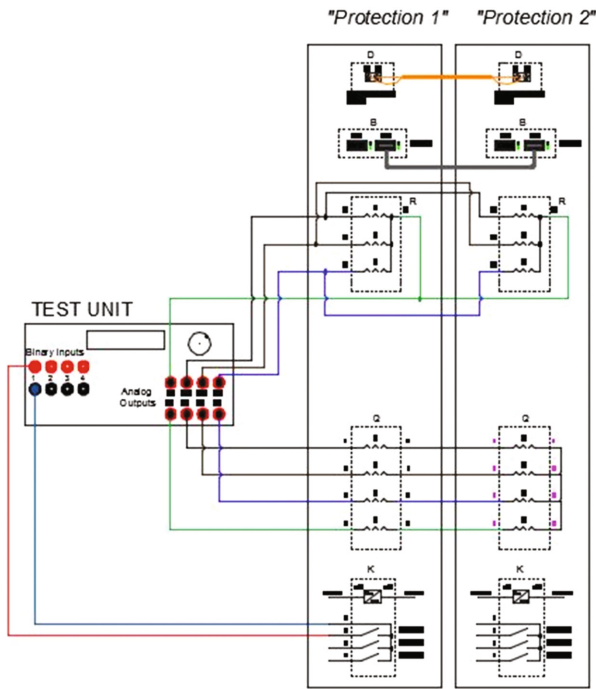


Fig. 1. Experimental test scheme.

The tests were made with two IEDs connected with fiber-optic cables and Ethernet link to exchange GOOSE messages, for the operation of the ground fault protection (Fig. 1). In this experimental setting were used Line Differential Protection IEDs. In this case the IED used fiber-optic to transmit differential type of data (like current, voltage, frequency etc.) with the opposite device. For GOOSE communication between the IEDs is used Ethernet channel (the scheme assumes two IEDs installed on two outgoing feeders in one substation). The “busbar voltage” was supplied to both devices from the respective analog outputs of the testing device. Two main groups of experiments were made – one with current supplied to the protection devices flowing “straight” for both and another when the current is fed in “reversed” direction to one of the IEDs.

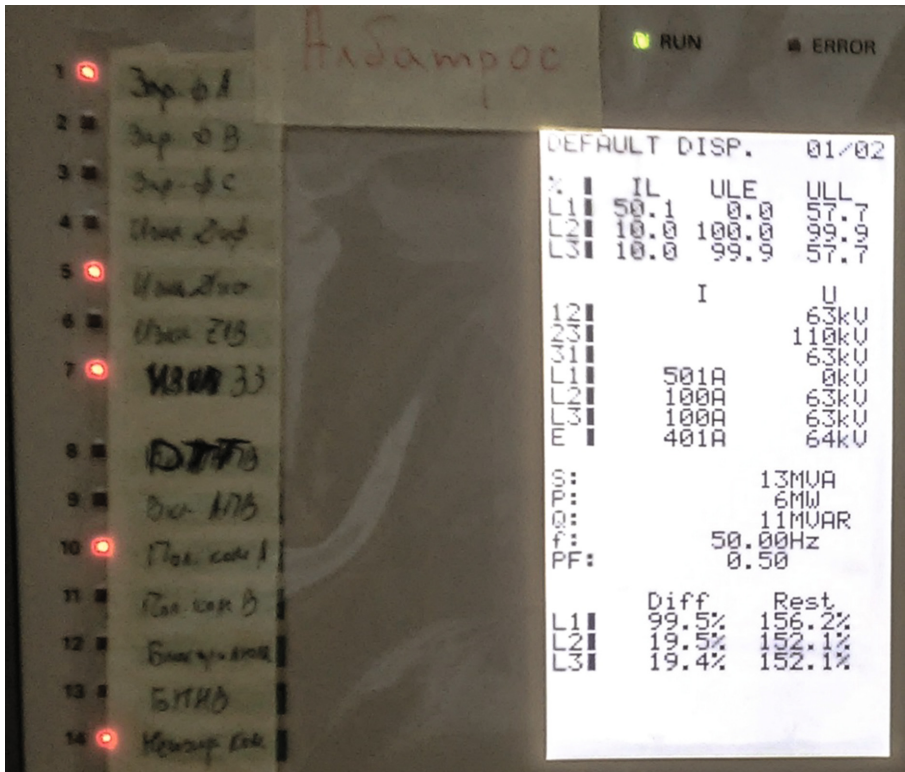


Fig. 2. Display of the IED.

In Fig. 2 is presented the measurement of the line protection IED in the case of currents injected as presented in Fig. 3, in order to simulate internal busbar fault. The two directional overcurrent functions both recognize “fault in the back” with respect to the power lines and the generated tripping commands are correct (selective).

With this scheme of exchange of GOOSE message between the IEDs, when both relays pick-up, but “fault in the back” is recognized, fault within the zone of the busbar

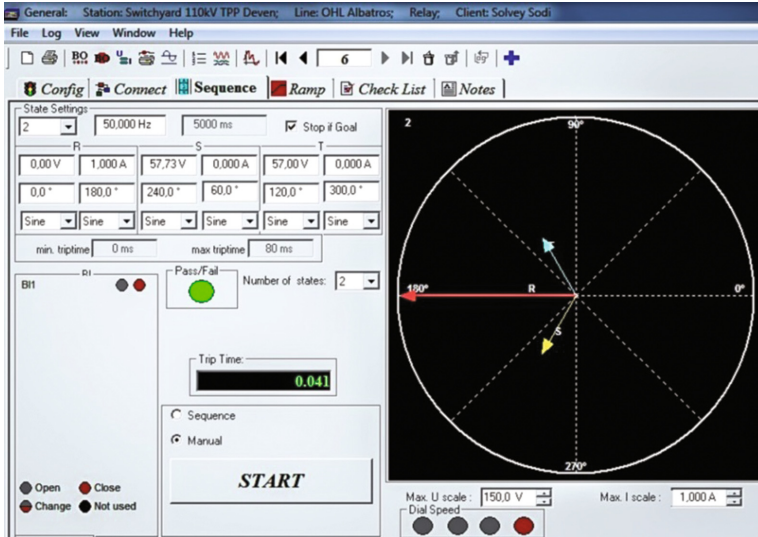


Fig. 3. Testing device signals phasor view.

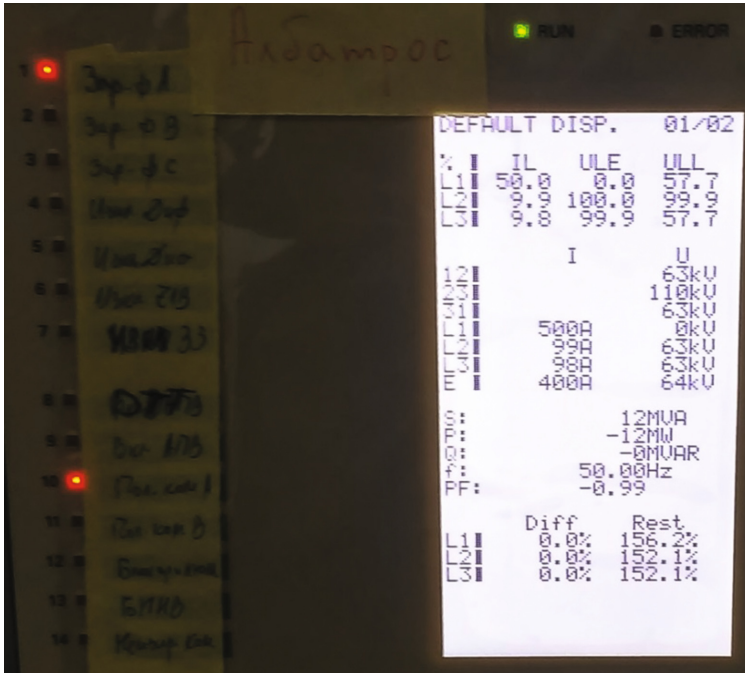


Fig. 4. Display of the IED.

system is identified. Such scheme can help to form busbar protection function (or with some compromise in the physical basis of the operation “artificial differential function”).

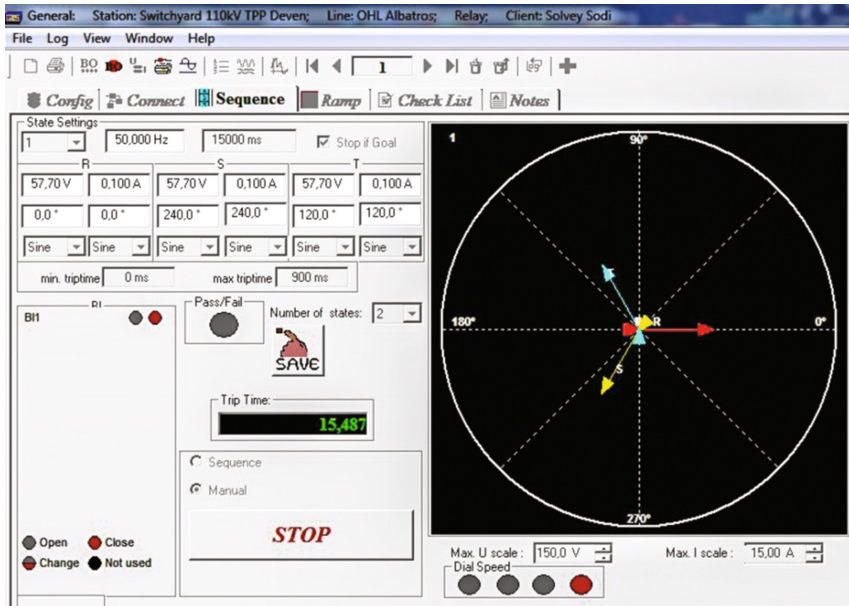


Fig. 5. Testing device signals phasor view.

The proposed scheme operation was tested for the case of fault occurring along one of the power lines [4, 6]. In Fig. 4 the behavior of the IED, which has received a blocking signal for ground fault recognized “towards the line” from the other IED, in order not to provide erroneous tripping function is presented. The primary currents were physically simulated with electronic IED testing device, directly connected to the respective analog signal inputs (Fig. 5). The IEDs providing protection of the power line correctly generated trip signal, and the other IED was blocked by the received GOOSE message, that the fault current flows “outwards” the busbar system. The tested principle can give improvement of the protection system functionality for small substations, or “node points”.

In relation to detection of single phase ground faults, the scheme is applicable for solid grounded networks. For resonance earthed or isolated star point networks, the scheme would be applicable for two or three phase short circuits, based on overcurrent element + directional criterion.

For solidly (effectively) grounded neutral networks with sufficient fault current to be selectively recognized for not being a load current, the power flow could be sufficient as criteria, but for low values of ground fault currents the complexly accounted criteria:

$$3I_0 = \dot{I}_A + \dot{I}_B + \dot{I}_C \tag{1}$$

$$3U_0 = \dot{U}_A + \dot{U}_B + \dot{U}_C \tag{2}$$

The specific angles characterizing the zero sequence power flow $\varphi_{(S_0)}$ shall be taken into account as well. Precise measurement of the residual voltage and current would be necessary for resonance earthed or isolated star point networks.

As limitation condition for the proposed scheme the specifics of the overcurrent protection used as basis shall be counted.

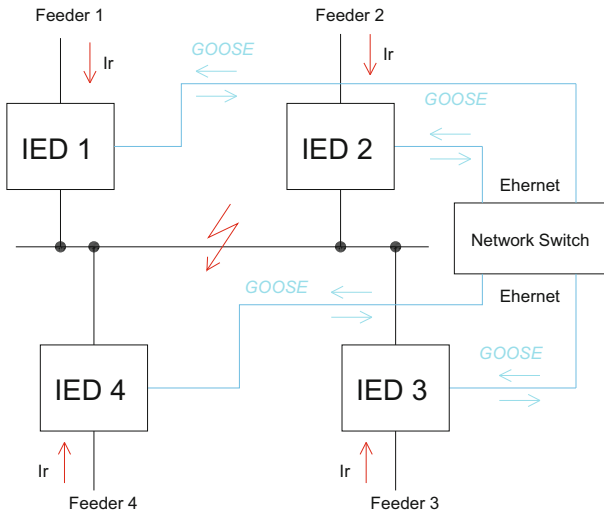


Fig. 6. Scheme to realize a bus protection for busbar with 4 feeders.

The typical setting of ground fault function (ANSI 67/67 N), which practically is used to form busbar protection “artificial differential” function is calculated as follows:

$$I_{pick-up} = \frac{\kappa_S \cdot \kappa_{rest} \cdot \kappa_{sh}}{\kappa_V \cdot \kappa_m} I_{m.l.}, \tag{3}$$

where:

- $I_{m.l.}$ maximum permissible load current;
- κ_S security factor;

κ_{rest}	factor of restart of induction machines;
κ_v	reset factor of the overcurrent functions;
κ_m	current transformer ration;
κ_{sh}	scheme coefficient;

In this case for determination of $I_{pick-up}$ is taken the maximum permissible normal current, which can be fed from the respective feeder to the bus section, at the worst in this case current distribution. The trip delay of the proposed bus protection function shall be coordinated with the settings of the outgoing feeders.

The fact that as initial “sensitive” element an overcurrent function is used, imposes some limitations towards the sensitivity of the functionality for low imbalanced currents, that may occur in case of high resistance faults in the busbar zone. If high start currents of induction machines have to be taken into account, this will make the scheme even more non-sensitive to high resistance faults in the protected zone. Exchange of GOOSE messages with measured values via the local Ethernet based network can help to improve the sensitivity, but still the delay of the scheme may be higher than dedicated bus differential (ANSI 87) protection scheme (Fig. 6). On other hand ultra-fast 87 function may impose overloading on the breakers, as the tripping will be in “relatively early” transient conditions, with significant DC component in the fault current.

3 Comparison of the Proposed Logic for Bus Protection with Available on the Market Industrial Products

The leading companies provide two typical schemes for bus differential protection:

“Centralized bus differential protection” - configuration with one central module (without bay units). All CTs signals are routed to one panel - “Busbar protection”, comprising the housing of the IED for centralized protection. The central unit collects also binary signal for position status of the respective commutation devices in the switchgear bays. This is the “classical” configuration, used in past for electromechanical and solid state devices. The producers use this concept in contemporary design IEDs [5, 14, 18] and the tendency is in the near future significant percent of world producers of “relay” protections to continue to use it. In this scheme there are no separate differential protection bay units as in “Distributed bus differential protection”, which means that bigger reliability can be expected from the “hardware”. As a disadvantage can be outlined, that when prophylaxis performed for some bays could be more difficult to render safe. Another disadvantage is the big length of copper cables and potential issues with cabling failures.

“Distributed bus differential protection” - the structure is based on the following concept: for every switchgear bay a separate bus differential bay unit is foreseen (peripheral module). The bay unit receives the signals from the CTs, position signals for commutation equipment, etc. and transmits the data to central processing module, typically via fiber optic cable. The main logic is in the central module. When fault is recognized, commands are distributed to the peripheral (bay) modules. This concept is applied in some of the new digital protection structures [13, 15, 17]. The distributed

IEDs concept provides flexible functionality and reduction of conventional instrumental copper cables is achieved. The disadvantage of this concept is the higher cost and some aspects of complexity of maintenance.

Exists one innovation variant [16], which represents that in every IED (like Overcurrent protection, Distance protection etc.) the bay control functionality, needed for differential protection function is integrated. In such design the Central module, which forms the bus differential protection is in permanent communication mode via dedicated channel with the IEDs for the respective bays. This concept is a variant to “Distributed bus differential protection”, but costs significantly less, as there are no special separate peripheral modules.

The proposed solution can be used as bus protection system, for places where the “classical” bus differential protection is not obligatory.

The provide solution can help realize fast responding and cost effective protection scheme, without dedicated hardware.

The proposed scheme can be used also as back-up of the bus differential function.

4 Conclusions

The provided application of GOOSE messages to form busbar protection function (of ground faults) on the basis of the power line protection IEDs is applicable for small “node points” on the grid, where the busbar differential protection realized with dedicated hardware may not be obligatory. Application of the proposed scheme can be realized in step-up substations of PVPPs, wind farms, small distribution substations in HV grids, etc., [3, 7].

In general, the provided solution can be realized with auxiliary contacts of the protection devices and conventional cables, but this will increase the complexity of the scheme and will reduce its reliability. Electromagnetic compatibility issues, galvanic separation benefit and simplicity of the design can be achieved by utilization of fiber-optic based communication [8]. The IEC 61850 GOOSE based communication and respectively acceleration /interlocking gives flexibility, noise immunity, and integrated solution [3, 12]. External events can be identified and register for transmission of data to higher level protection /grid control system. Some “external factors” still impede on some substations preferable utilization of shielded Ethernet cables than optics. These obstacles result of the necessity of more precise cable tracing, protection of rodents, some maintenance issues.

The obtained results give justification for the opportunity of GOOSE exchange IEC 61850 implementation in order to obtain reliable bus protection.

The proposed approach can give positive financial effect for investment designs, as additional functionality can be gained, without extra investments for high-cost equipment.

References

1. Apostolov, A.: Integration of distributed energy resources. PAC World Mag. **25**, 18–25 (2013)
2. Velez, J., Ward, S., Elizondo, D.: System Integrity Protection System (SIPS). PACWorld Mag. **27**, 38–43 (2014)
3. Adamiak, M., Baigent, D., Mackiewicz, R.: IEC 61850 communication networks and systems in: substations, pp. 61–68 (2009)
4. Application manuals for SIPROTEC Protection Relays, SIEMENS
5. Buyer's Guide Busbar differential protection IED REB 670, ABB (2005)
6. Fernandes, C., Borkar, S., Gohil, J.: Testing of goose protocol of IEC61850 standard in protection IED. Int. J. Comput. Appl. **93**(16), 30–35 (2014)
7. Falk, H.: IEC 61850-90-5 – an overview (2008)
8. Fries, S., Seewald, M.: Information security for energy automation: IEC 62351 – challenges and Solutions. Magazine for the energy industry (2008)
9. Hoyos, J., Dehus, M., Brown, T.: Exploiting the GOOSE Protocol: A Practical Attack on Cyber – Infrastructure, 1508-1513. University of Colorado, USA (2012)
10. Kriger, C., Behardien, S., Retonda-Modiya, J.: A Detailed Analysis of the GOOSE Message Structure in an IEC 61850 Standard – Based Substation Automation System. University of Technology South Africa, Cape Town (2013)
11. Kush, N., Ahmed, E., Branagan, M., Foo, E.: Poisoned GOOSE: Exploiting the GOOSE Protocol, pp. 17–22. Queensland University of Technology (2014)
12. Seeley, N.: Automation at Protection Speeds: IEC 61850 GOOSE Messaging as a Reliable, High – Speed Alternative to Serial Communications, Spokane, Washington (2008)
13. ABB Switzerland Ltd Power Systems: Distributed busbar protection REB500 including line and transformer protection Product Guide
14. ABB Power Technologies AB: Substation Automation Products Technical reference manual. Busbar differential protection IED REB 670
15. Siemens, A.G.: Department of EV S PSN, D–13623. SIPROTEC Manual, Distributed Busbar/Breaker Failure Protection 7SS52, Berlin, Germany
16. SIPROTEC 5 Low-Impedance Busbar Protection 7SS85
17. Protecta Electronics Ltd. Distributed busbar protection OGYD manuals, Hungary
18. Protecta Electronics Ltd. Centralized busbar protection DGYD manuals, Hungary

Author Index

A

Aleksieva, Veneta, 228
Alexandrova, Mariela, 312, 420
Andreev, Simeon, 239
Arabiat, Sereen, 106
Arustamov, Sergey, 50
Atanasov, Nasko R., 420
Atanasov, Nasko, 312

B

Barkovskii, Simon, 21
Bataineh, Omar, 106
Belyak, O.A., 171
Blokhin, Yury M., 11
Bogdanov, Dimitar, 459
Borisova, Lyudmila, 96
Bulgakov, Mikhail, 178
Burdo, Georgy, 67
Butakova, Maria A., 128

C

Cechulin, Andrey, 178
Chernov, Andrey V., 128
Chirikov, Victor A., 210
Chislov, Oleg N., 161

D

Demirova, Siyka, 271
Dimitrov, Georgi, 459
Dimitrov, Valery, 96
Dimitrova, Ekaterina, 376
Dimitrova, Krasimira, 410
Dimitrova, Neli, 201
Docekal, Tomas, 57
Dovramadjiev, Tihomir, 42

F

Fedosovsky, Michael, 50

G

Ganchev, Todor, 323
Garipova, Julia, 340
Georgiev, Anton, 201, 340
Georgieva, Todorka, 271
Gerasimov, Krum, 396
Gibner, Ya.M., 146
Gonzalez-Longatt, Francisco, 459
Grigorov, Ivan V., 420
Grigorov, Ivan, 312
Guda, Alexander N., 161
Gurjanov, Andrey, 50
Guskov, Gleb, 3
Gyurov, Valentin, 247

H

Hadzhidimov, Iliya, 191
Haka, Aydan, 228
Hendrych, Jakub, 332
Hjeelah, Dina Abu, 106

I

Ilicheva, Vera V., 161

K

Kabanov, Aleksey A., 32
Kabanova, Ekaterina N., 32
Kalinkov, Kalin, 323
Kamenov, Yoncho, 396
Kartashov, Oleg O., 128
Kartiev, S.B., 76
Klimenko, A., 84
Kochin, Alexander E., 349
Kolesnikov, M.V., 146
Kolpakhchyan, Pavel G., 349
Korobeynikov, Anatoly, 50
Korobkin, V., 84
Kotenko, Igor, 178
Kovachev, Dimitar, 376

Kovalev, Sergey M., 119
Kovářová, Kateřina, 332
Kumpová, Ivana, 332
Kunčický, Radim, 332
Kureychick, V.M., 76

L

Larin, A.E., 171
Ličev, Lačezar, 332
Lyabakh, N.N., 138

M

Markova, Valentina, 323
Mechkarova, Tatyana, 403
Mehmed-Hamza, Mediha, 220, 264, 386
Melnik, E., 84
Mrovec, Tomas, 428

N

Namestnikov, Alexey, 3
Neches, I.O., 449
Nikolaev, Nikolay, 301, 396
Nikolov, Nikolay, 201, 340
Nikov, Nikolay, 254
Nurutdinova, Inna, 96

P

Panov, Emil, 264, 280, 290
Papanchev, Toncho, 340
Pirogova, N.D., 449
Polyakov, Vladimir, 50
Przeczek, Samuel, 428

R

Rangelov, Yulian, 396
Rosenov, Emil, 191
Rybin, Victor M., 11
Rybina, Galina V., 11

S

Sergienko, Elena S., 11
Shabelnikov, Alexander N., 119, 138
Shaikhiev, Alexey R., 349

Shukalov, Anatoly, 50
Simeonova, Anna, 254
Simonik, Petr, 428
Skulev, Hristo, 42
Slanina, Zdenek, 57, 439
Slavov, Stoyan, 365
Stanchev, Plamen, 386
Stanev, Petar, 323
Stoianov, Plamen, 359
Stoyanov, Svilen, 32
Stoyanova, Aneliya, 403
Sukhanov, Andrey V., 119
Suvorova, T.V., 171
Svecova, Lucie, 439

T

Taran, Vladimir, 154
Trofimenko, Vladimir, 154
Tselykh, Alexander, 21
Tselykh, Larisa, 21

V

Vala, David, 439
Valchanov, Hristo, 239
Valchev, Vencislav, 376
Vasilev, Rosen, 42
Vasilev, Vladislav, 21
Vasileva, Margreta, 201, 386
Vereskun, Vladimir D., 128

Y

Yarushkina, Nadezda, 3
Yordanov, Krastin, 403
Yordanov, Yuliyani, 247
Yordanova, Marinela, 220, 264

Z

Zharinov, Igor, 50
Zhekov, Zhivko, 312, 420
Zhekova, Tatyana, 254
Zlatev, Dimitar, 340
Zlateva, Penka, 271, 403